GEOLOGICAL EVOLUTION OF WESTERN H.U. SVERDRUPFJELLA, DRONNING MAUD LAND, ANTARCTICA

By

GEOFFREY HUGO GRANTHAM

Submitted in partial fulfilment of
the requirements for the degree of
Doctor of Philosophy
in the Department of Geology
University of Natal
Pietermaritzburg
South Africa

Pietermaritzburg 1992

This is to certify that this thesis has not been
submitted to any other University and that,
unless specifically acknowledged, the work
in this thesis is the candidates own original work.

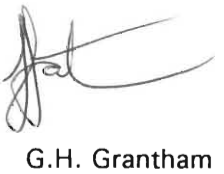

G.H. Grantham

Discussion between R. Messner and his young daughter on his return from Antarctica

- What did you find down there ?
- Infinity.
- What's infinity like ?
- White, peaceful, still, and everything moves slowly.
- So, is that like Heaven ?
- Perhaps that is Heaven.

-Did you look for Heaven in the Antarctic?

-No, I wasn't looking for anything there, but I discovered white infinity there.

-What do I have to do to see white infinity?

-Fight all your life to make sure that people don't put up buildings and electricity pylons, or burrow around or divide up the last wilderness amongst themselves.

From "Antarctica, Both Heaven and Hell" by Reinhold Messner. Translated by Jill Neate. The Crowood Press. Ramsbury, Wiltshire. 381pp.

TABLE OF CONTENTS

List of Maps and Enclosures

The maps and enclosures listed below are contained in sleeves at the back of the thesis. Maps 2-7 were compiled on aerial photographs flown by the German Antarctic Expedition in 1985. The photographs were used to compile outlines of the nunataks using a radial line plotter loaned from the Geography Department, University of Natal, Pietermaritzburg.

Map 1. Simplified general geological map of the study area.

Map 2. Geological Map of Jutulrora and Brekkerista.

Map 3. Geological map of Roerkulten.

Map 4. Geological map of Fuglefjellet.

Map 5. Geological map of Straumsvola.

Map 6. Geological map of Storjoen and Joungane.

Map 7. Geological map of Tvora.

ACKNOWLEDGEMENTS

This thesis was started while I was in the employ of the University of Natal, Pietermaritzburg. Much of the compilation was completed at the University of Pretoria.

From Pietermaritzburg, I wish to acknowledge and thank the following people.

Prof. D.R. Hunter for his support and guidance during this study and particularly his efficient and constructive criticism of countless earlier versions.

Dr. A.H. Wilson is thanked for reading the chapter on the Jutulrora Granite.

Mr. P.B. Groenewald is thanked for numerous discussions.

Freda Richards and Olive Anderson for assistence with the draughting of diagrams is gratefully acknowledged.

Mr. R. Seyambu, Mr. P. Suthan and Mr. M. Seyambu for thin section preparation, sample preparation, photography and XRF analyses.

From the University of Pretoria I would like to thank and acknowledge the assistence of Marina van Leeuwen for drafting, Sabine Verryn (electron microprobe and X-ray diffraction assistence) and Josiah Mahlangu for thin sections.

The electron microprobe analyses at the University of Cape Town were conducted with the assistence of Dick Rickard.

The companionship and assistance in the field of Mark St. Quentin, Leigh Ducasse, David Sleigh, Cow Preston and Bob Thomas is also greatly appreciated.

The friendly assistance of the helicopter crews of 30 Squadron is greatly appreciated. Without them movement in the field would have been a lot slower and far more hazardous.

I gratefully acknowledge the financial support of the Departments of Transport and Environmental Affairs who funded the research.

I wish to thank my parents for their unfailing support during my undergraduate and post graduate years of study.

Finally I wish to thank Lisa for her long suffering patience with my involvement in Antarctica, her unfailing assistance and support.

GEOLOGICAL EVOLUTION OF WESTERN H.U. SVERDRUPFJELLA, DRONNING MAUD LAND, ANTARCTICA

ABSTRACT

The oldest rocks of western H.U. Sverdrupfjella, the Jutulrora Formation, consist of interlayered mafic to felsic ortho- and paragneisses thought to represent calc-alkaline volcanic and clastic sedimentary rocks. These rocks are structurally overlain by the largely paragneissic, carbonate- dominated Fuglefjellet Formation which may represent a miogeosynclinal shelf facies. This sequence is structurally overlain by the dominantly para-gneissic Sveabreen Formation which may comprise a eugeosynclinal facies.

Three granitic bodies, the Roerkulten, Jutulrora and Brekkerista Granites intrude the Jutulrora Formation. The trace element chemistry of these granites suggest that accessory minerals played significant roles during their generation and crystallization. Various mafic intrusions, now discordant amphibolites, and a phase of diorite veining are present.

The Dalmatian Granite was emplaced syntectonically with the 470Ma Pan-African (or Ross) orogeny during D_3. This granite was generated by crustal anatexis at >5kb.

Jurassic age intrusions include alkaline complexes at Straumsvola and Tvora and numerous dolerite dykes, some of which postdate the alkali intrusions.

Five episodes of deformation are recognised. The first two resulted in folds (F_1 and F_2) which are co-planar and coaxial resulting in type 3 interference structures. Low angle thrust faulting occurred during D_2. Fold vergence and associated lineations suggest tectonic transport from the southeast during D_1 and D_2.

D_3 involved folding and reverse faulting. The orientations of the fault and axial planes of these structures suggest transport from the west and north-west. D_4 involved open dome and basin folding.

D_6 involved normal faulting and jointing, adjacent and parallel to the Jutulstraumen Glacier in the west. The joints affect the Tvora Alkaline Complex.

Three phases of metamorphism, related to the deformation, are recognised. The dominant mineral assemblages are typical of medium to high grade metamorphism and define S_1 and S_2 planar fabrics. Discordant mafic intrusions provide evidence of a long history of metamorphism. M_3 mineral development, commonly represented by biotite, is oriented axial planar to D_3 folds.

Comparison of the geology of the area with that of southern Mozambique reveals many similarities. These support reconstructions based on geophysical data which juxtapose Dronning Maud Land and southern Africa prior to the break up of Gondwanaland.

CHAPTER 1
INTRODUCTION

REGIONAL SETTING

The field work on which this study is based was conducted during the austral summers of 1983/1984, 1984/1985 and 1985/1986 under the auspices of the South African National Antarctic Program. A total of 88 days was spent in the field with fieldwork being possible on 69 days. In addition, two field seasons (1987/1988 and 1988/1989) were spent in the Sverdrupfjella to the southeast of the study area. The data collected during these subsequent trips are not considered here but have provided more insight into the geology of the Sverdrupfjella.

Each nunatak was mapped on a scale of approximately 1:10000 using either enlarged segments of 1:250000 topographical sheets or aerial photographs having a scale of approximately 1:10000. The geological maps are contained in a folder at the back of the thesis.

The study area is bordered in the west by the 40km wide Jutulstraumen Glacier which occupies the northern portion of the Pencksokket (Penck Trough)(Fig. 1.1). West of this glacier relatively undeformed sedimentary and volcanic rocks of the Ritcherflya Supergroup (Wolmarans and Kent, 1982) are exposed in the Ahlmanryggen and Borgmassivet (Fig. 1.1).

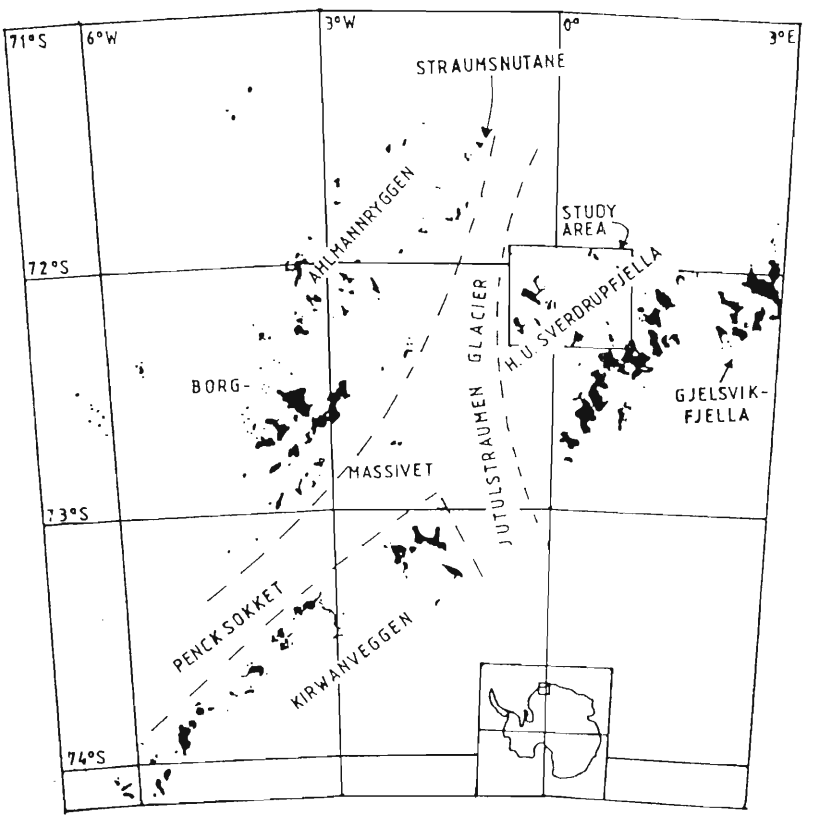

Figure 1.1. Locality map of the study area.

Mineral assemblages in the Ritcherflya Supergroup indicate that they have been metamorphosed at greenschist facies (Ferreira, 1986).

The study area extends from 0°35'W to 1°E and from 71°57'S to 72°20'S and constitutes the northwestern part of the H.U. Sverdrupfjella. The areal extent of the terrane is approximately 2400 square kilometres (Fig. 1.2). Exposure is limited to isolated nunataks which form less than 5% of the area, thus representing a maximum of 120 square kilometres of exposure (Fig. 1.2.).

Gneissic terranes similar to those in the study area have been described in the Sverdrupfjella main range (Hjelle, 1972; Roots, 1953,1969), to the east in the Gjelsviksfjella (Ravich and Solo'vev, 1966, van Autenboer, 1972) and to the southwest in the Kirwanveggan (Fig. 1.1, Roots, 1953, 1969; Ravich and Solo'vev, 1966; Wolmarans and Kent, 1982).

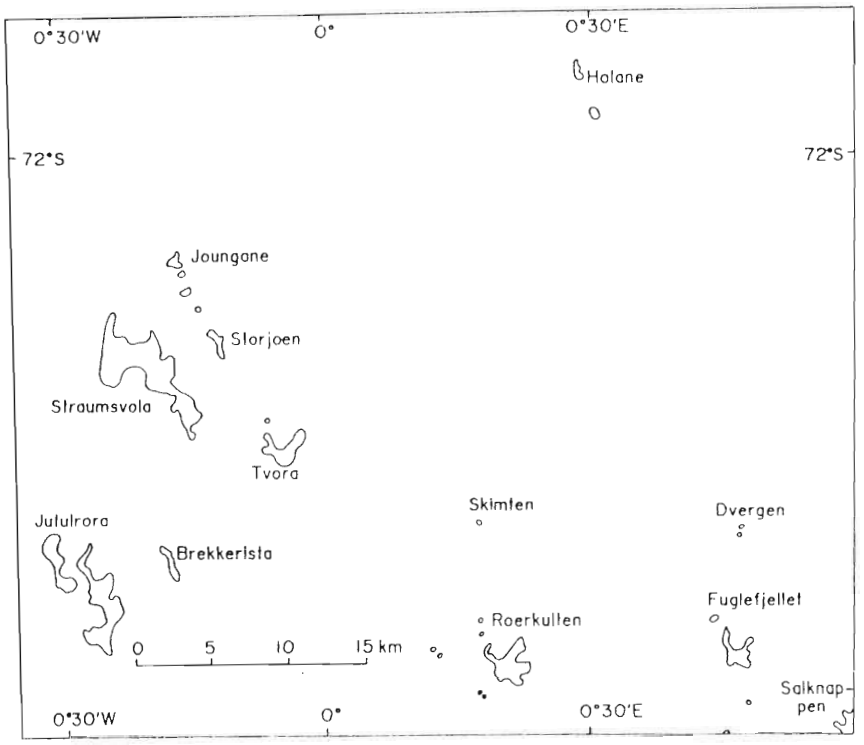

Figure 1.2. Map of distribution and location of nunataks in the study area.

PREVIOUS WORK IN AND ADJACENT TO THE STUDY AREA

The first geological investigation in the Sverdrupfjella was undertaken by the Norwegian-British-Swedish Antarctic Expedition during the period 1949-1952 (Roots, 1953,1969). This work was of a reconnaissance nature, covering the metamorphic terranes of the Sverdrupfjella and the Kirwanveggan east of the Penck Trough, as well as the relatively

undeformed sedimentary and volcanic rocks and intrusions of the Ahlmannryggen terrane, west of the Penck Trough (Fig. 1.1). Roots (1953, 1969) placed the metamorphic rocks of the Sverdrupfjella and Kirwanveggan in the Sverdrupfjella Group. A thickness of at least 2000m for the group was proposed. Roots (1953) indicated that the metamorphic rocks range from chloritic slate and schist to migmatite and pegmatite and from amphibolite to acid gneisses. He estimated that 80% of the rocks consist of banded gneisses of acid to intermediate composition. The distribution of garnet was found to be highly variable, being ubiquitous in some areas and rare in others. The garnets were reported to be grossular based on refractive index studies.

Roots (1953,1969) described the overall structure of the gneissic terrane as variable with foliations dipping between 10° and 40° to the southeast and northeast. Two generations of pegmatite were recorded. The first generation was considered to comprise "replacement pegmatites" developed during metamorphism and the second as "fracture-filling pegmatites" which are undeformed. Roots (1953) reported the occurrence of hornblende syenite at Gburektoppane. The nunataks at Gburektoppane were subsequently renamed and include Tvora, Straumsvola, Storjoen and Joungane (Fig. 1.2). The hornblende syenite referred to by Roots (1953) is exposed at Tvora. A poorly exposed angular unconformity at Barkleyfjella was interpreted by Roots to represent either two periods of deformation separated by an interval of erosion or a large scale thrust fault from the south. The name Barkleyfjella, used by Roots (1953), refers to an area southeast of the study area in the central portion of the Sverdrupfjella main range.

Studies by Russian workers between 1959 and 1961 were of a broad regional nature (Ravich and Solo'vev, 1966). The only nunataks in the study area to which reference was made are the Gburek Peaks (Tvora and Straumsvola, map 1,2.) where post-tectonic syenites were noted. Ravich and Solo'vev (1966) reported that the rocks in the study area are compositionally similar to granulite grade gneisses in the Gjelsvikfjella to the east but noted that they have amphibolite grade metamorphic assemblages. These authors reported that the rocks in the study area include schists, gneisses, and migmatites as well as boudinaged layers of "calciphyres" (carbonate-bearing rocks) and sheeted bodies of "metabasite". Ages of approximately 500Ma (K-Ar) have been obtained from biotites from the gneisses whereas ages of between 170 and 200Ma were recorded for the Tvora and Straumsvola Alkaline Complexes (Ravich and Solo'vev, 1966).

van Autenboer (1972) reported on the geology of Dronning Maud Land east of the study area. Two generations of gneisses were recognized in the metamorphic terrane of Dronning Maud Land. In general, the younger sequence comprises marbles, dolomites, calc-silicates, pyroxenites, graphitic schists, micaceous quartzites and amphibolites. The younger sequence (structurally?) overlies a gneiss complex which is virtually devoid of calcareous rocks. The

gneiss complex is dominated by medium-grained homogeneous augen or banded gneisses of granitic to granodioritic composition comprising biotite-, biotite-hornblende and biotite-hornblende-garnet gneisses. These gneisses were considered to be of sedimentary origin. The rocks were reported to show strong small scale folding. The migmatisation of the gneisses reportedly involved at least two stages in which the formation of veinlets, lenses and eyes of granitic leucosome were followed by later intrusion of aplite, granite and pegmatite. The only reference to nunataks in the study area was the report of a faulted zone characterized by chlorite and epidote on Jutulrora (Fig. 1.1).

The most detailed previous work in the study area was that conducted in 1971 by Hjelle (1972). Besides reporting similar rock-types to those described by earlier workers, Hjelle (1972) recognized two periods of folding, namely, F_1 folds with shallow plunges toward the north-northeast and south-southwest and F_2 folds with plunges of 10-30° toward the south-east overprinting F_1. Hjelle (1972) also noted an apparent increase in metamorphic grade toward the southeast which contrasted with the observation that stratigraphically higher lithological units appeared to be present as one traversed towards the southeast.

In the Kirwanveggan (Fig. 1.1) a well-stratified suite, consisting predominantly of leucogneisses, garnet-biotite plagiogneisses, amphibolites and hornblende plagiogneisses, has been reported (Wolmarans and Kent, 1982). Calc-silicate rocks have a restricted development. Within the metamorphic rocks there are minor granitic pegmatites, augen gneisses, pre- or syn-tectonic plutonic bodies of gabbroic and charnockitic compositions. A large scale thrust dipping 20° to the southeast is present at Tverrega in the Kirwanveggan and indicates thrusting toward the northwest (Wallace, 1980). This thrusting is related to an earlier phase of folding (Wallace, 1980). High angle normal or reverse faults with northeasterly and northwesterly strikes were also recognized (Gavshon and Erasmus, 1975; Heard, 1976; Meinecke, 1976). Rb/Sr whole rock isochrons indicate ages between 1173 and 876 Ma for gneisses from the Kirwanveggan (Wolmarans and Kent, 1982). K- Ar ages on biotite from the Kirwanveggan indicate a later metamorphic episode at approximately 500 Ma (Wolmarans and Kent, 1982).

STRATIGRAPHY

Formal steps to draw up a stratigraphic column in the study area were initiated by Roots (1953,1969) who placed all the metamorphic lithologies in the Sverdrupfjela Group without subdivision into formations. Hjelle (1972) considered that the Sverdrupfjella Group could be subdivided into four formations (Table 1.1) of which all but the Rootshorga Formation are represented in the study area.

Hjelle (1972) suggested that a discrete Fuglefjellet Formation might not be justified because it was distinguished from the Jutulrora Formation only by the presence of calcareous rocks.

Wolmarans and Kent (1982) subdivided the metamorphic terrane into the Sverdrupfjella Group and the Basic Meta-intrusive Suite which includes syn-tectonic charnockites, gabbros and dolerites intrusive into the Sverdrupfjella Group.

Sveabreen Formation	Mainly almandine-bearing (augen-) granite gneisses in part sillimanite-bearing.
Rootshorga Formation	Pelitic and granitic gneisses with some sillimanite almandine and cordierite.
Fuglefjellet Formation	Biotite-hornblende plagiogneisses with discontinuous beds and layers of marbles and skarns.
Jutulrora Formation	Biotite-hornblende gneisses with epidote, biotite gneisses, and granite gneiss. Calcareous rocks not recorded.

Table 1.1. Stratigraphic units recognized by Hjelle (1972) in the H.U.Sverdrupfjella.

LATE INTRUSIONS
Kirwanveggan Dolerites
Straumsvola/Tvora Alkaline Complexes
Sheet Granites
Dalmatian Granite

METAMORPHOSED INTRUSIVE ROCKS
A3 Amphibolite
Diorite Dykes
A2 Amphibolite
A1 Amphibolite
Jutulrora Granite
Roerkulten Granite
Brekkerista Granite

SVERDRUPFJELLA GROUP
Sveabreen Formation (pelitic gneisses)
Fuglefjellet Formation (carbonates)
Jutulrora Formation (tonalitic Grey Gneiss and heterogeneous Banded Gneiss)

Table 1.2. Stratigraphic units recognized in the northwestern Sverdrupfjella.

Grantham et al. (1988) further classified the rock units into four broad groupings, namely, (i) the Sverdrupfjella Group, (ii) Tabular granitoids, (iii) Mafic and intermediate intrusions and (iv) Late- and post-tectonic intrusions. The separate status of the Fuglefjellet Formation was maintained and the metamorphosed intrusive rocks were subdivided according to their temporal relations to deformational events.

The stratigraphic table presented in Table 1.2 broadly follows Grantham et al. (1988) and has been compiled using the suggestions of previous workers and expanded further where necessary. This stratigraphic table will be used as a framework for the discussion of the field characteristics, petrography and geochemistry of the various units recognized.

ANALYTICAL METHODS

The major and trace element analyses presented in this thesis were made at the University of Natal, Pietermaritzburg. The analytical techniques for these analyses are presented in appendix 1. The rare earth element (REE) analyses were undertaken at the University of Stellenbosch and the electron microprobe analyses (discussed in chapter on the metamorphic history) were done at the Universities of Cape Town and Pretoria. The normalizing values for the REE's are those of Wakita et al. (1971) and are used on the recommendation of Henderson (1984a, pp 9). A compilation of partition coefficients (K_d) is presented in appendix 3 along with the references from which the K_ds were derived. The K_ds used in the modelling in this thesis are, where possible, largely average values for the types of rock involved, eg. acid or basic.

The Fe_2O_3/FeO contents were estimated using the method of Le Maitre (1976) for plutonic rocks. The abbreviations of mineral names used in the thesis are those recommended by Kretz (1983).

CHAPTER 2
LITHOSTRATIGRAPHY

INTRODUCTION

The field relations of the rock types, described in this chapter, have been used to construct the stratigraphic table presented in Chapter 1. The oldest rocks in the study area are represented by the Sverdrupfjella Group which consists in the study area of the Jutulrora, Fuglefjellet and Sveabreen Formations. Intrusive into these formations are numerous bodies displaying a great diversity of compositions including amphibolites, granitoids, syenites and dolerites. These intrusive rocks are broadly divided into a) the metamorphosed intrusive rocks and b) the late intrusions. The former incorporates those intrusions which display evidence of deformation and the development of metamorphic minerals defining a planar fabric. The late intrusions include those which appear to be undeformed and which display primary igneous mineralogies.

THE SVERDRUPFJELLA GROUP

Introduction

The relative ages of the Jutulrora, Fuglefjellet and Sveabreen Formations of the Sverdrupfjella Group cannot be determined because of the paucity of exposure and the fact that primary structures in the Sverdrupfjella have been virtually totally destroyed by superimposed deformation and metamorphic events. These formations display similar structural histories and are therefore described from the structurally lowest to the structurally highest.

Jutulrora Formation

Two major lithological units are distinguished in the Jutulrora Formation and are termed the Grey Gneiss Complex and the Banded Gneiss Complex, respectively. The distribution of the two types is shown on map 1 (maps are located in a pocket at the back of the thesis). The rocks of these two units are conformably intercalated and therefore no relative age between the units is implied. The criteria for distinguishing the two unit types can best be described with reference to figure 2.1. The Grey Gneisses are typically relatively homogeneous, dominantly intermediate in composition (see chapter 3) and display a coarse layering with individual layers typically being tens of metres thick. The compositional variation between layers in the Grey Gneiss Complex is commonly minor and subtle, being defined by variations in the proportions of felsic and mafic minerals. The Banded Gneisses show great compositional variation ranging from ultramafic to felsic (see chapter 4) with layers commonly only a few metres thick.

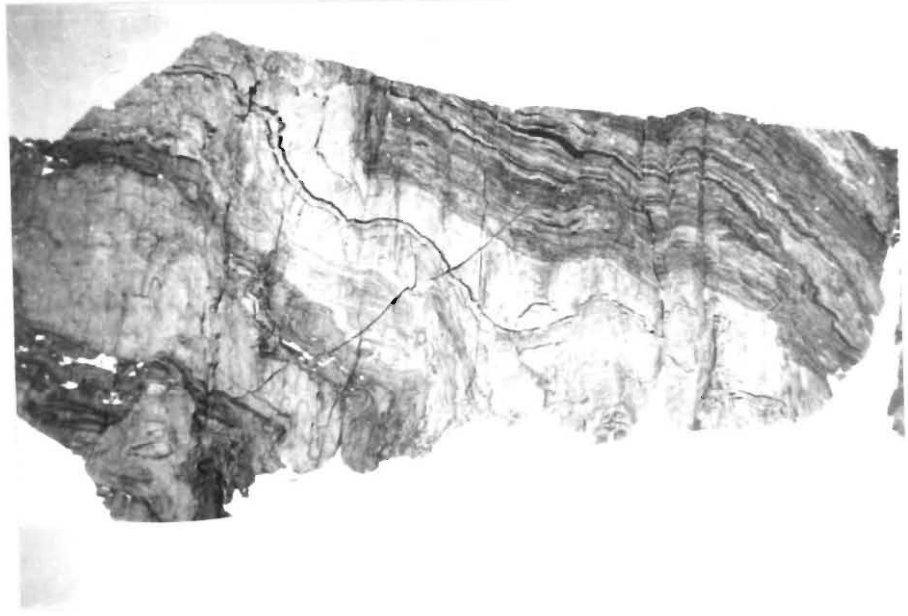

Figure 2.1. An east-west vertical exposure on southern Jutulrora in which the sheet- like Jutulrora Granite separates Banded Gneisses in the hanging wall from Grey Gneisses in the foot wall. The exposure is approximately 400m high.

Figure 2.2. Deformed carbonates of the Fuglefjellet Formation at Fuglefjellet. Person at top right for scale.

Rocks of granitic composition that intrude the Jutulrora Formation include the Jutulrora, Roerkulten and Brekkerista Granites. At least three generations of rocks of mafic composition, termed A1, A2 and A3 amphibolites, respectively, were emplaced into the Jutulrora Formation. Post-metamorphic intrusions into the Jutulrora Formation include the Dalmatian Granite, the Kirwanveggan Dolerites, the Sheet Granites and the Straumsvola and Tvora Alkaline Complexes.

The Fuglefjellet Formation

Exposures of this formation are restricted to Fuglefjellet and Dvergen; the former nunatak being the type locality (see maps 1,4). The dominant characteristic of this formation is the presence of calcareous and calc- silicate rocks. Interlayered with the carbonates are layers of amphibolite, quartzofeldspathic gneiss, a metaconglomerate and tonalitic gneisses similar in appearance and composition to those of the Grey Gneiss Complex (Fig. 2.2). The Fuglefjellet Formation is intruded by mafic sheets which are classified as A2 amphibolites (see below). Post-metamorphic intrusions into the Fuglefjellet Formation include the Dalmatian Granite and the Kirwanveggan Dolerites.

The Sveabreen Formation

This formation forms a very small portion of the geology of the study area being exposed only in the southeastern corner at Salknappen (Map 1). It is best exposed at Romlingane (1° 10'E , 72° 10'S) which lies to east of the study area. The rocks of the Sveabreen Formation within the study area are typically pelitic in composition with minor amphibolitic and quartzofeldspathic layers. The Sveabreen Formation contains a porphyroclastic granitoid sheet which may form part of the Vendeholten Granite Suite (Grantham *et al.* 1988). No contact between the sheet and the enclosing gneisses is seen because of a high degree of shearing. Post- metamorphic intrusions into the Sveabreen Formation include the Kirwanveggan Dolerites and the Dalmatian Granite.

THE META-INTRUSIVE ROCKS

Introduction

Within this group, rocks of basic, dioritic and granitic composition are distinguished.

Granitic intrusions

The earliest intrusive rocks recognized are granitic in composition and include the Jutulrora, Brekkerista and Roerkulten Granites which are sufficiently extensive to form mappable units (see maps 1, 2 and 3). Numerous smaller intrusions similar in appearance to these granites are also present in the study area. It is not possible to determine the relative ages of the various intrusions because they are never in contact and all display planar foliations concordant with

those in the surrounding gneisses. Broadly, two varieties of granite may be distinguished, namely equigranular medium-grained varieties (eg. Jutulrora and Roerkulten Granites) and porphyroclastic varieties (eg. Brekkerista Granite).

The Jutulrora Granite

The Jutulrora Granite is a sheet-like body intruded between Banded Gneisses and Grey Gneisses of the Jutulrora Formation and is well exposed on a vertical cliff face on the southeastern portion of Jutulrora (Fig. 2.1). The areal extent of the granite in plan is small, of the order of 5000m^2 (map 2). The contacts of the granite with the country rock are not well exposed, however at the northern contact (ie. the contact with the underlying Grey Gneisses) xenolithic fragments of Grey Gneiss and amphibolite were noted in the granite. The granite is intruded by mafic sheets up to 2m thick which have a planar foliation parallel to that in the granite which serves to identify the mafic sheet as an A1 amphibolite. Kirwanveggan Dolerite dykes of the Post-metamorphic Suite also intrude the Jutulrora Granite.
The Jutulrora Granite is medium-grained, equigranular, and pale pink to orange in colour and is characterized by a strong planar foliation defined by biotite and hornblende.

The Roerkulten Granite

The Roerkulten Granite consists of two bodies, a westerly body which is poorly exposed and an easterly body which forms a tabular body approximately 120m thick (Fig. 2.3). The granite is, in appearance, very similar to the Jutulrora Granite but shows clear discordant contacts with the enclosing Grey Gneiss at Roerkulten. The western contact of the easterly body is highly irregular with numerous apophyses intruding the Grey Gneisses whereas the eastern contact is relatively smooth and regular. However, just above the snow line in figure 2.3 at A, the contact is deformed by a fold considered to be of F_3 age (see later). The closure of this fold is visible at B (Fig. 2.3) where the Grey Gneiss is folded. The upper limb of this fold dips westward at approximately 60° whereas the lower limb dips at a shallow angle (approximately 25°) to the east defining a fold with an approximately horizontal fold axis and an axial plane which dips approximately 25°W (see figure B on map 5). The western body is poorly exposed with only its eastern contact being seen.

Mafic sheets, classified as A1 amphibolites, also intrude the Roerkulten Granite and are indistinguishable from those intruding the Jutulrora Granite in terms of their foliation. The Roerkulten Granite is intruded by undeformed pegmatites which are grouped with the Sheet Granites of the Late Intrusions.

These granites are similar to the Jutulrora Granite, being medium- grained, equigranular, and

pale pink to orange in colour. They are also characterized by a strong planar foliation defined by biotite and hornblende.

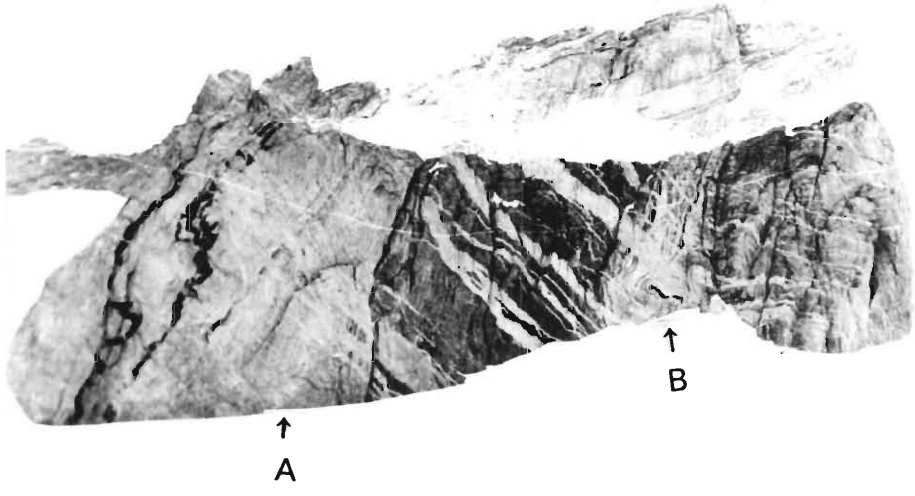

Figure 2.3 Photograph of the eastern sheet of the Roerkulten Granite. The granite underlies the left portion (leucocratic) of the buttress in the foreground and contains the folded mafic-sheets. The right portion of the buttress and the background are underlain dominantly by Grey Gneisses, crosscut by inclined pegmatitic sheets. The height of the fore-ground exposure is approximately 100m.

Provisional Rb/Sr isotopic data from whole rock samples suggest an age of approximately 926 $\pm$ 31Ma (R_o =0.70939) for the Roerkulten Granite (Moyes and Barton, 1990).

The Brekkerista Granite

The Brekkerista Granite is pink to orange coloured, porphyroclastic and displays rodded crystals of microcline up to 2cm in diameter. The rodded microcline grains define a strong lineation which plunges steeply (40°) to the east (Fig.2.4 and stereonet K on map 2). The granite is exposed in two discrete intrusions at Brekkerista. Their contacts with the enclosing Banded Gneisses are concordant with the planar foliation and lithological layering of the Banded

Gneisses. No unequivocal intrusive contacts were seen. The two bodies of Brekkerista granite are considered to represent portions of the same sheet repeated at the level of exposure by folding.

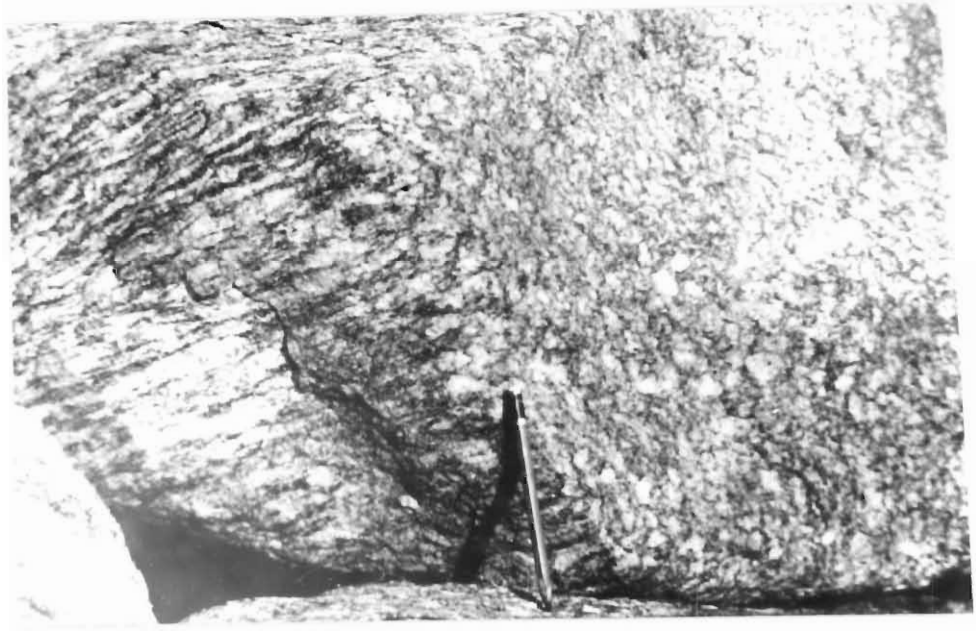

Figure 2.4. Porphyroclasts in the Brekkerista Granite. The pencil is approximately 10cm long. The left hand part of the photograph shows the foliation defined by the rodded feldspars whereas the right hand side displays a different orientation perpendicular to the feldspar rods.

This conclusion is based on the recognition of M folds in the Banded Gneisses separating the two bodies. These M folds are interpreted to indicate the existence of a major antiformal closure separating the two bodies. The Brekkerista Granite is intruded by mafic sheets, pink granitic veins and grey dioritic veins. Foliations in the mafic sheets are parallel to both those in the Brekkerista Granite and in the surrounding gneisses. The mafic sheets are therefore considered to be belong to the A1 amphibolites (see below). The mafic sheets are themselves cut by grey dioritic veins which are in turn cut by pink granitic veins. The latter have a chemical composition similar to the Dalmatian Granite (see later).

Mafic Intrusions

Three generations of discordant mafic sheets and one generation of discordant mesocratic grey dioritic aplite have been identified, all of which have been metamorphosed to varying degrees. These bodies are not large enough to be shown on any of the maps.

A1 Amphibolite

The recognition of the first generation mafic sheets is based on the development of a planar fabric, S_1, which is parallel to the enclosing gneisses. A sketch of an example of this generation is shown in figure 2.5. The stereographic projection showing the structural data pertaining to this mafic sheet is presented on map 2 as stereonet H. Although this sheet was not seen to be discordant, the orientation of the various portions of the boudinaged sheet suggest that the body is discordant because they are oriented at right angles to the planar foliation which is generally concordant to the layering. Quartz veins developed in this amphibolite define folds which have axial planar foliations. Other examples of the A1 amphibolites include the mafic sheets which cut the Jutulrora, Roerkulten, and Brekkerista Granites.

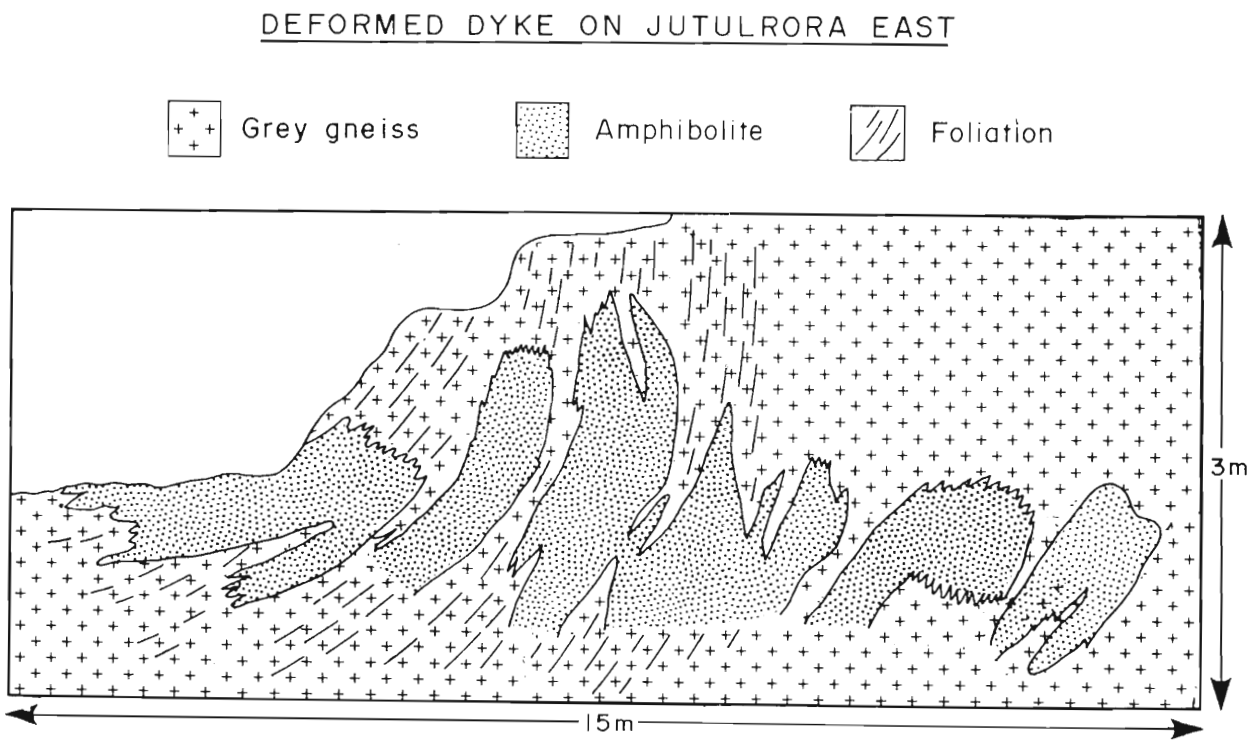

Figure 2.5. Sketch of a mafic sheet discordant to foliation in Grey Gneisses at Jutulrora.

A2 Amphibolite

The second generation of mafic sheets is recognized by having either foliations which are discordant to the S_1 planar foliation in the intruded host rocks or the mafic sheets clearly cut quartzofeldspathic leucosomes in the gneisses (Fig. 2.6). These leucosomes are either arranged parallel to the S_1 foliation in the gneisses or define F_1 folds indicating that the leucosomes were pre- or syntectonic. Examples of this variety of mafic sheet are recognized at Brekkerista, Roerkulten, Fuglefjellet and Straumsvola. These mafic intrusions may include more than one generation but it has not been possible to distinguish them using their field relations. Attempts to distinguish these amphibolites based on their chemistry will be made in chapter 10.

Figure 2.6. A2 amphibolite intruded discordantly to layering and foliation in Grey Gneiss at Roerkulten.

A3 Amphibolites

The recognition of this generation of amphibolite is based on the absence or local development of a planar fabric. The third generation of discordant mafic sheets is represented by examples at Brekkerista and Straumsvola. The amphibolite at Brekkerista locally has a planar

fabric defined by hornblende and biotite but elsewhere it is not foliated. A coarse fracture cleavage is also developed. The mafic sheet has relict plagioclase phenocrysts up to 2cm long (Fig. 2.7) which have been recrystallized to an aggregate exhibiting granoblastic textures and consisting of plagioclase and garnet. These garnets are restricted to area of the relict plagioclase phenocrysts.

The A3 amphibolites from Straumsvola show no planar fabric and have relict sub-ophitic textures.

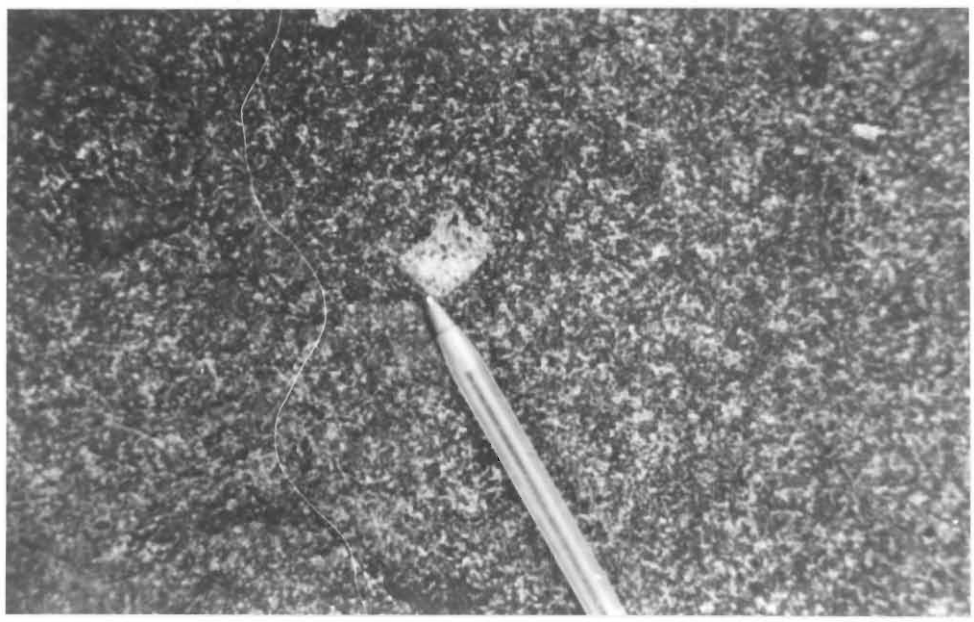

Figure 2.7. Relict plagioclase phenocryst in A3 amphibolite at Brekkerista.

Dioritic sheets

The dioritic sheets are up to 30 cm thick and intrude the Brekkerista Porphyroclastic Granite. The diorite is a medium-grained grey rock which displays a weak planar fabric defined by biotite and amphibole.

SYN TO POST-TECTONIC INTRUSIONS

Introduction

The post-tectonic intrusions include rocks of granitic, basic and alkaline (nepheline-bearing syenites to alkali granites) compositions. The ages of these intrusions range from approximately 450Ma to 170Ma (Moyes and Barton, 1990).

The Dalmatian Granite

On Brekkerista discordant sheets of leucogranite up to 10m thick cross-cut both the Grey Gneiss and Banded Gneiss (Map 2). A feature of this granite is the development of nodular structures up to 10cm in diameter having a melanocratic core and a leucocratic rim (Fig. 2.8). The mafic mineral in the dark cores is tourmaline. The leucocratic rim is characterized by muscovite, whereas the granite typically contains both muscovite and biotite.

Similar granites have been recognized at Fuglefjellet and Dvergen. At Dvergen a granite sheet was found to contain poikilitic tourmaline nodules where the granite intruded carbonates of the Fuglefjellet Formation. The granite is devoid of tourmaline away from the carbonate-rich country rocks and is characterized by porphyritic magnetite crystals surrounded by a leucocratic rim of quartz, feldspar and muscovite. Preliminary whole rock Rb/Sr isotopic data from the Dalmatian Granite suggest an age of approximately 470Ma.

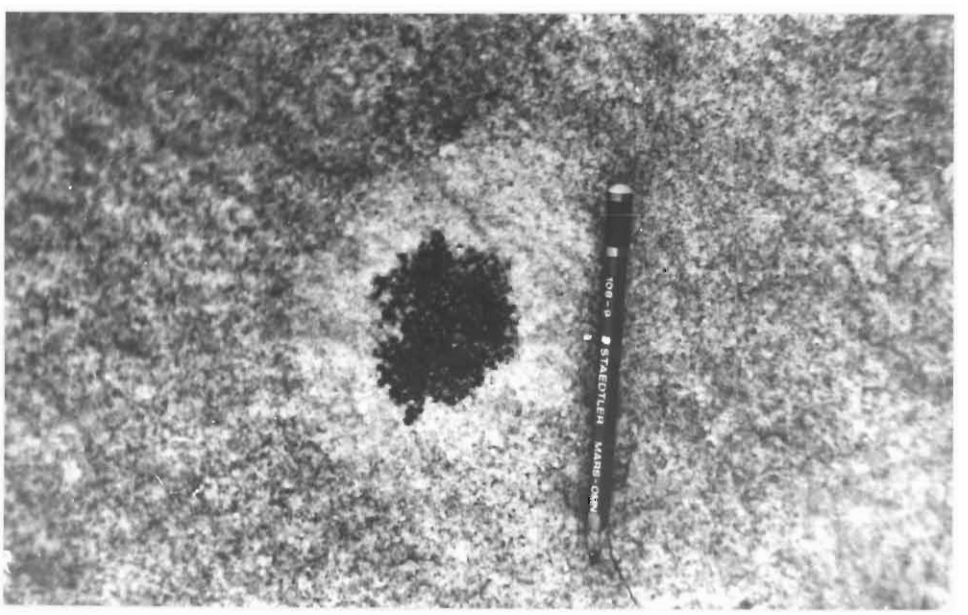

Figure 2.8. Nodular structure in the Dalmatian Granite.

Sheeted Granites

Granitic sheets occur as discordant layers up to 2 m thick (see Fig. 2.3 where pegmatites cut the Roerkulten Granite), are aplitic to pegmatitic in texture, and vary in colour from white to dark pink. The aplite veins are up to 30cm thick and intrude as dykes and subhorizontal sheets

into the Grey Gneisses at Jutulrora, Salknappen and Dvergen. Preliminary geochemistry shows that some samples of these rocks and the Dalmatian Granite are compositionally very similar. Others, however, have distinctive chemistries suggesting that there is possibly more than one generation of aplitic granites.

Included in the group of sheeted granites are pegmatites which locally are tourmaline-bearing. Granitic phases in these pegmatites are chemically distinct from the pink aplite veins and pink granite sheets by virtue of their more sodic compositions (see later). These pegmatites are best exposed at Jutulrora where they intrude the Grey Gneisses, at Roerkulten where they intrude the Grey Gneisses and the Roerkulten Granite, and at Holane where they intrude the Grey Gneisses. These sheet granites will be described and discussed in the same chapter as the Dalmatian Granite (Chpt. 10).

Kirwanveggan dolerites

Although some of these dykes clearly intrude the Straumsvola Alkaline Complex (Fig. 2.9), the presence of xenoliths of dolerite in the Straumsvola Complex provides evidence that other dolerite dykes predate the complex as well. These undeformed dykes vary from a few centimetres to 30m in width (Map 2). The wider dykes commonly display a strong textural variation from fine grained margins to coarse olivine gabbros in the centres of the dykes. The thin, fine-grained dykes commonly display vesicles which typically are filled by calcite or prehnite or a combination of both these minerals. Two varieties of dyke are recognized, namely an olivine-bearing variety and an olivine-poor variety. The olivine-bearing dykes are distinguished from the olivine-poor types by their high content of opaque minerals, zonation in titanaugite grains, and the presence of euhedral to anhedral olivine and accessory red brown biotite. The olivine- bearing dykes display only incipient alteration which contrasts with the more intense alteration of the olivine-poor dykes which are characterised by extensive saussuritization of plagioclase.

The Straumsvola and Tvora Alkaline Complexes

The Straumsvola Alkaline Complex underlies Storjoen, much of Straumsvola, and a small portion of Joungane whereas the Tvora Complex is restricted to Tvora (Maps 1, 5, 6 and 7). The ages of the Straumsvola and Tvora Complexes are approximately 170-180Ma (170-200Ma K/Ar, Ravich and Solo'vev, p220, 1966; 170$\pm$4 Ma. unpublished Rb/Sr whole rock data, A.R. Allen, 182Ma Ar/Ar age on amphibole from Straumsvola, unpublished data, I. Evans). The Straumsvola and Tvora Alkaline complexes are clearly intrusive with numerous veins of syenite intruding the metasomatised gneisses surrounding the complexes. Xenoliths of the gneisses are common although sparsely distributed. At Tvora two generations of syenite are recognized, namely, an earlier mesocratic variety and a later leucocratic variety.

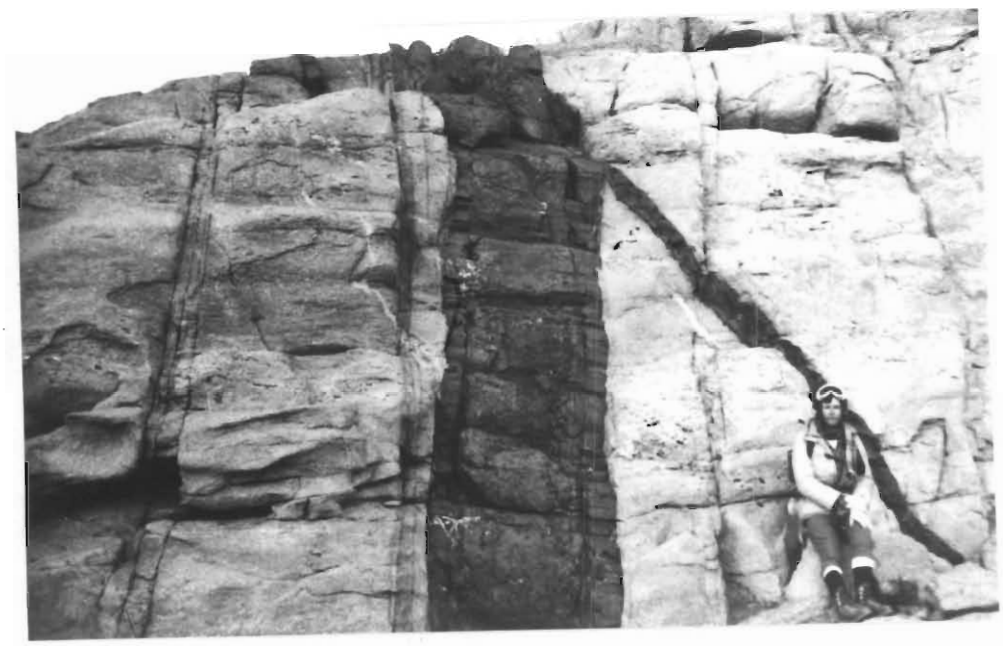

Figure 2.9. Dolerite dyke intruding the Straumsvola Complex.

Figure 2.10. Layering in the central portion of the Straumsvola Alkali Complex. The layers have a mean thickness of ~5m (C. Harris, unpublished data) and therefore the slope shown in the photograph is ~100m high.

Coarse-grained veins of leucocratic syenite intrude the mesocratic syenite and xenoliths of the mesocratic syenite are commonly found in the leucocratic syenite. Mineralogically the two varieties of syenite are similar with the darker colour of the mesocratic variety resulting from the presence of dark brown feldspars. The brown colour of the feldspars is considered to result from alteration because adjacent to the contacts of trachyte dykes intruded into the syenite, the feldspar grains become lighter in colour.

At least three intrusive phases have been identified in the Straumsvola Alkaline Complex. A central layered phase (Fig. 2.10). An inner and outer coarse-grained leucocratic phase and a mesocratic phase which separates the inner and outer coarse-grained leucocratic phase from each other. The age relations of the various phases will be discussed later in the appropriate chapter.

Associated with the alkaline complexes are numerous dykes which intrude the Straumsvola and Tvora Alkaline Complexes and adjacent country rocks. These dykes range in composition from alkali granites to lamprophyres and trachytes.

CHAPTER 3
THE GREY GNEISS COMPLEX

INTRODUCTION

The scale of banding in, and the field relationships of, the Grey Gneiss Complex were described in Chapter 2. In this chapter the general field appearance, petrography and chemistry of the Grey Gneisses and associated granitic gneisses will be described and these data utilised to propose an origin for the Grey Gneisses.

FIELD APPEARANCE

The gneisses of the Grey Gneiss Complex are dominantly leucocratic, although they vary from mafic to felsic. The gneisses are generally medium-grained and equigranular, consisting of varying proportions of plagioclase, K-feldspar, quartz, hornblende, biotite, epidote, zoisite, sphene, apatite and, in some samples, opaque minerals. Rare layers containing coarse plagioclase feldspar grains (1cm) have been observed (Fig. 3.1). The coarse feldspars are found only in layers. The Grey Gneiss Complex is characterised by lenticular epidote + magnetite-bearing pegmatites which are typically approximately 15cm long but may be up to 1m long (Fig. 3.2). The pegmatites display consistent orientations which locally are discordant to the lithological layering. At Roerkulten measurements of the pegmatite lenses indicate that they are oriented axial planar to F_2 folds (stereonet D on map 3). At Fuglefjellet the lenticular pegmatites are clearly folded by an F_3 fold (Fig. 3.3).

The Grey Gneisses contain concordant interlayers of two types. Amphibolite layers, typically 2m thick, constitute less than 5% of the total volume of the Grey Gneiss. The amphibolite layers are commonly boudinaged (Fig. 3.4) and display textural variations. Some layers are banded, reflected by differences in grain size but others are homogeneous. A crude foliation is present, aligned concordantly with that in the enclosing Grey Gneisses.

The second type of interlayered gneiss is granitic in composition. These gneisses are distinguished by their pale pink colour in the field as well as the absence of hornblende in thin section (see later). The contacts and planar foliations in the granitic gneisses are conformable with those in the enclosing Grey Gneisses.

Inclusions are rarely distributed in the Grey Gneisses although zones rich in inclusions are present (Fig. 3.5). One such zone is located stratigraphically very close to a contact with the Banded Gneiss Complex. The compositions of the inclusions are, however, unlike the Banded Gneisses but are similar to, and span the range of compositions represented in the Grey Gneisses. Other than the inclusions, the concordantly layered nature and the presence of porphyroclastic layers, no other structures of possibly primary origin were recognised in the Grey Gneisses.

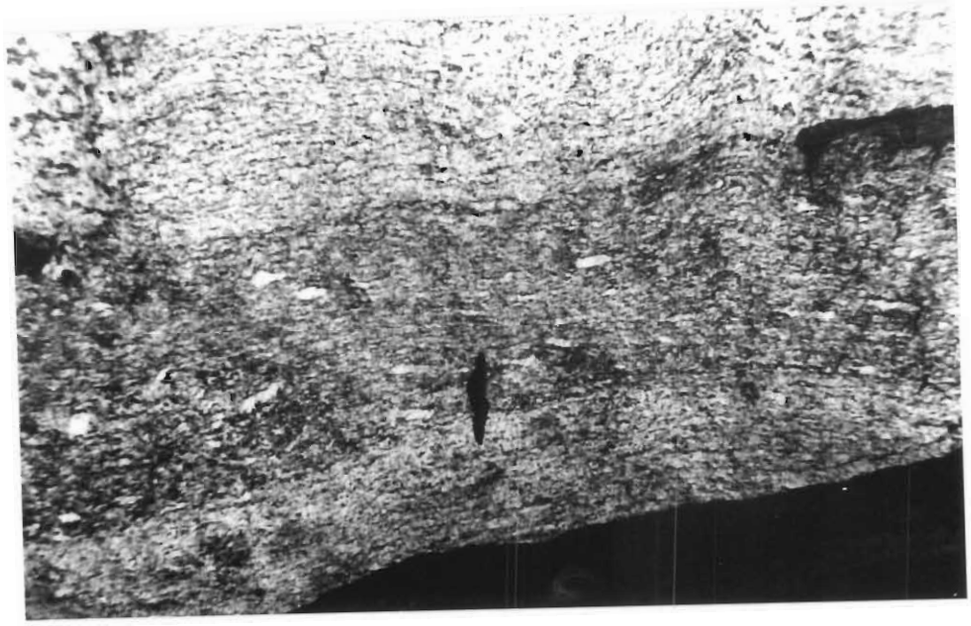

Figure 3.1. A thin layer of Grey Gneiss containing coarse grains of feldspar at Jutulrora. Pen at centre for scale.

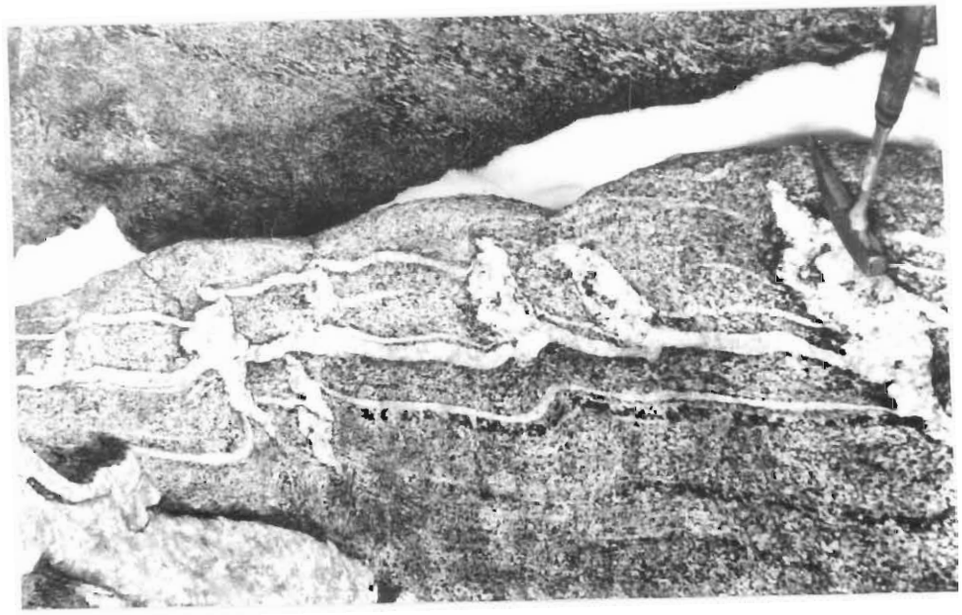

Figure 3.2. Lenticular epidote-bearing pegmatites in Grey Gneiss at Roerkulten. These pegmatites are probably the replacement pegmatites described by Roots (1953).

Figures 3.3. Lenticular pegmatites folded by F_3 at Fuglefjellet.

Figure 3.4. Boudinaged concordant amphibolite in Grey Gneiss at Jutulrora. The amphibolite is approximately 2m thick.

Figure 3.5. Inclusions or autoliths in Grey Gneiss at Jutulrora.

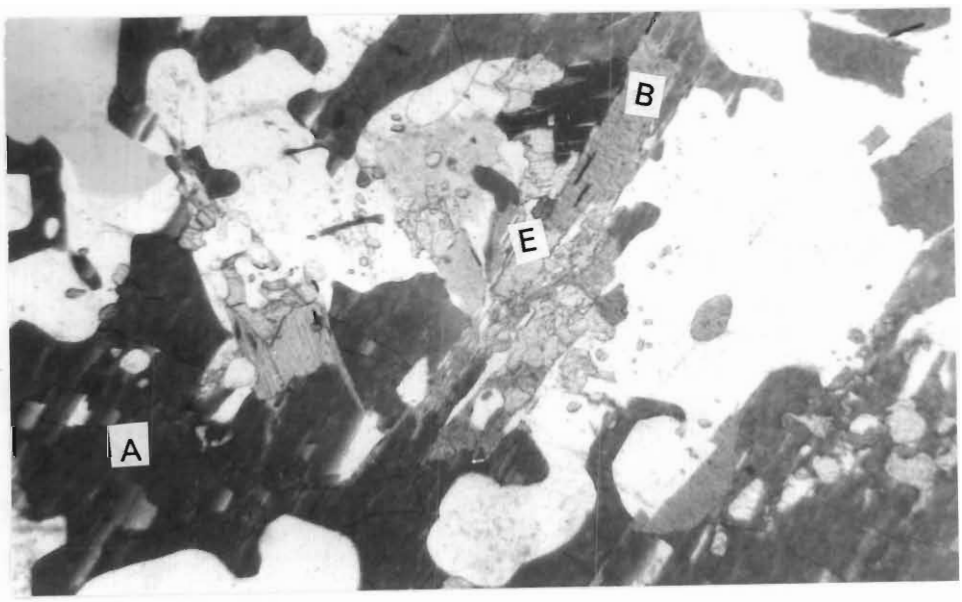

Figure 3.6. Photomicrograph of Grey Gneiss showing biotite partially replacing hornblende (Sample JE9). Field of view is 4mm. E = epidote, B = biotite, A = amphibole. The colourless (white) minerals are quartz and feldspar.

PETROGRAPHY

Representative modal analyses (based on approximately 1000 points per thin section) of the dominant minerals in the Grey Gneiss are presented in table 3.1. Mineralogically, the Grey Gneisses are fairly monotonous, the dominant minerals being plagioclase, K-feldspar, quartz, hornblende, biotite, epidote, and sphene. Varying proportions of these minerals result in some samples being amphibolitic or hornblende-rich (JE12, JE57), others granitic (JE10, JE25) with most being tonalitic (Table 3.1). In summary, the quartz content ranges from 4 to 32%, hornblende 1 to 28%, biotite 4 to 32%, sphene 0 to 3.5%, epidote 0 to 5.6% and feldspar 37 to 68%.

Sample No.	Qtz	Feld	Hbl	Bt	Spn	Ep		
JE9	15.0	57.8	12.2	12.7	0.5	1.8		
JE10	24.3	54.4	8.8	10.9	0.0	1.6		
JE12	9.3	53.0	27.8	6.0	1.2	2.7		
JE13	15.3	49.9	13.6	17.3	0.6	3.3		
JE16	20.4	52.6	10.1	14.5	0.4	2.0		
JE18	11.5	59.3	10.2	17.3	0.3	1.4		
JE24	13.2	58.6	8.8	16.8	0.4	2.2		
JE25	32.0	57.1	1.1	7.0	0.0	2.8		
JE26	24.0	47.3	8.1	17.9	0.3	2.4		
JE41	14.0	66.1	12.1	4.0	1.0	2.8		
JE42	15.3	37.7	11.9	31.7	2.0	1.4		
JE43	8.3	55.1	12.3	21.7	0.2	2.4		$\bar{x}$=2.4
JE57	7.5	47.7	26.5	14.3	3.5	0.5		s=1.08
JW11	9.0	55.0	13.0	19.7	0.3	3.0		n=22
JW2	10.6	52.0	12.0	22.0	0.3	3.1		
JW3	14.6	52.0	12.1	17.1	0.3	3.9		
JW4	9.1	50.1	21.7	16.7	0.2	2.4		
JW5	1.6	58.7	22.2	10.8	0.9	5.6		
JW6	13.9	53.6	8.3	20.9	0.3	3.0		
JW9	12.7	55.7	13.4	15.6	0.4	2.2		
JW17	13.8	63.0	10.1	11.1	0.5	1.5		
BK3	21.5	61.0	9.0	7.3	0.1	1.1	---	
RK11	28.8	65.4	1.4	4.1	0.2	0.1		
RK12	23.3	67.4	3.5	5.8	-	-		
RK13	4.3	33.2	28.0	32.5	2.0	-		$\bar{x}$=0.23
RK18	6.8	68.0	16.3	8.3	-	0.6		s =0.26
RK25	13.8	62.8	12.6	10.6	-	0.2		n=6
RK27	10.7	63.8	6.3	18.6	0.1	0.5	---	
H2	9.1	54.8	22.3	13.2	0.1	0.5		
H9	15.3	56.0	19.0	9.7	-	-		$\bar{x}$=0.38
H10	7.1	60.3	21.6	10.7	-	0.3		s =0.4
H12	9.7	59.1	22.7	8.3	0.1	0.1		n=5
H13	6.7	61.3	19.1	11.7	0.2	1.0	---	

Table 3.1. Modal mineralogy (vol%) of samples of Grey Gneiss. Plagioclase and orthoclase are combined under feldspar. The numbers on the right of the column represent the number of samples (n), the mean epidote content ($\bar{x}$) and its standard deviation (s). Feld = feldspar

In the modal estimates alkali feldspar and plagioclase are considered together because, without resorting to staining techniques, it is difficult to estimate their relative proportions. The reasons for this are that albite twinning is not present in all sections thus preventing easy

identification of plagioclase and, secondly, the alkali feldspar in many sections is orthoclase which is largely indistinguishable from the untwinned plagioclase. The granitic gneisses associated with the Grey Gneisses are distinguished from the more acid Grey Gneisses by the absence of hornblende.

The Grey Gneisses typically have a granoblastic texture with a strong planar foliation defined by aligned grains of amphibole and biotite. Hornblende occurs as xenomorphic poikiloblastic grains typically pleochroic light green to dark green locally exhibiting a blueish tinge.

Khaki-brown to olive-green biotite appears to replace the amphibole and, when this occurs, the alignment of the biotite flakes is oblique to that of the earlier amphibole (Fig. 3.6). The planar fabrics typically defined by amphibole are axial planar to F_1 and/or F_2 folds, whereas the axial planar fabrics to F_3 folds are commonly defined by aligned biotite flakes only (see chapter on structure).

Biotite is locally partially to completely altered to green chlorite with the chlorite and biotite commonly forming interstratified layers. Sphene is present in varying proportions whereas opaque ore minerals are present in very few samples. Sphene is commonly poikiloblastically enclosed in hornblende and plagioclase.

Plagioclase has compositions of $An_{26\text{-}30}$ (determined by the Michel-Levy method) and locally shows partial to complete sericitisation. Plagioclase exhibits patch antiperthite and locally encloses quartz poikiloblastically. Replacement of plagioclase by microcline is observed locally and is indicated by coalescence of patch antiperthite. Myrmekitic intergrowths are also present.

The K-feldspar is commonly microcline with characteristic cross-hatched twinning but locally orthoclase is dominant, showing no twinning. Quartz, plagioclase, and microcline are commonly poikiloblastically included in laths of hornblende. Quartz occurs as rounded grains and exhibits undulatory extinction.

Epidote occurs as idiomorphic to xenomorphic grains and is commonly (Fig. 3.6) adjacent to, or included in, biotite. The epidote is typically zoned and appears to partially replace hornblende locally.

METAMORPHISM

The mineral assemblage of the Grey Gneiss may be defined as hornblende + epidote + biotite + plagioclase + K-feldspar within which two mutually exclusive assemblages occur. Assemblage 1 consists of K-feldspar + hornblende + plagioclase and is characteristic of the hornblende amphibolite facies or medium grade of metamorphism. Assemblage 2 consists of biotite + epidote. These assemblages are shown in figure 3.7 where it may be seen that the tie-lines linking epidote and chlorite/biotite intersect the tie-line linking plagioclase and hornblende.

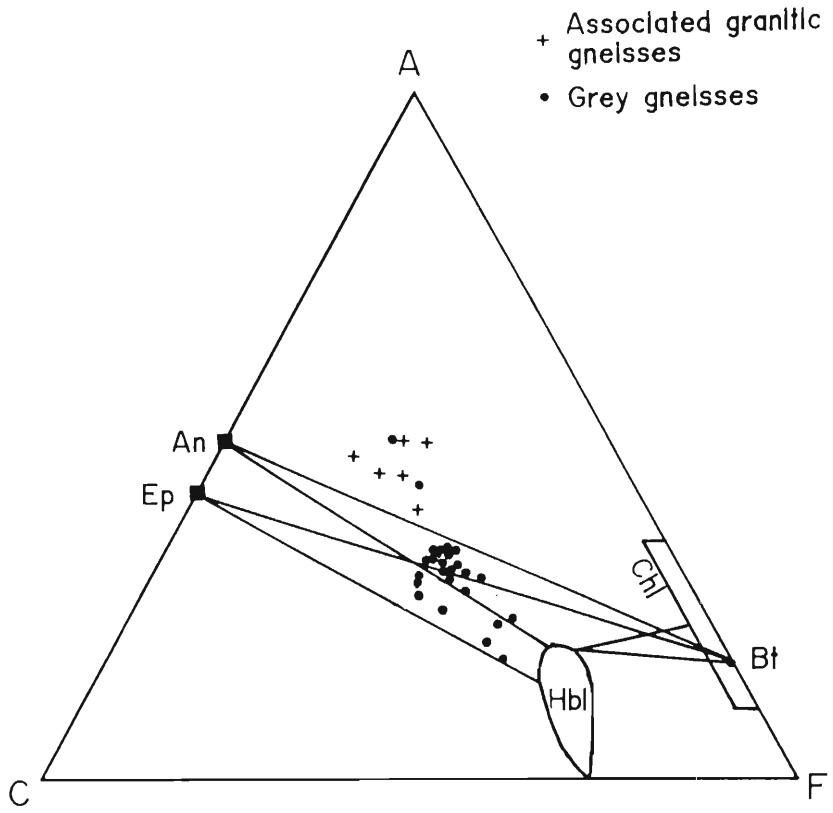

Figure 3.7. ACF diagram for the Grey Gneisses.

From the regional map (Map 1) it may be seen that Grey Gneisses are exposed at most of the nunataks in the area. The proportion of epidote in the Grey Gneiss appears to decrease from the west toward the north and east such that samples of Grey Gneiss at Jutulrora, Straumsvola and Brekkerista (in the west) have a mean epidote content of 2.4% (n = 22, s = 1.08, Table 3.1). At Holane (in the north) and at Roerkulten (to the east) the mean epidote contents are 0.38% (n = 5, s = 0.4,) and 0.23% (n = 6, s = 0.26) respectively (see table 3.1). The common association of biotite and epidote replacing amphibole retrogressively suggests the following reaction:

$6CaAl_2Si_2O_8 + Ca_2(Mg_2Fe_2Al)Si_7AlO_{22}(OH)_2 + 2KAlSi_3O_8 + 3H_2O \rightarrow$
$K_2(Mg_2Al_4)Si_6Al_2O_{20}(OH)_4 + 2Ca_2FeAl_2Si_3O_{12}(OH)_2 + 2Ca_2Al_3Si_3O_{12}(OH)_2 + 7SiO_2$
ie. 6 An + Hbl + 2 Or + 3 water -> Bt + 2 Ep + 2 Zo + 7 Qtz

Modelling of this reaction using the program THERMO developed by Powell and Holland (1988) yields the following reactions:-

I Phl + Zo = An + Hbl + Kfs + Qtz + H_2O ($aH_2O = 1$)

II Ann + Zo = An + ferro-hbl + Kfs + Qtz + H_2O ($aH_2O = 1$)

III Phl + Zo = An + Hbl + Kfs + Qtz + H_2O ($aH_2O = .01$)

IV Ann + Zo = An + ferro-hbl + Kfs + Qtz + H_2O ($aH_2O = .01$)

V Phl + Zo = An ($aAn = .3$) + Hbl + Kfs + Qtz + H_2O ($aH_2O = 1$)

which occur under the physical conditions shown in figure 3.8.

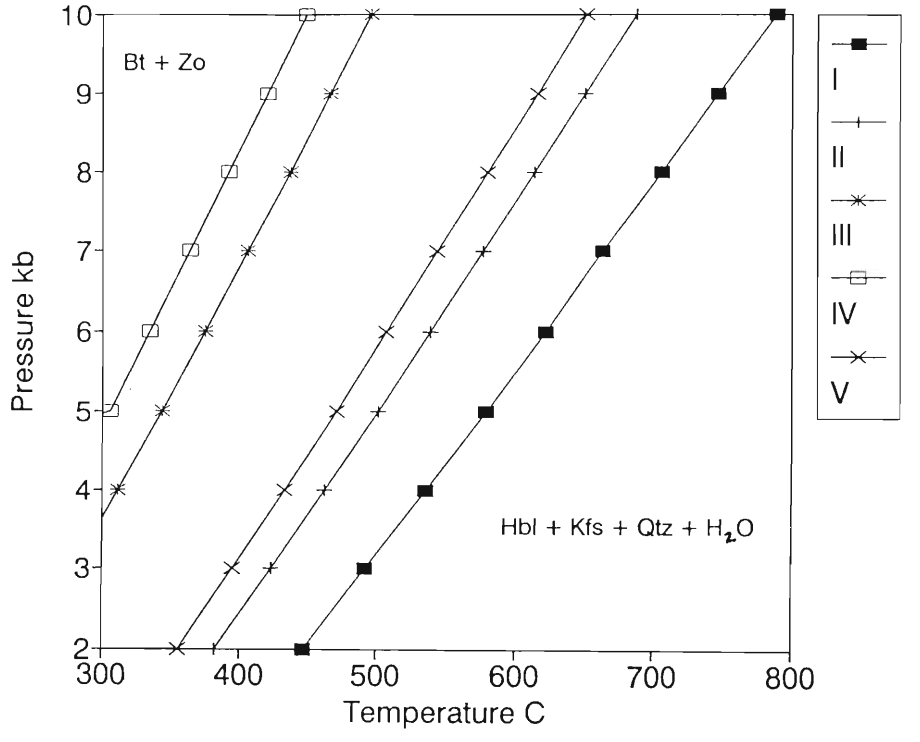

Figure 3.8. Physical conditions for the reactions I-V described above.

The presence of both the reactants and products of this reaction shows that the reaction has not proceeded to completion. Possible causes for this are that $pH_2O < P_{load}$ and therefore the reaction may have been buffered by the activity (a) of H_2O or alternatively the reaction was frozen by a rapid rate of cooling. If the activity of $H_2O < 1$ then the temperatures of reaction can be adjusted to lower levels. The possible influence of the MgO/MgO + FeO ratio of the Grey Gneisses is shown with the reaction being displaced to higher temperature with increasing Mg content. Another factor influencing this reaction would be the activity of An in the plagioclase. The reactions are modelled with an activity of 1 except for reaction V (Fig.3.8) which shows that with a more sodic, plagioclase the reaction is displaced to lower temperatures. These alternatives will be explored further in Chapter 14 on the metamorphic history.

GEOCHEMISTRY

Introduction

Forty-five samples of Grey Gneiss were analyzed for 9 major and 15 trace elements. Also included are data for seven samples of the granitic gneisses which form concordant layers within the Grey Gneiss. The major element data are shown in order of increasing SiO_2 content in table 3.2.

Major element chemistry

The major element analyses for the Grey Gneisses and associated granitic gneisses (table 3.2) reveal that the Grey Gneisses include rocks of a broad range of compositions with SiO_2 contents ranging from 49 to 75%. Based on SiO_2 contents six samples may be described as being basaltic in composition having SiO_2 contents between 49% and 55%. Thirty two samples have SiO_2 contents between 55% and 66% and may therefore be described as intermediate in composition. Five samples of Grey Gneiss have SiO_2 contents >66% and may therefore be described as acid.

On the basis of SiO_2 content therefore, the Grey Gneisses are dominantly intermediate in composition with subordinate basic and acid varieties.

Harker diagrams show systematic variations of elements with SiO_2 as do the major element oxides plotted against the Differentiation Index (D.I.) of Thornton and Tuttle (1960) (Figs. 3.9 and 3.10). The D.I. was selected because it is based on the variation of normative alkali-bearing minerals with the alkalis generally being enriched in residual liquids of crystallization. The use of the Mg number (Mg/Mg + Fe) and related indices would have been of little use since the Mg number varies very little between samples (see AFM diagram later).

The Harker and the D.I. diagrams show FeO, TiO_2, MgO, MnO, P_2O_5 and CaO contents decreasing with increasing SiO_2 or D.I. respectively whereas K_2O shows a sympathetic increase with SiO_2 (Fig. 3.9). The decreasing contents of FeO, TiO_2, MgO, MnO and CaO in relation to SiO_2 are described by negative correlation coefficients <-0.7 (table 3.3). Na_2O and Al_2O_3 show no coherent variations with SiO_2 or D.I. (Fig. 3.10). However strong correlation between these two oxides (r = 0.84, table 3.3) suggests that plagioclase dominated the distributions of these elements.

From table 3.3 it may be seen that FeO, CaO, MnO, and MgO have correlation coefficients >0.7 showing coherent linear variations with one another. These coherent linear variations are consistent with the varying mafic mineralogy where these elements form a structural or trace component in biotite, hornblende and epidote. TiO_2 varies linearly with FeO, MnO, SiO_2 and P_2O_5.

	SiO_2	Al_2O_3	Fe_2O_3	FeO	MnO	MgO	CaO	Na_2O	K_2O	TiO_2	P_2O_5	TOTAL
JE44	49.75	14.04	2.84	11.62	0.22	5.91	9.34	2.41	1.58	2.44	0.42	100.57
RK15	53.55	12.20	2.31	9.48	0.25	9.66	9.07	1.50	1.88	0.87	0.12	100.89
JW5	53.79	19.71	1.92	5.79	0.15	3.52	7.77	4.38	2.46	0.85	0.27	100.61
JE42	54.02	15.14	2.77	8.85	0.22	4.87	6.34	2.40	3.41	1.28	0.45	99.75
RK28	54.64	15.08	2.62	7.89	0.21	4.39	6.73	2.87	3.52	2.02	0.58	100.55
SV44	54.81	16.28	2.00	7.20	0.17	4.75	8.65	3.12	1.69	0.94	0.34	99.95
H9	57.75	17.67	1.66	5.96	0.14	3.48	6.89	3.60	1.83	0.78	0.31	100.07
H10	58.40	18.07	1.65	5.57	0.14	3.04	6.65	3.77	1.84	0.73	0.33	100.19
JE26	58.93	17.29	1.75	5.57	0.15	2.98	5.85	3.38	2.93	0.87	0.30	100.00
JW4	59.15	17.13	1.68	5.70	0.14	3.23	6.00	3.15	2.79	0.81	0.26	100.04
RK18	59.48	17.46	1.58	5.36	0.13	2.82	6.34	3.60	2.24	0.76	0.31	100.08
JW2	59.54	16.44	1.69	5.72	0.14	3.42	5.55	3.09	2.65	0.80	0.27	99.31
JW16	59.91	16.71	1.73	5.21	0.12	3.76	4.87	3.43	3.15	0.73	0.22	99.84
RK22	60.03	17.61	1.50	5.07	0.13	2.75	6.25	3.95	2.04	0.71	0.30	100.34
JE13	60.15	16.69	1.64	5.56	0.12	3.13	5.75	3.20	2.73	0.77	0.18	99.72
JE41	60.21	17.50	1.57	4.74	0.14	2.98	5.13	3.99	2.66	0.66	0.30	99.88
H2	60.22	16.60	1.71	5.80	0.14	3.34	6.03	3.44	2.12	0.61	0.26	100.27
H13	60.26	16.66	1.61	5.74	0.14	2.89	6.20	3.42	2.05	0.77	0.28	100.02
SV43	60.58	16.32	1.47	4.96	0.21	2.47	6.29	3.74	2.30	0.71	0.24	99.29
JE18	60.87	16.79	1.46	4.66	0.11	2.50	5.04	3.63	3.01	0.70	0.26	99.03
JE43	60.89	17.52	1.43	4.85	0.13	2.60	5.12	3.39	2.75	0.69	0.32	99.69
JE16	60.90	16.75	1.45	4.91	0.11	2.85	5.66	3.18	2.64	0.73	0.25	99.43
JE18	60.94	17.40	1.42	4.53	0.11	2.47	4.90	3.46	3.15	0.69	0.26	99.33
JE24	61.28	17.40	1.52	4.84	0.12	2.71	5.00	3.48	2.76	0.69	0.30	100.10
JW9	61.31	16.99	1.52	5.14	0.12	2.84	5.52	3.20	2.63	0.75	0.25	100.27
JW3	61.37	15.96	1.54	5.21	0.12	3.27	5.60	3.22	2.62	0.68	0.22	99.81
JE28	61.56	15.99	1.58	5.02	0.12	2.87	5.16	3.04	3.12	0.75	0.23	99.44
JE9	61.69	16.96	1.45	4.64	0.11	2.48	5.00	3.44	3.08	0.71	0.23	99.79
JE12	61.90	16.03	1.41	4.77	0.11	2.71	5.15	3.01	2.71	0.68	0.25	98.73
JW15	62.15	16.91	1.36	4.88	0.11	2.67	5.01	3.34	2.36	0.65	0.26	99.70
JW15	62.55	16.59	1.33	4.78	0.11	2.88	5.11	3.11	2.42	0.65	0.27	99.80
H12	62.66	17.60	1.36	4.11	0.08	2.28	4.56	4.10	2.90	0.61	0.27	100.53
JW6	62.77	16.33	1.39	4.45	0.11	2.55	4.66	3.12	3.43	0.65	0.22	99.68
JW17	63.06	16.45	1.38	4.41	0.11	2.25	4.96	3.08	3.26	0.65	0.25	99.86
RK25	63.85	15.73	1.31	4.43	0.11	2.20	5.00	3.10	3.02	0.66	0.25	99.66
JW1	64.94	15.36	1.23	3.91	0.09	2.40	4.26	2.84	3.40	0.56	0.19	99.18
JG10	65.24	14.73	1.22	3.67	0.09	2.89	4.23	3.65	3.19	0.72	0.35	99.98
BK3	66.48	15.39	1.09	3.27	0.07	1.78	3.09	3.19	3.65	0.48	0.18	98.67
JE15	66.56	12.92	1.29	5.06	0.09	2.52	6.38	0.98	3.88	0.71	0.23	100.62
JE25	71.64	14.22	0.55	1.58	0.04	0.69	1.97	2.32	5.43	0.28	0.09	98.81
JE10	72.92	14.92	0.28	0.67	0.01	0.26	1.03	3.74	5.54	0.18	0.06	99.61
					Granitic gneisses associated with the Grey Gneisses							
JE17	75.00	12.81	0.35	0.95	0.02	0.46	1.20	2.06	5.97	0.22	0.06	99.10
JE21	74.68	13.66	0.30	0.77	0.02	0.36	0.89	2.26	6.54	0.19	0.05	99.72
JE32	74.06	14.42	0.32	0.85	0.02	0.32	1.17	3.54	4.74	0.18	0.06	99.67
JE6	72.73	13.85	0.52	1.41	0.04	0.60	1.76	3.01	4.96	0.26	0.08	99.22
JE7	76.01	13.50	0.22	0.57	0.01	0.17	1.14	2.55	6.18	0.09	0.02	100.46
H8	74.74	13.36	0.41	1.17	0.02	0.42	1.49	2.24	5.60	0.20	0.05	99.70
JE4	73.43	14.05	0.36	1.01	0.02	0.65	1.98	2.13	5.56	0.18	0.07	99.44

Table 3.2. Major element chemistry (wt%) of the Grey Gneiss Complex. FeO/Fe_2O_3 contents were estimated after le Maitre (1976).

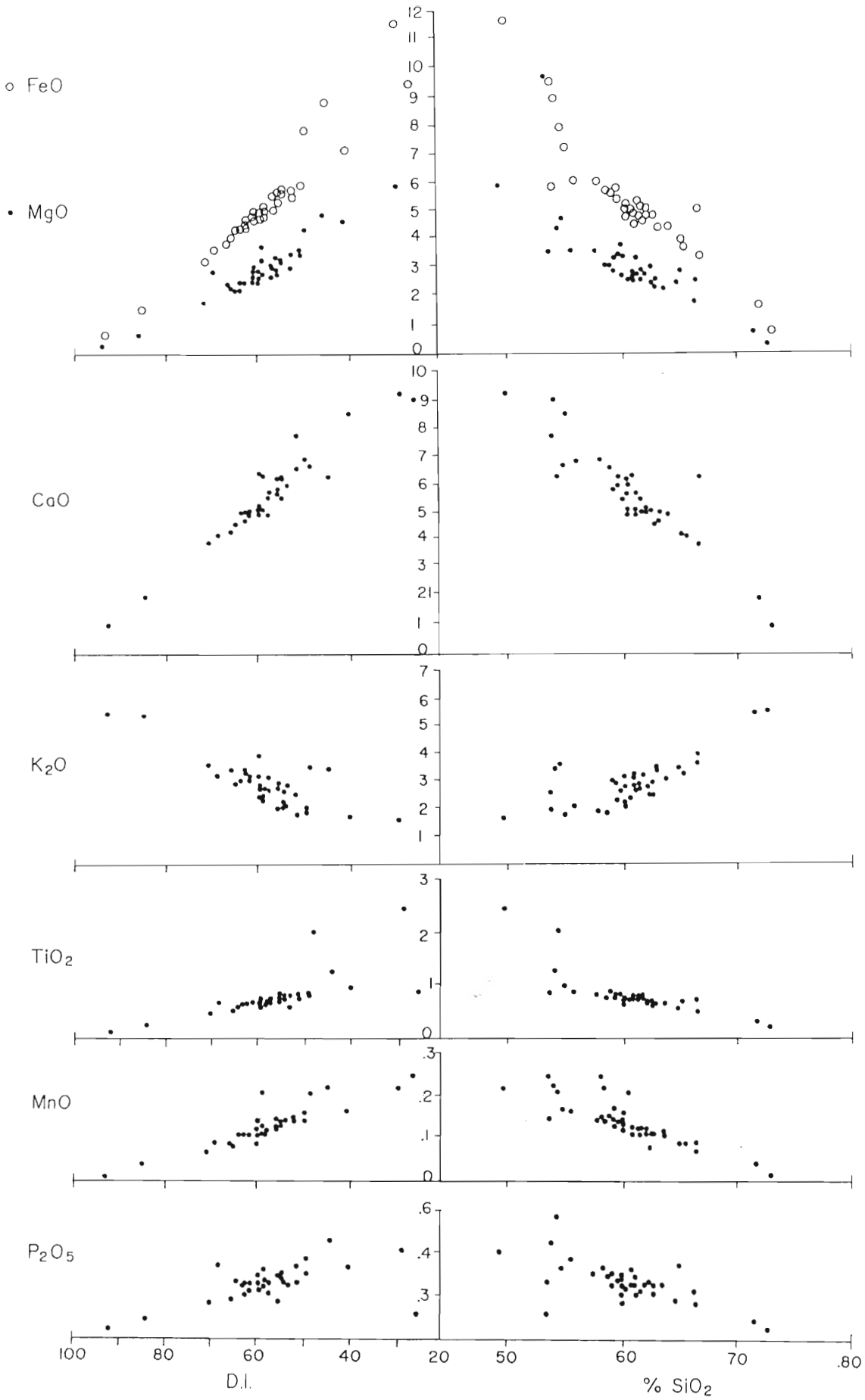

Figure 3.9. SiO_2 and D.I. vs FeO, MgO, CaO, K_2O, MnO, P_2O_5 and TiO_2 for the Grey Gneisses.

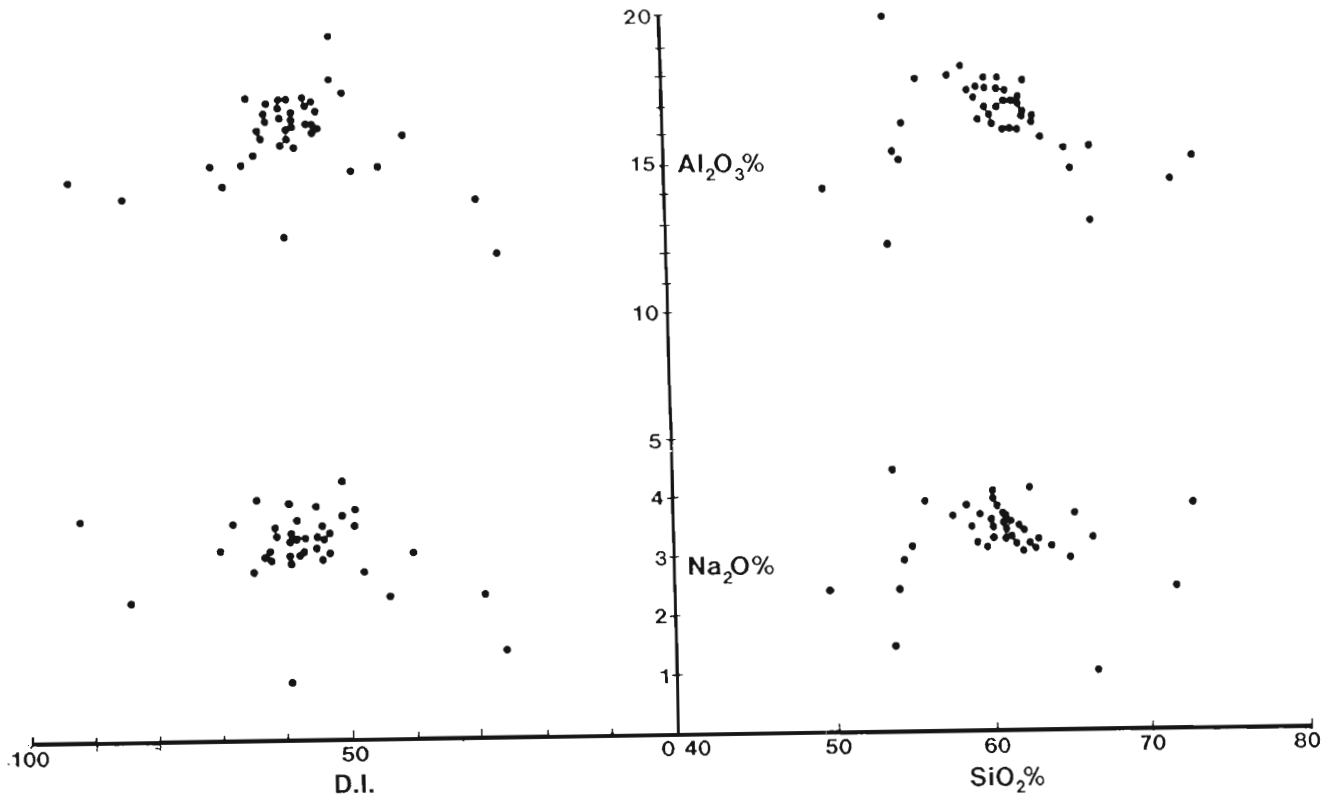

Figure 3.10. SiO_2 and D.I. vs Na_2O and Al_2O_3 for the Grey Gneisses.

	Al_2O_3	FeO	MnO	MgO	CaO	Na_2O	K_2O	TiO_2	P_2O_5
SiO_2	-0.19	-0.91	-0.90	-0.79	-0.90	-0.01	0.75	-0.75	-0.65
Al_2O_3	XXXX	-0.17	-0.08	-0.32	0.02	0.84	-0.37	-0.20	0.19
FeO		XXXX	0.90	0.87	0.89	-0.33	-0.64	0.84	0.60
MnO			XXXX	0.83	0.85	-0.19	-0.64	0.71	0.58
MgO				XXXX	0.81	-0.39	-0.56	0.58	0.31
CaO					XXXX	-0.18	-0.80	0.66	0.51
Na_2O						XXXX	-0.22	-0.24	0.11
K_2O							XXXX	-0.36	-0.42
TiO_2								XXXX	0.75

Table 3.3. Table showing inter-element correlation coefficients for the Grey Gneisses (excluding the associated granitic gneisses). Those values >0.7 or <-0.7 are underlined.

Trace element chemistry

The trace element chemistry of the Grey Gneisses is shown in Table 3.4. The data are organised in the same sequence as the major elements thus permitting easy comparison. In Table 3.5 inter-element correlation coefficients for the trace elements are shown. Al_2O_3 and Na_2O vary linearly with Sr suggesting control by plagioclase whereas K_2O varies linearly with Rb, Th and to a lesser degree, Ba, suggesting control by K-feldspar and/or biotite.

No.	Rb	Sr	Rb/Sr	Th	Zr	Y	Nb	Ba	Sc	Cr	La	V	Cu	Ni	Zn
JE44	23	285	0.08	2.2	182	34	11.4	202	41.6	106	15	449	62	60	134
RK15	43	174	0.25	4.2	84	27	9.5	229	42.6	78	20	288	15	84	123
JW5	45	860	0.05	9.8	222	29	15.1	1092	17.6	22	29	154	1	12	96
JE42	124	426	0.29	14.8	230	43	27.6	1206	26.7	24	46	225	47	16	139
RK28	100	416	0.24	7.2	223	38	20.7	1069	24.6	39	42	221	162	33	128
SV44	50	582	0.09	4.3	71	29	11	662	28.1	88	27	187	23	23	90
H9	50	718	0.07	3.9	158	28	18.4	953	20.1	25	43	153	20	10	88
H10	44	834	0.05	2.0	154	34	14	672	18.4	15	40	159	5	6	84
JE26	74	475	0.16	4.6	184	29	16	1195	16.9	24	29	153	91	8	75
JW4	72	466	0.15	10.9	160	34	20.3	1240	21.4	19	32	172	26	9	76
RK18	56	754	0.08	9.6	154	23	4.3	881	15.7	15	56	130	16	6	74
JW2	90	416	0.22	12.7	174	28	13.7	928	16.8	31	39	147	16	11	80
JW16	82	473	0.17	8.6	155	23	12.6	1250	16.7	50	31	155	5	19	84
RK22	56	842	0.07	1.6	163	23	12.9	933	14.3	15	42	146	23	6	82
JE13	79	437	0.18	5.7	170	26	15	1029	17	32	25	171	33	11	75
JE41	90	663	0.14	11.1	142	23	15.8	1011	13.1	15	27	113	4	6	90
H2	70	468	0.15	12.1	167	28	14.4	613	22.4	27	48	164	21	13	85
H13	55	621	0.09	4.7	145	23	14.6	1004	20.9	10	45	190	29	9	84
SV43	61	500	0.12	3.6	150	27	14	1150	16.6	10	31	124	4		76
JE18	82	475	0.17	7.7	183	27	14.5	1356	13	24	41	101	37	8	63
JE43	74	625	0.12	3.8	171	21	10.9	1373	11	11	25	114	3	6	77
JE16	79	455	0.17	7.6	155	27	13.9	995	18.1	26	28	155	21	10	65
JE18	76	476	0.16	3.1	177	28	14.3	1276	15	23	27	96	43	8	60
JE24	74	707	0.10	5.9	148	19	8.8	1484	12.1	16	36	108	41	7	71
JW9	77	439	0.18	10.7	183	25	15.1	1077	16.9	24	31	142	25	10	71
JW3	74	468	0.16	5.4	163	25	11.8	1004	20.9	10	45	190	29	9	84
JE28	87	392	0.22	8.2	168	30	16.5	994	17.3	26	29	143	47	9	68
JE9	72	478	0.15	7.4	181	28	15.6	1415	16.1	16	32	116	30	8	67
JE12	111	409	0.27	5.2	155	27	13.9	1068	14.5	27	37	132	12	11	70
JW15	96	762	0.13	8.5	135	24	14.8	1079	11.6	7	25	147	5	7	71
JW15	93	754	0.12	8	133	43	15.8	1106	12.7	12	30	128	6	6	74
H12	84	818	0.10	20.7	248	25	18.7	1367	9.1	29	96	85	4	19	70
JW6	92	414	0.22	9.7	156	25	15.2	1285	13	21	30	118	14	8	62
JW17	87	608	0.14	11.6	143	22	10.5	1339	10.8	2	37	120	2	4	64
RK25	66	572	0.12	11.9	152	24	14.2	1270	12.2	5	37	83	5	4	65
JW1	87	403	0.22	14.4	154	23	14.4	1041	14.3	19	36	100	15	9	62
JG10	114	491	0.23	6.3	207	25	9	1032	12.7	78	33	121	22	30	76
BK3	83	646	0.13	5.7	114	17	11.1	2009	9.4	7	56	84	3	2	41
JE15	129	262	0.49	10.3	187	24	14	609	18.4	28	37	164	27	11	69
JE25	97	583	0.16	30.5	196	11	6.5	3137	1.6	1	77	18	11	2	23
JE10	142	203	0.70	22.4	157	7	12.2	1082	0.9	1	20	17	2	2	25
Granitic gneisses associated with Grey Gneisses															
JE17	142	282	0.50	33.5	129	10	9.2	1541	2.9	4	46	16	2	3	15
JE21	147	241	0.61	25.9	100	9	9.6	1034	1.9	ND	33	ND	3	2	14
JE32	126	221	0.57	27.3	104	28	11.8	1013	2.1	ND	53	12	1	3	20
JE6	131	275	0.48	15.7	198	15	17.2	1155	3.9	2	48	17	4	2	32
JE7	123	134	0.92	24.5	88	7	9.9	308	2.4	9	3	10	2	3	15
H8	113	325	0.35	17.7	175	11	5.4	1601	3.4	1	74	16	7	2	23
JE4	106	449	0.24	17.5	125	8	5.5	2700	0.8	ND	24	20	28	3	19

Table 3.4 Trace element chemistry (ppm) of the Grey Gneiss Complex. ND = Not detected.

The Rb/Sr ratio for the Grey Gneisses has a mean value of 0.18 (n = 44) and varies from 0.05 to 0.7. There appears to be a very weak tendency for the higher values to be associated with the more siliceous gneisses. This trend is consistent with increasing Rb content with SiO_2 (r = 0.63, Table 3.5) whereas the Sr content shows no obvious variation with SiO_2. The

interlayered granitic gneisses have a mean Rb/Sr value of 0.52 (n = 7), significantly higher than the mean value for the Grey Gneisses. Zinc, V, Sc and, to lesser degrees, Ni, Y and Cr show strong positive correlations with FeO, MgO, MnO, TiO_2 and CaO and strong negative correlations with SiO_2. These particular trace elements also show strong linear variations with each other eg. Y/Zn, V/Ni, V/Zn, V/Sc, V/Cr, Sc/Ni, Sc/Zn and Cr/Ni. These consistent variations generally involve major and trace elements which are either structural components in or are compatible in the dominant mafic mineral in the Grey Gneisses, namely, amphibole (see appendix 3).

The consistent linear variations in the chemistry of the Grey Gneisses should enable the identification and characterisation of the original precursors of the Grey Gneisses. This question is addressed below.

	Rb	Sr	Th	Zr	Y	Nb	Ba	Sc	Cr	La	V	Cu	Ni	Zn
SiO_2	0.63	-0.06	0.57	0.04	-0.76	-0.32	0.60	-0.81	-0.53	0.29	-0.81	-0.36	-0.53	-0.90
Al_2O_3	-0.33	0.73	-0.21	0.10	0.07	0.20	0.06	-0.28	-0.40	0.06	-0.27	-0.19	-0.56	-0.08
FeO	-0.50	-0.19	-0.49	-0.04	0.75	0.28	-0.63	0.91	0.65	-0.29	0.95	0.43	0.71	0.93
MnO	-0.51	-0.12	-0.52	-0.10	0.73	0.30	-0.55	0.83	0.46	-0.31	0.79	0.39	0.59	0.90
MgO	-0.45	-0.28	-0.42	-0.24	0.56	0.09	-0.61	0.88	0.70	-0.32	0.81	0.25	0.87	0.82
CaO	-0.68	0.02	-0.62	-0.19	0.67	0.15	-0.70	0.85	0.57	-0.30	0.83	0.25	0.58	0.82
Na_2O	-0.23	0.63	-0.12	0.10	-0.13	0.05	0.08	-0.40	-0.31	0.08	-0.38	-0.22	-0.46	-0.18
K_2O	0.76	-0.34	0.73	0.33	-0.49	-0.06	0.66	-0.58	-0.35	0.24	-0.58	0.04	-0.30	-0.59
TiO_2	-0.31	-0.21	-0.36	0.23	0.68	0.29	-0.43	0.71	0.60	-0.23	0.85	0.68	0.58	0.80
P_2O_5	-0.17	0.22	-0.40	0.29	0.68	0.43	-0.33	0.42	0.29	-0.03	0.50	0.59	0.17	0.72
Rb	XXXX	-0.34	0.53	0.31	-0.25	0.19	0.32	-0.49	-0.28	0.11	-0.47	0.04	-0.30	-0.36
Sr		XXXX	-0.10	0.01	-0.09	0.00	0.22	-0.31	-0.38	0.39	-0.28	-0.33	-0.44	-0.08
Th			XXXX	0.36	-0.39	0.05	0.55	-0.44	-0.31	0.52	-0.48	-0.20	-0.22	-0.43
Zr				XXXX	0.28	0.45	0.25	-0.17	-0.06	0.40	-0.05	0.37	-0.08	0.09
Y					XXXX	0.67	-0.44	0.66	0.39	-0.14	0.64	0.51	0.34	0.77
Nb						XXXX	-0.13	0.20	-0.14	0.11	0.16	0.36	-0.11	0.40
Ba							XXXX	-0.64	-0.50	0.51	-0.66	-0.10	-0.48	-0.62
Sc								XXXX	0.69	-0.34	0.89	0.34	0.75	0.81
Cr									XXXX	-0.27	0.70	0.29	0.82	0.56
La										XXXX	-0.36	-0.07	-0.22	-0.24
V											XXXX	0.40	0.74	0.84
Cu												XXXX	0.30	0.43
Ni													XXXX	0.64

Table 3.5. Inter-element correlation coefficients for the Grey Gneisses. The correlation coefficients >0.7 and <-0.7 are underlined.

Rare Earth Element Chemistry

Five samples from the Grey Gneisses were analyzed for the rare earth element contents (REE). The samples were selected so as to represent rocks with a range of SiO_2 contents in intermediate compositions similar to those recorded in the Grey Gneisses.

It may be seen from table 3.6 and figure 3.11 that the REE contents generally decrease with increasing SiO_2 contents. Broadly, the samples are characterised by relatively steep LREE and flat HREE patterns. Samples JW6, JE42, BK3 and JE13 are characterised by weak negative Eu anomalies whereas sample JE10 has no Eu anomaly.

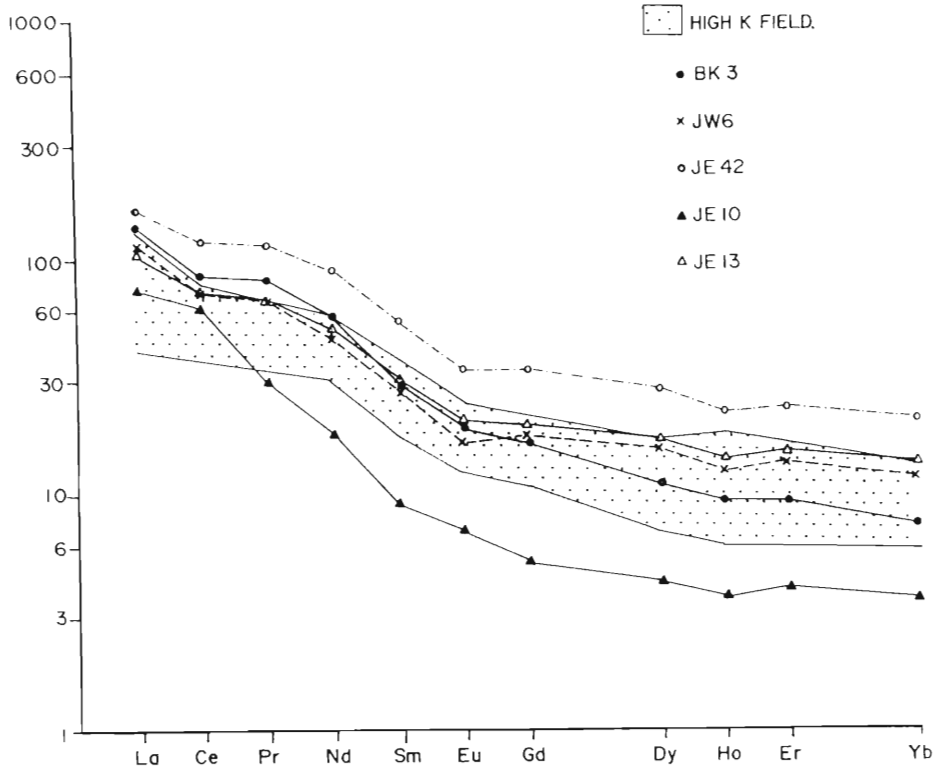

Figure 3.11. REE profiles for 5 samples of Grey Gneiss. The shaded area represents the range of REE values recorded for orogenic andesites with SiO_2 contents 55-62% SiO_2 from Gill (1981).

	La	Ce	Pr	Nd	Sm	Eu	Gd	Dy	Ho	Er	Yb	SiO_2
JE42	53.74	105.11	13.5	56.46	10.5	2.37	8.45	8.16	1.69	4.56	4.31	54.02
JE13	35.88	64.29	7.96	31.75	5.94	1.45	5.02	5.02	1.07	2.93	2.83	60.15
JW6	39.94	65.23	8.03	29.76	5.60	1.22	4.43	4.55	0.94	2.58	2.48	62.77
BK3	48.5	78.2	9.82	37.22	5.78	1.4	4.23	3.27	0.72	1.82	1.59	66.48
JE10	24.95	56.5	3.69	11.86	1.8	0.51	1.35	1.3	0.29	0.80	0.77	72.92

Table 3.6 REE chemistry of the Grey Gneiss Complex. The SiO_2 contents are shown for comparison.

ORIGIN OF THE GREY GNEISSES

Introduction

The question of the origin of the Grey Gneisses must begin with a discussion of their field characteristics and field relationships because these factors influence the interpretation of the gneisses as ortho- or paragneisses and, if the former, whether the gneisses can be interpreted as being originally intrusive or extrusive in origin.

Discussion of field characteristics and relationships.

Although the Grey Gneisses are layered, the thicknesses of layers (up to 50m) and the compositional homogeneity within layers are considered more likely to represent orthogneisses rather than paragneisses. This conclusion is also supported by the consistency of the chemistry (described above).

Acceptance of the Grey Gneisses as orthogneisses raises the question whether they were intrusive or extrusive. The concordant compositional layering is consistent with an extrusive origin if it is assumed that the layering is a primary feature. The presence of porphyroclasts of plagioclase in some layers suggests that the layering is primary (Fig. 3.1). These porphyroclasts could be interpreted as relict volcanic phenocrysts in a finer matrix. On the contrary presence of autolithic fragments (Fig. 3.5) in the Grey Gneisses could be used to argue in favour of an intrusive origin but their mineralogical consanguinity with the enclosing Grey Gneisses suggests that they are not xenoliths of adjacent Banded Gneisses. They may represent agglomeratic fragments which is the preferred interpretation at present. The lack of unequivocal evidence for either an intrusive or extrusive origin mitigates against drawing conclusions from field evidence alone.

Comparison of the Grey Gneisses with modern volcanic rocks.

Chemically, the Grey Gneisses display coherent chemical trends (Fig. 3.9, see above) which display strong similarities with trends for calc-alkaline rocks (Gill, 1981). Figure 3.12 shows that the Grey Gneisses define a consistent calc-alkaline trend. Brown (1982) states that "Calc-alkaline granitoids from magmatic arcs have geochemical characteristics paralleled by the characteristics of associated volcanic rocks" and thus are chemically indistinguishable. Ewart (1982) calculated correlation coefficients for the chemistry of calc-alkaline volcanic suites. Comparing these coefficients with those for the Grey Gneisses (Tables 3.3 and 3.5), positive correlations are seen for FeO vs MgO, V vs FeO, MgO vs V, MnO vs V, MgO vs Ni, TiO_2 vs P_2O_5 and Cr vs Ni. Correlations greater than 0.5 calculated by Ewart (1982) but not found in the Grey Gneisses include K_2O vs P_2O_5, Ba and Sr, TiO_2 vs Rb, Rb vs Sr and Ba, Sr vs Ba, and Zr vs Ba and La.

These discrepancies may suggest that the Grey Gneisses are not comparable with calc-alkaline volcanic rocks.

However, the positive correlations recognised by Ewart (1982) are for unmetamorphosed rocks, and largely involve trace elements generally accepted as being mobile in the medium to high metamorphic grades eg Ba, Sr and Rb (Heier and Thoresen, 1971; Barbey and Cuney, 1982). Therefore the lack of significant correlations for these elements is not unexpected. The original definition of calc-alkaline rocks was based on Peacock's (1931) alkali-lime index.

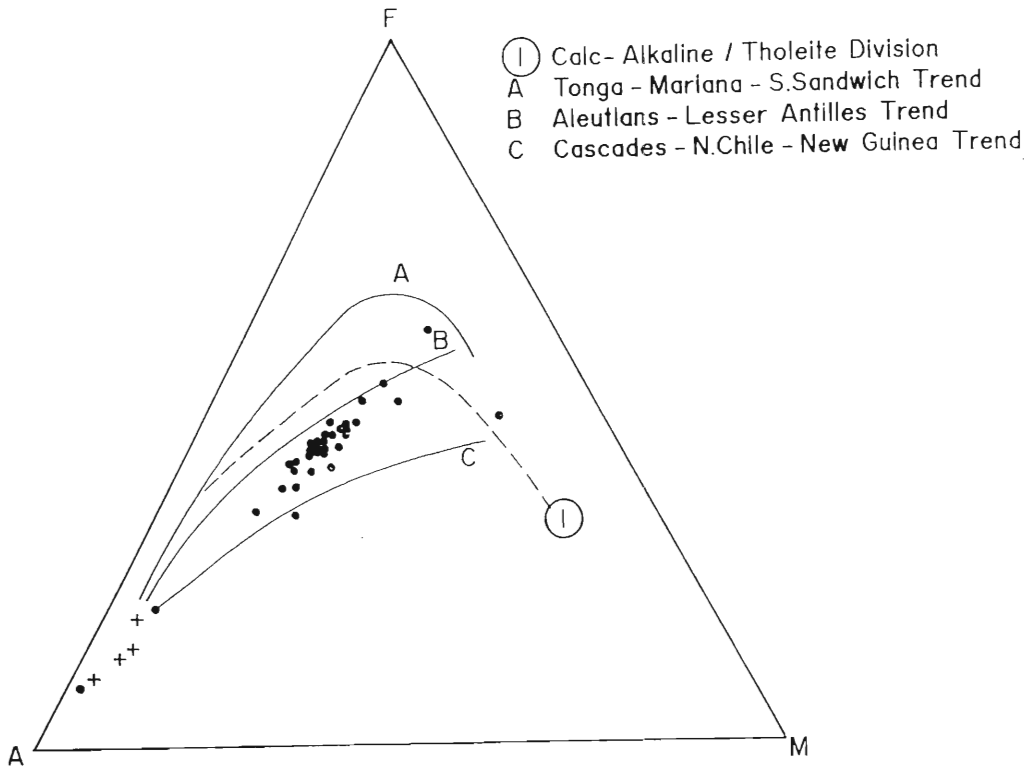

Figure 3.12. AFM diagram with calc-alkaline tholeiite division after Irvine and Barager (1971) for the Grey Gneisses. The trendlines A,B and C are from Brown (1982). The + symbols are the granitic gneisses associated with the Grey Gneisses.

Calc-alkaline rocks were defined as those rocks having SiO_2 contents between 56% to 61% and $CaO/(Na_2O + K_2O) = 1$. The Grey Gneisses have alkali-lime index values of between 54% and 62% SiO_2 (Fig. 3.13). Also shown in figure 3.13 is the field of normal calc-alkaline andesites from Brown (1982). Figure 3.13 indicates that the Grey Gneisses are comparable to calc-alkaline andesites in terms of their silica contents and alkali/lime ratios.

Brown (1982) recognises an increasing arc maturity from AFM diagrams with curve A (Fig. 3.12) representing the least mature arcs whereas curve C, having a higher Mg/Mg + Fe ratio, is representative of more mature arcs. Brown (1982) related the maturity of the arc to the crustal thickness at the time of genesis. The intermediate SiO_2 contents of the Grey Gneisses in general suggests that in terms of volcanic rocks, they are likely to have been andesitic to dacitic in composition.

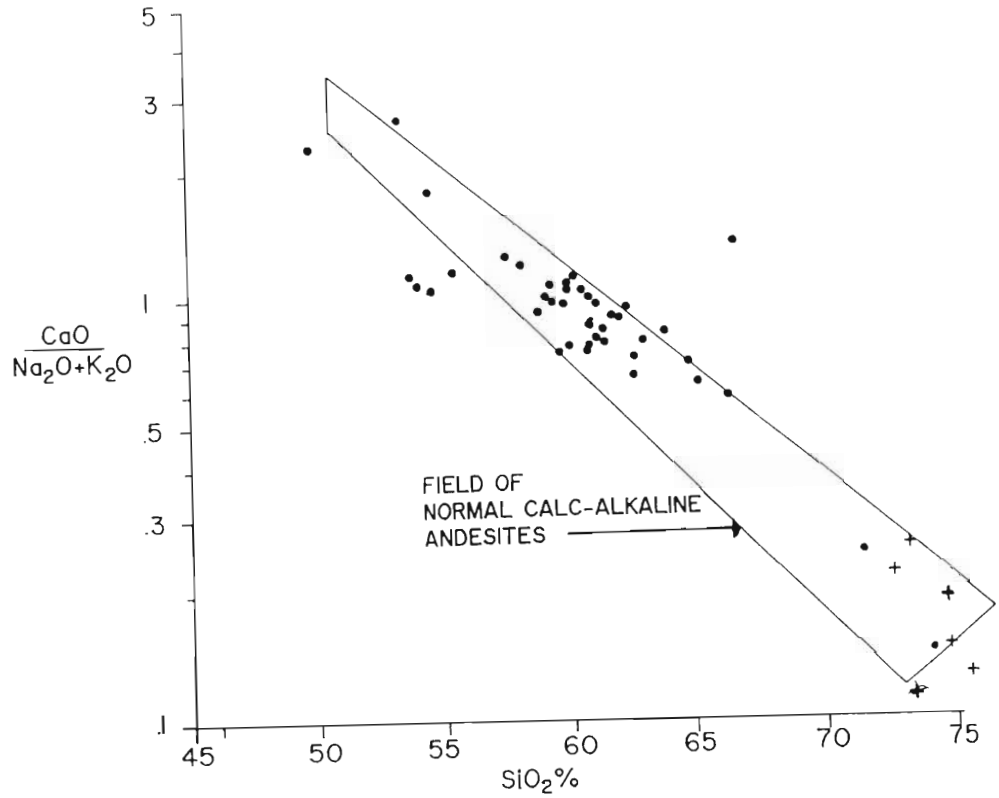

Figure 3.13. CaO/Na_2+K_2O vs SiO_2 for the Grey Gneisses. The field for normal orogenic andesites is from Brown (1982).

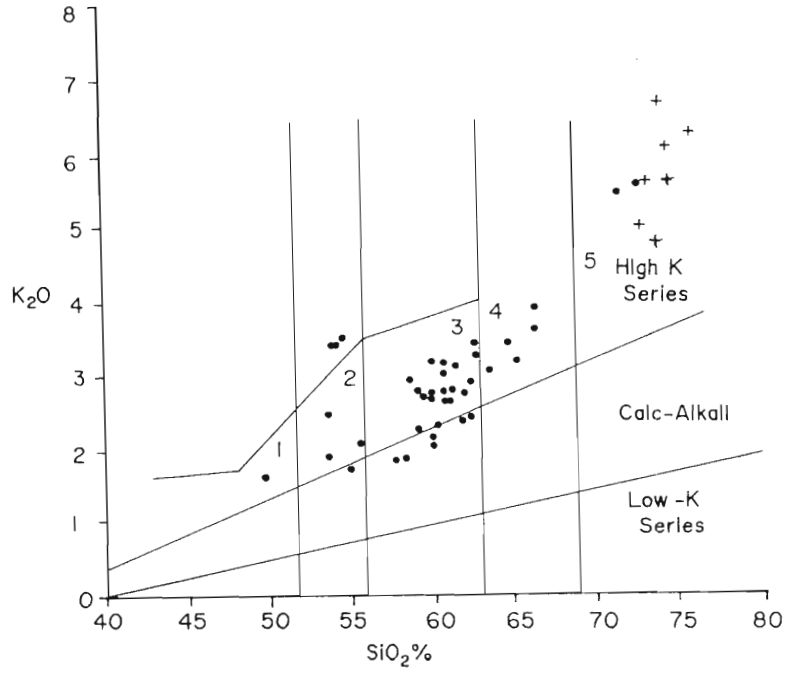

Figure 3.14 K_2O vs SiO_2 for the Grey Gneisses. The figures 1,2,3,4,5 define fields for basaltic, basaltic andesitic, andesitic, dacitic and rhyolitic rocks respectively.

	FeO	MnO	Na_2O	K_2O	TiO_2	P_2O_5	Rb	Sr	Zr	Ba	Cr	Ni
MnO	0.63	XXXX										
TiO_2			0.35		XXXX							
P_2O_5			0.37	0.71	0.495	XXXX						
Rb					0.64	0.49	XXXX					
Sr				0.54		0.49	0.60	XXXX				
Zr			0.45	0.33	0.42	0.38	0.38	0.33	XXXX			
Ba				0.53		0.43	0.58	0.73	0.57	XXXX		
Cr		0.66									XXXX	
V	0.54	0.40										
Ni											0.81	XXXX
La								0.32	0.57	0.49		
MgO												0.65

Table 3.7. Table showing inter-element correlation coefficients for Tertiary to Recent orogenic volcanic rocks (from Ewart, 1982).

Brown (1982) states that the volume ratio of basic to intermediate and acidic members increases with arc maturity with andesitic and dacitic lavas being characteristic of the more mature western American continental arcs. Based on these criteria (Brown, 1982), the Grey Gneisses have compositions which are comparable to calc-alkaline rocks from a mature arc environment.

Ewart (1982) has studied the chemistry of basaltic to andesitic (52-63% SiO_2) orogenic volcanic rocks of Tertiary to Recent age and has recognised three subdivisions based on K_2O vs SiO_2 contents (Fig. 3.14). The Grey Gneisses have K_2O vs SiO_2 contents comparable with those from the high K series (Fig. 3.14). Comparison of the contents of Ba, Sr and Zr in the Grey Gneisses with Ewart's (1982) data for basaltic and andesitic lavas (Fig. 3.15) reveals that the contents in the Grey Gneisses are similar.

Nickel contents in the Grey Gneisses are typically lower than those reported by Ewart (1982) for Tertiary to Recent basalts and andesites (Fig. 3.14) whereas Cr contents of the Grey Gneisses straddle Ewart's field. The concentrations of MgO and Ni in the Grey Gneisses are, however, similar to those recorded for orogenic andesites by Gill (1981) (Fig. 3.16).

The REE patterns of the Grey Gneisses are similar to those for high-K orogenic andesites reported by Gill (1981) but samples from the Grey Gneisses have slightly steeper LREE slopes than those reported by Gill (1981)(Fig. 3.11). The five Grey Gneiss samples exhibit a greater range of REE contents than the data from Gill (1981). A possible reason for this is that the Grey Gneiss samples represent rocks with SiO_2 contents between 54 and 72% whereas the data of Gill (1981) include rocks with SiO_2 contents of 55% to 62% SiO_2.

It was noted above that the REE contents decreased with increasing SiO_2 contents. If it is assumed that the variation of the SiO_2 values are the consequence of fractional crystallization, then the increasing depletion of REE in general would reflect the crystallization of a phase or phases in which the REE are compatible.

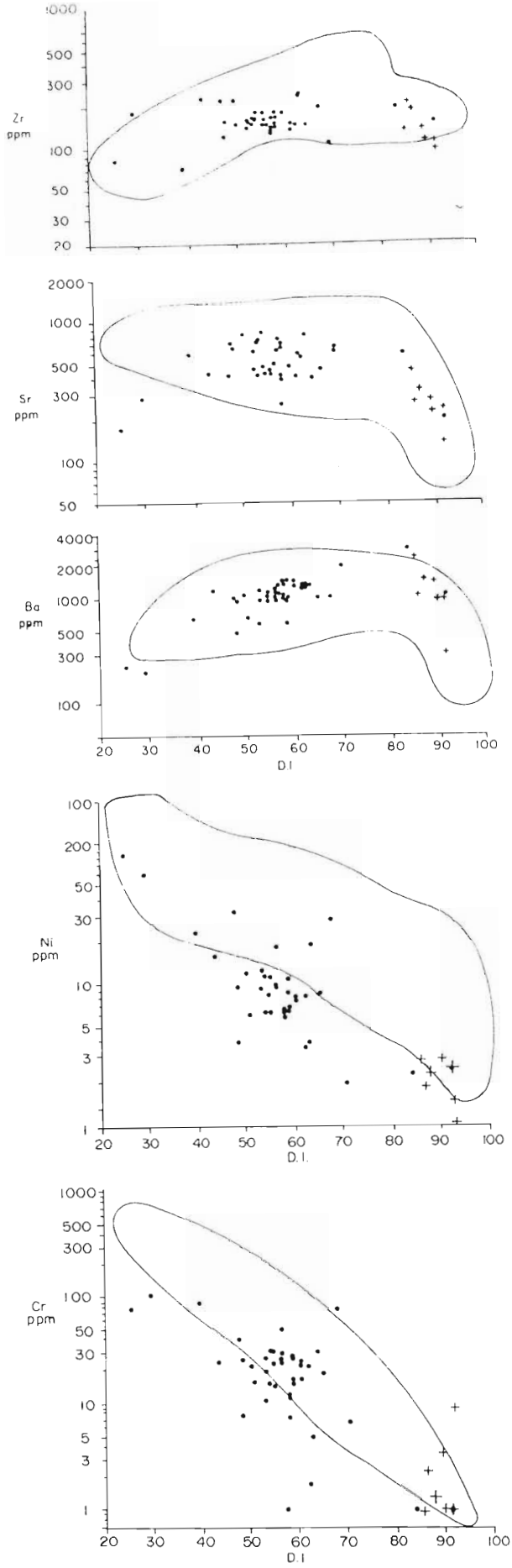

Figure 3.15. Sr, Ba, Zr, Cr and Ni vs D.I. for the Grey Gneisses. The fields for Tertiary to Recent volcanics are shown in solid lines and are taken from Ewart (1982).

The greater variation of the HREE may reflect the involvement of either garnet or hornblende because both these minerals preferentially accommodate the HREE, garnet to a far greater extent than hornblende (see K_d's for garnet and hornblende in appendix 3). However the relatively flat HREE patterns suggests that garnet was neither a fractionating nor residual phase. The greater HREE variation with relatively flat HREE profiles may reflect minor hornblende fractionation or the presence of residual hornblende. The REE patterns for samples JE42, JE13, JW6, and BK3 are also characterised by small negative Eu anomalies which may indicate that plagioclase was also a fractionating or residual phase.

The above discussion has indicated that the Grey Gneisses are chemically similar to calc-alkaline igneous rocks. The genesis of such rocks is beyond the scope of this thesis and is addressed to varying degrees in Gill, (1981); Brown, (1982) and Ewart (1982).

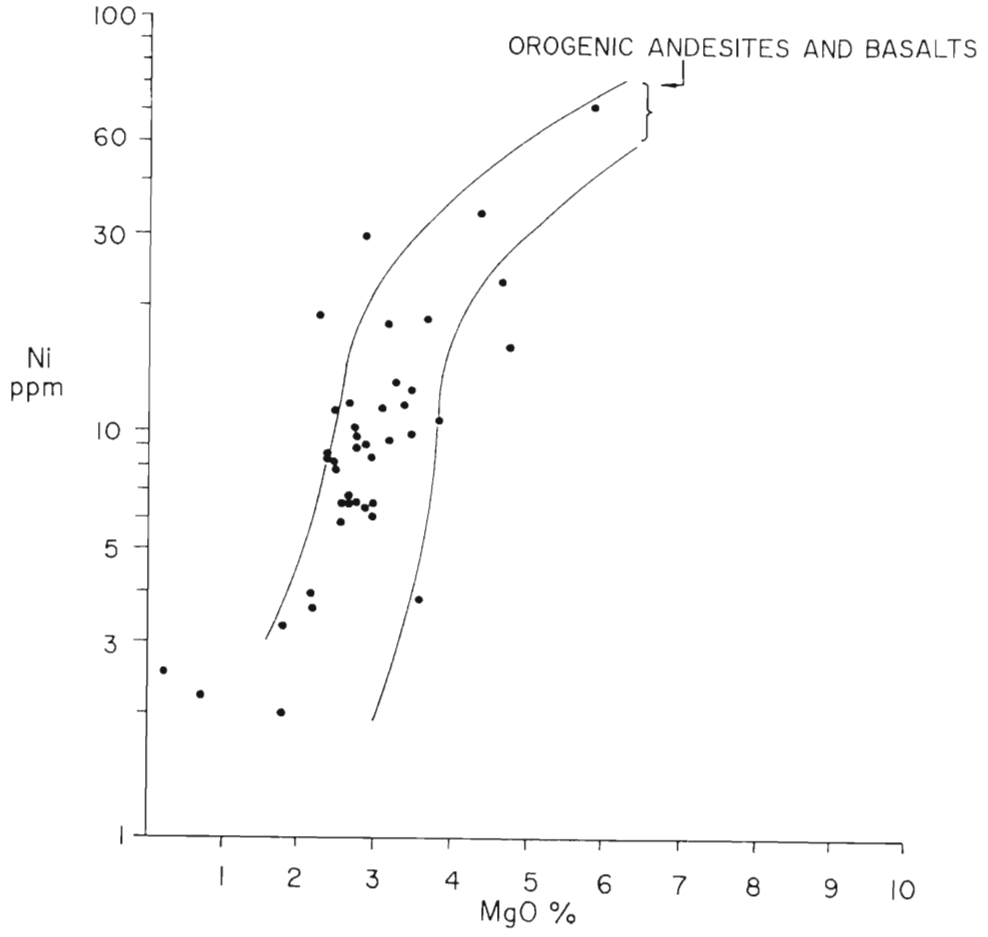

Figure 3.16. MgO vs Ni for the Grey Gneisses. The field of orogenic andesites is taken from Gill (1981). Those samples with SiO_2 contents between 60 and 66% lie within the andesitic field defined by Gill (1981).

Conclusion

The Grey Gneisses show wide ranges in chemical composition. Within the widely varying chemistry, coherent linear relationships between many of the trace and major elements are seen. The chemistry broadly reflects the varying proportions of minerals, the number of mineral species in the Grey Gneisses being relatively few.

Broadly, variation diagrams demonstrate that, compositionally, the Grey Gneisses show many similarities to calc-alkaline rocks of volcanic and plutonic origin. Interpretation of field characteristics and relationships suggest that a volcanic rather than a plutonic origin is more likely.

CHAPTER 4
BANDED GNEISS COMPLEX

INTRODUCTION

The field relationships of the Banded Gneiss Complex (BGC) were described in Chapter 2. The field appearance of the BGC is shown in figure 4.1. from which it can be seen that the Banded Gneisses are characterised by a great variety of lithologies including amphibolites, and various quartzofeldspathic, magnesian and calcareous rocks. The latter two lithologies are typically subordinate.

Figure 4.1 Photograph showing the field appearance of the Banded Gneisses at the northern part of Brekkerista. The fold is D_3 in age.

The description and discussion of the various rock-types will be initiated with a broad summary of the chemistry of the Banded Gneisses followed by a more detailed description of the petrography and chemistry of the various compositional classes present. The variety of rock-types facilitates a better understanding of the metamorphic history of the area. Therefore, the stability and history of the metamorphic assemblages recorded from the various rock types will

also be discussed.

CHEMISTRY, PETROGRAPHY AND METAMORPHISM

Introduction

The chemistry of the Banded Gneisses, like that of the Grey Gneisses, is highly varied. SiO_2 contents range from 44% to 81%, Al_2O_3 from 1.67% to 21.76%, FeO from 0.4% to 16.87%, MgO from 0.25% to 27%, CaO between 1.1% to 15.34%, Na_2O from below the limits of detection to 5.35% and K_2O from 0.12 to 5.6% (Table 4.1). However the Banded Gneisses do not show the same coherent linear relationships which characterised the Grey Gneisses and therefore no Harker diagrams or D.I. variograms are shown. On an AFM diagram the Banded Gneisses describe a broad calc-alkaline trend (Fig.4.2) although most mafic samples lie in the tholeiitic field. The samples which are largely tholeiitic in character constitute the mafic group (see later).

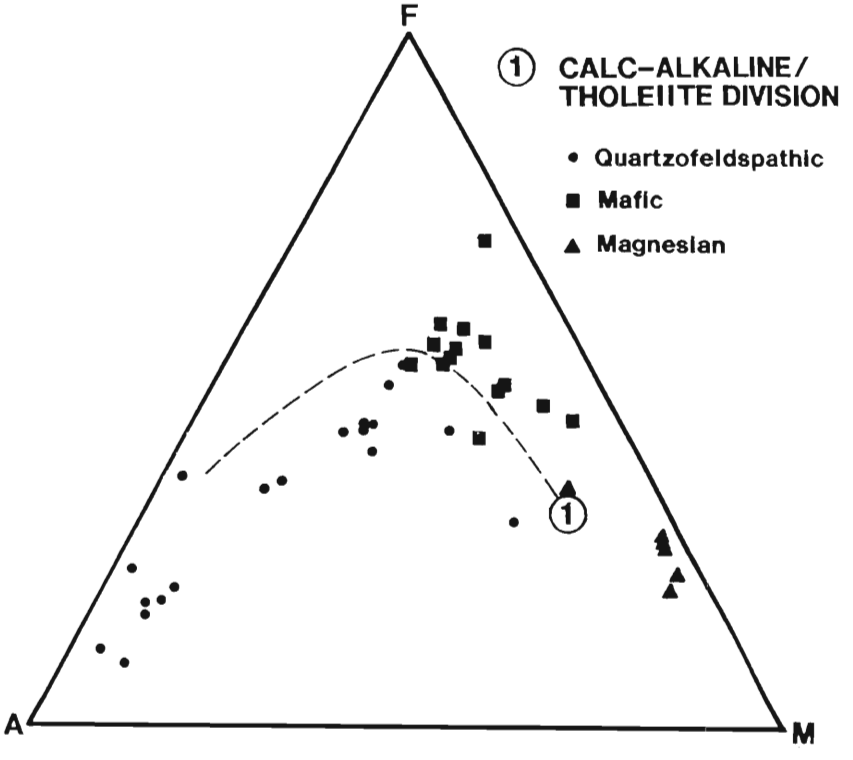

Figure 4.2. AFM diagram of the Banded Gneisses with the calc-alkaline- tholeiite division after Irvine and Barager (1971).

	SiO_2	Al_2O_3	Fe_2O_3	FeO	MnO	MgO	CaO	Na_2O	K_2O	TiO_2	P_2O_5	TOTAL
MAGNESIAN ASSEMBLAGES												
SV16	55.82	1.95	1.29	6.11	0.31	19.28	15.34	0.45	0.12	0.21	ND	100.88
BK23	57.30	1.67	1.94	7.46	0.22	24.02	6.17	0.12	0.63	0.13	0.04	99.70
BK11	56.04	3.14	1.89	5.68	0.16	27.27	3.55	0.05	1.79	0.15	0.01	99.73
BK10	57.61	2.67	1.75	6.31	0.18	26.87	2.83	ND	0.95	0.13	0.02	99.32
SV3	51.00	12.26	2.02	7.27	0.23	14.14	9.80	2.24	0.93	0.33	0.07	100.29
SV7	55.61	4.34	0.97	7.82	0.20	24.93	4.04	0.14	2.03	0.17	0.01	100.24
MAFIC ASSEMBLAGES												
JE37	48.15	14.28	3.21	9.14	0.18	10.88	7.71	2.19	3.41	1.11	0.32	100.58
JE40	47.55	17.03	2.89	9.80	0.21	5.48	8.55	3.39	2.19	1.91	0.60	99.60
JW19	50.34	14.22	2.47	10.11	0.20	6.45	9.98	2.85	1.00	1.87	0.22	99.71
JW23	50.96	15.93	1.85	7.09	0.16	7.95	11.31	2.83	1.18	1.06	0.23	100.55
SV5	51.19	13.57	2.68	10.98	0.22	5.67	9.56	2.72	1.12	1.71	0.25	99.67
SV13	49.19	13.22	2.91	11.93	0.31	7.07	9.90	2.63	0.92	1.70	0.21	99.99
SV15	49.09	13.86	2.39	10.21	0.20	9.43	11.44	2.38	0.55	0.82	0.10	100.47
SK5	51.80	7.95	2.21	10.45	0.35	13.96	11.23	0.60	1.04	0.57	0.08	100.24
SV1	49.55	14.31	2.21	10.46	0.29	7.26	11.06	2.23	0.34	1.39	0.17	99.27
TV29	49.66	13.59	2.79	10.71	0.30	6.04	10.62	3.35	1.06	2.08	0.23	100.43
JG8	53.30	9.40	2.04	9.63	0.23	10.99	11.13	1.54	0.45	0.81	0.12	99.64
BK8	56.13	10.18	2.07	9.08	0.18	8.43	10.05	1.96	0.87	0.86	0.16	99.97
BK12	46.92	16.61	2.83	10.19	0.19	6.47	10.22	3.07	1.50	1.33	0.45	99.78
S4	53.27	14.68	2.80	16.87	0.68	6.75	2.22	0.10	1.29	0.60	0.15	99.41
S3	48.08	21.76	2.36	9.60	0.25	6.24	6.47	1.53	2.27	0.37	0.07	99.00
QUARTZOFELDSPATHIC ROCKS												
JW18	73.01	13.73	0.70	1.88	0.05	0.25	1.31	2.55	5.62	0.31	0.06	99.47
JW24	73.97	14.46	0.30	0.82	0.03	0.37	1.37	3.01	5.36	0.17	0.05	99.91
BK13	72.59	15.51	0.38	1.22	0.02	0.57	2.42	4.65	2.08	0.29	0.09	99.82
JW26	72.65	12.71	1.20	3.42	0.06	0.34	1.57	3.28	4.28	0.55	0.11	100.17
JW20	72.19	14.77	0.50	1.42	0.02	0.84	2.30	3.38	4.12	0.34	0.10	99.98
BK9	72.84	15.32	0.46	1.46	0.02	0.89	2.45	5.29	1.37	0.30	0.12	100.52
JE36	80.95	11.91	0.09	0.40	ND	0.38	2.53	4.08	0.20	0.05	0.03	100.62
JG9	70.76	12.65	1.36	4.86	0.10	3.80	1.10	1.86	3.38	0.28	0.05	100.20
BK7	72.57	15.03	0.39	1.18	0.02	0.63	1.90	5.35	1.66	0.30	0.10	99.13
JW11	58.17	17.91	1.74	5.54	0.16	3.24	5.62	3.49	2.71	0.78	0.35	99.71
SK2	65.19	14.74	1.59	5.72	0.04	3.70	3.18	2.29	3.13	0.77	0.15	100.50
JE33	64.79	14.33	1.61	5.80	0.12	3.84	2.63	2.19	3.18	0.76	0.16	99.41
JW27	63.93	10.99	1.44	4.89	0.08	9.95	2.83	1.33	2.99	0.68	0.17	99.28
JW25	60.66	13.66	1.68	6.44	0.18	6.27	5.47	2.13	2.07	0.73	0.17	99.46
JE33	64.45	14.88	1.70	5.76	0.13	3.79	2.57	2.54	3.17	0.75	0.17	99.91
SK1	61.68	14.30	2.25	7.63	0.14	4.45	2.56	1.87	3.72	0.86	0.16	99.62
SK3	68.57	15.93	0.93	3.36	0.04	1.75	3.20	3.68	2.07	0.71	0.19	100.43
JE35	69.18	12.15	1.64	7.21	0.13	3.85	1.86	1.70	2.26	0.70	0.18	100.86
JW10	65.37	16.41	1.10	3.50	0.10	1.82	4.05	3.53	3.17	0.52	0.24	99.81
CALC-SILICATE												
SV12	81.57	1.92	0.29	2.35	0.38	4.12	7.89	0.57	0.10	0.25	0.04	99.49

Table 4.1. Major element chemistry of the Banded Gneisses. ND = not detected. Oxides in weight percent.

The discussion of the Banded Gneisses will be arranged according to the following groups namely Magnesian Rocks, Mafic Rocks, Quartzofeldspathic Rocks and Calc-silicate Rocks.

Chemistry, Petrography and Metamorphism of the Magnesian Rocks

Introduction

Magnesian rocks are defined as those having >14% MgO contents. The rocks may have high Ca or Al contents but not both. Generally rocks of this nature originate from ultramafic igneous precursors.

Petrography

The mineralogy of these rocks (table 4.2) is dominated by the following minerals; phlogopite, diopside, olivine, tremolite-actinolite, cummingtonite, talc, and anthophyllite with subordinate plagioclase, carbonate, and chlorite. Table 4.2 shows that the rocks generally contain moderately high contents of colourless to pale-green amphiboles including anthophyllite, cummingtonite, and tremolite. The amphiboles exhibit granoblastic textures and are either randomly oriented or show a weak planar foliation. Phlogopite, present in almost all samples in variable proportions, is pleochroic from pale brown to colourless.

	Phl	Act	Cum	Ath	Di	Tlc	Pl	Mgs	Ol
SV16					80		20		
BK23	5		5			90			
BK11	40					60			
BK10	10		70			17		3	
SV3	7			3	90				
SV7	40	50				10			
BK6	5	50		12				8	25
JG4	5				80	15			
JG5	5		92			1	2		

Table 4.2 Table of the estimated modal mineralogy (vol%) of the magnesian gneisses

The textural relationships of phlogopite differ widely. In some samples the phlogopite laths are subparallel but clearly crosscut amphibole grain boundaries. In others phlogopite is randomly oriented whereas in still others phlogopite laths are aligned parallel to the amphibole grains. Talc replaces anthophyllite in sample BK23 whereas in sample BK10 the assemblage talc + anthophyllite + phlogopite defines a strong schistose fabric. In the latter sample, a later generation of talc is oriented across the planar fabric.

Olivine, present only in sample BK6, is partially replaced by phlogopite and anthophyllite and locally contains inclusions of carbonate presumed to be magnesite. Carbonate in sample BK6 also occurs interstitially and is intergrown with tremolite (Fig. 4.3). Considering the highly magnesian nature of these rocks the carbonate is likely to be either dolomite or magnesite.

Diopside, present only in sample SV16, defines an equigranular granoblastic texture with

cummingtonite. Plagioclase forms accessory phases in the gneisses and is commonly partially saussuritised.

Chemistry

The chemistry of this group is characterised by high MgO (14-28%) with low to high contents of CaO (2-15%) and typically low Al_2O_3 contents (except for SV3) (Table 4.1). The SiO_2 contents in this group have a limited range from 51% to 57%.

The magnesian gneisses are characterised by high contents of Cr and Ni which vary between 1825ppm to 3010 and 326 to 1683ppm, respectively. The gneisses have low Zr, Ba, La and Sr contents (see Table 4.3).

	Rb	Sr	Th	Zr	Y	Nb	Ba	Sc	Cr	V	Cu	Ni	Zn
SV16	1	32	ND	12	19	3	ND	52	2809	174	13	326	121
BK10	64	6	1	12	19	4	96	7	1855	37	3	1595	151
BK11	64	5	1	12	15	5	106	17	3010	58	3	1205	115
BK23	33	7	ND	11	19	1	25	6	2427	41	3	1683	165
SV3	33	145	1	47	16	4	167	33	1825	154	8	605	125
SV7	121	7	ND	5	4	3	117	20	2316	74	ND	1408	124

Table 4.3 Trace element chemistry in ppm of the magnesian gneisses. ND = not detected.

Figure 4.3. Microphotograph of carbonate intergrown with tremolite in sample BK6. Field of view is 2mm wide. The intergrowth (I) shows diamond-shaped amphibole (white) enclosed in (grey) carbonate. T = tremolite.

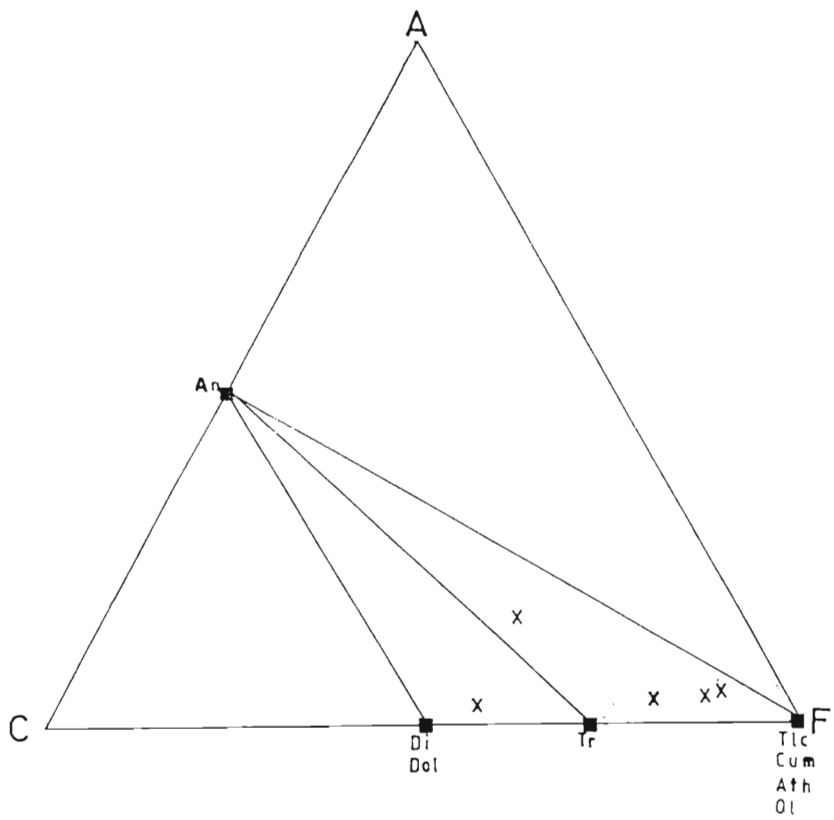

Figure 4.4. ACF diagram of the Magnesian Gneisses showing the bulk rock compositions and the various mineral phases recorded in these gneisses.

Metamorphism

The assemblages present are broadly characteristic of medium grade or amphibolite facies metamorphic conditions. Generally, the mineral assemblages developed in magnesian-rich rocks can be useful indicators of the nature of the fluid phase present during metamorphism. If it is assumed that the rocks were originally igneous in origin and had typical igneous mineral assemblages, then such assemblages may broadly approximate the C.I.P.W. normative or catanorm mineralogy. The normative minerals are shown in table 4.4. from which it may be seen that the original rocks were possibly pyroxenitic (SV16, BK23, BK11, BK10 and SV7) and gabbroic (SV3). Of the major normative phases, olivine, clinopyroxene and plagioclase are the only minerals still present in the gneisses although this does not imply that they are necessarily relics of primary igneous minerals.

	C.I.P.W.						CATANORM					
	SV16	BK23	BK11	BK10	SV3	SV7	SV16	BK23	BK11	BK10	SV3	SV7
Ap		0.10	0.02	0.05	0.17	0.02		0.09	0.02	0.05	0.16	0.02
Ilm	0.40	0.25	0.29	0.25	0.62	0.32	0.28	0.18	0.20	0.17	0.45	0.23
Or	0.70	3.73	10.61	5.65	5.48	11.96	0.69	3.63	10.10	5.41	5.36	11.49
Pl	6.69	3.18	3.49	4.51	39.49	6.38	6.81	3.15	3.35	4.32	39.77	6.20
Mag	1.85	2.82	2.75	2.55	2.92	1.40	1.31	1.98	1.89	1.76	2.06	0.97
Cpx	57.61	22.59	11.49	7.57	22.23	11.74	57.03	21.99	11.08	7.28	21.47	11.32
Opx	30.56	61.62	70.25	74.14	11.03	63.13	31.89	63.77	72.68	76.28	12.34	65.01
Qtz	1.93	5.57		5.15			1.99	5.21		4.72		
Fo			0.86		13.17	3.93			0.62		14.72	4.07
Fa			0.12		4.77	0.95			0.06		3.68	0.68
	99.74	99.86	99.88	99.87	99.88	99.84	100.00	100.01	100.00	100.01	100.02	100.00

Table 4.4. C.I.P.W. and catanorm mineralogy of the magnesian gneisses.

Figure 4.5 was calculated using the computer program GEOCALC (Brown *et al.* 1988) for the system Ca, Mg, Al, Si, O, H, C and K at 5kb. A pressure of 5kb was chosen because thermobarometers applied (see the chapter on metamorphism) indicate pressures of this magnitude. The following reactions (abbreviations after Kretz, 1983) are numbered in figure 4.5:-

1. 5 Srp = 6 Fo + 1 Tlc + 9 H_2O
2. 5 Ath + 4 H_2O = 9 Tlc + 4 Fo
3. 8 Fo + H_2O + 9 CO_2 = Ath + 9 Mgs
4. 2 Srp + 3 CO_2 = 1 Tlc + 3 Mgs + 3 H_2O
5. Ath + H_2O + CO_2 = Mgs + Tlc
6. 6 Fo + 13 Di + 4 H_2O + 10 CO_2 = 5 Dol + 4 Tr
7. 4 Fo + H_2O + 5 CO_2 = 5 Mgs + Tlc
8. 5 Kfs + 3 Tr + 6 CO_2 + 2 H_2O = 24 Qtz + 5 Phl + 6 Cal
9. 8 Fo + 2 Dol + H_2O + 9 CO_2 = 13 Mgs + Tr
10. 5 Tr + 12 Fo + 8 H_2O + 2 Qtz = 10 Dol + 13 Tlc
11. Tr + 3 Mgs + H_2O + CO_2 = 2 Dol + 2 Tlc
12. Tr + 4 CO_2 = Tlc + 4 Qtz + 2 Dol
13. Tlc + 3 CO_2 = 4 Qtz + 3 Mgs + H_2O
14. 2 Fo + 11 Di + 3 H_2O + 5 CO_2 = Cal + 3 Tr

Table 4.2 shows that the mineralogy of the magnesian rocks is dominated by anthophyllite, cummingtonite or tremolite. Figure 4.5 shows that tremolite + dolomite + calcite would form from diopside + forsterite + H_2O + CO_2 at between approximately 600°C to 680°C (reactions 6 and 14). Anthophyllite $\pm$ magnesite $\pm$ tremolite would form from olivine (forsterite) $\pm$ dolomite at temperatures of 550°C to 670°C (reactions 2,3 and 9). These reactions could therefore have been responsible for the formation of the observed Mg-rich amphibole-dominated

assemblages. The presence of anthophyllite indicates temperatures during the earlier stages of metamorphism of greater than approximately 600°C (Fig. 4.5). The low content of carbonate in these rocks may be indicative of a relatively H_2O-rich fluid phase because, if this phase had contained significant quantities of CO_2, most of the reactions shown in figure 4.5 (eg. reactions 3-12) would result in the generation of carbonate - dolomite and/or magnesite.

Reactions 1 and 4 constrain the stability field of serpentine. The absence of serpentine in thin section shows that either the fluid phase had $X_{CO2} > 0.06$ or that retrogressive reactions ceased before the stability field of serpentine was reached.

The interpretation from thin section that phlogopite developed late in the genesis of the mineral assemblage could be due to a reaction such as tremolite + 5 K-feldspar + 6 CO_2 + 2 H_2O = 5 phlogopite + 24 quartz + 6 calcite (Fig. 4.5) which occurs at temperatures between 500°C and 580°C. A problem with this reaction is that no free quartz nor calcite are observed. A possible reason for this is that the generation of phlogopite is the consequence of open system behaviour resulting from introduction of K^+ + water and that K-feldspar was not present as an independent phase.

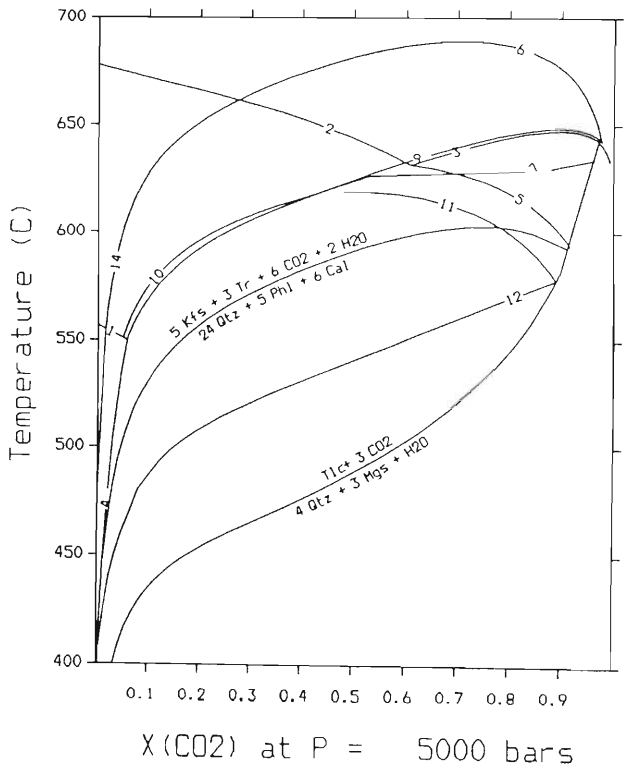

Figure 4.5. T-X_{CO2} diagram showing reactions of relevance to the magnesian gneisses.

However, reaction 8 does serve to provide some idea of the physical conditions related to the stability of phlogopite in these rocks. The stable presence of talc in some of the rocks indicates temperatures at least in excess of 450°C and less than approximately 650°C (Fig. 4.5).

The reactions discussed above suggest that the fluid phase was a mixture of H_2O and CO_2 and that the temperatures prevailing during the formation of the amphibole-dominated assemblages were of the order of 600°C. The formation of phlogopite and talc would appear to require slightly lower temperatures, of the order of 450-580°C and may be interpreted to have formed from a retrogressive influx of H_2O and K^+.

The system discussed above contains no Fe. Table 4.1 shows that the Fe content of the magnesian rocks is not insignificant. The presence of Fe in the magnesian rocks would result in lower temperatures of reaction of the order of 10°C (Winkler, 1976, p163). Therefore it is concluded that the reactions in figure 4.5 provide a reasonable estimate of the physical conditions under which the observed mineral assemblages may have formed.

The Petrography, Chemistry and Metamorphism of the Mafic Rocks

Petrography

The dominant minerals of the mafic rocks are hornblende and plagioclase with varying proportions of subordinate diopside, garnet, quartz, sphene, biotite, chlorite, epidote, cummingtonite, and opaque minerals (Table 4.5; Fig. 4.6). The rocks are medium- to fine-grained (0.5mm to 2mm grain size).

	Hbl	Pl	Di	Ep	Spn	Grt	Bt	Qtz	Chl	Opaque
TV25		50	30				20			
TV23		40	40				20			
TV27	30	39	20				7	3		1
JE37	45	34					20	1		
JE40	50	30			1		3		15	1
JW19	55	36			3			5		1
JW23	37	55		2	2			3		1
SV5	50	40				1	5	2		2
SV13	50	42					1	5		2
SV15	80	16	3					1		
SK5	93						2	5		
SV1	60	32						5		3
SV9	45	40	10					4		1
TV29	65	25	3				3			2
JG8	70	20			2		5	3		
BK8	49	30	5		1			15		
BK12	55	38			1		3	2		1
S4						20	20	15	45	
S3						1	25	15	59	

Table 4.5. Estimated modal mineralogy (vol%) of the mafic rocks.

Hornblende and plagioclase generally define a granoblastic texture. The weakly to strongly developed foliation, interpreted as an S_1 and/or S_2 foliation, is defined by aligned hornblende

laths. Biotite typically crosscuts this foliation suggesting its development occurred at a later stage. Pleochroic light to dark green hornblende commonly forms subidiomorphic laths and exhibits a poikiloblastic texture resulting from inclusions of quartz, plagioclase and sphene. Plagioclase is generally untwinned but exhibits variable extinction resulting from zoning. Measurements of extinction angles of rare albite twins yielded compositions in the range An_{26} to An_{36}. Plagioclase is commonly partially to completely saussuritized and commonly includes small (0.2mm) grains of quartz.

Diopside, when present, is rimmed by hornblende which appears to be replacing diopside. Diopside is pale green in colour and defines a planar fabric. Sphene forms small (0.5mm) subidiomorphic grains which are commonly included in hornblende. Garnet when present forms ragged poikiloblastic grains which are not seen in contact with hornblende. Associated with garnet are biotite, magnetite and a pale green mineral considered to be zoisite. In samples S3 and S4 garnet is partially altered to chlorite.

Pleochroic, light to dark brown biotite is commonly partially chloritized. Biotite shows variable textural relationships; in some sections it crosscuts the planar fabric defined by hornblende whereas in others biotite is oriented parallel to the foliation. Chlorite is colourless to pale green and occurs commonly along fractures. It also partially replaces hornblende and biotite. Accessory minerals include small idiomorphic sphene grains and an idiomorphic to xenomorphic opaque mineral, presumed to be magnetite.

The mineralogies of the first two samples listed in Table 4.5 (TV25 and TV23), are considered to be anomalous because of their high contents of clinopyroxene and biotite and absence of hornblende. A possible cause of the anomalous mineralogies is the close proximity of the Tvora Syenite intrusion (see map 7).

Chemistry

The major element chemistries of the mafic gneisses are typical of basic rocks, having SiO_2 contents of 47 to 56%, a wide range in Al_2O_3 (8 to 22%) and high FeO + MgO contents (table 4.1). The FeO content is approximately constant, varying between 9 and 11%, whereas the MgO content shows great variation ranging from 5 to 14%. The high MgO content of sample SK5 may be related to the fact that rock consists almost entirely of hornblende. CaO contents are mostly high ranging from 6 to 12%, except for sample S4 which has ~2% CaO. Na_2O contents are low varying between 0.6 and 3.35% except for sample S4. Trace element contents are highly variable (table 4.6). Rb/Sr ratios vary from 0.04 to 2.4, Nb from 3 to 26ppm, Ba 47 to 518ppm, Cr 46 to 2105 ppm, Cu 3 to 223ppm and Zn 9 to 172ppm. The Cr content of 2105ppm in sample SK5 correlates with the high MgO content in the rock.

Metamorphism

The characteristic assemblage of the mafic rocks is shown in figure 4.6 and consists of hornblende ± plagioclase ± clinopyroxene ± quartz ± garnet ± sphene ± biotite ± chlorite ± cummingtonite ± opaque minerals.

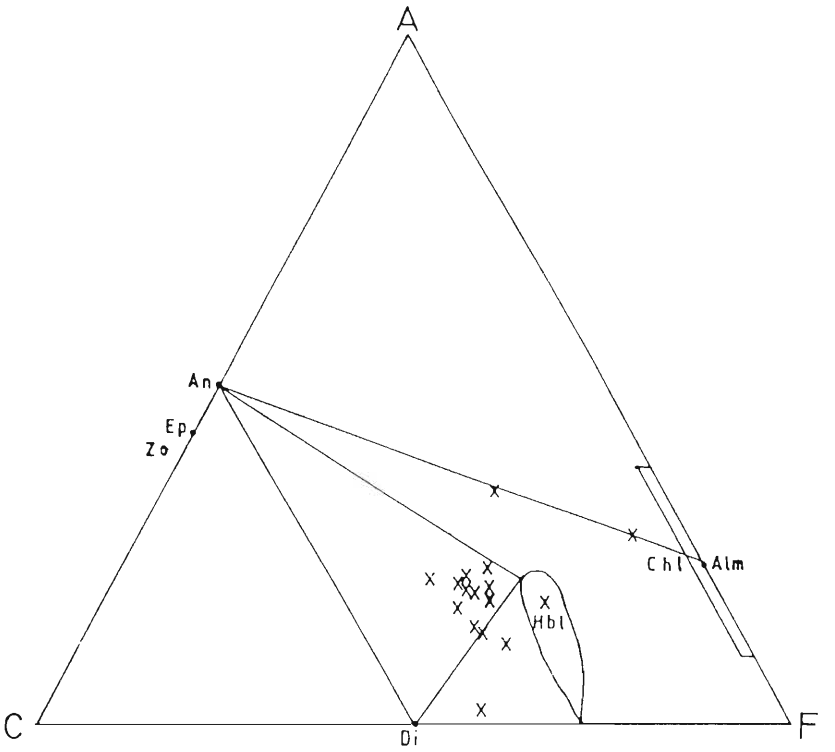

Figure 4.6. ACF diagram of the mafic gneisses showing the characteristic minerals.

It is difficult to attach specific conditions of metamorphism to the above assemblage for the following reason, outlined by Yardley (1989, pp. 100- 101), that mafic "rocks generally contain few phases and these are made up of a large number of components (Na_2O, K_2O, CaO, MgO, FeO, Fe_2O_3, Al_2O_3, SiO_2, H_2O, CO_2)". Consequently, reactions are likely to be continuous and will vary because of solid solutions involving the dominant minerals eg. CaO and Na_2O in plagioclase and amphiboles, FeO, Fe_2O_3, Al_2O_3 and MgO in amphiboles and biotite.

The mineral assemblage of plagioclase + diopside + hornblende represented in figure 4.6 is typical of medium grade or amphibolite facies metamorphism and, more particularly, the presence of clinopyroxene and the absence of epidote indicate upper amphibolite facies. The assemblage clinopyroxene + plagioclase + quartz, present in samples TV27, SV9, BK8 and SV15, is significant for barometry because of increasing solubility of Ca-Tshermacks molecule in clinopyroxene with pressure. This aspect will be explored further in the chapter on the

metamorphic history.

	Rb	Sr	Th	Zr	Y	Nb	Ba	Sc	Cr	La	V	Cu	Ni	Zn
JE37	173	242	1.5	136	24	10.3	572	14	652	25	127	10	468	128
JE40	75	530	1.3	158	39	26.3	518	23	25	51	355	57	125	147
JW19	24	261	1.8	114	29	8.8	122	43	159	1	392	59	55	105
JW23	25	469	3	69	20	4.8	149	42	464	3	254	45	104	80
SV5	30	156	3	155	37	9	190	31	131	17	315	223	96	127
SV13	25	93	0.8	97	30	7.3	93	44	197	6	352	72	82	132
SV15	11	94	ND	39	21	3	85	47	445	10	307	15	188	122
SK5	37	15	4	131	48	11	47	35	2105	9	209	3	391	111
SV1	9	170	ND	81	25	5.7	50	41	257	6	305	46	133	97
TV29	22	217	1.2	125	34	10	135	42	121	7	398	44	60	172
JG8	7	48	1.7	69	27	5.2	31	34	1130	ND	274	33	274	99
BK8	6	139	1.7	79	17	5.4	81	33	574	14	284	3	115	112
BK12	23	423	ND	103	29	11.3	252	30	46	22	348	240	52	97
S4	49	50	16	133	35	17	249	16	856	32	134	22	234	128
S3	72	520	29	135	36	20	504	20	860	49	100	30	166	9

Table 4.6. Trace element chemistry of the mafic rocks (Values in ppm). ND = not detected.

The Petrography, Chemistry and Metamorphism of the Quartzofeldspathic rocks

Petrography

The mineralogy of the quartzofeldspathic gneisses is presented in table 4.7. rocks are medium to fine-grained (0.5 to 2mm grain size). The gneisses generally display granoblastic textures with a planar foliation defined by the mafic minerals. The characteristic feature of these rocks is their quartz content which is associated with a high feldspar content. In some samples microcline, displaying typical tartan twinning, is common whereas in other samples twinning is rare making it difficult to distinguish untwinned plagioclase and orthoclase. Feldspar grains commonly show incipient sericitisation.

Pink to colourless garnet, when present, is generally sub-idiomorphic and typically poikiloblastic containing numerous inclusions of quartz and opaque minerals. The inclusions in the garnet do not define any planar fabrics. The planar foliation is wrapped around the garnet porphyroblasts suggesting that the garnet grew pre-tectonically.

Hornblende is pale-green to dark green in colour and forms subidiomorphic grains. Biotite is light brown to reddish brown in colour. Muscovite replaces plagioclase and is interpreted as a secondary retrogressive product. The presence of muscovite + quartz in some of the samples is significant for thermobarometry because it indicates that the reaction of muscovite + quartz -> K-feldspar + Al_2SiO_6 + H_2O was not reached.

Sample TV26 consists largely of perthitic feldspar, xenomorphic poikiloblastic hornblende and biotite. The rock is highly recrystallized. The perthitic nature of the feldspars and the recrystallization are considered to result from fenitization caused by the intrusion of the Tvora Alkaline Complex.

	Qtz	Pl	Or	Mc	Bt	Grt	Hbl	Chl	Aln	Ms	Spn	opaque
JW18	35	20		30	9		5				1	
JW24	20	20		50	7			2			1	
BK13	20	50		20	5					5		
JW26	30	15		20	10	10	.5				5	5
JW20	30	23		35	10				2			
BK9	20	75			5							
JE36	20	30*			25	20		2				3
JG9	30	40*			30							
BK7	20	60		10	5					5		
JW12	25	60			10					3		2
SK2	25	68			5	2						
JE33	20	45*			25			10				
JW27	30	20*			30		20					
JW25	25	23			15		25				2	
JE32	25	20		50	2			1		2		
SK1	25	58*			25	2						
JE27	30	22		35				3				10
SK3	25	68*			10					2		
JE39	25	25*			12	15	15	3				5
JE38	40	45*			10	5						
BK25	30	25		35	5			5				
BK21	28	35		35	1			1				
BK19	25	30	31		8	5			1			
BK17	30	30	31							1		
SV10	10	75			15							
SK4	35	25		30	5	3						2
JG7	35	30					35					
BK15	25	32	33		5					1		4
JE34	20	30*			20	25	5					
TV26	20	60*			10		5		5			
S1	30	40*			30						5	5
SV11	30	35*			20	10		5				

Table 4.7. Estimated modal proportions of minerals (vol%) in the quartzofeldspathic gneisses. * indicate samples in which the feldspars show no twinning and therefore the proportion for plagioclase includes that for K-feldspar.

Chemistry

The quartzofeldspathic gneisses have intermediate to high SiO_2 contents ranging between 58% and 81% with twelve of the eighteen samples having between 65% and 75% SiO_2 (Table 4.1). Like the Grey Gneisses, the major element oxides in these rocks display a wide range of concentrations. FeO varies from 0.4% to 7.63%, MgO from 0.25% to 9.95%, CaO from 1.1% to 5.62%, Na_2O from 1.33 to 5.35%, and K_2O from 0.2% to 5.62%. Whereas the Grey Gneisses were characterized by coherent linear variations with correlation co-efficients > 0.7 or <-0.7, systematic co-variance between oxides is less common in the quartzofeldspathic banded gneisses (Table 4.8). Negative coherent linear variations between SiO_2 and FeO, MgO, CaO, TiO_2 and P_2O_6 are indicated by correlation coefficients <-0.7. These may be related to the closure effect recognised by Chayes (1964). FeO shows positive linear relationships with MgO and TiO_2 and a negative relationship with Na_2O. MgO shows a negative relationship with Na_2O whereas CaO and TiO_2 show positive relationships with P_2O_6.

	Al_2O_3	FeO	MnO	MgO	CaO	Na_2O	K_2O	TiO_2	P_2O_5
SiO_2	-0.33	-0.81	0.35	-0.69	-0.69	0.49	-0.10	-0.88	-0.82
Al_2O_3	XXXX	-0.09	-0.34	-0.36	0.48	0.49	0.00	0.16	0.53
FeO		XXXX	-0.15	0.72	0.37	-0.74	0.05	0.88	0.58
MnO			XXXX	-0.07	0.10	0.06	-0.51	-0.29	-0.21
MgO				XXXX	0.37	-0.71	-0.07	0.64	0.40
CaO					XXXX	-0.01	-0.34	0.52	0.78
Na_2O						XXXX	-0.43	-0.54	-0.14
K_2O							XXXX	0.05	-0.12
TiO_2								XXXX	0.75

Table 4.8. Inter-element correlation coefficients for the major element chemistry of the quartzofeldspathic gneisses.

	Rb	Sr	Th	Zr	Y	Nb	Ba	Sc	Cr	La	V	Cu	Ni	Zn
BK7	45	396	2.8	135	7.4	3.8	223	2	8	12	20	2	4	29
JW18	117	169	13	295	36	23	2262	5.1	ND	117	13	1	ND	61
JW24	149	214	20	93	9.1	6.1	1349	2.3	1	20	16	1	1.7	17
BK13	47	408	16	176	35	27	717	3	5	101	11	1	8.4	25
JW11	86	725	ND	184	28	11	1502	17	29	23	159	1	11	106
JW10	72	617	5.7	114	17	8.5	1560	9	9	28	78	1	5	54
JE33	150	249	8.8	168	30	23	512	21	33	39	151	13	124	74
JW26	91	158	24	613	89	44	1145	6.2	8	117	12	9	4	56
JW25	62	283	5.3	156	26	12	507	18	449	28	149	14	127	135
JW27	87	114	8.1	140	31	11	374	19	372	24	139	3	114	67
JE36	106	234	ND	121	40	14	52	1	19	3	20	1	10	5
JE33	144	271	9.6	193	32	23	513	22	364	39	142	16	143	82
JW20	78	423	15	191	7	9	1092	3	11	57	17	10	7	35
SK3	83	404	17	409	39	23	1477	12	36	133	65	33	12	64
BK9	41	548	9	172	11	6	312	3	6	51	31	5	7	42
JE36A	10	124	5	183	2	2	338	15	347	35	137	6	120	57
JG9	160	102	6	92	9	13	426	13	577	10	105	8	150	96
SK1	141	140	10	162	29	11	917	27	445	79	194	10	132	34
SK2	137	169	14	173	30	14	781	26	416	58	155	13	138	41

Table 4.9. Trace element chemistry of the quartzofeldspathic gneisses (Values in ppm). ND = not detected.

Trace elements show wide variations in concentrations. Rubidium ranges from 41 to 160ppm, Sr from 114 to 725ppm, Ba from 52 to 2262 ppm, Sc from 1 to 27 ppm, Cr from below detection to 577 ppm, La from 3 to 133 ppm, and Ni from 4 to 150 ppm (Table 4.9). There are however few linear relationships between the various major and trace elements as shown by correlation coefficients >0.7 or <-0.7 (Table 4.10).

The linear covariance of Na_2O with Rb may be related to the substitution of Rb for Na in the alkali feldspar lattice. Similar covariance between Th, Zr, Y, Nb, and La may be related to the concentration of these elements in accessory phases such as zircon, apatite and sphene (see appendix 3, high K_d's for these elements in zircon, apatite and sphene are given). The linear relationships between Sc, Cr, V, and Ni may result from the accommodation of the elements in the ferromagnesian minerals namely amphiboles, biotite and garnet. The linear variations of CaO and P_2O_5 together with the sympathetic behaviour of Th, Y, Nb, and La suggests that apatite influenced these linear relationships.

	Rb	Sr	Th	Zr	Y	Nb	Ba	Sc	Cr	La	V	Cu	Ni	Zn
SiO_2	-0.36	-0.24	0.31	0.17	-0.19	-0.04	-0.06	-0.64	-0.28	0.17	-0.65	-0.19	-0.34	-0.5
Al_2O_3	-0.06	0.84	0.00	-0.04	-0.14	-0.06	0.44	-0.03	-0.46	0.15	-0.01	0.09	-0.40	0.06
FeO	0.53	-0.18	-0.34	-0.11	-0.33	0.16	0.21	0.67	0.49	-0.21	0.65	0.25	0.54	0.35
MnO	-0.40	-0.24	-0.32	-0.08	-0.27	-0.30	-0.24	0.22	0.31	-0.19	0.35	-0.03	0.34	0.15
MgO	0.27	-0.27	-0.37	-0.31	0.06	-0.11	-0.37	0.62	0.61	-0.37	0.65	0.13	0.62	0.43
CaO	-0.28	0.56	-0.39	-0.12	-0.04	-0.19	0.10	0.42	0.12	-0.16	0.54	0.17	0.12	0.59
Na_2O	-0.70	0.58	0.06	0.13	-0.24	-0.15	0.02	-0.54	-0.57	0.17	-0.48	-0.13	-0.58	-0.27
K_2O	0.69	-0.24	0.53	0.18	0.37	0.33	0.64	-0.06	-0.14	0.25	-0.21	-0.15	-0.16	-0.09
TiO_2	0.40	0.05	-0.14	0.12	0.46	0.28	-0.01	0.66	0.23	0.04	0.59	0.42	0.34	0.31
Rb	XXXX	-0.41	0.20	-0.09	0.17	0.25	0.17	0.39	0.28	-0.05	0.26	0.15	0.38	0.05
Sr		XXXX	-0.25	-0.09	-0.19	-0.20	0.25	-0.27	-0.56	-0.07	-0.16	-0.11	-0.56	0.07
Th			XXXX	0.62	0.46	0.58	0.44	-0.16	-0.23	0.72	-0.27	0.41	-0.29	-0.07
Zr				XXXX	0.79	0.78	0.38	-0.10	-0.28	0.77	-0.27	0.41	-0.29	0.07
Y					XXXX	0.89	0.21	0.06	-0.17	0.57	-0.12	0.20	-0.14	0.04
Nb						XXXX	0.26	0.01	-0.19	0.67	-0.19	0.30	-0.09	0.10
Ba							XXXX	-0.10	-0.38	0.55	-0.20	0.01	-0.45	-0.07
Sc								XXXX	0.71	-0.05	0.96	0.41	0.83	0.49
Cr									XXXX	-0.26	0.72	0.25	0.90	0.45
La										XXXX	-0.26	0.41	-0.27	-0.10
V											XXXX	0.29	0.82	0.56
Cu												XXXX	0.32	0.32
Ni													XXXX	0.46

Table 4.10 Inter-element correlation coefficients for the major and trace element chemistry of the quartzofeldspathic banded gneisses.

Metamorphism

The dominant mineral assemblage of the quartzofeldspathic gneisses is K-feldspar + plagioclase ± garnet ± hornblende ± biotite (table 4.7, Fig. 4.7). The presence of hornblende and plagioclase ($An_{>20}$) indicates that the rocks have been metamorphosed under medium grade or amphibolite facies conditions. In the A'KF diagram (Fig. 4.7) the dominant assemblage is garnet + biotite + K-feldspar ± muscovite. The coexistence of muscovite and biotite in some samples is a product of retrogression as is indicated by the intersecting tie-lines of biotite-muscovite and garnet-K-feldspar in the A'KF diagram (Fig. 4.7). This relationship suggests the reaction:-

$$Ms + Bt + 3Qtz \rightarrow Alm + Kfs + 2H_2O$$

This reaction has been modelled using the computer program THERMO (Powell and Holland, 1988) in a Fe-bearing system (Fig. 4.8). Figure 4.8 shows two curves, one where $aH_2O = 1$ (squares) and another where $aH_2O = 0.5$ (asterisks). An additional factor which would shift the reaction to higher temperature is the MgO content of the biotite. Figure 4.8 shows that $aH_2O < 1$ would shift the reaction to lower temperatures. A preliminary estimate of metamorphic temperature and pressures derived from figure 4.8 is of the order of 500-600°C. A full discussion of metamorphic temperature will be given in chapter 14.

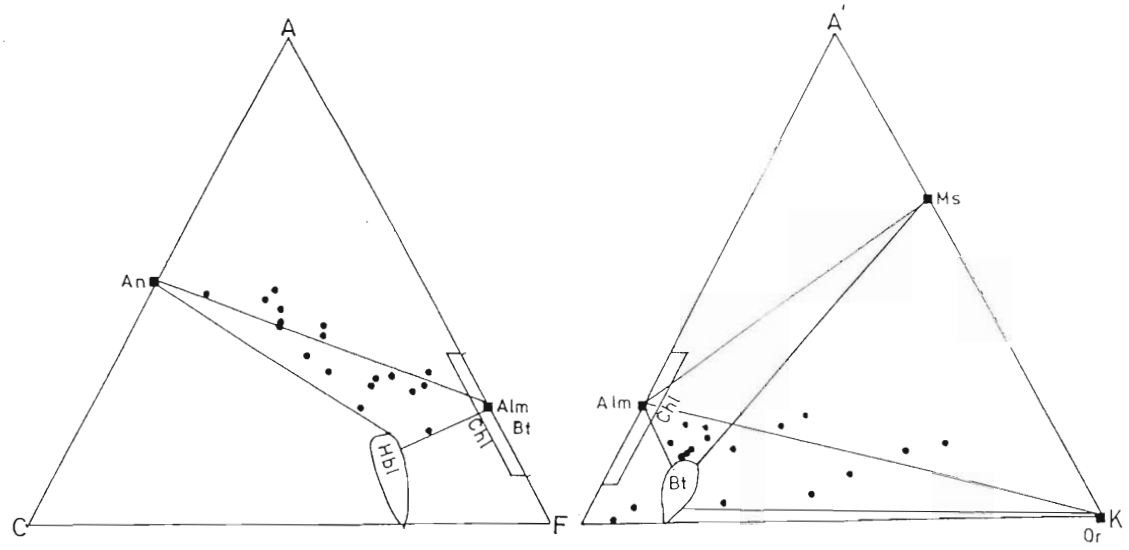

Figure 4.7. ACF and A'KF diagrams of the quartzofeldspathic gneisses.

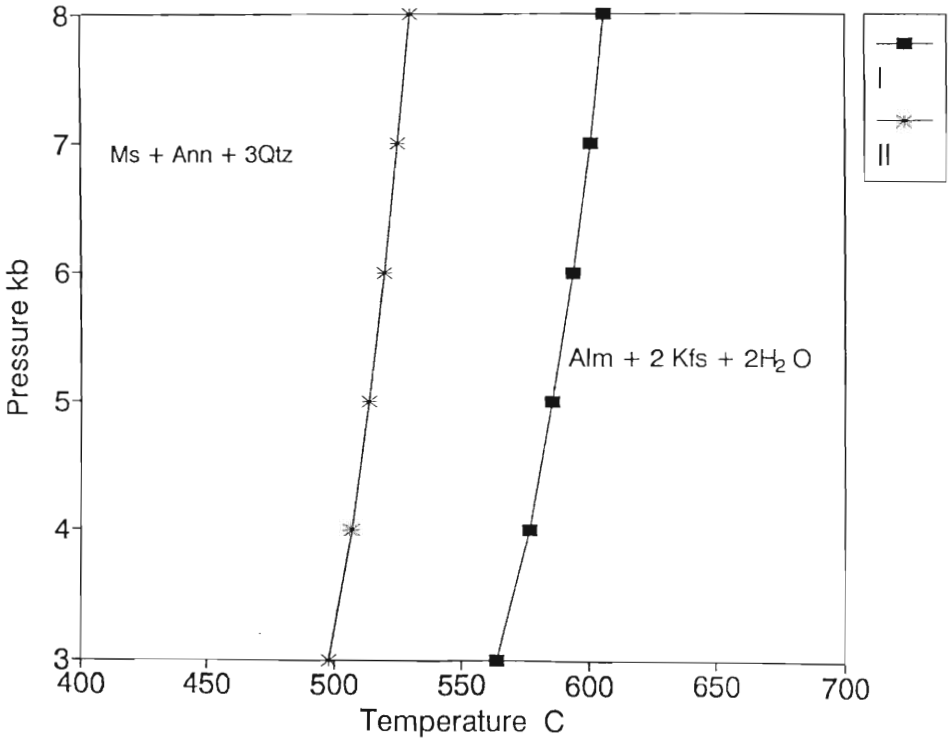

Figure 4.8. Physical conditions of metamorphism for mineral assemblages in the quartzofeldspathic gneisses.

Petrography and chemistry of the calc-silicate gneisses

Petrography

These rocks are medium to fine-grained (0.5-2mm grain size). Their mineralogical composition comprises variable proportions of diopside, quartz, hornblende, plagioclase and a green isotropic mineral considered to be grossular (table 4.11).

	Di	Grs	Qtz	Hbl	Pl	Spn
SV12	30	15	50	4		1
JG3	20		5	5	70	1

Table 4.11. Estimated modal mineralogy (vol%) of the calc-silicate gneisses.

The rocks have a granoblastic texture. Grossular is characterized by a green colour and locally is partially replaced by hornblende (Fig. 4.9). Pale green diopside is partially replaced by hornblende which is characterized by a dark green colour. Plagioclase is partially saussuritized. Sphene is an accessory mineral occurring as small (<0.3mm) subidiomorphic grains.

Chemistry

The single analysis of a calc-silicate gneiss (SV12) does not permit a detailed discussion of the chemistry of this group. SV12 has high SiO_2 and CaO accompanied by low contents of Al_2O_3, Na_2O, and K_2O (see table 4.1). The trace element chemistry of the calc-silicate gneisses is characterized by high Cr and Ni and low contents of Sr and Ba (Table 4.12).

	Rb	Sr	Th	Zr	Y	Nb	Ba	Sc	Cr	La	V	Ni	Zn
SV12	6	32	1	18	7	2	21	12	1241	3	67	297	26

Table 4.12. Trace element chemistry of sample SV12 (Values in ppm).

Metamorphism

The calc-silicate gneisses have a mineral assemblage consisting of plagioclase + clinopyroxene + hornblende + quartz $\pm$ grossular (table 4.11). This assemblage is shown in figure 4.10. The bulk composition of sample SV12 falls on the diopside-grossular tie-line, consistent with the low content of hornblende and absence of plagioclase. The presence of grossular is surprising in view of the low Al_2O_3 content in sample SV12 but its presence is significant with respect to the conditions of metamorphism. Figure 4.11 was calculated using the program GEOCALC developed by Brown *et al.* (1988).

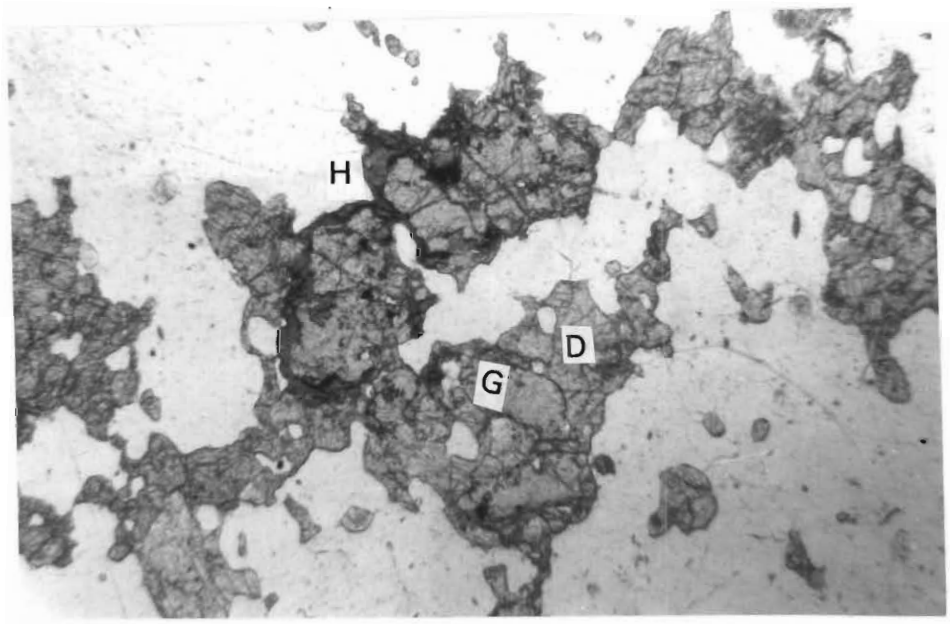

Figure 4.9. Microphotograph of grossular (G) enclosed by diopside (D)(right) and hornblende (H)(dark)(left) in sample SV12. Field of view is approximately 2mm.

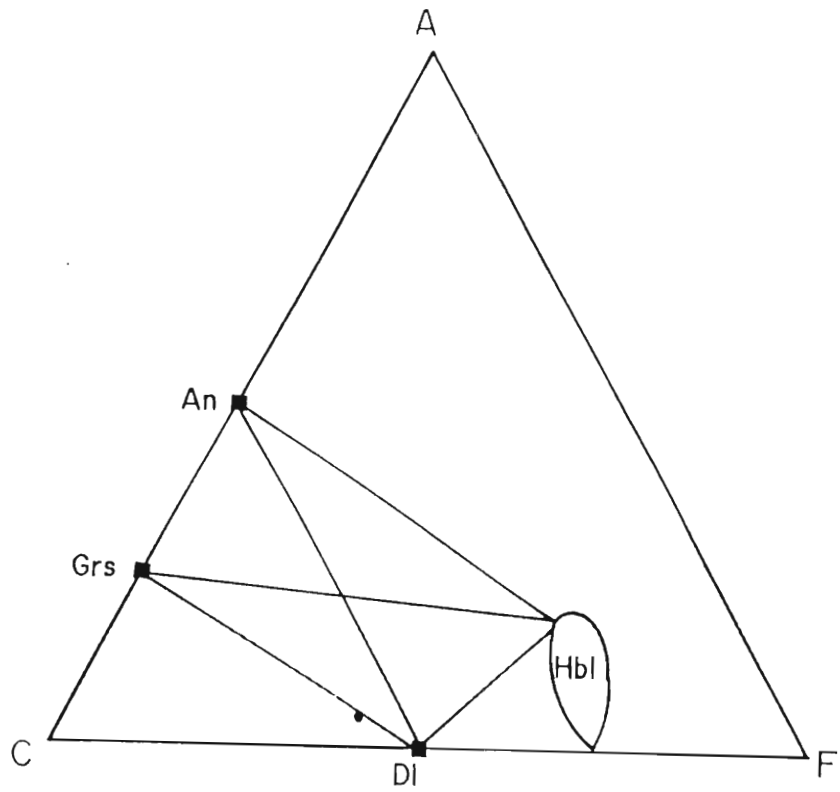

Figure 4.10. ACF diagram for the calc-silicates.

The presence of grossular is defined by the following reactions which are labelled or numbered on figure 4.11.

1. 4 Zo + Qtz = 5 An + Grs + 2 H_2O

3. Qtz + 2 Cal + An = Grs + 2 CO_2

8. 5 Cal + 3 Qtz + 2 Zo = 3 Grs + H_2O + 5 CO_2

The following reactions may constrain the coexisting diopside and amphibole.

5. 2 Qtz + Tr + 6 Zo = 5 Di + 9 An + 4 H_2O

9. 6 Zo + Tr + 2 CO_2 = 9 An + 4 Di + Dol + 4 H_2O

At a pressure of 5kb grossular is stable above approximately 550°C (reactions 5 and 8, Fig. 4.11) and its stability is also restricted to H_2O-rich conditions (Fig. 4.11).

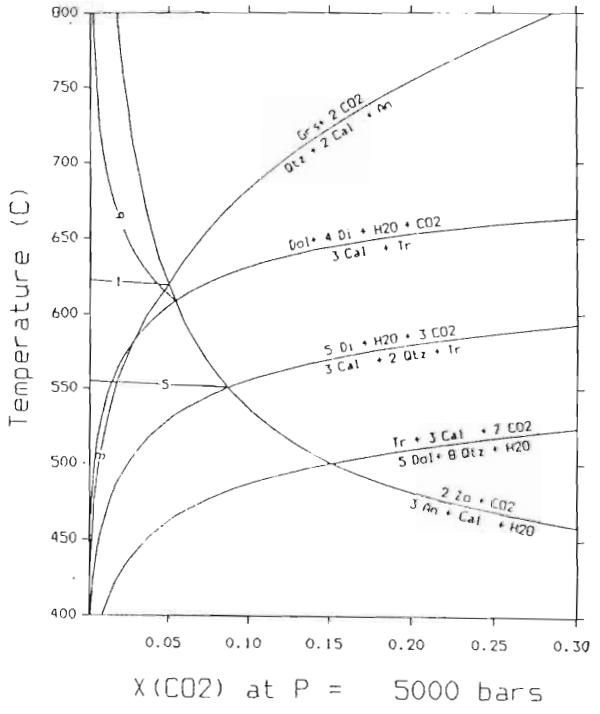

Figure 4.11. Stability field of grossular-bearing assemblages calculated using the program GEOCALC developed by Brown *et al.* (1988).

ORIGIN OF THE BANDED GNEISSES

It has been emphasised that the Banded Gneisses are characterised by a great variety of lithologies including amphibolites (basic rocks), quartzofeldspathic rocks (including semi-pelitic gneisses), magnesian rocks and calcareous rocks. On an ACF diagram (Fig.4.12) analyses of the

Banded Gneisses lie in fields which are considered to be characteristic of ultramafic rocks, basic to intermediate igneous rocks, greywackes and pelitic rocks.

Magnesian Gneisses

The compositions of the magnesian gneisses lie in the field for ultramafic igneous rocks on an ACF diagram (Figs. 4.4 and 4.12). Paragneissic calc-silicate rocks could conceivably yield similar chemistries, particularly those characterised by high concentrations of both CaO and MgO. Distinguishing between a paragneissic or an orthogneissic origin for these rocks is assisted by a study of their trace element chemistries. The magnesian-rich nature of these rocks suggests either an ultramafic igneous origin or a paragneissic calc-silicate origin. The former alternative is preferred and is supported by the high contents of Cr and Ni which vary from 1825 to 3010ppm and 326 to 1683ppm, respectively (table 4.3). The low Ba and Sr contents are also characteristic of ultramafic rocks rather than paragneissic calc-silicate rocks because the latter would be expected to have relatively high contents of these elements. The low La contents are also characteristic of ultramafic rocks (see table 4.3).

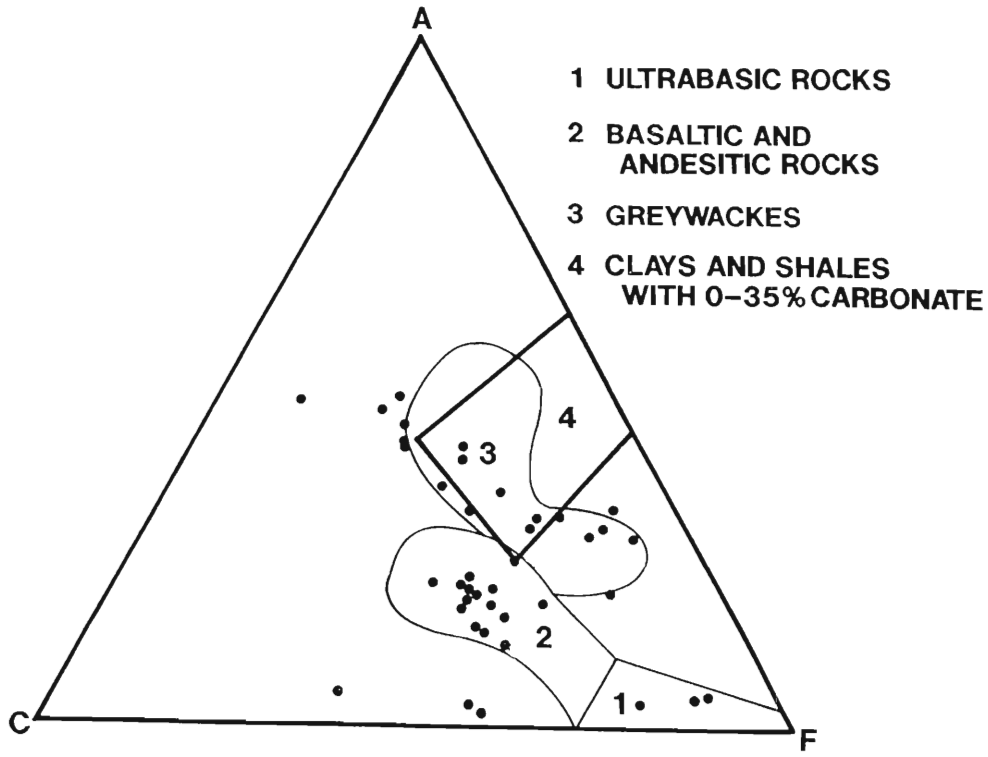

Figure 4.12. ACF diagram of the Banded Gneisses with boundaries for ultramafic rocks (field 1), basic to intermediate igneous rocks (field 2), greywackes (field 2, thin boundary line) and pelitic rocks (field 4, thick boundary line) after Winkler (1976, p.46).

Accepting an igneous origin for the magnesian gneisses raises the question of their source and whether they were extrusive or intrusive. The magnesian rocks are not seen to crosscut the general layering of the gneiss complex and therefore do not appear to be intrusive and the magnesian gneisses may represent volcanic rocks. Alternatively, the apparent absence of intrusive contacts may be the result of high strains resulting in intrusive sheets of ultramafic material being rotated into parallelism with the gneissic layering.

Mafic Gneisses

The bulk compositions of the mafic gneisses are plotted in figures 4.6 and 4.12 from which it may be seen that the rock compositions plot in the area typical of basic to intermediate rocks. Taking the heterogeneous layered nature of the Banded Gneisses into consideration, rocks of this composition are most likely to have been volcanic in origin.

Quartzofeldspathic gneisses

The compositions of the quartzofeldspathic gneisses lie in fields (Fig. 4.7 & 4.12) characteristic of greywackes and shales (Winkler,1976, p. 46). However, the Al_2O_3 contents are not as high as would be expected in pelitic rocks. The high SiO_2 content of sample JE36 is atypical of an orthogneiss and it is possibly more characteristic of a sandstone. In view of the intermediate to acid compositions of these rocks greater coherency might have been expected between Na_2O, K_2O and CaO, if the rocks had a common origin.

Calc-silicates gneisses

The high CaO contents are typical of the calc-silicate gneisses and, together with their high SiO_2, suggest that the rocks originated as a calc-arenite. However the trace element chemistry of the calc-silicate gneisses are unusual in that they are characterized by high Cr and Ni concentrations and low contents of Sr and Ba. High Cr and Ni concentrations are characteristic of ultramafic or Mg-rich assemblages whereas high Sr and Ba contents would be expected in paragneissic calc-silicate rocks. Assuming isochemical metamorphism, the high SiO_2 content of sample SV12 seemingly precludes an ultramafic origin and contrasts with its high Cr and Ni. A possibility which could satisfy the requirements of high CaO and SiO_2 contents as well as high Cr and Ni would be that the rocks are derived from a highly altered or silicified mafic to ultramafic rock.

CONCLUSIONS

The Banded Gneisses are highly variable in mineralogy and chemistry. The mafic and magnesian-rich assemblages are considered to be derived from igneous precursors, the strongly layered nature suggesting a volcanic origin. The quartzofeldspathic gneisses are chemically variable and do not show coherent linear relationships. This may indicate that they are, at least in part, of sedimentary as well as volcanic in origin. Mineral assemblages in the various rock types are broadly consistent with medium to high grade metamorphism with temperatures of the order of 550- 650°C being indicated by assemblages in the magnesian, quartzofeldspathic and calc-silicate gneisses. Temperatures of this magnitude for the mineralogy of the quartzofeldspathic gneisses suggest that $pH_2O \sim P_{load}$ (Fig. 4.8). The presence of grossular also indicates that the fluid composition was H_2O-dominated although the presence of carbonate in the magnesian gneisses also provides evidence of a minor component of CO_2.

CHAPTER 5
THE FUGLEFJELLET FORMATION

INTRODUCTION

The Fuglefjellet Formation is dominated by carbonate rocks with subordinate calc-silicate, quartzofeldspathic, mafic and magnesian-rich gneisses. Tonalitic gneisses similar to the Grey Gneiss Complex form a significant component of the quartzofeldspathic gneisses. The Fuglefjellet Formation is exposed at Fuglefjellet and Dvergen (maps 1 and 4). In this chapter, the mineral assemblages, metamorphism and chemistry of the various rock-types comprising the Fuglefjellet Formation will be described followed by a discussion of their origins.

PETROGRAPHY

The petrography and mineralogy for each of the various chemical classes will be described and discussed.

The quartzofeldspathic rocks

The mineralogy of these rocks, shown in table 5.1, is highly variable but is dominated by quartz and feldspar. The rocks display a gneissose fabric, typically defined by biotite and to a lesser extent, hornblende.

No.	Feldspar	Qtz	Bt	Hbl	Spn	Ep	Cpx	Grt	Chl	Mag	Cal	Ms
FG1	65	5	7	20	2		1					
FG5	63	30	2					2				3
FG7	45	20	15	15	3				2			
FG10	55	15	12	12	4						2	
FG12	60	15	15	5	5							
FG13	59	20	20					1				
FG15A	15	20		5	5	5	5	25		20		
FG22	70	25	3	2								
FG23	65	7	13	15								
FG24	65	28	5									2
FG28	60	25	13									2
FG50	50	25	15	10								
FG59	57	20	10	10	3							
FG60	55	15	7	20	3							
FG61	60	15	5	10	5	5						
FG62	55	20	12	8			2				1	2
DVG10	53	25	10							10		2
DVG11	60	25	10							5		
DVG12	57	30	10		1					2		

Table 5.1 Modal estimates (vol%) of the mineralogy of the quartzofeldspathic rocks.

The rocks are typically fine- to medium-grained (0.5-2mm grain diameters) and show granoblastic textures. Quartz and feldspar form rounded xenomorphic grains. Identification of

plagioclase is hampered by the fact that plagioclase is commonly untwinned. K-feldspar occurs dominantly as microcline with tartan twinning and less commonly as untwinned orthoclase. Locally single grains show both varieties. Muscovite occurs as minor alteration of feldspar. Biotite, the most common mineral after quartz and feldspar, is pleochroic brown to dark-brown and partially replaces hornblende, which builds pleochroic green to dark blue-green, poikiloblastic laths. Quartz inclusions in hornblende locally define a vermicular intergrowth. In some sections, relict cores of clinopyroxene are preserved in the hornblende.

Sample FG15A is unusual and consists of quartz, garnet, plagioclase, sphene, clinopyroxene, hornblende, epidote and an opaque phase presumed to be magnetite. The epidote and hornblende form vermicular masses which separate magnetite and/or clinopyroxene from plagioclase feldspar. Hornblende partially replaces clinopyroxene. Sphene forms rims around idiomorphic grains of magnetite. Locally, garnet adjacent to plagioclase is rimmed by zoisite-quartz symplectites.

In summary, the characteristic mineralogy of the quartzofeldspathic gneisses consists of quartz + feldspar + biotite $\pm$ hornblende $\pm$ sphene with local development of epidote, clinopyroxene, garnet, chlorite, magnetite, calcite and muscovite.

The carbonate rocks

The mineralogy of the carbonate rocks is shown in table 5.2.

Sample No.	Cal/Dol	Tr	Tlc	Phl	Brc	Mtc	Srp	Qtz
FG20	80	10	10					
FG11	80	9			10	1		
FG6	50/40		5	5				
FG54	35/40	10	10					5
FG56	70/0		10		10		5	5

Table 5.2 Estimates of the modal mineralogy (vol%) of the carbonate rocks.

The carbonate rocks range in grain sizes from fine- to coarse-grained (0.5 - 10mm) and are characterised by a granoblastic texture. The mineralogy is dominated by carbonates ie. calcite and dolomite with subordinate silicate minerals including tremolite, talc, phlogopite, monticellite and brucite. Talc rims tremolite and is partially intergrown with brucite in some samples. Serpentine and brucite form a zoned aggregate in sample FG56 with serpentine forming in the cores with marginal brucite. Textures in the serpentine mimic the fracture pattern of olivine suggesting that it was derived from olivine. Talc forms discrete grains and is also located adjacent to the brucite-serpentine aggregates. Monticellite is rimmed by brucite. The silicate minerals define a very weak planar fabric. Samples FG6, FG54 and FG56 were studied using X-ray diffraction to determine the nature of the carbonates present. Sample FG56 was found to contain only calcite whereas samples FG6 and FG54 contain dolomite and calcite in similar

proportions. The identification of the carbonates was done by Ms. S. Verryn in the Department of Geology, at the University of Pretoria.

In summary the characteristic mineralogy of the carbonate rocks is calcite ± dolomite ± tremolite ± talc with local development of phlogopite brucite, monticellite, serpentine, and quartz.

Calc-silicate rocks

The rocks are medium- to coarse-grained (0.5mm to 6mm). The mineralogy of the samples is shown in Table 5.3.

	Di	Hbl	Pl	Qtz	Spn	Scp	Mc	Cal	Bt	Ep/Zo	Chl
FG26	5	30		15	1	15	30	1		3	
FG53	40		14	2	1	1	40			1	1
FG58	13	15	5	2	2	3				60	
FG52	40	20	30	5	1			2	2		
FG16			10	24	1					65	
FG17	10	15	70	2	1				2		
FG18	10	4	80		1			1	4		
FG19	5	12	75	1	1			1	5		
DVG3	20	14	25	1	2		35	1			2
DVGA	70	20						10			
FG2	40	5	50		3	2					

Table 5.3. Estimates of the modal mineralogy (vol%) of the calc-silicate gneisses.

Diopside, calcite, amphibole, plagioclase, quartz, and sphene are present in almost all samples whereas epidote, scapolite, microcline, biotite and chlorite are present in some samples. The proportions of quartz, calcite and sphene are generally very low (<5%) whereas plagioclase is a major constituent. The gneisses typically have a granoblastic texture defined by hornblende, feldspar (plagioclase and/or microcline when present), scapolite and diopside. Pale-green diopside forms ragged poikiloblastic grains which enclose grains of quartz and plagioclase. Diopside is commonly partially replaced by amphibole. The amphibole is variable in colour, in some sections being pale-green to colourless whereas in others it is dark green. Plagioclase commonly shows albite twinning and, locally, albite/Carlsbad combination twins. Scapolite is partially to completely enclosed in zoisite suggesting that it is pseudomorphed, at least in part, by zoisite. Biotite is commonly pleochroic, colourless to pale-brown indicating a phlogopitic or magnesian composition. The biotite grains transect the granoblastic texture suggesting that they have grown later. Accessory minerals in these gneisses include subidiomorphic to idiomorphic sphene, and xenomorphic calcite and apatite. The apatite, present in two samples, occurs as relatively coarse grains up to 1mm in diameter. Calcite commonly fills voids between grains. Where epidote forms a major constituent of the rock, it occurs as fine to coarse grains 0.5 to 3mm in diameter but in other samples it forms a net-like mesh separating grains of plagioclase

from one another. Banding or layering in the gneisses on a centimetre scale is reflected by the presence of alternating hornblende-rich and diopside-rich layers.

In summary the characteristic mineralogy of the calc-silicate gneisses is diopside ± hornblende ± plagioclase ± quartz ± sphene ± calcite with local development of microcline, scapolite, biotite, epidote, zoisite and chlorite.

Basic Rocks

These rocks are generally medium-grained (2-3mm grain size) with a granoblastic texture. The mineralogy is dominated by plagioclase, hornblende and biotite with quartz, epidote, garnet, chlorite, calcite, apatite, tourmaline, clinopyroxene, sphene and opaque minerals forming minor phases (Table 5.4).

Sample No.	Pl	Bt	Hbl	Qtz	Spn	Ep	Cpx	Grt	Chl	Mag	Cal	Ap	Tml
FG3	22	20	40	5	1		10				1	1	
FG4	50	10	35	2						3			
FG31	20	5	50			3		1	5	1			15

Table 5.4. Modal estimates (vol%) of the mineralogy of the mafic rocks

Hornblende is green to dark-green, and partially replaces clinopyroxene. Plagioclase is characterised by zoning and albite twinning. Red-brown to brown biotite commonly defines a weak planar foliation and transects the granoblastic texture indicating a later development. Biotite is partially replaced by chlorite. Garnet forms poikiloblastic grains which are partially to completely replaced by an aggregate of chlorite, opaque minerals and epidote. Tourmaline is pleochroic, and has a yellow-brown colour toward the outer portions of grains whereas the cores are commonly blue-green in colour. Tourmaline locally contains inclusions of quartz.

In summary, the characteristic mineral assemblage of the mafic rocks is plagioclase + biotite + hornblende ± quartz with local development of sphene, epidote, clinopyroxene, garnet, chlorite, magnetite, calcite, apatite and tourmaline.

Magnesian Gneisses

Modal estimates of the mineralogy of the Mg-rich rocks (table 5.5) show that the mineralogy is variable without a characteristic mineral assemblage being recognised. The olivine in sample FG59 occurs as coarse (5mm) poikiloblastic grains with inclusions of magnetite, cummingtonite and phlogopite. Phlogopite and cummingtonite define a planar fabric which cross-cuts grains of olivine, and serpentine. Olivine poikiloblasts are partially to completely replaced by

yellowy-brown serpentine. Carbonate, presumably magnesite, fills voids and cracks.

	Ol	Srp	Cum	Hbl	Mag	Mgs	Phl	Tlc	Pl
FG30				80			20		
FG51				70			15		15
FG55		49			2			49	
FG59	20	15	40		3	2	20		

Table 5.5. Modal estimates of the mineralogy (vol%) of the magnesian gneisses.

Sample FG51 and FG30 are similar, both being dominated by pale-green hornblende and red-brown phlogopite. They have a granoblastic texture with a strong planar fabric defined by the phlogopite laths. The plagioclase in sample FG51 is untwinned. Sample FG55 consists essentially of serpentine and talc and is devoid of a planar fabric. The talc and serpentine are completely intergrown.

METAMORPHISM

The quartzofeldspathic rocks

The characteristic mineral assemblage of the quartzofeldspathic gneisses is quartz + plagioclase + K-feldspar + biotite ± hornblende ± sphene (Fig. 5.1) with local occurrences of epidote, clinopyroxene, garnet, chlorite, muscovite, carbonates and opaque minerals.

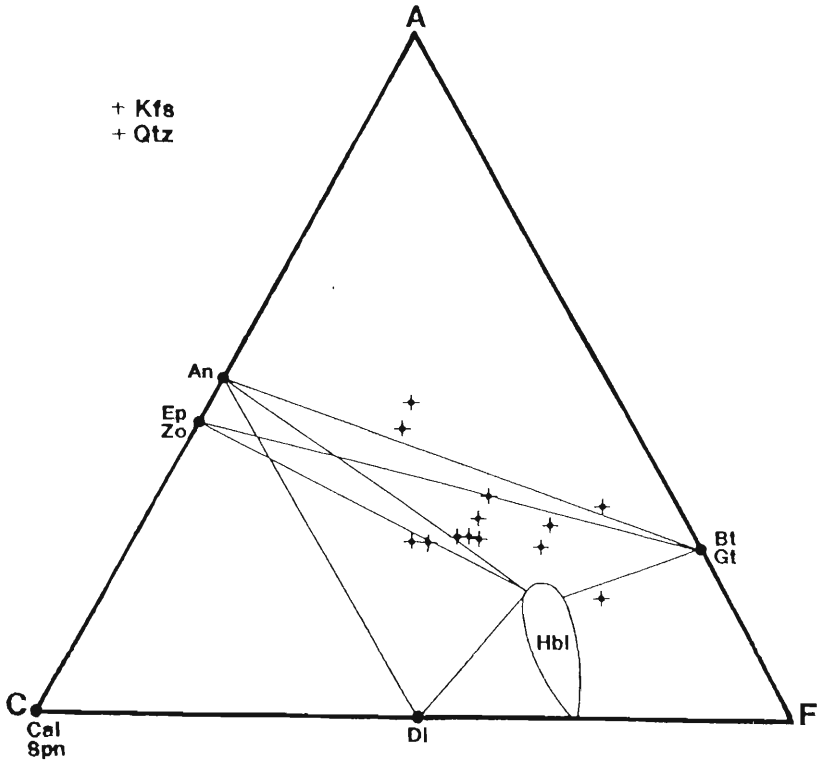

Figure 5.1. ACF diagram for the quartzofeldspathic gneisses.

The metamorphic mineral assemblage of these rocks is comparable to that of the Grey Gneiss Complex hence it is reasonable to assume that similar metamorphic conditions prevailed. However their are exceptions, marked by the general absence of epidote and the presence of clinopyroxene in some samples of the Fuglefjellet Formation.

The absence of epidote suggests that the reaction:-

(I) $6An + Hbl + 2\ Or + 3\ H_2O \rightarrow Bt + 2\ Ep + 2\ Zo + 7\ Qtz$

recognised in the Grey Gneiss Complex did not occur, possibly indicating a somewhat higher grade of metamorphism at Fuglefjellet. The presence of relict clinopyroxene is consistent with this conclusion.

In chapter 3 (Fig. 3.8, page 27) it was shown that the above reaction is displaced to lower temperatures where $aH_2O < 1$. It would be reasonable to expect the $aH_2O < 1$ in the Fuglefjellet Formation because of the significant production of CO_2 during metamorphism of carbonate rocks. Therefore, the preservation of clinopyroxene and the absence of epidote may imply a lower aH_2O or higher temperatures. These possibilities will be discussed further in the chapter 14.

The mineralogy and textures seen in sample FG15A suggest the following reactions:-

(II) $5An + Grs + 2H_2O \rightarrow 4Zo + Qtz$

(III) $10An + 4Hd + 4H_2O \rightarrow 3Qtz + Hbl + 6Zo$

(IV) $4Ilm + 9Grs + 31An\ 14H_2O \rightarrow Hbl + 4Spn + 26Zo$

(V) $3Ilm + 5Hd + 2An + 3Qtz + 2H_2O \rightarrow 2Hbl + 3\ Spn$

Modelling these reactions using the computer program THERMO by Powell and Holland (1988) indicates that all these reactions occur at similar physical conditions ie. at temperatures >500°C assuming pressures of the order of 5kb (Fig. 5.2, see later).

The carbonate rocks

The characteristic metamorphic assemblage of the carbonate rocks is calcite $\pm$ dolomite $\pm$ tremolite $\pm$ talc $\pm$ serpentine $\pm$ brucite $\pm$ monticellite (Fig. 5.3). The silicate minerals recognised as part of the characteristic assemblage described above are all hydrated to varying degrees. It is significant that wollastonite does not appear to have formed despite the availability of quartz because it suggests that the fluid phase was sufficiently dominated by CO_2 to inhibit the reaction calcite + quartz = wollastonite + CO_2 which would occur at >700°C at 5kb and $X_{CO2} > 0.15$.

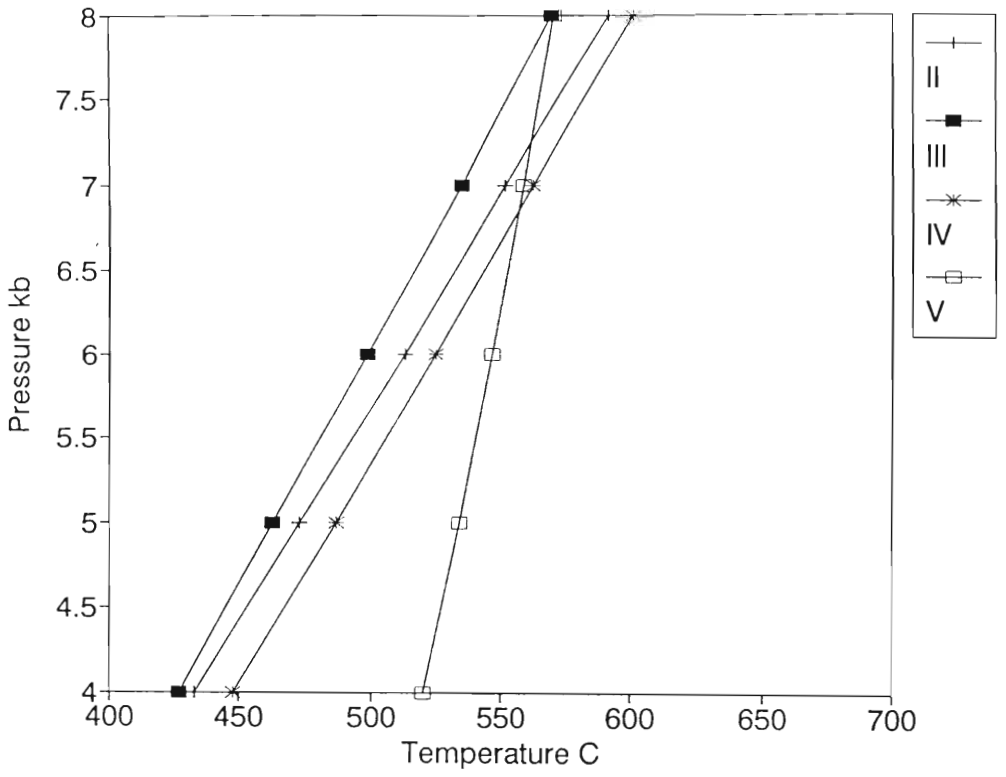

Figure 5.2. P-T diagram showing the physical conditions applicable to reactions II, III, IV and V described above.

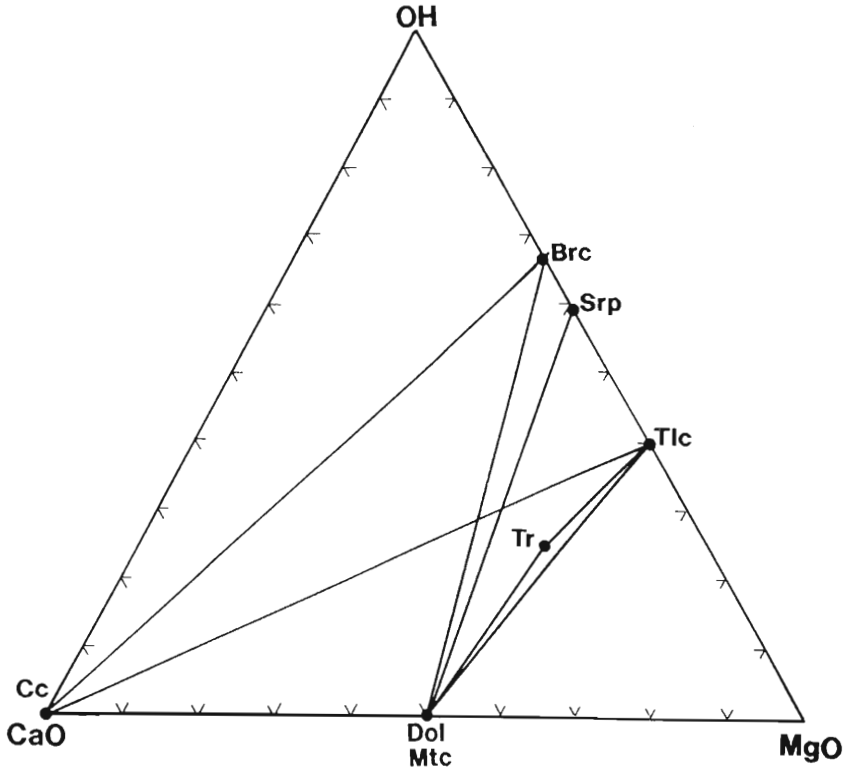

Figure 5.3 CaO, MgO and OH diagram for carbonate rocks.

The formation of forsterite (reaction 11 below Fig. 5.4) would have required temperatures of approximately 550 to 600 °C over a broad range of fluid compositions. Reaction 12 (Fig. 5.4 and list above) indicate that tremolite is stable above temperatures of ~500°C for most fluid compositions (X_{CO2} > 0.2). The more hydrated minerals (brucite, serpentine and talc) are interpreted to have involved retrogressive rehydration at the expense of tremolite, monticellite and, possibly, olivine at temperatures <500°C (Fig. 5.4 and reactions 1,3,6 and 9) because they either rim tremolite and monticellite (talc, brucite) or form pseumorphic textures after olivine (serpentine, brucite). The development of brucite and serpentine in particular is consistent with the prior existence of olivine (reaction 1, Fig. 5.4) and suggests that the fluid phase during cooling was increasingly dominated by H_2O. Serpentine was formed where it is stable under fluid compositions of X_{CO2} ~ 0.0 to 0.07 (Fig. 5.4).

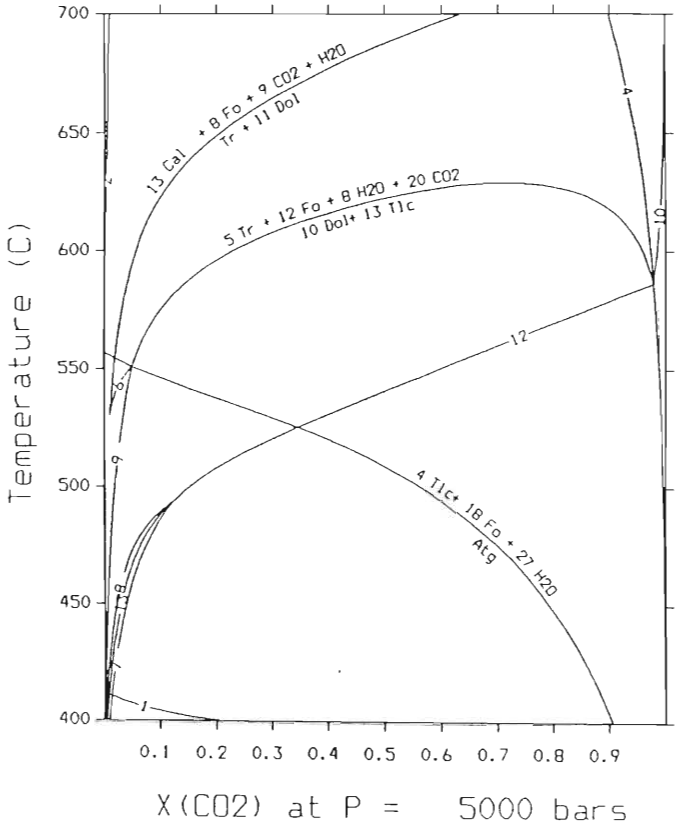

Figure 5.4. P-T-fluid conditions applicable to the system CaO-MgO-SiO_2-H_2O (for the carbonate rocks) modelled using the computer program GEOCALC by Brown *et al.* (1988). The relevant reactions are listed below.

(1). 34 Fo + 51 H_2O = 20 Brc + Atg

(2). Brc + Cal + CO_2 = Dol + H_2O

(3). Atg = 4 Tlc + 18 Fo + 27 H_2O

(4). 2 Tlc = 5 Qtz + 3 Fo + 2 H_2O

(5). 13 Cal + 8 Fo + 9 CO_2 + H_2O = Tr + 11 Dol

(6). 13 Atg + 40 Dol = 20 Tr + 282 Fo + 383 H_2O + 80 CO_2

(7). 3 Dol + 4 Qtz + H_2O = Tlc + 3 Cal + 3 CO_2

(8). 3 Cal + 2 Tc = Tr + Dol + H_2O + CO_2

(9). 2 Atg + 15 Tr + 60 CO_2 = 47 Tlc + 30 Dol + 30 H_2O

(10). 2 Tr + 8 CO_2 = 13 Qtz + 3 Fo + 4 Dol + 2 H_2O

(11). 10 Dol + 13 Tlc = 5 Tr + 12 Fo + 8 H_2O + 20 CO_2

(12). 2 Dol + 4 Qtz + Tlc = Tr + 4 CO_2

(13). 6 Cal + 4 Qtz + 5 Tc = 3 Tr + 2 H_2O + 6 CO_2

The calc-silicate gneisses

The characteristic metamorphic mineral assemblage of the calc-silicate gneisses is (Fig. 5.5) diopside + hornblende + plagioclase ± quartz ± sphene which is typical of the upper amphibolite facies or medium grade of metamorphism.

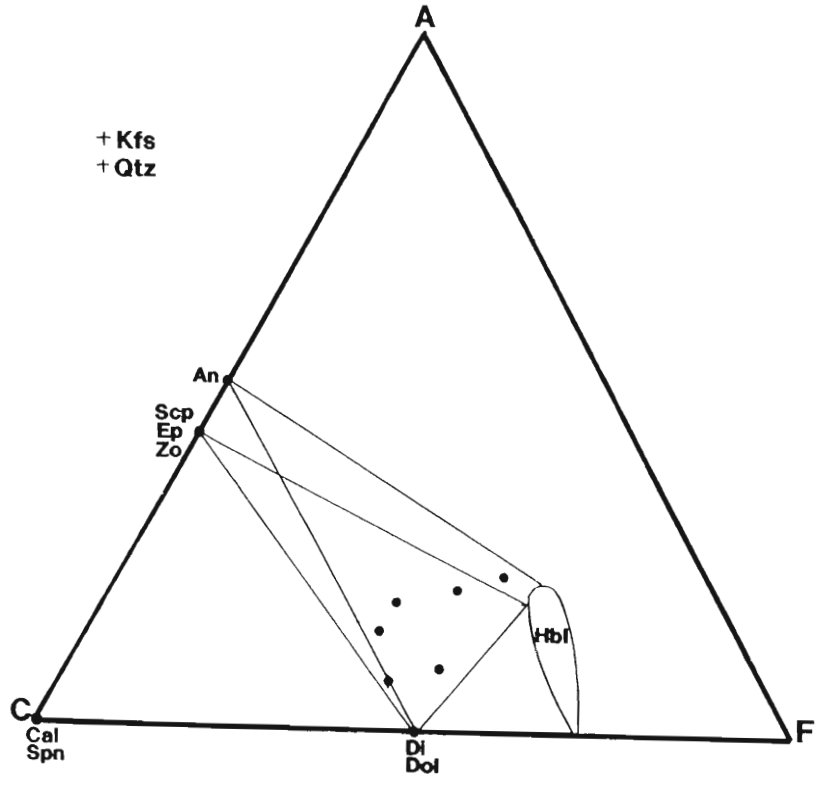

Figure 5.5. ACF diagram showing the mineralogy of the calc-silicate rocks.

Superficially, the mineralogy of the calc-silicate rocks suggests that they are basic in origin, as they are characterised by relatively high contents of hornblende, diopside and plagioclase. However, the presence of significant amounts of microcline (samples FG26, FG23, DVG3) and

quartz (FG26, FG16) serve to distinguish these rocks from basic rocks. The abundance of plagioclase in samples FG17, FG18 and FG19 is high which distinguishes these samples from basic rocks.

Many of the textures observed in these rocks may be interpreted to be the result of late-stage retrogressive hydration. Textures considered to indicate this are the net-like zoisite, the partial replacement of diopside by hornblende, and the development of transgressive biotite. Reactions 1-9 modelled using the computer program GEOCALC by Brown *et al.* (1988) are shown in the list below and figure. 5.6. Reactions 1,2,3,5,7 and 8 may have been responsible for the late stage formation of zoisite during cooling and/or due to variation of the fluid phase composition to a more H_2O-rich composition.

The development of amphibole during retrograde metamorphism may possibly be ascribed to reactions 5,6,7 and 8 that involve cooling and hydration (reaction 5 and 8), and/or cooling (reaction 6).

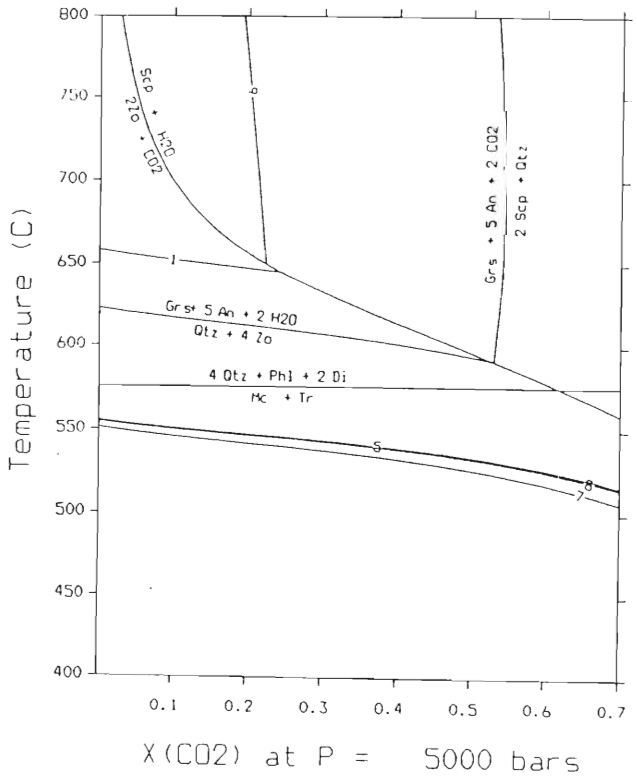

Figure 5.6. P-T-fluid conditions applicable to the mineralogy of the calc- silicate rocks.

1) An + 6Grs + Phl + $8H_2O$ = 18 Zo + Mc + 3 Di

2) Scp + H_2O = 2Zo + CO_2

3) Qtz + 4Zo = Grs + 5An + $2H_2O$

4) 2Scp + Qtz = Grs + 5An + $2CO_2$

5) Mc + 3Tr + 12Zo = Phl + 12Di + 18 An + $8H_2O$

6) Mc + Tr = 4Qtz + Phl + 2Di

7) 5Phl + 24Qtz + 12Zo = 3Tr + 5Mc + 18An + $8H_2O$

8) 2Qtz + Tr + 6Zo = 5Di + 9An + $4H_2O$

9) Phl + Grs + 21 An + $9CO_2$ = 3Di + 9Scp + 2Mc + $4H_2O$

The development of phlogopite may result from cooling and/or hydration involving reaction 7. The presence of calcite filling voids suggests that it formed late, hence the fluid phase can be assumed to have contained CO_2.

The presence of scapolite is particularly significant since figure 5.6 shows that scapolite + quartz is a stable assemblage in rocks when the fluid phase contains significant CO_2, ie X_{CO2} > 0.55 (reaction 4, Fig. 5.6). Under more hydrous conditions grossular $\pm$ zoisite is stable at higher temperatures (>620°C), whereas at lower temperatures (<600°C) zoisite + quartz are stable (reaction 6, Fig. 5.6). Figure 5.6 assumes that scapolite is pure meionite (Ca-rich). With an increasing marialite component (Na) in the scapolite, its stability field is increased under more H_2O-rich conditions. The presence of scapolite + diopside + microcline suggests temperatures of approximately >575°C at X_{CO2}=0.6 and at 5kb (Fig. 5.6).

The Basic rocks

The characteristic metamorphic assemblage in the basic rocks is plagioclase (>An23) + hornblende $\pm$ clinopyroxene $\pm$ sphene $\pm$ quartz $\pm$ garnet (Fig. 5.7). This assemblage is typical of the amphibolite facies or medium grade of metamorphism and as such may be stable between approximately 500°C and 650°C. As for the Banded Gneisses (Chpt. 4), it is difficult to attach more specific conditions of metamorphism to the above assemblage for the reason outlined by Yardley (1989, pp. 100-101) that mafic "rocks generally contain few phases and these are made up of a large number of components (Na_2O, K_2O, CaO, MgO, FeO, Fe_2O_3, Al_2O_3, SiO_2, H_2O, CO_2)". Consequently, reactions are likely to be continuous and will vary because of solid solutions involving the dominant minerals eg. CaO and Na_2O in plagioclase and amphiboles, FeO, Fe_2O_3, Al_2O_3 and MgO in amphiboles and biotite. An unusual constituent is tourmaline which also may occur in medium to high grade metamorphic conditions (Povondra and Novak, 1986). The tourmaline may have originated as a result of boron metasomatism from the adjacent carbonates.

The Magnesian gneisses

The metamorphic mineralogy of the magnesian gneisses (Fig. 5.8, table 5.7) is highly variable. Figure 4.5 (p. 49), is applicable to the Magnesian Gneisses in the Fuglefjellet Formation.

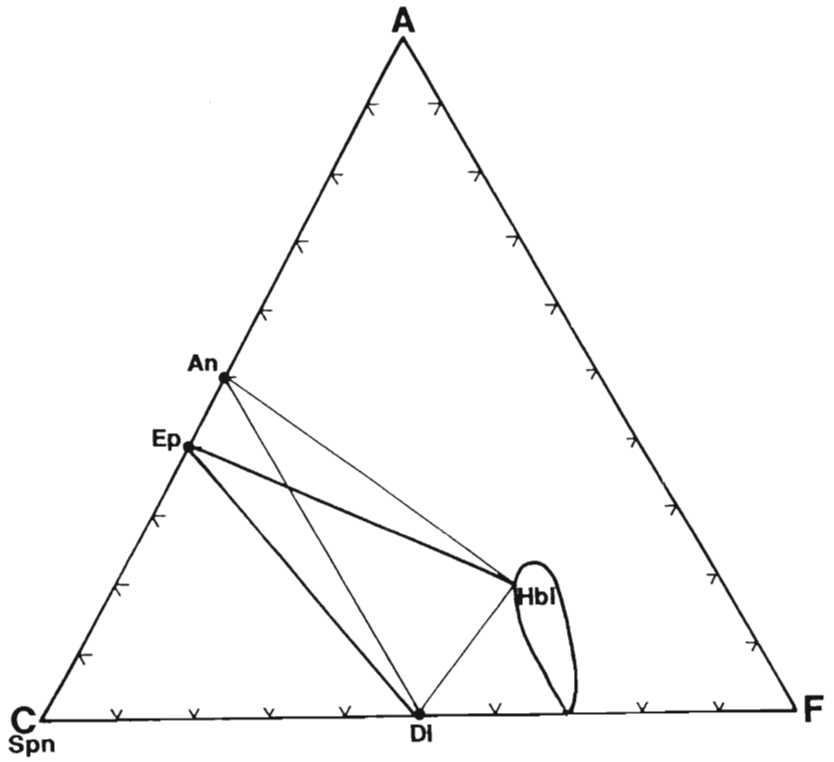

Figure 5.7 ACF diagram for the basic rocks.

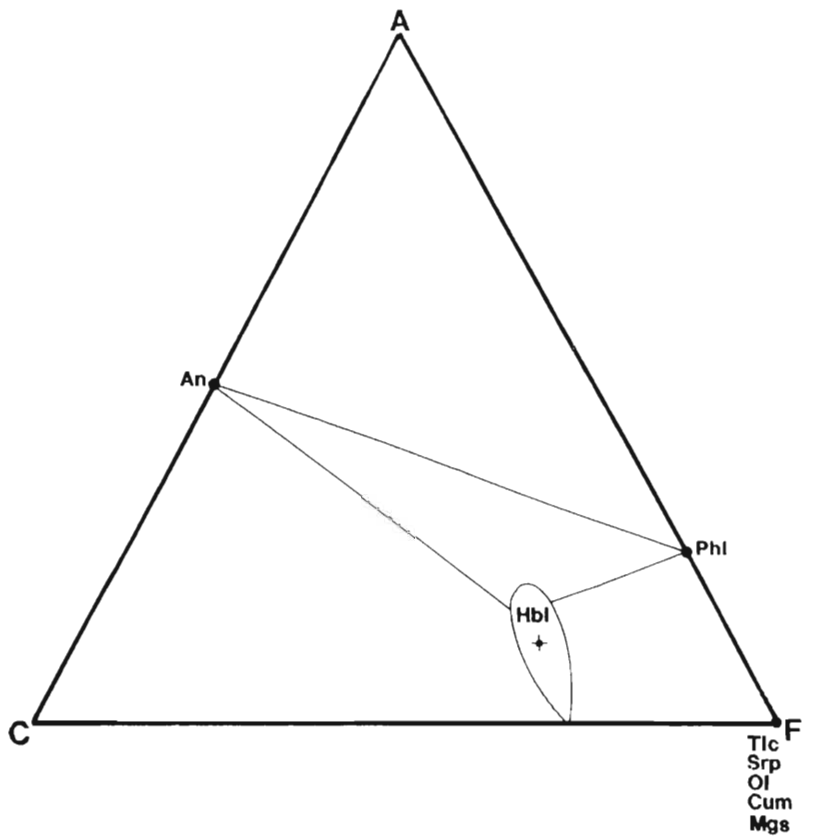

Figure 5.8. ACF diagram for the magnesian rocks.

Interpretation of the textures described above suggests that a planar fabric defined by phlogopite and cummingtonite clearly postdates and crosscuts the olivine. The partial to complete replacement of olivine by serpentine does not show a planar fabric and therefore appears to represent post-tectonic hydration. The magnesite, present with serpentine and occurring in voids and cracks, is also interpreted as a late feature and could result from reaction 4 (Fig. 4.5, p. 49; p. 48).

The textures of the rocks are typical of retrogressive hydration with the later development of hydrous minerals eg. phlogopite, cummingtonite, talc, and serpentine. The development of serpentine is particularly significant since the stability of serpentine is constrained by reactions 1 and 4 (figure 4.5). These reactions suggest a fluid phase with $X_{CO2} < 0.05$. The coexistence of serpentine + talc in sample FG55 and of magnesite and serpentine in sample FG59 suggests that the fluid phase was internally buffered by reaction 4 during the retrogressive hydration. Reactions 1 and 10 (Fig. 4.5, p. 51) constrain the stability field of olivine to >550°C with any fluid composition (ie pure CO_2 to pure H_2O) in the fluid phase.

CHEMISTRY

Nineteen samples of quartzofeldspathic and calc-silicate gneisses and together with one magnesium-rich rock from the Fuglefjellet Formation were analyzed for major and trace elements. The analyses are presented in table 5.6.

The calc-silicate rocks are characterised by relatively low SiO_2 contents, comparable to those of basic to intermediate igneous rocks. The CaO contents are typically high whereas ΣFeO, MgO, Na_2O, K_2O and TiO_2 vary greatly. The trace element abundances in the calc-silicate rocks are highly variable with most showing wide ranges. The Cr, Cu and Ni contents are however consistently low. The quartzofeldspathic rocks have SiO_2 contents comparable with acid to intermediate igneous rocks. The ΣFeO and MgO abundances are low whereas CaO, K_2O and TiO_2 are highly variable. Sodium has a limited range between ~3.3 and 5.5%. The trace element contents of the quartzofeldspathic rocks are highly variable with most elements showing wide ranges. Barium is typically present in amounts >1000pm whereas the abundances of Zn, Cu, Ni, Cr are low (i.e. <50ppm).

Sample FG30, the only magnesian rock analyzed, has high MgO and CaO (18% and 10%) respectively and is characterised by low SiO_2 and Al_2O_3 contents as may be expected. Sample FG30 is characterised by high Cr, Ni and Ba and low Th, Zr and La.

ORIGIN OF THE FUGLEFJELLET FORMATION

The Fuglefjellet Formation consists predominantly of metamorphosed chemical sedimentary rocks and thus differs from the other stratigraphic units of the Sverdrupfjella Group. The presence of highly deformed conglomerates supports the sedimentary origin of these rocks.

	SiO_2	Al_2O_3	Fe_2O_3	FeO	MnO	MgO	CaO	Na_2O	K_2O	TiO_2	P_2O_5	TOTAL
						CALC-SILICATE ROCKS						
FG2	53.76	13.85	2.67	10.96	0.21	3.58	7.32	2.13	2.25	2.26	0.53	99.52
FG17	59.39	12.72	0.6	1.63	0.07	7.91	9.1	6.06	0.8	0.71	0.22	99.21
FG26	57.31	13.90	1.37	5.83	0.07	4.27	9.55	1.98	3.77	0.76	0.21	99.02
FG53	56.76	13.47	1.30	5.90	0.12	4.50	10.39	2.13	4.26	0.69	0.17	99.69
FG58	50.63	16.56	2.20	9.39	0.25	4.51	8.75	2.81	3.04	0.95	0.23	99.32
FG52	52.79	8.86	1.85	7.89	0.23	10.69	13.29	2.15	0.55	0.56	0.25	99.11
						QUARTZOFELDSPATHIC ROCKS						
FG1	71.12	15.06	0.52	1.27	0.04	0.5	1.74	3.32	5.54	0.35	0.09	99.55
FG23	60.88	16.68	1.88	4.14	0.22	1.77	3.59	4.38	5.16	0.59	0.31	99.60
DVG10	71.28	13.79	0.51	4.17	0.04	1.01	1.62	4.99	1.81	0.53	0.11	99.86
DVG11	73.69	14.72	0.09	0.76	0.02	0.19	0.89	3.88	5.50	0.11	0.04	99.89
DVG12	66.87	15.89	0.48	3.88	0.09	1.58	2.92	4.42	2.79	0.63	0.22	99.77
FG7	61.35	16.46	1.4	3.58	0.11	2.51	4.91	4.48	3.86	0.86	0.28	99.80
FG50	61.64	17.21	0.61	4.94	0.14	1.87	2.66	4.7	4.99	0.53	0.3	99.59
FG61	60.70	17.52	0.53	4.32	0.08	2.65	4.72	5.54	2.46	0.87	0.34	99.73
FG62	63.36	14.38	0.82	6.65	0.13	3.64	2.56	4.77	2.89	0.66	0.22	100.08
FG59	64.39	16.69	0.45	3.61	0.06	1.71	3.13	4.42	4.29	0.69	0.27	99.71
FG10	62.25	15.65	1.23	3.7	0.08	2.44	5.8	5.64	0.99	1.43	0.47	99.68
FG13	66.72	14.14	1.42	4.04	0.08	2.83	1.46	4.43	2.42	0.58	0.25	98.37
FG60	61.14	17.49	0.53	4.31	0.08	2.56	4.42	5.24	3.01	0.86	0.29	99.93
						MG-RICH ROCKS						
FG30	49.15	8.95	2.33	7.44	0.19	18.35	9.75	0.6	2.75	0.5	0.29	100.3

No.	Rb	Sr	Th	Zr	Y	Nb	Ba	Sc	Cr	La	V	Cu	Ni	Zn
						CALC-SILICATE ROCKS								
FG2	45	595	8	357	45	26	1039	19	ND	84	363	17	5	109
FG17	14	215	11	200	23	11	58	14	104	4	122	1	46	15
FG26	131	495	9	137	37	11	974	22	135	nd	189	13	100	100
FG53	186	694	4	122	31	11	1315	14	136	nd	179	14	96	99
FG58	75	338	nd	102	25	7	1571	25	101	nd	191	12	46	237
FG52	10	123	nd	84	33	9	156	28	181	nd	232	9	114	30
						QUARTZOFELDSPATHIC ROCKS								
FG1	163	392	38	431	5	8	1663	1	ND	127	19	3	1	32
FG23	126	232	7	73	21	6	1840	14	14	28	107	11	7	72
DVG10	89	203	7	355	75	15	313	16	ND	28	37	ND	16	16
DVG11	191	315	26	110	11	5	1377	1	ND	61	6	2	ND	39
DVG12	103	368	13	179	38	8	1127	12	5	54	65	ND	1	54
FG7	84	584	8	153	19	5	1724	15	30	22	120	5	1	27
FG50	122	297	6	72	23	4	1779	14	10	35	83	ND	5	53
FG61	72	601	5	151	22	4	895	17	17	31	128	5	4	39
FG62	60	273	4	74	20	4	1228	34	116	22	219	3	19	48
FG59	95	621	13	160	21	6	1762	12	4	46	83	13	1	28
FG10	25	265	8	253	31	9	282	19	6	11	184	15	3	21
FG13	53	269	3	74	17	5	1283	24	81	ND	175	3	22	40
FG60	113	463	8	146	21	5	1044	14	23	30	112	16	7	42
						MG-RICH ROCKS								
FG30	125	128	1	31	13	3	695	34	1725	ND	235	1	603	87

Table 5.6. Major and trace element chemistry (concentrations in wt% and ppm respectively) of the Fuglefjellet Formation. ND = not detected. nd = not determined.

The origin of the interbedded mafic, calc-silicate, magnesian and quartzofeldspathic gneisses is less clear. The high MgO and CaO and low SiO_2 and Al_2O_3 contents of the single analyzed sample of magnesian rock are consistent with an ultramafic igneous origin even though

the bulk composition falls in the field for basaltic and andesitic rocks (Fig. 5.9). This conclusion is supported by the high Cr and Ni contents (table 5.6). Relatively high Rb, Sr and Ba contents in the sample appear to conflict with this conclusion because ultramafic rocks are characterised by low contents of these elements. The elements in question are however known for their mobility in high grade metamorphic environments (Heier and Thoresen, 1971; Barbey and Cuney, 1982). More specifically Sr and Ba are commonly enriched in carbonates and therefore could have been introduced in sample SV30 from adjacent carbonates.

Three of the calc-silicate gneisses lie within the field for basaltic and andesitic rocks (field 2, Fig. 5.9). whereas the remainder lie outside and below this field indicating Al_2O_3 concentrations less than those typical of volcanic rocks. The low Cr, Cu and Ni contents of the calc-silicate gneisses could be taken as evidence that these rocks are sedimentary in origin because igneous rocks would normally have greater abundances of these elements.

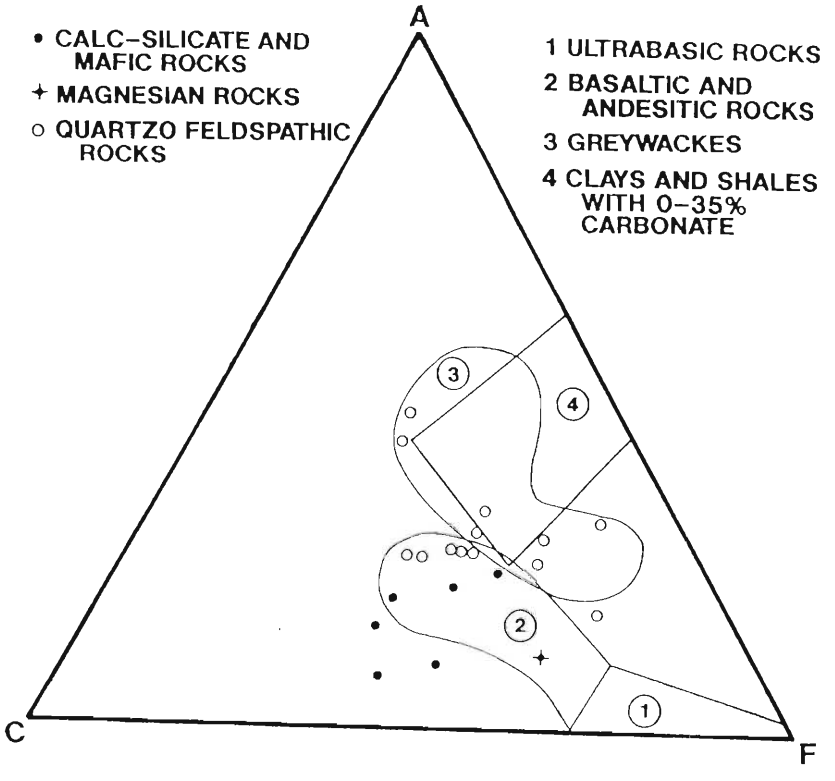

Figure 5.9. Bulk composition of the rocks of the Fuglefjellet Formation plotted on an ACF diagram with the fields of various compositions shown. The fields are those defined by Winkler (1976, p. 46).

The SiO_2 contents of the calc-silicate gneisses are, at most, 10-15% higher than might be expected for basaltic rocks. It is possible that silicification may have occurred. Whereas this process may have affected the abundance of Al_2O_3 it is unlikely to have had a similar effect on elements such as Cr, Ni, and Cu. Consequently, it is proposed that the calc-silicate rocks may

represent impure calc-arenites.

All but three of the samples of quartzofeldspathic gneiss lie in the sedimentary fields (3 and 4) whereas the remainder plot in the basaltic/andesitic field (field 2, Fig. 5.9). Some of these rocks are indistinguishable from the Grey Gneisses in the field, forming relatively homogeneous layers. It is concluded that the quartzofeldspathic gneisses in the Fuglefjellet Formation were derived from a mixed assemblage of volcanic and sedimentary protoliths.

CONCLUSIONS

The lithologies comprising the Fuglefjellet Formation are dominated by carbonates with subordinate quarztofeldspathic, calc-silicate, mafic and magnesium-rich rocks. The rocks are considered to represent a sediment- dominated sequence with subordinate intercalated volcanic material. The rocks have been altered by medium grade or amphibolite facies metamorphism with temperatures >550°C followed by retrogressian involving partial hydration of the medium grade mineral assemblages. The fluid composition during the medium grade metamorphism contained a significant CO_2 content (X_{CO2} >0.30). During the later retrogression the fluid composition appears to have been almost pure H_2O with X_{H2O} ~ 0.93 or X_{CO2} ~ 0.07.

CHAPTER 6
THE SVEABREEN FORMATION

INTRODUCTION

The Sveabreen Formation underlies Salknappen, the most easterly nunatak in the area. These rocks form a small part of the geology of the study area (Map.1). The Sveabreen Formation in the study area comprises three dominant rock types, namely, biotite-rich gneisses, mafic rocks and a porphyroclastic granitoid body. The mafic rocks occur as boudinaged masses within the biotite-rich gneisses. The contacts of the porphyroclastic granitoid body with the other rocks are highly sheared. In the cores of the granitic bodies, the rocks display virtually undeformed porphyritic textures but become more sheared and finer-grained towards their margins. Associated with the shearing, the grain size of the coarse feldspars (up to 2 cm) decreases until it is no longer possible to recognise relict phenocrysts, at which point the appearance of the granitoid resembles adjacent sillimanite-bearing, biotite-rich gneisses.

PETROGRAPHY AND MINERALOGY

The mineralogy of the Sveabreen Formation is presented in table 6.1.

BIOTITE-RICH GNEISSES

	Bt	Sil	Qtz	Grt	Ms	Chl	feldspar
SA1	30	15	25	10			20
SLK55	25	5	25	3			42
SA7	5		40	10		5	40
SA3	15		24	10	1		50
SAA	55			40		5	
SA12	5		20	10		5	60
SA6	5	5	50	15		5	20
SA5	10		20		5	2	63
SA4	30	15	20	5		5	25

MAFIC ROCKS

	Bt	Qtz	Grt	Hbl	Cpx	Spn	feldspar	opaque
SLK50	1	5	50	20	12	1	10	1
SA13	1	5	15	40			37	2
SLK52	10	10		50			27	3

GRANITOID ROCKS

	Bt	Opx	Qtz	Grt	Hbl	feldspar
SA8	15		30	5		50
SA9	15		25	10	7	45
SA10	10	3	25	2	5	45

Table 6.1. Modal estimates of the mineralogy (vol%) of the Sveabreen Formation.

Biotite-rich gneisses

These rocks are medium to fine-grained (0.5-2mm) and generally have a strong foliation defined by aligned flakes of biotite and needles of sillimanite (where present). The mineral assemblage of these rocks is biotite + quartz + feldspar ± garnet ± sillimanite ± muscovite ± chlorite (Table 6.1). The sillimanite is generally fibrolitic but also forms prismatic crystals (Fig. 6.1).

Two textural varieties of garnet have been recognised. In the first type garnet is intergrown with quartz (sample SAA, table 6.1). This intergrowth forms knots displaying no planar fabric and about which the S_1/S_2 foliation is wrapped. In the second type, the garnets are poikiloblastic with small inclusions of quartz, biotite and opaque minerals. These inclusions show evidence of rotation and thus appear to have grown syn-tectonically either during D_1 or D_2. Both types of garnet are partially surrounded and replaced by green biotite. In these rocks the biotite which is not spatially associated with garnet is typically red-brown in colour, which is reportedly characteristic of high grade metamorphism and also high TiO_2 contents (Jackson, 1976; Binns, 1969). Two generations of muscovite are recognised. In sample SA4 muscovite coexists with quartz apparently in stable equilibrium. The rock also contains fibrolitic sillimanite which is partially replaced by muscovite.

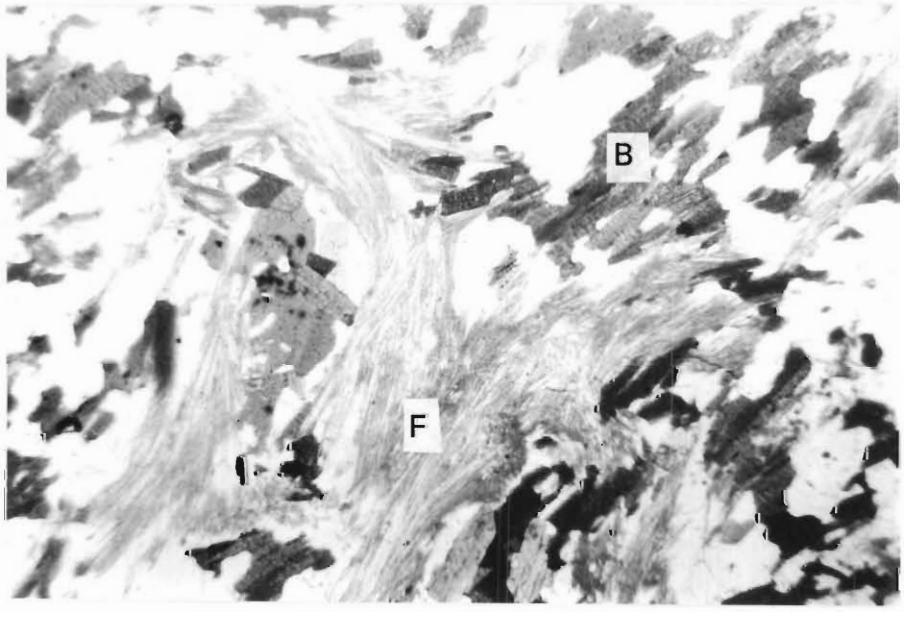

Figure 6.1. Fibrolite sillimanite (F) in the biotite-rich gneisses (sample SA4). Field of view is 4mm. B = biotite. The clear (white) areas are quartz and feldspar.

Mafic rocks

These rocks are generally slightly finer-grained than the biotite-rich gneisses (0.5-1mm) and do not display a planar fabric. Samples SLK13 and SLK52 have similar mineralogies which differ from that in SLK50 which is characterised by abundant garnet. The characteristic assemblage of the mafic gneisses is hornblende + plagioclase + quartz ± garnet ± clinopyroxene ± biotite (Table 6.1). Red-brown biotite is randomly oriented. Garnet, when present, forms xenomorphic poikiloblastic grains enclosing quartz. Sphene forms xenomorphic accessories. Hornblende is commonly intergrown with quartz suggesting that these two minerals are possibly the product of a reaction such as clinopyroxene + plagioclase -> hornblende + quartz. Opaque minerals form vermicular structures spatially associated with biotite or hornblende. Plagioclase is equigranular, untwinned, zoned and locally intergrown with quartz. Sample SLK50 contains the assemblage garnet + clinopyroxene + hornblende + plagioclase + quartz. Plagioclase forms zoned xenomorphic grains and is present as vermicular grains in symplectitic intergrowths with amphibole. Clinopyroxene is partially replaced by brown-green hornblende and is clouded with fine inclusions which are characterised by low birefringence. These inclusions are interpreted to be the result of orthopyroxene exsolution. Small xenomorphic garnets are separated from clinopyroxene by symplectitic intergrowths of anorthite plagioclase and a pale green amphibole indicating an unstable reaction relationship between garnet and clinopyroxene (see Fig. 14.2). Accessory biotite partially replaces hornblende and may represent a late stage introduction of K-bearing fluids. The assemblages garnet + hornblende + plagioclase + quartz and clinopyroxene + plagioclase + quartz in SLK50 have granoblastic textures and are interpreted to be stable associations. These assemblages are useful for thermobarometry and have been chemically analyzed using an electron microprobe, the results of which are discussed in chapter 14.

Granitoid rocks

These rocks are medium- to coarse-grained (0.5mm-10mm). The rocks have a strong planar foliation defined by biotite ± hornblende. The characteristic mineral assemblage of the granitic rocks is quartz + plagioclase + K-feldspar + garnet + biotite ± hornblende ± hypersthene. Garnet occurs as ragged poikiloblastic grains with inclusions of quartz. K-feldspar forms porphyroclasts up to approximately 10mm in diameter with rims of myrmekite.

Plagioclase in the groundmass commonly shows a trellis pattern antiperthite where K-feldspar exsolution lamellae commonly form up to 30% of the mineral. Hypersthene, seen only in thin section SA10, is partially rimmed by hornblende suggesting that the hornblende is replacing orthopyroxene (Fig. 6.2).

Figure 6.2. Hypersthene (H) partially replaced by hornblende (A) in the granitic gneisses (Sample SA10). Field of view is 4mm. The clear areas are quartz and feldspar.

CHEMISTRY

Ten samples from the Sveabreen Formation have been analyzed. Major and trace element analyses are given in table 6.2. The granitic rocks are characterised by SiO_2 contents of 64 to 67% with $TiO_2 \geq 1.0\%$, $Al_2O_3 \sim 14\%$, and $P_2O_6 \sim 0.35\%$. The granitoid has high Fe/Fe + Mg ratios. The average C.I.P.W. normative composition of the granitoid is orthoclase 25%, plagioclase 37%, quartz 22%, apatite ~0.9%, ilmenite 2.3%, corundum.01%, magnetite 2.5%, diopside 1.5% and orthopyroxene 9%. The relative proportions of quartz, orthoclase and plagioclase indicate that the rock is granodioritic or enderbitic in composition.

The chemistry of the biotite-rich gneisses is variable with some samples having Al_2O_3 and TiO_2 >16% and >1% respectively (SLK55 and SA4). Samples SA6 and SLK54 are more siliceous with SiO_2 >71% In addition they have high Fe/Fe + Mg ratios. The mafic rocks are characterised by SiO_2 contents of ~50%, relatively higher FeO, MgO, TiO_2 and CaO concentrations than the other rock types. They are typically basic in composition.

	SiO_2	Al_2O_3	Fe_2O_3	FeO	MnO	MgO	CaO	Na_2O	K_2O	TiO_2	P_2O_5	TOTAL
BIOTITE-RICH GNEISSES												
SLK55	63.4	16.11	0.8	6.51	0.07	3.10	2.22	3.18	3.49	1.16	0.15	100.19
SA4	64.86	16.91	0.96	7.78	0.12	2.96	0.61	0.26	3.84	1.15	0.20	99.65
SA6	72.01	13.23	0.81	6.55	0.20	1.03	0.85	2.30	2.80	0.32	0.04	100.14
SLK54	71.39	14.91	0.33	2.67	0.14	0.76	1.53	2.47	5.54	0.13	0.06	99.93
MAFIC ROCKS												
SLK50	50.45	15.65	1.22	9.91	0.21	7.96	12.44	0.78	0.53	1.07	0.11	100.33
SLK51	50.07	15.77	1.26	10.19	0.27	7.97	12.37	0.51	0.68	1.04	0.10	100.23
SLK52	50.08	15.97	1.17	9.49	0.19	8.83	11.46	0.79	0.74	0.91	0.04	99.67
GRANITOIDS												
SA8	67.39	14.17	1.50	4.52	0.12	0.95	2.96	2.47	4.54	1.00	0.32	99.94
SA9	64.45	14.25	1.88	6.00	0.20	1.33	3.65	2.67	3.87	1.34	0.41	100.05
SA10	64.3	14.21	1.97	5.93	0.13	1.33	3.83	2.65	4.19	1.35	0.40	100.29

	Rb	Sr	Rb/Sr	Th	Zr	Y	Nb	Ba	Sc	Cr	La	V	Cu	Ni	Zn
BIOTITE-RICH GNEISSES															
SLK55	144	258	0.55	10	228	24	13	720	28	189	17	271	23	67	152
SA4	191	60	3.18	13	256	42	16	689	37	198	23	212	22	78	158
SA6	64	107	0.59	16	429	89	10	2273	18	19	28	22	ND	3	18
SLK54	116	344	0.34	64	329	54	3	2139	15	16	74	38	13	12	29
MAFIC ROCKS															
SLK50	5	120	0.04	ND	62	24	3	18	57	140	ND	308	ND	64	137
SLK51	15	64	0.23	ND	53	24	4	56	63	141	ND	297	49	50	209
SLK52	14	51	0.27	3	38	23	1	31	51	182	ND	262	9	12	79
GRANITOIDS															
SA8	108	274	0.39	2.8	564	35	19	1828	17	14	41	41	9	5	118
SA9	111	300	0.37	ND	464	49	21	1854	22	23	39	53	11	6	160
SA10	107	293	0.36	8.7	466	56	20	1681	20	21	46	52	10	5	151

Table 6.2. Major and trace element chemistry (concentrations in wt% and ppm respectively) of the Sveabreen Formation. ND = not detected.

Trace element chemistry

Abundances of trace elements appear to correlate with SiO_2 concentrations. Thus Cr (~190ppm), Ni (~70ppm), Zn (~150ppm) and V (>200ppm) are enriched in the gneiss with ~64% SiO_2 relative to the gneiss with ~72% SiO_2. The latter gneisses have low concentrations of these trace elements but contain >2000ppm Ba and >300ppm Zr (table 6.2). Chromium, Ni, and Zn abundances in the low SiO_2 gneisses are similar to those in mafic gneisses which are distinguished by low contents of Ba, Rb, and La.

Chromium concentrations in the granitoids are comparable to those in the high SiO_2 gneisses despite the granite having ~64% SiO_2 similar to the low SiO_2 gneisses. Nickel in the granitoids is however low (~5ppm). Barium contents are high (>1800ppm) as are those of Zr (>400ppm).

METAMORPHISM

Biotite-rich gneisses

Typical mineral assemblages of these gneisses consist of biotite + quartz + feldspar ±

garnet ± sillimanite ± muscovite ± chlorite (Table 6.1)(Figs. 6.3 and 6.4).
The co-existence of sillimanite and muscovite together with the replacement of the former by muscovite can be accounted for by a reaction such as :-

sillimanite + K feldspar + H_2O -> muscovite + quartz.

In SA4, the apparently stable association of muscovite + quartz + biotite + sillimanite suggests that the sillimanite originated from a reaction other than that given above or that the partial pressure of H_2O was $<P_{load}$ with the result that the reaction of muscovite + quartz -> K feldspar + sillimanite was buffered by $pH_2O<P_{load}$. An AFM diagram for the pelitic rocks shows that they lie in the field defined by the assemblage sillimanite + biotite + garnet (Fig. 6.4).

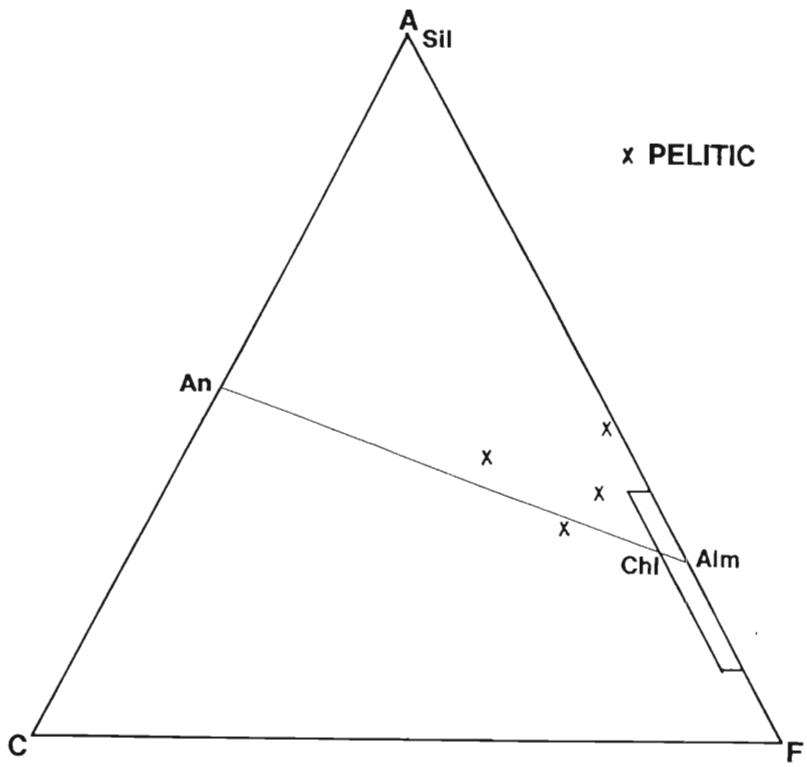

Figure 6.3 ACF diagram for the biotite-rich gneisses showing the compositions of the analyzed samples.

The AFM projection used is that of Reinhardt (1968) where $A = (Al_2O_3-(K_2O + Na_2O + CaO))$. The reason for using this projection is that muscovite and K-feldspar are both present. The AFM diagrams of Thompson (1957) and Barker (1961) project from either the muscovite or the K-feldspar compositions whereas the Reinhardt projection provides a general case.

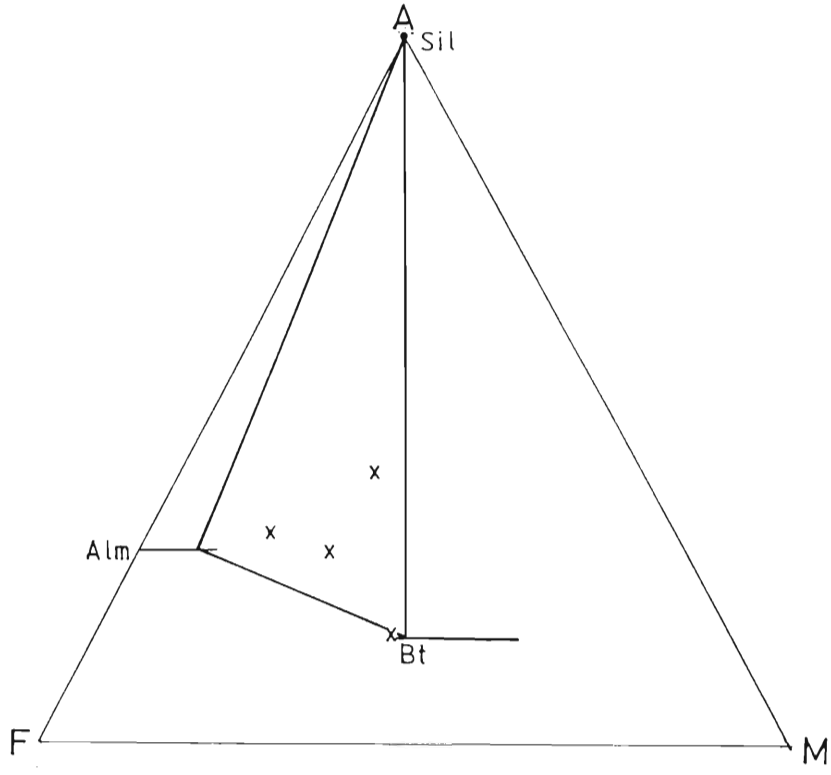

Figure 6.4 AFM diagram for the biotite-rich gneisses showing the compositions of the analyzed samples.

The physical conditions relevant to the observed mineral assemblages in the biotite-rich gneisses are shown in figure 6.5. The reactions shown in figure 6.5 were calculated using the computer program THERMO developed by Powell and Holland (1988). In addition to the stability fields of sillimanite, kyanite and andalusite, 6 reactions in the KFASHC system (K_2O, FeO, Al_2O_3, SiO_2, H_2O and CO_2) are shown and are numbered I to VI. These reactions are:-

I And = Sil

II Ky = And

III Ky = Sil

IV Qtz + Ms = Sil + Kfs + H_2O

V 3Qtz + Ms + Ann = 2Kfs + Alm + $2H_2O$

VI 2Ms + Alm = 3Sil + Ann + Kfs + H_2O

The reactions are shown for water saturated conditions ($aH_2O = 1$). With $aH_2O = \sim 0.5$ (assuming dilution by CO_2) reactions IV, V and VI would shift to lower temperatures by approximately 50°C. The presence of MgO in the rocks (average MgO/MgO + FeO + Fe_2O_3

ratio = 0.33) would result in the reactions V and VI shifting to higher temperatures. The replacement of sillimanite by muscovite represents the reversal of reaction 1 and suggests pressures of between 3 and approximately 10kb. Temperatures in excess of approximately 650°C are implied for the earlier phases of metamorphism represented by the assemblage Sil + Kfs + Ann + Alm.

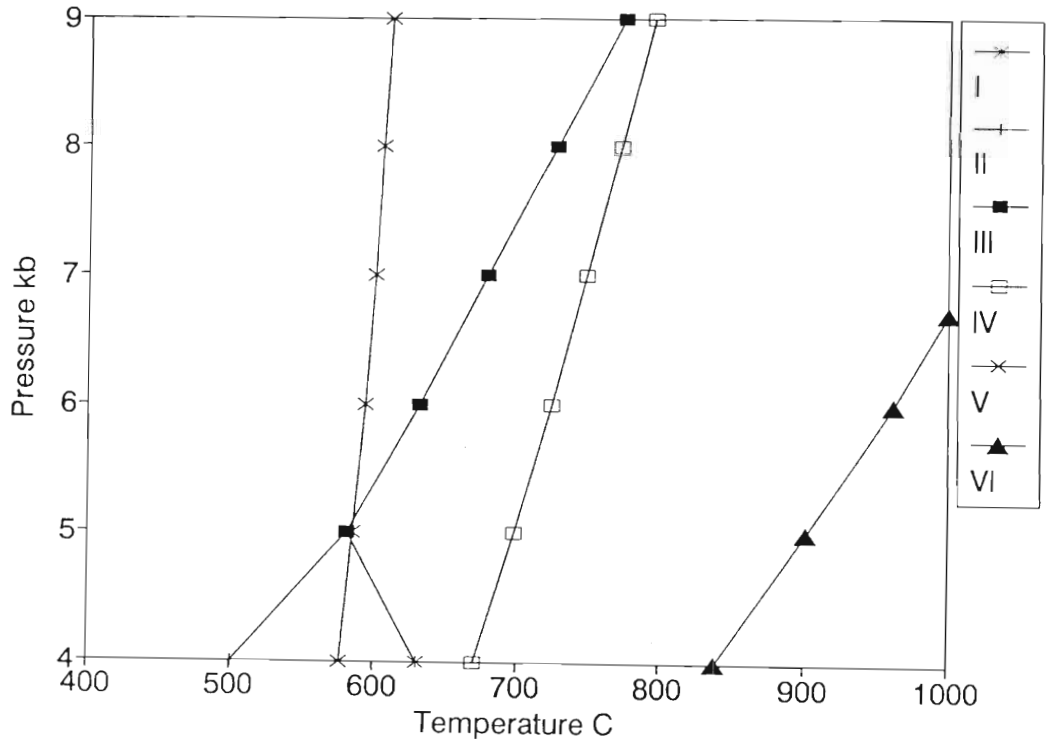

Figure 6.5. Physical conditions pertaining to the mineral assemblages of the biotite-rich gneisses.

Declining temperature and hydration are suggested by the partial sericitisation of sillimanite and the replacement of garnet by biotite (reversal of reaction 2).

Mafic rocks

The metamorphic assemblage of sample SLK50 was described above as hornblende + plagioclase + quartz + garnet + clinopyroxene and is shown in figure 6.6. The history of sample SLK50 may be interpreted as follows:-

M_1 (1 = first phase of metamorphism) represented by the granulitic assemblage Cpx + Grt + Pl + Qtz

M_2 represented by the assemblage Hbl + Pl + Qtz + Cpx.

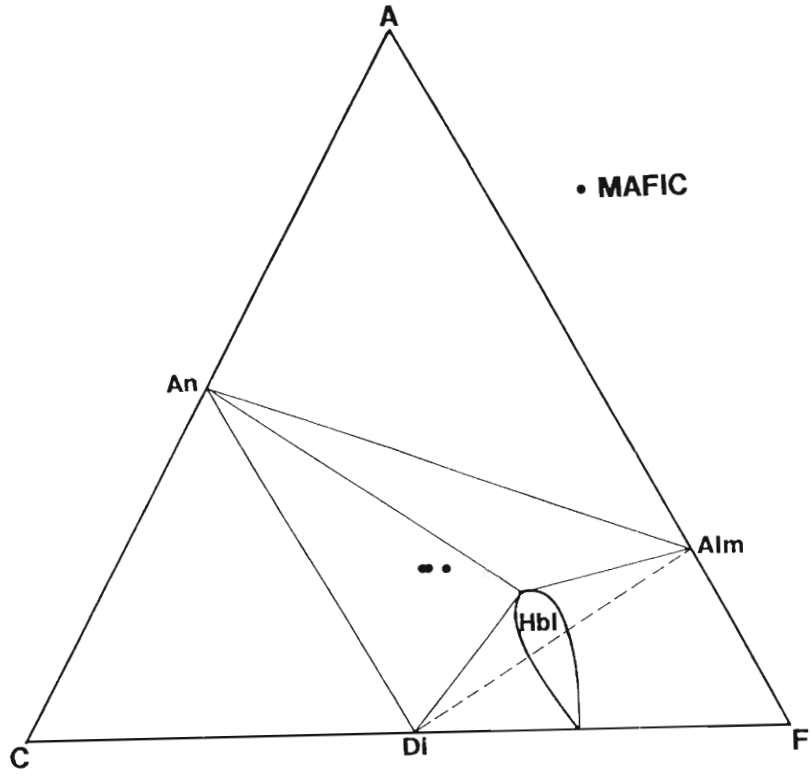

Figure 6.6. ACF diagram for the mafic rocks showing the mineralogy and bulk composition of the samples.

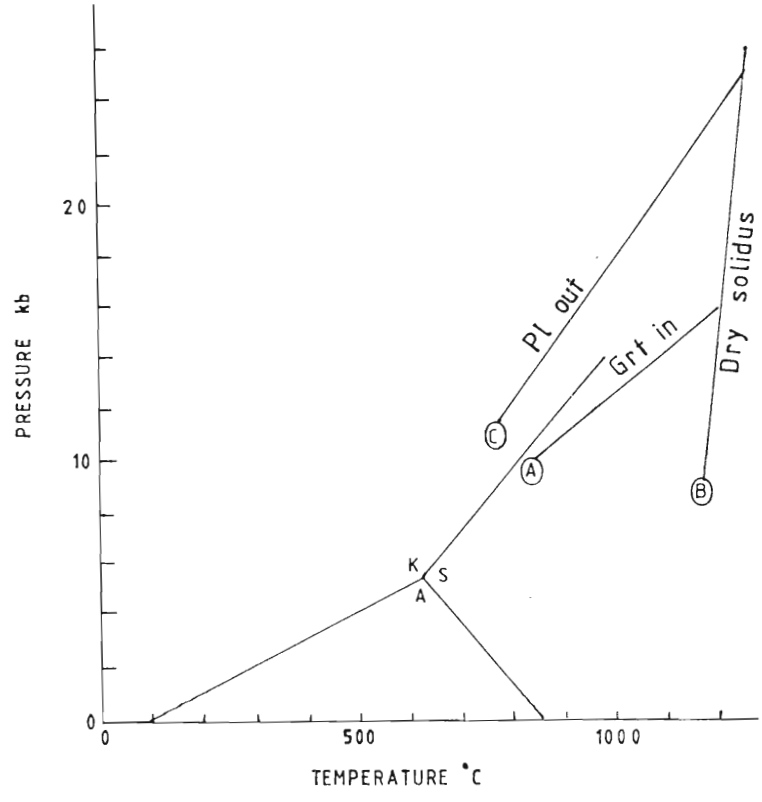

Figure 6.7. Physical conditions pertaining to the mineral assemblages in the mafic rocks. See text for details. K = kyanite, S = sillimanite, A = andalusite.

An idea of the physical conditions prevailing during M_1 can be gained from the work of Green and Ringwood (1967) who studied the transformation of quartz-tholeiite to eclogitic compositions. The relevant aspects of their work are shown in figure 6.7. The curve labelled A represents the first appearance of garnet in a quartz-tholeiite having $Fe^{2+}/Fe^{2+} + Mg = 0.4$, curve B is the approximate solidus under dry conditions and curve C marks the disappearance of plagioclase with increasing pressure.

The mafic rocks have an average $Fe^{2+}/Fe^{2+} + Mg$ ratio $= 0.38$. Figure 6.7 shows that at a temperature of approximately 800°C garnet would be stable at a pressure greater than approximately 9-10 kb. The enclosing biotite-rich gneisses would still be within the sillimanite stability field but the presence of plagioclase implies that the pressure cannot have been significantly higher than 10kb under these temperature conditions.

Granitic rocks

The metamorphic assemblage of the granitic rocks is quartz + plagioclase + K-feldspar + garnet + biotite ± hornblende ± hypersthene (figure 6.8). The rocks have a strong planar foliation defined by biotite ± hornblende.

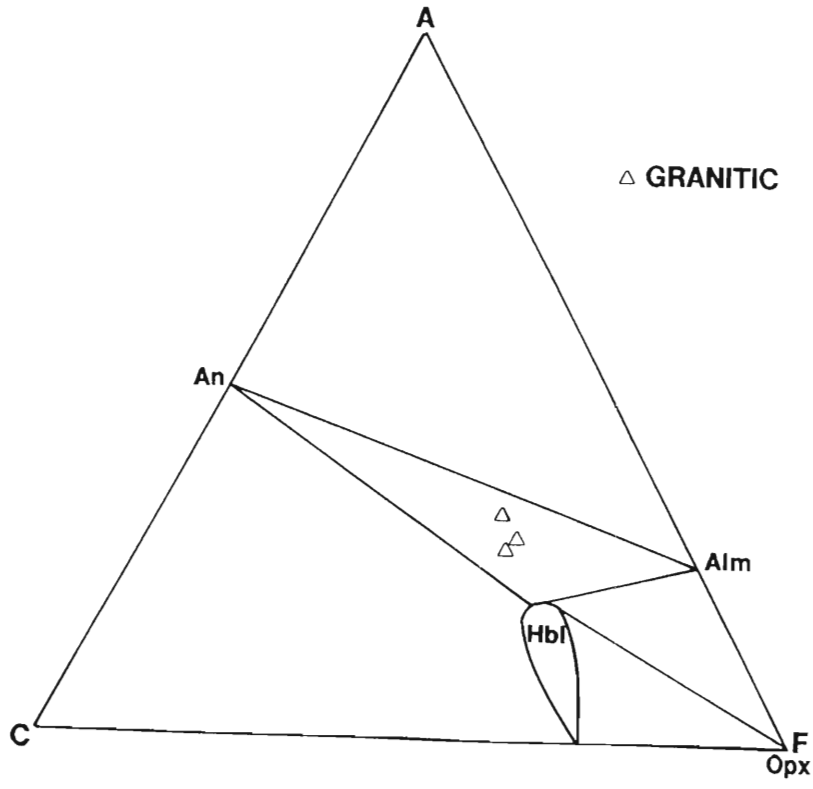

Figure 6.8. ACF diagram for the granitic gneisses showing the mineralogy and bulk composition of the samples.

The presence of hypersthene + K-feldspar + biotite + quartz is important because it suggests the following reactions (shown in figure 6.9):-

1) 2 Phl + 6 Qtz = 2 San + 3 En + 2 H_2O

3) 2 Ann + 6 Qtz = 2 San + 3 Fs + 2 H_2O

The presence of these four minerals implies that pH_2O has either been buffered with aH_2O < 1.0 or that retrogressive hydration and cooling prevented the reaction from going to completion. The former alternative is preferred because, if aH_2O = 1 at the temperatures indicated, large scale partial melting would have occurred and there is no evidence of this in the field.

The rimming of hypersthene by hornblende observed in sample SA10 suggests the following reactions (figure 6.9):-

2) 2 Hbl = 2 An + 2 Di + 3 En + 2 H_2O

4) 2 ferro-Hbl = 2 An + 2 Hd + 3 Fs + 2 H_2O

These reactions (2 and 4, Fig. 6.9) may also represent buffer reactions with aH_2O < 1.0 or that retrogressive hydration and cooling prevented complete reaction. Figure 6.9 shows that the mineral assemblages do not constrain the metamorphic pressures but suggest that the temperatures were approximately 700°C to 900°C.

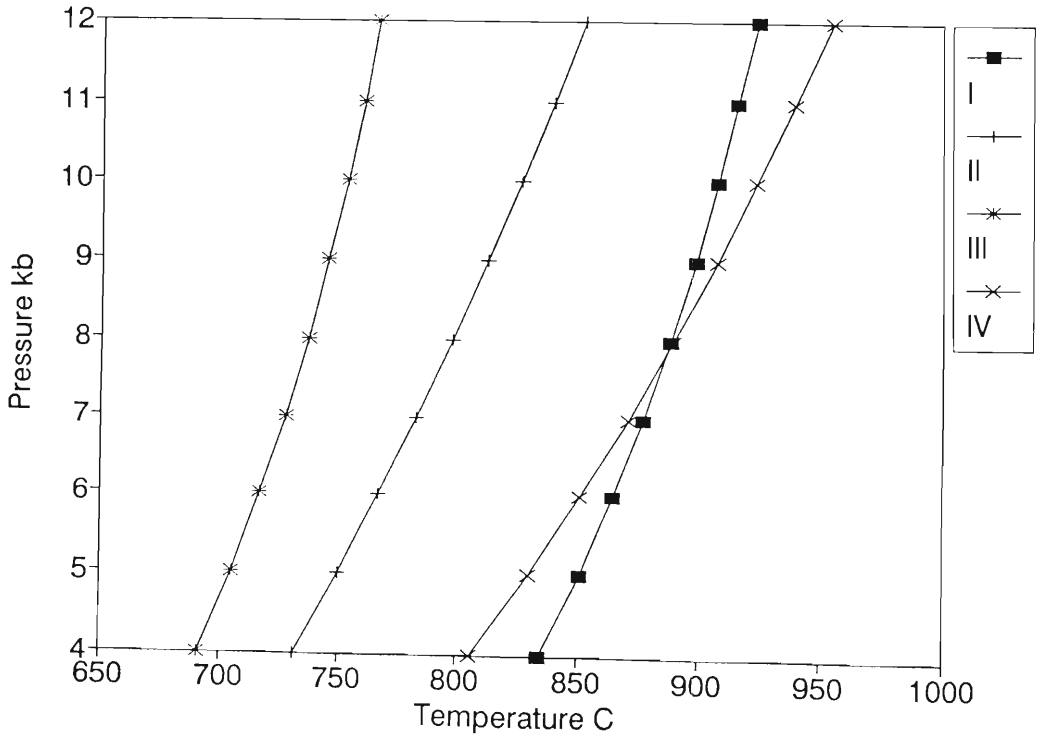

Figure 6.9. Reactions constraining the metamorphic assemblages seen in the granitic gneisses.

ORIGIN OF THE SVEABREEN FORMATION

An ACF diagram (Fig. 6.10) compares the bulk compositions of the Sveabreen Formation gneisses with compositional fields from Winkler (1979, p. 46). Two biotite-rich samples and the granitic samples lie in the fields for pelites and greywackes (fields 2 and 3). Granitoids and greywackes would be expected to show similar mineralogies. In the Sveabreen Formation, some of the biotite-rich gneisses were clearly formed as a result of highly strained (sheared) granite. The two remaining biotite rich samples show lower CaO (C component) contents typical of pelitic rocks.

The relatively high contents of sillimanite, biotite, feldspar and garnet in the pelitic to semipelitic rocks indicate an aluminous protolith of typical sedimentary origin.

The orthopyroxene recognised in one sample of the granite is particularly significant because it indicates that these granitic rocks may have been charnockitoid. Charnockites, sharing similar characteristics, have been recognised east of the study area (Ravich and Solo'vev, p156-197, 1966). Still further east in Enderby Land, a "charnockite magma suite" characterised by high TiO_2, P_2O_6, K_2O and CaO has recently been defined (Kilpatrick and Ellis, 1991). Enderbites exposed in the Natal Structural and Metamorphic Province show similar chemical characteristics (Grantham, 1984; Eglington *et al.*, 1986, Thomas 1988).

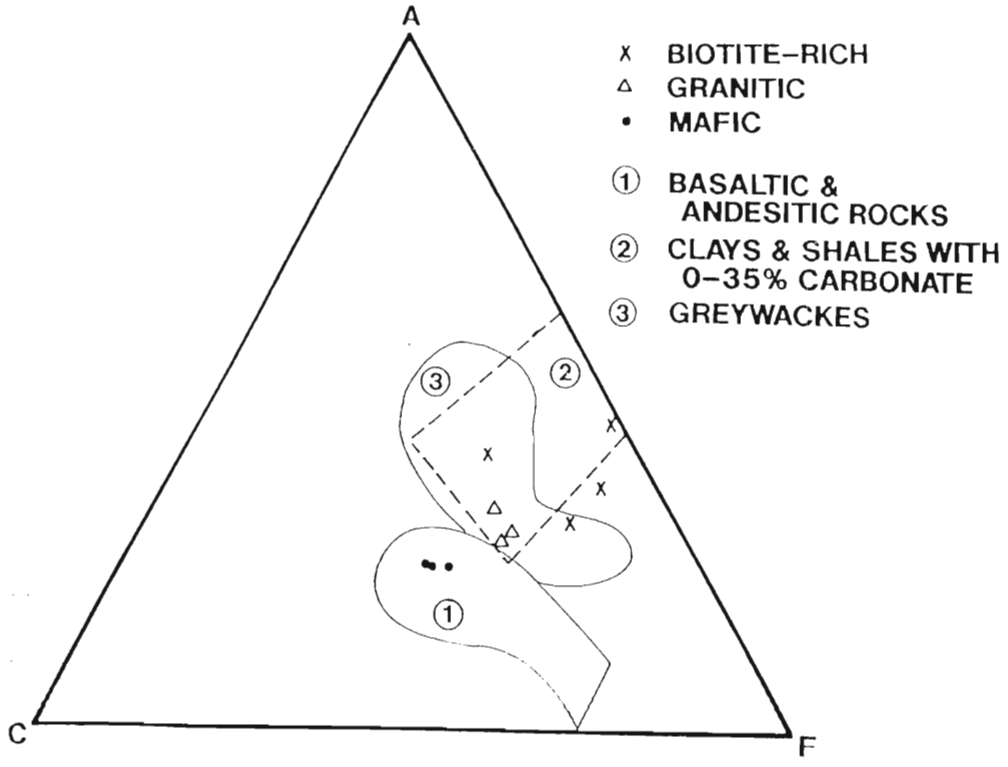

Figure 6.10. ACF diagram for the gneisses of the Sveabreen Formation.

It is uncertain whether the mafic boudins in the pelitic rocks originated as interlayered mafic volcanic rocks or as mafic intrusions into the sedimentary pile.

CONCLUSIONS

The rocks exposed at Salknappen represent pelitic, mafic and granitic compositions. The mineral assemblages in the pelitic rocks indicate metamorphic temperatures of >650°C and pressures between 3kb and ~10kb. Mineral assemblages in the mafic rocks indicate that at a temperature of 800°C, pressures during M_1 were of the order of ~10 kb. Mineral assemblages in the granitic rocks suggest temperatures of approximately 700-900°C for M_1. All the mineral assemblages show evidence of partial rehydration during subsequent retrogression.

CHAPTER 7

THE PETROGRAPHY AND CHEMISTRY OF THE JUTULRORA, ROERKULTEN AND BREKKERISTA GRANITES

PETROGRAPHY

Introduction

The proportions of quartz, plagioclase and K-feldspar are approximately 30 vol. %, 25 vol.%, and 35% respectively in the Jutulrora and Roerkulten Granites and 30 vol.%, 30 vol.% and 30 vol.% respectively in the Brekkerista Granite. Approximately equal proportions of biotite and hornblende constitute the major portion of the remaining 10% in the Jutulrora and Roerkulten Granites whereas biotite dominates the remaining 10% in the Brekkerista Granite.

	Hbl	Bt	Aln	Spn	Ap	Zrn	Grt	Mag	Ms	Ep	Cal	Chl
BK27		1	4	2	5	8		3	6	7		
BK28		1	3	2	5	6		2				
BK53		1	4	2	5	6		3				
BK52		1	3	2	5	7		2	6			
BK54		1	3	2	5	6		4				
BK50		1	4	2	5	6		3				
BKA		1	4	2	5	6		3				
BKB		1	4	2	5	6		3				
BKC		1	3	2	5	6		3				
JE50	1	2	3	4	5	6	7	8				
JE56	1	2	3	4	5	6						
JE104	1	2	3	4	5	6	7					
JE105	1	2	3	4	5	6	7					
JE106	1	2	3	4	5	6						
JE107	1	2	3	4	5	6	8					
RK58		1	2		4	5		3				
RK59	1	2	4		5	6	7	2				
RK60	7	1		5	8	9		3	2		6	4
RK61	1	2	4		5	6	7	3				
RK62	1	2	4		5	6	7	3				
RK6	1	2	4		5	6	7	3				
RK7	1	2	4		5	6	7	3				
RK8	1	2	4	7	5	6	8	3				
RK16		6			4	5		2	1		7	3
RK30	1	2		8	7	9		4	3		6	5
RK11	2	1	5		4	7		3		6		
RK12	2	1	5		4	6	7	3				

Table 7.1 Mafic and accessory mineralogy (from the top down) of the Brekkerista, Jutulrora and Roerkulten Granites respectively. The numbers reflect the relative mineral contents. 1 represents the mineral with the highest proportion and 9 the least. Equal numbers for different minerals in the same sample indicate approximate equal proportions of those minerals. Modal estimates were not carried because most of the accessory and minor minerals form less than 1%. For such minerals, one thousand point counts would have a relative error of ~50% and an absolute error of ~1% (Van der Plas and Tobi, 1965).

The relative proportions of accessory and secondary minerals in the Jutulrora, Roerkulten and Brekkerista Granites are shown in table 7.1. Allanite, apatite and zircon are common to all the granites whereas sphene is present in the Jutulrora and Brekkerista Granite but is typically absent from the Roerkulten Granite (see later). Trace quantities of garnet were recorded in the Roerkulten and Jutulrora Granites but are absent in the Brekkerista Granite. Opaque ore minerals are present in the Brekkerista and Roerkulten Granites but are largely absent from the Jutulrora Granite. Besides these minerals, epidote, muscovite, chlorite and calcite were recorded in some thin sections and are considered to be the products of secondary alteration.

Samples JE104 to JE107 were collected across the southerly dipping Jutulrora granitic sheet from south (top) to north (bottom) at approximately 30m intervals with the intention of identifying possible mineralogical and chemical variations across the sheeted granite. The remaining samples were collected randomly through the sheet. Similarly, samples RK58 to RK62 were collected at approximately 30m intervals across the westerly dipping Roerkulten Granite sheet from east (bottom) to west (top); the remaining samples (except RK11 and RK12) being collected randomly through the sheet. Samples RK11 and RK12 were collected from the western granitic sheet. The samples of Brekkerista Granite were collected at random.

Jutulrora Granite

No systematic mineralogical variations were noted in the samples through the sheet-like body. The quartz and feldspars are equigranular, medium grained (2-3 mm) and display granoblastic textures. Potassium feldspar is typically microcline, characterized by tartan twinning. Plagioclase rarely shows albite twinning and is partially saussuritized locally. Hornblende displays a blue-green colour and forms medium-grained (1-2 mm) irregular grains partially including quartz, feldspar and sphene grains. Hornblende also contains inclusions of allanite, zircon and apatite (Fig. 7.1) suggesting that it may have been a late crystallizing phase. Light to dark brown pleochroic biotite forms discrete aligned plates as well as grains which crosscut and replace hornblende. The cross-cutting biotite which partially replaces hornblende is interpreted to be of secondary metamorphic origin. Allanite occurs as small <0.5mm) xenomorphic grains commonly included in hornblende, biotite, and plagioclase. Larger discrete grains of allanite typically form subidiomorphic prismatic grains which are metamict and dark brown in colour, and rarely show rims of light brown crystalline allanite. Sphene is present in all rocks as xenomorphic grains and is commonly included in hornblende and plagioclase.

Garnet occurs as fine (<1mm) anhedral, inclusion-free grains which are enclosed in feldspar, quartz and hornblende. Zircon forms idiomorphic to subidiomorphic grains and is commonly included in hornblende, feldspar, quartz and allanite. Apatite is present as small (<0.5mm) idiomorphic to subidiomorphic inclusions in hornblende and feldspar.

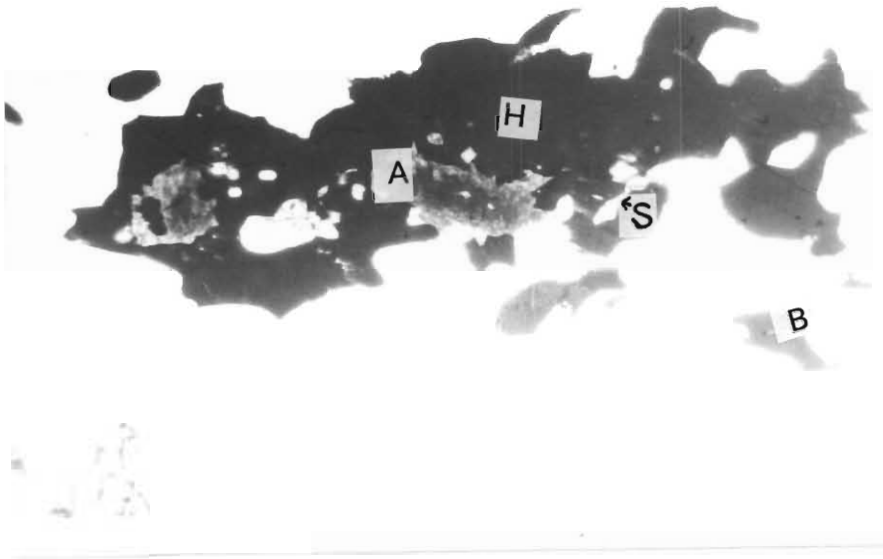

Figure 7.1 Thin section photograph of sphene, allanite and hornblende in the Jutulrora Granite. Field of view is 4mm. H = hornblende, A = allanite, B = biotite, S = sphene. The clear areas are quartz and feldspar.

The textures described above suggest that apatite, zircon, allanite and sphene were early crystallizing phases followed by quartz and the feldspars, and, finally, hornblende and biotite. Experimental studies of the influence of pH_2O on the crystallization sequences in granitic magmas (Wyllie *et al.* (1976) and Naney (1983)) have shown that, where $pH_2O < P_{load}$, the crystallization of biotite and hornblende follows the crystallization of quartz and/or the feldspars whereas at higher H_2O pressures hornblende and/or biotite commonly crystallizes before or crystallizes simultaneously with quartz and feldspar. The crystallization sequence proposed above suggests therefore that the H_2O contents of the magma were relatively low (~2%) but that the temperature of the magma was relatively high (see later).

Roerkulten Granite

The quartz and feldspars are equigranular, medium grained (2-3 mm), and display granoblastic textures. Potassium feldspar is generally microcline characterized by tartan twinning. Plagioclase rarely shows albite twinning and is partially saussuritized in some samples. Samples RK30 and RK60 show incipient sericitisation of plagioclase and also contain calcite which locally forms an

anastomosing network of veinlets. Alteration in these two samples may be related to intense jointing associated with a dolerite dyke crosscutting the granite sheet. Myrmekitic intergrowths are developed rarely at the margins of microcline plates. Samples RK60, RK30, and RK16 differ from the other samples in that they are coarser-grained and also show evidence of varying degrees of alteration. RK16 shows the highest degree of alteration with chlorite pseudomorphing and completely replacing biotite and amphibole.

Blue-green hornblende forms irregular grains commonly partially enclosing quartz, feldspar and opaque ore grains. Hornblende also contains inclusions of allanite, zircon and apatite. Biotite forms discrete grains as well as those which cross-cut and replace hornblende. The latter commonly forms symplectitic intergrowths with a colourless mineral presumed to be quartz. The cross-cutting and symplectitic biotites are interpreted as secondary metamorphic products. Allanite occurs as small grains typically included in hornblende and, rarely, in opaque ore grains.

Figure 7.2 Inclusions of zircon and apatite in magnetite (M) grains in the Roerkulten Granite. Field of view 4mm. A = allanite, G = garnet, H = hornblende, B = biotite. The clear areas are quartz and feldspar.

Larger grains of allanite occur as discrete grains, are generally metamict, and, rarely, show rims of unmetamict allanite. Opaque ore occurs as idiomorphic to subidiomorphic grains which commonly include zircon, apatite and less commonly, allanite (Fig. 7.2). Zircon forms idiomorphic grains, commonly included in amphibole. Garnet is found as fine (<0.5 mm),

anhedral, inclusion-free grains enclosed in microcline or plagioclase grains. Sphene commonly forms thin rinds to the opaque minerals. This texture suggests that the sphene formed as a consequence of reaction possibly between calcic plagioclase and titaniferous magnetite or ilmenite.

No mineralogical variation through the Roerkulten Sheet is obvious but the opaque ore content appears to be inversely proportional to that of hornblende. Sample RK58 is characterised by a high opaque content but contains no hornblende whereas in the other samples with significant hornblende content, opaque ore is subordinate. Another difference between RK58 and the other samples is the absence of garnet.

From the above description of the petrography, the following sequence of crystallization may be inferred for the Roerkulten Granite assuming that effects of deformation and metamorphic recrystallization have been minor. Texturally, zircon, apatite and allanite appear to have crystallized early, occurring as inclusions in virtually all phases. Garnet is also interpreted as an early, if not xenocrystic, mineral phase occurring as inclusions in feldspar. The early crystallisation of zircon and apatite suggests that the magma was saturated with regard to Zr and P. Opaque ore crystallization occurred after the early phases but appears to have preceded feldspar. Subsequent to the crystallization of opaque minerals, quartz, feldspar and biotite appear to have followed being succeeded in turn by hornblende. The partial replacement of hornblende by biotite-quartz symplectites is interpreted as a post-kinematic metamorphic feature because such intergrowths are unlikely to survive deformation.

Brekkerista Granite

In thin section the K-feldspar porphyroclasts consist of recrystallised aggregates of microcline characterised by tartan twinning. Albite twinning is only locally developed but permitted a determination of the plagioclase composition of An_{20} based on the Michel-Levy method. Some grains of plagioclase exhibit zoning. Quartz exhibits undulatory extinction. Biotite defines a weak planar fabric and is typically pleochroic from light to dark brown but also occurs as green varieties reflecting local alteration to chlorite.

The rock is characterized by a high content of sphene which occurs as idiomorphic to xenomorphic grains (Fig. 7.3). The opaque ore minerals are idiomorphic to subidiomorphic, and commonly contain inclusions of apatite, allanite and zircon. The opaque ore minerals are enclosed in places by narrow rims of sphene. Medium to fine-grained yellow-brown xenomorphic grains of allanite are ubiquitous. The medium-sized grains commonly are metamict and semi-opaque whereas the smaller grains are more typically found enclosed in sphene, biotite and opaque ore grains. Muscovite and epidote are rarely present and occur as alteration products of microcline and plagioclase respectively.

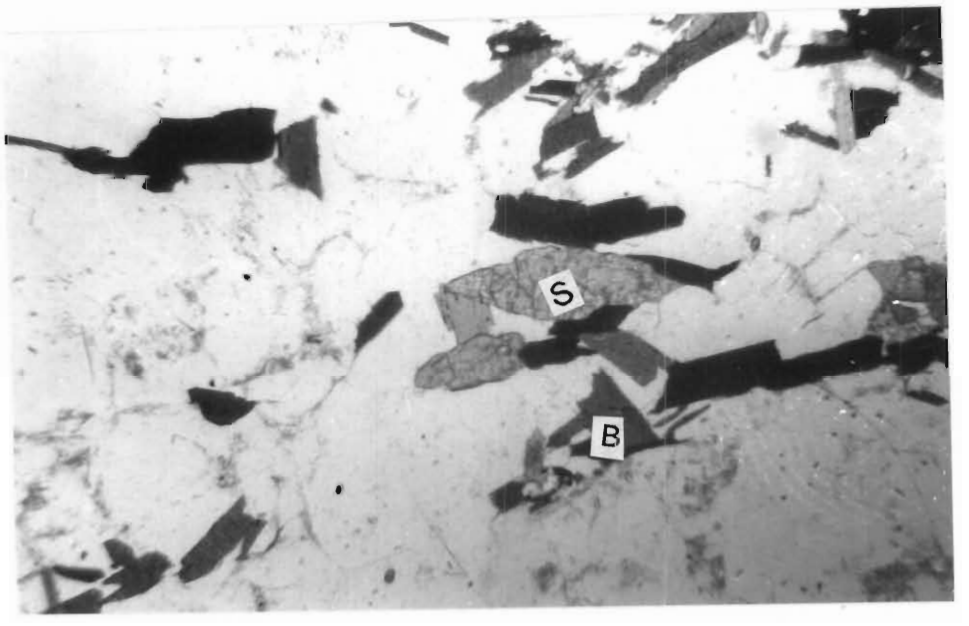

Figure 7.3. Idiomorphic sphene grain in the Brekkerista granite interpreted as products of primary magmatic crystallisation. Field of view is 4mm. S = sphene, B = biotite. The clear areas are quartz and feldspar.

The crystallisation of microcline porphyroclasts was followed by quartz and biotite. The idiomorphic shape of the opaque mineral grains suggests early crystallization. Prior crystallization of apatite, allanite and zircon is indicated by the presence of inclusions of these minerals in the opaque grains. Recognition of early apatite and zircon grains suggest a magma saturated with respect to P and Zr. The idiomorphic grains of sphene are interpreted to indicate a primary magmatic origin (Fig. 7.3) whereas the rims of sphene developed around opaque ore grains are interpreted to be the products of reaction of Ca (presumably from plagioclase) with Ti in the magnetite.

The relatively euhedral sphene may suggests that it was an early phase to crystallise although inclusions of small allanite grains in sphene, biotite and opaque ore grains implies that allanite was a liquidus if not xenocrystic phase.

GEOCHEMISTRY

Major element chemistry

Introduction

The major element analyses of the Jutulrora, Roerkulten and Brekkerista Granites are shown in table 7.2 from which it may be seen that the major element variations within and between these granite bodies are minor. The Jutulrora and Roerkulten Granites have very similar major element chemistry but the Brekkerista Granite has lower SiO_2 and K_2O contents and higher CaO, Na_2O, TiO_2, P_2O_6 and MgO contents than the Jutulrora and Roerkulten Granites.

	SiO_2	Al_2O_3	Fe_2O_3	FeO	MnO	MgO	CaO	Na_2O	K_2O	TiO_2	P_2O_5	TOTAL
JUTULRORA GRANITE												
JE50	74.83	12.53	0.66	1.77	0.04	0.27	1.18	2.38	5.5i	0.25	0.05	99.47
JE56	72.99	13.23	0.80	2.04	0.05	0.31	1.33	2.68	5.75	0.30	0.06	99.54
JE104	74.61	13.00	0.63	1.79	0.06	0.21	1.06	2.47	5.41	0.24	0.04	99.52
JE105	72.44	13.08	0.79	2.10	0.05	0.14	1.17	2.62	5.50	0.20	0.05	98.13
JE106	72.23	13.25	0.94	2.53	0.11	0.46	1.88	2.83	5.42	0.43	0.09	100.17
JE107	71.95	13.83	0.93	2.46	0.06	0.31	1.66	2.99	5.22	0.27	0.08	99.75
ROERKULTEN GRANITE (EASTERN SHEET)												
RK58	72.64	13.27	1.04	2.37	0.11	0.26	1.35	2.60	5.72	0.40	0.05	99.65
RK59	71.73	13.73	0.83	2.54	0.15	0.20	1.48	2.86	6.03	0.43	0.06	100.25
RK60	71.3	13.96	0.92	2.23	0.10	0.20	2.27	3.80	4.23	0.44	0.06	99.42
RK61	70.91	14.39	0.70	2.23	0.11	0.11	1.29	2.81	6.02	0.35	0.05	99.19
RK62	73.51	13.05	1.06	1.70	0.12	0.11	1.23	2.68	6.26	0.32	0.05	99.73
RK6	70.16	14.39	1.07	2.58	0.09	0.31	1.55	3.01	6.12	0.43	0.07	99.77
RK7	69.61	13.89	0.93	2.61	0.10	0.30	1.61	2.64	6.49	0.43	0.07	98.82
RK8	70.83	13.88	0.59	2.26	0.08	0.19	1.30	2.92	6.20	0.33	0.06	98.98
RK16	72.0	15.54	0.65	1.43	0.02	0.42	1.01	3.43	5.98	0.32	0.08	100.82
RK30	70.4	15.34	0.59	1.66	0.06	0.27	1.98	4.14	4.42	0.38	0.05	99.35
(WESTERN SHEET)												
RK11	71.38	15.03	0.74	1.68	0.05	0.70	2.25	3.05	4.80	0.25	0.09	99.85
RK12	70.06	15.19	0.88	2.10	0.05	0.97	2.60	3.40	3.96	0.34	0.12	99.53
BREKKERISTA GRANITE												
BK28	72.93	13.61	0.67	1.92	0.03	0.52	1.48	3.37	4.31	0.58	0.13	99.05
BK27	68.37	14.69	1.09	3.10	0.06	0.98	2.35	3.24	4.24	0.79	0.22	99.13
BK54	71.52	14.18	0.71	2.14	0.02	0.91	2.21	4.09	2.95	0.67	0.17	99.57
BK53	69.93	13.71	0.94	2.68	0.04	0.87	2.20	3.20	4.45	0.74	0.21	98.97
BK52	70.36	13.99	0.96	2.59	0.05	0.92	1.95	3.29	4.80	0.71	0.18	99.8
BK50	69.78	13.63	1.07	3.23	0.06	0.98	2.29	3.18	4.03	0.87	0.23	99.35
BKA	69.84	14.27	0.40	3.22	0.05	0.81	2.08	3.48	4.55	0.76	0.20	99.64
BKB	71.31	13.61	0.38	3.04	0.04	0.7	1.79	3.60	4.29	0.68	0.17	99.61
BKC	70.69	13.70	0.38	3.06	0.03	0.75	2.09	3.68	3.99	0.73	0.19	99.31

Table 7.2 Major element (wt%) chemistry of the Jutulrora, Roerkulten and Brekkerista granites.

Jutulrora Granite

Although data are sparse, minor systematic variations in major elements across the Jutulrora Granite sheet are observed (Fig. 7.4).

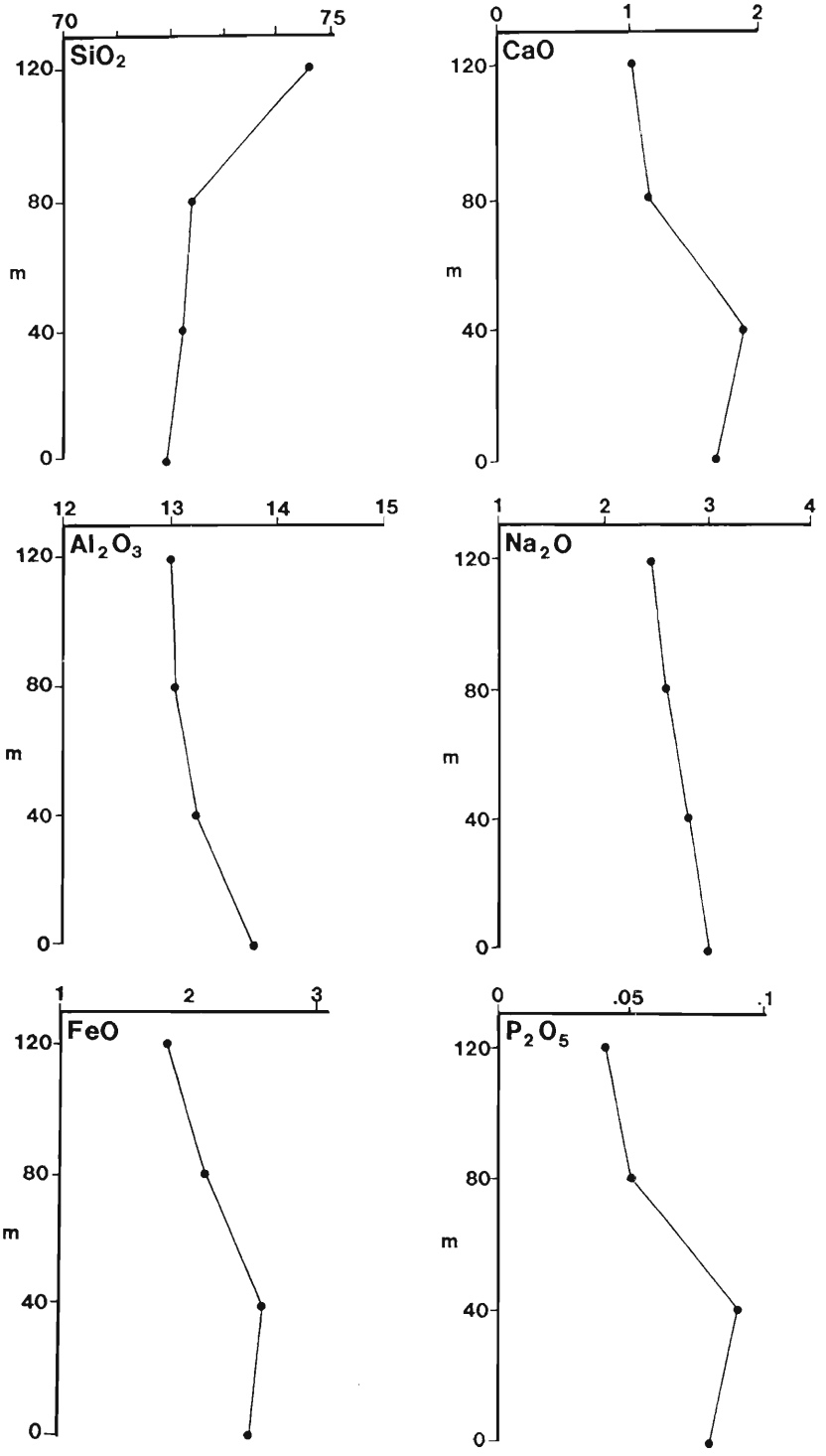

Figure 7.4. Variation diagrams showing major element variation across the Jutulrora Granite Sheet. The thickness values are measured from south (top) to north (bottom).

SiO_2 increases upwards whereas Al_2O_3, Na_2O, FeO, CaO and P_2O_5 decrease, but small deviations from these trends do occur (Fig. 7.4)

			SOUTH (top) ----------> NORTH (bottom)				
	JE50	JE56	JE104	JE105	JE106	JE107	MEAN
Qtz	35.88	30.77	35.78	32.43	28.8	28.84	32.19
Or	32.63	34.00	32.02	32.99	31.82	30.78	32.49
Ab	20.19	22.71	20.94	22.51	23.81	25.26	22.65
An	5.54	6.21	5.01	5.56	7.4	7.7	6.26
Opx	3.59	4.12	3.53	4.04	4.68	4.95	4.17
Mag	0.96	1.16	0.92	1.16	1.36	1.35	1.15
Crn	0.63	0.32	1.25	0.82		0.43	0.58
Ilm	0.48	0.57	0.46	0.38	0.81	0.51	0.54
Ap	0.11	0.13	0.09	0.11	0.19	0.17	0.14
Di					1.11		0.19

Table 7.3 C.I.P.W. norm values for the Jutulrora Granite.

No systematic variations in the concentrations of MnO, MgO, and TiO_2 are evident from the analyses. These trends suggest that the proportions of plagioclase and mafic minerals increase upwards with antipathetic increase in quartz and K-feldspar, but their normative mineralogy shows that these variations are not of a great magnitude (table 7.3). For example, normative orthopyroxene and plagioclase decrease from 4.95% to 3.53% and 32.96% to 25.95% respectively whereas normative quartz and orthoclase increase from 28.84% to 35.78% and 30.78% to 32.02% respectively.

Roerkulten Granite

The chemical data presented in table 7.2 shows that the western sheet of the Roerkulten Granite is characterised by higher MgO, P_2O_5 and CaO contents than the eastern sheet. Attention was drawn to the fact that samples RK16, RK30 and RK 60 showed evidence of alteration, characterised by partial to complete chloritisation of biotite and hornblende, incipient sericitisation of plagioclase and the presence of calcite in voids. Samples RK60, RK30, RK11 and RK12 contain slightly higher contents of normative plagioclase. In the latter two samples this is considered to be real whereas in the former two samples the increase may relate to alteration associated with the introduction of calcite, and therefore Ca, resulting in higher normative plagioclase content.

Table 7.2 and figure 7.5 demonstrate that systematic variations across the Roerkulten Granite exist. Fe and Mg display trends reflecting moderate increases upwards (west to east). SiO_2 and Al_2O_3 have antipathetic trends. The uppermost sample has higher contents of SiO_2 in contrast to the general upward depletion found in the lower part of the sheet.

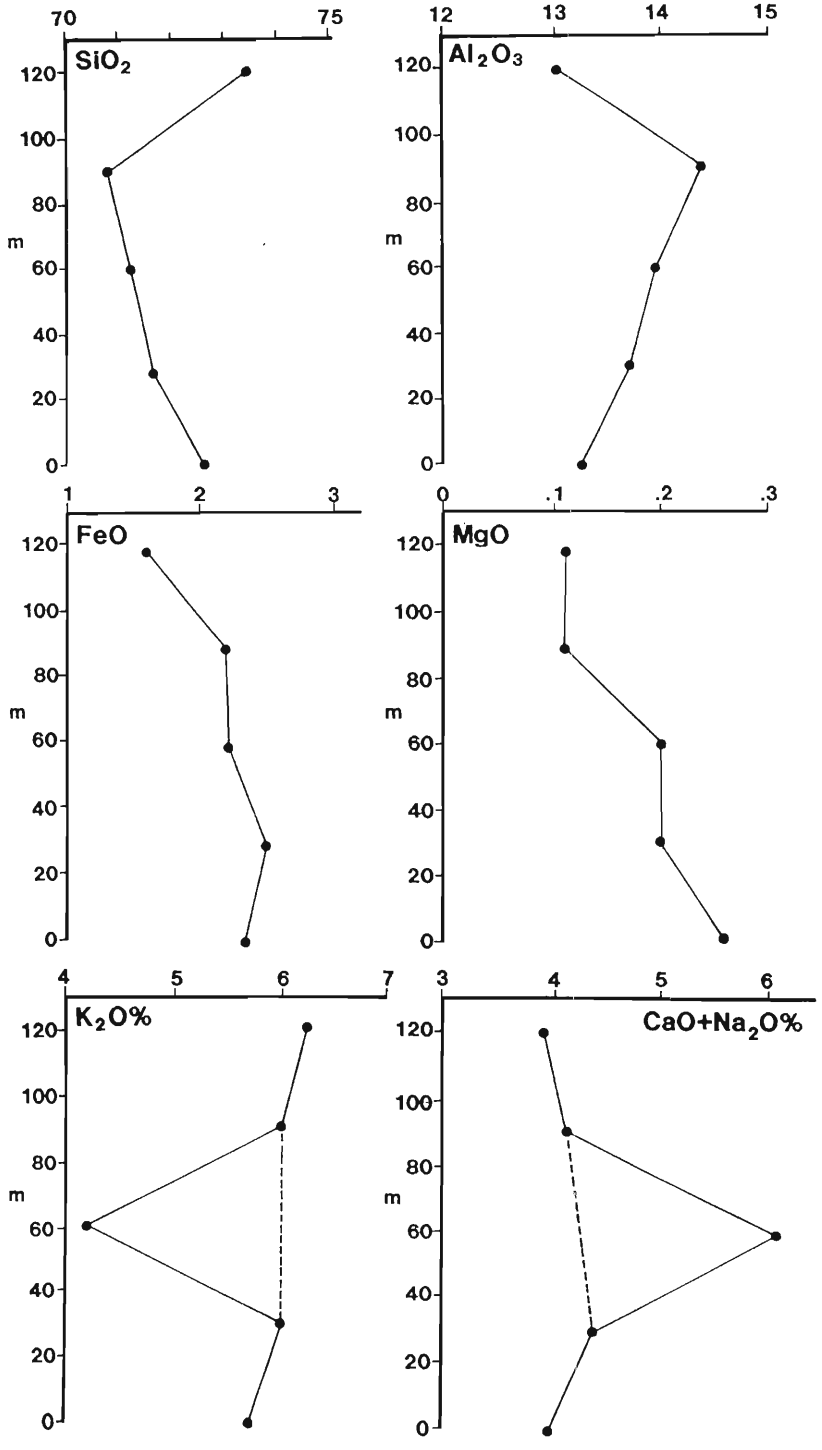

Figure 7.5 Major element variations across the eastern Roerkulten Granite sheet. The thickness values are measured from east (bottom) to west (top).

Al_2O_3 in the same samples shows a sudden decrease, whereas this oxide shows a steady increase through the underlying 100m of the sheet. The alkalis show little variation except sample RK60 which is relatively depleted in K_2O and relatively enriched in $CaO + Na_2O$. The chemical variation in sample RK60 is presumed to reflect the partial alteration of the sample.

	RK58	RK59	RK60	RK61	RK62	RK6	RK8	RK7	RK16	RK30	RK11	RK12	MEAN
Qtz	30.71	26.64	27.24	27.16	30.17	23.69	25.67	24.09	25.48	23.99	28.46	27.05	26.98
Or	33.78	35.37	25.12	35.71	36.97	36.07	36.85	38.61	35.03	26.31	28.36	23.48	36.34
Ab	21.22	24.03	32.31	23.88	22.67	25.41	24.86	22.5	28.77	35.28	25.80	28.86	23.72
An	6.37	6.77	8.58	6.10	5.09	7.22	6.10	6.93	4.81	9.79	10.98	12.70	6.39
Opx	4.54	4.64	2.12	4.01	2.77	4.96	4.25	4.76	2.62	2.74	3.89	5.09	4.29
Mag	1.28	1.50	1.34	1.34	1.01	1.53	1.36	1.56	0.93	0.86	1.07	1.28	1.37
Ilm	0.76	0.81	0.84	0.67	0.61	0.81	0.63	0.82	0.60	0.73	0.47	0.65	0.73
Co	0.46	0.12		1.03		0.16	0.15		1.63	0.18	0.79	0.67	0.26
Di	0.60		2.28	0.57				0.18					
Ap	0.11	0.13	0.14	0.11	0.11	0.15	0.13	0.15	0.19	0.12	0.21	0.29	0.13

Table 7.4. C.I.P.W. norm values for the from the Roerkulten Granite. Values in percent. The mean value is for the unaltered samples from the eastern sheet.

Brekkerista Granite

The Brekkerista Granite has moderately variable SiO_2 (68-73%), high $\Sigma FeO/\Sigma FeO + MgO$, $K_2O/Na_2O \sim 1.2$ and moderately high TiO_2. The C.I.P.W. norms (table 7.5), reveal that the granite has a mean plagioclase to K-feldspar ratio of 1.55:1.

No.	BK28	BK27	BK54	BK53	BK52	BK50	BKA	BKB	BKC
Qtz	31.99	25.60	29.66	27.43	26.19	28.23	25.01	27.60	27.12
Or	25.70	25.26	17.50	26.56	28.41	23.96	26.97	25.44	23.73
Ab	28.79	27.65	34.76	27.36	27.89	27.08	29.55	30.56	31.36
An	6.55	10.31	9.90	9.64	8.51	9.92	9.04	7.80	9.14
Mag	0.98	1.59	1.03	1.37	1.39	1.56	0.58	0.55	0.55
Ilm	0.15	1.51	1.28	1.42	1.35	1.66	1.45	1.30	1.40
Ap	0.29	0.48	0.37	0.46	0.39	0.51	0.42	0.37	0.42
Opx	4.79	7.00	5.15	6.00	5.98	7.09	6.79	6.30	6.36
Co	1.3	1.03	0.65	0.13	0.27	0.43	0.32	0.20	
Di									0.04

Table 7.5. Values for C.I.P.W. norm for the Brekkerista Granite.

Strong linear variations between various elements are seen in Table 7.6. Correlation coefficients between >0.7 and <-0.7 for the major elements are reflected by linear variations in figure 7.6. Iron oxide, MnO, MgO, CaO, TiO_2 and P_2O_5 decrease sympathetically with increasing SiO_2. The coherent variation of other elements with SiO_2 may be viewed as possibly resulting from the constant sum effect recognised in acid rocks (Chayes, 1964) particularly in view of the high and restricted range in SiO_2 values (68- 73%).

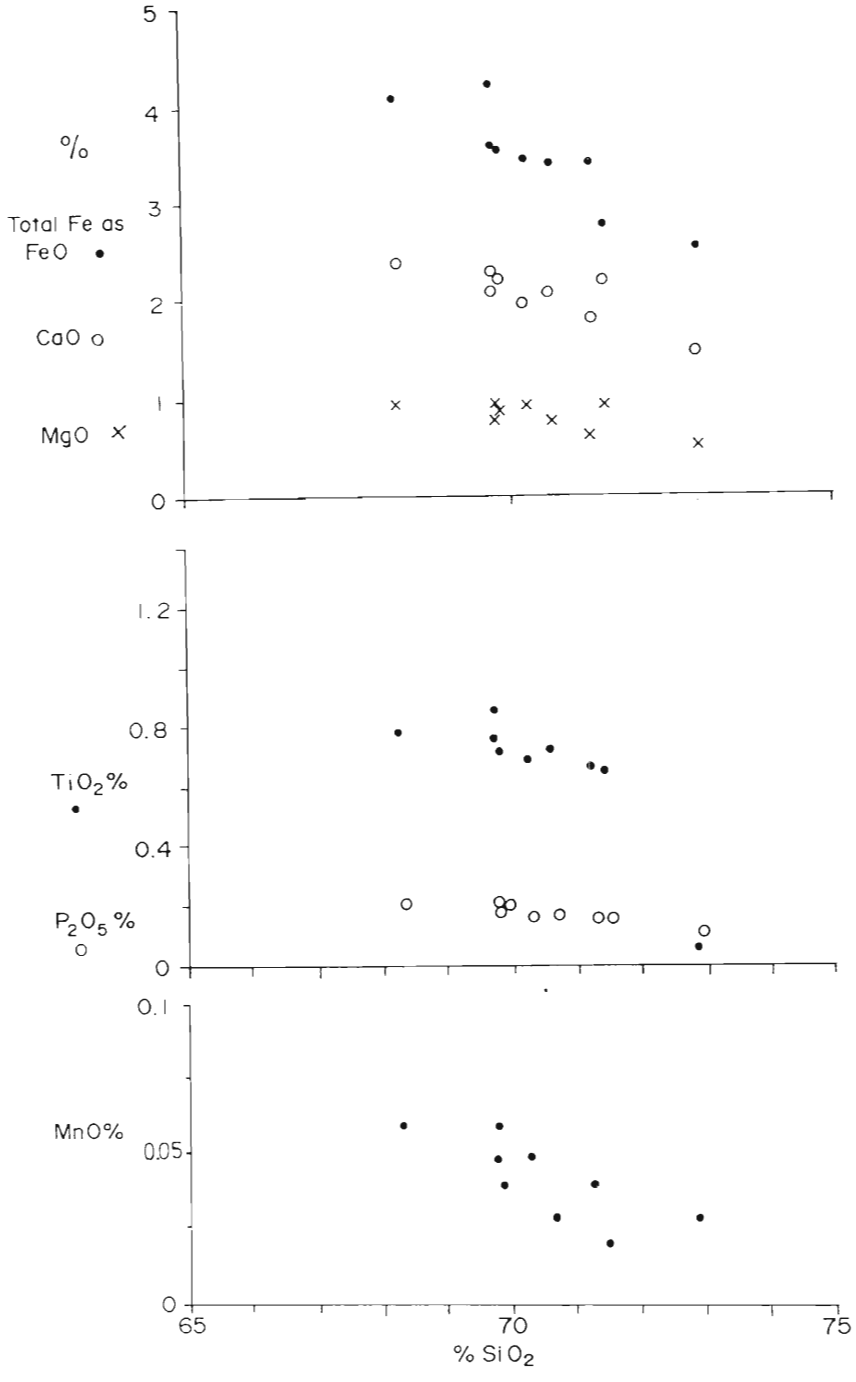

Figure 7.6 Harker variation diagrams for the Brekkerista Granite for FeO, MnO, MgO, CaO, TiO_2 and P_2O_6.

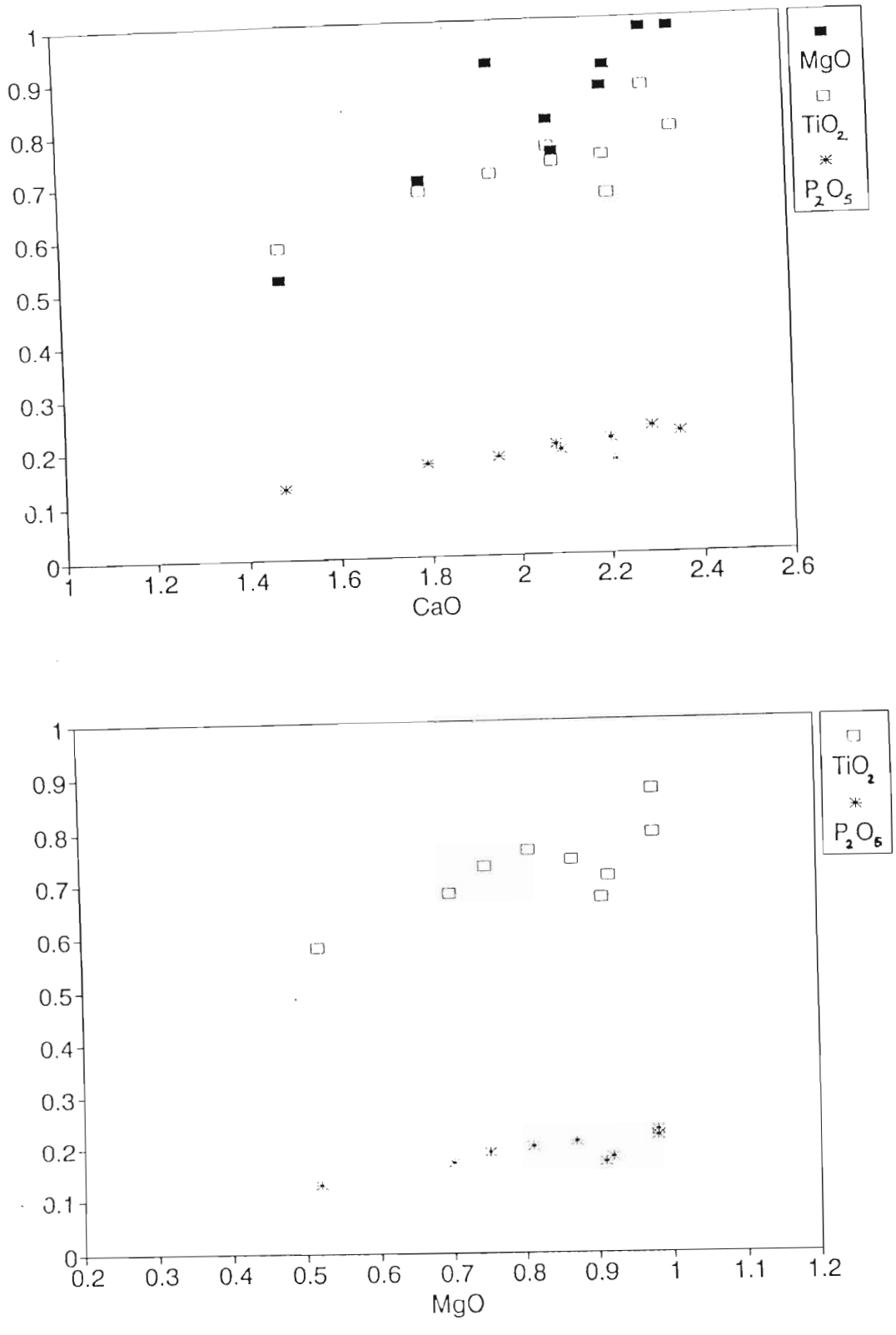

Figure 7.7. Variation diagrams for CaO/MgO, CaO/TiO_2, CaO/P_2O_5 (above) and MgO/TiO_2, MgO/P_2O_5 (below) for the Brekkerista Granite. Values in wt%.

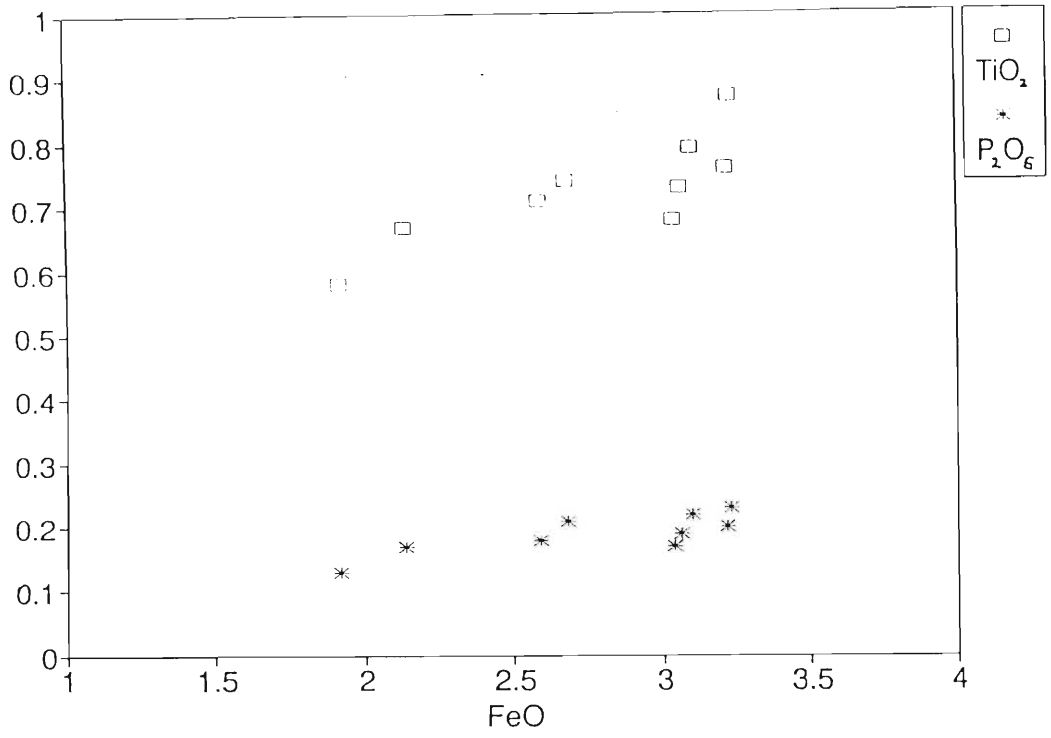

Figure 7.8. FeO vs TiO_2 and FeO vs P_2O_6 (wt%) for the Brekkerista Granite.

Whereas the constant sum effect may be significant, the lack of variation in K_2O and Na_2O suggests that this effect does not play a dominant role and that the linear variations are valid. Positive correlations >0.7 are seen for CaO/MgO, CaO/TiO_2, CaO/P_2O_6, MgO/TiO_2, MgO/P_2O_6, FeO/TiO_2 and FeO/P_2O_6 in Table 7.6 (Figs. 7.7 and 7.8). The strong sympathetic correlation between CaO and TiO_2 provides some support for the interpretation that sphene was a primary magmatic mineral.

	Al_2O_3	FeO	MnO	MgO	CaO	Na_2O	K_2O	TiO_2	P_2O_5
SiO_2	-0.59	-0.74	-0.77	-0.80	-0.82	0.46	-0.26	-0.81	-0.92
Al_2O_3	XXXX	0.16	0.32	0.52	0.51	0.07	-0.09	0.32	0.32
FeO		XXXX	0.68	0.42	0.53	-0.32	0.31	0.77	0.78
MnO			XXXX	0.54	0.40	-0.77	0.57	0.51	0.71
MgO				XXXX	0.9	-0.17	-0.15	0.83	0.81
CaO					XXXX	-0.05	-0.29	0.85	0.88
Na_2O						XXXX	-0.77	-0.07	-0.43
K_2O							XXXX	-0.03	0.10
TiO_2								XXXX	0.87

Table 7.6. Table showing correlation coefficients describing variation between various elements for the Brekkerista Granite.

Trace element chemistry

Introduction

The transition element and large ion lithophile element (LILE) contents of the various granites are shown in table 7.7 whereas the rare earth element (REE) analyses from the three granite bodies are shown in table 7.9. Although the major elements in the granites do not vary greatly, certain trace elements and REE exhibit significant variation.

	Rb	Sr	Zr	Th	Y	Nb	Ba	Sc	La	V	Zn
JUTULRORA GRANITE											
JE50	103	160	281	11.7	35.6	23	2158	3.1	137.6	0.3	65.4
JE56	109	170	355	15.6	45.1	27.1	2183	5.1	174.1	0.0	82.9
JE104	113	148	319	16.5	37.2	24.1	2173	4.5	156.5	7.7	46.3
JE105	109	151	311	15.4	47	25.7	2112	5.0	156	2.6	55.7
JE106	113	196	385	18.3	55	27	2312	6.3	158.8	7.8	86.1
JE107	110	170	348	12.8	78	37.5	2167	7.1	126.3	14.4	96.4
ROERKULTEN GRANITE (EASTERN SHEET)											
RK58	134	205	564	16.3	26	14	1198	5.1	153.6	1.7	43.7
RK59	99	140	590	14.9	37.1	21.2	1238	5.6	150.8	0.9	87.5
RK60	62	189	554	13.7	26	19.4	979	5.4	122.9	2.8	65.9
RK61	102	138	528	13.1	30.1	17.1	1293	6	131.7	0.0	81.7
RK62	112	171	436	8.2	25	13	1305	4.1	107	0.0	46.8
RK6	91	147	614	15.9	35.5	20.1	1251	6.1	145	0.0	86.8
RK7	101	167	635	19.6	38.6	21.4	1315	6.8	166.6	3.1	86.4
RK8	94	143	486	12.1	29.5	16.9	1221	5.7	140	0.0	73.5
RK16	189	434	228	36.4	7.9	8.3	1586	2.9	75.9	14.5	32.8
RK30	77	249	363	9.4	17.8	15.2	1020	5.9	79.6	2.5	58.4
(WESTERN SHEET)											
RK11	100	362	130	0.0	12.5	11	1377	3.1	39.4	30.4	36.9
RK12	88	369	154	14.7	11.7	8.6	1286	6.2	44	38.3	48.9
BREKKERISTA GRANITE											
BK28	73	226	263	14	45.4	14.4	1514	3.4	106.6	21.1	33.5
BK27	102	352	421	9.9	69.3	21.6	2584	7.9	92.9	44.9	56
BK54	56	356	367	24.4	61.7	16.8	1305	5.9	160.7	37.6	31.4
BK53	102	319	407	13.3	69.8	20.6	2337	8.1	94.8	41.3	60.9
BK52	99	301	360	9.5	63.4	19.2	2303	7.1	89.7	32.2	52.5
BK50	102	308	406	12	83.3	25.8	2010	9.3	134.5	38	67.7
BKA	123	293	407	14.3	66.9	19.7	2122	8.6	103.8	31.9	51.9
BKB	129	149	353	15.7	66.8	18.6	1706	5.4	112.5	31.9	45.3
BKC	85	317	391	15.9	75.5	20.4	2043	7.1	117	34.7	37.2

Table 7.7. Transition element and large ion lithophile element chemistry of the Jutulrora, Roerkulten and Brekkerista Granites. Concentrations in ppm.

Jutulrora Granite

Small but systematic variations in major element contents can be recognised across the Jutulrora Granite sheet and similar trends are recognised in some of the trace elements (Fig. 7.9).

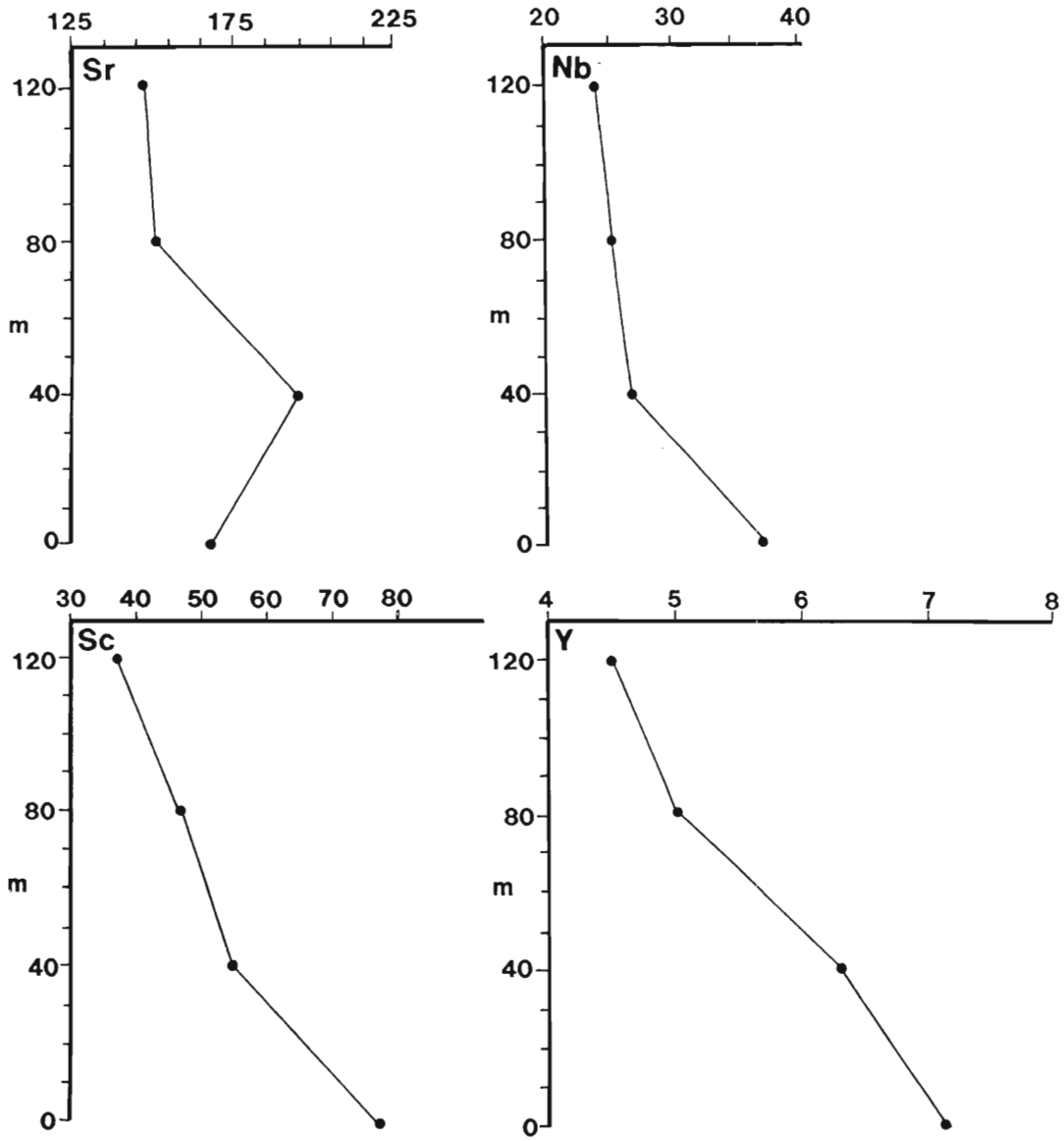

Figure 7.9. Diagrams showing trace element variation across the sheet-like Jutulrora Granite. The thickness values are measured from the bottom (north) to the top (south) of the granite sheet.

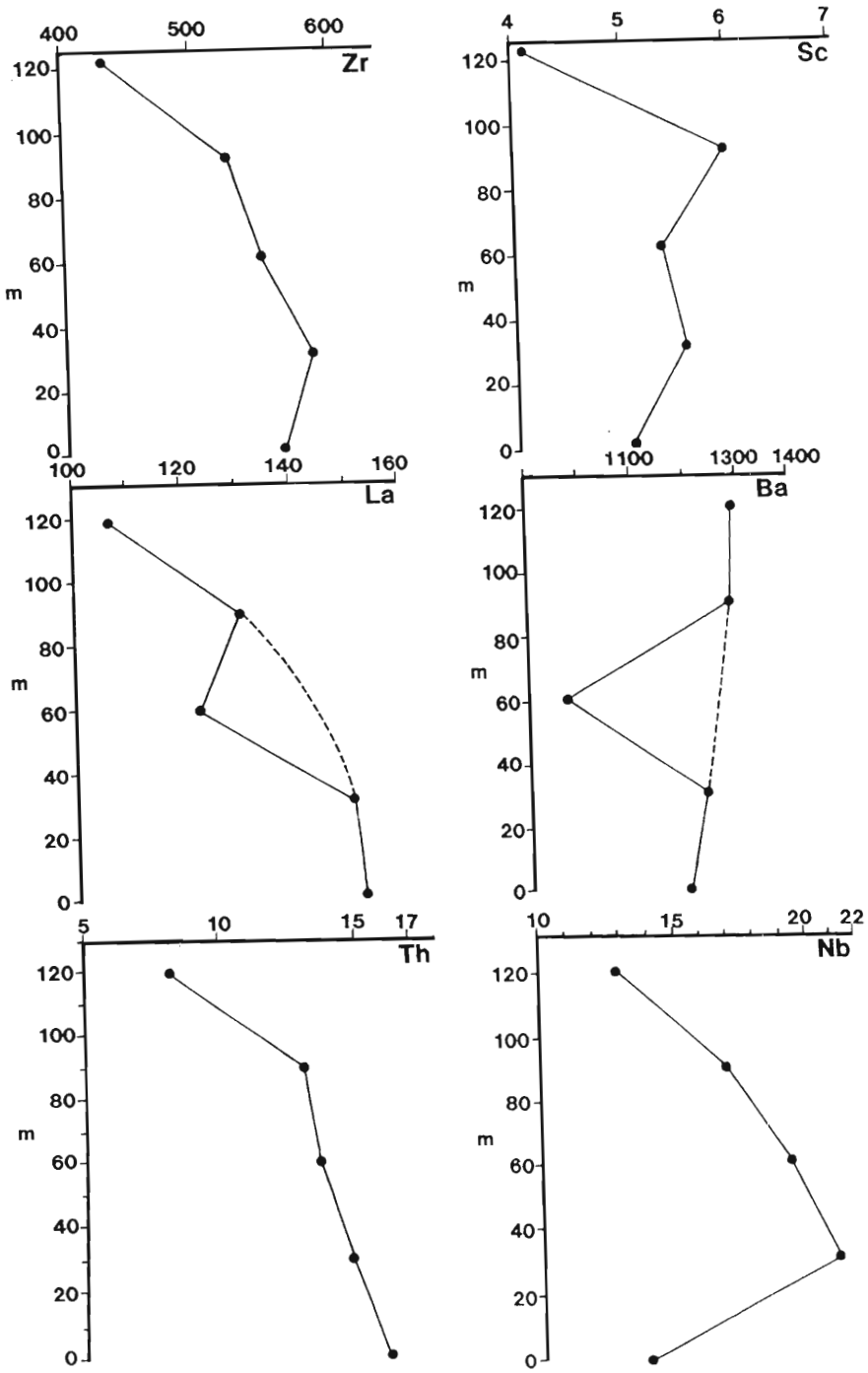

Figure 7.10 Trace element variation across the eastern Roerkulten Granite sheet. The thickness values are measured bottom (west) to top (east).

Niobium, Y, Sc and Zn display sympathetic decreases upwards through the sheet (Fig. 7.9, Zn not shown). Strontium shows moderate relative upward enrichment, sample JE106 being markedly enriched in relation to other samples. The slight upward increase in plagioclase content is consistent with the Sr data (except JE107) because Sr is readily accommodated in the plagioclase lattice (K_d for Sr in plagioclase ~6 Henderson, 1982, p. 92).

Partition coefficients for Y, Nb, Sc, and Zn (see appendix 3) show that these elements are all partitioned to varying degrees in amphibole and/or biotite. Thus the variations in these elements may be related to increasing mafic mineral content in the base of the sheet that is also reflected by a sympathetic increase in Fe content. Rubidium, Th, Ba, La and V do not show any systematic variation.

Roerkulten Granite

Only two samples were collected from the western Roerkulten Granite sheet (RK11 and RK 12) sheet and thus little can be said other than noting that compositionally the western sheet differs from the eastern sheet by virtue of its lower Zr and La and higher Sr concentrations.The trace elements show consistent trends across the granite sheet (Fig. 7.10) except sample RK58 and sample RK60 which shows alteration in thin section. Thorium, Nb and La decrease whereas Ba increases up through the sheet.

Alteration of plagioclase to muscovite, deposition of intergranular calcite and the partial alteration of hornblende to an unidentified brown mineral have been noted in sample RK60. This alteration could be responsible for the anomalous Ba and Ca concentrations in RK60. The low content of La in sample RK60 is difficult to ascribe to alteration in that the REE are normally considered to be relatively unaffected by alteration and low to intermediate grade metamorphism. A possible cause for the low La content is that allanite was not noted in thin sections of RK60. The partition coefficient (K_d) for La in allanite is 820 (Henderson, 1984,p 94) and therefore the high La contents in the other samples may be related to the allanite content. The differences in sample RK58 may be related to the absence of hornblende.

Brekkerista Granite

Zirconium, Nb, Ba, Sc and V have antipathetic relationships with correlation coefficients <-0.7. (table 7.8). Coherent variations are seen between the following trace elements with positive correlations (r> 0.7) being observed; La vs Th, Y vs Zr, Nb vs Zr, Sc vs Zr, V vs Zr, Y vs Nb, Y vs Sc, Nb vs Sc, Nb vs Zn, Sc vs Zn and Sc vs V.

Strong negative correlations (r less than -0.7) between Th vs Ba and La vs Ba indicate antipathetic relationships. Partition coefficients for Y, Zr, Nb, Sc and Zn in biotite are all >1

(appendix 3) and thus crystallisation of biotite may exert significant control on the variations shown by these elements.

	Rb	Sr	Th	Zr	Y	Nb	Ba	Sc	La	V	Cu	Ni	Zn
iO_2	-0.47	-0.42	0.51	<u>-0.90</u>	-0.69	<u>-0.78</u>	<u>-0.86</u>	<u>-0.87</u>	0.34	<u>-0.82</u>	0.32	0.23	<u>-0.75</u>
l_2O_3	0.00	0.53	-0.07	0.45	-0.01	0.06	0.39	0.30	-0.13	0.49	-0.16	-0.02	-0.07
eO	<u>0.76</u>	-0.11	-0.40	<u>0.77</u>	<u>0.82</u>	<u>0.80</u>	0.60	<u>0.76</u>	-0.21	0.47	-0.11	-0.43	0.63
nO	0.65	0.04	<u>-0.81</u>	0.52	0.50	<u>0.74</u>	<u>0.75</u>	0.68	-0.48	0.38	-0.25	-0.31	<u>0.87</u>
gO	0.09	0.58	0.12	<u>0.80</u>	0.66	<u>0.71</u>	0.52	<u>0.79</u>	0.11	<u>0.84</u>	-0.19	0.33	0.62
aO	0.05	0.65	0.14	<u>0.92</u>	<u>0.76</u>	<u>0.73</u>	0.49	<u>0.83</u>	0.20	<u>0.93</u>	-0.27	0.24	0.53
a_2O	-0.47	0.01	<u>0.93</u>	-0.16	-0.19	-0.49	<u>-0.71</u>	-0.39	<u>0.71</u>	-0.11	0.39	0.39	-0.78
O	0.68	-0.34	<u>-0.85</u>	0.00	-0.04	0.13	0.64	0.18	<u>-0.92</u>	-0.22	-0.26	-0.61	0.48
$_2O_2$	0.43	0.25	-0.12	<u>0.94</u>	<u>0.89</u>	<u>0.8</u>	0.53	<u>0.87</u>	0.07	<u>0.80</u>	-0.06	0.04	0.62
O_5	0.42	0.40	-0.38	<u>0.93</u>	<u>0.87</u>	<u>0.93</u>	<u>0.71</u>	<u>0.95</u>	-0.10	<u>0.83</u>	-0.34	-0.03	<u>0.83</u>
)	XXXX	-0.55	0.53	0.40	0.39	0.43	0.52	0.43	-0.54	0.11	0.17	-0.58	0.60
:		XXXX	0.06	0.42	0.18	0.23	0.29	0.42	0.16	0.52	-0.67	0.45	0.10
1			XXXX	-0.17	-0.18	-0.44	-0.8	-0.36	0.82	-0.07	0.38	0.56	-0.68
:				XXXX	<u>0.84</u>	<u>0.79</u>	0.65	<u>0.92</u>	-0.04	<u>0.87</u>	-0.25	-0.03	0.64
					XXXX	<u>0.93</u>	0.47	<u>0.84</u>	0.14	0.68	-0.17	-0.03	0.64
)						XXXX	0.60	<u>0.88</u>	-0.02	0.66	-0.29	-0.04	<u>0.83</u>
1							XXXX	0.68	-0.74	0.55	-0.47	-0.49	<u>0.72</u>
:								XXXX	-0.10	<u>0.70</u>	-0.46	0.08	<u>0.80</u>
1									XXXX	0.05	0.26	<u>0.72</u>	-0.37
										XXXX	-0.06	0.04	0.53
1											XXXX	-0.09	-0.25
												XXXX	-0.10

Table 7.8. Table showing correlation coefficients describing variation between various elements for the Brekkerista Granite. Correlation coefficients >0.7 or <-0.7 are underlined.

Similarly, the K_d's for Nb, Sc, and Zr in sphene are high (>>1) and thus crystallisation of sphene would also exert significant control on the variation of these elements. The relationship La vs Th may be related to the influence of varying proportions of sphene and allanite with these elements being strongly partitioned into these minerals.

REE Chemistry

Introduction

In addition to two samples from the Brekkerista Granite, the four samples collected across the Jutulrora Granite sheet and three of the five samples collected across the Roerkulten Granite sheet were analyzed for REE (JE104 - JE107 and RK58, RK60, RK62; table 7.9).

Jutulrora Granite

The chondrite normalised REE patterns of samples JE104, JE105, JE106 and JE107 are steep with La_{cn}/Yb_{cn} varying between 30.75 and 14.28 (Fig. 7.11). All samples have negative Eu

anomalies although the magnitude of the anomaly decreases from sample JE107 to JE104. This is more a function of changing abundances of Gd and the other HREE rather than differences in Eu concentrations.

	La	Ce	Pr	Nd	Sm	Eu	Gd	Dy	Ho	Er	Yb
JUTULRORA GRANITE											
JE104	164.48	285.69	31.87	119.86	15.77	3.12	11.01	8.43	1.75	4.25	3.46
JE105	147.23	245.72	29.44	107.67	16.14	2.76	10.56	9.46	1.83	4.59	3.39
JE106	150.16	244.2	30.54	114.62	18.12	2.81	12.75	11.62	2.20	5.57	4.04
JE107	123.22	217.65	27.79	105.97	20.81	2.55	16.75	15.62	3.19	7.44	5.58
ROERKULTEN GRANITE											
RK58	177.88	298.97	35.55	129.0	17.31	1.95	10.12	6.33	1.28	2.92	1.98
RK60	123.47	213.98	26.05	97.31	13.6	1.86	8.42	5.65	1.16	2.72	2.07
RK62	116	194.94	23.81	88.62	12.45	1.98	7.69	5.29	1.07	2.66	2.18
BREKKERISTA GRANITE											
BK28	124.36	206.18	21.39	72.48	10.99	2.14	8.51	8.81	1.87	4.94	4.87
BKA	141.3	248.35	27.4	100.67	16.7	3.71	13.78	15.5	3.3	9.17	8.84

Table 7.9. REE chemistry (ppm) of the Jutulrora, Brekkerista and Roerkulten Granites.

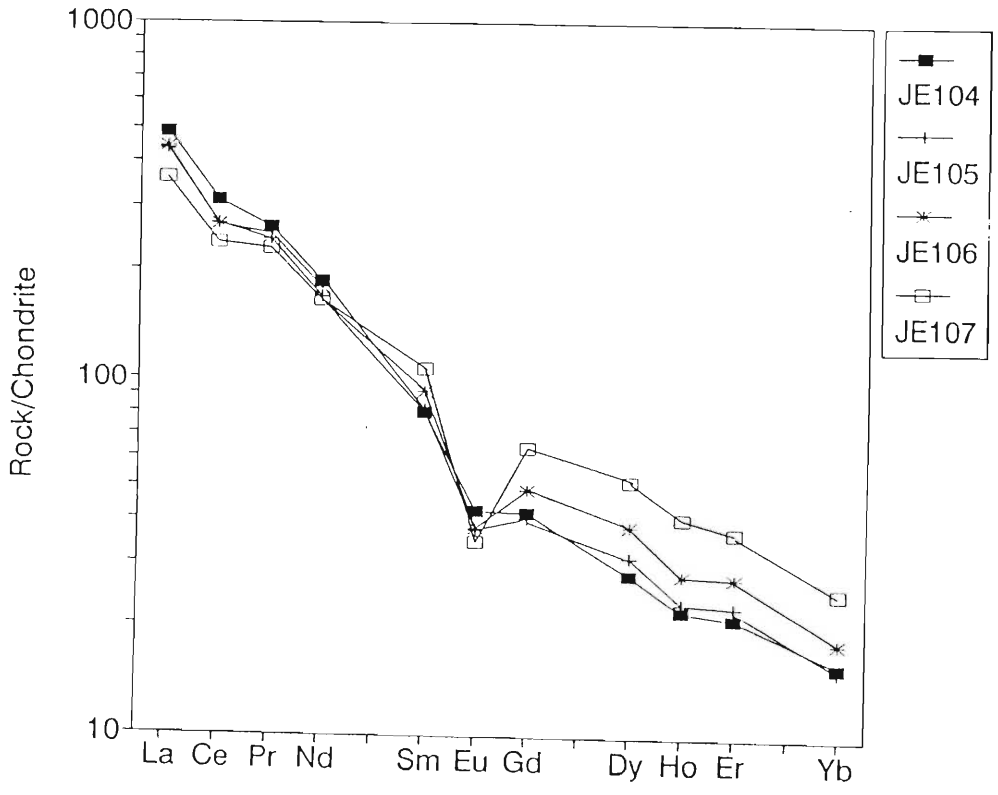

Figure 7.11 Chondrite normalised REE patterns for the Jutulrora Granite.

The light REE (La, Ce, Pr, Nd and Eu) except Sm, increase upwards whereas the heavy REE (Gd, Dy, Ho, and Er) and Sm decrease sympathetically. Yb values also increase from the top to the base of the sheet except for sample JE105.

The systematic variation shown by samples JE104, JE105, JE106 and JE107 may reflect crystal fractionation of a single body of magma or multi-phase intrusion of different magmas to form the sheet-like body. The regular trends shown by major, trace and RE elements do not support the latter suggestion. The possibility of crystal fractionation controlling the REE variation will be explored in the next chapter.

Roerkulten Granite

The three REE patterns in the Roerkulten Granite are broadly parallel and steep with La_{cn}/Yb_{cn} ratios between 58 (RK58) and 34 (RK62) (Fig. 7.12). All three samples show pronounced negative Eu anomalies. Contents of REE decrease from sample RK58 to RK62 except Eu and Yb. Sample RK60 is partially altered and this alteration appears to manifest itself in certain of the major and trace elements.

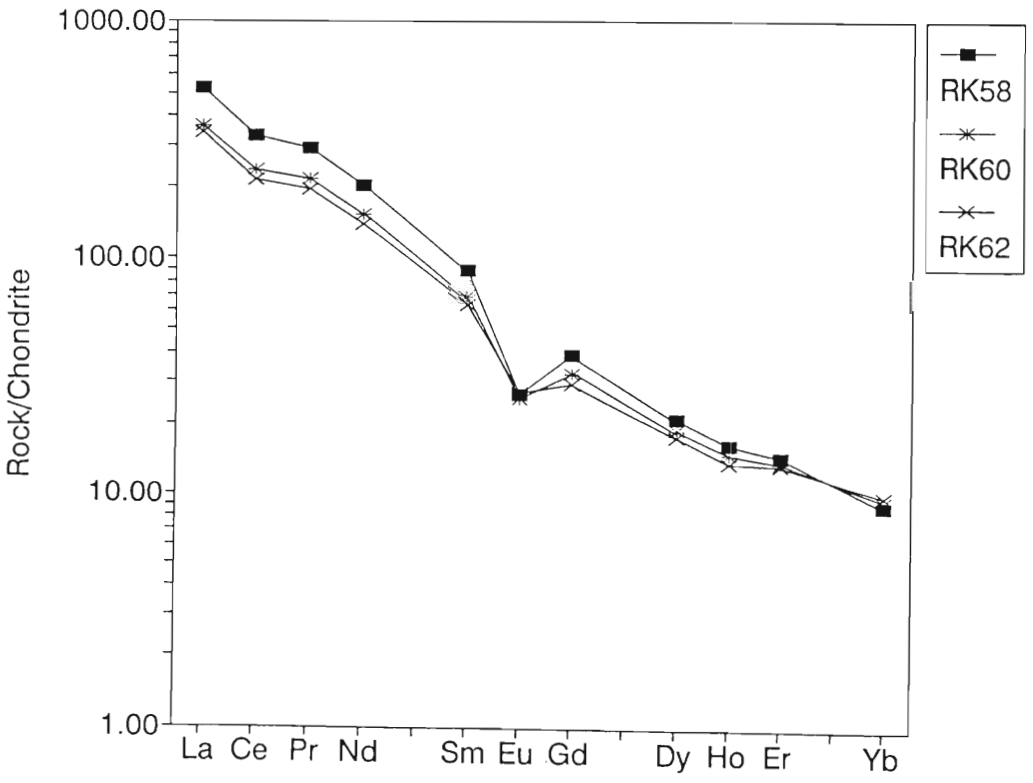

Figure 7.12 Chondrite normalised REE patterns for the Roerkulten Granite sheet.However, the REE pattern for RK60 does not show obvious differences compared to RK58 and RK62 suggesting that the alteration did not noticeably affected the REE content.

Brekkerista Granite

The Brekkerista Granite is characterised by steep LREE (La_{cn}/Sm_{cn} = 4.85-6.48) and relatively flat HREE (Dy_{cn}/Yb_{cn} = 1.29-1.33) patterns with small negative Eu anomalies (Fig. 7.13). The Brekkerista Granite has flat heavy REE patterns that contrast with the steeper slopes in the Roerkulten and Roerkulten Granites. This difference may be due to the common presence and sphene in the Brekkerista granite.

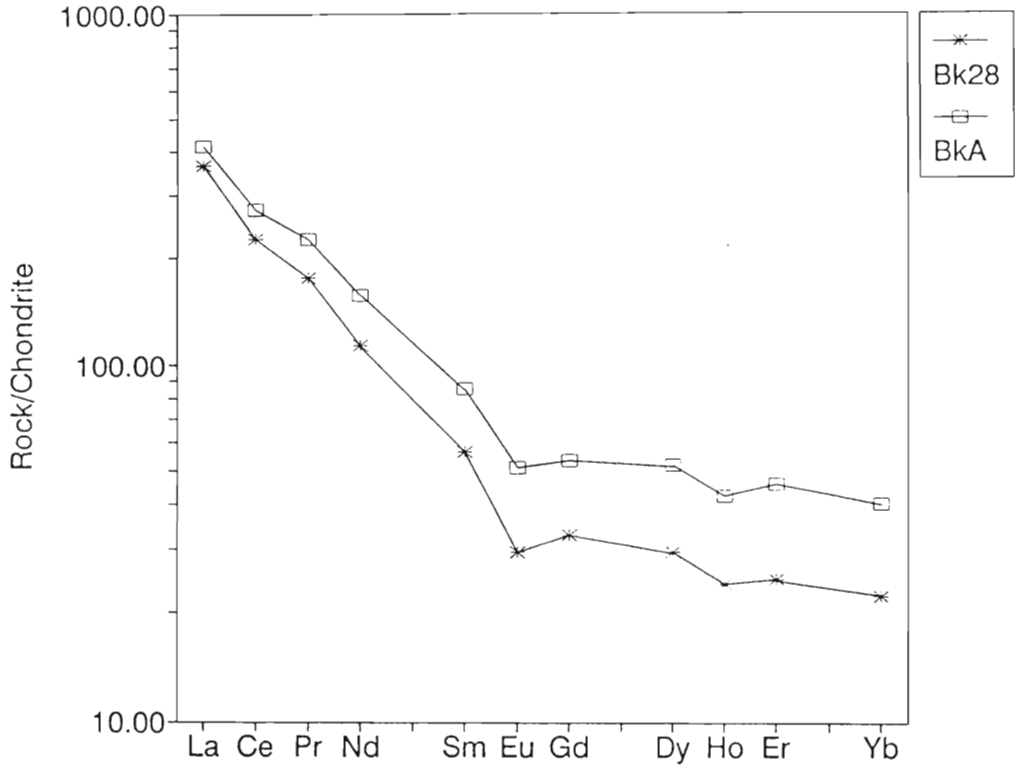

Figure 7.13. Chondrite normalised REE profiles for the Brekkerista Granite.

CHAPTER 8
THE GENERATION AND CRYSTALLISATION OF THE JUTULRORA, ROERKULTEN AND BREKKERISTA GRANITES

GENERATION OF THE GRANITES

Nature of the sources of the granites

Recent studies have attempted to relate granites to various types of source material (Louiselle and Wones, 1979: White, 1979; Chappel and White, 1974; Chappel *et al.*, 1987). These authors maintain that differences in granites may be related to their source material allowing recognition of I- type (derived from igneous sources) and S-type granites (derived from sedimentary sources, Chappel and White, 1974), A-type (anorogenic, Louiselle and Wones, 1979; Creaser *et al.*, 1991) and M-type (mantle derived, White, 1979). The characteristics of the various types are summarised as follows (Pitcher, 1982; Clarke, 1992):

1. I-type granitoids have $Na_2O > 3.2\%$ in felsic varieties, Mol $Al_2O_3/(Na_2O + K_2O + CaO)$(A/CNK) < 1.1, C.I.P.W. normative diopside or $< 1\%$ corundum, felsic to mafic range of compositions, regular inter-element, linear or near-linear variations, Sr^{87}/Sr^{86} (R_o) = 0.704 - 0.706 and are generally hornblende-bearing and commonly sphene-bearing.

2. S-type granitoids have $Na_2O < 3.2\%$ in rocks with approx 5% K_2O A/CNK > 1.1, $> 1\%$ C.I.P.W. normative corundum, restricted in composition to high SiO_2, variation diagrams more irregular, $R_o > 0.708$ and commonly contain muscovite, biotite and monazite. Alumino-silicates such as garnet/cordierite may be present.

3. M-type granitoids have A/CNK < 1.0, $R_o < 0.705$, hornblende, biotite or pyroxene-bearing.

4. A-type granitoids have A/CNK > 1.0, R_o = 0.703 -0.712, are characterised by low CaO, high Fe/Mg, enrichment in high field strength elements (HFSE; Ta, Nb, Zr) REE (and F), are anorogenic in their tectonic setting and contain green biotite, alkali amphiboles and alkalic pyroxenes. A-type granites are considered to have been water undersaturated and consequently generated at relatively elevated temperatures; the higher temperatures contributing to greater dissolution of the HFSE.

Table 8.1.Properties proposed for discrimination of between various granites.

	I-type	S-type	M-type	A-type
Na_2O >3.2%	B			
Na_2O <3.2%		R,J		
A/CNK <1.1	R,J,B			
A/CNK >1.1			R,J,B	
A/CNK <1.0		R,J		
Normative Crn				
Normative Di				
Mineralogy				
Hbl	R,J			
Bt		B,R,J	B,J,R	
Spn	J,B,			
Pyx				
Cd				
Grt		R,J		
Ms				
Regular inter-element ratios	R,J,B			
Restricted high SiO_2		R,J,B		
R_o $^{87}Sr/^{86}Sr$ 0.704 - 0.706				
R_o $^{87}Sr/^{86}Sr$ >0.708	R			
R_o $^{87}Sr/^{86}Sr$ <0.705				
HFSE				R,J,B

Table 8.2. Summary of characteristics of the Brekkerista (B), Jutulrora (J) and Roerkulten (R) Granites.

The various granites of the H.U. Sverdrupfjella display a combination of I-type, S-type and A-type characteristics (table 8.2). The mean values for A/CNK for the three granite bodies are between 1.0 and 1.1 however some samples in all three granites have values <1.0 and therefore also show M type characteristics. Whereas these characteristics may have served as a useful basis for distinguishing various granites studied by Chappel and White (1974), application to the granites of the NW. H.U. Sverdrupfjella does not permit the distinctions made by these authors. Asmeron *et al.* (1988) have shown that S-type granites may be derived by partial melting of I-type granitoids and thus the connotations of source attached to S- and I-type granites may be incorrect. Alternatively, the recognition of both I and S type characteristics may indicate a heterogenous source for the granites.

Creaser *et al.* (1991) and Clarke (1992) have questioned the A-type classification because the I, M and S granite classification conveys genetic information. The A-type classification describes characteristics of the magma and also identifies a specific anorogenic tectonic environment. Clarke (1992) states that the classification system does not take the effects of igneous differentiation or sub-solidus alteration into account and further points out that "Given the chemical and genetic complexity of the crust, granitoids with hybrid sources must be the rule".

Physical conditions of granite petrogenesis

Temperature of Magma

The results of experimental work on the solubilities of P and Zr in acid lavas (Watson, 1979a; Watson, 1979b; Watson and Harrison, 1983) have indicated that the solubilities of Zr and P are dependant on temperature and the bulk composition of the magmas. These authors have calibrated the following thermometers based on the solubilities of these elements :- for Zr contents $\ln D_{Zr}^{zircon/melt} = (-3.80-(0.85(M-1))) + 12900/T$ where $D_{Zr}^{zircon/melt}$ is the concentration ratio of Zr in stoichiometric zircon to that in the melt, T is the absolute temperature and M is the cation ratio (Na + K + 2Ca)(Al x Si) and for P $\ln D_{P}^{apatite/melt} = ((8400 + (SiO_2-0.5)2.64 \times 10^4))/T)-(3.1 + (12.4(SiO_2-0.5)))$ where SiO_2 is the weight fraction in the melt and $D_{P}^{apatite/melt}$ is the ratio of P in stoichiometric apatite to that in the melt. Comparison of the temperatures provided by the Zr solubility with those yielded by thermometry using opaque mineralogies yield similar values (Nash and Crecraft, 1985). Ellison and Hess (1986) have also found the Zr solubility-based temperatures to be reliable. Mendonides and Grantham (1989) have found temperatures calculated from the P contents in charnockites to be comparable with those yielded by two-pyroxene thermometry. Interpretation of the temperatures is dependant on the nature of the zircon and apatite in these granitoids. Rocks which are not saturated with regard to either Zr or P will yield anomalously low temperatures whereas those rocks which contain inherited or xenocrystic (undissolved) zircon or apatite will be saturated and will yield temperatures which are anomalously high. Application of these solubility calculations to granitic rocks is based on the assumption that there is no significant crystal settling in granitic intrusions and, secondly, that crystallisation in such magmas is likely to be eutectic ie. involving all phases.

It was noted in chapter 7 that zircon and apatite in the Roerkulten and Jutulrora Granites appear to have crystallized relatively early suggesting that the magma was saturated with regard to these elements. Application of these thermometers to the Roerkulten Granite (eastern sheet) provide almost identical temperatures (876°C for Zr and 866°C for P, average of 10 samples for Roerkulten Granite and 836°C for Zr and 885°C for P for the Jutulrora Granite, average of 6 samples). These temperatures are higher than those normally considered for granitic liquids, however it is unlikely that the high temperatures are the result of xenocrystic zircon and apatite because the chance of xenocrystic inclusions co-incidentally providing similar temperatures is small.

Application of the saturation surface thermometers of Watson and Harrison (1983, using Zr) and Harrison and Watson (1984, using P contents) to the Brekkerista Granite yield average temperatures of 839°C and 976°C, respectively. Whereas the similarity of temperatures for the Jutulrora and Roerkulten Granites suggest that the temperatures may be valid, the higher

temperature suggested by P for the Brekkerista Granite would appear to be anomalous and suggests that apatite may be a xenocrystic phase in the granite.

Comparison of the C.I.P.W. normative compositions of the Brekkerista Granite with compositions derived from minimum melt compositions (Fig. 8.1), shows that the Brekkerista Granite plots between the loci for minimum melts with Ab/An = infinity and Ab/An = 2.9, with $pH_2O = P_{load}$ (Fig. 8.1). The mean Ab/An ratio of the Brekkerista Granite is 2.83. The position of its field suggests that the Brekkerista Granite had a relatively high pH_2O.

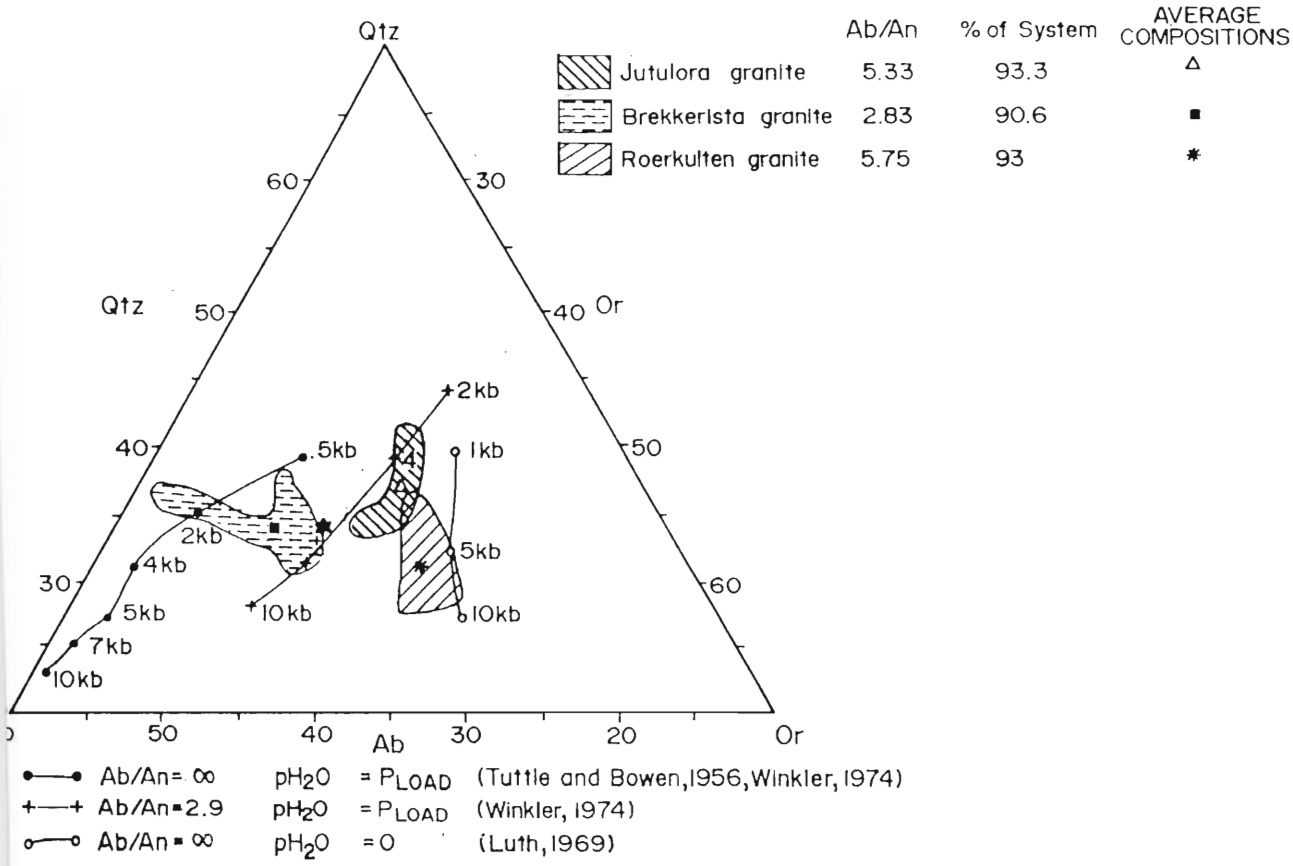

Figure 8.1. The composition of the samples of Brekkerista, Jutulrora, and Roerkulten Granites in terms of minimum melt experiment compositions. Data for the various points are from Tuttle and Bowen (1958), Luth(1969), Winkler (1976, pp. 290).

The compositions of the Brekkerista Granites vary greatly and thus no estimation of pressures of formation can be made except noting that the average for the samples suggests approximately 6kb. The apparently high pH_2O and high temperature (suggested by Zr thermometry) suggests that the Brekkerista Granite cannot be viewed as a minimum melt. This conclusion is supported by its porphyroclastic nature which implies that orthoclase was on the

liquidus prior to other minerals.

Comparison of the C.I.P.W. normative quartz, orthoclase, and plagioclase contents of the Jutulrora and Roerkulten Granites with minimum melt compositions (Fig. 8.1) shows that the compositional fields of the Jutulrora and Roerkulten Granites lie between Ab/An = 2.9 with $pH_2O = P_{load}$ and Ab/An = infinity with $pH_2O = 0$ (Fig. 8.1). This suggests that both these granites had pH_2O contents less than P_{load}, supporting the relatively high temperatures calculated by Zr and P thermometry. The average composition of the Jutulrora Granite suggest a pressure of approximately 3kb. The average composition of the unaltered samples of the Roerkulten Granite implies a high pressure of ~6kb. The data in figure 8.1 points to generation of the Roerkulten Granite at a significantly greater pressure or depth than the Jutulrora Granite and Brekkerista Granites.

Partial melt modelling

It is possible to model the potential sources of granitic magmas utilising the melting model of Arth (1976). Requirements of such models are (1) an estimate of the mineralogy of the source rocks, (2) the degree of melting, and (3) a knowledge of the K_ds of the elements in minerals likely to be residual phases.

Various types of melting have been postulated (Arth, 1976), the simplest being equilibrium melting which assumes that the restite will be in equilibrium with the partial melt until the magma is separated from the source. In equilibrium melting the following assumptions are made: (1) constant mineral proportions in the residue (modal melting), and (2) constant partition coefficients during melting. Haskin (1984, pp.127) has expressed the opinion that melting processes will approximate equilibrium conditions only for small degrees of partial melting.

Whereas it is not possible to identify the source of the granitic magmas, various rock compositions can be tested to determine whether they are suitable parental material. Other factors which have to be considered are the mineralogies of the source regions and the degrees of partial melting necessary before magmas may be separated from their sources. Possible potential sources for the tabular granitoid intrusions include the Grey Gneiss Complex and the Banded Gneiss Complex.

In selecting a possible source, the average composition of the Grey Gneiss Complex will be used for the following reasons:- (1) the Grey Gneiss constitutes a significant proportion of the older (i.e. pre-granite) basement exposed in the area, (2) the Grey Gneiss is fairly uniform, and (3) data are available for the trace element contents including REE analyses of five samples of the Grey Gneisses and associated rocks. Furthermore, the Grey Gneiss is intermediate in composition and as such could be viewed as approximating a mixture between basic and acid end members.

Partial melting is commonly assisted by the presence of H_2O which is released into the fluid

phase during the dehydration reactions which characterise the transition from amphibolite or medium-grade metamorphism to granulite or high-grade metamorphism. Thus it is reasonable to postulate that the residual phases of partial melting will be largely anhydrous in such cases. The catanorm mineral proportions of the average chemical compositions of the Grey Gneiss Complex will be used as a restite composition because the catanorm is anhydrous and yields mineral proportions based on cation percent and not weight percent. These mineral proportions are presented in table 8.3 together with partition coefficients for the elements constituting the main minerals. Two alternative sources will be considered in the partial melt models. Model A (table 8.3) is calculated with a source consisting of quartz, orthoclase, plagioclase, orthopyroxene, clinopyroxene and magnetite whereas in model B proportions of apatite, zircon and sphene have been included in the source assemblage. The proportion of sphene is estimated using the mesonorm. A comparison of models A and B allows a study of the influence of accessory minerals on partial melt models.

	MINERAL PROPNS. %		PARTITION COEFFICIENTS %									
PHASE	A	B	K_2O	Rb	Ba	Th	Nb	Ce	Zr	Sm	Y	Yb
Qtz	13	11	.011	.016	.015	.01	.001*	.018	.38	.004	.001*	.024
Pl	52	51.38	.19	.09	.5	.04	.01	.24	.1	.13	.1	.08
Kfs	17	17	1.4	.38	6.6	.1	.01*	.04	.06	.02	.1*	.012
Opx	13	13	.002	.09	.02	.02	.15	.46	.2	.7	.9	.34
Cpx	3	3	.002	.09	.02	.13	.1	.9	.6	2.7	4	2.1
Mag	2	2	.001*	.8*	.07	.11	.4	.61	.1	.9	2	.4
Ap		0.6	.001*	.001*	.001*	.001*	.001*	53	.1	63	40	24
Zr		0.02	.001*	.001*	.001*	1.0*	.001*	4.2	280	3	60	280
Spn		2	.001*	.001*	.001*	.001*	7.6	80	.01*	150	1	100

Table 8.3 Table showing the mineral proportions calculated for the restite in models A and B as well as the partition coefficients used. * denotes an assumed value. The sources of all other partition coefficients are given in Appendix 3.

Wickham (1987) suggests that at least 30% partial melting is required to generate sufficient granitic magma to permit extraction from its parent.This is because of the viscous nature of granitic magmas and the increased porosity resulting from higher proportions of intergrain melt. Thus the models of partial melt compositions of the Grey Gneisses presented below show the range of compositions resulting from a minimum of 30% partial melting to 90% although the latter is most unlikely in nature. The elements modelled are those used in spider diagrams by Pearce *et al.* (1984) and for which data are available for the various Sverdrupfjella granites.

In figure 8.2 the ocean ridge granite (ORG)(Pearce *et al.* 1984) normalised compositions of partial melt arising from 30%, 60% and 90% melting of source compositions A and B are shown.

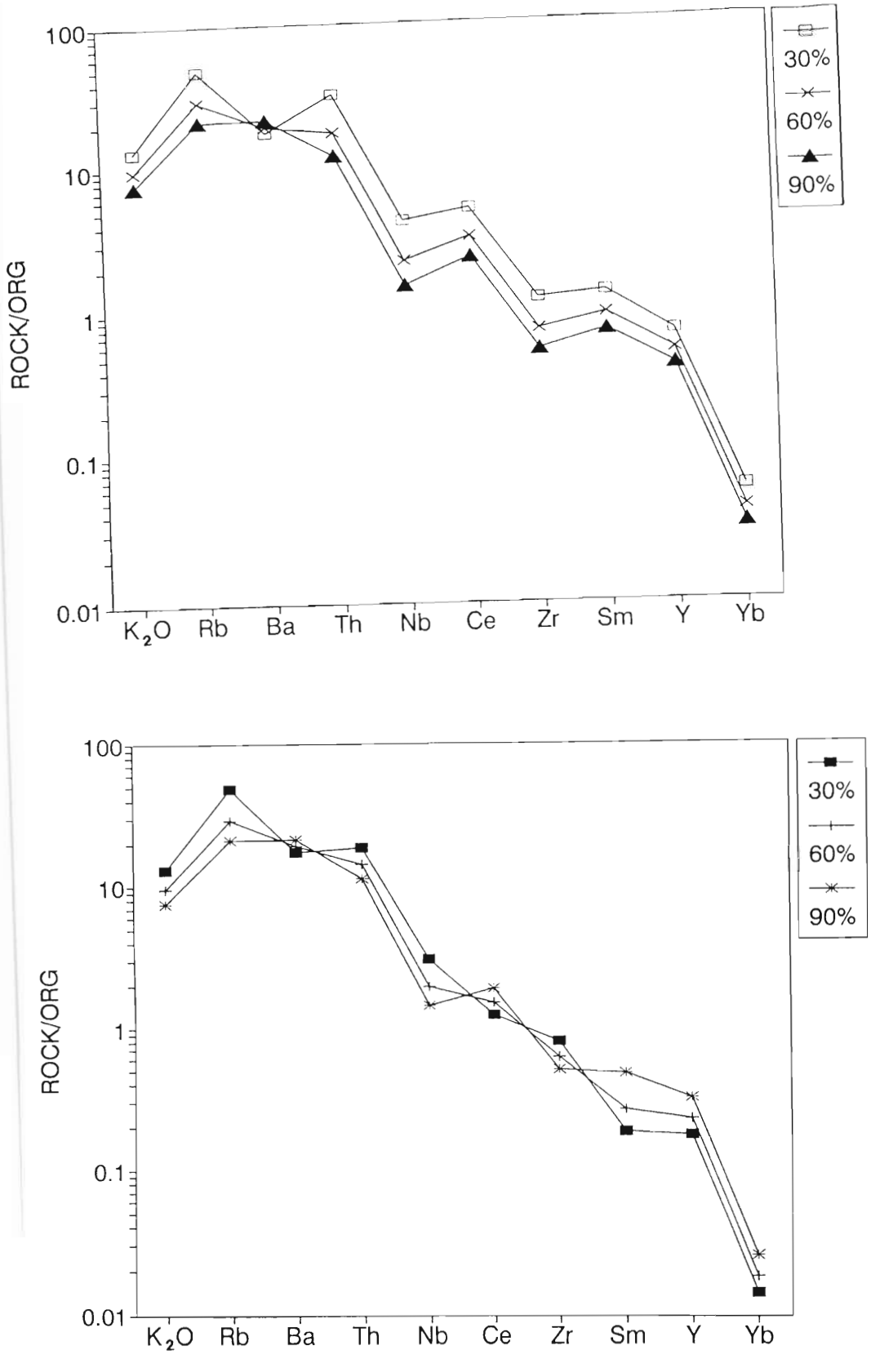

Figure 8.2. ORG normalised partial melt models of average compositions of the Grey Gneiss Complex. The differences between model A (above) and B (below) are explained in the text.

No differences between the models is seen for K_2O, Rb, Ba and Th but model B, which includes accessory minerals in the restite, shows significant differences in Ce, Sm and Yb contents with smaller differences in Zr and Y contents. Model B is considered to be more realistic because it includes accessory minerals in the source. Model A could represent the compositions generated if the partial melt is not in contact with the accessory minerals. Models A and B will now be compared with the ORG-normalised compositions of the Jutulrora, Brekkerista and Roerkulten Granites.

Comparison of the mean ORG-normalised patterns for the Roerkulten, Jutulrora and Brekkerista Granites shows that broadly, they are similar with minor differences (Fig. 8.3). Differences between the Jutulrora and Roerkulten Granites are higher Ba and Nb and lower Zr in the former.

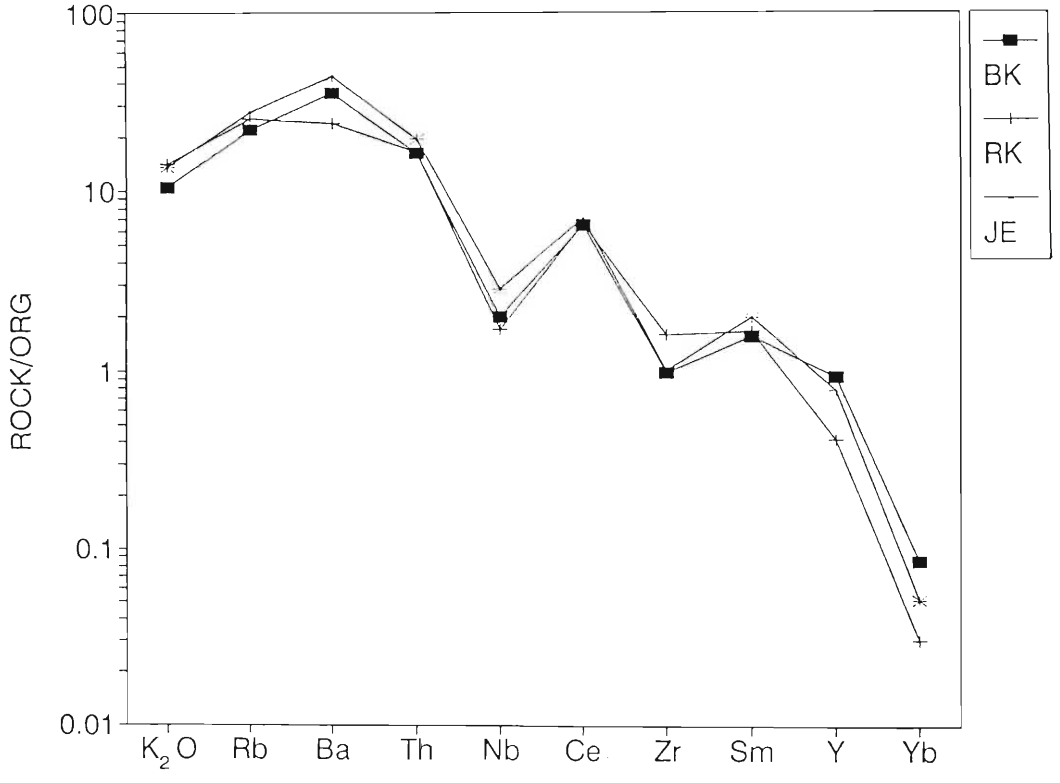

Figure 8.3. Mean ORG-normalised patterns for the Roerkulten, Jutulrora and Brekkerista Granites.

Differences between the Jutulrora and Brekkerista Granites are higher K_2O, Rb, Sm and Nb in the former. The minor extent of these differences may suggest that the sources of the granites were similar and that the differences are the result of processes after the granites migrated from their sources.

Discussion of partial melt models

The modelled patterns are plotted with the patterns for the Jutulrora, Roerkulten and Brekkerista Granites for comparison in figures 8.4, 8.5, and 8.6 respectively. For all three granite partial melting of between ~30% to 60% satisfies most of the elements under consideration except in model B where the Ce, Sm and Yb values are significantly lower than the analyzed concentrations. This would suggest that the accessory phases which were assumed to form part of the residue in model B did not remain in the residue and could have been incorporated in to the melt.

An unsatisfactory aspect of both models is that both models have Ba/Th ratios <1 (ie. ORG-normalised) at reasonable degrees of partial melting (~30%) whereas all three granites have Ba/Th ratios >1. The variation of Ba in the partial melt models is controlled by the relatively high proportion of orthoclase postulated to be present in the source coupled with the high K_d (6.6) for Ba in orthoclase. The assumption of equilibrium or modal melting is simplistic in this case because orthoclase is likely to be completely melted and therefore will not form part of the residue.

CRYSTALLISATION OF THE GRANITES

The aim of this section is to determine to what extent the systematic variations, described in chapter 7, may be ascribed to igneous crystallization. Hildreth (1981) presents strong evidence for vertical zonation in volcanic magma chambers and suggests that granite plutons may be zoned in a similar fashion. However, the tabular Jutulrora and Roerkulten Granites are only approximately 120m thick. The highly viscous nature of granitic magma (McKenzie, 1985) is likely to have prevented crystal fractionation. It is unlikely that this process contributed greatly to chemical variations in a relatively small granitic body. Any observed geochemical variations may instead reflect local temperature differences and/or chemical gradients.

Various models of crystallization are considered. Equilibrium crystallization assumes that after a mineral has crystallized from a magma the mineral remains in equilibrium with the melt. This model is clearly unrealistic because zoning in minerals demonstrates that it is unlikely that minerals maintain equilibrium with the magmas from which they crystallized. Rayleigh crystallization, on the other hand, assumes that once a phase has crystallized it is removed from the magma and no longer interacts with the magma (see McCarthy and Hasty, 1976, Tindle and Pearce, 1981). The high viscosity of acid magmas (McKenzie, 1985) implies that it is unlikely that minerals which have crystallized from granitic magmas will settle out to any great degree. Equilibrium crystallization results in the least degree of fractionation whereas Rayleigh crystallization results in the highest degree of fractionation.

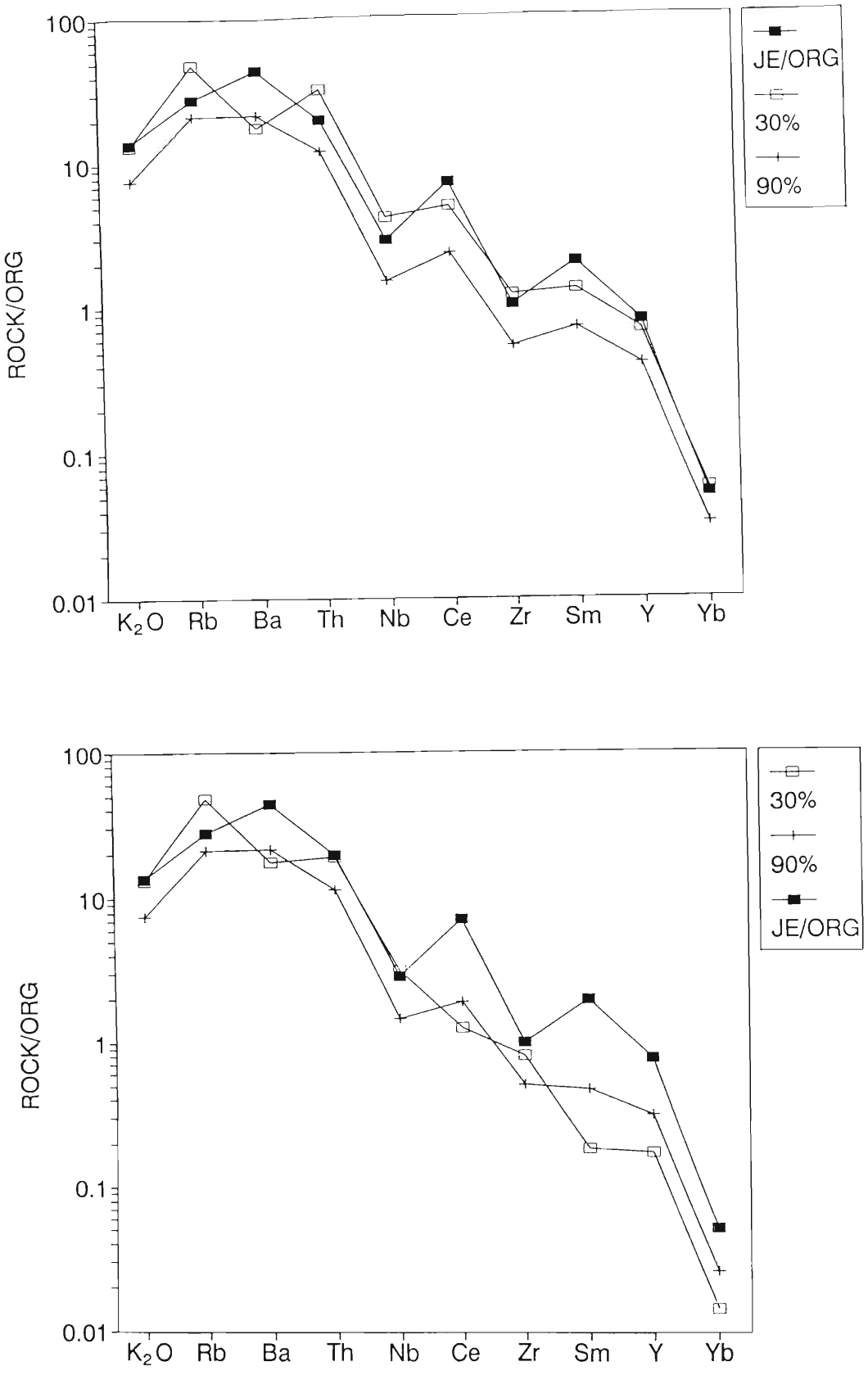

Figure 8.4 Mean ORG-normalised profile of the Jutulrora Granite compared to the partial melt models. Model A above and B below.

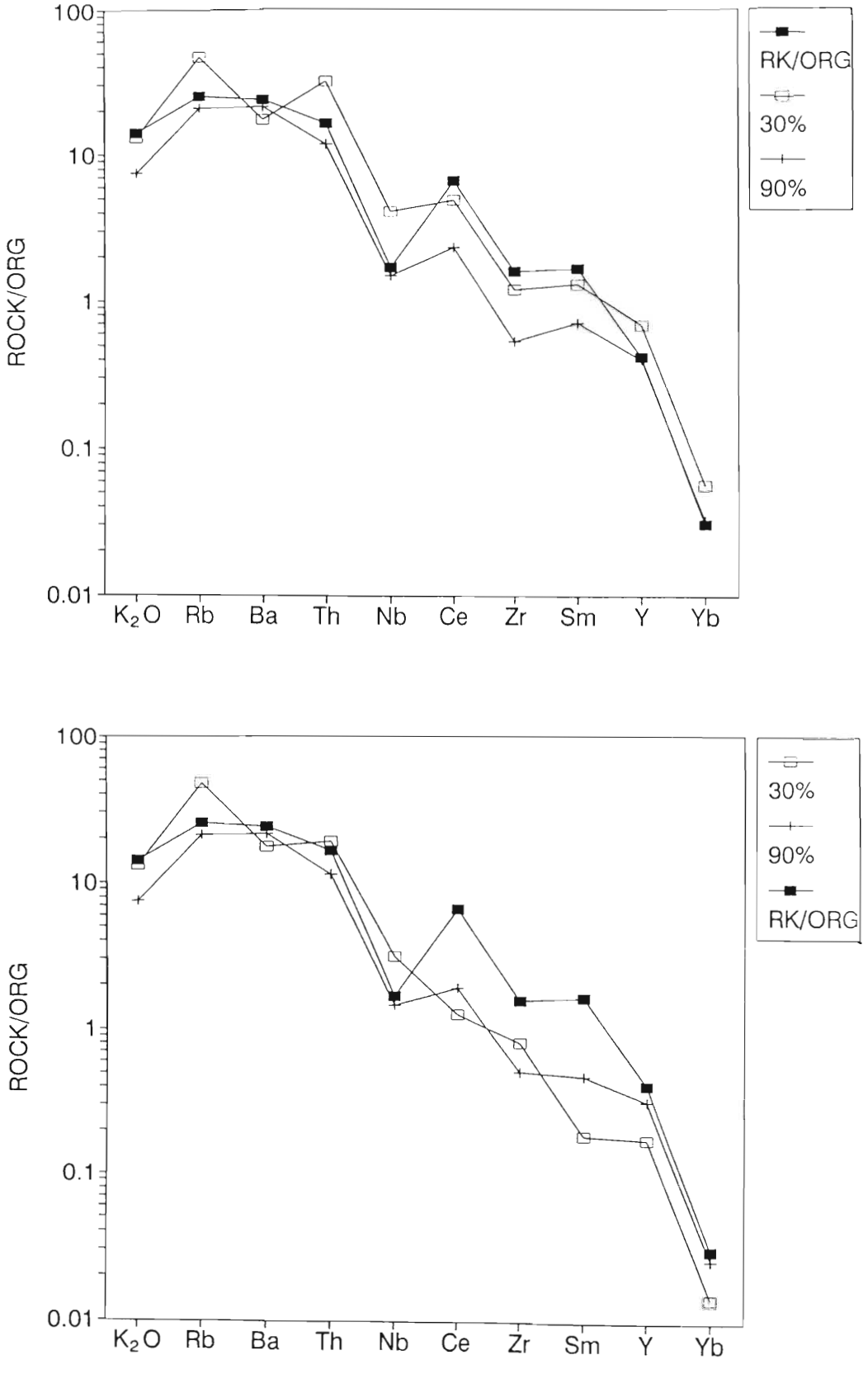

Figure 8.5 Mean ORG-normalised profile of the Roerkulten Granite compared to the partial melt models. Model A above and B below.

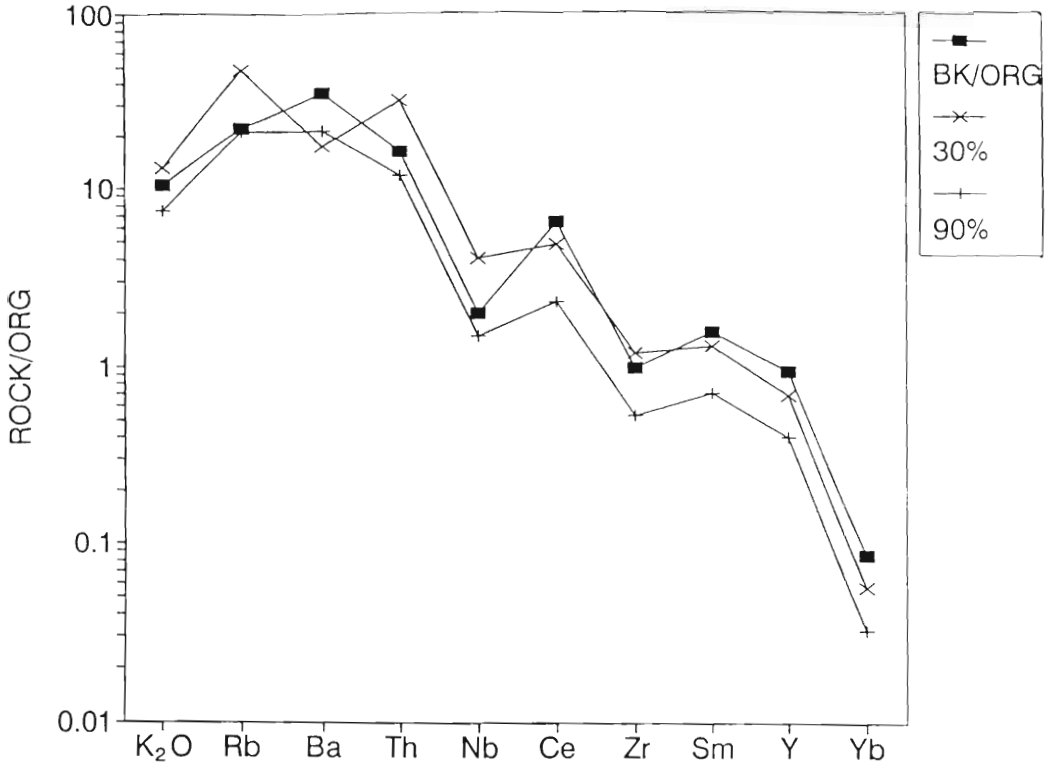

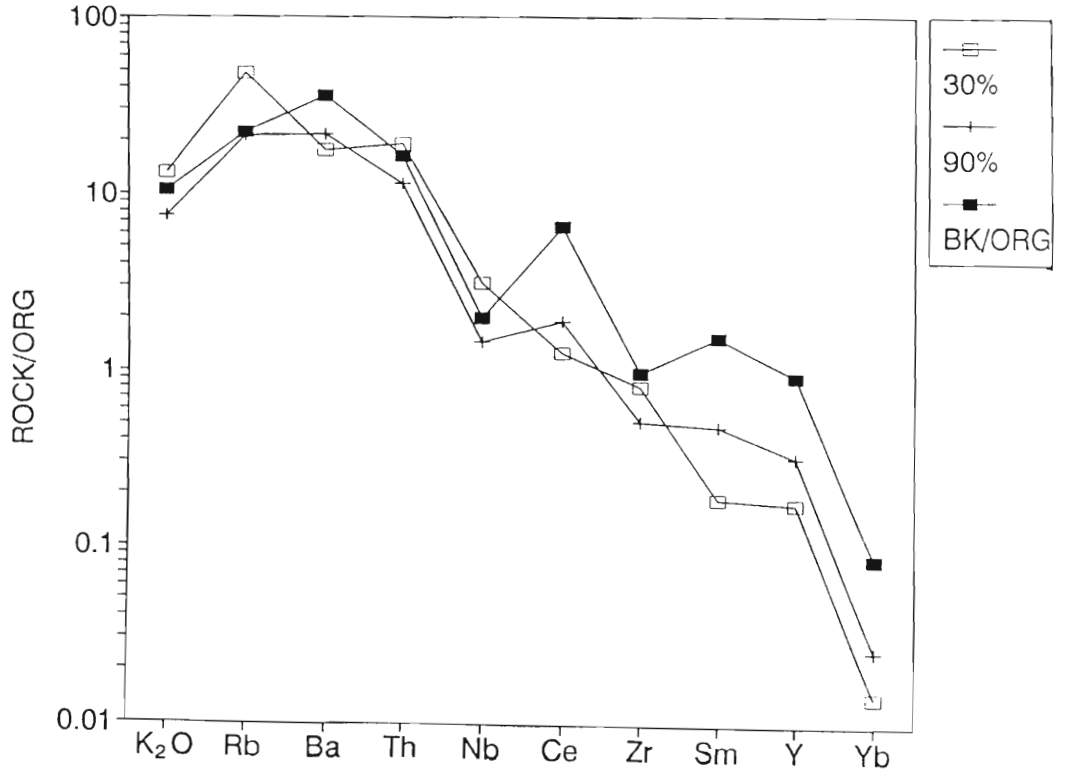

Figure 8.6. Mean ORG-normalised profile of the Brekkerista Granite compared to the partial melt models. Model A above and B below.

McCarthy and Hasty (1976) developed an incremental fractionation model which results in intermediate degrees of fractionation and therefore may approximate granitic magmas more closely than either the equilibrium model or the Rayleigh model. The incremental fractionation model is used here unless stated otherwise.

Before the models are discussed, it is necessary to briefly consider the requirements of, and assumptions made during, modelling. The requirements of the modelling may be summarised as follows:-

(1) a knowledge of K_ds for the various elements in the minerals fractionated.

(2) a reasonable estimate of the initial composition of the magma fractionating.

(3) a reasonable estimate of the proportions of the minerals which crystallized.

Regarding the first requirement, published data for K_ds for most elements in most common rock-forming minerals are available for acid to mafic magmas. However, the data for accessory minerals are less complete. Another problem regarding K_ds is that they are calculated from mineral/matrix pairs in volcanic rocks and thus their applicability to deep-seated plutonic rocks can be questioned.

For the Roerkulten and Jutulrora tabular Granites, samples taken closest to the opposing contacts with the country rock were considered as possible starting compositions. This assumption is made in the absence of a better alternative. In the case of the Brekkerista Granite an average content is utilised merely to determine whether the element in question was compatible or incompatible during crystallization. The estimate of mineral proportions is relatively easy for the common rock-forming minerals where point- counting yields reasonable estimates. However, the margins of error for point-counts for accessory minerals are very high. To overcome this problem, the estimates used here are based on catanorm and mesonorm calculations. The catanorm is used in preference to the C.I.P.W. norm because it is calculated on a cation basis in contrast to the C.I.P.W. which is calculated on a weight percent basis. Calculations on a weight percent basis would tend to overestimate the proportions of minerals with higher than normal specific gravities eg apatite, zircon and opaque minerals. The mesonorm also has the advantage of calculating biotite, amphibole, and sphene.

Modelling was based on the following assumptions that:-

(1.) the proportions of phases crystallising remained constant,

(2.) the mineral/matrix K_d's remained constant during crystallization, and

(3.) the deformation and metamorphism which have affected the granites have not materially altered the trace element and REE distributions used in the modelling.

The assumptions are clearly simplistic. Assumption (1.) relies on crystallization of constant mineral proportions and ignores possible fluctuations in pressure and fluid phases, both of

which may affect the mineral proportions crystallizing. During crystallization, the phases crystallizing are unlikely to remain constant except possibly under eutectic or minimum melt type compositions. Fortunately, crystallization in granites is most likely to approximate eutectic conditions. Another uncertainty arises from the fact that xenocrystic phases may be present in the granite magmas.

Assumption (2.) is questionable in that work by Watson (1978) and Green and Pearson (1986) amongst others have shown that K_d's are affected by temperature and liquid compositions and hence are liable to vary during crystallization. The compositions of phases which involve solid solutions eg. plagioclase, amphiboles, biotite etc. also commonly show varying K_d's. Where possible, these factors were taken into account when K_d's were selected. Assumption (3) is based on the observation that texturally the granites display many igneous characteristics and thus it appears that the mineral phases present appear to be largely primary. Such an interpretation does not however preclude the diffusion of elements like Rb, Sr, K, Na subsequent to crystallization.

REE modelling

The K_d's used for the REE modelling are shown in table 8.4. In selecting values for K_d's, values recorded from acid rocks were chosen where possible.

Jutulrora Granite

The mesonorms and catanorms of the Jutulrora Granite are shown in table 8.5. These values may be compared with the values used in the modelling (table 8.6). Not all the minerals present in the Jutulrora Granite are calculated in the mesonorm or catanorm (eg. allanite, hornblende) and therefore the contents of these minerals were estimated in the following manner.

The allanite content is estimated at approximately 1% because in thin section it is seen that the allanite content slightly exceeds that of sphene. The hornblende content is estimated to be twice that of mesonormal biotite.

In figure 8.7 four models of REE distributions are presented to explore the possibility that fractionation of some or all of the minerals present in the Jutulrora Granite could result in chondrite-normalised REE patterns reported in Chapter 7 (see Fig. 7.11). Figures 8.7a-c present the results of incremental fractionation of a granitic assemblage using K_d's and mineralogies given in table 8.4 and 8.6, respectively. Models 8.7a and 8.7b are based on fractionation of the same mineral proportions (model 1, table 8.6) but using the REE content of JE104 as a starting composition for model 8.7a whereas model 8.7b uses JE107 as a starting composition.

Fractionation of minerals in the proportions presented in table 8.6 and using JE104 and

JE107, respectively, as starting compositions results in substantial decreases of all the REE in the residual liquid, particularly the LREE (Fig. 8.7a and 8.7b). These patterns bear no resemblance to Fig. 7.11 and therefore models 8.7a and 8.7b are rejected. In model 8.7c, a proportion equal to that of allanite (1%) is assigned to quartz (model 2, table 8.6) ie. allanite is assumed to be xenocrystic. With this exception the same mineralogy and K_d's are used with the REE content of JE107 as the starting composition.

This model (no.2, table 8.6) generates REE patterns (Fig. 8.7c) similar to the observed patterns (Fig. 7.11). In model 8.7c most of the REE variation may be attributed to the fractionation of sphene because of the high K_d's for REE in sphene (see table 8.4 and appendix 3). However, in model 8.7c allanite is assumed to be xenocrystic and, therefore, the REE contained in the allanite would not have been involved in fractionation.

PHASE	La	Ce	Pr	Nd	Sm	Eu	Gd	Dy	Ho	Er	Yb
Qtz	0.012	0.018	0.018	0.024	0.017	0.08	0.08	0.017	0.017	0.017	0.017
Or	0.1	0.04	0.04	0.03	0.02	1.13	0.07	0.006	0.006	0.006	0.012
Pl	0.49	0.24	0.24	0.19	0.13	2	0.16	0.13	0.05	0.05	0.08
Hbl	0.85	1.2	1.2*	3.2	5.4	3.6	1.1	9	8*	8	6.2
Bt	0.32	0.03	0.38*	0.04	0.39	0.33	0.44	0.1	0.16*	0.16	0.67
Mag	0.88	0.61	0.61	0.88	0.9	0.58	1.9	1.7	1.7	1.2	0.4
Ilm	0.02	9	8	8	8	2	8	7	6	5	4
Ap	21	31	31	50	54	30	22	42	42	31	24
Spn	45	80	80	80	200	180	200	200	200	150	100
Zrn	2*	4.2	4.2*	3.6	3	3	5	48	60*	140	300
Aln	820	635	535*	460	205	80	130	90*	50*	20*	8.9

Table 8.4 Table of the K_d's used in the modelling of the Jutulrora, Roerkulten and Brekkerista Granites. * indicates K_d's values assumed for those minerals. The reference sources for the K_d's are shown in appendix 3.

Several studies have shown that in granitoids, accessory minerals contain most of REE, U, and Th (Fourcade and Allegre, 1981; Gromet and Silver, 1983; Rapp *et al.*, 1986; Harrison and Watson, 1986; Sawka and Chappel, 1988). Thus, xenocrystic accessory minerals may "impose" their distributions on the observed patterns. Noting the high K_d's for REE in allanite (table 8.4 and appendix 3.), it can be deduced that allanite hosts significant proportions of REE and thus, if allanite is xenocrystic, use of the composition of JE107 as a starting composition is invalid.

Figure 8.7d shows the modelled variation of REE resulting from Rayleigh fractionation in a granite crystallizing minerals in the same proportions and K_d's as those used in model 8.7c, with a starting composition the same as JE107. In this model it is assumed that 50% of the REE are contained in xenocrystic allanite. Thus the proportion of REE involved in fractionation is modelled at 50% of the abundance reported for JE107. In model 8.7d it can be seen that the REE patterns are similar to those observed in figure 7.11. As was the case with model 8.7c the REE patterns are greatly influenced by fractionation of sphene resulting in depletion of middle

and HREE with increasing, and therefore incompatible, LREE with fractionation.

MESONORM

	JE50	JE56	JE104	JE105	JE106	JE107	MEAN
Qtz	37.76	32.94	37.61	34.43	31.34	31.36	34.40
Or	29.63	30.55	29.11	29.81	27.35	26.79	29.01
Ab	20.17	22.68	20.92	22.49	23.77	25.22	22.65
An	4.66	5.16	4.17	4.86	7.18	6.76	5.49
Bt	5.15	5.94	5.04	5.58	7.67	6.92	6.08
Mag	0.96	1.16	0.91	1.16	1.35	1.34	1.15
Crn	0.95	0.71	1.56	1.08	0.07	0.77	0.86
Spn	0.61	0.74	0.59	0.49	1.05	0.66	0.69
Ap	0.11	0.13	0.09	0.11	0.19	0.17	0.14

CATANORM

	JE50	JE56	JE104	JE105	JE106	JE107	MEAN
Qtz	34.25	29.36	34.12	30.96	27.56	27.55	30.64
Or	33.41	34.71	32.76	33.72	32.52	31.39	33.09
Ab	21.94	24.59	22.73	24.41	25.81	27.33	24.47
An	5.67	6.34	5.12	5.69	7.56	7.85	6.37
Opx	2.81	3.19	2.74	3.00	3.64	3.80	3.20
Mag	0.71	0.85	0.68	0.86	1.00	0.99	0.85
Crn	0.7	0.36	1.40	0.92		0.48	0.64
Ilm	0.36	0.43	0.34	0.28	0.61	0.38	0.4
Ap	0.12	0.14	0.1	0.12	0.22	0.19	0.15
Di					1.05		0.17
Zrn	0.026	0.033	0.03	0.036	0.035	0.032	0.032

Table 8.5 Mesonorm and catanorm values for the Jutulrora Granite.

PHASE %	Model 1	Model 2
Qtz	30.97	31.97
Or	30	30
Pl	30	30
Hbl	4	4
Bt	2	2
Mag	1.15	1.15
Ap	0.15	0.15
Spn	0.7	0.7
Zrn	0.03	0.03
Aln	1.00	0.00

Table 8.6 Mineral proportions used for modelling the fractionation in the Jutulrora Granite.

Two features of the observed REE patterns are not apparent in the modelled REE distributions in figure 8.7d. The first is that Eu remains compatible in the fractionation model. However, the REE profiles for JE104 and JE107 suggest that Eu behaved incompatibly if JE107 is a valid starting composition because the Eu contents of JE107 are the lowest and increase across the granite sheet. This would imply that the K_d's for Eu, particularly in feldspar, were far lower than published estimates. Moller and Muecke (1984) concluded that melt composition and structure play the major role in determining Eu^{2+}/Eu^{3+} ratios and the partitioning of Eu into mineral phases. These workers attributed anomalously low Eu K_d's to medium- dependent reduction of Eu^{3+} and the formation of stable Eu^{2+}- alumino-silicate complexes in the melt. They stated further that this mechanism does not apply to feldspar-rich melts.

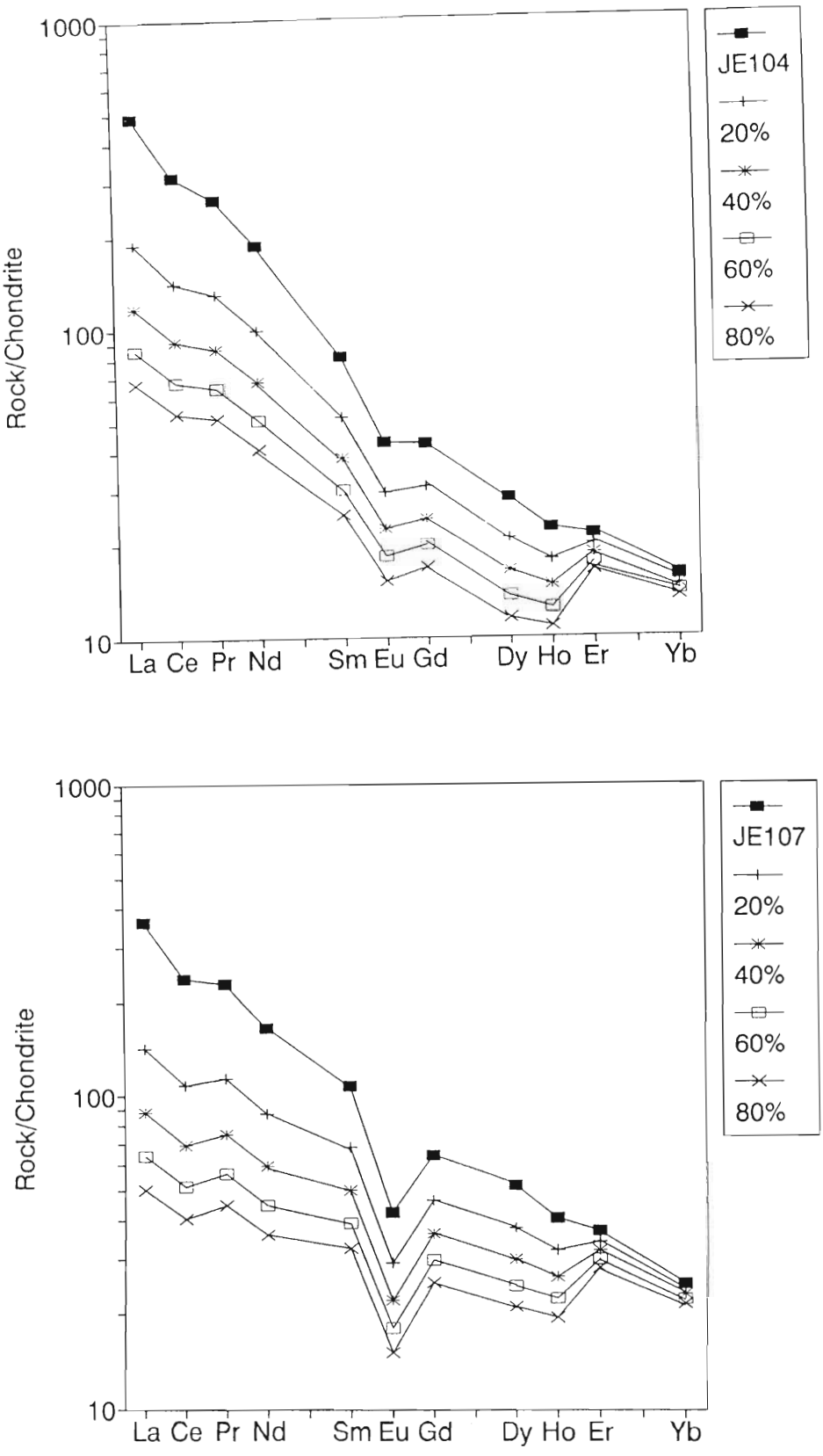

Figures 8.7a (above) and 8.7b (below). Various modelled REE distributions for the Jutulrora Granite. The different models are discussed in the text.

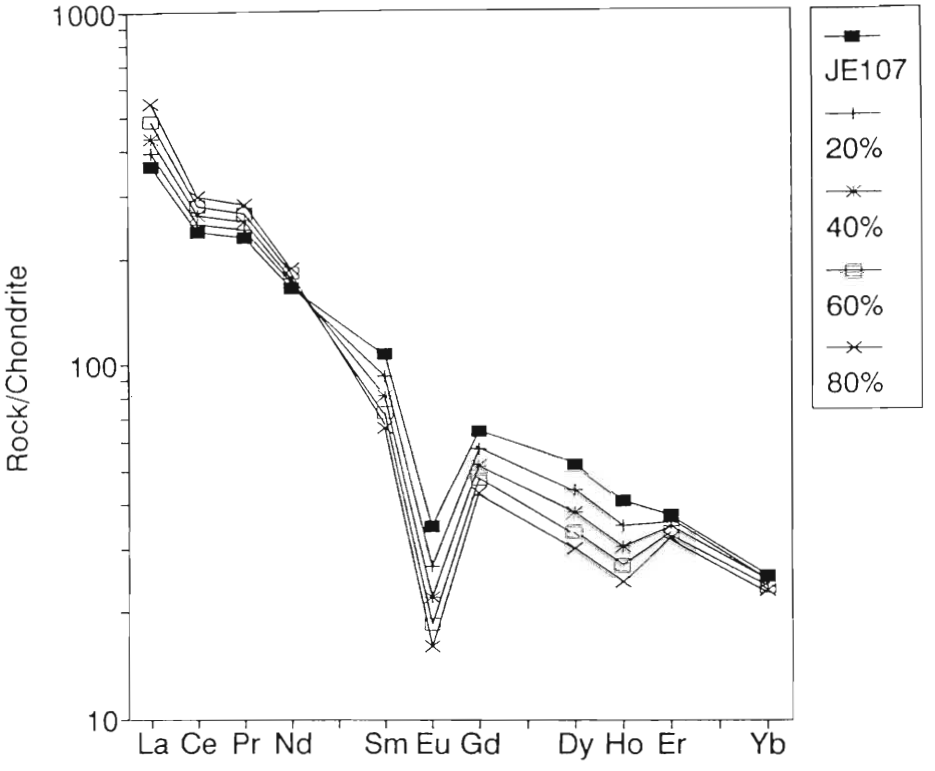

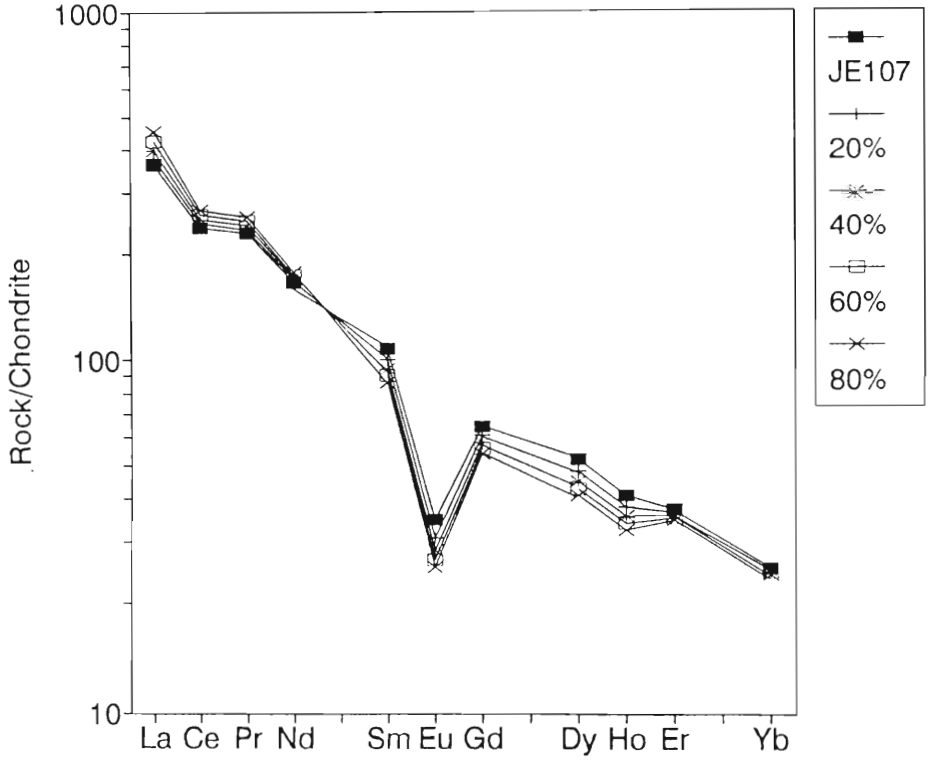

Figures 8.7c (above) and 8.7d (below). Various modelled REE distributions for the Jutulrora Granite. The different models are discussed in the text.

Studies by Drake (1976) and Weill and Drake (1973) have shown that partitioning of Eu into feldspars is affected by the O_2 fugacity of the magma. In relatively O_2- rich magmas Eu is partitioned into the magma whereas under reducing conditions Eu is partitioned into feldspars. Thus K_d's for Eu are subject to great variation because of the effects of O_2, melt composition, and volatile content of the magma (Moller and Muecke, 1984).

The second difference between the model in figure 8.7d and the observed patterns is that the heavy REE (Yb,Er) do not vary in the model to the degree observed in the measured profiles. This suggests that the relatively low K_d's for the HREE in sphene recorded by earlier workers may be in error.

The REE modelling has shown that the observed REE patterns across the Jutulrora Granite sheet could not have resulted from allanite fractionation alone even though the Jutulrora Granite has a significant allanite content (figs. 8.7a&b). The REE variation may have resulted from Rayleigh fractionation of approximately 1% sphene with a significant proportion of the REE in the rock being contained in xenocrystic allanite.

Harrison and Watson (1986) state that the solubilities of many accessory minerals (apatite, zircon, sphene, monazite, allanite and thorite) are low in granitic rocks and dissolve to the limit of saturation in geologically short times. The implication of their work is that these elements may form significant fractions in the restite and also may be xenocrystic in a magma. Rapp and Watson (1986) have shown that the solubility of the LREE in granitic magmas is low and is dependant on the H_2O content and temperature of the magma. The interpreted crystallization sequence for the Jutulrora Granite, like that of the Roerkulten Granite (see later), suggests that hornblende crystallized late, enclosing quartz and feldspars. Wyllie *et al.* (1976) have interpreted such crystallization sequences as evidence that H_2O contents in the magma were low, possibly of the order of 2%.

The saturation surface geothermometers of Watson and Capobianco (1981) and Watson and Harrison (1983), using the P and Zr contents, both suggest magma temperatures of approximately 850°C for the Jutulrora Granite. Rapp and Watson (1986) have shown that granitic magmas at temperatures of approximately 850°C and water contents of approximately 6% and 2% would be saturated with total LREE contents of the order of 400ppm and 150 ppm, respectively.

The Jutulrora Granite has total LREE contents of 495ppm (sample JE 107) thus if the postulated low water content in the granite is valid, a significant proportion of the REE in the Jutulrora Granite may have been contained in xenocrystic allanite.

Roerkulten Granite

Modelling has been undertaken using RK62 and RK58 as starting compositions to determine

whether fractionation may have occurred in the Roerkulten Granite (Figs. 8.8a and 8.8b). The mineralogical composition, presented in table 8.7, is based on catanorm and mesonorm calculations (table 8.8) of the unaltered samples of the eastern Roerkulten Granite Sheet. The proportion of allanite was estimated. The equilibrium crystallization model was used.

PHASES	%
Pl	30.5
Hbl	3.5
Kfs	30
Bt	3.5
Qtz	30
Ilm	0.56
Mag	0.94
Ap	0.12
Zr	0.05
Aln	0.83

Table 8.7 Mineral proportions used in the modelled REE distributions of the Roerkulten Granite.

MESONORM

	RK58	RK62	RK59	RK6	RK8	RK61	RK7	MEAN
Qtz	33.12	31.68	29.10	26.34	27.89	29.26	26.64	29.30
Or	29.94	34.33	31.41	31.87	33.33	32.37	34.34	32.69
Ab	21.96	22.65	24.00	25.37	24.83	23.85	22.47	23.72
An	4.97	4.66	5.41	5.71	4.93	4.87	6.07	5.26
Bt	6.67	4.62	6.90	7.27	6.15	5.86	7.40	6.45
Mag	1.27	1.01	1.50	1.53	1.36	1.34	1.56	1.37
Spn	0.98	0.78	1.05	1.05	0.81	0.86	1.06	0.95
Ap	0.11	0.11	0.13	0.15	0.13	0.11	0.15	0.13
Co	0.98	0.16	0.50	0.71	0.57	1.48	0.31	0.67

CATANORM

	RK58	RK62	RK59	RK6	RK8	RK61	RK7	MEAN
Qtz	29.38	28.72	25.53	22.67	24.51	25.93	23.12	25.70
Or	34.55	37.69	36.12	36.70	37.51	36.38	39.40	36.91
Ab	23.87	24.52	26.04	27.44	26.85	25.81	24.35	25.56
An	6.51	5.18	6.91	7.34	6.20	6.21	7.07	6.49
Opx	3.47	1.95	3.39	3.71	3.12	2.87	3.51	3.14
Mag	0.94	0.75	1.10	1.12	1.00	0.98	1.15	1.01
Ilm	0.57	0.45	0.61	0.61	0.47	0.49	0.62	0.55
Co	0.52			0.18	0.16	1.14		0.28
Di		0.56	0.11				0.53	0.17
Ap	0.12	0.12	0.14	0.17	0.14	0.12	0.17	0.14
Zr	0.052	0.040	0.054	0.056	0.045	0.049	0.059	0.051

Table 8.8 Mesonorm and catanorm values for the unaltered samples from the Roerkulten sheet. Values in percent.

The modelled REE patterns in figure 8.8a and b show that REE variation greatly exceeds the actual variation in figure 7.12. Causes for this overestimation of variation are difficult explain. Figure 8.8b has a pattern which is comparable to that seen in figure 7.12 and therefore RK58 appears to be a better candidate as a starting composition than RK62.

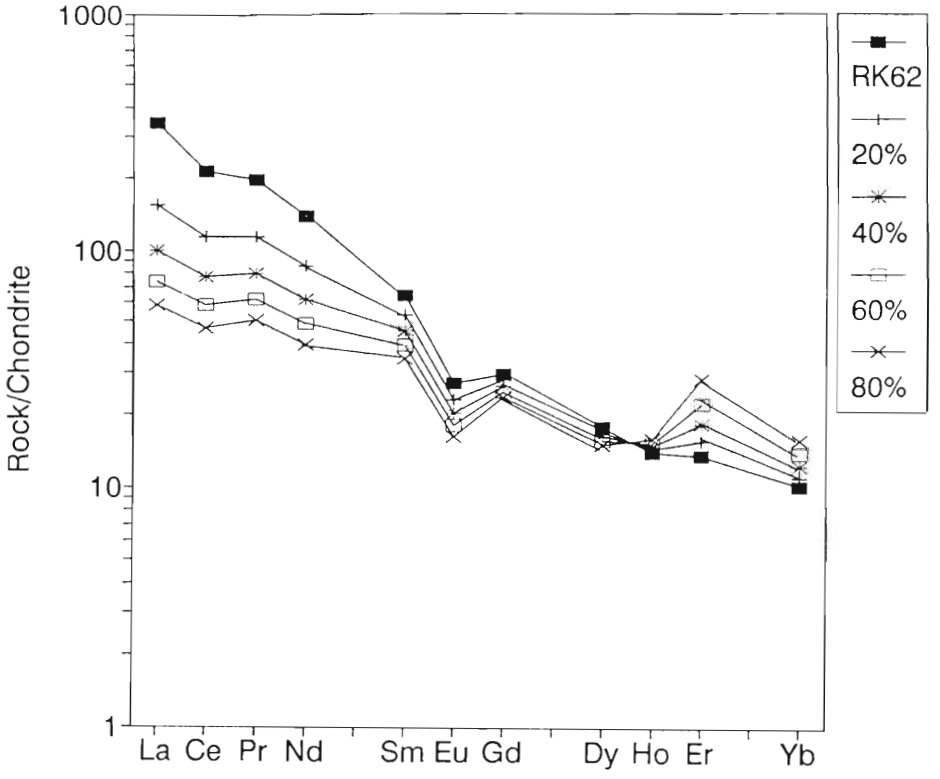

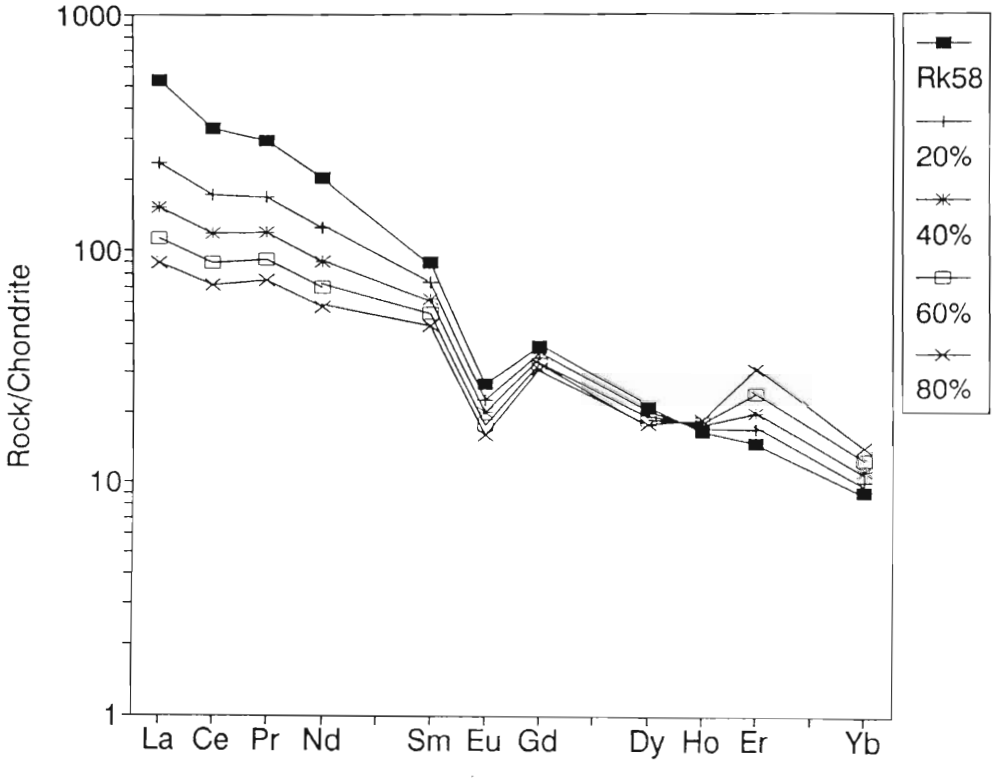

Figures 8.8a (above) and 8.8b (below). Modelled REE variations based on starting composition the same as RK58 and assuming equilibrium crystallization.

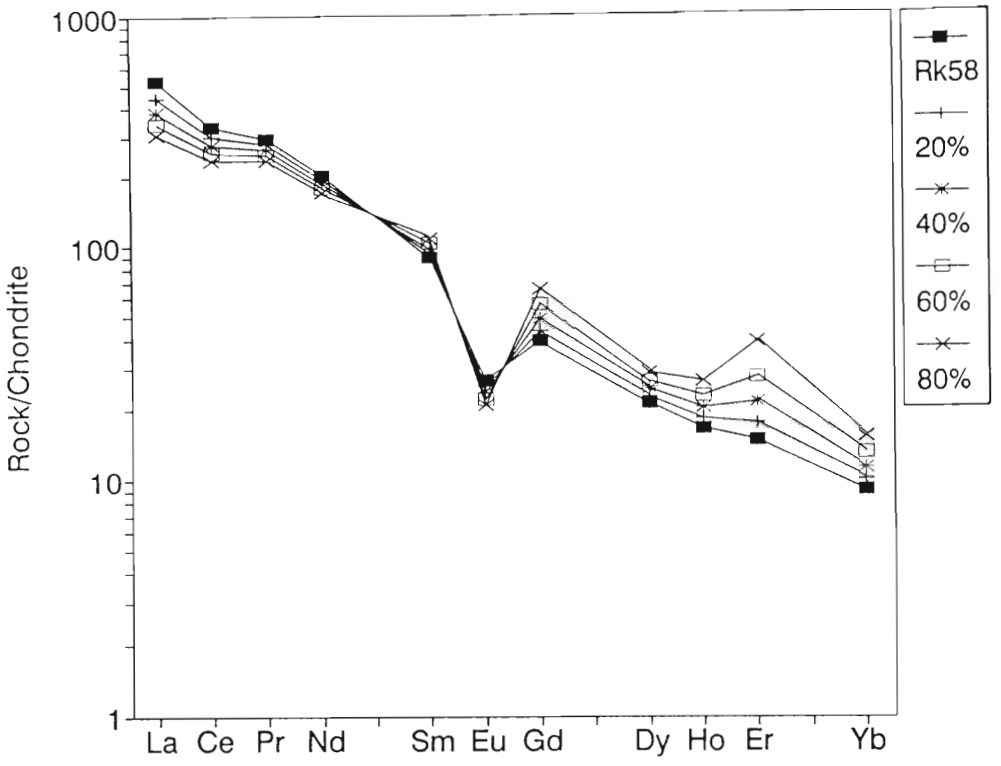

Figure 8.8c. Modelled REE variations based on starting composition the same as RK58 and assuming equilibrium crystallisation.

Equilibrium crystallization results in the least possible variation and therefore the low degree of variation (ie. less than equilibrium crystallization) cannot be ascribed to the choice of crystallization mechanism. Overestimation of the allanite content is possible but considered unlikely. A model using only 0.2% allanite (fig 8.8c) still resulted in an overestimate of the degree of REE variation.The proportion of allanite in the granite far exceeds the apatite and opaque minerals and therefore the estimate of the allanite content is considered to be realistic. A possible reason of the deviation of the modelled patterns is that the published K_d's are themselves in error. This possibility cannot be assessed but all studies that discuss the K_d's of REE in allanite emphasise the extreme fractionation of REE into allanite.

Alternatively, another possible reason for the inexactitude of the modelled patterns is that much of the allanite in the granite may have been xenocrystic, and that in fact little or no fractionation occurred. This alternative implies that the REE variation seen in the samples is merely due to (slightly ?) varying proportions of xenocrystic allanite. This possibility receives some support from the presence of clear rims of allanite around the metamict cores.
The concept of xenocrystic allanite is relevant to current debates regarding the origins of

various types of granites.

Chappel *et al.* (1987) suggest that varying proportions of restite or xenocrysts in a magma are largely responsible for linear chemical variations in granite and that restite or xenocrystic material may form a significant portion of a magma.

Wall *et al.* (1987) suggest that neither restite incorporation nor restite unmixing can be considered as major factors contributing to the chemical variation of many granitoids and suggest that fractional crystallization and magma mixing may contribute to the observed chemical variations.

Another factor supporting incorporation of xenocrysts is that Rapp and Watson (1986) have shown that the solubilities of the LREE in granitic magmas are low and are dependant on temperature and water content. These authors found that a granitic magma at 750°C with a water content of 6% would be saturated by LREE at levels of the order of 60ppm total LREE. RK58 has total LREE contents of 658ppm. The temperature of the Roerkulten Granite magma is estimated at ~860°C using the thermometers of Watson and Harrison (1983) and Watson and Capobianco (1981). At 860°C a granitic magma with 6% H_2O would be able to absorb approximately 400ppm total LREE before saturation. Wyllie *et al.* (1976) have used interpreted crystallization sequences to estimate H_2O contents of granitic magmas and conclude that the H_2O contents of large batholithic bodies of granite are unlikely to exceed 1.5%. The crystallization sequence deduced for the Roerkulten Granite has hornblende crystallizing after quartz and feldspar. Late crystallization of amphibole would occur under conditions of low H_2O, possibly of the order of 2% H_2O. A factor which would support this is the relatively high temperature indicated by the Zr and P thermometers of Watson and Harrison (1983) and Watson and Capobianco (1981), respectively. At H_2O contents of the order of 2% and a temperature of 860°C, a granitic magma would be saturated in total LREE contents of approximately 170 ppm (Rapp and Watson, 1986). Thus the high LREE contents of the Roerkulten Granite may indicate that much of the allanite is xenocrystic.

The model presented here predicts that the heaviest REE's (Ho to Yb) were incompatible during fractionation and their concentrations would be expected to increase with fractionation. In the observed data, only Yb appears to have been incompatible, the concentration of Yb increasing slightly in samples RK58-RK62. This suggests that at least one of the phases used in the modelling had higher K_d values for the HREE than the K_d's used in the models.

It was noted above that the REE patterns of the Roerkulten Granite are steep. Steep REE patterns are commonly interpreted to mean that garnet was a significant component in the residue of partial melting or fractional crystallization (Pride and Muecke, 1980). The presence of garnet inclusions in plagioclase was noted and interpreted to be xenocrystic. Xenocrystic garnet would confirm the existence of garnet in the residue at depth. However, steep REE patterns may also be due to the presence of xenocrystic allanite since the LREE are strongly partitioned

into allanite (see table 8.2 and appendix 3). Both alternatives may explain the steep REE patterns of the Roerkulten Granite. Miller and Mittlefehldt (1982) have suggested that entrainment of minerals like allanite and monazite will substantially obscure REE petrogenetic interpretations and may also influence Sm-Nd and Th-Pb geochronometers. Harrison and Watson (1986) report that the solubilities of zircon, apatite, monazite, sphene, allanite and thorite in felsic magmas are low. These minerals commonly host high concentrations of U, Th and REE. The low solubilities of these minerals in felsic melts implies that these minerals will commonly be residual during melting and remain in the lower crust resulting in an increase in the heat productivity of the lower crust (Harrison and Watson, 1986). These authors also state that a portion of the generally refractory accessory minerals may be entrained in the departing melt.

The modelled REE patterns predict a higher degree of variation in Eu content than that which is observed. A possible reason for this is that the significant opaque mineral content in the granite implies a relatively high oxygen fugacity. Drake (1976) has shown that the partitioning of Eu is dependant on oxygen fugacity and under reducing conditions Eu^{2+} is easily accommodated in the plagioclase crystal lattice. Under more oxidising conditions Eu^{3+} is the stable form and is less easily accommodated in the plagioclase lattice. Consequently, fractionation of plagioclase from a relatively oxidised magma will generate a smaller negative Eu anomaly than plagioclase fractionation in a reduced magma.

Brekkerista Granite

Modelled REE patterns in the Jutulrora Granite showed that 1% fractionation of sphene results in the depletion of the middle and heavy REE in the residual magma whereas the LREE are enriched in the residual magma. The higher sphene content of the Brekkerista Granite could result in depletion of all the REE in the residual magma with greater depletion of the middle and HREE. This could result in the type of REE patterns seen in the Brekkerista Granite with smaller variations in the LREE and greater variations in the HREE. Alternatively, the LREE distribution of the Brekkerista Granite could be controlled by allanite whereas the middle and HREE could be controlled by sphene for reasons discussed previously. The crystallisation of approximately 1.65% sphene and 0.5% allanite would result in depletion of REE in the magma with continuing crystallization. This is consistent with the presently available data. Total REE in BK28 (~73% SiO_2) is less than the ΣREE in BK50 (~69.75% SiO_2) suggesting depletion of the REE with increased fractionation.

Modelling of other trace elements

The requirements of the trace element modelling are similar to those for the REE modelling.

With these data it is possible to compare the trace element variations described in chapter 7 with modelled trends. To facilitate these comparisons, the effects of crystallising major, minor and accessory minerals have been calculated and are presented as vectors in figures 8.9a, 8.10a and 8.11a. These vectors were calculated in the following manner. The starting compositions for the modelling are an average of the contents of samples RK58, JE107 and the average of the Brekkerista Granite. For the major minerals quartz and feldspar (plagioclase and orthoclase are treated as one for the trace elements under consideration) the vectors were determined assuming equilibrium monomineralic crystallization of a specific phase (ie 100% fractionation of that phase).

The vectors for the accessory minerals (apatite, allanite) were determined assuming that the accessory phase forms 1% of the phases crystallizing with the remaining 99% having an assumed bulk K_d of 1. Accessory minerals by definition constitute very small proportions of a rock, commonly $<1\%$ and unless the K_d's for the various elements are particularly high, crystallization of these minerals will not result in great variations. Therefore to identify the effects of crystallization of accessory minerals on magma compositions it is necessary to assume that, besides the accessory mineral in question, the bulk K_d for the other minerals crystallizing is 1 because crystallization of any phase with a K_d of 1 will neither deplete nor enrich the magma in the elements concerned. Thus any variation may be attributed to the accessory mineral. Based on these assumptions and taking published partition co-efficients (K_d) of the various phases, only sphene and allanite were found to have appreciable effects on the variation of certain trace elements.

Similarly, the vectors for the minor minerals (biotite and hornblende) were determined assuming that the minor minerals form 10vol% of the phases crystallizing with the remaining 90% having an assumed bulk K_d of 1. The minor minerals rarely exceed 10% in granitoids and therefore such a calculation will provide an indication of the degree of influence these minerals may have on crystallisation.

The lengths of the vectors for both major, minor and accessory minerals reflect the degree of variation expected after 50% crystallization of the phase with each symbol along the length of the vector representing an increment of 10% fractionation. Table 8.9 shows the partition coefficients used for the modelling of the trace elements. The trace elements considered include those which are normally considered to be relatively immobile and therefore least affected by metamorphism.

	K_d's					
PHASES	La	Th	Zr	Sc	Y	Nb
Pl	.32	.04	.3	.2	.1	.01
Hbl	.85	.22	.5	20	1	.8
Or	.4	.1	.3	.2	.01	.1
Bt	.32	.31	2	20	1	9.5
Qtz	.03	.004	.38	.015	.001	.001
Ilm	.02	.001*	3	11	0.2	2.3
Mag	.53	.11	8.6	15	2	2.5
Ap	21	.001*	7.4	0.45	20	0.01
Zrn	2	.001*	280	10	60	.001*
Aln	820	420	.001*	0.46	9*	0.01
Spn	45	17	9	10	80*	7.6

Table 8.9. K_d's used for the modelled trace element variations. The reference sources for the K_d's are shown in appendix 3. * represents assumed values for the K_d's.

Lanthanum-Thorium variation in the granites.

In figure 8.9a, the calculated mineral vectors are shown. Fractionation of the following minerals is likely to have an appreciable effect on La/Th distribution namely allanite (depletion) and sphene to a lesser degree (depletion) and quartz and feldspar (enrichment). Figure 8.9b shows the distributions of La vs Th for the Roerkulten, Jutulrora and Brekkerista Granites. The La/Th variation in the granites is relatively restricted.

The Roerkulten Granite shows the greatest variation, followed by the Brekkerista and finally the Jutulrora Granites. The samples from all the granites broadly define a linear grouping which has a positive slope. This would suggest that either fractionation of quartz and feldspar resulted in enrichment of La and Th in the residual magmas or fractionation of allanite caused depletion of these elements in the residual magma. The broad similarity in La and Th values from the three granite bodies suggests that the granites may have a common source.

Zirconium-scandium variation in the granites

Figure 8.10a. shows the calculated mineral vectors. Fractionation of quartz and feldspar are likely to result in fractionation of both Zr and Sc into the magma resulting in enrichment whereas fractionation of biotite and hornblende are likely to result in depletions of scandium but have minimal influence on Zr contents. Fractionation of sphene and allanite have virtually no effect on these trace elements.

Figure 8.10b shows the Zr vs Sc variation in the three granite bodies. The Brekkerista and Jutulrora Granites show similar contents of these elements whereas the Roerkulten Granite shows higher Zr contents.

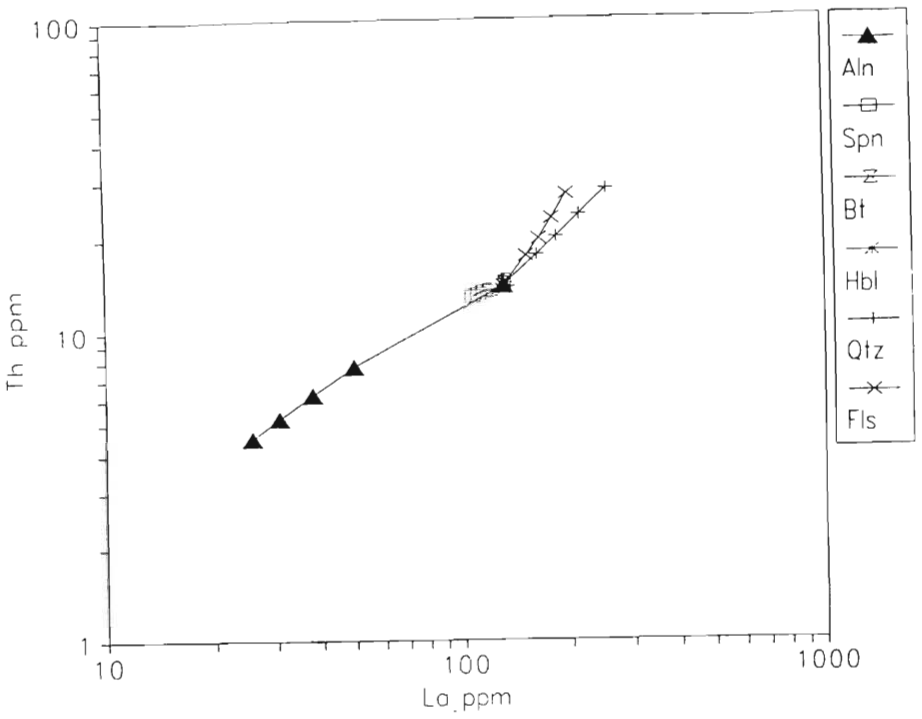

Figure 8.9a. Calculated mineral vectors for the mineralogy of the granites. Each symbol along the length of the vector represents an increment of 10% fractionation.

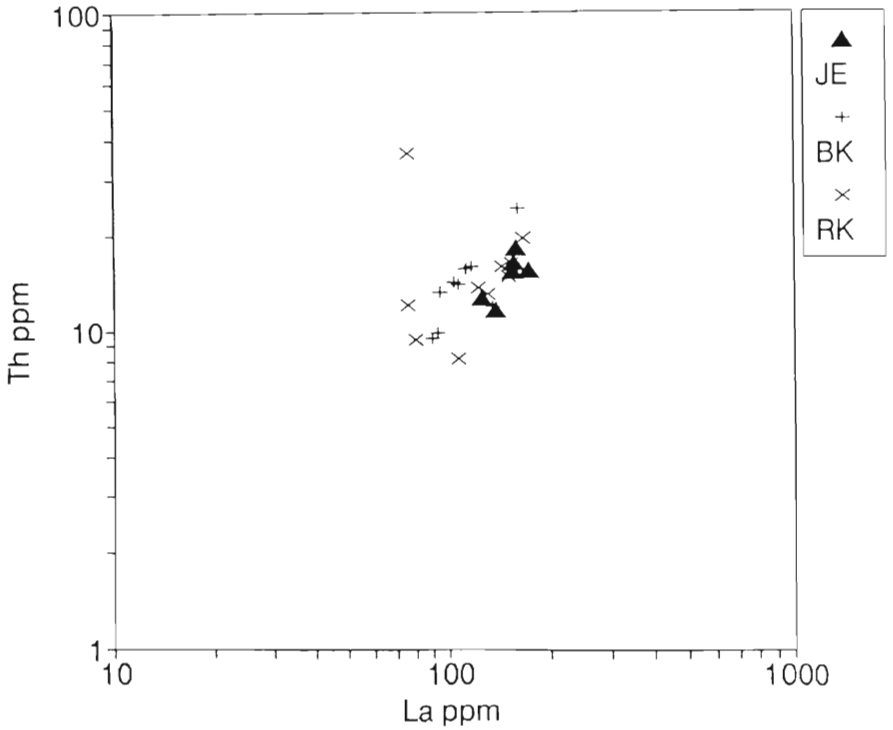

Figure 8.9b. La/Th variation diagram for the Roerkulten, Jutulrora and Brekkerista Granites. The symbols JE,BK and RK are analyzed concentrations.

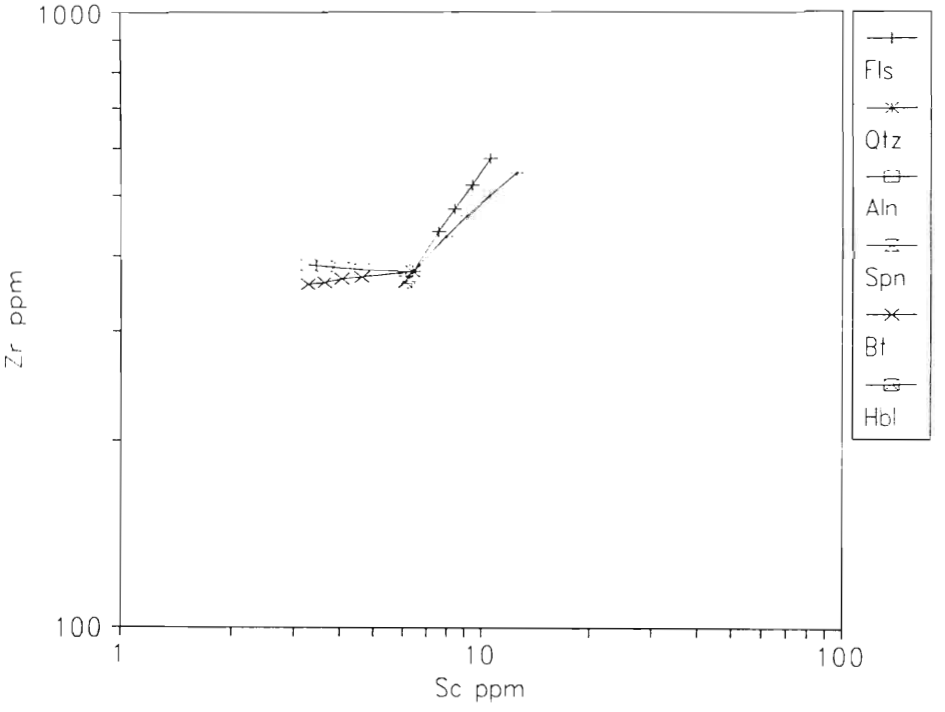

Figure 8.10a. The calculated mineral vectors for Zr vs. Sc.

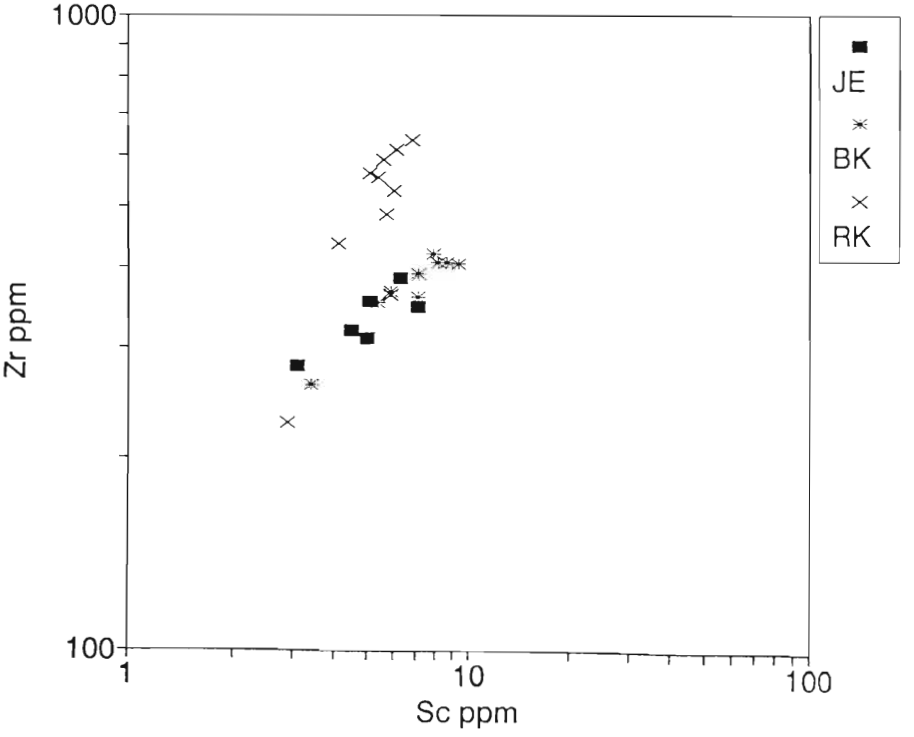

Figure 8.10b. Zirconium vs. Sc variation for the granites and modelled fractionation vectors for the granites.

In the Zr versus Sc plot a correlation coefficient of 0.8 for the Jutulrora Granite indicates a reasonably strong sympathetic relationship from which it may be concluded that both elements behaved similarly ie either as compatible or incompatible elements. The orientation of the trends for the granites are similar to that which would be expected from fractionation of quartz and feldspar.

Niobium-Yttrium variation in the granites

The modelled mineral vectors (fig 8.11a) show the following :- fractionation of quartz and/or feldspar are likely to partition Nb and Y into the residual magma. Crystallization of sphene is likely to deplete the magma in Y and Nb, the latter to a lesser degree than the former. Fractionation of biotite could deplete the magma in Nb but have little effect on Y contents. Allanite and hornblende are unlikely to affect Nb and/or Y contents to any great degree.

The distributions of Nb and Y in the three granite bodies are broadly similar although Y concentrations in the Brekkerista Granite are marginally higher (Fig. 8.11b). These similarities may suggest that the granites were derived from a common source. The distributions of Y and Nb in the Jutulrora Granite show a strong linear relationship with a correlation coefficient of 0.96 with the Y content varying significantly and the Nb content remaining almost constant. The variation of these elements in the Roerkulten and Brekkerista Granites are greater than that in the Jutulrora Granite. The variations in the Roerkulten and Brekkerista Granites also show linear patterns with positive slopes. This would suggest that in all three granites, Nb and Y were either compatible or incompatible. A study of the mineral vectors suggests that fractionation of quartz and feldspar is likely to have been dominant and therefore these trace elements were probably incompatible.

Conclusions

Modelling of the REE data of the Jutulrora Granite suggests that the observed variations could have been derived by sphene-dominated fractionation of a magma with a REE content similar to that of JE107 and that this magma may have had a significant proportion of its REE contained in xenocrystic allanite. Modelling of the REE data of the Roerkulten Granite suggests that the observed pattern may result from the allanite content. The variation is less than can be explained by any fractionation model. A possible cause for this is that much of the allanite may be xenocrystic.

Modelling of La/Th, Zr/Sc and Nb/Y distributions suggests that the variation of these trace elements were probably largely controlled by quartz and feldspar fractionation although in some cases accessory minerals may have played a significant role.

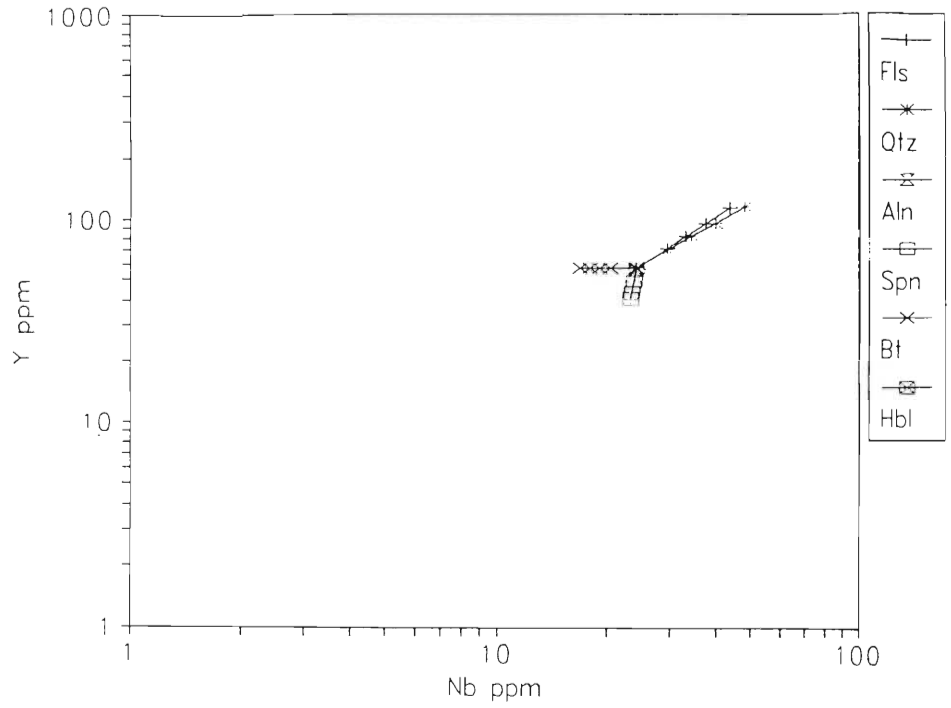

Figure 8.11a. Calculated mineral vectors for Nb and Y.

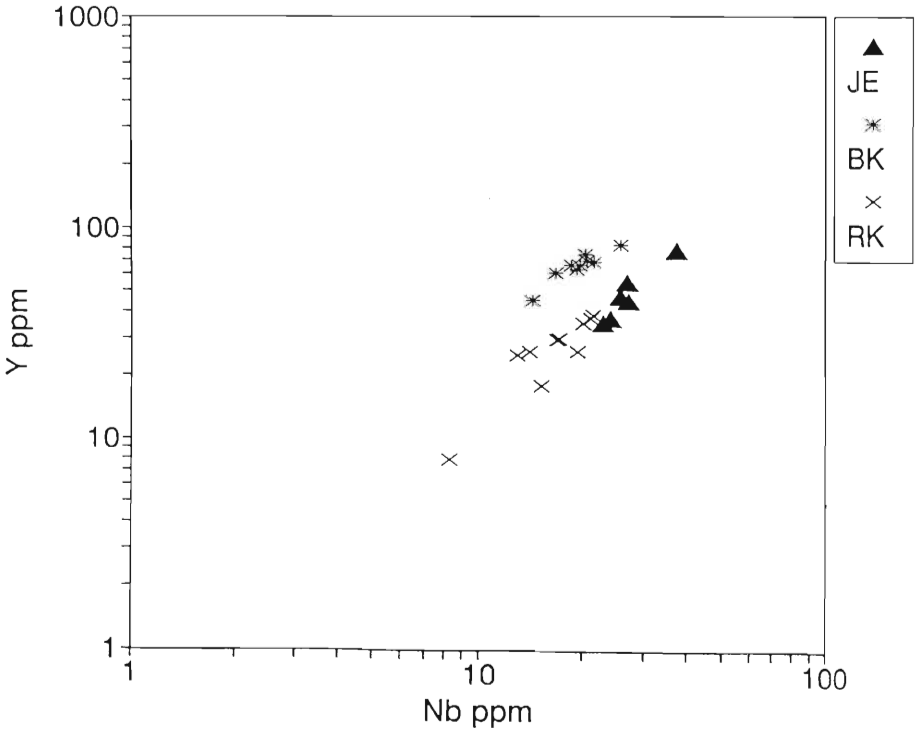

Figure 8.11b. Nb vs Y for the Roerkulten, Jutulrora and Brekkerista Granites.

Broadly, the three granite bodies show fairly similar major and trace element contents which may suggest that they shared a common origin. The differences between them may reflect local fractionation processes involving the crystallisation of different quantities and or species of minerals, in particular the accessory phases.

CHAPTER 9
THE METAMORPHOSED INTRUSIONS

INTRODUCTION

The field relationships of these intrusions were described in chapter 2. Four varieties are recognised, namely (i) at least three generations of mafic intrusions, A1, A2 and A3 amphibolites, and (ii) diorite. The petrography and metamorphic history of these rocks will be considered after which the chemistry of the various types will be described and discussed.

PETROGRAPHY

A1 Amphibolite

These mafic intrusions are defined as having contacts discordant to layering considered to be of primary origin but having planar fabrics which are parallel to S_1. Generally, the discordant contacts are difficult to identify because high strains during D_1 have rotated the intrusions parallel to the layering. One possible example of this type of discordant mafic intrusion has been recognised at Jutulrora. The structural measurements are presented on stereonet H, map 2. The stereonet shows that the contact of the amphibolite and the planar foliation within the amphibolite are parallel to the planar foliation in the host Grey Gneisses.

Sample JE14 is the only sample of an A1 amphibolite. The mineralogy is shown in table 9.1. Sample JE14 is equigranular, medium-grained, and has a strong planar foliation defined by olive-green to dark green pleochroic hornblende. Plagioclase locally displays albite twinning and is normally zoned. Biotite and chlorite form interstratified intergrowths and crosscut the planar fabric. Sphene is included poikiloblastically in hornblende.

A2 Amphibolite

The A2 amphibolites are defined as being discordant to lithological banding and to S_1 foliation. Based on these criteria, it is possible that more than one generation of these amphibolites exist but it is not possible to distinguish more than one generation in the field. The mineralogy of the samples is shown in table 9.1.

One of these amphibolites, exposed at the southern end of Straumsvola, is garnet-bearing (Sample S2) whereas another amphibolite exposed at the southeastern corner of Roerkulten (Samples RK19-21 and RK50-56) is garnet-free. Samples JE55, BK55, BK51 and BK26, collected from Jutulrora (JE) and Brekkerista (BK), are also garnet-free but are more mafic than those from Roerkulten. The amphibolites from southeastern Roerkulten are fine- to medium-grained (approximately 0.5 to 1mm). The mineralogy includes plagioclase, biotite, hornblende, quartz, and sphene with accessory magnetite, chlorite, and epidote.

	Qtz	Pl	Hbl	Bt	Spn	Chl	Mag	Ep	Grt	Cpx	Kfs
A1 AMPHIBOLITE											
JE14	10	35	50	2	2		1				
A2 AMPHIBOLITES											
RK19	10	53	10	25	2						
RK20	10	50	13	10	2	14	1				
RK21	10	55	13	20	2						
RK50	10	55	15	16	2		2				
RK51	10	55	12	19	2		2				
RK52	10	55	13	15	2			5			
RK53	10	55	18	13	2		2				
RK54	10	55	15	16	2		2				
RK55	10	55	10	21	3		1				
RK56	10	55	15	16	2		2				
RK2	10	45	20	20	3		2				
S2	3	10	65		1		1		20		
JE55	5	15	75	1	2		2				
BK55	5	15	55	10						15	
BK51	4	15	70	10	1						
BK26	2	55	25		2		1			15	
A3 AMPHIBOLITES											
BK100	15	45	16	16			8				
BK18	10	50	1	16			8				
BK14	10	60	10	10			5		5		
SV17		10	70	10			2			8	
GREY APLITE DYKES											
BK29	10	60	15	8	1	1		4			2
BK22	10	60	15	8	1	1		4			2

Table 9.1 Modal estimates (vol%) of the mineralogy of the metamorphosed intrusions.

Pleochroic light to dark brown biotite defines a planar fabric whereas the other minerals show a granoblastic texture. Pleochroic olive to dark green hornblende is poikiloblastic and encloses fine grains of quartz. Plagioclase is largely untwinned and is locally antiperthitic. In sample RK20 biotite is extensively chloritised and plagioclase is partially saussuritised.

Sample S2 shows a granoblastic texture defined by olive-green to dark green hornblende, plagioclase and garnet with accessory quartz, sphene, and opaque minerals. Garnet is typically poikiloblastic with inclusions of quartz and opaque minerals. The inclusions do not show any preferred orientation. Plagioclase is largely untwinned and shows normal zonation ie. becoming more sodic toward the rim.

Samples JE55, BK55 and BK51 are similar texturally in that they are medium to coarse-grained and have a strong planar fabric defined by olive-green to dark green hornblende. Other minerals (table 9.1) include untwinned plagioclase, pale-green clinopyroxene and minor proportions of quartz, sphene, biotite, and opaque minerals. The biotite is red-brown in colour and crosscuts the planar fabric.

Sample BK26 is fine-grained and has a granoblastic texture.

A3 Amphibolites

This generation of amphibolite is defined as having no planar fabric and a mineralogy that is partially or completely metamorphic. One example of this amphibolite is exposed at Brekkerista (samples BK14, BK18 and BK100) and another on the southern ridge of Straumsvola (SV 17). The mineralogy of these rocks is shown in table 9.1. The amphibolites from Brekkerista are medium-grained (2mm) with relict plagioclase phenocrysts up to 2cm long (see Fig. 2.7, chapter 2, p. 15). The plagioclase phenocrysts commonly enclose small (<1mm) pink garnets (Sample BK14). Secondary biotite crosscuts blue-green to pale green poikiloblastic hornblende and plagioclase. Opaque ore minerals, presumed to be magnetite and/or ilmenite form a significant constituent. Plagioclase is largely untwinned but locally shows Carlsbad/albite combination twins. Inclusions of quartz are also present in the plagioclase. The plagioclase has a composition of An_{22} and shows normal zoning. The relict plagioclase phenocrysts consist of a granoblastic mosaic which includes quartz and garnet and randomly oriented biotite. The plagioclase in the vicinity of the garnet is saussuritised. Apatite is a common accessory.

Sample SV17 displays a relict porphyritic texture with partially saussuritised plagioclase grains up to 3mm in length. The plagioclase is set in a fine-grained matrix (<.1mm) of hornblende and biotite. Locally grains of hornblende contain relict cores of clinopyroxene. Larger (>1mm) grains of partially altered clinopyroxene retain relict zonation structures and a light purple colour reminiscent of titanaugite.

Grey aplite dykes

These dykes are exposed at Brekkerista where they intrude the Banded Gneisses of the Jutulrora Formation and the Brekkerista Granite. The dykes are typically about 30cm wide. Their mineralogy comprises plagioclase, hornblende, and quartz, with subordinate biotite, sphene, microcline, and secondary epidote (Table 9.1). The rock has a granoblastic texture indicating a degree of metamorphic annealing subsequent to intrusion. A weak planar fabric is defined by oriented khaki-brown biotite grains which crosscut hornblende laths. The plagioclase is largely untwinned. Epidote and zoisite are associated with the breakdown of hornblende to biotite. The opaque mineral content is subordinate to the sphene content. The mineralogy of these rocks is typical of diorite.

METAMORPHISM

The assemblage of the A2 Amphibolites is hornblende + plagioclase $\pm$ quartz $\pm$ garnet $\pm$ clinopyroxene $\pm$ biotite $\pm$ sphene $\pm$ opaque minerals (Table 9.1, Fig. 9.1) which is characteristic of medium-grade or amphibolite facies metamorphism of basic rocks. This assemblage would be stable at temperatures between about 500° and 650°C. The garnet-bearing assemblage of sample S2 is particularly useful since it permits the application of

thermobarometry (see chapter on metamorphism).

Except for sample S2 it is difficult to attach specific conditions of metamorphism because the rocks contain few mineral phases and these are made up of a large number of components (Na_2O, K_2O, CaO, MgO, FeO, Fe_2O_3, Al_2O_3, SiO_2, H_2O, CO_2).

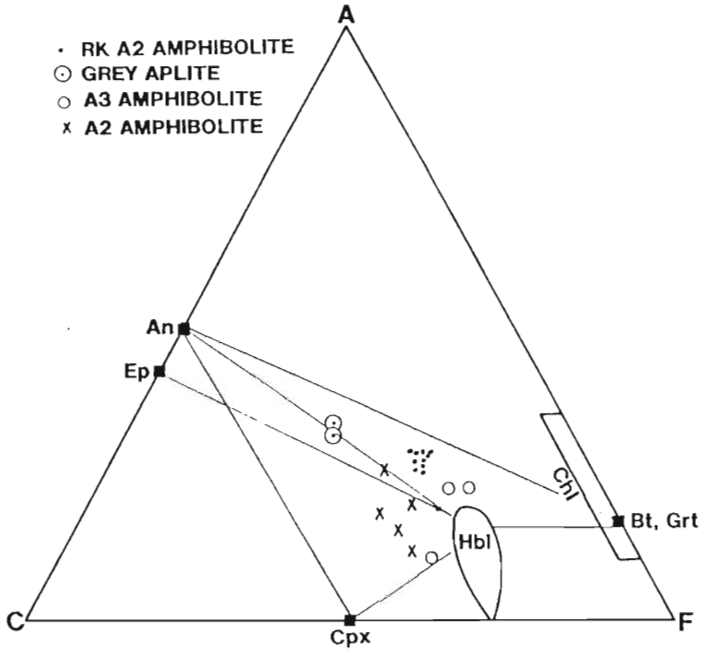

Figure 9.1. ACF diagram for the A2 and A3 metamorphosed intrusions. The RK A2 amphibolites (.) are those collected from Roerkulten whereas the A2 amphibolites (X) refer to all the other amphibolites.

Consequently, reactions are likely to be continuous and will vary because of solid solutions involving the dominant minerals eg. CaO and Na_2O in plagioclase and amphiboles, FeO, Fe_2O_3, Al_2O_3 and MgO in amphiboles and biotite (Yardley, 1989, pp. 100- 101).

The typical mineral assemblage of the A3 Amphibolites is similar to that of the A2 amphibolites and consists of hornblende + plagioclase + quartz + opaque minerals $\pm$ garnet (Table 9.1, Figure 9.1). This mineralogy is similarly typical of medium grade or amphibolite facies metamorphism of mafic rocks and reflects temperatures of between 500 and 650 °C. One difference between the A2 and A3 amphibolites is that, in the A2 amphibolites, when garnet is present, it occurs in contact with hornblende. In sample BK14, the only garnet-bearing A3 amphibolite, the garnet is completely enclosed within plagioclase. The restriction of garnet to the relict plagioclase phenocrysts suggests that the garnet is probably Ca-rich and probably contains minimal Fe,Mg and Mn. A possible reaction resulting in the above described relationship

is:-

$13An + 2Ab + 8Ed + 2H_2O \rightarrow 19Qtz + 3Grs + 10Prg$

Plagioclase + Al-poor edenite + water = quartz + grossular + Al-rich pargasite

This reaction will be considered further in chapter 14.

CHEMISTRY

Twenty-one samples of these rocks were analyzed for the major and trace elements. The major and trace element analyses are shown in Table. 9.2 and REE analyses in Table 9.3.

The chemistry of the A2 amphibolites from southeastern Roerkulten does not vary greatly. All the samples have intermediate SiO_2 (~56%), and high Al_2O_3 (~15%) and TiO_2 (>1.5%) contents. The trace element chemistry of these amphibolites is characterised by high contents of Sr, Zr and Ba. contents.

The A2 amphibolites from southern Straumsvola (S2) and Brekkerista (BK26, BK55 and BK51) are distinguished from the Roerkulten samples by their lower contents of SiO_2 (~50%) and higher concentrations of iron and calcium. The concentrations of trace elements, Sr, Zr and Ba in the Straumsvola and Brekkerista A2 amphibolites are lower than those reported in the Roerkulten samples. The higher MgO contents of two of the Brekkerista samples is matched by Cr concentrations >500ppm.

The Jutulrora A2 amphibolite has close similarities with respect to major, minor and trace elements to the Roerkulten amphibolites but is slightly more siliceous.

The A3 amphibolites from Brekkerista (BK18,BK100) have SiO_2 contents similar to those of A2 amphibolites from the same area but have lower MgO and CaO but higher total Fe. Although the Brekkerista A3 amphibolites have high Ba contents like those in the A2 amphibolites, Sr is lower.

The two A3 amphibolite samples are readily distinguished by virtue of their anomalously high Zr contents (~750ppm). The A3 amphibolite from Straumsvola (SV17) has close similarities to the A2 amphibolites at Brekkerista with respect to MgO, CaO and total Fe but has SiO_2 of only 43.6%.

The chondrite-normalised REE profile for A2 amphibolite (RK54) steep slope ($La_{cn}/Yb_{cn} = 16.2$), with a small negative europium anomaly ($Eu/Eu^* = 0.81$) (Fig. 9.2). This contrasts with the pattern of the A3 amphibolite (BK100) that has a gentler slope ($La_{cn}/Yb_{cn} = 5$) and a prominent negative Eu anomaly (Fig. 9.2).

	SiO_2	Al_2O_3	Fe_2O_3	FeO	MnO	MgO	CaO	Na_2O	K_2O	TiO_2	P_2O_5	TOTAL
A2 AMPHIBOLITES												
S2	50.57	13.31	2.51	12.8	0.35	6.21	9.75	2.06	0.61	1.67	0.2	100.04
RK21	57.21	15.99	1.70	5.13	0.14	4.12	5.98	3.46	2.82	1.57	0.94	99.06
RK19	57.21	15.49	2.10	6.69	0.14	4.02	5.64	2.93	2.92	1.52	0.85	99.51
RK20	56.72	15.70	2.00	6.76	0.15	4.10	5.93	2.96	2.76	1.57	0.89	99.54
RK56	56.40	15.39	2.16	6.88	0.19	3.99	6.10	2.86	2.95	1.54	0.89	99.35
RK53	56.55	15.39	2.16	6.89	0.17	4.05	6.32	3.10	2.96	1.55	0.86	100.0
RK55	56.49	15.27	2.15	6.87	0.18	3.95	6.04	3.10	2.78	1.60	0.90	99.33
RK54	56.30	15.73	2.17	6.92	0.24	3.87	6.22	3.44	2.72	1.62	0.92	100.15
RK50	55.18	15.61	2.20	7.00	0.22	4.12	6.27	3.42	2.60	1.53	0.89	99.04
RK51	56.85	15.74	2.10	6.69	0.23	3.94	6.24	3.20	2.79	1.52	0.83	100.13
RK52	56.91	15.39	2.14	6.44	0.16	3.75	6.03	3.58	2.74	1.50	0.83	99.47
RK2	52.1	13.51	2.7	9.15	0.21	5.77	7.06	2.95	2.72	2.27	0.66	99.1
BK26	49.64	14.23	2.41	9.23	0.20	7.43	11.06	3.17	1.03	1.49	0.14	100.03
BK55	49.29	12.54	2.24	8.59	0.18	11.22	11.94	2.13	1.29	0.94	0.35	100.71
BK51	48.21	10.16	2.70	9.14	0.22	12.40	12.30	1.50	2.49	0.89	0.55	100.56
JE55	60.02	15.07	1.59	5.39	0.13	3.93	6.17	3.11	2.60	0.72	0.27	99.0
GREY APLITE DYKES												
BK22	59.87	19.4	1.26	3.79	0.15	1.18	5.77	6.41	0.7	0.43	0.26	99.22
BK29	58.32	19.38	1.32	3.75	0.1	2.05	6.01	6.13	1.08	0.75	0.39	99.28
A3 AMPHIBOLITES												
BK18	50.98	13.44	3.02	10.88	0.23	3.81	6.64	2.25	2.71	4.12	0.92	99.01
BK100	50.24	12.82	2.98	11.42	0.32	3.71	7.35	2.16	2.41	4.04	1.81	99.26
SV17	43.59	10.81	3.39	10.81	0.32	12.43	10.96	2.92	1.71	2.62	0.19	99.75

No.	Rb	Sr	Th	Zr	Y	Nb	Ba	Sc	Cr	La	V	Cu	Ni	Zn
A2 AMPHIBOLITE DYKES														
S2	16	170	11	94	39	7	187	44	141	2	354	73	43	82
RK21	64	815	2	284	35	26	1602	17	101	52	181	40	38	139
RK19	86	925	ND	297	32	25	1602	17	222	48	173	92	69	137
RK20	100	783	ND	301	33	26	1262	20	89	53	197	60	40	135
RK56	82	888	ND	274	31	24	1637	19	103	47	180	42	28	112
RK53	88	849	ND	271	31	24	1541	17	102	46	165	62	40	140
RK55	73	850	3	284	34	27	1540	19	95	44	154	58	37	130
RK54	66	872	ND	292	33	27	1465	19	80	54	208	50	34	135
RK50	57	898	4	262	32	24	1503	20	103	39	194	94	39	134
RK51	79	889	4	282	32	24	1427	19	91	48	177	66	38	137
RK52	65	830	1	277	31	24	1517	18	85	50	195	47	36	131
RK2	62	411	1	203	39	10	734	30	92	16	213	132	55	130
BK26	11	388	1	97	28	7	159	47	327	6	378	71	99	94
BK55	42	279	2	114	20	6	228	42	523	23	272	9	120	111
BK51	131	168	3	135	25	11	418	45	672	75	316	27	192	127
JE55	57	682	2	143	21	14	1470	20	72	25	170	1	27	79
GREY APLITE DYKES														
BK22	4	609	4	197	37	22	128	3	2	60	41	32	1	93
BK29	21	468	5	122	24	15	116	8	2	35	90	7	14	71
A3 AMPHIBOLITE DYKES														
BK18	114	313	7	754	103	29	1021	33	81	59	120	17	19	210
BK100	24	294	2	760	101	28	1039	32	55	57	146	14	1	139
SV17	106	497	3	83	20	14	399	25	784	15	469	91	476	145

Table 9.2. Major and trace element chemistry (concentrations in wt% and ppm respectively) of the metamorphosed intrusions. ND = not detected.

	La	Ce	Pr	Nd	Sm	Eu	Gd	Dy	Ho	Er	Yb
RK54	69.81	126.01	16.36	62.4	10.95	2.56	7.88	6.49	1.32	3.3	2.78
BK100	73.85	154.25	21.65	99.71	21.34	4.04	20.01	19.46	4.01	10.78	9.46

Table 9.4. REE composition of the sample RK54 from the A2 amphibolite from southeastern Roerkulten. Concentrations in ppm.

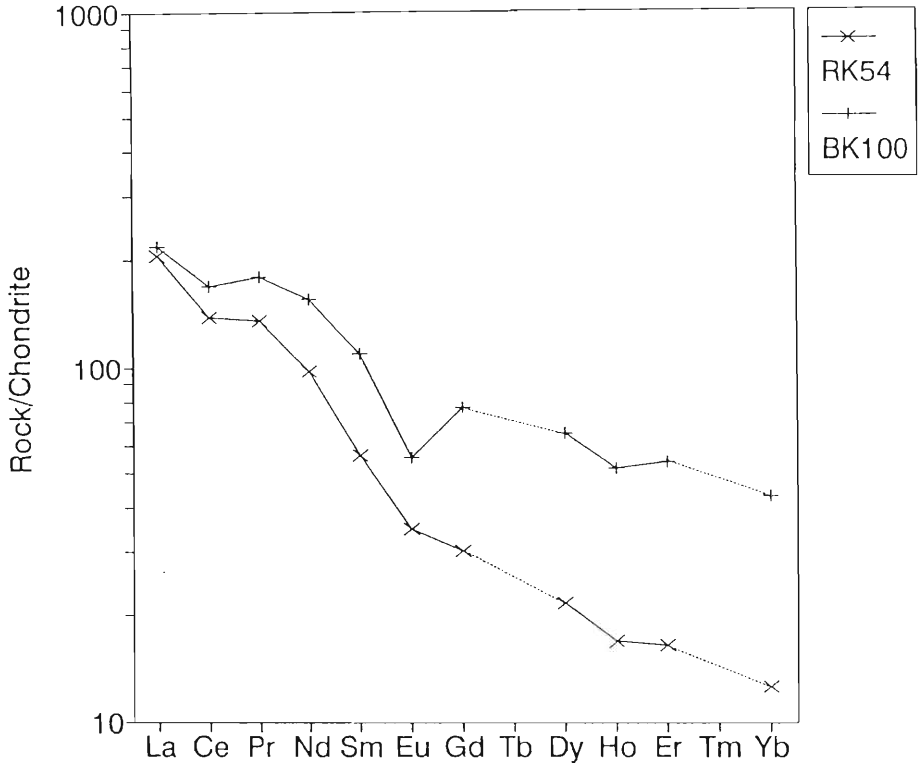

Figure 9.2. Chondrite normalised REE patterns for the metamorphosed intrusions.

The Roerkulten A2 amphibolites lie in the calc-alkaline (Irvine and Barager, 1971) field of the AFM diagram (Fig. 9.3). The remaining A2 and A3 amphibolites are tholeiitic with one exception (JE55).

The Grey Aplites have intermediate SiO_2, high Al_2O_3, CaO, and Na_2O and low K_2O contents. This chemistry is consistent with the classification of these rocks as diorite on the basis of mineralogy. The Grey Aplites have high Sr and Zr and low contents of Rb, Cu, Ni, Zn, Cr and V and plot within the calc-alkaline field (Fig. 9.3).

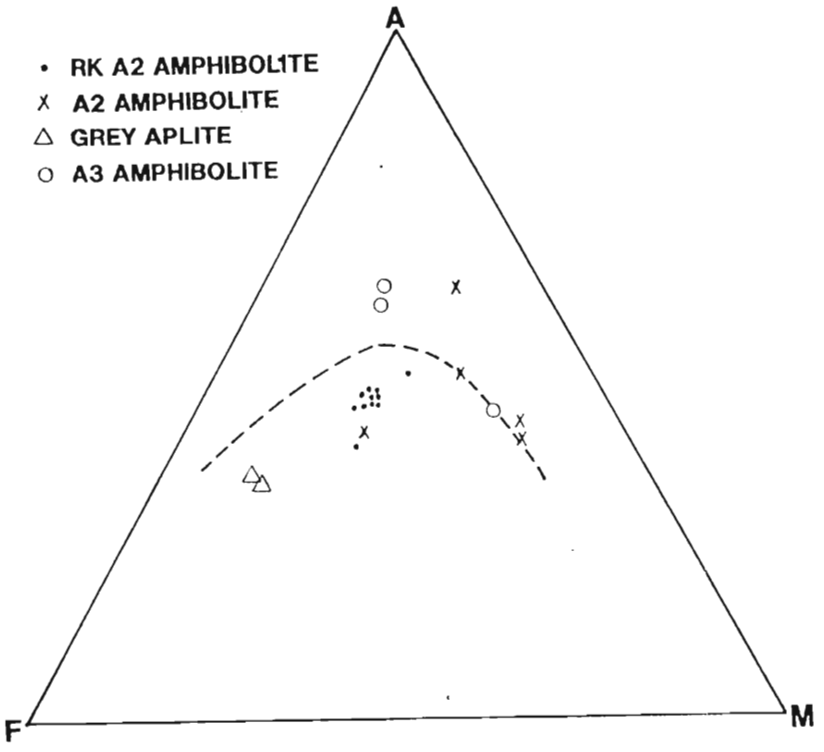

Figure 9.3. AFM diagram for the metamorphosed intrusions. The dashed line is the calc-alkaline tholeiite dividing line after Irvine and Barager (1971). The RK A2 (.) amphibolites are those collected from Roerkulten whereas the A2 amphibolites (X) refer to all the other amphibolites.

Discussion

The relevance of the chemistry of the Grey Aplite Dykes will be discussed in chapter 15 with the chemistry of the Roerkulten, Jutulrora and Brekkerista granitoids.

To facilitate discussion of the chemistries of the amphibolites, the compositions of these various intrusions have been plotted on spider diagrams normalised to island-arc calk-alkaline basalt (IACA), island-arc tholeiite (IAT) and within plate tholeiite (WPT) compositions (Fig. 9.6) with the normalising factors being taken from Sun (1980).

The compositions of the mafic intrusions may provide some indication of the tectonic environments in which they were emplaced. Two groups of A2 amphibolites are recognised (Fig. 9.4), namely those from Roerkulten and the mean of A2 amphibolites from Brekkerista and Straumsvola (samples BK55, BK26, S2 and BK51). The RK samples are not strictly basaltic in composition having mean SiO_2 contents of ~57% whereas the samples forming the A2 group are typically basaltic having SiO_2 contents of ~50%.

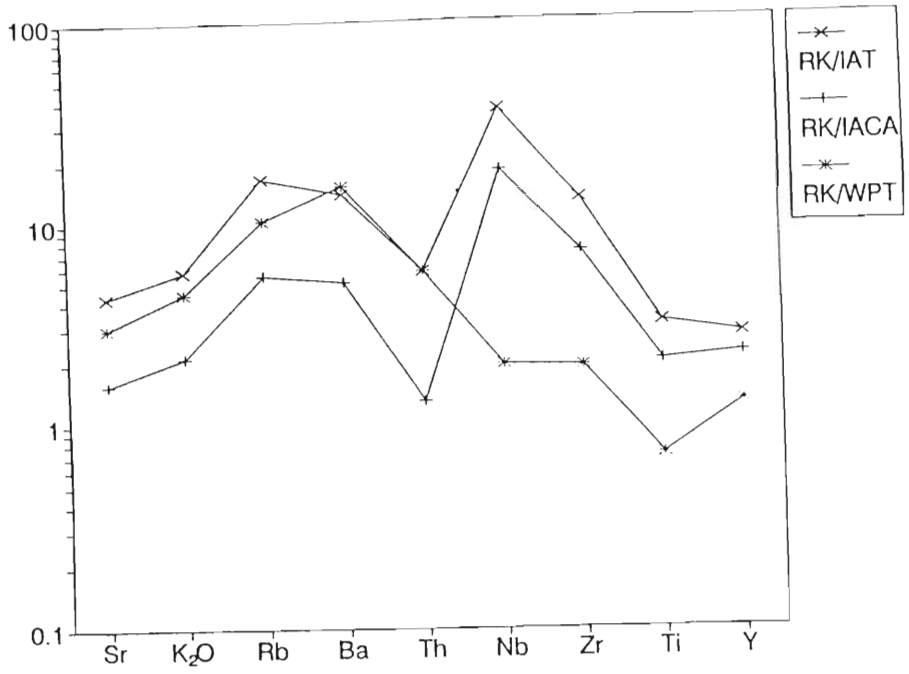

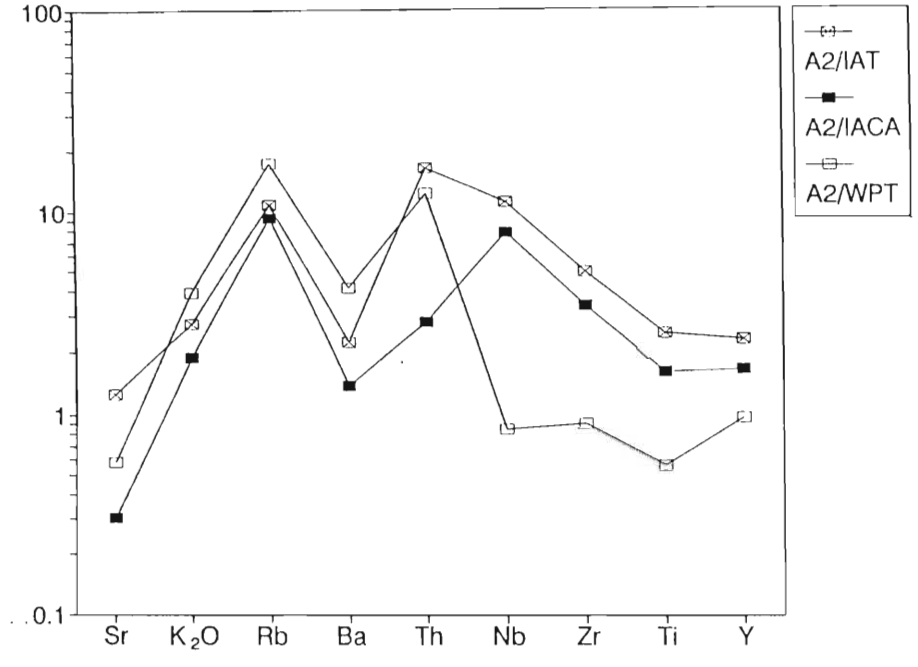

Figure 9.4. Spider diagrams of the A2 amphibolites from Roerkulten (RK)(above) and remainder of A2 (below) amphibolites. Normalising values for island arc tholeiite (IAT), island arc calc-alkaline basalt (IACA) and within plate tholeiite (WPT) are from Sun (1980).

Figure 9.4 shows that, for the immobile elements (eg Nb, Zr, Ti and Y), all the A2 amphibolites are comparable to within-plate compositions. For the mobile elements the RK composition is closest to island arc calc-alkaline basalts whereas the A2 composition is closest to island-arc tholeiite compositions except for Sr (Fig. 9.4).

The A3 amphibolites have immobile element distributions similar to within plate tholeiites and mobile element distributions closest to island arc calc-alkaline basalts.

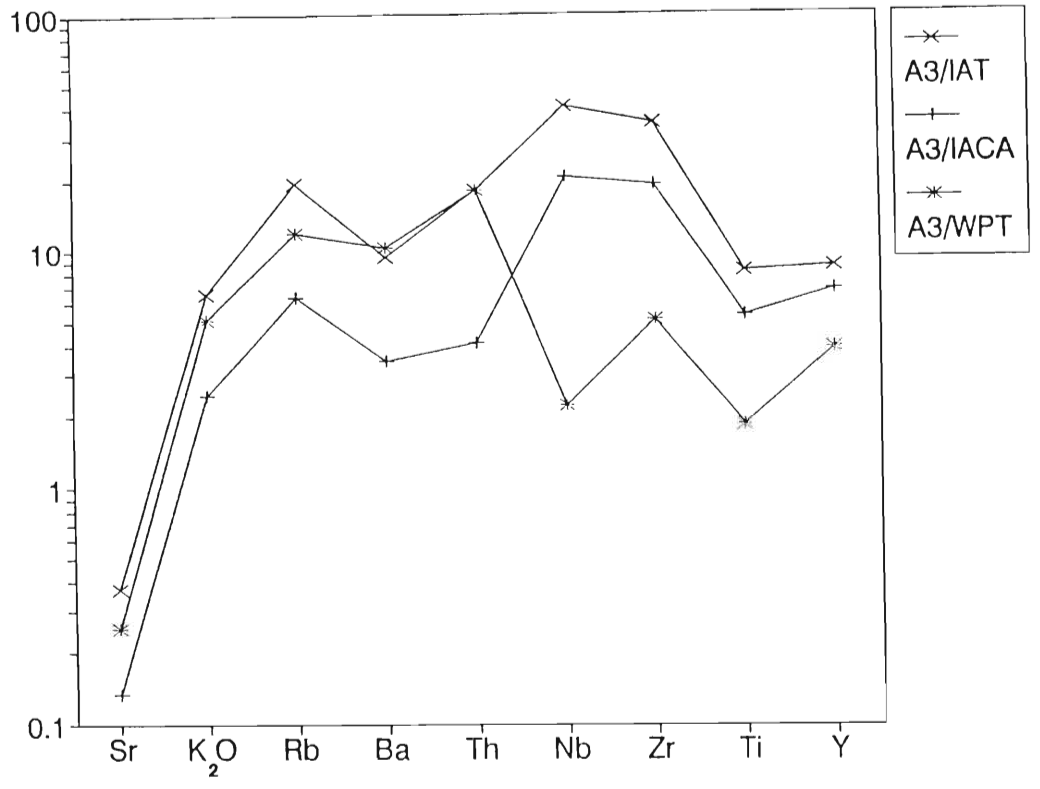

Figure 9.5. Spider diagrams for the A3 amphibolites. Abbreviations are the same as for figure 9.4.

The small europium anomaly in the A2 amphibolite (from Roerkulten) and the strong europium anomaly in the A3 amphibolite (from Brekkerista) (Fig. 9.2) indicate that both these intrusions either experienced fractionation of plagioclase or had plagioclase in their residues. The presence of relict plagioclase phenocrysts in the A3 amphibolite provides some evidence for plagioclase fractionation. If plagioclase was present in the source, it would suggest that the magmas from which A2 amphibolites formed were not generated at great depths. The relatively steep REE pattern of the Roerkulten A2 amphibolite may indicate that hornblende and/or garnet were in the residue or garnet and/or hornblende fractionation may have depleted these magmas in HREE. The relatively flat pattern of the A3 amphibolite suggests that neither garnet and/or hornblende

fractionation nor garnet and/or hornblende restites played significant roles in the composition of the A3 amphibolite.

Tectonic significance of the metamorphosed intrusions.

Besides providing some indication of the tectonic evolution of the Sverdrupfjella Metamorphic Province, the intrusions have also provided strain markers which, if successfully dated by isotopic methods, could provide time constraints on the deformation history. Ten samples from the A2 amphibolite were analyzed for their Rb and Sr isotope contents. The data are presented in table 9.4.

These data provide a poorly constrained errorchron which yields an age of ~720Ma. Exclusion of three samples from this errorchron yields a seven point isochron defining a date of 795 $\pm$ 110 Ma with an initial ratio of (R_o) 0.704712 (Fig. 9.6). The large margin of error arises as a consequence of the limited spread of $^{87}Sr/^{86}Sr$ values.

A detailed study of the structural relationships of the A2 amphibolite shows that the intrusion occurred after D_1 because the amphibolite clearly crosscuts the D_1 foliation and leucosomes developed parallel to that foliation (Fig. 9.7).

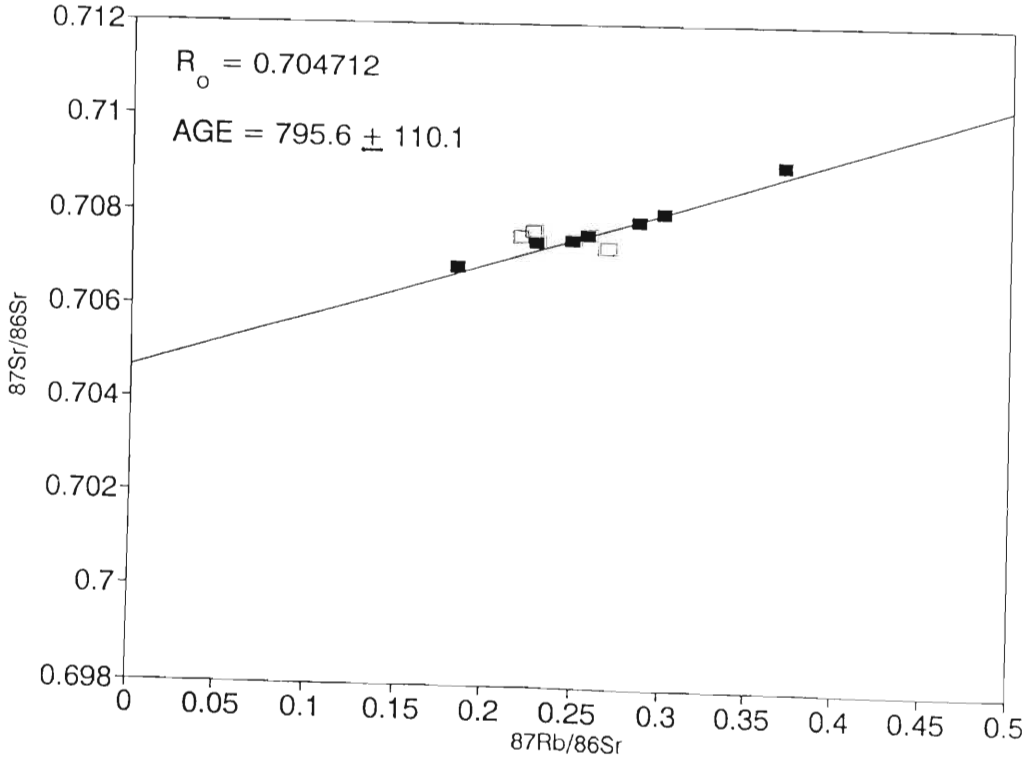

Figure 9.5. Rb/Sr isotope data for the A2 amphibolite from southeastern Roerkulten. The open symbols are excluded from the isochron calculation.

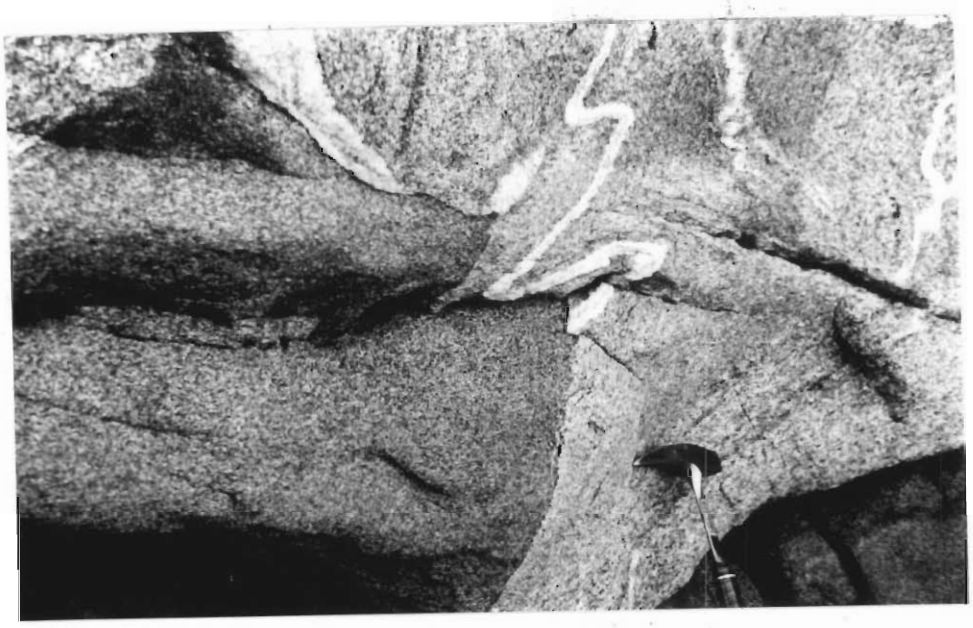

Figure 9.6. Photograph of A2 amphibolite transecting leucosome (M_1?).

Sample No.	Rb	^{87}Rb	Sr	^{86}Sr	$^{87/86}$Sr	±	^{87}Rb/^{86}Sr
RK19	91.4	25.88	925	89.46	0.707856	.000008	0.286
RK20	100	28.32	783	75.72	0.709049	.000005	0.369
RK21	64.3	18.21	815	78.83	0.707418	.000006	0.228
RK50	57	16.14	898	86.86	0.706872	.000006	0.184
RK51	79	22.37	889	85.98	0.707579	.000005	0.257
RK52	65	18.41	830	80.28	0.707654	.000013	0.227
RK53	88	24.92	849	82.11	0.708034	.000004	0.300
RK54	66	18.69	872	84.34	0.707517	.000006	0.219
RK55	73	20.67	850	82.21	0.707462	.000006	0.248
RK56	82	23.22	888	85.89	0.707301	.000012	0.267

Table 9.5. Rb/Sr isotope data for the A2 amphibolite from Roerkulten. The isotope analyses were conducted by Dr. A. Moyes at the Bernard Price Institute, University of the Witwatersrand. Rb and Sr values were obtained by I.D.

The A2 amphibolites are highly deformed by D_2 folds and also contain a planar fabric which is deformed about open D_3 folds. The provisional age of the A2 amphibolite therefore provides a minimum age for D_1 deformation and a maximum age for D_2.

CONCLUSIONS

The metamorphosed intrusions contain a wide variety of compositions, some being tholeiitic in character and others calc-alkaline. Their mineral assemblages are typical of medium grade or amphibolite facies metamorphism ie. temperatures of between 500°C and 650°C. The presence of garnet in some samples helps to constrain the physical conditions of formation but

insufficiently to provide an indication of pressures of metamorphism. The emplacement of the A2 amphibolite provides a minimum age for D_1 (> 796 Ma $\pm$ 110) and a maximum age for D_2 (<796 Ma $\pm$ 110). The distribution of immobile trace elements in the A2 and A3 amphibolites reflect affinities with within-plate sources.

CHAPTER 10
THE DALMATIAN GRANITE AND OTHER POST-TECTONIC GRANITOID INTRUSIONS

INTRODUCTION

The field relationships of the Dalmatian Granite were described in chapter 2. Apparently undeformed granite sheets, up to 10m thick, with varying orientations intrude the Banded Gneiss Complex at Brekkerista, the Fuglefjellet Formation at Fuglefjellet and Dvergen, and the Sveabreen Formation at Salknappen (Map 1).

Two varieties of granite are recognised. The first is characterised by nodular structures, up to 15cm in diameter, which have a leucocratic rim enclosing a melanocratic core (Fig. 2.9, chapter 2). The latter owe their colour to the presence of tourmaline. Locally, where the density of the nodules is high, the leucocratic rims coalesce to form bands enclosing adjacent melanocratic cores.

The second type of granite is characterised by magnetite phenocrysts which are typically only 1-2mm in diameter but rarely may be up to 1cm in diameter. These two varieties of granite are clearly part of the same intrusive phase because, at Dvergen, a granite sheet displaying both varieties, intrudes discordantly across quartzofeldspathic gneisses interlayered with marbles. Where this sheet intrudes the quartzofeldspathic gneisses it is characterised by magnetite phenocrysts but, where it intrudes the marble layers, tourmaline nodules are developed.

The nodules in the Dalmatian Granite are spherical and in this respect they resemble orbicular granites but significant differences are also observed. These differences will be discussed in a later section dealing with the origin of the nodules.

PETROGRAPHY

The granite is evenly medium-grained and is composed of the following minerals (vol. % given in parentheses) quartz (33%), microcline (32%), plagioclase of composition An_{20} (28%), muscovite (4%) and biotite (2%). Accessory minerals, constituting less than 1 vol.% of the rock, include apatite, magnetite and zircon. Some of the muscovite is clearly an alteration product of plagioclase in which it occurs as small patches. The remaining muscovite has the same habit as biotite and appears to be primary (Fig. 10.1). Biotite shows incipient alteration to pale green chlorite. Plagioclase commonly shows zoning.

Contacts between the leucocratic zones of the tourmaline-bearing nodules and the host granite are diffuse as are the contacts between the melanocratic cores and the leucocratic rims. The absence of biotite and tourmaline, respectively, define the boundaries of rims and cores.

Mineralogically, the leucocratic rim of the nodules is similar to the granite host except for an increase in the modal proportion of plagioclase that compensates for the absence of biotite.

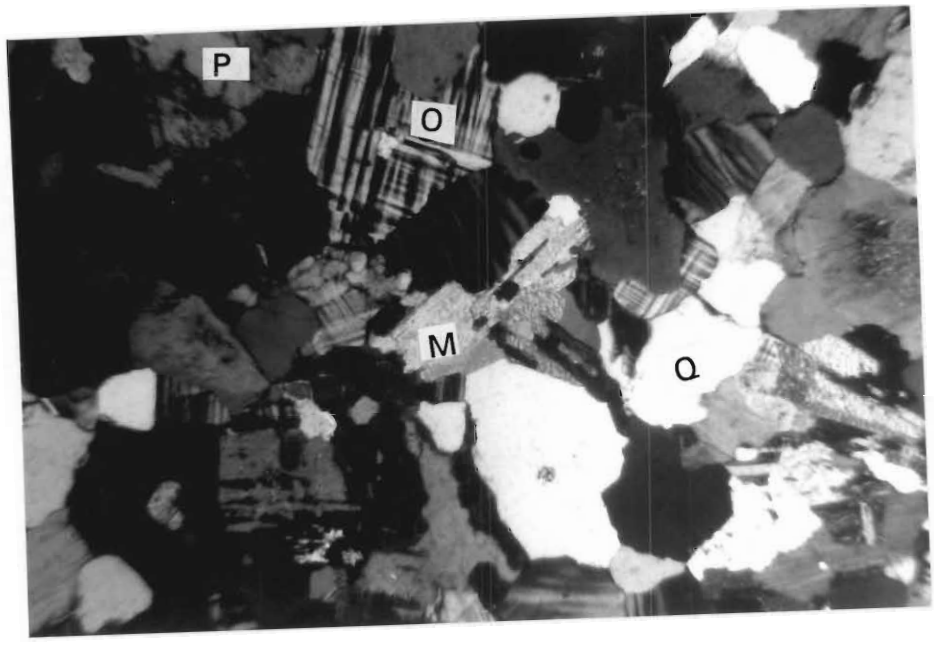

Figure 10.1. Photomicrograph showing the textural nature of muscovite in the granite. Field of view is 4mm. M = muscovite, O = microcline, Q = quartz and P = plagioclase.

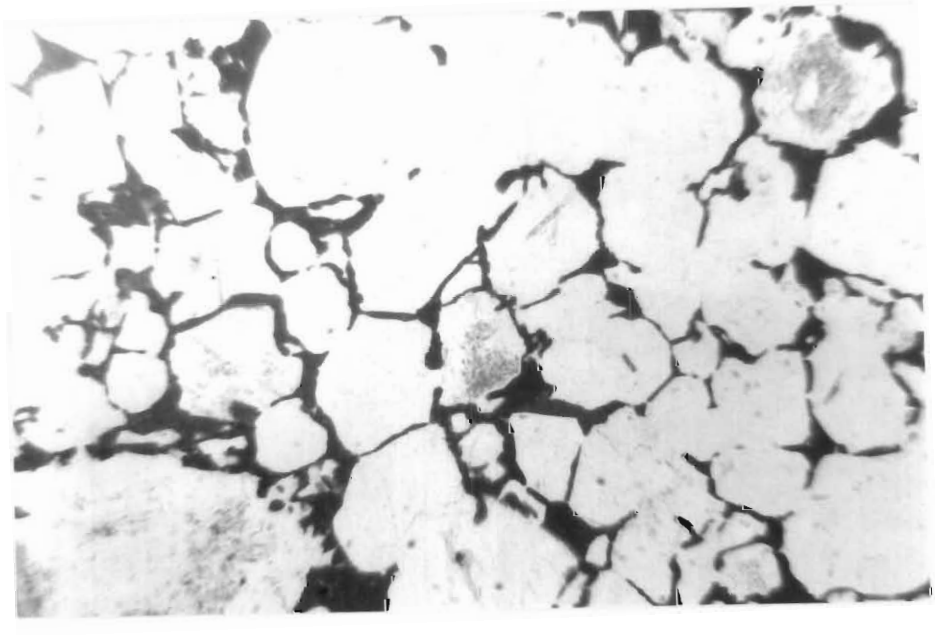

Figure 10.2. Photomicrograph of skeletal tourmaline in the nodules. Field of view is 4mm. The colourless (white) minerals are quartz and feldspar.

The rims consist of quartz (29%), plagioclase (43%), microcline (25%) and muscovite (3%). The melanocratic cores are characterised by tourmaline having a slight colour zonation from pale blue to dark green. The tourmaline is poikilitic and occurs as almost skeletal crystals (see Fig. 10.2) filling the interstices between the other minerals which include quartz (31%), microcline (25%) and plagioclase (30%). The tourmaline grains are optically continuous although apparently unconnected in thin section.

CHEMISTRY

Analyses of the major and trace element chemistry of the granite, the leucocratic rim and the melanocratic core are presented in table 10.1. The mean normative (C.I.P.W.) composition of the granite is quartz (31%), orthoclase (29%), plagioclase (36%), corundum (1%), and hypersthene (1%). The normative plagioclase composition is An_{13}. The granite is iron-rich with an Fe/Fe + Mg ratio of 0.85.

	SiO_2	Al_2O_3	Fe_2O_3	FeO	MnO	MgO	CaO	Na_2O	K_2O	TiO_2	P_2O_5	TOTAL
DVG2	74.63	14.08	0.28	0.65	0.06	0.17	1.02	3.69	5.74	0.08	0.03	100.43
BK56	74.35	14.40	0.20	0.51	ND	0.25	0.97	3.36	5.22	0.09	0.06	99.41
BK57	74.84	14.10	0.20	0.51	0.01	0.24	0.92	3.29	5.22	0.09	0.05	99.47
BK58	74.95	14.64	0.19	0.49	0.01	0.36	0.89	3.44	5.29	0.09	0.07	100.42
BK59	74.47	14.17	0.18	0.46	0.01	0.23	0.94	3.31	5.05	0.09	0.06	98.97
BK6O	75.02	13.77	0.20	0.50	0.01	0.24	0.83	3.39	5.23	0.09	0.05	99.33
BK61	74.31	14.98	0.19	0.47	ND	0.15	1.16	3.95	5.07	0.09	0.06	100.43
BK62	74.41	14.50	0.23	0.57	0.01	0.30	1.08	3.47	5.47	0.09	0.07	100.20
DVGD	74.63	13.65	0.23	0.59	0.05	0.09	1.03	3.43	5.32	0.08	0.05	99.15
BK4	73.98	14.79	0.21	0.53	0.01	0.14	1.05	3.68	4.94	0.13	0.06	99.52
BK4[1]	76.44	14.47	0.04	0.10	ND	0.00	0.31	4.17	4.71	0.03	0.06	100.33
BK4[2]	71.15	14.51	0.50	1.41	0.01	0.70	0.35	2.99	4.22	0.11	0.90	96.04
mean	74.56	14.31	0.21	0.53	0.02	0.22	0.99	3.50	5.26	0.09	0.06	99.75

	Rb	Sr	Th	Zr	Y	Nb	Ba	Sc	La	Zn
DVG2	184	236	18.7	82	7	7	1127	2.9	31	28
BK56	207	224	8.6	67	3.8	5.9	1203	1.2	13.4	32
BK57	222	217	9.7	63	4.4	6.2	1125	2.0	12.2	27
BK58	220	185	6.1	53	4.9	7.1	1001	1.6	13.9	23
BK59	200	190	8.4	64	3.7	4.8	1121	0.8	16.8	31
BK6O	201	187	9.5	65	4.4	6.8	1129	2.1	10.8	35
BK61	180	209	9.3	72	4.1	4.6	925	2.4	12.7	24
BK62	200	220	8.1	71	4.0	4.8	1133	0.3	11.4	32
DVGD	231	244	23	85	4.8	12.9	1097	2.6	45.3	48
BK4	212	209	4.7	47	2.6	4.6	1164	1.1	7.5	24
BK41	171	184	9.8	61	3.3	2.0	1168	ND	12.1	20
BK42	151	155	7.5	59	6.4	0.8	1036	2.7	13.2	121

Table 10.1. Whole rock analyses of the Dalmatian Granite. BK4[1] represents an analysis of a leucocratic rim of a nodule. BK4[2] represents an analysis of a tourmaline-bearing nodule. The low total is due to Boron. ND = not detected. Major element concentrations (above) in wt% and trace element concentrations (below) in ppm.

Trace element chemistry

The only variations in the trace element chemistry of the Dalmatian Granite appear to be related to differences between the sample localities. Most of the samples were collected at from Brekkerista (table 10.1, BK samples) and show very little variation. The two samples from Dvergen (DVG samples) have somewhat higher Th, Zr, Y, Nb, and La contents than the Brekkerista samples.

These differences are not sufficiently large to imply that the granites from the two localities are not cogenetic. The subtle increase in some trace elements might merely reflect minor source rock differences or minor crystal fractionation.

Rare earth element chemistry

The REE analyses of two samples of the Dalmatian granite are given in table 10.2. Chondrite normalised patterns of these samples (Fig. 10.3) are characterised by a small positive Eu anomaly and moderately steep slopes with Ce_{cn}/Yb_{cn} ratios of 12.75 and 16.09.

	BK59	BK60
La	18.85	19.87
Ce	29.95	31.12
Pr	3.4	3.59
Nd	11.98	12.81
Sm	2.19	2.41
Eu	0.7	0.74
Gd	1.54	1.78
Dy	0.94	1.2
Ho	0.19	0.25
Er	0.51	0.63
Yb	0.45	0.59

Table 10.2 REE analyses of the Dalmatian Granite (ppm).

Whereas the major minerals of granites typically have K_d's $<<1$, under reducing conditions Eu is partitioned into both orthoclase and sodic plagioclase. Positive Eu anomalies are therefore commonly recognised in rocks which are interpreted to be either feldspar-rich cumulates or restites in which residual plagioclase forms a significant proportion.

Granites with small positive Eu anomalies are relatively rare. Cullers and Graf (1984, p 295) state that positive Eu anomalies are less common in monzogranites and syenogranites than the more plagioclase-rich granodiorites, quartz diorites, tonalites or trondhjemites. Various models have been proposed for the development of positive Eu anomalies. Pride and Muecke (1980) suggested that positive anomalies might result from the melting of plagioclase-rich restites or plagioclase cumulates. Cullers and Graf (1984) have summarised REE chemistry of granitoids noting that those with positive Eu anomalies, low REE contents and moderately large LREE/HREE ratios could be produced by hornblende and/or garnet fractionation.

The HREE pattern in the Dalmatian Granite suggests that some fractionation of garnet and/or hornblende or the presence of minor amounts of garnet and/or hornblende in the restite are probable. In the case of the Dalmatian Granite, the presence of magnetite is considered to be significant in that its presence implies a relatively high oxygen fugacity. Under oxidising conditions Eu is present as Eu^{3+} and is preferentially partitioned into the melt whereas under reducing conditions, Eu^{2+} is strongly partitioned into plagioclase and K-feldspar (Philpotts, 1970; Weill and Drake, 1973; Drake and Weill, 1975; Drake, 1976; Henderson, 1982,pp. 91-94). Thus the positive Eu anomaly may result from the oxygen-rich nature of the Dalmatian Granite resulting in Eu being partitioned into the liquid. A possible alternative method of generating positive Eu anomalies may be related to the suggestion by Chappel *et al.* (1987) that granites may contain a significant content of xenocrystic or restite material. If the Dalmatian Granite contains a significant proportion of feldspar xenocrysts or feldspathic restite fraction, such material could contain "excessive Eu" and thus result in a positive Eu anomaly. No features have been noted in thin section which could be used to suggest or confirm that a significant restite or xenocryst fraction is present.

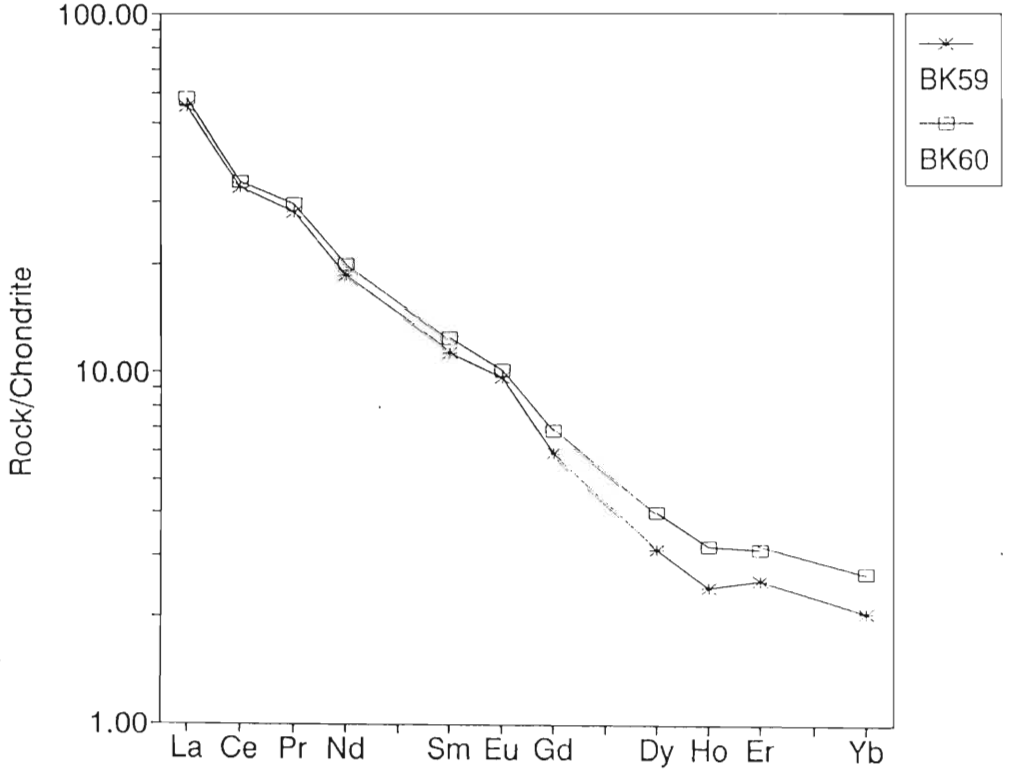

Figure 10.3. Chondrite-normalised REE variation diagrams for two samples of Dalmatian Granite.

EMPLACEMENT OF THE DALMATIAN GRANITE

The mechanism of emplacement of the Dalmatian Granite is best discussed with reference to figure 10.4 which represents a vertical face at Salknappen. Here sheets of tourmaline-free Dalmatian Granite up to 2m thick intrude the gneisses of the Sveabreen Formation. The granite sheets are generally concordant to the layering in the enclosing gneisses.

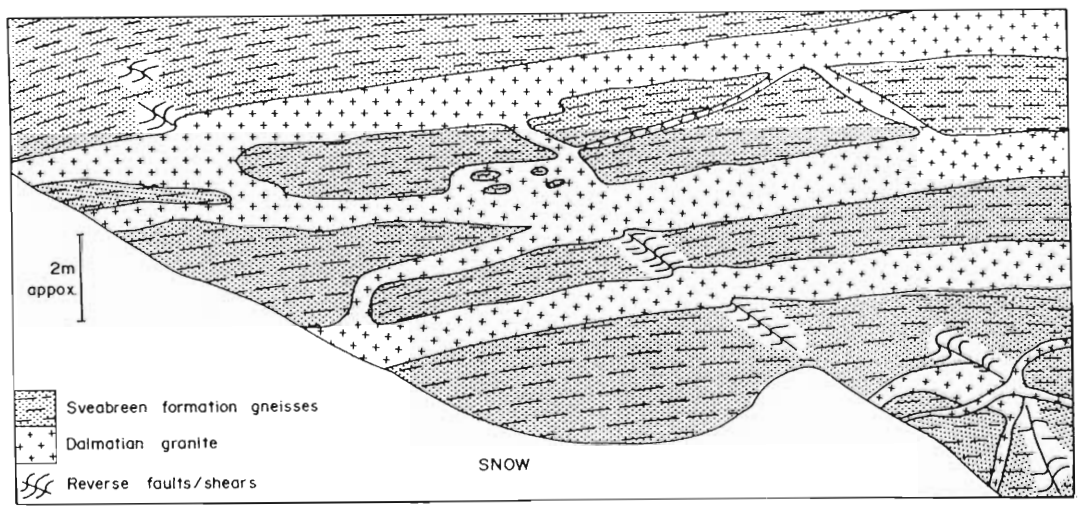

Figure 10.4. Sketch of a locality at Salknappen showing the layers of Dalmatian Granite intruded into Sveabreen Gneisses at Salknappen. The exposure is ~30m wide with and is oriented southeast (left) northwest (right).

Numerous small reverse faults with fault planes dipping to the northwest are seen in the enclosing pelitic gneisses (Figs. 10.4,10.5). These faults displace the margins of the sheets of Dalmatian Granite (see figure 10.5) but do not deform the granite within the sheets. The thin veins of granite linking the granite sheets are oriented parallel or near parallel to the reverse faults. The orientations of these reverse faults are similar to the NW dipping axial planes of D_3 folds further west (see structural chapter).

These features are interpreted to indicate that the granites were emplaced syntectonically during D_3. A planar fabric, defined by biotite, is associated with, and oriented parallel to the NW dipping axial planes of the D_3 folds. K/Ar dating on biotite from the Sverdrupfjella (Ravich and

Solov'ev, 1966, pp. 273-277) yielded ages of approximately 500Ma suggesting that this age represents the timing of D_3 and hence that of the syntectonic emplacement of the Dalmatian Granite.

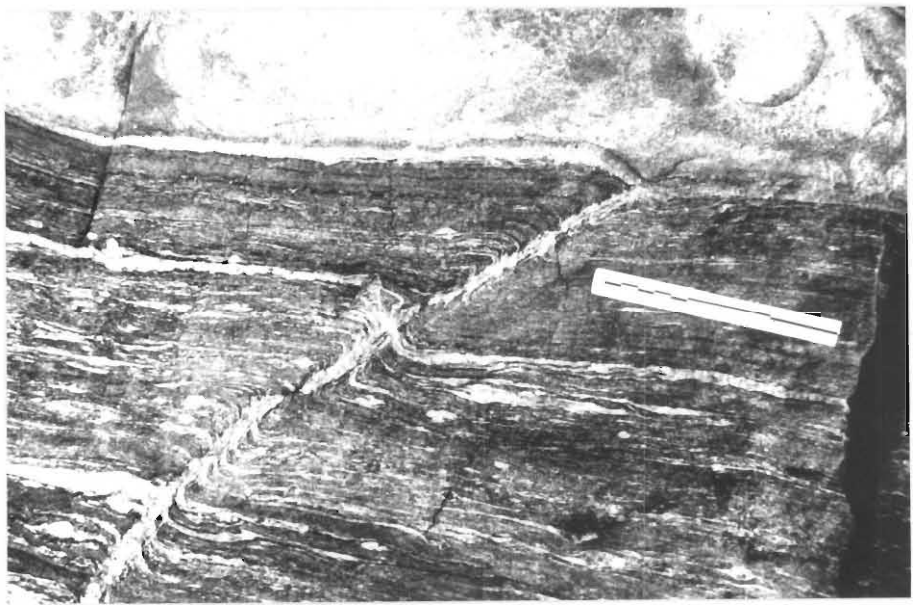

Figure 10.5. Photograph of the margin of the granite sheets at Salknappen showing the shear zones deforming the gneisses, displacing the granite sheet margin but not affecting the granite. Orientation the same as figure 10.4.

PETROGENESIS OF THE DALMATIAN GRANITE

The potential source for the Dalamatian Granite is essentially the same source as for the Jutulrora, Roerkulten and Brekkerista Granites (the Grey Gneiss and Banded Gneiss Complex). Therefore, the partial melt models, presented in chapter 8 (Fig. 8.1), which take the average composition of the Grey Gneiss Complex to represent an estimate of the composition of the source region, are equally applicable to the Dalmatian Granite.

Profiles A and B (Fig. 8.1) are compared to the ORG normalised profile for the Dalmatian Granite in figure 10.6. In terms of these models, partial melting between 30% and 90% (although 90% melting is unlikely in nature) could generate the observed variations in the concentration of K_2O (~30% partial melting), Rb (~30% partial melting) and Ba (~90% partial melting) but Th slightly exceeds the range predicted by the partial melt models.

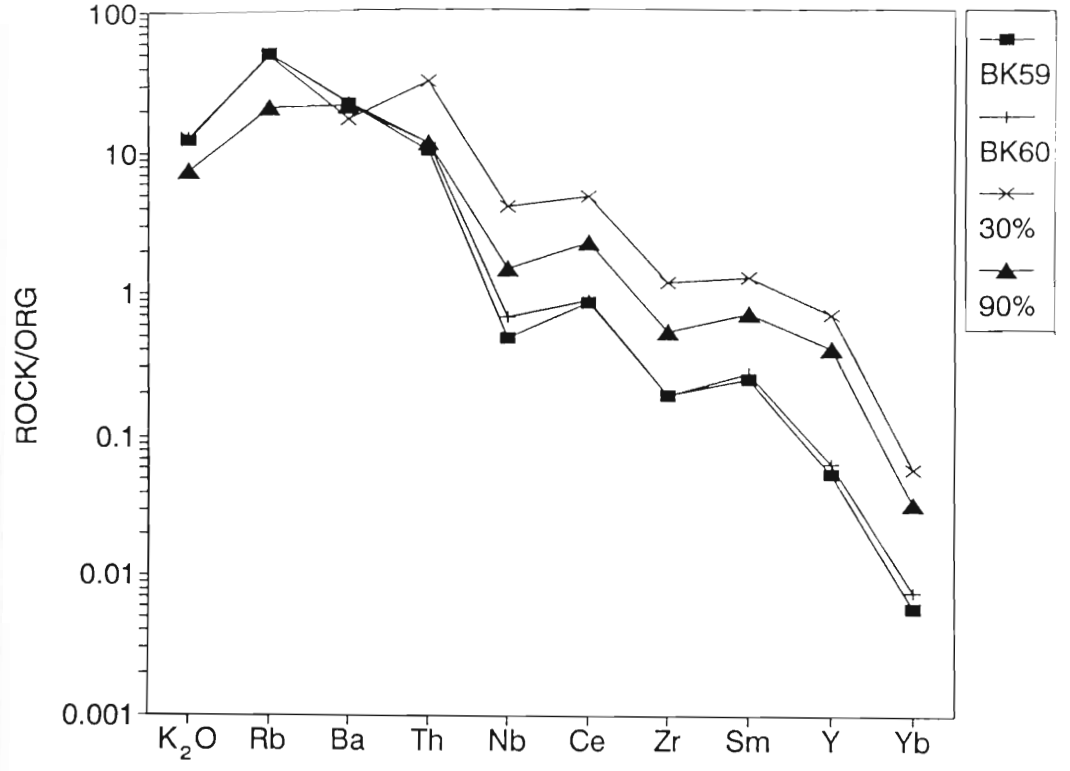

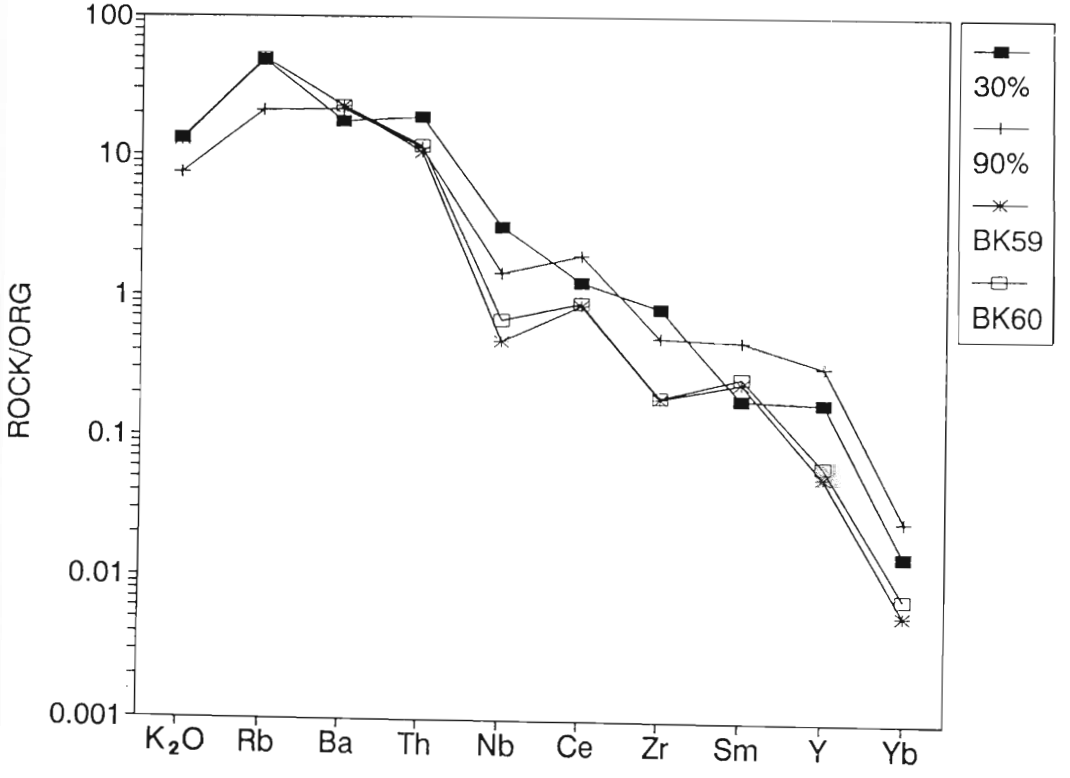

Figure 10.6. ORG normalised profile of samples BK59 and BK60 compared to the partial melt models (A above and B below).

The model shows that the differences between 30 and 90% melting are small and therefore moderate differences in the concentration of Ba in the source region may result in lower fractions of partial melting being required to fulfil the requirements of the model. Variation of Nb is less than in either of the partial melt models or the assumed residuum. Such a situation might arise from a Nb compatible phase in the restite or the concentration of Nb in the assumed source is too high. Cerium, Zr, Sm, Y and Yb contents of the Dalmatian Granite are all lower than those predicted by the partial melt models however the differences between the Dalmatian Granite and partial melt model B (containing accessory minerals in the source) are less than those for partial melt model A. This could imply that the source of the Dalmatian Granite may have had a significantly higher accessory mineral content with the REE remaining largely in the restite after partial melting.

Utilising the granite classification schemes of various authors (Chappel and White, 1974; Louiselle and Wones, 1979; Creaser *et al.*, 1991; White, 1979) described in chapter 8 (p. 115), the Dalmatian Granite has S- type characteristics in that A/CNK > 1.1, normative corundum >1.1%, high SiO_2 content that is restricted in range, irregular variation in chemistry, and common presence of biotite and muscovite. However, the Na_2O content is >3.2% and is more typical of I-type granites. Grantham *et al.* (1991) have reported that the initial $^{87}Sr/^{86}Sr$ ratio (R_o) of the Dalmatian Granite is 0.7353, typical of S-type granites. The low CaO is an A-type characteristic. The high R_o of the granite precludes the Dalmatian Granite being an M-type or I type granite. The Dalmatian Granite is yet another example of a granite having chemical and mineralogical features common to more than one type of granite (see also chapter 8).

Physical conditions of Petrogenesis

Application of the saturation surface thermometers of Watson and Harrison (1983, using Zr) and Harrison and Watson (1984, using P contents) to the Dalmatian Granite yield average temperatures of 704°C and 894°C respectively. Clearly the temperature suggested by the P thermometer appears to be too high as muscovite in the presence of quartz (primary minerals in the Dalmatian Granite) would not be stable at such high temperatures (see later and Fig.10.8). This suggests that a proportion of P in the rock is possibly xenocrystic in the form of apatite, assuming that the geothermometer calibration is valid. In figure 10.7 the C.I.P.W. normative compositions of the samples of Dalmatian Granite are compared to the minimum-melt compositions derived from experiments conducted under a range of physical conditions.

The average composition of the Dalmatian Granite with a normative Ab/An ratio of 6.9 suggests that the Dalmatian Granite was generated at approximately 6-7kb (Fig. 10.7). The presence of primary muscovite in the granite is significant for barometry.

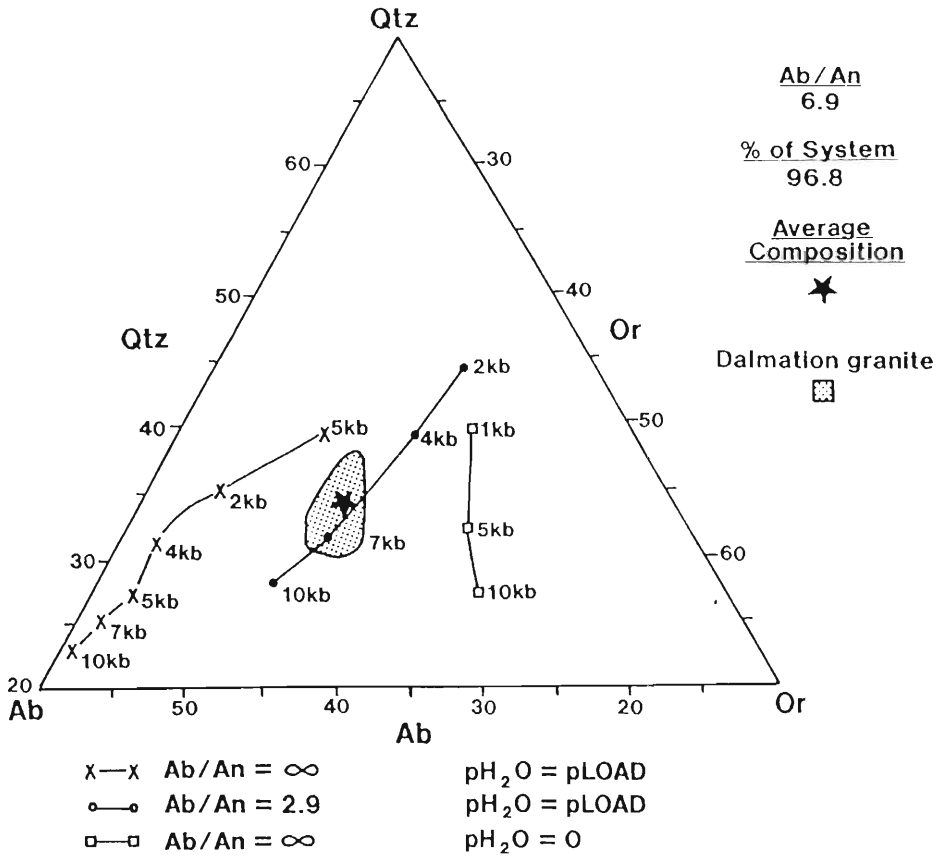

Figure 10.7. The composition of the Dalmatian Granite in terms of minimum melt experiment compositions. Data for the various points are from Tuttle and Bowen (1958), Luth(1969), Winkler (1976, p. 290).

Curves 1a and 1b (Fig. 10.8) represent the conditions for the reaction muscovite + quartz > K-feldspar + aluminosilicate + water with mole fraction of water $X_{H2O} = 1$ and $X_{H2O} = 0.25$, respectively (from Powell, 1978, p 135). Curve 1a shows that muscovite + quartz would be expected on the granite solidus shown by curve 2 (from Johannes, 1985, p 44) and be stable above the solidus at pressures >4kb for the granite system (Qtz-Ab-Or-H_2O). For the system Ab-An-Qtz-H_2O with a plagioclase composition of An_{20} (curve 3, from Johannes 1985, p 44), muscovite + quartz are stable above the solidus at pressures > ~5kb. At pressures below 4 and 5kb, respectively for these systems the granite would be characterised by K-feldspar + sillimanite.

Another implication of figure 10.8 is that the X_{water} in the magma must approach unity because, if it were significantly lower, the stability of muscovite + quartz is reduced to lower temperatures (curve 1b, from Powell, 1978, p 135). In contrast the granite solidus would be significantly increased to higher temperatures (curve 4, from Johannes, 1985, p 41).

The solidi for granites with $pH_2O = P_{load}$ (curves 2 and 3) show that granites will solidify after ascending to higher crustal levels due to decreasing pressure.

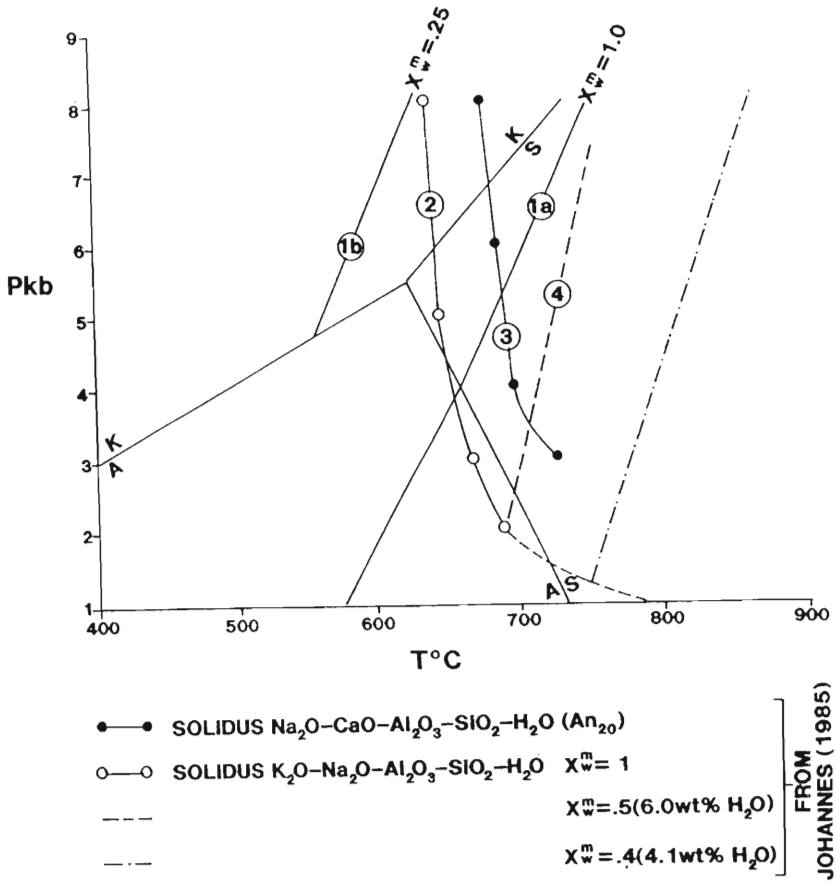

Figure 10.8. Physical conditions pertaining to the petrogenesis of the Dalmatian Granite. The reference sources of the various curves are discussed in the text. Curves 1a and 1b reflect the physical conditions for the reaction of muscovite + quartz = K-feldspar + Al_2SiO_6 + H_2O with X_{H2O} = 1.0 and X_{H2O} = 0.25 respectively. K = kyanite, S = sillimanite and A = andalusite.

There is no evidence of local or large scale melting at the various exposures of Dalmatian Granite and thus the Dalmatian Granite must have risen a small distance from its source probably assisted by syn-tectonic emplacement.

ORIGIN OF THE NODULAR TOURMALINE STRUCTURES

The quartz content is approximately constant in the host granite, the leucocratic rims and the melanocratic cores. The host granite has a slightly higher microcline content than in the nodules. In contrast, leucocratic rims and the tourmaline-rich cores of the nodules are enriched in plagioclase relative to the host granite. Tourmaline and biotite are antipathetic, the former being confined to the cores of nodules and the latter to the host granite. This distribution appears to reflect a chemical zonation toward the core of the nodules marked by decreasing K and increasing Na, Fe and Mg. This zonation might result from variable diffusion rates, liquid immiscibility or local enrichment.

The spherical nature of the tourmaline nodules suggests a similarity to orbicular granites but

there are important differences that distinguish the nodules from orbs. These differences are (see Eliston, 1984) :-

(1) orbs in orbicular granite are described as being so profuse that they are commonly in contact and deform adjacent orbs whereas in the Dalmatian Granite, the nodules seldom make contact and are randomly dispersed through the granite. When contact between two nodules occurs, the leucocratic outer rims and, more rarely, the cores coalesce.

(2) orbs in orbicular granite commonly show nucleation about a core consisting of some pre-existing particle whereas this is not evident in the nodules of the Dalmatian Granite. Eliston (1984) provided evidence for the mobility of minerals in the cores of the orbs after orbicule formation. No such evidence is seen in the Dalmatian Granite. The apparently even-grained mineral fabric defined by quartz and feldspar throughout both the granite and nodules implies that the Dalmatian Granite was at least semi-solid at the time the nodules formed.

The origin of the large poikilitic tourmaline crystals in the cores of the nodules appears to be intimately related to the genesis of the nodules themselves. Tourmaline is confined to the nodules and is not found disseminated in the granite host. Benard *et al.* (1985) have described a granite in which magmatic tourmaline occurs randomly distributed as euhedral crystals. The experimental work of Benard *et al.* (1985) demonstrated that the solubility of tourmaline in granite magmas is fairly low with tourmaline commonly being an early liquidus phase and stable to relatively high temperatures. These properties suggest that liquid immiscibility and/or low rates of diffusion did not contribute to the formation of either the tourmaline or the nodules. Perhaps the most significant observation relative to the origin of the tourmaline nodules is that at Dvergen they are confined to those parts of the Dalmatian Granite intruding into carbonates. Similar relationships have been recorded at Fuglefjellet and Kvitkjolen (east of the study area) and imply that slow or poor diffusion of boron through the sheet was not a factor. The intimate association of tourmaline nodules in the granite with carbonates strongly suggests that the ingredients to form the nodules were derived from the country rocks.

That the carbonates and associated gneisses could be sources of boron is supported by the occurrence of tourmaline in a sample of quartzofeldspathic gneiss interlayered with carbonates at Fuglefjellet. (see Chapter 5).

Povondra and Novak (1986) have reported the presence of tourmaline in metamorphosed carbonate rocks from western Moravia, Czechoslovakia indicating that the association of boron with carbonates is not unusual. The concentration of tourmaline in nodules rather than as disseminated grains in the granite suggests some form of local physico-chemical control.

Assuming that the granite was intruded as a semi-crystalline mush of quartz and feldspar (Chappel *et al.* 1987) in which magnetite phenocrysts already existed with a proportion of intercrystalline melt, it would be reasonable to suggest that the granite emplaced in the vicinity of carbonates would be affected by increased pCO_2 and therefore reduced partial pressures of

O_2 and H_2O. Pichavant (1981) and London *et al.* (1988) have shown that boron is partitioned into the vapour phase in melt-vapour systems. Under conditions of lowered pO_2 conditions, magnetite in the Dalmatian Granite would be unstable and would react with the intercrystalline fluid and the boron-enriched vapour of the magma. The following reaction can then be proposed for the development of tourmaline around nuclei of magnetite :-

$Fe_3O_4 + 3K_2(Fe)_6Al(Si_5Al_3O_{20})(OH)_4 + K_2Al_4(Si_6Al_2O_{20})(OH)_4 + 6NaAlSi_3O_8 + 9B_2O_3 \rightarrow$
$6Na(Fe)_3Al_6Si_6O_{18}(BO_3)_3(OH)_4 + 5SiO_2 + 2K_2 + 3.5O_2 + 4H_2O$
Magnetite + annite + muscovite + albite + Boron (from carbonates) ->
Tourmaline + quartz + K_2^+ + oxygen + water

It is suggested that magnetite, biotite, albite (in plagioclase) and muscovite reacted with a boron-rich fluid phase to produce tourmaline. The original presence of muscovite in the cores of the nodules is presumed because this mineral is found in the leucocratic rims. Significantly, magnetite, as a reactant, requires that oxygen is released into the fluid phase as a product along with K_2 and water. Under these conditions it would be reasonable to expect to find poikilitic tourmaline with partially corroded magnetite nuclei. Although this model is attractive, no remnant magnetite has yet been observed in the cores of the nodules to substantiate this hypothesis. Another feature which may be expected is that the tourmaline could display zoning with iron-rich cores becoming more magnesian to the rims. A traverse across tourmaline from one of these nodules (Table 10.3) showed no major compositional variation despite the colour zonation seen in thin section.

A mineral separate of tourmaline from a nodule is very similar to the probe analyses (Table 10.3) suggesting that the tourmaline in the nodules is relatively homogeneous. Chorlton and Martin (1978) have shown that addition of boron to a granitic liquid results in depression of the solidus by up to 125°C. Thus the nodules may represent small sub-liquidus domains which equilibrated and solidified after the rest of the granite. If the model proposing derivation of tourmaline from magnetite and biotite is correct, the tourmaline should be extremely iron-rich. Whereas the Fe/Fe + Mg ratio in the tourmalines is quite high at 0.62 (average of 3 analyses, table 10.3), the relatively high proportion of Mg is surprising because the granite host has an Fe/Fe + Mg ratio of 0.85 and therefore is less magnesian than the tourmaline. Attainment of a Fe/Fe + Mg ratio of 0.62 in tourmaline (derived from magnetite and biotite) would require the presence of biotite of a highly magnesian or phlogopitic composition. This is considered to be unlikely.

Benard *et al.* (1985) noted that the Mg/Mg + Fe ratio in tourmalines is commonly higher than the associated rock with K_dFe in tourmaline being 0.81-0.97.

	1	2	3	4
SiO_2	35.74	35.32	35.62	36.71
Al_2O_3	32.82	32.30	32.59	34.18
$B_2O_3^*$	10.58	10.50	10.50	10.94
FeO	11.45	12.09	11.13	12.24
MnO	0.12	0.13	0.12	0.10
MgO	3.97	3.91	3.99	4.46
CaO	0.42	0.44	0.34	0.50
Na_2O	2.34	2.30	2.42	1.82
TiO_2	0.82	0.92	0.68	0.6496
TOTAL	98.26	97.85	97.39	101.61
	no.ions	no.ions	no.ions	no.ions
SiO_2	5.874	5.851	5.896	5.8363
$Al_2O_3^T$	0.126	0.149	0.104	0.164
$Al_2O_3^Z$	6.000	6.000	6.000	6.000
$Al_2O_3^X$	0.231	0.157	0.256	0.241
FeO	1.574	1.674	1.541	1.6272
MnO	0.017	0.018	0.017	0.013
MgO	0.972	0.965	0.985	1.057
CaO	0.074	0.078	0.060	0.085
Na_2O	0.745	0.739	0.777	0.561
TiO_2	0.101	0.115	0.085	0.077
TOTAL	18.714	18.746	18.725	18.664

Table 10.3. Analyses (wt%) of tourmaline from the tourmaline nodules. Analysis 4 is anhydrous and is from a bulk mineral separate that was analyzed by X-Ray fluorescence spectrometry (with Fe_2O_3 recalculated to FeO) whereas analyses 1-3 are electron microprobe analyses from core to rim. *B_2O_3 content was calculated on the basis of 3 cations in the mineral structural formula after Henry and Guidotti (1985). The microprobe analyses were done by P.B. Groenewald at Rhodes University using a Jeol Microprobe.

Benard *et al.* (1985) also stated that the K_d will be dependant on pO_2 with a higher K_d for Mg in tourmaline being related to a higher pO_2. It is not improbable that magnesium was introduced together with boron in a fluid phase. When the latter reacted with magnetite, K was released into the fluid phase (see reaction above). The incipient alteration of plagioclase to sericite observed in the Dalmatian Granite may be evidence for the presence of a K-enriched fluid phase.

Henry and Guidotti (1985) related the compositions of tourmalines to different petrological environments. In the system Al-Fe-Mg, tourmalines in the Dalmatian Granite are comparable to tourmalines from Fe^{3+}-rich quartz-tourmaline rocks, calc-silicates and metapelites (Fig. 10.9). In the Ca-Fe-Mg system, tourmalines in the Dalmatian Granite have compositions considered to be characteristic of Li-poor granitoids, associated pegmatites and aplites (Fig. 10.9). Henry and Guidotti (1985) demonstrated that, in tourmalines whose compositions fall below the schorl-dravite line in the Al-Fe-Mg diagram (as the Dalmatian Granites do), Fe^{3+} may be a major substituent of Al in Z sites of the tourmaline mineral lattice provided the uvite component is insignificant. In the case of the Dalmatian Granite this suggests that replacement of magnetite by tourmaline occurred without the Fe^{2+}/Fe^{3+} ratio being affected.

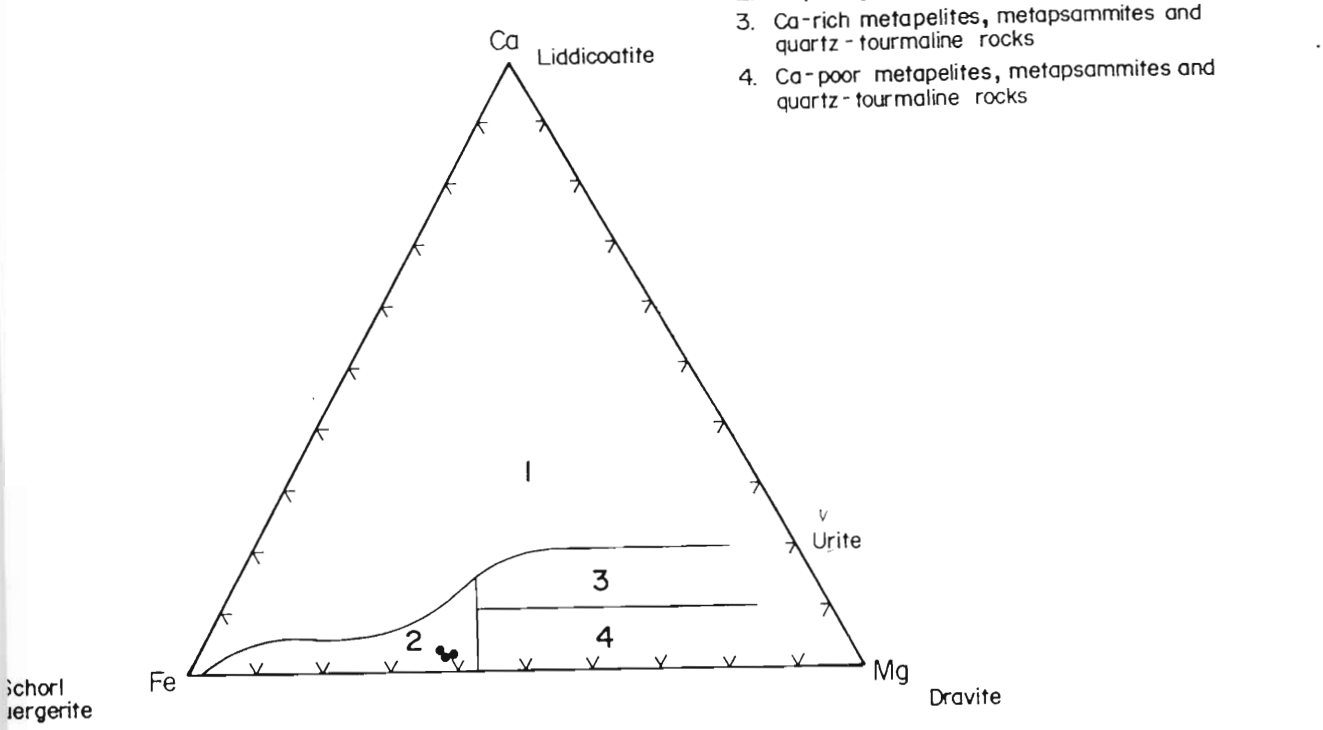

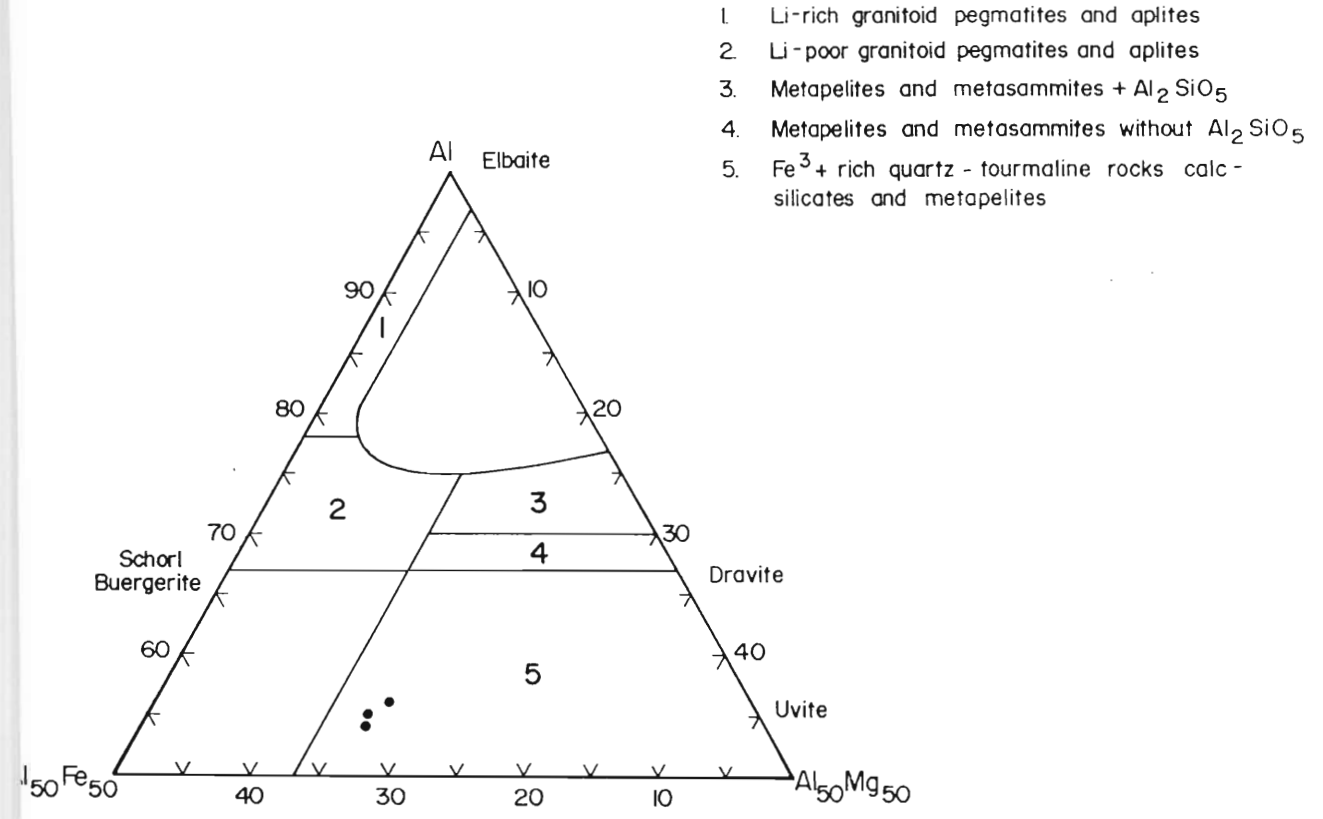

Figure 10.9. Compositions of the tourmaline from the Dalmatian Granite in the Ca-Mg-Fe (above) and Al-Fe-Mg (below) systems.

This is in conflict with the reaction given above because it allows for no Fe^{3+} in the tourmaline and essentially involves de-oxidation. The presence of a significant uvite component in the Dalmatian tourmalines is also in conflict with this interpretation. Examination of the analyses in Table 10.3 shows that there is sufficient Al to fill the Z sites and contribute to the T and Y sites. Therefore it is suggested that Fe^{3+} was not a significant substituent for Al in the Dalmatian tourmalines. It is concluded from the fore-going discussion that the tourmaline developed sub-liquidus and resulted from the replacement of magnetite grains in the presence of a boron-magnesium-bearing fluid introduced from adjacent carbonates.

Tourmaline-bearing granites similar to the Dalmatian Granite have been recorded in the Darling Granite Batholith of the Cape Province, South Africa (Schoch, 1975) which has been dated at 600 $\pm$20 Ma (U-Pb method) (Schoch *et al.*, 1975). Schoch (1975) concluded that the nodules were a result of either late segregation processes or local additions of boron to the melt. He based this conclusion on the size and distribution of the nodules in the Darling Batholith.

In Antarctica, granites containing tourmaline nodules have been recorded in the central Transantarctic Mountains (Stump *et al.*, 1986). At this locality undeformed granites, of which the tourmaline-bearing Mount Mooney granite is a phase, intrude the volcanogenic Wyatt Formation which has been dated at 545$\pm$ 59 Ma. (R_o=0.7114 $\pm$0.003) (Stump *et al.*, 1986). It may be significant that tourmaline overgrowths are found in the Wyatt Formation at Mount Mooney although Stump *et al.* (1986) do not name the mineral(s) on which tourmaline has grown.

OTHER POST-TECTONIC INTRUSIONS

These intrusions are granitic in composition but, texturally, include aplitic to pegmatitic varieties. The veins are up to 2m wide and, with one exception, do not display planar mineral fabrics. Except for local displacement by faults, the veins do not show any evidence of deformation in the field and are therefore considered to be post-tectonic. It is possible that some or all of these veins are related to the Dalmatian Granite, the only other phase of post-tectonic granites thus far recognised. Field relationships do not permit such a correlation but this is suggested by chemical similarities between the veins and the Dalmatian Granite.

Sample JE31 was sampled from a fine-grained portion of a late pegmatite and on chemical grounds is not considered to be related to the Dalmatian Granite. The remainder of the samples are similar in grain size and appearance to the Dalmatian Granite although no tourmaline nodules have been seen in these veins.

Petrography

Nine samples from these intrusions were collected. Their mineralogy is summarised in table 10.4. The rocks are typically granitic having approximately equal modal proportions of quartz, plagioclase and K- feldspar. The rocks are generally medium- to coarse-grained and show a

hypidiomorphic granular texture. Sample H6 shows a weak planar fabric defined by biotite. Sample H6 also differs in that it is the only sample to contain hornblende and allanite.

In the remaining samples muscovite commonly partially replaces plagioclase and, in most cases, is secondary. Light to dark-brown biotite is typically partially altered to pale-green chlorite. Opaque minerals, present in samples RK3, RK9, RK10, RK17 and H6, commonly show subhedral cubic forms and are therefore considered to be magnetite. In all the samples K-feldspar is present as microcline. Plagioclase is commonly untwinned.

Compared to the Dalmatian Granite, mineralogical differences are the presence of amphibole and allanite in sample H6, lower biotite contents in general, and the absence of primary muscovite and of tourmaline.

	JE20	JE19	BK21	RK9	RK10	RK17	RK3	H6	JE31
Qtz	30	30	30	30	35	30	30	30	30
Pl	35	30	30	25	24	30	25	30	40
Mc	30	30	35	40	35	35	35	30	20
Ms	9	10	1	2	2	6	3		9
Bt	1		3	2	3	8	6	7	1
Aln								<1	
Mt			1	1	1	1	1	1	
Hbl								1	

Table 10.4. Estimated modal mineralogy (vol%) of the granitic veins.

Chemistry

The major and trace element analyses of the samples of the granitic veins are shown in table 10.5. Included in table 10.5 for comparison are average values for the Dalmatian Granite (MDG).

All the samples are typically granitic, having SiO_2 contents in excess of 70%. Most samples have $K_2O > Na_2O$ except sample JE31. Sample H6 has CaO marginally in excess of Na_2O. All the samples are weakly corundum normative (Table 10.6). Barium contents are generally high (>1000ppm) except for samples JE31, RK9 and RK10. Lanthanum contents are mostly low, varying between 6 and 32ppm except for samples H6 and RK17 which are relatively enriched in La (124 and 221ppm respectively). Rubidium and Sr contents in the samples are broadly similar, except for samples JE31 and H6. JE31 has high Rb and low Sr whereas H6 has high Sr. These differences result in JE31 having a Rb/Sr ratio of ~7 and H6 a low Rb/Sr ratio (0.23). Zirconium contents are low ($\leq$ 80ppm) except for samples H6 and RK17 (220ppm and 64ppm respectively). The high Zr, La and relatively high Th contents in samples H6 and RK17 may be related to the presence of allanite and zircon in these rocks.

	JE20	JE19	BK21	RK9	RK10	RK17	RK3	H6	JE31	MDG
SiO_2	73.71	74.31	74.62	76.28	76.43	70.63	75.23	71.41	75.06	74.56
Al_2O_3	14.43	14.76	14.19	13.40	13.37	14.24	13.34	15.08	14.46	14.31
Fe_2O_3	0.17	0.19	0.28	0.14	0.17	1.11	0.34	0.67	0.16	0.21
FeO	0.42	0.49	0.73	0.34	0.43	2.70	0.86	1.90	0.40	0.53
MnO	0.01	0.01	0.01	ND	ND	0.08	0.01	0.03	0.02	0.02
MgO	0.11	0.20	0.17	0.09	0.07	0.14	0.23	0.91	0.15	0.22
CaO	1.12	0.56	0.95	0.96	1.01	1.49	1.01	2.32	0.63	0.99
Na_2O	3.45	3.27	3.45	2.74	2.25	2.57	2.41	2.30	4.61	3.50
K_2O	5.48	5.62	5.24	6.25	6.19	6.39	6.11	5.53	3.79	5.26
TiO_2	0.05	0.13	0.13	0.06	0.07	0.48	0.10	0.33	0.04	0.09
P_2O_5	0.05	0.04	0.03	0.02	0.02	0.07	0.03	0.10	0.08	0.05
TOTAL	99.00	99.58	99.80	100.28	100.01	99.90	99.67	100.58	99.40	99.74
Rb	187	192	129	109	108	115	127	119	320	206
Sr	193	180	197	131	208	139	331	507	47	212
Th	4	8	16	18	14	21	ND	19	4	11
Zr	30	32	67	68	80	648	53	220	46	67
Y	2	4	17	3	3	42	3	18	8	4
Nb	4	6	20	3	2	26	3	12	14	7
Ba	1109	1012	1001	266	479	1354	2277	2552	240	1103
Sc	1	2	1	ND	1	8	ND	3	ND	2
Cr	ND	ND	ND	4	4	ND	6	2	ND	ND
La	12	8	32	6	23	221	6	124	ND	18
V	7	8	5	6	2	7	15	36	3	ND
Cu	4	2	1	3	ND	67	4	7	3	ND
Ni	2	1	ND	1	2	1	2	3	ND	ND
Zn	13	20	17	6	8	51	21	25	26	305
A/CNK	1.06	1.18	1.09	1.03	1.09	1.03	1.07	1.08	1.13	
Rb/Sr	0.97	1.06	0.65	0.83	0.52	0.83	0.38	0.23	6.81	0.97

Table 10.5. Major and trace element chemistry (in wt% and ppm respectively) of the granitic veins. ND = not detected.

Source materials of the granites

Based on the criteria for recognising various granite-types described in chapter 8 (p. 115), the granite veins show variable affinities. None of the samples show M-type characteristics.

Samples JE20, JE19, JE31 and BK21 show S-type characteristics having $Na_2O > 3.2\%$ whereas samples RK9, RK10, RK17, RK3 and H6 have I-type characteristics with $Na_2O < 3.2\%$. All the samples except RK9 and RK 17 show S-type characteristics with A/CNK >1.05, the exceptions showing I-type characteristics. The presence of hornblende in sample H6 suggests that it is not an S-type granite. The high HFSE's in samples H6 and RK17 suggest A-type affinities for these samples.

The limitations of I, S, A and M type granite classification was discussed briefly in chapter 8. From the above it may be seen that the various granitic veins display I-, S- and A-type characteristics as defined above. Whereas these various characteristics may have served as a useful basis for distinguishing various granites studied by Chappel and White (1974), application to the granites of the NW. H.U. Sverdrupfjella does not permit the distinctions made by these authors. Asmeron *et al.* (1988) have shown that S-type granites may be derived by partial melting of I-type granitoids and thus the connotations of source attached to S- and I-type

granites may be incorrect. Alternatively, the recognition of both I and S type characteristics may indicate a heterogenous source for the granites.

MESONORM	JE20	JE19	BK21	RK9	RK10	RK17	RK3	H6	JE31
Ap	0.12	0.10	0.07	0.05	0.05	0.17	0.07	0.24	0.19
Spn	0.11	0.27	0.27	0.13	0.15	1.02	0.21	0.70	0.08
Or	32.15	32.55	30.06	36.69	36.55	35.14	35.31	28.73	21.72
Ab	31.45	29.68	31.27	24.83	20.54	23.52	22.05	20.84	41.63
Mag	0.18	0.20	0.30	0.15	0.18	1.18	0.36	0.71	0.17
An	5.13	2.09	4.10	4.46	4.71	5.36	4.55	9.80	2.48
Crn	1.08	2.80	1.49	0.56	1.41	1.30	1.25	1.93	2.05
Bt	1.15	1.61	1.91	0.91	1.00	5.33	2.37	6.78	1.28
Qtz	28.64	30.71	30.53	32.23	35.41	26.99	33.82	30.31	30.42
TOTAL	100.01	100.01	100.01	100.01	100.01	100.02	100.01	100.03	100.02
CIPW									
Ap	0.12	0.10	0.07	0.05	0.05	0.17	0.07	0.24	0.19
Ilm	0.10	0.25	0.25	0.11	0.13	0.91	0.19	0.62	0.08
Or	32.71	33.35	31.03	36.83	36.57	37.80	36.22	32.49	22.53
Ab	29.49	27.78	29.25	23.12	19.04	21.77	20.46	19.35	39.24
An	5.51	2.71	4.66	4.71	4.97	7.26	4.97	11.25	2.99
Crn	0.83	2.32	1.14	0.40	1.15	0.44	0.95	1.16	1.70
Mag	0.25	0.28	0.41	0.20	0.25	1.61	0.49	0.97	0.23
En	0.28	0.50	0.42	0.22	0.17	0.35	0.57	2.25	0.38
Fe	0.57	0.55	0.91	0.41	0.53	3.40	1.16	2.43	0.58
Qtz	30.19	32.20	31.88	33.97	37.16	26.30	34.93	29.32	32.15
TOTAL	100.04	100.03	100.02	100.02	100.02	100.00	100.02	100.07	100.06

Table 10.6. C.I.P.W. and Barth mesonorms for the granitic vein samples (%).

Creaser *et al.* (1991) and Clarke (1992) have questioned the A-type classification because the I, M and S granite classification conveys interpreted genetic information whereas the A-type classification describes characteristics of the magma and also implies an anorogenic tectonic environment. Clarke (1992) states that the "alphabetic" classification system does not take the effects of igneous differentiation or sub-solidus alteration into account and ignores the heterogeneous nature of the lower crust.

Correlation of the granitic veins

The major element chemistries of samples JE19, JE20 and BK21 are almost identical to that of the Dalmatian Granite. Samples RK9, RK10, RK17 and RK3 are similar except for slightly higher K_2O and lower Na_2O contents whereas JE31 and H6 are characterised by higher Na_2O and CaO than the Dalmatian Granite, respectively. Samples JE19, JE20 and BK21 have similar trace element contents to the Dalmatian Granite. Samples JE31 and H6 have higher Rb and Sr than the Dalmatian Granite respectively. Ba contents in samples JE31, RK9 and RK10 are lower than in the Dalmatian Granite whereas Ba contents in samples RK3, RK17 and H6 are higher than the

Dalmatian Granite. RK17 and H6 have higher La and Zr contents than the Dalmatian Granite.

The C.I.P.W. normative compositions of the granitic veins are plotted on a Qtz-Ab-Or diagram (Fig. 10.10) which shows that 3 samples have comparable compositions to the Dalmatian Granite (JE19, JE20 and BK21), 5 samples scatter outside the Dalmatian Granite field and Sample H6 does not plot within the limits of the diagram. It might be reasonable that pegmatitic phases of a granite might reflect lower pressures, however they could equally be expected to reflect more hydrous compositions.

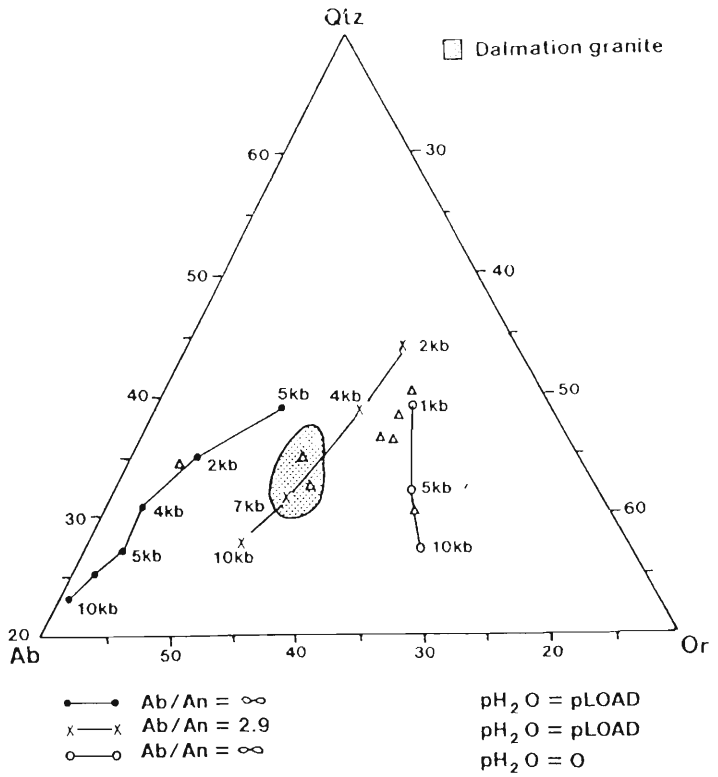

Figure 10.10. Composition of the granite veins on a Qtz-Ab-Or diagram.
Data for the various points are from Tuttle and Bowen (1958), Luth(1969), Winkler (1976, p. 290).

CONCLUSIONS

Field relationships suggest that the Dalmatian Granite was emplaced syntectonically during D_3 at 469 $\pm$5 Ma (Rb/Sr data, Grantham *et al.*, 1991). The significance, if any, of the occurrence of tourmaline-rich nodules in granites emplaced between ~450 and 600Ma is not known but may be a feature of the Pan-African (or Ross) orogeny with which the granites are associated.

Field relationships indicate that the development of the tourmaline nodules in the Dalmatian Granite, at least at Dvergen, is a localised phenomenon and is spatially related to areas where the granite intrudes carbonate-rich paragneissic sequences. The boron required for the

tourmaline nodules is therefore considered to be derived from the carbonates. Whereas the above model may apply where a ready source of boron is present from adjacent carbonates, the broader occurrence of tourmaline nodules may also involve other mechanisms.

Samples JE19, JE20 and BK21 collected from the granitic veins have almost identical major and trace element contents to those of the Dalmatian Granite and therefore are probably related to this phase of intrusion. Samples RK3, RK9, RK10 and RK17 are broadly similar to the Dalmatian Granite except for Ba (RK3, RK9, RK10), La (RK17) and Zr (RK17). Consequently these samples may be related to the Dalmatian Granite with minor differences in chemical composition arising from local source variations (Grantham, *et al.* 1991). Samples H6 and JE31 show significant differences in major and trace element contents and are therefore considered to be unrelated to the Dalmatian Granite.

CHAPTER 11
THE KIRWANVEGGAN DOLERITES

INTRODUCTION

No radiometric dating has been undertaken on the dolerite dykes from the H.U. Sverdrupfjella; however Wolmarans and Kent (1982) report an age of 192± Ma for a dolerite dyke at Nils Jorgenutane, to the west of the study area. The Straumsvola Alkaline Complex has been provisionally dated at ~182 Ma(Ar-Ar, I. Evans., pers. comm.) and 170±4Ma (Rb/Sr, A. R. Allen, pers comm). The presence of dolerite xenoliths in the Straumsvola Alkaline Complex as well as dolerite dykes which intrude the Straumsvola Complex (fig. 2.9, chpt. 2, p.18) indicate that the intrusion of the dykes occurred over an extended period pre- and post- ~170Ma. The dykes are generally vertical in orientation although steeply inclined dykes are known. Two orientations of dykes have been recognised in the study area; a suite striking slightly west of north and a northeast striking suite (Hjelle, 1972; Grantham and Hunter, 1991). The dolerite dykes are up to 30m wide.

PETROGRAPHY

Twenty-two samples were collected from the dolerite dykes. The petrography and mineralogy of the dykes are summarised in table 11.1. The medium- to coarse-grained, equigranular samples described below are from the central portions of relatively thick dykes. Some of the narrower dykes in the study area contain amygdales filled with prehnite and/or carbonate (JW51, H14 and JE58) (fig. 11.1). The samples from Tvora (indicated by prefix TV, table 11.2) are recrystallised and altered to varying degrees and contain significant biotite and/or amphibole. The alteration may be a consequence of the intrusion of the Tvora Syenite Complex (chapter 13). Consequently in the subsequent discussion, the altered and unaltered dolerites will be considered separately.

The unaltered dolerites (table 11.1) are generally fine to medium grained, mostly inequigranular, porphyritic, and contain variable proportions of olivine, orthopyroxene, clinopyroxene, plagioclase, and accessory opaque minerals assumed to be magnetite and/or ilmenite. The porphyritic phases are contained in a medium- to fine-grained equigranular groundmass characterised by a sub-ophitic to ophitic texture.

The groundmass contains clinopyroxene + plagioclase + opaque minerals (magnetite and or ilmenite) ±olivine ± orthopyroxene. The porphyritic phases include, most commonly, olivine (most samples), clinopyroxene (four of sixteen samples), and plagioclase (three of sixteen samples). Olivine is commonly partially serpentinised and is generally porphyritic with anhedral to euhedral grain shapes. Clinopyroxene is anhedral to euhedral, pinkish in colour, and is commonly zoned.

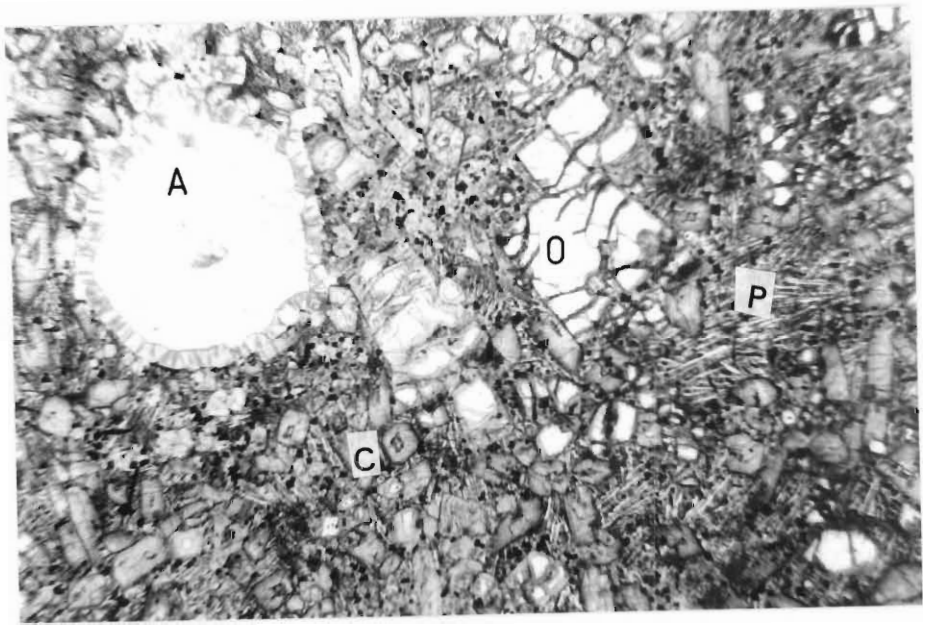

Figure 11.1. Amygdale (A) in dolerite filled with calcite (core) and prehnite (thin rim). Note the adjacent porphyritic olivine (O), hollow skeletal clinopyroxene (C) and needle-like plagioclase (P). Diameter of amygdale is ~1mm.

No.	Texture	Ol	Pyx	Pl	Mt,Ilm	Comments
FG57	f, in	10 p,e	70	5	5	radiating Cpx + glass?
JW51	m, in	5 p,a	60 p,a	30	5	vesicular
JE58	f, in	15 p,e	50 p,s	30	5	ves, Cpx includes Ol
JW57	m, eq	10 s	60 s	27 a	3	Cpx zoned titanaugite
RK5	f, in	5 (sp)	40	50 p,s	5	
RK23	m, eq	5 a	40 e	50 s	5	Qtz xenocryst?
JE54	f, eq	15 (sp)	30	50	5	Pl altered, Cpx hollow
RK4	f, in	5 p,e	40	50 p,s	5	trachytic texture
JW52	m, eq	10 p,a	60	25	5	Phl present
JW60	c, in	10 p,a	60 p,a	25 s	5	Cpx coarse + Ol incl.
JE53	f, in	15 p,a	60	20 p,a	5	Pl oscillatory zones
JE52	f, in	15 p,a	60	20	5	Pl radiating
JE59	f, in	15 p,a	50	30	5	
H3	m, eq	5 a	45 s	45 s	5	
H4	f, in		65	30	5	Cpx zoned
H14	f, in	15 p,a	50 p,e	28	7	Pl skeletal, cpx cores

Table 11.1. Table showing estimated mineral composition (vol%) and texture of the unaltered dolerite samples. p = porphyritic a = anhedral, s = subhedral and e = euhedral phenocrysts. in = inequigranular, eq = equigranular, m = medium grained, f = fine grained, ves = vesicular, (sp) = completely serpentinised.

Olivine forms inclusions in clinopyroxene in some samples (JW60, JE58). Skeletal (hollow) clinopyroxene and plagioclase grains are seen in samples JE54 and H14, respectively. Radiating crystals of clinopyroxene and plagioclase are seen in samples FG57 and JE52 respectively. Sample FG57 contains isotropic zones interstitial to clinopyroxene which may be devitrified volcanic glass.

The altered dolerites (table 11.2) are generally fine to medium grained, mostly inequigranular, porphyritic and contain variable proportions of olivine, clinopyroxene, plagioclase, hornblende, biotite, saussurite, serpentine, and accessory opaque minerals assumed to be magnetite and/or ilmenite, calcite, and sericite.

	TV3	TV4	TV5	TV6	TV22	TV50
Texture	re	p,f	p, f	re	re	p ,f
Ol		15,p	15,p			5,p
Pl	20	5,p,a	15,p	35	37	15
Cpx	25	25,p,e		10	40	20
Hbl	25	10	30	15	10	
Tr						10
Serp						40
Saus		35	30	20		
Cc			3			
Mt/Ilm	2	10	6		3	10
Sc			1			
Bt	25			15	10	

Table 11.2. Table showing the estimated mineral compositions (vol%) and textural characteristics of the altered dolerite samples from Tvora. p = porphyritic a = anhedral, s = subhedral and e = euhedral phenocrysts. in = inequigranular, eq = equigranular, m = medium grained, f = fine grained, ves = vesicular, (sp) = completely serpentinised, re = recrystallised

In some samples a porphyritic texture is still clear (TV4, TV5, TV50) whereas in others the original igneous texture is poorly preserved having been destroyed by extensive recrystallisation (TV3, TV6, TV22).

Interpretation of textures

Unaltered dolerites

The presence of the amygdales in certain dykes is of interest. The development of vesicles is a function of the dissolved fluids in a melt (Fyfe, 1970; Moore, 1965). With decreasing pressure, dissolved fluids may be exsolved from the melt to form vesicles. The size of the vesicles will be governed by the fluid species and molar volume of the fluid phase. At 1000°C, the molar volume of H_2O varies from approximately 50cm^3/mole at 8kb to

180cm^3/mole at 2kb and to >1000cm^3/mole at 0.5kb (Burnham *et al.*, 1969). At 1000°C the molar volume of CO_2 varies from 43cm^3/mole at 8kb to 83cm^3/mole at 2kb to approximately 160cm^3/mole at 0.5kb (van den Kerkhof, 1988). These data show that exsolved fluids are most likely to develop volumetrically large vesicles at pressures less than 0.5kb. Moore (1965) studied the development of vesicles in submarine basalts, and found that vesicles were developed in basalts extruded up to 5000m below sea-level, equivalent to a load pressure of approximately 0.5kb. The presence of amygdales in dykes of the Kirwanveggan Dolerite Suite provide evidence that at the time of emplacement, the cover was probably of the order of $\leq$0.5kb.

The skeletal and radiating clinopyroxene and plagioclase crystals are indicative of rapid crystallisation and nucleation and also support crystallisation at shallow depths.

Altered dolerites

Samples TV2, TV4, TV3 and TV5 intrude the Tvora Alkaline Complex whereas samples TV22 and TV50 intrude the adjacent country rock. Three of the samples (TV4, TV5, TV50) are porphyritic. However the original minerals which formed the phenocrysts have been partially to completely altered and hydrated to form saussurite (after plagioclase) and serpentine $\pm$ tremolite (after olivine and/or clinopyroxene?). These three samples also have significant proportions of hornblende in the groundmass.

The other three samples (TV3, TV6 and TV22) show extensive recrystallisation and the development of biotite and hornblende. The alteration has therefore involved extensive hydration as indicated by the development of hydrous assemblages.

CHEMISTRY

Twenty-three samples were analyzed for major and fifteen trace elements (Table 11.3). The values for U and Th are not shown because, for most samples, neither of these elements was detected. The dolerites are typically basic in composition, having SiO_2 contents between 45 and 54% SiO_2. The dykes show significant variation in composition. Al_2O_3 ranges from 7 to ~18%, MgO 5 to 18%, CaO 6 to 14%, Na_2O <1 to 5%, and K_2O 0.4 to 3%. ΣFeO, TiO_2, MnO and P_2O_6 do not vary so significantly. Unaltered dolerites are characterised by widely ranging contents of Ba (150-1400ppm), Cr (57-2100ppm) and Ni (75-800ppm) contents whereas concentrations of Rb, Sr, Zr, Y, Nb, Sc, La, V, Cu, and Zn are less variable. The major element chemistries of the altered dolerites from Tvora are not significantly different to the other dolerites except for K_2O which is higher and CaO, which is lower in the altered dolerites. Concentrations of trace elements in altered dolerites sampled from Tvora differ from unaltered dolerites. Niobium, Ba, La, Sr are all enriched compared to the unaltered dykes (Table 11.4).

The dolerites are typically tholeiitic in composition except a number of samples from Tvora are calc-alkaline (Fig 11.2).

Unaltered dolerites

Harris *et al.* (1991) have made a detailed study of dolerite dykes east and west of the study area. Following Harris *et al.* (1991), the analyses have been divided into two groups, those with MgO ≥ 10% and those with MgO < 10%. Harris *et al.* (1991) noted that the high Mg-dykes are distinguished by a positive correlation between MgO and Ni and antipathetic relations between MgO and CaO, consistent with the chemistry of this group of dykes being controlled by olivine fractionation. The positive correlation of MgO and CaO in dykes with <10%MgO was interpreted to indicate olivine + clinopyroxene fractionation. Harris *et al.* (1991) also recognised a negative correlation between Al_2O_3 and MgO, from which they concluded that fractionation of plagioclase had not occurred.

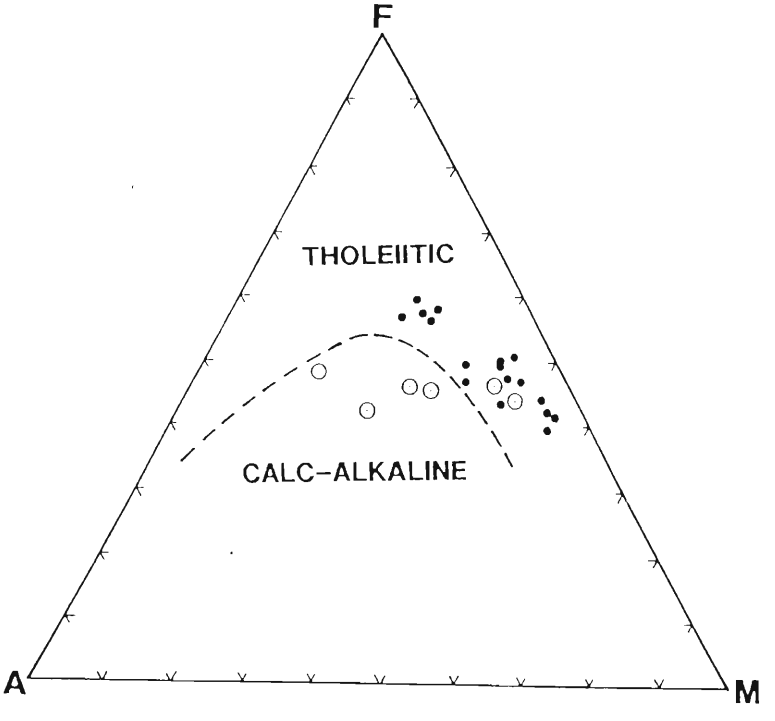

Figure 11.2. AFM diagram for the dolerites. The tholeiite/calc-alkaline dividing line is from Irvine and Barager (1971). The open circles are the altered dolerites from Tvora and the dots represent the unaltered dolerites.

Harris *et al.* (1991) also recorded negative correlations between Na_2O and P_2O_5 and MgO in the dolerites.

	SiO_2	Al_2O_3	Fe_2O_3	FeO	MnO	MgO	CaO	Na_2O	K_2O	TiO_2	P_2O_5	TOTAL
						MgO> 10%						
FG57	47.25	9.43	1.43	11.55	0.19	17.48	8.09	1.64	0.41	1.62	0.21	99.3
JW51	50.15	11.10	2.21	10.46	0.21	10.66	10.26	1.31	0.74	2.16	0.20	99.46
JE58	47.72	11.12	2.58	9.90	0.30	12.84	9.88	2.56	0.53	1.54	0.20	99.17
JW57	46.24	7.31	2.86	12.13	0.31	17.31	10.04	1.12	0.49	1.63	0.14	99.58
JW52A	47.38	10.52	2.67	11.74	0.21	12.15	9.77	1.48	0.69	2.12	0.25	98.98
JW60	45.24	9.42	2.73	12.91	0.22	13.25	12.33	1.20	0.50	2.32	0.18	100.3
JE53	50.41	12.53	2.17	10.27	0.18	11.26	10.05	1.69	0.49	1.52	0.15	100.72
JE52	49.80	11.50	2.19	10.35	0.18	12.41	9.49	1.40	0.42	1.45	0.14	99.33
JE59	49.14	9.44	2.44	10.70	0.19	16.33	8.49	0.98	0.52	2.00	0.20	100.43
H14	46.69	8.15	2.82	11.58	0.20	18.49	8.47	0.85	0.50	1.99	0.22	99.96
						MgO <10%						
RK5	53.02	13.99	2.09	9.88	0.17	6.22	9.96	2.27	0.72	1.79	0.20	100.31
RK23	45.98	13.39	2.93	12.02	0.21	7.17	13.01	3.30	0.49	2.03	0.28	100.81
JE54	50.41	12.60	2.71	9.19	0.18	9.72	9.10	3.02	1.54	1.66	0.23	100.36
RK4	48.64	13.76	2.48	10.17	0.18	9.25	9.79	2.47	0.90	1.85	0.34	99.83
H3	45.99	13.57	3.28	11.81	0.23	6.46	12.19	4.01	0.69	2.11	0.34	100.68
JW52B	50.34	14.59	2.57	11.27	0.21	5.75	9.78	2.76	0.82	2.40	0.29	100.78
H4	46.11	12.61	2.75	12.08	0.21	7.30	13.51	2.54	0.56	2.16	0.29	100.12
						Altered dykes						
TV3	45.37	13.53	1.41	11.38	0.25	8.67	8.95	3.37	2.89	2.47	0.78	99.06
TV4	43.60	14.89	1.27	10.28	0.23	7.43	9.63	5.14	3.28	1.86	1.23	98.84
TV5	44.51	13.49	1.42	11.48	0.21	9.68	9.73	3.45	2.28	2.40	0.64	99.29
TV6	50.36	17.47	1.17	9.45	0.22	3.78	6.67	4.86	2.76	1.98	0.86	99.59
TV22	49.72	11.77	1.38	11.17	0.21	11.64	9.66	1.84	0.96	1.74	0.20	100.28
TV50	50.15	11.55	1.35	10.93	0.20	13.16	8.76	1.30	1.17	1.52	0.20	100.30

	Rb	Sr	Zr	Y	Nb	Ba	Sc	Cr	La	V	Cu	Ni	Zn
						>10% MgO							
FG57	11	264	95	25	4	206	22	1045	11	278	108	868	95
JW51	25	280	124	31	5	1387	24	753	6	297	86	269	106
JE58	18	256	86	25	6	282	21	754	11	274	108	507	92
JW57	22	263	105	19	9	218	28	2112	8	372	122	803	98
JW52A	13	372	147	26	8	287	22	803	22	341	100	398	108
JW60	14	362	94	18	4	267	33	1143	3	557	147	472	90
JE53	16	209	95	22	7	150	24	897	6	342	120	384	99
JE52	19	199	95	22	8	153	22	919	4	293	120	460	92
JE59	22	245	127	24	8	236	23	1083	11	296	100	768	116
H14	14	278	132	18	5	169	22	995	13	384	134	958	104
						<10% MgO							
RK5	17	288	142	21	6	239	24	197	20	353	141	79	101
RK23	13	489	106	20	5	173	20	116	13	487	264	115	88
JE54	49	246	132	28	9	723	21	950	14	322	84	257	108
RK4	14	429	135	18	5	853	21	387	18	347	82	234	109
H3	19	552	126	22	4	257	18	57	19	470	263	98	94
JW52B	25	258	162	23	6	128	27	127	11	387	95	75	137
H4	20	494	116	22	5	246	24	73	11	562	224	128	92
						Altered dykes							
TV3	130	1147	164	24	70	1248	20	451	66	275	63	199	164
TV4	88	2087	236	25	86	2595	14	371	153	226	75	142	122
TV5	65	1081	202	22	58	1423	18	649	65	258	75	231	112
TV6	108	1482	218	32	64	1486	10	117	68	160	34	12	117
TV22	49	286	105	27	8	393	38	1086	7	324	119	322	188
TV50	31	302	102	30	9	563	18	982	18	275	82	504	108

Table 11.3 Major and trace element (concentrations in wt% and ppm respectively) chemistry of the dolerite dykes.

The analyses of dolerite reported here show the same relationships as those described by Harris *et al.* (1991)(table 11.4).

In addition to the relationships in the Mg-rich dolerites described by Harris *et al.* (1991), the Mg-rich dolerites also show strong positive relationships between Ca, Sc and V, Al_2O_3 and SiO_2, K_2O and Ba, Sr and TiO_2, La and P_2O_5, Zr and Zn, and Ba and Y (Table 11.4). Strong negative correlations are seen between Al_2O_3 and Cr and Ni, and Cu and Y (table 11.4).

Modelling by Harris *et al.* (1991) has shown that the low Mg dolerites could be derived from the high Mg dolerites by 36% fractionation of olivine and clinopyroxene in the proportions 63:37. The strong correlations between CaO, Sc and V in the Mg-rich dykes, are consistent with clinopyroxene fractionation with both these trace elements being easily accommodated in that phase (see appendix 3). The correlation between K_2O and Ba is to be expected because these elements are likely to be partitioned into the liquid phase.

	SiO_2	Al_2O_3	Fe_2O_3	FeO	MnO	MgO	CaO	Na_2O	K_2O	TiO_2	P_2O_5	Rb
SiO_2												
Al_2O_3	0.746											
Fe_2O_3	-0.443	-0.394										
FeO	-0.842	-0.699	0.331									
MnO	-0.463	-0.380	0.502	0.120								
MgO	-0.538	-0.855	0.067	0.420	0.137							
CaO	-0.244	0.138	0.396	0.398	0.207	-0.543						
Na_2O	0.160	0.569	-0.265	-0.519	0.355	-0.434	-0.010					
K_2O	0.194	0.199	0.269	-0.082	0.071	-0.508	0.249	-0.018				
TiO_2	-0.333	-0.261	0.376	0.531	-0.162	-0.062	0.411	-0.501	0.604			
P_2O_5	-0.227	-0.104	0.023	0.130	-0.149	0.111	-0.307	0.027	0.510	0.549		
Rb	0.437	0.009	0.206	-0.380	0.286	-0.195	0.093	-0.166	0.350	0.025	-0.368	
Sr	-0.653	-0.303	0.398	0.710	0.134	-0.146	0.459	-0.160	0.500	0.796	0.618	-0.340
Zr	0.017	-0.240	0.329	0.167	-0.247	0.110	-0.234	-0.541	0.644	0.601	0.650	0.081
Y	0.571	0.514	-0.460	-0.553	-0.114	-0.495	-0.212	0.394	0.648	0.071	0.410	0.308
Nb	0.326	0.033	0.366	-0.227	0.125	-0.068	-0.089	-0.178	0.036	-0.273	-0.362	0.447
Ba	0.357	0.209	-0.115	-0.213	0.000	-0.448	0.219	-0.040	0.755	0.424	0.177	0.571
Sc	-0.522	-0.342	0.367	0.697	0.254	-0.006	0.813	-0.318	-0.095	0.399	-0.394	0.065
Cr	-0.475	-0.735	0.325	0.531	0.527	0.551	0.118	-0.396	-0.329	-0.138	-0.489	0.227
La	-0.194	-0.157	0.168	0.077	0.036	0.198	-0.458	0.068	0.374	0.182	0.795	-0.359
V	-0.645	-0.347	0.515	0.784	0.060	0.047	0.748	-0.398	-0.062	0.563	-0.103	-0.268
Cu	-0.582	-0.333	0.374	0.553	0.054	0.291	0.402	-0.242	-0.591	0.013	-0.365	-0.433
Ni	-0.477	-0.790	0.022	0.332	0.099	0.993	-0.607	-0.376	-0.558	-0.139	0.104	-0.226
Zn	0.316	-0.117	0.130	-0.131	-0.284	0.122	-0.390	-0.463	0.523	0.413	0.462	0.342

	Sr	Zr	Y	Nb	Ba	Sc	Cr	La	V	Cu	Ni	Zn
Sr												
Zr	0.440											
Y	-0.010	0.236										
Nb	-0.314	0.245	-0.109									
Ba	0.143	0.259	0.706	-0.260								
Sc	0.407	-0.270	-0.519	-0.078	-0.026							
Cr	-0.027	-0.126	-0.555	0.352	-0.268	0.542						
La	0.435	0.684	0.252	0.149	-0.165	-0.511	-0.191					
V	0.590	-0.049	-0.660	-0.227	-0.166	0.857	0.294	-0.273				
Cu	0.117	-0.373	-0.930	-0.175	-0.583	0.586	0.339	-0.372	0.778			
Ni	-0.127	0.072	-0.487	-0.067	-0.493	-0.087	0.488	0.200	-0.015	0.287		
Zn	0.086	0.836	0.365	0.415	0.264	-0.324	-0.097	0.508	-0.287	-0.570	0.108	

Table 11.4. Correlation coefficient matrix for the Mg-rich dolerite dykes.

The strong negative correlations between Al_2O_3 and Cr and Ni support the interpretation that

plagioclase fractionation did not play a major role. The correlations between Sr and TiO_2, La and P_2O_5, Zr and Zn, Ba and Y, and Cu and Y are less easily explained.

Dolerites with <10%MgO

Correlation coefficients calculated for all seven of these samples were found to be spurious because sample JE54, which contains abnormally high K_2O, Ba, Cr, Ni and V contents, generated high correlation coefficients for these elements. The anomalous values in JE54 may possibly suggest contamination in that sample.

SiO_2	SiO_2											
Al_2O_3	0.694	Al_2O_3										
Fe_2O_3	-0.881	-0.382	Fe_2O_3									
FeO	-0.837	-0.529	0.823	FeO								
MnO	-0.752	-0.251	0.921	0.897	MnO							
MgO	-0.294	-0.370	-0.045	-0.219	-0.333	MgO						
CaO	-0.830	-0.855	0.675	0.854	0.625	0.001	CaO					
Na_2O	-0.646	-0.099	0.916	0.623	0.825	-0.233	0.459	Na_2O				
K_2O	0.549	0.676	-0.425	-0.709	-0.418	0.223	-0.892	-0.320	K_2O			
TiO_2	-0.285	0.143	0.429	0.647	0.726	-0.502	0.197	0.305	-0.087	TiO_2		
P_2O_5	-0.671	-0.157	0.675	0.363	0.541	0.485	0.163	0.518	0.248	0.291	P_2O_5	
Rb	0.236	0.391	-0.009	0.175	0.350	-0.661	-0.211	-0.026	0.257	0.802	-0.017	Rb
Sr	-0.910	-0.767	0.805	0.619	0.568	0.391	0.783	0.641	-0.505	-0.071	0.594	-0.458
Zr	0.760	0.854	-0.520	-0.557	-0.294	-0.362	-0.864	-0.357	0.794	0.260	-0.155	0.674
Y	0.169	0.216	0.070	0.340	0.432	-0.871	0.056	0.088	-0.117	0.747	-0.266	0.906
Nb	0.947	0.714	-0.872	-0.707	-0.702	-0.329	-0.762	-0.669	0.420	-0.150	-0.717	0.241
Ba	0.015	-0.033	-0.215	-0.528	-0.476	0.900	-0.377	-0.291	0.600	-0.544	0.469	-0.486
Sc	0.597	0.386	-0.619	-0.222	-0.277	-0.391	-0.419	-0.676	0.288	0.430	-0.443	0.719
Cr	0.404	0.291	-0.574	-0.786	-0.764	0.725	-0.666	-0.546	0.690	-0.604	0.107	-0.438
La	0.292	0.150	-0.135	-0.607	-0.386	0.188	-0.355	0.119	0.356	-0.752	-0.029	-0.439
V	-0.799	-0.816	0.654	0.901	0.690	-0.089	0.965	0.394	-0.818	0.394	0.191	0.029
Cu	-0.728	-0.654	0.748	0.767	0.659	-0.198	0.902	0.699	-0.868	0.091	0.090	-0.259
Ni	-0.236	-0.252	-0.065	-0.273	-0.329	0.986	-0.119	-0.243	0.371	-0.433	0.552	-0.553
Zn	0.544	0.809	-0.378	-0.333	-0.132	-0.254	-0.747	-0.314	0.723	0.486	0.036	0.693
Sr	Sr											
Zr	-0.837	Zr										
Y	-0.354	0.434	Y									
Nb	-0.967	0.713	0.196	Nb								
Ba	0.141	0.015	-0.790	-0.105	Ba							
Sc	-0.808	0.688	0.616	0.683	-0.276	Sc						
Cr	-0.281	0.265	-0.726	0.350	0.882	-0.009	Cr					
La	0.099	0.046	-0.443	0.035	0.436	-0.520	0.397	La				
V	0.689	-0.716	0.251	-0.728	-0.440	-0.216	-0.736	-0.502	V			
Cu	0.769	-0.806	0.071	-0.707	-0.486	-0.611	-0.734	-0.064	0.810	Cu		
Ni	0.314	-0.217	-0.824	-0.283	0.944	-0.321	0.774	0.193	-0.182	-0.317	Ni	
Zn	-0.767	0.917	0.403	0.601	0.019	0.720	0.250	-0.276	-0.579	-0.792	-0.106	Zn

Table 11.5. Correlation coefficient matrix for the dolerite samples (excluding JE54) with <10% MgO. Values <-0.7 and >0.7 are underlined.

Exclusion of sample JE54 from the data set resulted in correlations listed in Table 11.5. Strong negative correlations between SiO_2 and MnO, CaO, ΣFeO and P_2O_5 are seen (Table 11.5, fig. 11.3). The correlation matrix shows that there are broadly four groups of associated elements. Group 1 consists of Ca, Sr, V and Cu, Group 2 of Zr, Nb, Zn, SiO_2, $Al2O_3$ and K_2O, Group 3 of MgO, Cr, Ni and Ba and Group 4 of TiO_2, Na_2O, Sc, Rb, Y. Elements in group 1 typically show

negative correlations with those in group 2 suggesting that group 1 is related to clinopyroxene fractionation (Ca and Sr) as suggested by Harris *et al.* (1991). The elements in group 2 are enriched in the residual magma. The elements in group 3 (except Ba) are typically related by olivine fractionation (Harris *et al.* 1991).

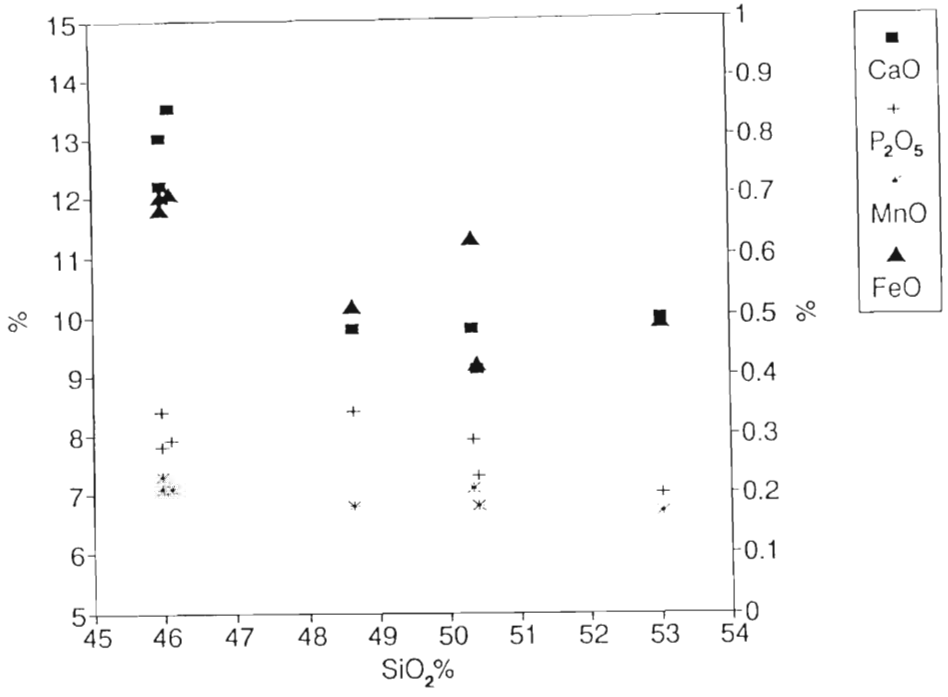

Figure 11.3. Harker variation diagrams for CaO, P_2O_5, MnO and FeO for the dykes with MgO $<10\%$. P_2O_5 and MnO values are scaled on the right axis whereas CaO and FeO are scaled on the left axis of the figure.

The correlation with Ba may be spurious because of the high Ba concentration in RK4. Elements in group 4 are normally considered to be incompatible and would be expected to be concentrated in the residual magma. It is surprising therefore that they do not show a relationship with elements in group 2.

Harris *et al.* (1991) provide evidence (high $\delta^{18}O$ values) to indicate that the dykes have been affected by alteration with Na, K, Ba, Sr, Rb and possibly Ca being most likely to be affected. They state that large variations in some of these elements cannot be explained by magmatic processes alone, eg Ba, Sr, Rb and K_2O. Harris *et al.* (1991) concluded that the lack of correlation between $\delta^{18}O$ and initial $^{87}Sr/^{86}Sr$ values for six samples from the Ahlmannryggen to the west of the study area suggested that the high $\delta^{18}O$ values did not result from contamination and suggested they might arise from alteration.

It is uncertain to what extent this conclusion can be applied to the Sverdrupfjella dolerites

and it is also uncertain to what extent the dykes have been affected by alteration.

Altered dolerites

A correlation matrix for the six analyses of altered dolerites is shown in table 11.6 from which it is deduced that the following elements have positive correlations with one another :- MnO, Na_2O, K_2O, P_2O_5, Rb, Sr, Ba, Zr, La and Nb (figs. 11.4, 11.5 and 11.6). These same elements appear to have an inverse relationship with ΣFeO, MgO, CaO, Sc, V, Cu, Ni and Y. The former group includes elements normally considered to be mobile (Na_2O, K_2O, Rb, Sr and Ba) but also includes Zr, La and Nb, elements commonly regarded as immobile. The latter group is dominated by the transition elements. The variations may arise as a consequence of either primary igneous processes or from alteration. Most of the elements in the former group are normally partitioned into the residual magma (except MnO) during fractionation of olivine and pyroxene. Elements in the latter group are accommodated in olivine and pyroxenes (except Y) during fractionation. Therefore it is possible that the chemistry reflects igneous processes and that the alteration recognised in thin section has had minimal effect on the chemistry.

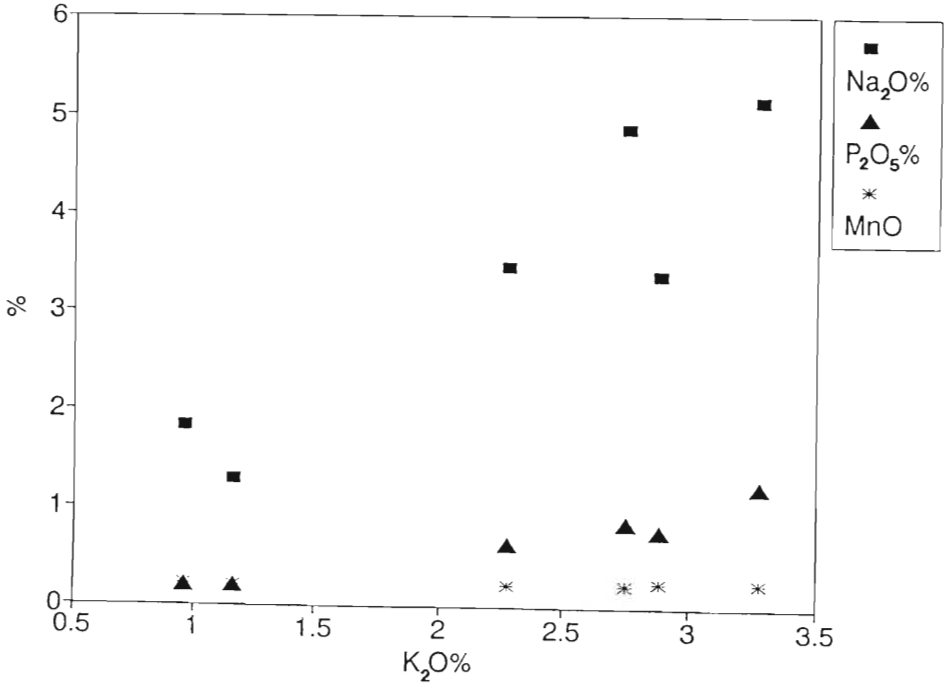

Figure 11.4. Na_2O, P_2O_5 and MnO versus K_2O for the altered dolerite dykes.

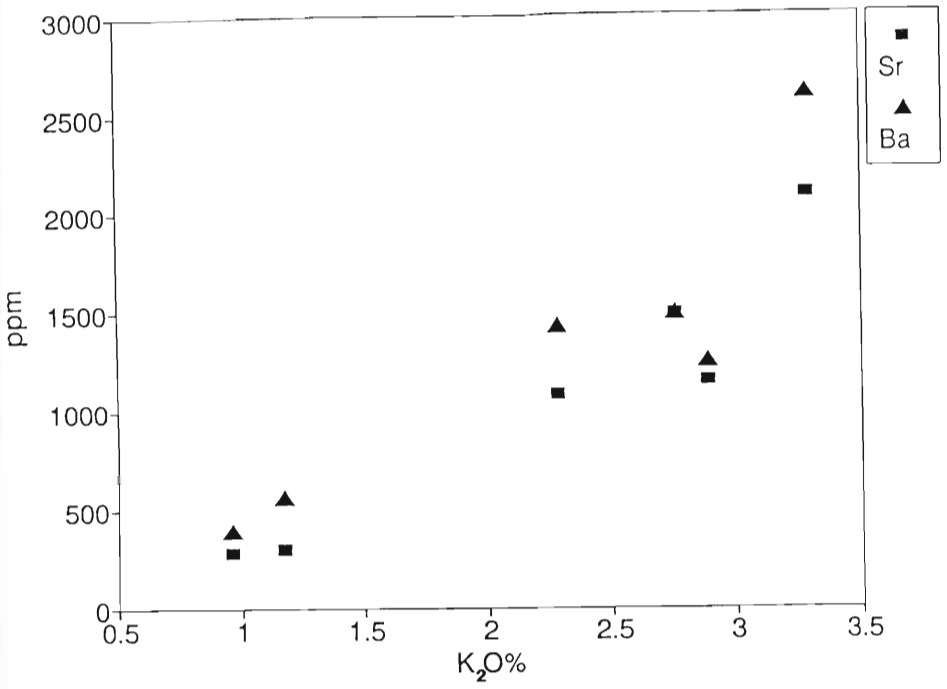

Figure 11.5. Sr and Ba versus K_2O for the altered dykes.

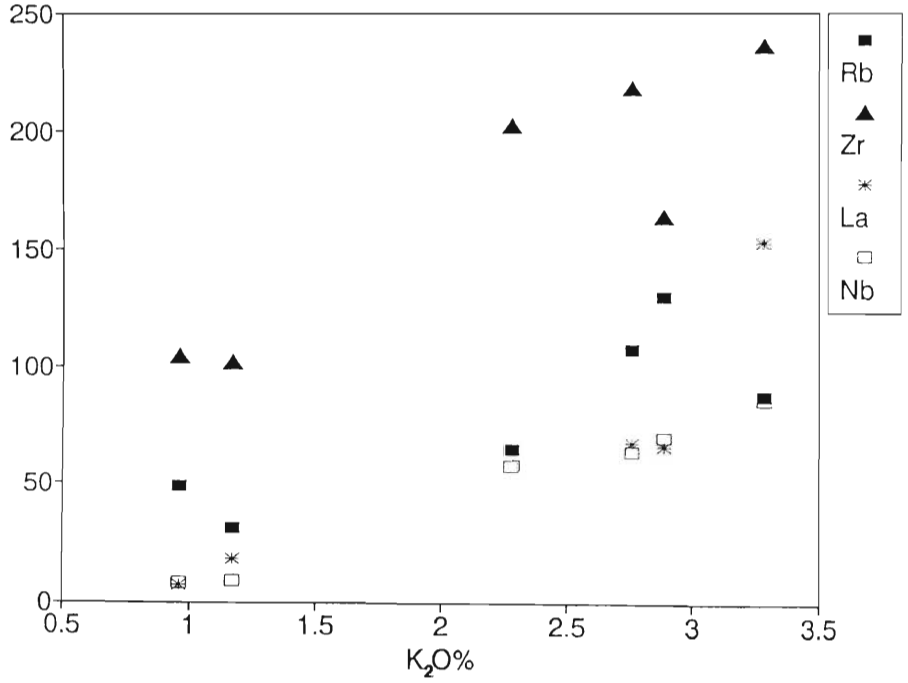

Figure 11.6. Rb, Zr, La and Nb versus K_2O for the altered dolerite dykes. Values in ppm.

When the concentrations of elements in the altered dolerites are compared with those of the unaltered rocks, the former include samples with MgO contents > and <10%. However, the altered dolerites have significantly higher K_2O, Rb, Sr, Ba and Nb irrespective of MgO contents. Zirconium and yttrium are marginally different to the unaltered rocks. If the differences were the result of fractionation processes, the Zr and Y concentrations should also be significantly higher. It is concluded that K_2O, Rb, Sr, Ba and Nb have been added to the altered dolerites, rather than resulting from fractionation processes.

SiO_2	SiO_2											
Al_2O_3	-0.075	Al_2O_3										
Fe_2O_3	-0.343	-0.803	Fe_2O_3									
FeO	-0.339	-0.811	1.000	FeO								
MnO	-0.609	0.387	-0.068	-0.078	MnO							
MgO	0.128	-0.987	0.740	0.750	-0.494	MgO						
CaO	-0.579	-0.696	0.759	0.767	0.027	0.648	CaO					
Na_2O	-0.482	0.892	-0.609	-0.616	0.611	-0.905	-0.315	Na_2O				
K_2O	-0.653	0.751	-0.380	-0.390	0.802	-0.784	-0.208	0.919	K_2O			
TiO_2	-0.633	0.279	0.345	0.330	0.545	-0.366	0.080	0.403	0.574	TiO_2		
P_2O_5	-0.648	0.751	-0.468	-0.474	0.748	-0.773	-0.139	0.955	0.970	0.415	P_2O_5	
Rb	-0.370	0.676	-0.268	-0.284	0.863	-0.766	-0.384	0.706	0.826	0.684	0.714	Rb
Sr	-0.615	0.777	-0.520	-0.525	0.679	-0.787	-0.161	0.968	0.949	0.364	0.995	0.659
Zr	-0.581	0.832	-0.500	-0.506	0.505	-0.826	-0.216	0.969	0.899	0.466	0.929	0.602
Y	0.873	0.284	-0.715	-0.712	-0.373	-0.205	-0.787	-0.095	-0.270	-0.666	-0.237	-0.144
Nb	-0.719	0.723	-0.314	-0.324	0.781	-0.759	-0.123	0.921	0.992	0.624	0.968	0.796
Ba	-0.704	0.646	-0.423	-0.425	0.617	-0.643	0.010	0.902	0.895	0.301	0.966	0.514
Sc	0.018	-0.835	0.727	0.734	-0.186	0.756	0.739	-0.683	-0.649	-0.149	-0.607	-0.465
Cr	0.304	-0.943	0.642	0.654	-0.613	0.949	0.581	-0.922	-0.909	-0.462	-0.865	-0.827
La	-0.726	0.584	-0.381	-0.383	0.666	-0.589	0.067	0.866	0.886	0.276	0.959	0.513
V	-0.014	-0.940	0.848	0.854	-0.200	0.876	0.753	-0.792	-0.665	-0.109	-0.667	-0.491
Cu	0.057	-0.834	0.597	0.609	-0.350	0.797	0.766	-0.670	-0.706	-0.381	-0.599	-0.673
Ni	0.273	-0.923	0.592	0.603	-0.564	0.967	0.465	-0.918	-0.797	-0.493	-0.794	-0.792
Zn	0.099	-0.355	0.380	0.377	0.266	0.215	0.298	-0.302	-0.280	0.092	-0.289	0.142
	Sr											
Zr	0.950	Zr										
Y	-0.196	-0.217	Y									
Nb	0.950	0.921	-0.365	Nb								
Ba	0.976	0.918	-0.294	0.909	Ba							
Sc	-0.637	-0.695	-0.382	-0.597	-0.558	Sc						
Cr	-0.864	-0.873	-0.084	-0.877	-0.748	0.839	Cr					
La	0.962	0.871	-0.318	0.895	0.993	-0.497	-0.706	La				
V	-0.708	-0.772	-0.416	-0.623	-0.611	0.959	0.881	-0.544	V			
Cu	-0.602	-0.658	-0.285	-0.651	-0.480	0.947	0.890	-0.424	0.891	Cu		
Ni	-0.799	-0.846	0.002	-0.798	-0.666	0.594	0.898	-0.617	0.744	0.663	Ni	
Zn	-0.346	-0.449	-0.188	-0.267	-0.408	0.745	0.354	-0.351	0.627	0.559	0.059	Zn

Table 11.6. Correlation coefficient matrix for the altered dolerite dykes. Values >0.7 or <-0.7 are underlined.

The altered samples are all from Tvora and these samples except TV22 and TV50 are from dykes intruding the Tvora Alkaline Complex. A study of the analyses of the syenites exposed at Tvora shows that the syenites have higher contents of Na_2O, K_2O, P_2O_5, Rb, Sr, Ba, Zr, La and Nb compared to the unaltered dykes whereas the syenites have equivalent or lower contents of ΣFeO, MgO, CaO, Sc, V, Cu, Ni and Y. It appears likely that emplacement of the dykes into the

syenite has been responsible for the alteration and/or contamination of the mineralogy and chemistry in the dykes (samples TV3, TV4, TV5 and TV6 in particular).

IMPLICATIONS OF THE DOLERITE DYKES FOR THE EVOLUTION OF THE STUDY AREA

Grantham and Hunter (1991) compared the two orientations of dykes in the study area,(ie suites striking slightly west of north and northeast) with those in Dronning Maud Land and southern Africa. They concluded that the orientations of these dyke swarms were similar to those in Vestfjella and northern Ahlmanryggen (in Antarctica), and the Lebombo mountains, southeastern Zimbabwe and Mozambique (in Africa) using the reconstruction of Gondwana by Martin and Hartnady (1986). Cox (1992) has postulated a two stage break up of Gondwana with Antarctica moving eastwards from Africa initially and then southward (fig. 11.7).

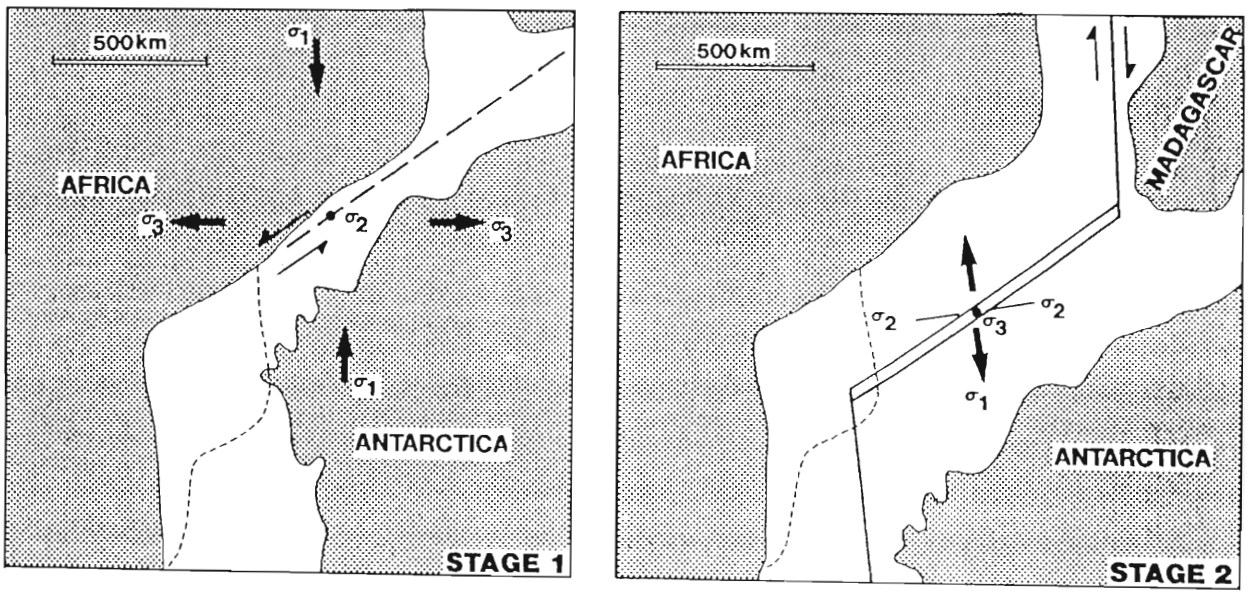

Figure 11.7. Two stage break up of Gondwana modified after Cox (1992) showing the probable orientations of the strain axes.

The orientation of the dolerite dykes in the study area is approximately parallel to the σ_1 orientation of the transpressional strain in the north and perpendicular to the extensional σ_3 orientation in the west postulated in stage 1 (Cox, 1992) (fig. 11.7). This suggests that the dykes were emplaced during the first stage proposed by Cox (1992). Dykes emplaced during the

second stage would be expected to be oriented parallel to σ_3 and perpendicular to the tensional σ_1 and have an east-west strike in an African framework.

Cox *et al.* (1967) showed that the Karoo basalts of Nuanetsi, Swaziland and Lesotho could be divided into a northern province enriched in K, Ti, P, Ba, Sr and Zr (HTZ) and a southern province with normal tholeiitic compositions. Sweeney and Watkeys (1990) have shown that the Archaean cratonic areas in southern Africa are characterised by HTZ whereas the dykes which are emplaced into Proterozoic metamorphic terranes are characterised by low Ti and Zr (LTZ). Harris *et al.* (1991) have compared the chemistry of dykes east and west of the study area with dykes from southern Africa. They concluded that dolerite dykes from the Ahlmannryggen were dominantly characterised by high Ti and Zr (HTZ or enriched) whereas those from the Sverdrupfjella were characterised by low Ti and Zr (LTZ, normal). Harris *et al.* (1991) have suggested that the Jutulstraumen Glacier, which separates the Ahlmannryggen (in the west) from the H.U. Sverdrupfjella (in the east), marks part of the HTZ/LTZ boundary. Using TiO_2 vs P_2O_5, TiO_2 vs Zr and Zr vs Y variation diagrams after Sweeney and Watkeys (1990) the dykes from the study area are typical of the LTZ chemistry (figs. 11.8, 11.9 and 11.10).

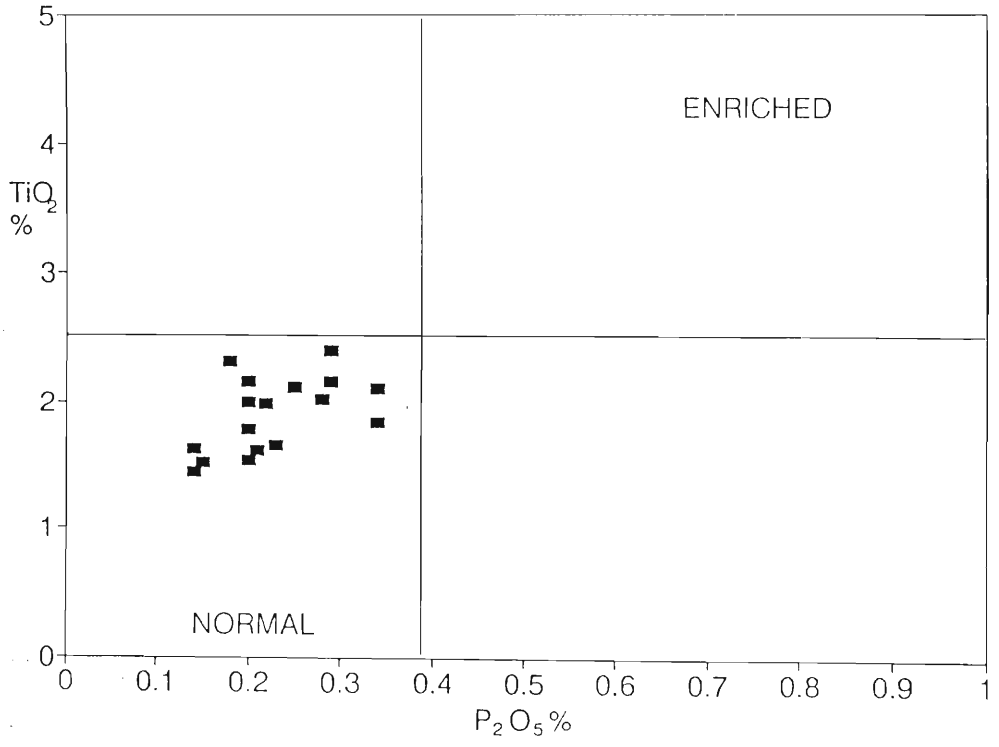

Figure 11.8. Figure showing the "normal" or LTZ TiO_2 versus P_2O_5 characteristics of the dolerites from the study area. SV = Sverdrupfjella

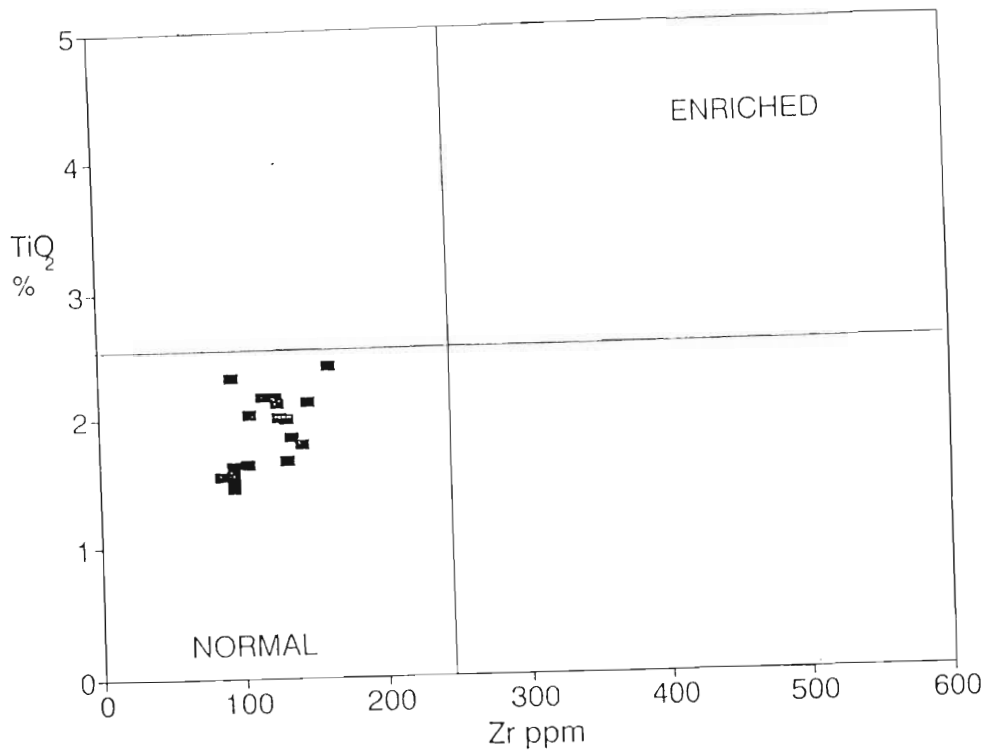

Figure 11.9. Figure showing the "normal" or LTZ TiO_2 versus Zr characteristics of the dolerites from the study area.

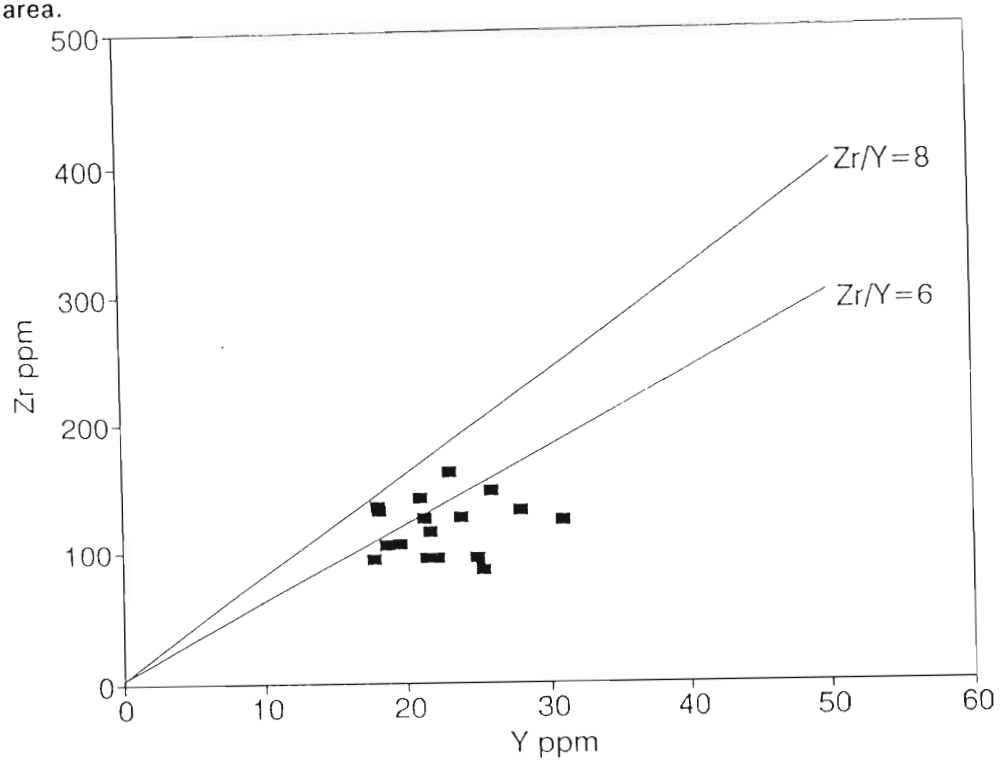

Figure 11.10. Figure showing the "normal" or LTZ Zr versus Y characteristics of the dolerites from the study area. Sweeney and Watkeys (1990) suggested that Zr/Y = 6 represented the discriminating value between "normal" and enriched rocks.

CONCLUSIONS

The dolerite dykes in the study area are petrographically and chemically similar to those studied by Harris *et al.* (1991) and support their conclusions regarding early olivine fractionation followed by later olivine + clinopyroxene fractionation. The dykes sampled from Tvora are altered and show chemical characteristics which suggest that they have been contaminated extensively by the Tvora Alkaline Complex. The unaltered dykes show typically "normal" chemistry as defined by Sweeney and Watkeys (1990). The presence of skeletal textures and amygdales indicate rapid cooling and crystallisation close to the surface probably at lithostatic pressures of <0.5kb.

CHAPTER 12
THE STRAUMSVOLA AND TVORA ALKALINE INTRUSIONS

INTRODUCTION

The Straumsvola and Tvora Alkaline Intrusions will be described separately after which possible relationships will be discussed. The field relationships and distribution of the Straumsvola and Tvora Alkaline Complexes were described in chapter 2. The Straumsvola Alkaline Complex (maps 1,5 and 6) appears to be roughly circular with an approximate diameter of 5km and probably underlies an area of approximately 20km^2, although only a small portion of this is exposed.

The Tvora Alkaline Complex (map 7) has a minimum diameter of 2km which yields a minimum area of 9.86km^2 (assuming a spherical shape) and a perimeter of ~3 km. Its contact with the country rock is exposed for only 400m along one sector of the intrusion.

The Straumsvola Alkaline Complex has been provisionally dated at ~182 Ma(Ar-Ar, I. Evans,pers. comm.) 170$\pm$4Ma (Rb/Sr, A. R. Allen, pers. comm.) and 170-200 Ma (Ravich and Solo'vev, 1966, p. 220). No age determinations have been attempted on the syenites from Tvora.

THE STRAUMSVOLA ALKALINE COMPLEX

Field relationships and appearance

At least four zones have been identified in the Straumsvola Alkaline Complex, namely, a central layered zone (CLZ) which includes a mafic lens (ML), an inner and outer coarse-grained homogeneous leucocratic zone (COZ) and a mesocratic zone (MZ) separating the inner and outer coarse-grained leucocratic phases (Maps 5 and 6). This distribution of rock types differs from that reported by Ravich and Solo'vev (1966, p220) who reported that "the central part of the intrusion is occupied by uniform coarse-grained syenites, while its periphery is occupied by less coarse- grained, trachytic syenites".

The CLZ and ML are exposed only at Straumsvola whereas the COZ and MZ are exposed at Straumsvola and Storjoen. The COZ is also exposed at Joungane. Field relationships along the southern ridge of Straumsvola suggest that the syenites of the CLZ intrude the inner coarse-grained leucocratic zone (Fig. 12.1) (COZ).

The layering in the CLZ forms a shallow saucer-like structure which plunges shallowly (~20°) toward 30°(Harris, unpubl. data). Approximately 66 layers have been recorded (Harris, unpubl. data). The layers in the CLZ are rhythmic, some showing reverse modal grading (being leucocratic at the base and becoming mesocratic toward the top of each layer, Fig. 12.2) and normal modal grading (mesocratic at the base and becoming leucocratic at the top, Fig. 12.3) (terminology after Irvine, 1982) whereas others show no grading.

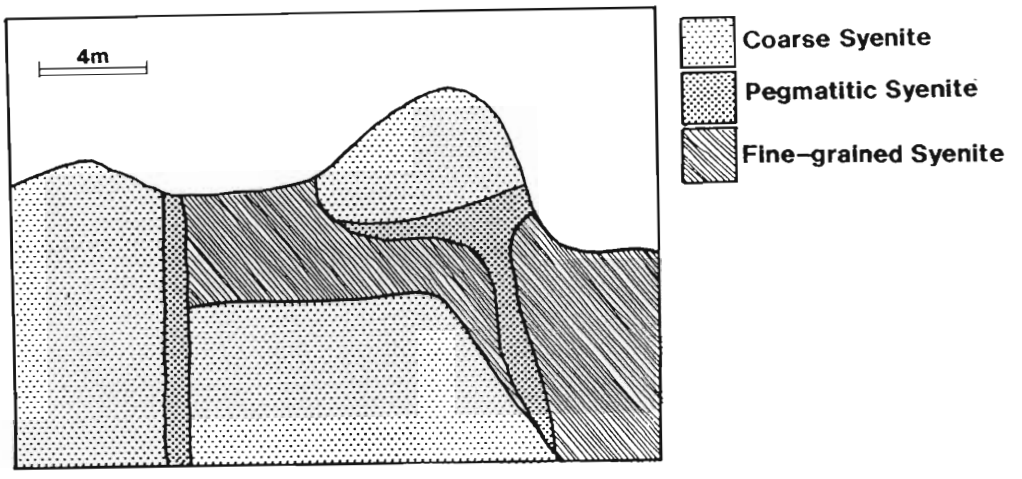

Figure 12.1. Sketch of field relationships at the contact between the central layered syenite (fine) and outer coarse syenite along the southern ridge of Straumsvola. The section is oriented approximately north (right) south (left). The height of the section is approximately 5m.

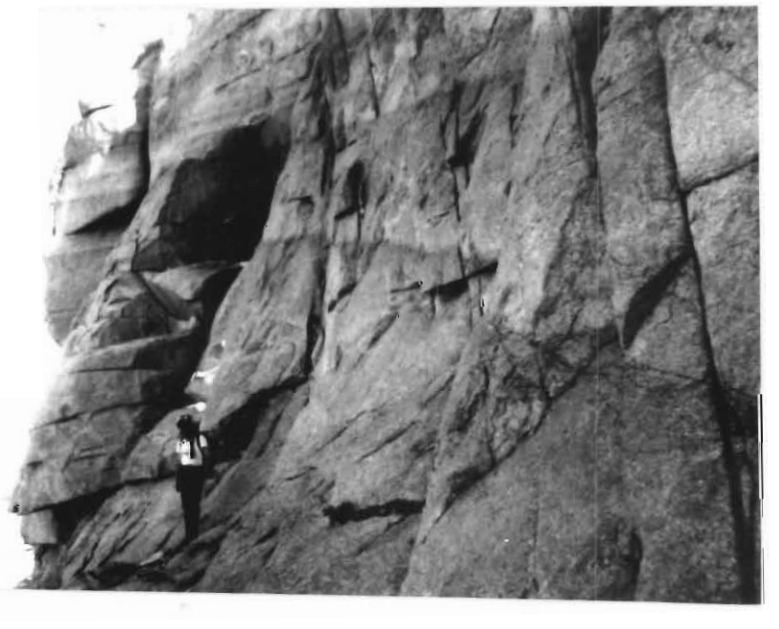

Figure 12.2. Layer at Straumsvola showing the increasing mafic content up the sequence. Person at lower left for scale.

Some layers near the base of the CLZ have a blotchy appearance defined by roughly spherical clots of mafic minerals (Fig.12.4).

The mafic lens (ML) is seen to form a discontinuous layer near the peak of Straumsvola. The margins of the lens are poorly exposed due to extensive scree but the impression gained is that the mafic layer dips parallel or near parallel to the enclosing layered nepheline syenites of the CLZ. Layering is developed in the ML and is defined by varying proportions of mafic and leucocratic minerals. The layering is not as sharply defined as the layering in the CLZ. Locally, near the margins of the ML small (up to 4cm in diameter) ultramafic spherical structures are seen.

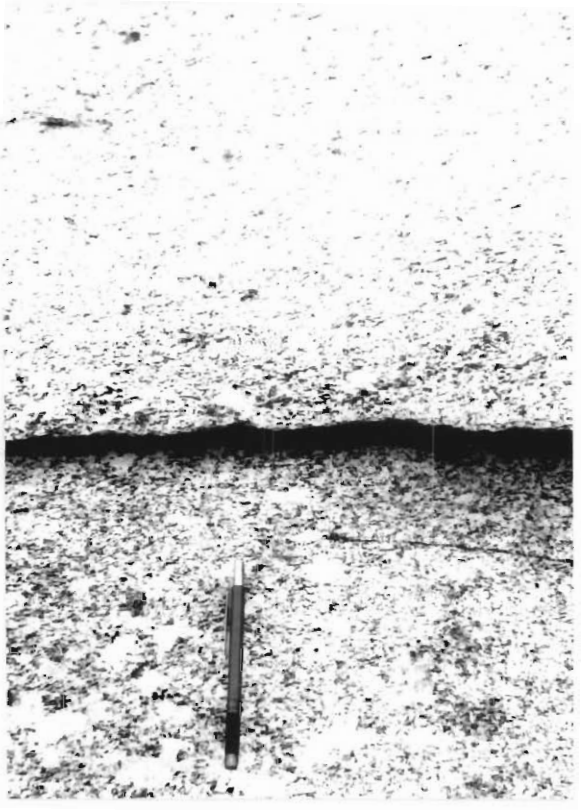

Figure 12.3. Normal graded modal layering in the CLZ of the Straumsvola Alkaline Complex

At Storjoen,the mesocratic phase (MZ) is near vertical and discordant to coarse layering in the inner coarse grained phase (figure 12.5, map 6). The mesocratic zone is ~5m wide and appears to represent a ring dyke-like body emplaced into the coarse-grained leucocratic phase thus forming inner and outer zones. The mesocratic zone is coarse-grained. Perthite defines a strong planar fabric, oriented parallel to the contact of the MZ with the COZ. At Storjeon, the mesocratic zone is characterised by lenticular, leucocratic segregations, oriented perpendicular to the contact and therefore discordant to the planar fabric described above.

Figure 12.4. Spherical blotchy structures near the base of the CLZ of the Straumsvola Alkaline Complex. Pencil is approximately 20cm long.

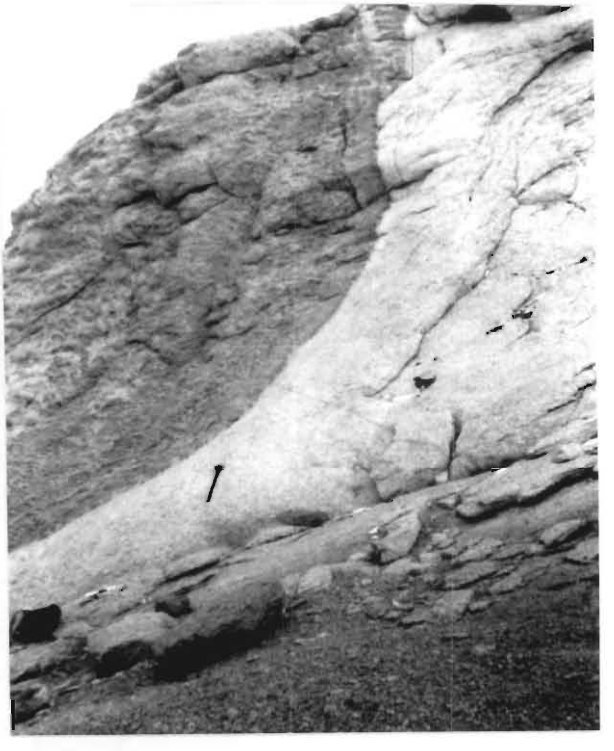

Figure 12.5. Contact between the COZ (right) and the MZ (left) at Storjoen. Hammer at middle lower left is approximately 1m long.

Within these lenticular segregations perthite laths are oriented perpendicular to the contact, parallel to the orientation of the lenticular segregations (Figs. 12.6 and 12.7).

Associated with the alkaline complexes are numerous dykes which intrude the Straumsvola and Tvora Alkaline Complexes and adjacent country rocks. These dykes range in composition from alkali granites to lamprophyres and trachytes.

Figure 12.6. Lenticular leucocratic segregations in the MZ perpendicularly oriented to the contact with the COZ at right.

Petrography

Central Layered Zone (CLZ)

The mineralogy of the Straumsvola Alkaline Complex is shown in Table 12.1. Rocks from the CLZ are characterised by a strong planar fabric defined by perthite laths up to 1cm long having a length/breadth ratio of ~7:1 (fig 12.8). The perthite grains are enclosed commonly by a narrow rim of plagioclase. Nepheline and amphibole occupy the interstices between the feldspar, with nepheline commonly being included poikilitically in the mafic minerals. Nepheline is locally partially replaced by cancrinite which forms an intergranular network. The mafic mineralogy is

dominated by amphibole which locally partially replaces clinopyroxene (aegerine augite). The amphibole is poikilitic, commonly containing numerous inclusions of apatite. Analyses of the amphibole (table 12.4) show that it has arfvedsonitic to katophoritic compositions (Harris, unpubl data).

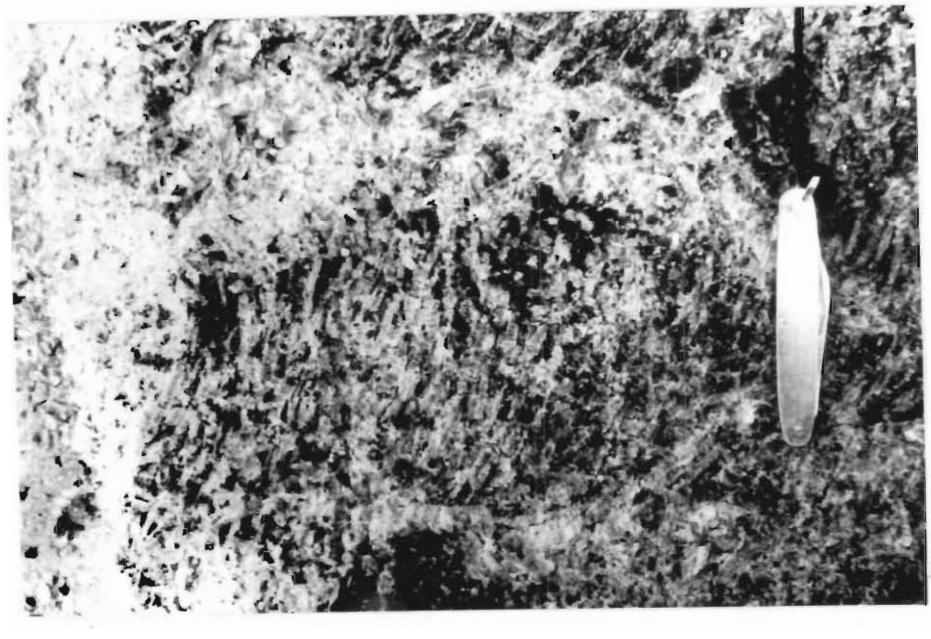

Figure 12.7 Lenticular leucocratic segregation showing the changes in orientation of perthite laths. Contact with COZ at right.

The CLZ commonly shows delicate textures in which perthite and plagioclase are intergrown with amphibole (Fig. 12.9). Biotite partially replaces amphibole, locally forming a network throughout the amphibole grain with all the stringers of the network in optical continuity.

Mafic Lens (ML)

The mineralogy of the ML is dominated by nepheline, dark green clinopyroxene (aegerine), amphibole, and biotite. Nepheline and amphibole form relatively coarse grains (1-2mm) whereas clinopyroxene and biotite are generally finer-grained (.1mm).

	felds	Ne	Bt	amph	Cpx	opaq	Sdl	Ccn	Ap	Spn
CLZ										
SV26	73	10		15				2		
SV31A	85	7	3	3	1			1		
SV33	95			4	1					
SV22	85	8		6	1			1		
SV23	80	10		10						
SV24	75	10		15						
SV27	80	5	5	5	2			10		
SV29	80	8	6	6	3			4		
SV28	65	10	1	20					2	
SV19	83	10	2		2					
SV21	70	10		18				1	1	
COZ										
ST2	91		1	4	3	1				
ST8	76	14	1	5	2	1			<1	
SV20	82	9	2	4	2					1
SV41	86	4	2	6	1	1				
ST5A	90	4	15							1
JG1	85					1	4	10		
ML										
SV35		10	30	10	30		20			
SV34	3	20	25	25	25					
SV37	5	25	20	20	20					
MZ										
ST6	74		3	4	11	6			2	
SV42	66	5	4	5	10	7			2	

Table 12.1. Estimate of modal mineralogy (vol%) of the Straumsvola Alkaline Complex. felds = feldspar, amph = amphibole opaq = opaque minerals.

Locally, coarser grains of clinopyroxene (1mm) are present comprising texturally homogeneous rims with cores full of fine- grained inclusions of biotite and amphibole. The spherical structures described above similarly have rim zones consisting dominantly of clinopyroxene and cores which are dominated by biotite. The rock enclosing the spherical structures consists of nepheline enclosed in an isotropic mineral thought to be sodalite. Intergranular amphibole is present. Nepheline is locally partially replaced by cancrinite.

Coarse Outer Zone (COZ)

The rocks of the COZ are characterised by coarse perthite (>5mm), medium grained nepheline (2-3mm), dark blue-green amphibole, pleochroic light to dark red brown biotite and pale green clinopyroxene (aegerine- augite). The perthite forms anhedral rounded grains with length/width ratio of ~2:1 and commonly has a thin rim of plagioclase.

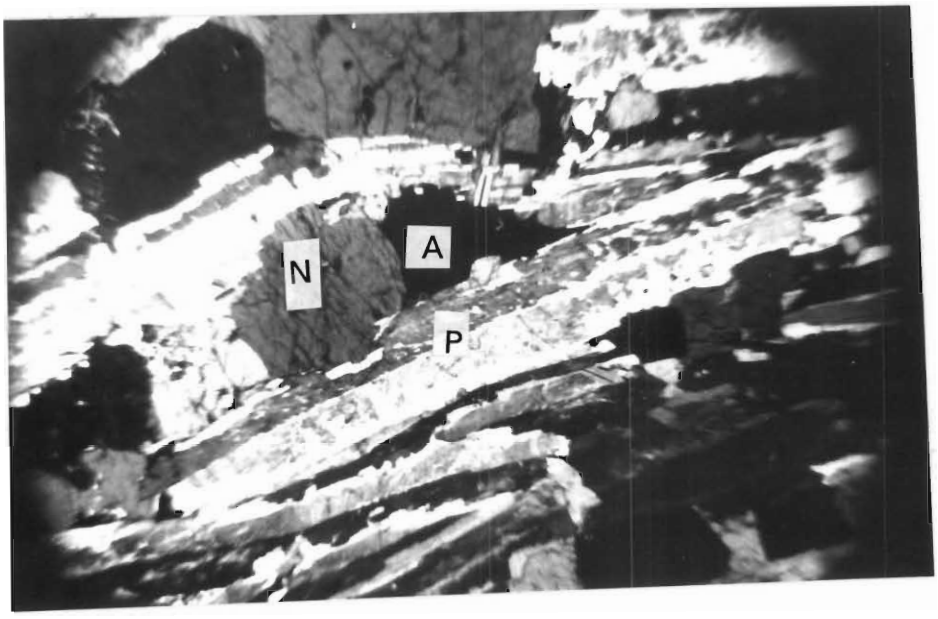

Figure 12.8. Strong planar fabric defined by perthite. Crossed Nicols. Field of view is 8 mm. P = perthite, A = amphibole and N = nepheline.

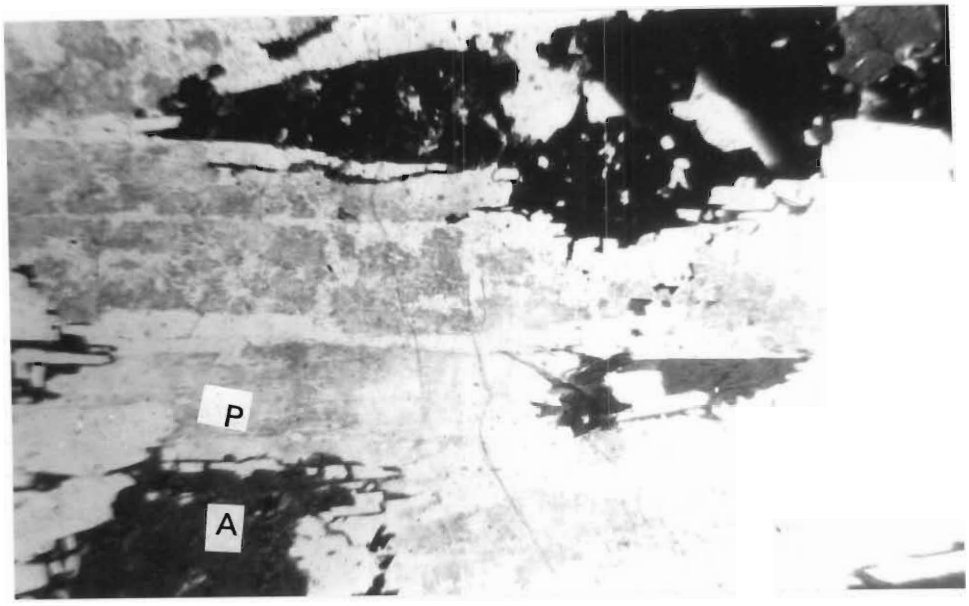

Figure 12.9. Delicate textures in which perthite and plagioclase are intergrown with amphibole. Field of view is 4mm. P = perthite and A = amphibole. Note the clear rim of plagioclase around the perthite grain.

The mafic minerals occupy the interstices between perthite and nepheline. Clinopyroxene is commonly partially to completely enclosed in amphibole with which appears to have been partially replaced. Biotite partially replaces amphibole and also occurs as discrete grains.

Mesocratic Zone (MZ)

The mesocratic zone is distinguished from the COZ and CLZ by significantly higher contents of opaque minerals and ferromagnesian silicate minerals which have a higher cpx/amphibole ratio than the COZ and CLZ. Perthite is coarse-grained (up to 3cm long), defines a planar fabric and contains inclusions of nepheline, clinopyroxene, biotite, opaque minerals. Green aegerine (up to 2mm) augite is the dominant ferromagnesian mineral and contains inclusions of apatite and biotite. The clinopyroxene is rimmed by vermicular amphibole. The opaque minerals are euhedral and are up to 0.5mm in size, commonly contain inclusions of apatite. Locally, clinopyroxene is radially distributed around opaque minerals. Two generations of biotite are present. Small (up to 0.1mm) randomly oriented inclusions of biotite occur in clinopyroxene and perthite, whereas larger grains of biotite (up to 1mm) are developed adjacent to clinopyroxene, amphibole, and opaque minerals.

Interpretation of Textures from the Straumsvola Alkaline Complex

Central Layered Zone

The textures in the layered zone may be interpreted as follows: cumulate laths of perthite and nepheline accumulated on the floor of the magma chamber trapping intercumulus liquid from which ferromagnesian minerals and their inclusions of apatite crystallised later. The delicate textures with perthite and plagioclase intergrown with amphibole and biotite are interpreted as an adcumulate growth during final cooling (fig 12.9). These delicate structures and the spherical mafic clots in layers (Fig. 12.4) near the base of the CLZ suggest that the ferromagnesian minerals crystallised from an intercumulus liquid which possibly originated as a result of liquid immiscibilty (see later). The mafic minerals cannot be viewed as a cumulate phase because they would have concentrated toward the base of the rhythmic layers and not at the top as is seen in some layers. Katophorite and arfvedsonite have densities of the order of 3.00 to 3.5 g/cm^3, aegerine-augite density of ~3.5 g/cm^3 whereas perthite and nepheline have densities of 2.5-2.65 and 2.56 to 2.66 g/cc^3 respectively (Deer, *et al.*,1966). Amphibole is the dominant ferromagnesian mineral. The local replacement of aegerine augite and amphibole by amphibole and biotite, respectively reflects either late stage residual volatile enrichment (H_2O) in the magma or a late stage influx of H_2O. Similarly, replacement of nepheline by cancrinite implies the presence of CO_2 in these late fluids (Deer *et al.*, 1966).

The thin rim of plagioclase around perthite is interpreted to be an exsolution phenomena with plagioclase having been exsolved from the perthite during cooling.

Mesocratic Zone (MZ)

The crystallisation sequence in the mesocratic zone appears to be different to the CLZ. Based on the textural relationships describe above, a probable order of crystallisation is as follows: the earliest phases include apatite, biotite and opaque minerals followed by clinopyroxene and nepheline. Finally there was crystallisation of perthite, amphibole, and a late generation of biotite.

Mafic Lens (ML)

The textures in the mafic lens, in which the spherical structures and local pyroxene grains have pyroxene rims and biotite cores, provide evidence of variable pH_2O or $pH_2O < P_{load}$. The partial replacement of nepheline by cancrinite suggests that the late stage fluid phase contained significant CO_2 (Deer *et al.*, 1966).

CHEMISTRY

Sixteen samples were analyzed from the Straumsvola Complex, nine from the central layered zone, four from the coarse outer zone, two from the mesocratic zone and one from the mafic lens (Table 12.2).

The samples from the CLZ and COZ are typically alkaline, being characterised by high concentrations of Al_2O_3, Na_2O, K_2O and $\Sigma FeO/(\Sigma FeO/MgO)$ and low contents of CaO and MgO. The CLZ shows widely varying chemistry with SiO_2 ranging between 53 and 65%, Al_2O_3 between 17 and 22%, CaO between 0.16 and 1.7%, K_2O between ~5 and ~9%, and Na_2O between ~5 and ~9%. Except for sample ST2, the composition of the COZ does not vary greatly. The Mesocratic Zone is distinguished by high TiO_2, P_2O_5, MgO and CaO and low Al_2O_3 in comparison to the other portions of the Straumsvola complex.

The concentrations of Sc, V, Ni and Cr were below detection limits. The CLZ is characterised by low Ba, despite its high perthite content, and high Rb/Sr ratios and abundance of Zr, Nb and La. The COZ and Mesocratic Zone have similar trace element contents and are characterised by lower Rb/Sr ratios, Zr and Y and higher Ba than the CLZ. The Mesocratic Zone is also distinguished from the COZ by a higher Nb content.

NO.	SiO_2	Al_2O_3	Fe_2O_3	FeO	MnO	MgO	CaO	Na_2O	K_2O	TiO_2	P_2O_5	TOTAL
CENTRAL LAYERED ZONE												
SV26	56.07	18.75	4.45	2.97	0.31	0.98	1.71	8.24	6.20	0.05	0.09	99.82
SV31A	55.76	21.44	3.36	1.96	0.22	0.30	0.65	9.23	6.23	0.47	0.09	99.71
SV33	64.74	18.16	1.02	0.65	0.06	0.15	0.63	5.49	8.85	0.08	0.02	99.85
SV22	60.86	20.13	1.65	0.97	0.15	0.31	0.68	7.23	7.80	0.07	0.06	99.91
SV23	57.67	17.62	4.04	2.91	0.35	0.84	1.58	6.82	6.80	0.44	0.07	99.14
SV24	61.00	20.23	1.36	0.80	0.15	0.10	0.16	6.85	8.24	0.25	0.01	99.15
SV27	59.52	19.56	2.42	1.48	0.20	0.36	0.73	7.33	7.51	0.27	0.06	99.44
SV29	55.81	20.28	3.33	2.10	0.24	0.73	1.43	9.45	6.05	0.29	0.08	99.79
SV28	53.31	19.69	2.98	4.66	0.41	0.92	1.89	9.38	5.58	0.47	0.17	99.46
COARSE OUTER ZONE												
ST2	65.25	17.85	0.90	0.58	0.13	0.41	0.98	5.81	7.57	0.24	0.21	99.93
ST8	57.37	21.36	2.82	1.82	0.12	0.69	1.31	8.79	5.86	0.60	0.23	100.97
SV20	57.25	22.09	1.78	1.14	0.14	0.67	0.94	9.08	6.15	0.47	0.19	99.90
SV41	57.60	21.24	2.01	1.32	0.20	0.58	0.83	8.06	6.47	0.52	0.18	99.01
MESOCRATIC ZONE												
ST6	57.84	16.09	3.67	3.38	0.31	1.42	2.73	5.80	5.62	1.59	0.78	99.23
SV42	48.45	16.22	6.50	6.17	0.52	1.54	3.53	6.12	5.54	3.23	1.30	99.12
MAFIC LENS												
SV35	46.37	14.40	6.36	6.35	0.52	6.60	6.52	7.95	3.40	0.88	0.29	99.64

SAMPLE	Rb	Sr	Rb/Sr	Th	Zr	Y	Nb	Ba	La	Cu	Zn
CENTRAL LAYERED ZONE											
SV22	325	203	1.60	10	218	18	103	76	56	4.1	68
SV23	266	143	1.86	4.5	389	20	154	66	57	5.8	121
SV24	376	187	2.01	7.6	384	9	141	79	22	1.2	58
SV27	302	226	1.33	6.7	369	13	183	103	41	3.6	95
SV29	267	207	1.28	23	322	22	139	129	88	nd	107
SV28	238	157	1.51	12	541	23	170	70	80	2	104
SV26	253	156	1.62	5	415	14	136	46	45	3	129
SV29	267	207	1.28	23	322	22	139	129	88	nd	107
SV31A	347	124	2.79	14	307	17	186	83	67	1	145
SV33	358	251	1.42	11	222	9	139	375	25	1	20
Mean			1.67								
COARSE OUTER ZONE											
ST2	187	301	0.62	6.3	103	13	34	1142	59	4.5	34
ST8	150	454	0.33	4.5	156	15	56	865	43	0.1	75
SV20	176	289	0.60	5.4	180	18	54	766	49	2.3	76
SV41	177	175	1.01	8.2	298	14	66	583	27	1.6	68
Mean			0.64								
MESOCRATIC ZONE											
ST6	158	194	0.81	3.8	111	31	45	685	104	1.2	77
SV42	175	222	0.78	4.4	77	39	70	800	171	1	97
Mean			0.80								
MAFIC LENS											
SV35	271	105	2.58	5.1	460	24	128	150	108	24	177

Table 12.2. Major and trace element chemistry (concentrations in wt% and ppm respectively) of the Straumsvola Alkaline Complex. nd = not detected

Plotting the normative mineralogy of the Straumsvola Syenites on the Petrogenys Residua Diagram shows that the samples from all the different sectors plot in the undersaturated part of the diagram (Fig. 12.10).

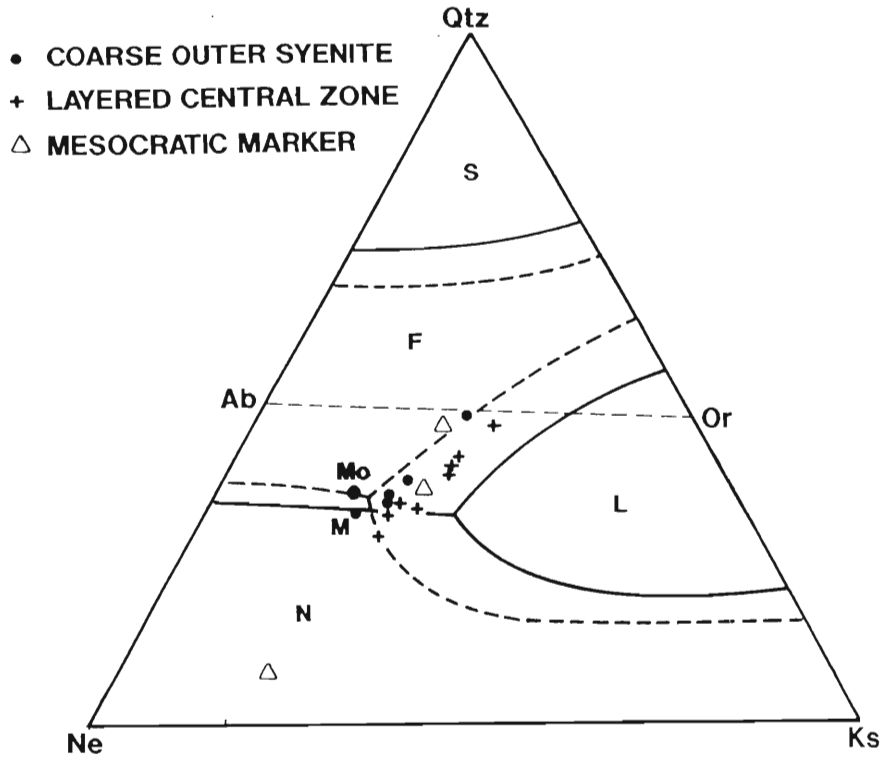

Figure 12.10. Normative mineralogy of the Straumsvola Complex plotted on the Petrogenys Residua System. The dashed lines represent phase boundaries at 1 atm (Schairer, 1950) whereas the solid lines represent phase boundaries at 1kb (Hamilton and Mckenzie,1965). S = quartz, F = perthitic feldspar, L = leucite and N = nepheline. M = temperature minimum at 1kb. M_o = temperature minimum at 1atm.

The compositions of the samples straddle the K-feldspar-nepheline phase boundary in the vicinity of the temperature minimum (M) at 1kb (Fig. 12.10).

The correlation coefficient matrix (Table 12.3) for the CLZ reveals that those elements which might be expected to be concentrated in nepheline (Na_2O) and the mafic minerals or fractionated into the intercumulus liquid (ΣFeO, MnO, MgO, CaO, P_2O_5, Zr, Y, La and Zn) have linear relationships (Figs. 12.11, 12.12 and 12.13). Those elements (K_2O, Rb and Sr) fractionated into perthite also show linear relationships (Fig. 12.14)(see appendix 3 for partition coefficients for K-feldspar and amphibole). The inverse relationship between Na_2O and K_2O is consistent with varying proportions of nepheline (Na_2O-rich) and perthite (K_2O-rich). In view of the many linear relationships between the major elements for the CLZ, it is surprising that so few correlations are seen for the trace elements.

SiO_2	SiO_2									
Al_2O_3	-0.297	Al_2O_3								
Fe_2O_3	-0.791	-0.125	Fe_2O_3							
FeO	-0.857	-0.138	0.705	FeO						
MnO	-0.874	-0.141	0.793	0.960	MnO					
MgO	-0.764	-0.333	0.840	0.878	0.893	MgO				
CaO	-0.723	-0.375	0.764	0.891	0.862	0.980	CaO			
Na_2O	-0.911	0.605	0.586	0.626	0.607	0.527	0.499	Na_2O		
K_2O	0.987	-0.243	-0.829	-0.852	-0.855	-0.805	-0.777	-0.907	K_2O	
TiO_2	-0.613	0.248	0.365	0.539	0.580	0.242	0.256	0.500	-0.554	TiO_2
P_2O_5	-0.872	0.151	0.583	0.916	0.834	0.739	0.777	0.774	-0.876	0.514
Rb	0.736	0.305	-0.750	-0.855	-0.861	-0.965	-0.964	-0.530	0.776	-0.240
Sr	0.727	-0.199	-0.709	-0.617	-0.700	-0.483	-0.403	-0.545	0.688	-0.601
Th	-0.243	0.545	-0.065	-0.029	-0.115	-0.034	0.037	0.545	-0.295	0.181
Zr	-0.704	-0.082	0.494	0.832	0.837	0.653	0.612	0.466	-0.627	0.522
Y	-0.768	0.147	0.561	0.708	0.725	0.682	0.711	0.709	-0.797	0.549
Nb	-0.418	0.195	0.292	0.358	0.341	0.070	0.083	0.345	-0.372	0.734
Ba	0.675	-0.331	-0.574	-0.470	-0.645	-0.456	-0.308	-0.554	0.598	-0.357
La	-0.800	0.344	0.544	0.631	0.616	0.596	0.630	0.843	-0.839	0.537
Cu	0.062	-0.499	0.199	0.138	0.291	0.211	0.180	-0.347	0.076	0.099
Zn	-0.847	0.313	0.835	0.598	0.706	0.551	0.479	0.748	-0.840	0.682

	P_2O_5									
Rb	-0.771	Rb								
Sr	-0.541	0.327	Sr							
Th	0.187	-0.025	0.164	Th						
Zr	0.666	-0.634	-0.503	-0.239	Zr					
Y	0.787	-0.729	-0.458	0.444	0.357	Y				
Nb	0.365	-0.104	-0.341	-0.041	0.463	0.092	Nb			
Ba	-0.448	0.423	0.698	0.197	-0.541	-0.461	-0.120	Ba		
La	0.774	-0.644	-0.411	0.645	0.281	0.951	0.175	-0.380	La	
Cu	0.033	-0.267	-0.150	-0.635	0.076	0.182	-0.016	-0.331	-0.081	Cu
Zn	0.617	-0.510	-0.800	0.116	0.429	0.648	0.544	-0.697	0.677	0.172Zn

Table 12.3. Correlation matrix for chemistry from the central layered zone of the Straumsvola complex. Correlations $<=-0.7$ and $>=0.7$ are underlined.

Interpretation of Chemistry

The compositions of the samples plotted on the Petrogenys Residua system are consistent with fractionation of a liquid at the temperature minimum. Experimental work shows that temperatures of between 750°C at 1kb (Hamilton and Mckenzie,1965) and ~1050°C at 1 atm (Schairer, 1950) may be expected at the temperature minimum.

The differences in chemistry between the various zones of the Straumsvola Alkaline Complex show that they do not appear to represent a continuum and that the CLZ, COZ and MZ are discrete intrusions with distinctive chemistry. The petrography study of the CLZ leads to the conclusion that perthite and nepheline were cumulus phases whereas amphibole crystallised from trapped intercumulus liquid. The strong linear variations defined by the major elements can be used to determine if these linear variations could have been controlled by the fractionation of the observed minerals.

Cox *et al.* (1979, pp. 147-160) describe a graphical method to test such hypotheses, making use of a series of variation diagrams on which the compositions of the whole rocks as well as mineral phases are plotted. The compositions of the three dominant mineral phases (nepheline, perthite and amphibole) form a triangle which is bisected by the trend-line defined by the whole rock chemistry. These triangles and trend-lines are then redrawn as equilateral triangles maintaining the proportionality of the trend-lines and the triangle intersections. The equilateral triangles are then superimposed or combined onto one triangle. "If the triangles are internally consistent then the superimposed bulk compositional trends will intersect in a point which gives the mineral proportions which will satisfy all the data" (Cox *et al.*, 1979, pp. 157-158).

These authors show that, in practice, a small field of uncertainty is defined yielding a restricted range of mixtures of the mineral phases which could have fractionated to yield the bulk compositional trends. Six variation diagrams have been drawn using the above described principles (figs 12.15 to 12.20) for K_2O vs Na_2O, K_2O vs SiO_2, Na_2O vs SiO_2, MgO vs SiO_2, Al_2O_3 vs SiO_2 and MgO vs K_2O, all of which yield correlation coefficients <-0.7 or >0.7, except for Al_2O_3 vs SiO_2. The mineral analyses used are those shown in table 12.4. These elements were selected because they comprise the dominant components in the minerals. Magnesium was used instead of Fe because of the uncertainties related to the variable oxidation states of Fe. The bulk trends were calculated using linear regression (least squares method).

	amph[1]	Or[2]	Ne[2]	amph[1]	Or[2]	Or[2]	amph[2]	Cpx[1]	Bt[1]	Cpx[1]	Cpx[2]
SiO_2	44.30	65.54	44.80	44.90	65.38	65.62	43.80	51.29	35.02	51.71	51.28
Al_2O_3	5.06	18.09	32.80	4.82	18.72	19.62	5.57	0.98	10.18	1.09	1.81
Fe_2O_3	12.77	0.43	0.18	8.12	0.38	0.26	10.81	15.17	0.00	23.39	23.53
FeO	18.26	0.00	0.00	22.71	0.00	0.00	19.36	12.34	35.17	5.10	5.40
MnO	1.74	0.00	0.00	1.33	0.00	0.00	1.35	0.77	1.43	0.75	0.50
MgO	2.80	0.09	0.34	3.09	0.00	0.10	2.82	1.52	2.91	1.33	0.79
CaO	1.81	1.15	0.33	4.25	0.86	0.16	4.35	10.92	0.00	5.95	5.53
Na_2O	8.02	5.60	15.85	6.57	6.29	5.84	6.33	7.03	0.32	10.34	9.59
K_2O	1.81	8.59	5.48	1.77	7.36	8.08	1.76	0.00	8.82	0.00	0.16
TiO_2	1.63	0.00	0.00	1.90	0.06	0.00	2.01	0.59	3.11	0.74	0.56
P_2O_5	0.00	0.05	0.02	0.00	0.05	0.00	0.03	0.00	0.00	0.00	0.03
	98.20	99.54	99.80	99.46	99.10	99.68	98.19	100.61	96.94	100.1	99.18

Table 12.4. Compositions of minerals from central layered zone (concentrations in wt%). The analyses are from C.Harris[1] (unpublished data) and Ravich and Solo'vev[2] (1966). amph = amphibole.

Figure 12.21 shows that fractionation of perthite:nepheline:amphibole in the proportions of 0.35:0.19:0.15 to 0.63:0.28:0.28 could result in the observed linear trends. However, textural data suggest that the amphibole crystallised from a late stage post- or intercumulus liquid, which may have originated as a consequence of liquid immiscibility.

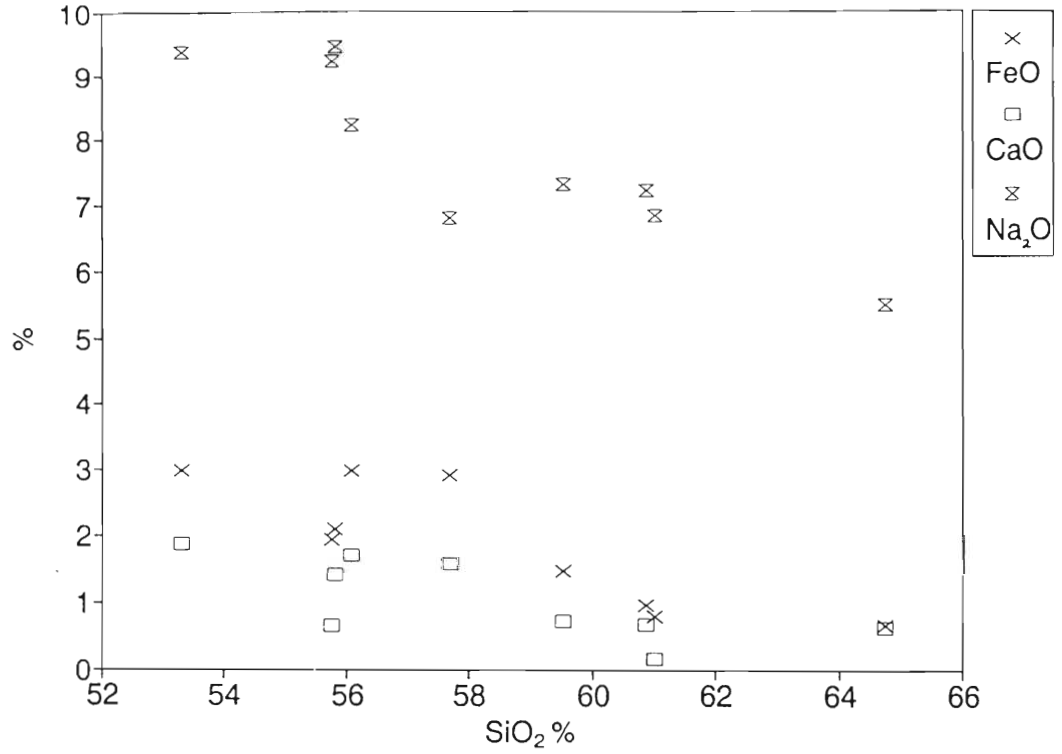

Figure 12.11. FeO, CaO and Na_2O vs SiO_2 for the CLZ.

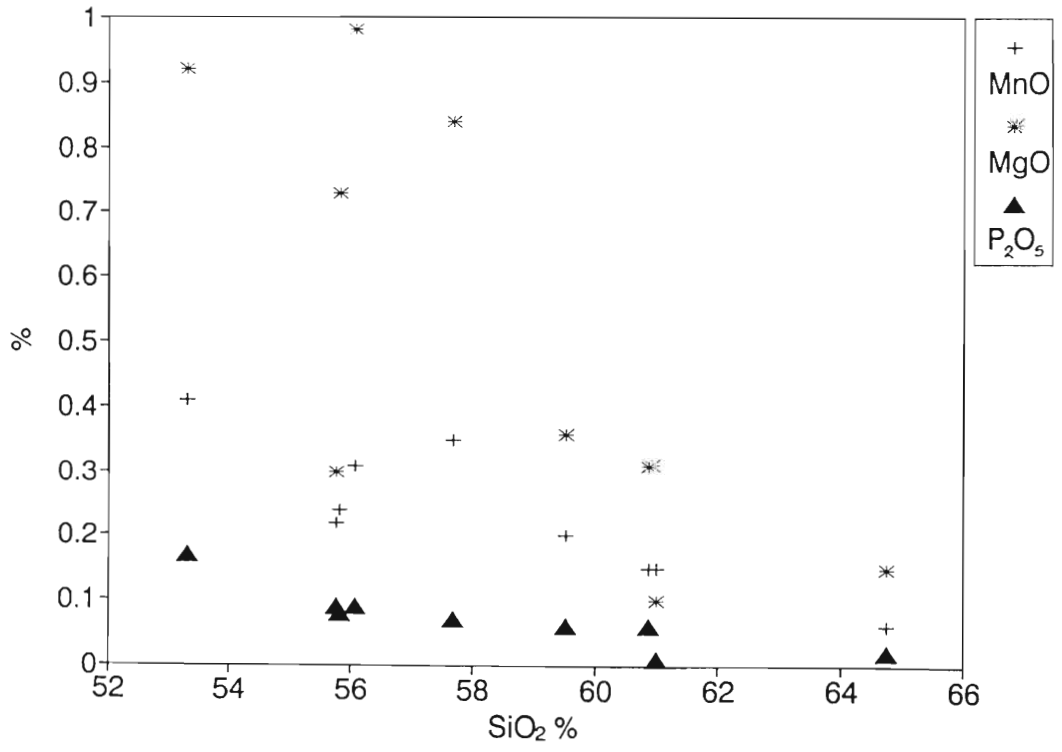

Figure 12.12. MnO, MgO and P_2O_5 vs SiO_2 for the CLZ.

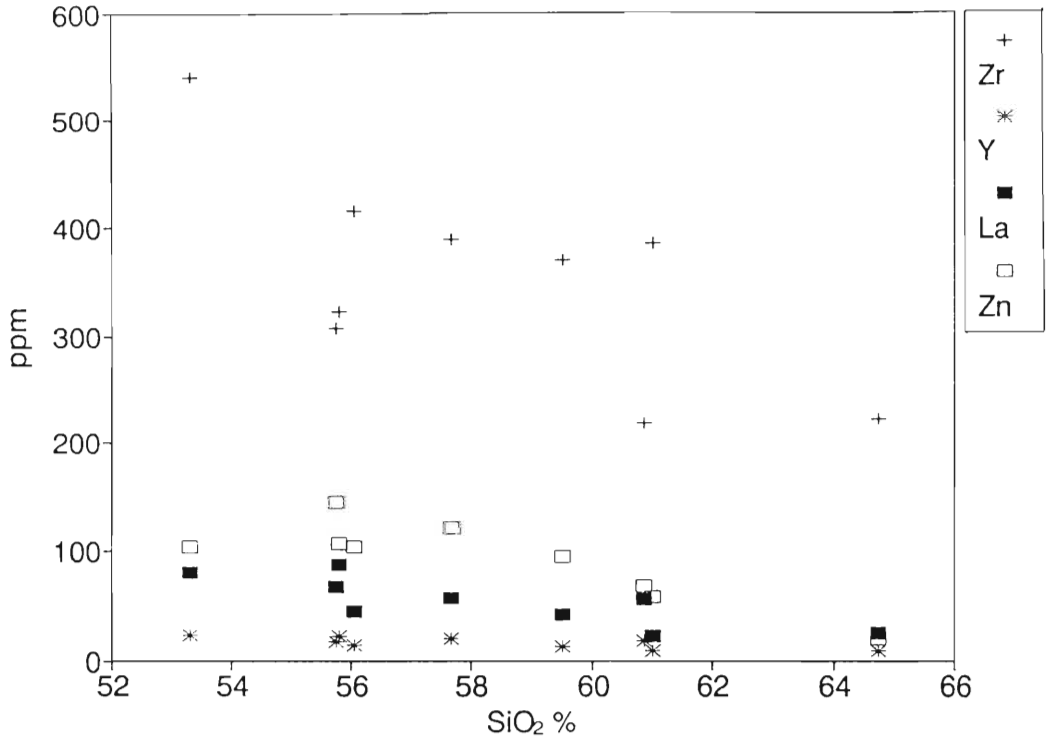

Figure 12.13 Harker variation diagrams for Zr, Y, La and Zn for the CLZ.

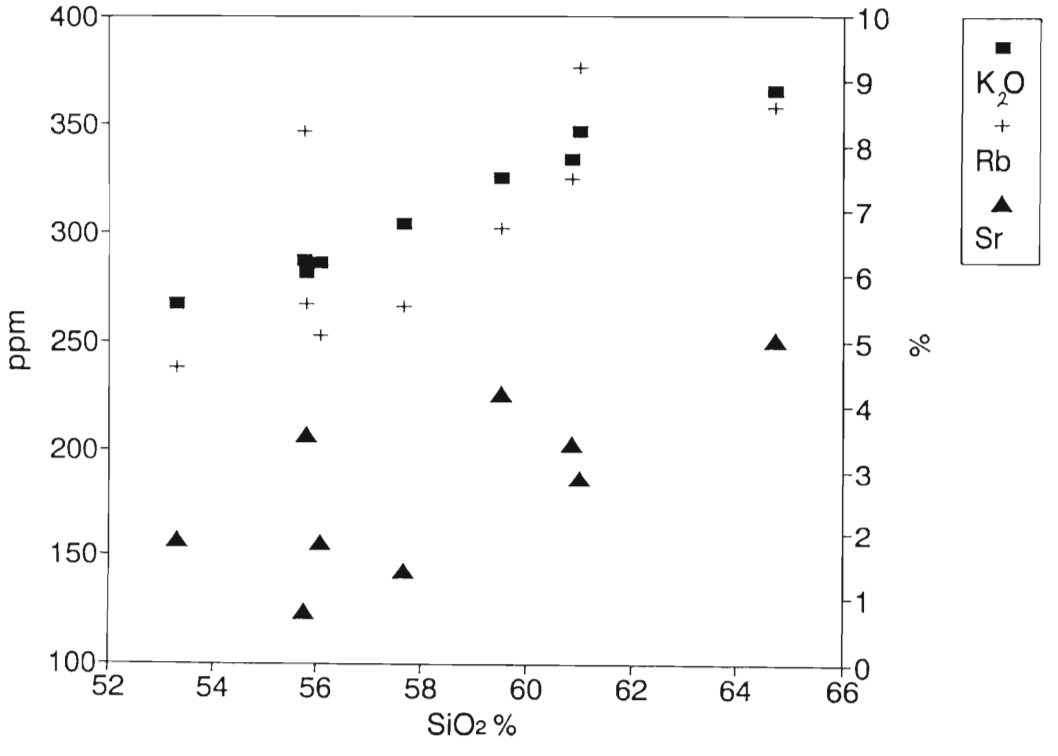

Figure 12.14. Harker variation diagrams for K_2O, Rb and Sr for the CLZ. K_2O is scaled on the right hand Y-axis and Rb and Sr on the left.

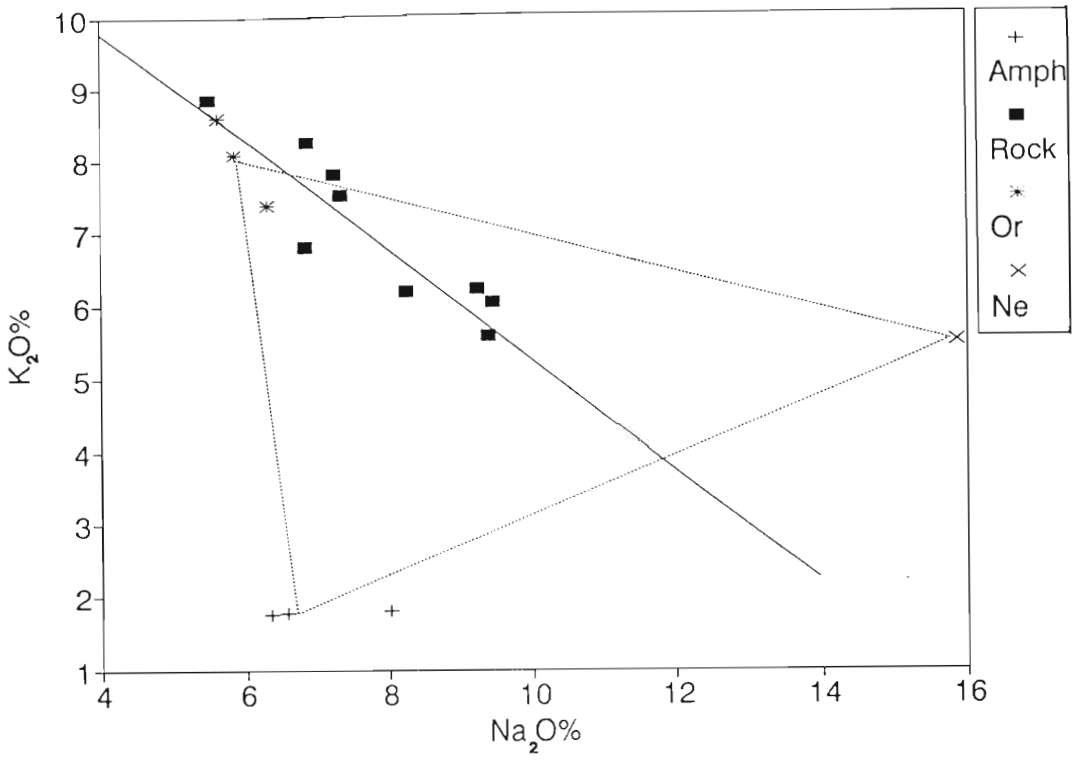

Figure 12.15. K_2O vs Na_2O for the whole rocks and dominant minerals from the CLZ of the Straumsvola Alkaline complex. The solid line represents the bulk trend calculated from linear regression whereas the dotted lines link the mineral phases to form the triangle.

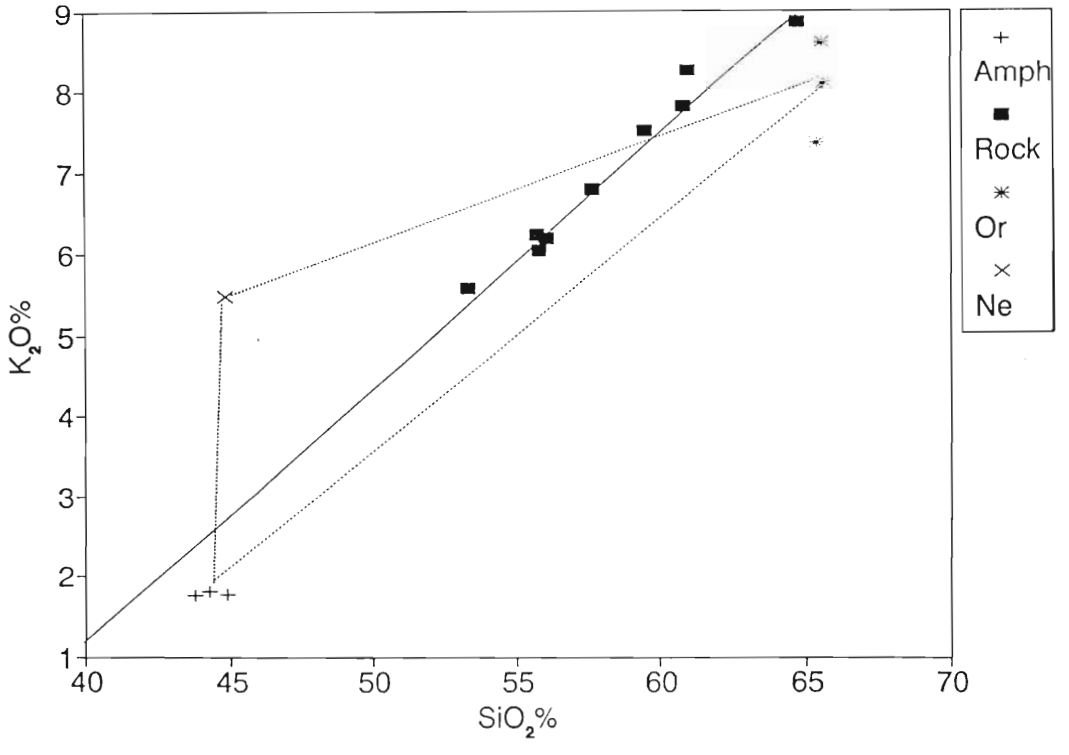

Figure 12.16. K_2O vs SiO_2 for the whole rocks and dominant minerals from the CLZ of the Straumsvola Alkaline complex. The solid line represents the bulk trend calculated from linear regression whereas the dotted lines link the mineral phases to form the triangle.

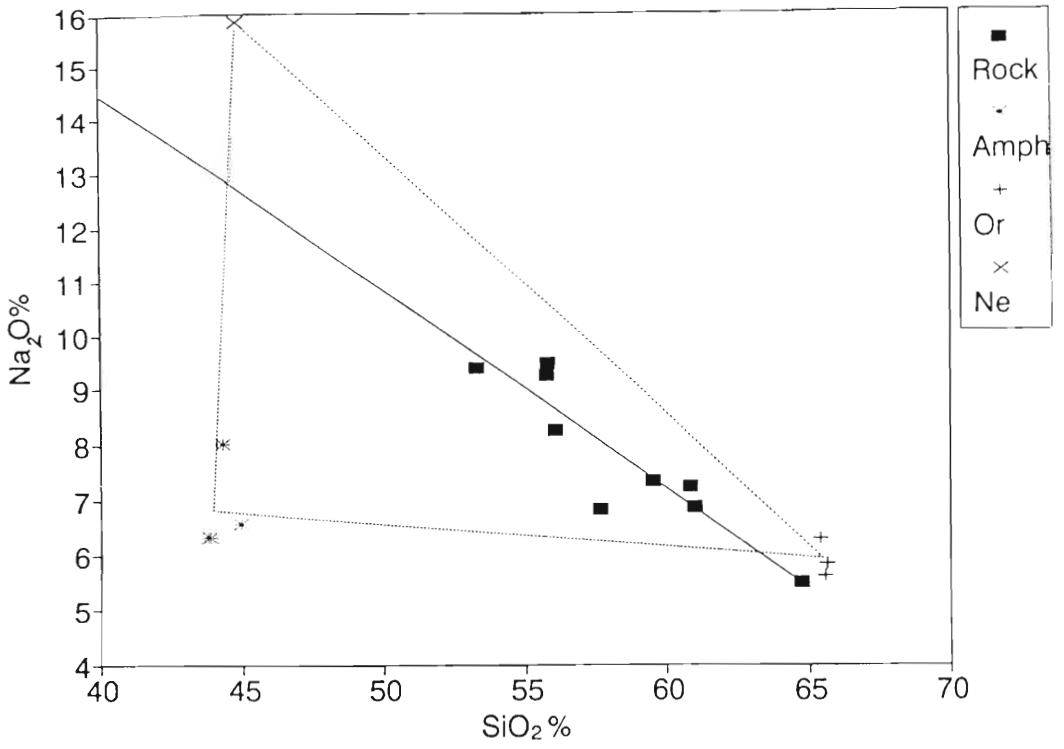

Figure 12.17. Na_2O vs SiO_2 for the whole rocks and dominant minerals from the CLZ of the Straumsvola Alkaline complex. The solid line represents the bulk trend calculated from linear regression whereas the dotted lines link the mineral phases to form the triangle.

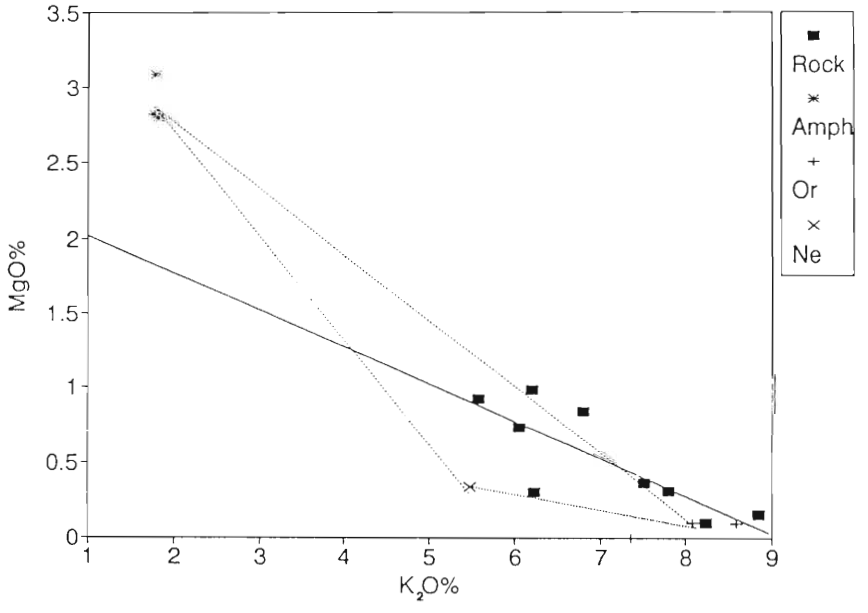

Figure 12.18. K_2O vs MgO for the whole rocks and dominant minerals from the CLZ of the Straumsvola Alkaline complex. The solid line represents the bulk trend calculated from linear regression whereas the dotted lines link the mineral phases to form the triangle.

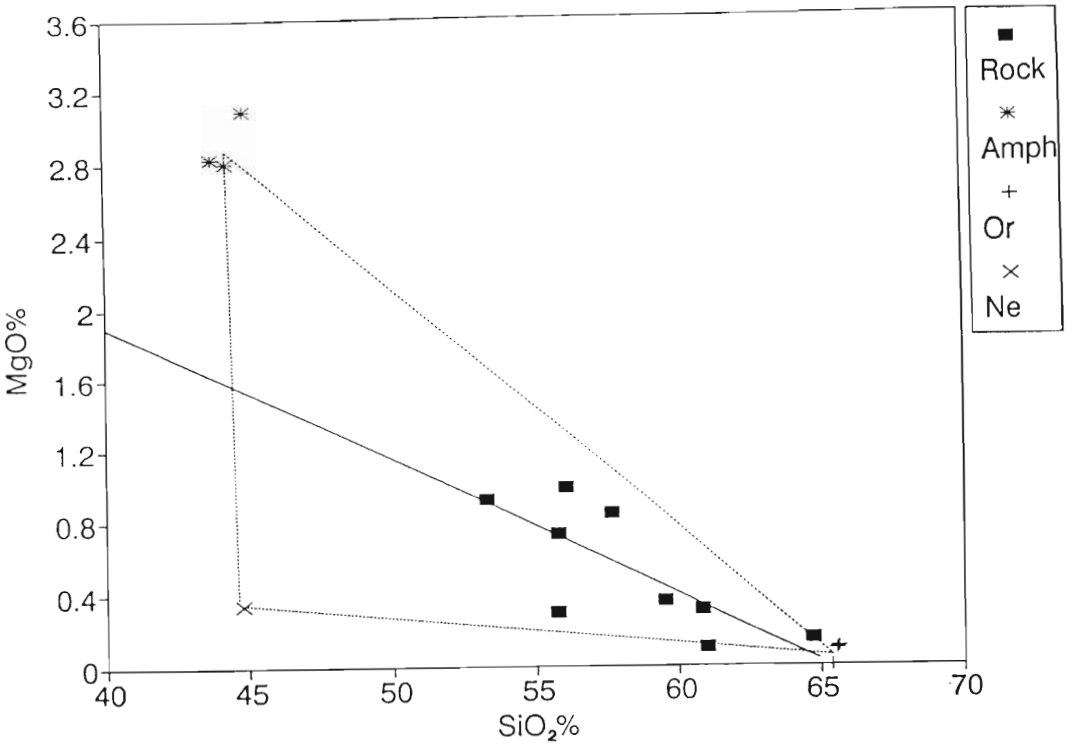

Figure 12.19. MgO vs SiO_2 for the whole rocks and dominant minerals from the CLZ of the Straumsvola Alkaline complex. The solid line represents the bulk trend calculated from linear regression whereas the dotted lines link the mineral phases to form the triangle.

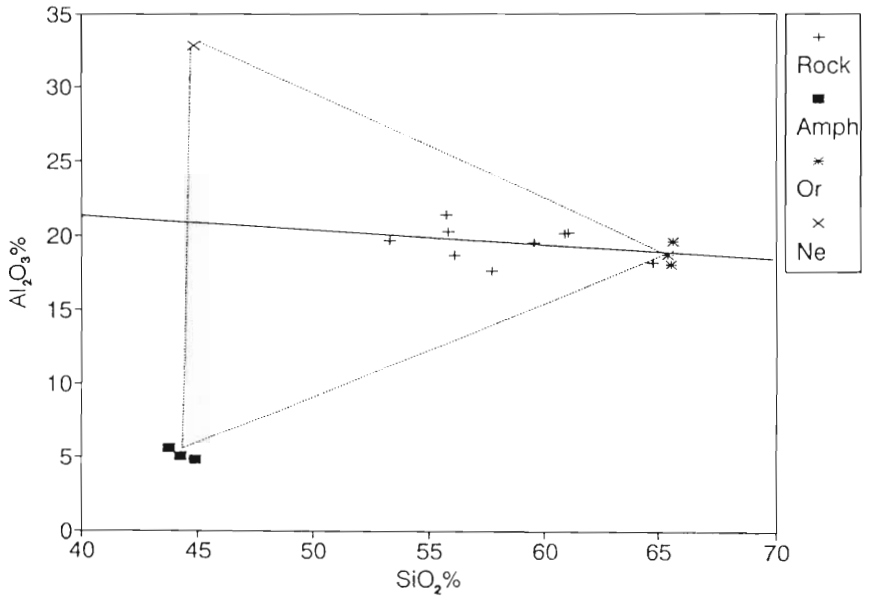

Figure 12.20. Al_2O_3 vs SiO_2 for the whole rocks and mineral analyses from the CLZ of the Straumsvola Alkaline complex. The solid line represents the bulk trend calculated from linear regression whereas the dotted lines link the mineral phases to form the triangle.

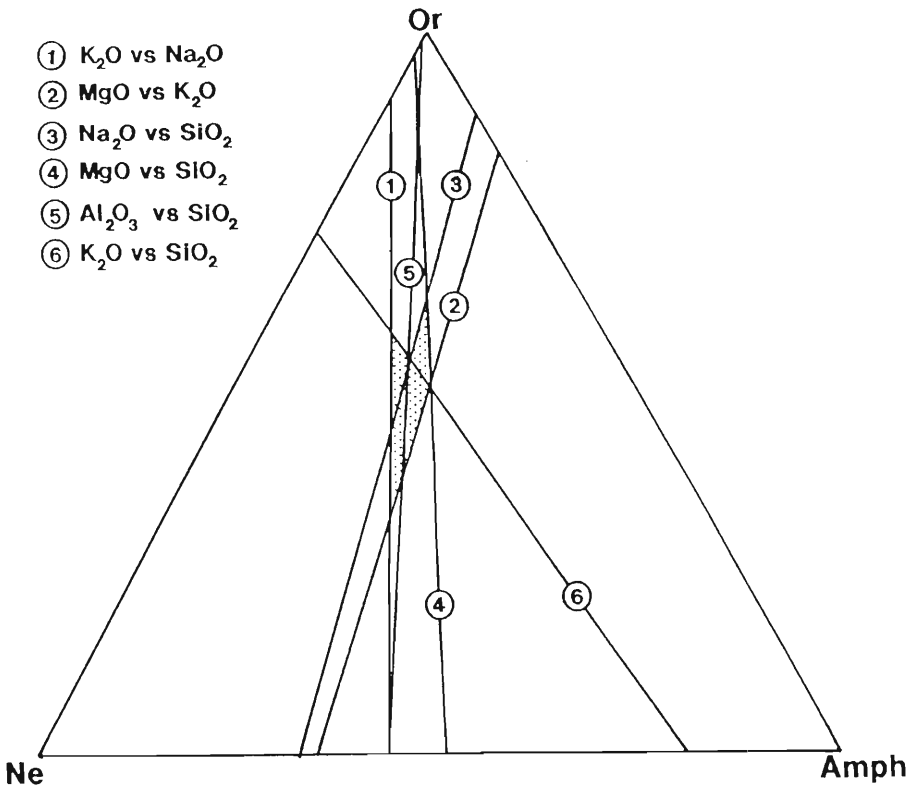

Figure 12.21. Superimposed transformed triangles from figures 12.15 to 12.20. The stippled area shows the possible variation in the proportion of minerals fractionated.

Naslund (1983) has shown that liquid immiscibility is possible in K, Na, Al-bearing Fe-rich silicate melts, the controlling factors being oxygen fugacity, and CaO, MgO, TiO_2 and P_2O_5 contents of the melts. Figures 12.22 to Figs 12.25 show the compositions of the ferromagnesian minerals from Table 12.4 plotted in the fields of liquid immiscibility defined by Naslund (1983).

The field of immiscibility for systems containing K_2O-FeO-Fe_2O_3-Al_2O_3-SiO_2 and Na_2O-FeO-Fe_2O_3-Al_2O_3-SiO_2 shows that the compositions of the amphiboles could represent that of an immiscible liquid at oxygen fugacities respectively between $fO_2 = 10^{-12}$ to $10^{-0.7}$ and $fO_2 = 10^{-6}$ to $10^{-0.7}$. The compositions of clinopyroxenes in the same system could reflect the composition of the immiscible liquid under more restricted conditions (ie $fO_2 = 10^{-5}$ to $10^{-0.7}$). Figure 12.23 shows that the compositions of the amphiboles could represent an immiscible liquid of similar composition with fO_2 varying between $fO_2 = \sim 10^{-6}$ to $fO_2 = 10^{-0.7}$. The composition of the clinopyroxene could only be viewed as such under fO_2 conditions between $< fO_2 = 10^{-5}$ and $fO_2 = 10^{-0.7}$.

At temperatures of 750°C to 1050°C the quartz- fayalite-magnetite buffer (QFM) is located at $fO_2 \sim 10^{-16}$ and $\sim 10^{-11}$ (Carmichael *et al.*, 1974, p. 331).

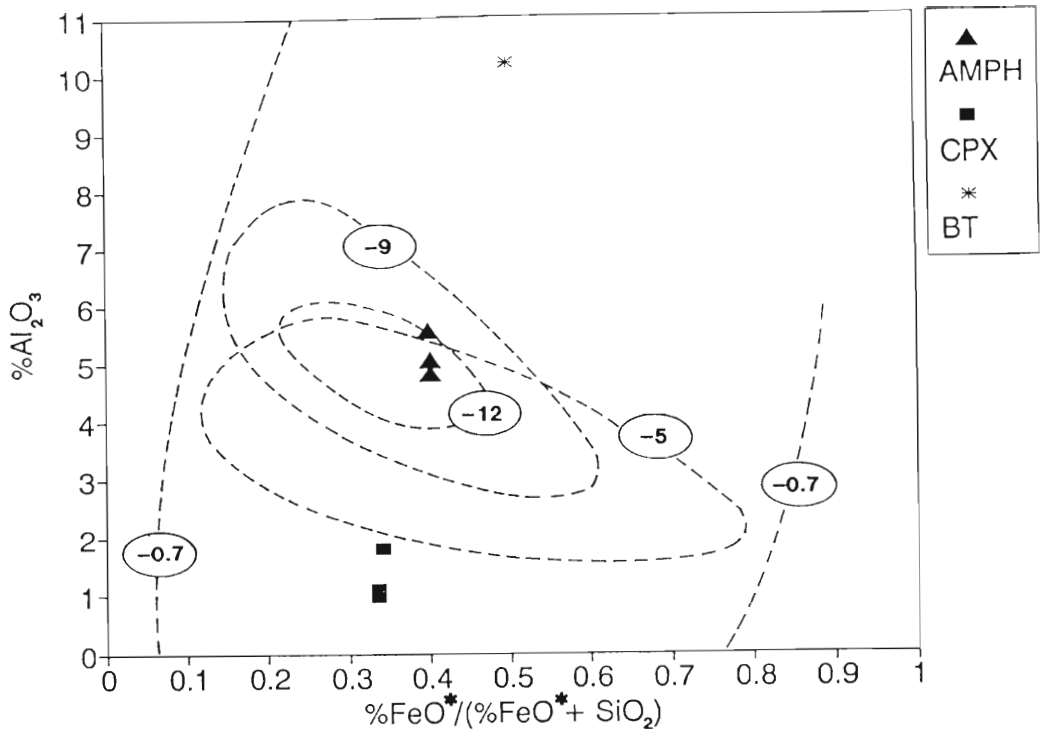

Figure 12.22. Mineral compositions shown with fields of immiscibility for a system containing K_2O-FeO-Fe_2O_3-Al_2O_3-SiO_2 with varying oxygen fugacities. The numbers attached to each fields are the exponential values of fO_2 to the base 10 (eg 10^{-9}).

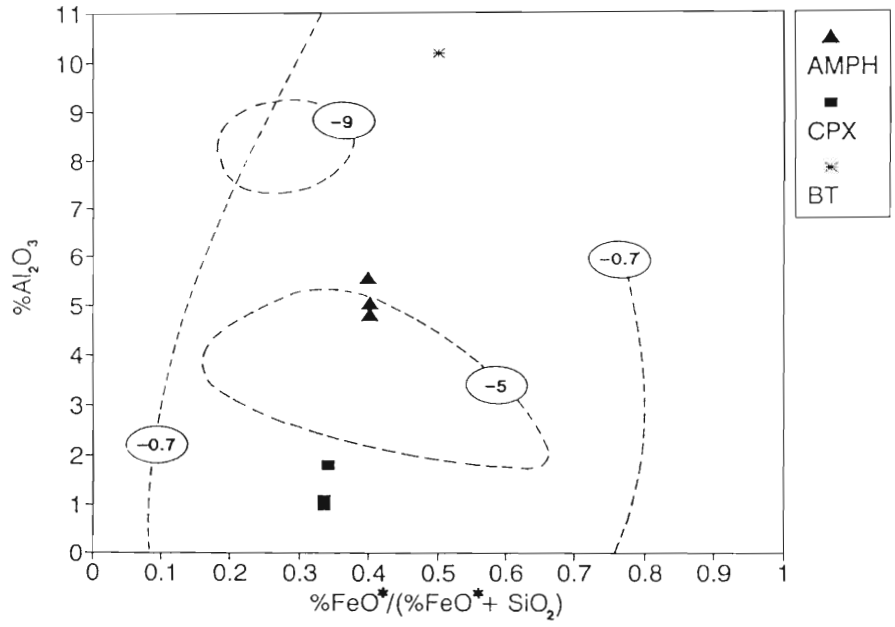

Figure 12.23. Mineral compositions shown with the fields of immiscibility for a system containing Na_2O-FeO-Fe_2O_3-Al_2O_3-SiO_2 with varying oxygen fugacities. The numbers attached to each fields are the exponential values of fO_2 to the base 10 (eg 10^{-8}).

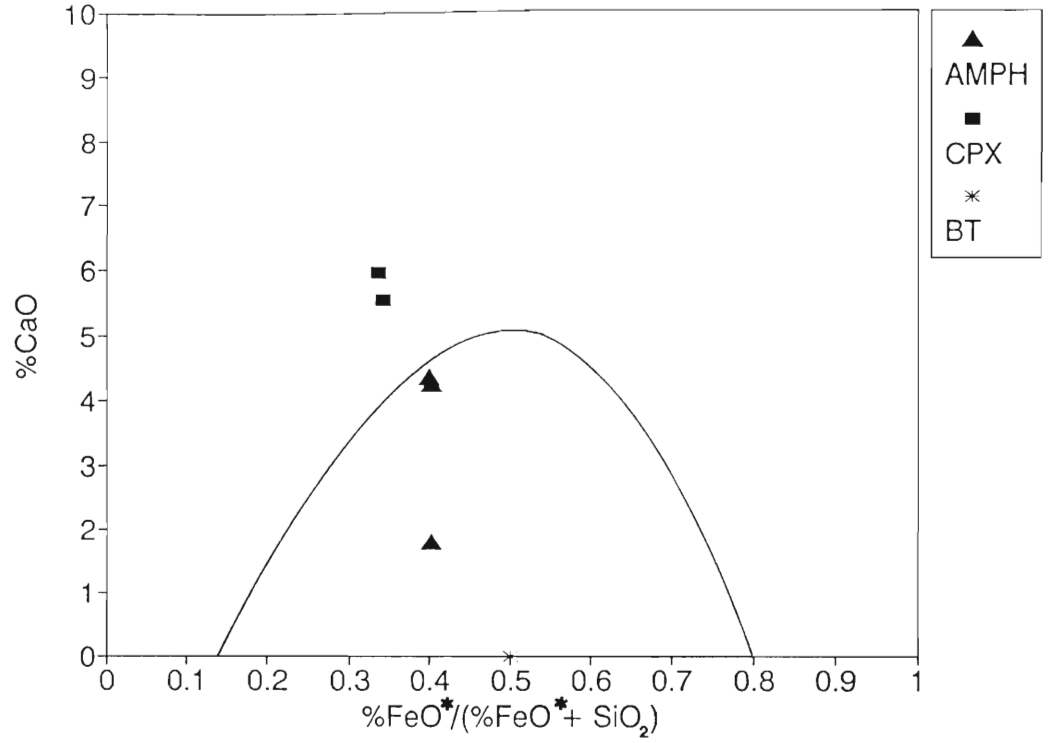

Figure 12.24. Mineral compositions shown with field of immiscibility for a system containing $CaO\text{-}K_2O\text{-}FeO\text{-}Fe_2O_3\text{-}Al_2O_3\text{-}SiO_2$. The area below the curved line is the field of immiscibilty.

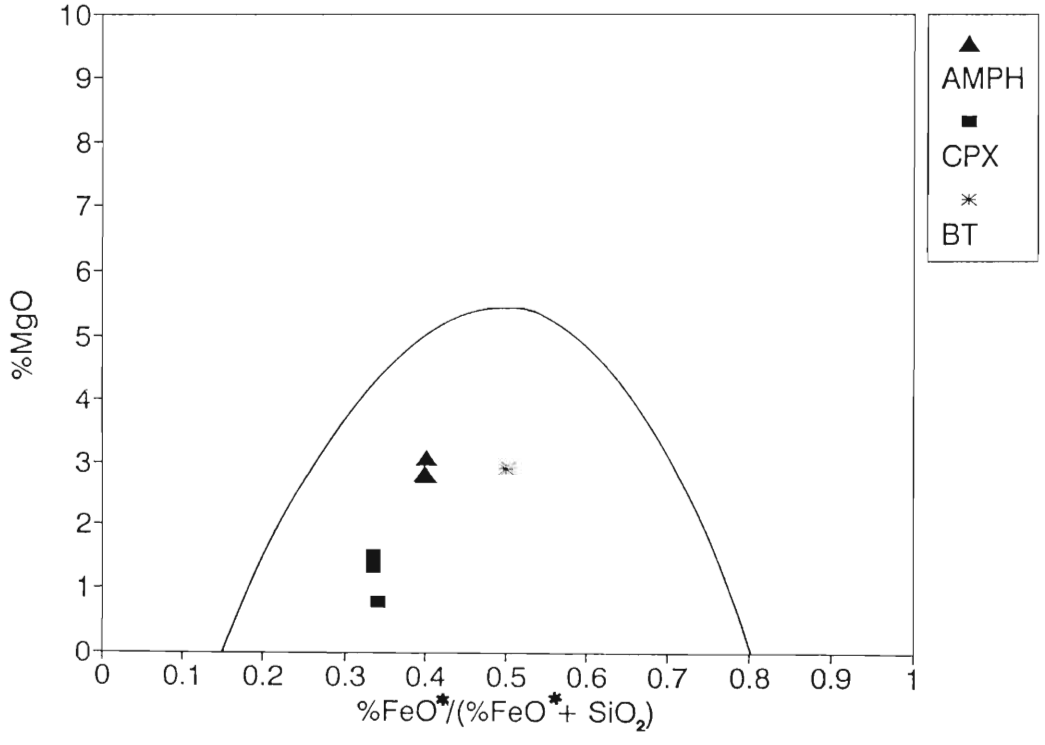

Figure 12.25. Mineral compositions shown with field of immiscibility for a system containing $MgO\text{-}K_2O\text{-}FeO\text{-}Fe_2O_3\text{-}Al_2O_3\text{-}SiO_2$. The area below the curved line is the field of immiscibilty.

Carmichael *et al.* (1974, p.332) state that in basaltic liquids values of fO_2 do not vary by more than two orders of magnitude on either side of the QFM buffer but that the range of fO_2 in salic magmas, like the Straumsvola Alkaline Complex, is probably greater. Consequently, in the Straumsvola Alkaline Complex, fO_2 values between $\sim 10^{-13 \text{ to } -19}$ at 750°C to $\sim 10^{-8 \text{ to } -14}$ at 1000°C may considered to be reasonable.

In addition Naslund (1983) studied the effect of additional components and found that the extent of liquid immiscibility was reduced by increasing CaO and MgO content whereas the presence of TiO_2 and P_2O_5 promoted immiscibilty. Figure 12.24 shows that the CaO content of the amphibole and biotite are consistent with liquid immiscibility whereas the clinopyroxene is not. Figure 12.25 shows that the MgO concentration of the amphibole, clinopyroxene and biotite are consistent with liquid immiscibilty. The amphiboles contain significant TiO_2 (table 12.4) and the numerous apatite inclusions in the amphibole indicate high P_2O_5 concentrations in the intercumulus liquid. Consequently, it appears that the composition of the amphibole is generally comparable with the immiscible liquid compositions defined by Naslund (1983).

Conclusions

The Straumsvola Alkaline Complex consists of four petrographically and chemically discrete units, the CLZ, COZ, MZ and ML. The COZ is the oldest part of the complex being intruded by the CLZ and the MZ. The CLZ appears to have resulted from fractionation of orthoclase and nepheline and an intercumulate liquid from which amphibole crystallised. This intercumulate liquid may have originated as a consequence of liquid immiscibilty. The ML is considered to constitute an integral part of the CLZ.

TVORA ALKALINE COMPLEX

Field relationships and appearance

At Tvora two generations of syenite are recognized, namely, an earlier mesocratic to melanocratic variety and a later leucocratic variety. Coarse- grained veins of leucocratic syenite intrude the mesocratic syenite and xenoliths of the mesocratic syenite are commonly found in the leucocratic syenite. Mineralogically, the two varieties of syenite are similar with the darker colour of the mesocratic variety resulting from the presence of dark brown feldspars. The brown colour feldspars are considered to result from alteration because the syenite becomes lighter in colour adjacent to the contacts of trachytic dykes intruding the syenite.

Petrography

The mineralogy of the samples from Tvora are shown in table 12.5. Mineralogically, the

leucocratic and melanocratic zones of Tvora are similar but with subtle differences. The samples contain varying proportions of perthite, amphibole, clinopyroxene, biotite and opaque minerals with accessory phases in some samples including sphene, quartz and olivine. The accessory quartz and olivine are present in the melanocratic zone but never in contact with one another. A separate plagioclase phase is also seen in the melanocratic phase. Texturally, the rocks are characterised by coarse, anhedral feldspar grains (2-3mm) with finer interstitial mafic and opaque minerals. In the leucocratic syenite the mafic mineral is dominantly amphibole whereas in the melanocratic phase a higher proportion of clinopyroxene (dark to light green aegerine-augite) is present. Clinopyroxene is commonly seen to form cores to amphibole grains. The mafic minerals commonly have small inclusions of apatite. The grain boundaries in the syenites are commonly irregular and ragged suggesting that the rocks have been slightly recrystallised.

	felds	Ol	Bt	amph	Cpx	opaq	Qtz	Sdl	Spn
LEUCO									
TV1	70		4	20	5	1			
TV8	70		2	23	4	1			
TV9	96			1	1	2			
TV11	75			20		3		1	1
TV14	85		2	10		2			1
MELANO									
TV7	65+10		4	4	15	2			
TV15	73+10			10	5	2			
TV16	80	1	1	10	6	2	1		
TV17	75+5	1		10	6	2			
TV19	75+5		2	10	4	2	1		

Table 12.5. Table showing the estimated modal proportions (vol%) of the Tvora Alkaline Complex. The two values in the feldspar column for the melanocratic syenite are for perthite + plagioclase. felds = feldspar, amph = amphibole, opaq = opaque minerals.

Discussion and interpretation of mineralogy and textures.

The dark colour of the melanocratic phase is thought to have resulted from alteration because the petrography shows that the proportion of mafic to felsic minerals between the leucocratic and melanocratic phases of the syenite does not differ greatly. The mafic and opaque minerals with their apatite inclusions appear to have crystallised after the feldspars, occurring as interstitial grains. Although olivine and quartz are seen in the same rock, but not in contact, their co-existence suggests that the olivine is either iron-rich (fayalitic) or that the minerals resulted from disequilibrium crystallisation. The partial replacement of clinopyroxene by amphibole suggests either a late stage fluid influx (H_2O) or concentration of H_2O in the residual magma.

Chemistry

Ten samples of the Tvora Syenite were analyzed, five from the leucocratic phase and five from the melanocratic altered phase (Table 12.6). The compositions of the samples do not vary greatly. The melanocratic and leucocratic syenites have similar SiO_2 contents but the melanocratic syenites have marginally higher ΣFeO, CaO, TiO_2 and P_2O_5 and marginally lower Al_2O_3, Na_2O and K_2O contents. The trace element contents of the leucocratic and melanocratic phases of the Tvora Syenites are similar except for Th and La which are higher in the leucocratic phase and Ba which is higher in the melanocratic phase. Rb/Sr is variable in the leucocratic phase but is relatively low and less variable in the melanocratic phase.

NO.	SiO_2	Al_2O_3	Fe_2O_3	FeO	MnO	MgO	CaO	Na_2O	K_2O	TiO_2	P_2O_5	TOTAL
LEUCO SYENITE												
TV1	59.53	18.60	2.78	3.13	0.14	1.09	3.56	6.18	3.97	0.85	0.32	100.15
TV8	63.08	19.13	2.07	1.81	0.14	0.27	1.46	5.86	6.64	0.34	0.11	100.91
TV9	64.11	19.08	1.79	1.39	0.11	0.09	0.71	6.61	6.23	0.13	0.02	100.27
TV11	62.91	19.21	1.81	1.42	0.15	0.27	1.53	6.01	6.66	0.40	0.1	100.47
TV14	61.95	19.56	1.70	1.46	0.14	0.40	2.05	6.26	5.61	0.32	0.11	99.56
MELANOSYENITE												
TV7	57.26	17.85	3.49	4.46	0.17	1.91	4.62	5.60	3.76	1.18	0.46	100.76
TV15	63.34	18.75	1.65	1.67	0.12	0.36	2.35	5.74	5.08	0.51	0.14	99.71
TV16	61.06	16.93	3.18	3.44	0.19	0.90	3.02	5.36	4.64	0.91	0.31	99.94
TV17	59.81	16.07	3.18	3.54	0.24	1.15	3.74	5.51	4.09	1.21	0.47	99.01
TV19	61.04	17.21	3.07	3.33	0.22	0.87	2.88	5.79	4.57	0.86	0.30	100.14

NO.	Rb	Sr	Rb/Sr	Th	Zr	Y	Nb	Ba	Sc	Cr	La	V	Cu	Zn
LEUCO SYENITE														
TV1	67	693	0.096	nd	240	39	80	1957	10	112	83	11	15	87
TV8	227	331	0.68	22	493	34	101	790	2	4	107	9	5	54
TV9	323	222	1.45	55	996	46	166	547	nd	92	106	nd	6	92
TV11	172	288	0.59	12	228	23	74	809	2	nd	74	1	5	60
TV14	184	647	0.28	24	8	27	92	826	1	nd	102	nd	5	71
MELANO SYENITE														
TV7	71	754	0.09	nd	235	28	42	2167	14	113	61	46	34	95
TV15	124	557	0.22	7	198	25	39	2829	5	nd	58	nd	3	44
TV16	131	504	0.26	10	383	45	68	2732	10	75	84	nd	15	100
TV17	83	694	0.12	6	15	40	56	2599	8	nd	80	nd	2	72
TV19	161	450	0.37	10	289	48	92	2604	10	132	81	nd	13	135

Table 12.6. Major and trace element chemistry (concentrations in wt% and ppm respectively) of the Tvora syenites. nd = not detected.

Plotting the normative mineralogy of the Tvora Syenites on the Petrogenys Residua Diagram shows that the samples from both the leucocratic phase and altered phase plot in the perthitic feldspar field in the region of the thermal divide between oversaturated and undersaturated systems (Fig. 12.26).

Comparison of Tvora and Straumsvola

Because no age determinations have been made on the Tvora syenites, it is uncertain to what extent the alkaline rocks of Tvora, Straumsvola and Storjeon may be related. Clearly, the rocks of Straumsvola and Storjeon are chemically similar and appear to be part of the same intrusion. The composition of the syenites from Tvora are different to those from the Straumsvola Alkaline Complex, being more SiO_2-rich and containing less K_2O and Na_2O. Locally, the jointing at Tvora is developed to a far higher degree than Storjeon. The mesocratic phase at Tvora appears to result from alteration whereas such alteration is not seen at Straumsvola or Storjeon.

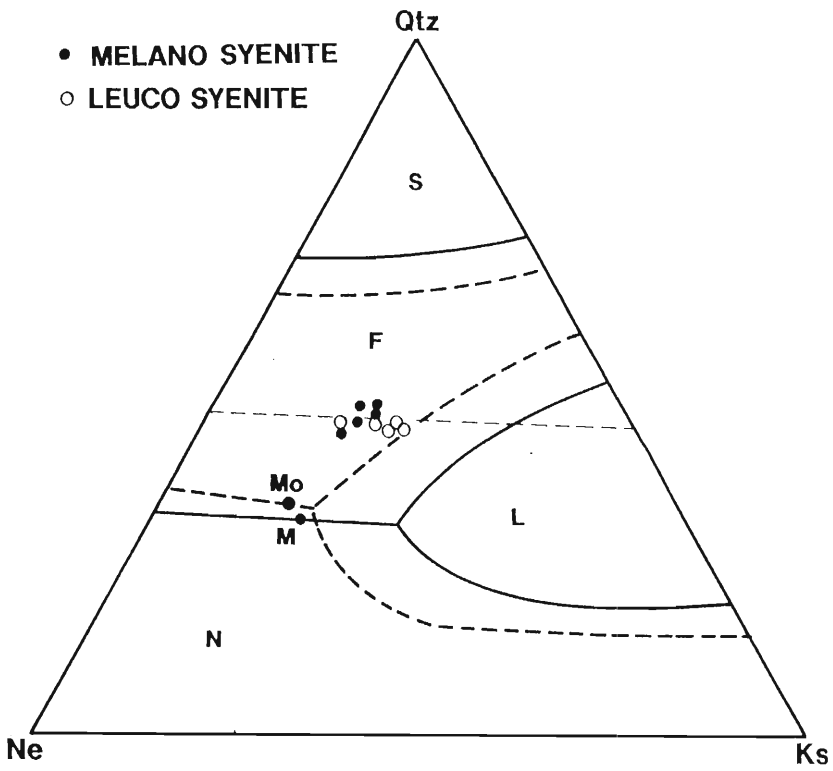

Figure 12.26. Normative mineralogy of the Tvora Syenites plotted on the Petrogenys Residua System. The dashed lines represent phase boundaries at 1 atm (Schairer, 1950) whereas the solid lines represent phase boundaries at 1kb (Hamilton and Mckenzie,1965). S = quartz, F = perthitic feldspar, L = leucite and N = nepheline. M = temperature minimum at 1kb. M_o = temperature minimum at 1atm.

Mechanisms of deriving the Straumsvola Syenites from magma of similar composition to the

Tvora Syenites would require crystallisation of oversaturated phases, depleting the magma in SiO_2. Comparing the composition of the Tvora Syenites (~57% to 64%) with the K-feldspar analyses in Deer *et al.* (1992, pp. 414-415) shows that the K-feldspar have SiO_2 contents in excess of 63% irrespective of whether the feldspar is anorthoclase ($Na_2O > K_2O$) or microcline (negligible Na_2O). The alkali feldspars with significant Na_2O contents in Deer *et al.* (1992, p. 414-415, compare also table 12.4 above) have average $Na_2O + K_2O$ contents of 13.8%. The Tvora syenites have an average SiO_2 content of 61.4% and average $Na_2O + K_2O = 11.01\%$. Therefore crystallization of perthitic K-feldspar (the most likely phase, Fig. 12.26) from a magma with composition similar to the Tvora syenites could result in SiO_2 depletion to produce an under-saturated magma but would also result in alkali-depletion. Therefore K-feldspar crystallisation alone is unlikely to generate magma similar to that from which the Straumsvola Alkaline Complex crystallised.

Derivation of rocks of compositions typical of the Tvora Syenites from magma similar that from which the Straumsvola Syenite crystallised would require extensive assimilation of siliceous country rock. The latter possibility could be tested by conducting stable (O) or radiogenic isotope studies.

THE DYKE SUITE

Petrography

Dykes intruded into the Straumsvola and Tvora Alkaline Complexes have a wide range of mineralogy and texture summarised in Table 12.7. Trachytic textures with strongly aligned platy minerals (generally feldspar) are common. Some samples consist of an extremely fine-grained groundmass in which sit euhedral feldspar phenocrysts. Sample TV20 is typically lamprophytic, containing phenocrysts of biotite and clinopyroxene in a fine-grained groundmass. Feldspar dominates most samples and is commonly perthite. Samples SV25 and ST3 both contain catapleite, a variety of eudialyte. Similar samples from Straumsvola were described by Harris and Rickard (1987).

Chemistry

Six samples were analyzed for the major elements and a variety of trace elements. The data for sample ST38, which is similar to SV25 and ST3, are from Harris and Rickard (1987). With exception of TV20 and ST3 most dykes have intermediate contents of SiO_2 and high concentrations of Al_2O_3, Na_2O and K_2O. Sample TV20 has ~ 47% SiO_2 which is accompanied by ~10% ΣFeO and CaO (respectively and ~5% MgO. The siliceous dyke ST38 with 71% SiO_2 has correspondingly lower contents of the major oxides (except Na_2O) compared to the other dykes. The dykes are mostly characterised by high Th, Zr, Nb, La and low Sc, V, Cu and Ni. Sample TV20 also contains high Sr and Ba.

Dykes	felds	Ne	Bt	amph	Cpx	opaq	Qtz	Edl	comments
TV2	75			25					t,mg
TV12	2,p								fg,i,t,gm
TV24	10,e				4,e				fg,i,gm,t
SV32	75		25						mg,t,
ST1	5,e								fg,t,i,gm
ST9	98				1	1			mg,t
TV21	5,p								fg,t
SV6	70		30						mg,t
SV31	75				25				mg
TV3	70				15	15			mg
TV18	90			10po					mg
TV20	60		20,p,r		20,p,e				mg
ST5	60	10	10 po	20					mg
SV30	70		5	10	15				mg,
ST2	90			5	5				mg
ST4	75			15,p,e			10		fg,i
SV25	70				15po,e			3	fg,i
ST3	70,p			13			10	2	fg, sugary
SV38	75			15,p,e			10		fg,i
TV10	5,p								fg,gm

Table 12.7. Estimated modal mineralogy (vol%) of the dykes associated with the Straumsvola and Tvora Alkaline Complexes. p = porphyritic, po = poikilitic, mg = medium-grained, fg = fine-grained, t = trachytic, i = inequigranular, gm = dominantly fine-grained groundmass, e = euhedral, felds = feldspar, amph = amphibole, Edl = eudialite, opaq = opaque minerals.

	SiO_2	Al_2O_3	Fe_2O_3	FeO	MnO	MgO	CaO	Na_2O	K_2O	TiO_2	P_2O_5	TOTAL
ST5	55.75	22.62	1.54	1.99	0.15	0.76	0.80	8.94	6.40	0.57	0.16	99.68
TV2	61.72	17.49	3.91	3.84	0.17	0.08	2.26	5.52	5.06	0.41	0.02	100.50
TV12	57.02	21.2	2.60	1.72	0.29	0.14	1.46	8.99	5.87	0.35	0.07	99.62
TV18	65.17	18.45	2.07	1.84	0.09	0.03	0.97	6.55	4.76	0.17	0.04	100.14
TV20	47.21	16.14	4.34	5.31	0.29	4.79	9.81	4.11	5.13	1.3	1.05	99.48
TV24	56.18	21.25	2.55	1.44	0.26	0.18	1.15	9.24	6.40	0.37	0.04	99.06
ST38	71.51	12.22	5.13*		0.06	0.00	0.46	6.00	4.44	0.20	0.00	100.02

	Rb	Sr	Th	Zr	Y	Nb	Ba	Sc	Cr	La	V	Cu	Ni	Zn
ST5	213	86	0.8	101	12	42	124	nd	1.1	33	nd	1.3	nd	76
TV2	148	17	25	3809	92	180	69	nd	20	239	nd	12	8	104
TV12	273	823	81	1222	39	440	34	nd	79	187	nd	6	nd	187
TV18	183	63	40	1010	63	102	237	nd	59	235	nd	nd	6	51
TV20	135	2178	11	326	29	100	3434	7	40	146	182	47	37	112
TV24	309	229	63	1003	29	349	99	nd	77	177	nd	nd	nd	163
ST38	144	23	ND	1305	29	108	ND	ND	ND	38	ND	ND	ND	ND

Table 12.8. Major and trace element chemistry (concentrations in wt% and ppm respectively) of the dykes analyzed. nd = not detected. ND = not determined. The data for sample ST38 are from Harris and Rickard (1987). * = all Fe as Fe_2O_3.

Discussion of Dyke chemistry

The high contents of Th, Zr, Nb and La suggest that the dykes represent late stage residual liquids in which the incompatible or high field strength elements were concentrated. To generate intermediate to high SiO_2 contents by fractionating compositions similar to the Straumsvola Alkaline Complex requires high temperatures permitting the composition of the magma to cross the thermal divide between the undersaturated and granitic systems. Similarly, fractionation of K-feldspar from a magma similar to the syenites from Tvora would generate, undersaturated low-alkali residues (see above). A possible mechanism to generate the siliceous dykes is assimilation of silica-rich country rock by incompatible element enriched residual magmas.

Conclusions

The Tvora Syenite Complex shows significantly different chemistry compared to the Straumsvola Complex. The nature of the alteration and deformation in the Tvora Complex as well as the chemical differences suggest that the Tvora Complex is unrelated to the Straumsvola Complex and that the former may well be older.

CHAPTER 13
THE NATURE AND HISTORY OF DEFORMATION

INTRODUCTION

Five episodes of deformation have been recognised. Not all episodes of deformation are recognisable at every nunatak. The identification of the various phases of deformation has been greatly assisted by the presence of numerous generations of intrusions of different ages. The degree and nature of deformation also varies greatly throughout the study area with the most intense deformation being recorded in the east.

DEFORMATION HISTORY

The First Deformation - D_1

The most obvious expressions of this deformation are mesoscale tight and isoclinal folds (limbs generally 1-2m long) defined by compositional layering in the Jutulrora and Fuglefjellet Formations, by quartzofeldspathic veins (Fig. 13.1) and by deformed amphibolite sheets (Fig. 13.2, Fig. 13.5). Examples of larger scale F_1 folds are rare with only one such fold being recognised (Map 4, north of sample locality FG11 at Fuglefjellet). This fold is defined by a layer of carbonate contained between two layers of quartzofeldspathic gneiss similar in composition to the Grey Gneiss. Generally, the compositional layering is interpreted to represent a primary feature because numerous structures (eg. xenolithic fragments, porphyroclasts in granitic rocks, discordant intrusions, deformed conglomerates) in the various rock types suggest that, although the rocks are highly deformed, the imposed strains have not been sufficiently high to totally destroy primary structures. This statement is considered to be particularly true in the western portion of the study area.

The F_1 folds develop prominent axial planar foliations which are commonly parallel to the lithological layering suggesting that the first fold episode involved isoclinal recumbent folding. The F_1 folds defined by the mafic sheets commonly show sharp angular contacts (Fig. 13.2) with axial planar foliations. The vergence of F_1 folds is commonly toward the west and northwest.

The timing of D_1 is difficult to constrain but obviously is limited by the age of the rocks involved. Isotopic work by Moyes and Barton (1990) has shown that the age of the Grey Gneiss Complex of the Jutulrora Formation is approximately 1000Ma and therefore D_1 must postdate this age.

The Second Deformation - D_2

The second deformation generated open to tight folds as well as thrust faults, the latter being recognised at Fuglefjellet and at Kvitkjolen, southeast of the study area.

Figure 13.1. F_1 fold defined by quartzofeldspathic vein in Grey Gneiss at Jutulrora.

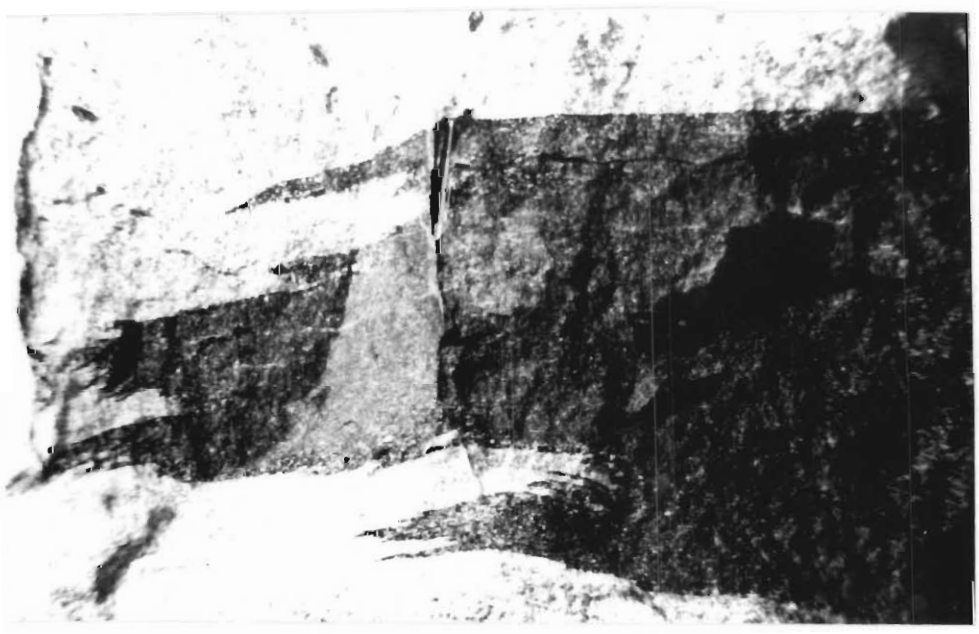

Figure 13.2. F_1 fold defined by A1 amphibolitic sheet in Grey Gneiss at Jutulrora. Pen for scale at top middle.

The mesoscale F_2 folds are commonly recognised by folding of the S_1 foliation about the D_2 folds.

The intensity of D_2 appears to increase toward the east. At Salknappen, zones of refoliation indicate that locally the S_1 planar foliation and primary layering is completely obliterated and is replaced by a similarly oriented S_2 foliation (Grantham *et al.*, 1987).

Ramsay type 3 (Ramsay, 1967;pp. 530-534) interference fold patterns indicate that D_1 and D_2 were almost co-axial. Examples of these interference patterns from various localities are shown in figures 13.3 and 13.4.

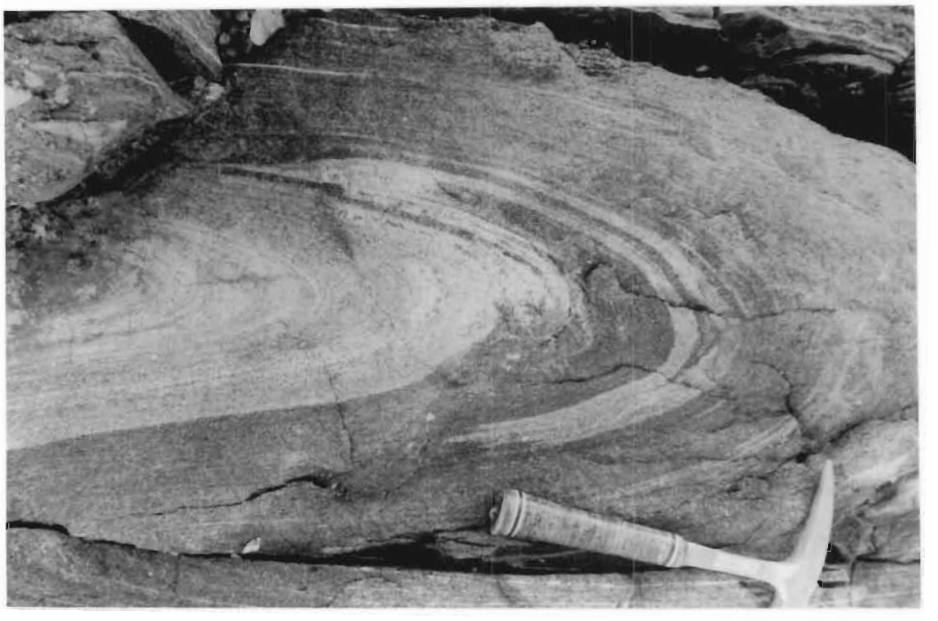

Figure 13.3. Type 3 fold interference patterns (Ramsay, 1967) between F_1 and F_2 in Banded Gneisses at the southern end of Straumsvola.

At Fuglefjellet an angular discordance, interpreted as a low angle thrust fault, is poorly exposed, due to surficial rubble, at the northeastern end of the nunatak. Stereonet A, Map 4 (Fuglefjellet) shows that, structurally below the discordance, the layering and planar foliation in the carbonates and gneisses strike northwards and dips eastward at ~30-60°. In the vicinity of, and above the assumed thrust, the gneisses strike southeastwards and dip steeply to the northeast and southwest. The rocks in the vicinity of the discordance have a strong lineation that plunges toward the east-southeast at ~20°.

Another feature of D_2 is that epidote-bearing pegmatites are oriented axial planar to F_2 folds. This relationship, recognised at Roerkulten, is shown in stereonet D, Map 3. The stereonet shows a fold with northeasterly dipping axial planes and a fold axis plunging to the northeast. The pegmatitic lenses are oriented axial planar to the fold. F_2 folds commonly show a stretching lineation which is oriented parallel to the fold axis (stereonet I and M, map 2, Jutulrora and Brekkerista). This feature suggests that F_2 was characterised by high strains. The vergence of F_2 folds is commonly toward the west and northwest.

Figure 13.4. Type 3 fold interference pattern between F_1 and F_2, in Banded Gneisses, at a small nunatak east of Tvora.

The timing of D_2 is slightly better constrained by the age of the A2 amphibolite sheet at Roerkulten. The amphibolite is clearly discordant to the S_1 foliation and also shows a folded F_2 fabric defined by amphibole and biotite (stereonets E and F, map 3). Isotopic data from samples from the sheet yield an age of 796$\pm$ 100Ma. The data define an isochron but the limited spread of values within the data result in the large margin of error.

The Third Deformation - D_3

Whereas D_1 and D_2 involved the development of isoclinal folds and thrust faults with near horizontal attitudes, D_3 resulted in folds and thrust faults with steep axial planes and steep planes of dislocation respectively (see Figs. 10.4 and 10.5, pp. 164-165). The axial planes generally dip steeply to the northwest in contrast to the D_1 and D_2 axial planes which display variable orientations but generally dip to the east or southeast. The hinges of the D_3 folds typically plunge at shallow angles to the northeast and southwest. The nature of the F_1, F_2 and F_3 folds may be seen with reference to figure 13.5 taken at Jutulrora. In the photo all three phases of folding may be seen.

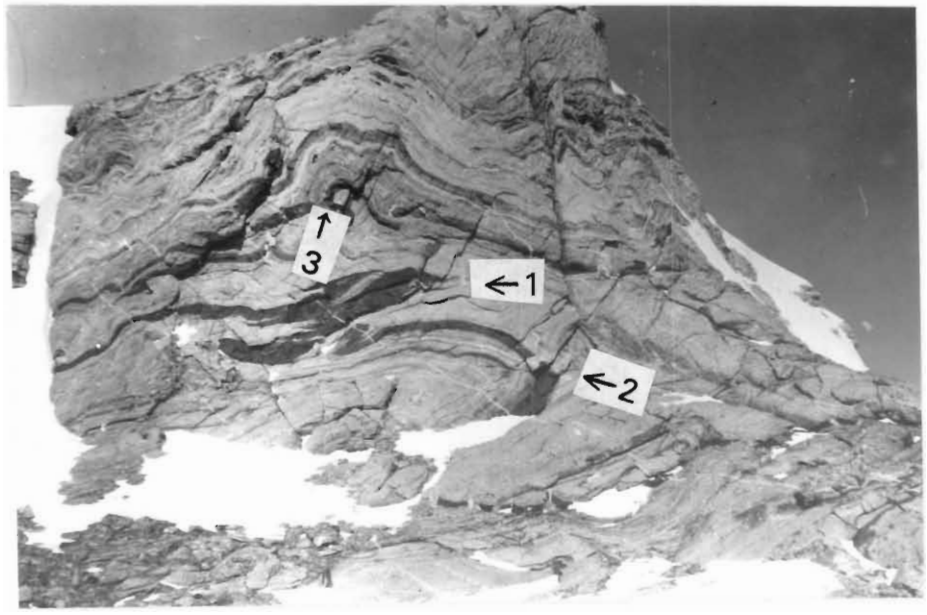

Figure 13.5. Three phases of folding at Jutulrora. The numbers refer to the generation of fold axes shown eg. $1 = F_1$. The F_1 and F_2 folds deform the same mafic sheet and have similar orientations, but may be distinguished by the sharp fold hinge zone displayed by the F_1 fold similar to figure 13.2 and a rounded hinge zone in the F_2 fold. The F_3 fold deforms the layering in the Grey Gneisses and also displays a rounded hinge zone but is characterized by a relatively steep axial plane dipping in the opposite direction to the axial plane of the F_1 and F_2 folds.

An axial planar cleavage defined by biotite is associated with the D_3 folding. This axial planar foliation is not developed in all rock types but is particularly prominent in biotite-rich rocks (Fig. 13.6). The thrust faults associated with D_3 are recognised at Salknappen where sheet-like intrusions of Dalmatian Granite occur. A sketch of the field relationships of this locality is shown

in figures 10.4 and 10.5, page 180. In this figure numerous small reverse faults can be seen disrupting the margins of the sheeted granite, yet the granites show no evidence of shearing. Such a relationship would suggest that the granites were emplaced syntectonically. It is also significant that the orientations of minor veins linking the sheeted granites commonly have an orientation which is parallel to or is nearly parallel to the orientations of the reverse faults.

Figure 13.6. F_3 fold with strong axial planar developed in Grey Gneisses at Jutulrora. Pen at centre for scale.

Stereonets B, map 3 (Roerkulten), J, map 2 (Brekkerista), and A, Map 7 (Tvora) are typical of D_3 folds in the field showing steeply inclined axial planes dipping toward the north-northwest and consequently verging toward the south-southwest. The fold axes of these folds are virtually horizontal and are oriented toward the east or, at Tvora, northeast. Stereonet C, map 2, Jutulrora shows F_1 axial planes with the same orientation as the gneissic layering. The layering is deformed about horizontal folds with axes oriented toward the east. The folding is therefore either F_2 or F_3 in age. The latter is preferred because there is no lineation developed parallel to the fold axis.

Ramsay type 1 and 2 interference patterns (Ramsay, 1967; pp. 521-530) are developed where D_1 and D_3 intersect (Fig. 13.7 and Fig. 13.8). The timing of D_3 is fairly well constrained by the syn-tectonic emplacement of the Dalmatian Granite as well as the biotite which is commonly developed axial planar to F_3 folds. K/Ar determinations on biotite yield ages of the order of 500 Ma (Ravich and Solo'vev, 1966, p. 220). Rb/Sr analyses of whole rock and mineral separates from the Dalmatian Granite yield an age of 469 Ma $\pm$5Ma (Grantham *et al.*, 1991).

The fourth episode of deformation - D_4

No mesoscale structures related to D_4 have clearly been identified. The nature of D_4 is inferred from a study of the orientations of the layering in the study area which is summarised below and shown on map 1. In the western part of the study area, the layering in the rocks at Jutulrora dips generally to the south, southwest and west. At Brekkerista, Joungane, Tvora and Straumsvola the layering dips generally toward the northwest, north and north east suggesting that between Jutulrora and the other nunataks an antiformal fold is developed, the axis of which strikes east-west. The gneisses underlying the western exposures at Roerkulten (map 3) strike west- northwest and dip generally toward the north-northeast. Progressing west to east, the strike swings around to the northeast and the gneissic layering dips toward the north-northwest.

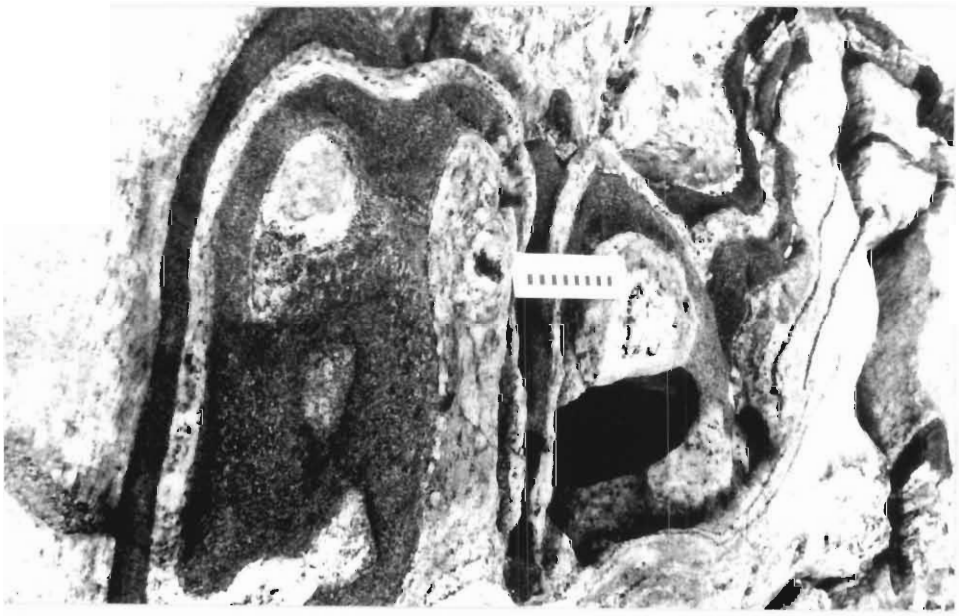

Figure 13.7. Type 1 fold interference pattern in Banded Gneisses at a small nunatak east of Tvora.

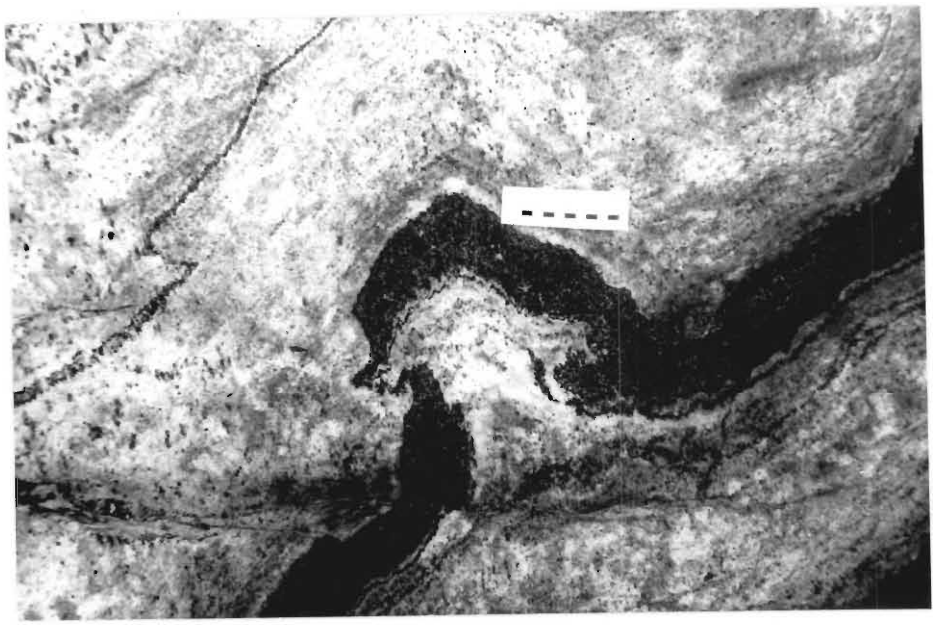

Figure 13.8. Type 2 fold interference pattern in Banded Gneisses at a small nunatak east of Tvora.

This change in strike and dip direction defines a northerly plunging synformal structure which may represent open folding associated with D_4. The nature of D_4 therefore appears to involve macroscale warping about northerly and easterly oriented axes suggesting relatively weak dome and basin folding.

The 5th episode of deformation - D_5

This deformation is represented by normal faulting and jointing. The strikes of the faults are shown in figure 13.9. The faults are steeply to vertically inclined. Most of the recognised faults are seen at Jutulrora. The occurrence of the faults decreases to the east possibly suggesting a relationship with the major tectonic structure interpreted by various workers (Ravich and Solo'vev, 1966; Grantham and Hunter, 1991) to underlie the Jutulstraumen Glacier. In the field the fault zones and joints are commonly marked by zones of pink alteration characterised in thin section by the chloritization of biotite and amphibole, the epidotization of plagioclase, and sericitization of microcline.

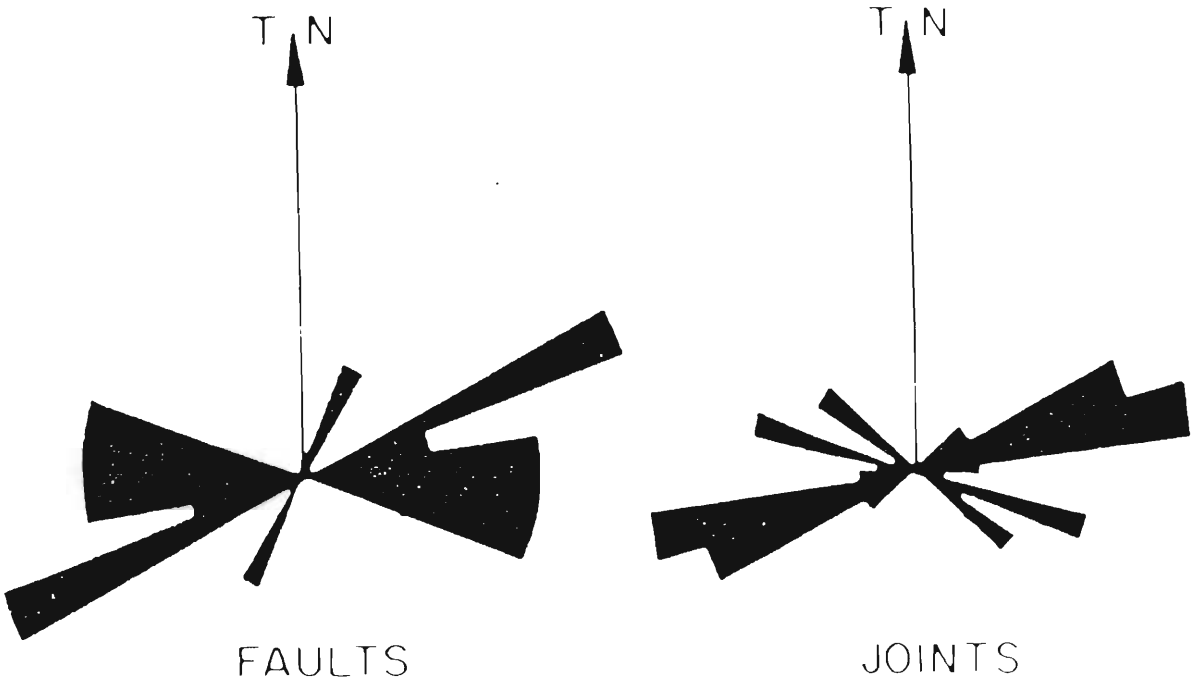

Figure 13.9. Rose diagram of the strikes of normal faults and joints recognised in the study area from Grantham and Hunter, (1991).

Joints measured throughout the study area show a similar trend to the faults (Fig. 13.9). The joints have steep to vertical dips. The orientations of joints measured by Hjelle (1972) throughout the Sverdrupfjella have an identical pattern to those of Grantham and Hunter (1991). The orientation of the joints and faults is parallel to the orientation of the spreading centre proposed for the second stage of the breakup of Gondwana proposed by Cox (1992) (see Fig. 11.7, p. 192).

An indication of the timing of D_5 is provided by the age of the Alkaline Complex at Tvora. The strong cleavage developed at Tvora indicates that D_6 post-dated the Tvora Alkaline Complex. Although it is uncertain whether the Tvora and Straumsvola Complexes are of similar age, the Straumsvola Alkaline Complex has yielded ages of ~170-180Ma (170 ± 4Ma,Rb/Sr, pers comm, A.R. Allen and ~182 Ar/Ar, pers comm I. Evans; 170-200, K/Ar, Ravich and Solo'vev, 1966). No age data for the Tvora Complex are available.

Discussion and Conclusions

Some structures seen in the field cannot easily be placed within the structural history described here. Examples are the mesoscale shear zones with displacements of a few centimetres which have been recorded in the Brekkerista, Jutulrora and Roerkulten Granites (stereonets A, map 3 and L, map 2). These shear zones commonly have sinistral and dextral

senses of movement. Those in the Roerkulten Granite define a pattern with sinistral and dextral shear zones plotting in different sectors of the stereonet and constrained by great circles, the intersection of which defines the σ_2 stress axis (Davidson and Park, 1978). This distribution suggests a southwesterly oriented, steeply plunging σ_2 axis and σ_1 plunging shallowly toward the northeast. No such pattern is shown by the shear zones in the Brekkerista Granite (stereonet L, map 2 Brekkerista). A possible reason for this is that the foliations in the Brekkerista Granite dip steeply to the north and south (stereonet K, map 2). If the folding which caused this variation in foliation orientation post-dated the shear zones then any pattern in the granite would similarly be disturbed.

Of the five periods of deformation that have been recognised, the first two involve high strains resulting in recumbent folding and, during D_2, thrust faulting from the southeast toward the northwest. D_3 and D_4 gave rise to more open folding with D_3 folds generally having horizontal fold axes and verging toward the southeast. D_4 appears to have resulted from gently dome and basin warping with northerly and easterly oriented axes. D_6 may be related to the tensional environment resulting from the breakup of Gondwana. The faulting may be related to the second stage of Gondwana breakup proposed by Cox (1992).

CHAPTER 14
THERMOBAROMETRY AND PRESSURE TEMPERATURE EVOLUTION OF THE STUDY AREA

INTRODUCTION

The purpose of this chapter is (a) to determine the metamorphic history of the study area, (b) to discuss results of thermobarometry of some of the assemblages described in the metamorphic history, (c) to identify variations in metamorphic assemblages in the area, particularly those which have not been considered in terms of the history or thermobarometry and (d) to construct a pressure-temperature-time loop for the area.

Four episodes of metamorphism have been distinguished, all of which appear to have involved medium grade metamorphism except for relict M_1 granulite grade assemblages partially preserved in mafic boudins in the Sveabreen Formation. The separation of the M_2 and M_3 events is based on the recognition of several generations of mafic intrusions. The grade attained during both M_2 and M_3 is identical. It follows that all the intrusions could also have been metamorphosed after a period of multiple intrusion, in which case the separate identity of the M_2 and M_3 events would not be valid. Hjelle (1972) studied a wider area than that of the present study and suggested that the metamorphic grade in the Sverdrupfjella increased to the south and east. This conclusion is based on the ubiquitous occurrence of garnet in almost all lithologies to the south and east whereas within the study area garnet is restricted to rare semi-pelitic rocks and garnet-amphibolites. Granulite grade assemblages are recognised to the east (Grantham *et al.*, 1988, Groenewald and Hunter, 1991).

METAMORPHIC HISTORY

The first metamorphic episode - M_1

The nature of the first episode of metamorphism is provided by the texture of garnets in the Banded Gneisses of the Jutulrora Formation, and the presence of anatectic veins axial planar to F_1 folds.

The garnets are porphyroblastic and contain inclusions of quartz, feldspar, biotite and rutile. The garnets display a pre-tectonic texture with the planar fabric being distorted about the garnets (Fig. 14.1). The inclusions are randomly distributed in the garnet and do not show any preferred orientation or distribution. The garnets therefore appear to have grown prior to significant deformation, hence M_1 is assumed to have preceded the first phase of deformation D_1. This conclusion is supported by the definition of F_1 folds by anatectic veins. The generation of the veins prior to F_1 similarly requires an increasing grade of metamorphism prior to deformation.

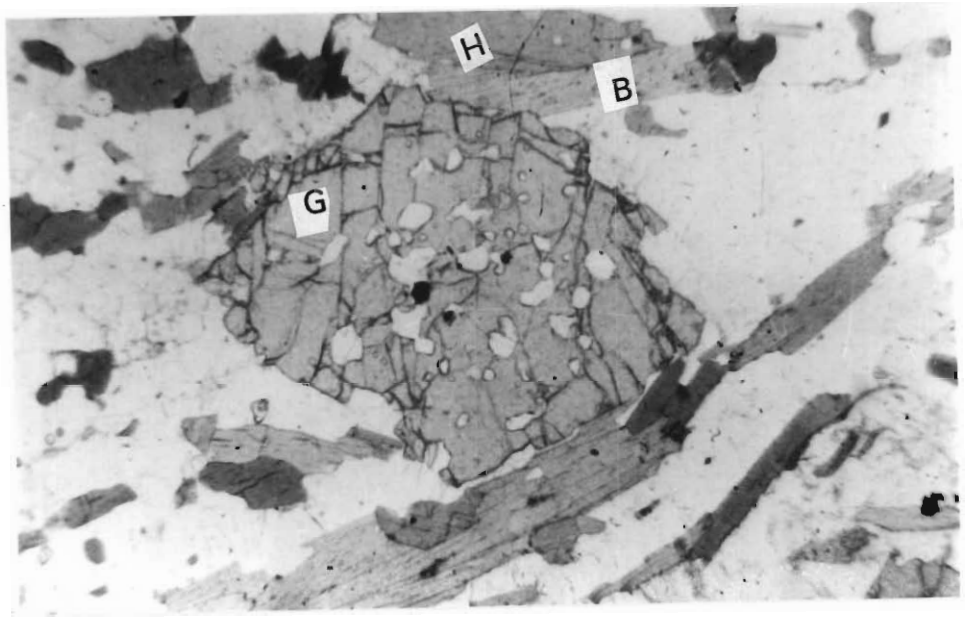

Figure 14.1. Pre-tectonic garnet in semi-pelite from Jutulrora. Field of view is 5mm across. G = garnet, B = biotite, H = hornblende whereas the clear areas are quartz and feldspar.

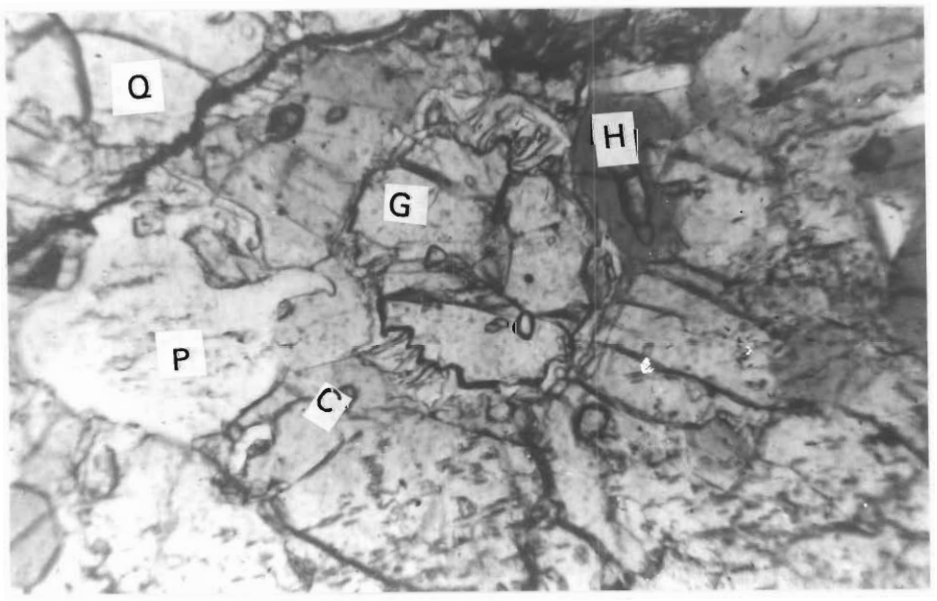

Figure 14.2 Hornblende plagioclase corona developed between garnet and clinopyroxene in sample SLK50 from Salknappen. Field of view is 1.5mm across. G = garnet, C = clinopyroxene, H = hornblende, P = plagioclase and Q = quartz.

Relict granulite grade assemblages preserved in mafic boudins in the Sveabreen Formation at Salknappen are also considered to represent M_1 assemblages because they do not contain a planar fabric. These assemblages consist of garnet, clinopyroxene, quartz, plagioclase and hornblende. The garnet commonly occurs as inclusions in clinopyroxene, however the two minerals are never in contact and are separated by corona structures consisting of symplectitic intergrowths of anorthitic plagioclase and hornblende (Fig. 14.2).

Assemblages in the Grey Gneiss Complex and Banded Gneiss Complex which define S_1 fabrics may reflect M_1 assemblages but it was noted above that S_1 and S_2 are difficult to distinguish from one another. Thus it is not possible to relate these assemblages to either M_1 or M_2.

The Second Metamorphism -M_2

Evidence for this metamorphic episode is derived from rocks in which new minerals were produced during D_2 or those mineral assemblages in intrusions recognisably discordant to S_1. An example of such an intrusion is a garnet amphibolite at the southern end of Straumsvola which is clearly discordant to the layering and foliation in the Banded Gneiss Complex. As in M_1, the M_2 conditions appear to have approached levels of anatexis indicated by the epidote-bearing lenticular pegmatites, commonly developed in the Grey Gneiss Complex, and oriented axial planar to F_2 folds.

The Third Metamorphism - M_3

The third episode of metamorphism is recognised largely by planar fabrics commonly defined by biotite, developed axial planar to D_3 folds. M_3 assemblages also include amphibolitised mafic intrusions which locally show no planar fabric (A3 amphibolites, chapter 9).

The Fourth Metamorphism - M_4

This episode of mineral development is characterised by the local development of chlorite and/or saussurite commonly replacing biotite/hornblende and plagioclase respectively. This alteration is commonly developed along cracks and involves retrogression

THERMOBAROMETRY BASED ON MINERAL CHEMISTRY

Introduction

This thermobarometric study must be viewed as a preliminary study because the amount of probe work completed was limited. Analyses of minerals used in the various thermobarometers are listed in appendix 2. Most geothermometers and geobarometers have been developed for granulite or high grade environments and thus few are applicable to amphibolite grade rocks. The experimental calibration of thermobarometers for amphibolite grade metamorphic rocks is

hampered by the relatively slow reaction rates under the applicable physical conditions. The slow reaction rates cause difficulties in demonstrating that the reactions (a) are reversible and (b) achieved equilibrium between the phases. Experimental calibrations are commonly conducted under physical conditions which are rarely realised in nature, thus introducing additional uncertainties. Highly variable lattice substitutions in most silicate minerals, particularly garnet, micas and the amphiboles create further unknowns because reliable thermodynamic solution models for these minerals are still being developed and refined. The mixing of solid solution components in pyroxenes, feldspars and garnet have been shown to be non-ideal. Under the relatively low temperatures normally ascribed to the amphibolite grade of metamorphism, the degree of deviation from ideality of these solutions increases. Thus thermobarometric calibrations utilising these minerals remain approximations. In addition to these sources of error, the inability of electron microprobes to distinguish between Fe^{2+} and Fe^{3+} requires assumptions to be made about the apportionment of ferrous and ferric oxides. This is a major problem, particularly in minerals which can accommodate significant quantities of Fe^{3+} eg. amphiboles, ferro-magnesian micas and sodic pyroxenes. Various attempts to overcome this by re-calculating mineral analyses using charge-balance techniques have met with only partial success. Uncertainties resulting from the possible presence of Fe in the Fe^{3+} state will obviously apply largely to exchange thermometers (see later) based on the exchange of Fe and Mg between various mineral species. They are also important where barometers are based on the substitution of Si by Al with which there is commonly a related substitution of Fe^{2+} by Fe^{3+} to maintain charge balances. Calibrated thermobarometers do have the advantage of being independent of fluid compositional influences.

Assemblages which lend themselves to the application of thermometers are garnet-biotite (Ferry and Spear, 1978; Perchuk and Lavrent'eva, 1983), garnet-clinopyroxene (Ellis and Green, 1979; Pattison and Newton, 1989; Krogh, 1988; Sengupta *et al.*, 1989) and garnet-hornblende (Graham and Powell, 1984). Assemblages for which barometers are available include clinopyroxene- plagioclase-quartz (Newton, 1986), garnet-rutile-plagioclase-ilmenite- quartz (Bohlen and Liotta, 1986), garnet-plagioclase -clinopyroxene-quartz (Moecher *et al.*, 1988) and garnet-hornblende-plagioclase-quartz (Kohn and Spear, 1989).

In the following table (table 14.1) a summary of the mineralogy of the thin sections studied is given with the interpreted metamorphic development of the various minerals. Full descriptions of the thin sections used for microprobe analysis are given in appendix 2.

Sample SLK50 (from a mafic boudin in the Sveabreen Formation) contains garnet + plagioclase + clinopyroxene + hornblende + quartz. The garnet and clinopyroxene are never in contact, being separated by symplectitic intergrowths of plagioclase + amphibole. Clinopyroxene, plagioclase, quartz and hornblende show a granoblastic texture. Clinopyroxene is commonly altered to hornblende. Hornblende/garnet grain boundaries appear to be stable

defining granoblastic textures. The formation of hornblende + plagioclase + quartz symplectites between garnet and clinopyroxene is clearly a later reaction and therefore the assemblage Grt + Cpx + Pl + Qtz + Hbl appears to have defined a partially hydrated M_1 assemblage whereas Cpx + Grt subsequently became unstable, possibly during M_2/D_2.

Samples JE39 and SK1 (from Banded Gneisses of the Jutulrora Formation) are characterised by porphyroblastic garnets which contain inclusions of quartz, feldspar, biotite and, in JE39, rutile and hornblende. The garnets display a pre-tectonic texture with the planar fabric being distorted about the garnets (Fig. 14.1). The inclusions are randomly distributed in the garnet and do not show any preferred orientation or distribution. The quartz, feldspar, hornblende, and biotite define a planar fabric which may be D_1 or D_2 in origin. Biotite partially replaces hornblende locally and is developed marginal to garnet. Therefore some of the biotite is considered to have formed later possibly during D_3.

Samples BK8 and SV9 (from Banded Gneisses of the Jutulrora Formation) are similar and show a weak planar fabric defined by plagioclase, clinopyroxene, hornblende and quartz. The grain boundaries are typically granoblastic. Hornblende partially replaces clinopyroxene and is itself locally partially replaced by biotite. The assemblage of Pl + Cpx + Hbl + Qtz is interpreted as being either M_1 or M_2.

SAMPLE NO.	MINERAL ASSEMBLAGE GENERAL	MINERALS DEVELOPED DURING VARIOUS PHASES M_1	M_2	M_3
SLK50	Grt Hbl Pl Qtz Cpx	Grt Cpx Pl Qtz $\pm$ Hbl	Hbl Pl Qtz	
JE39	Grt Hbl Pl Qtz Bt Kfs Ilm	Grt Hbl Pl Qtz Bt Kfs Ilm		Bt
BK8	Cpx Hbl Pl Qtz	Cpx Hbl Pl Qtz		Bt
S2	Grt Hbl Pl Ilm Qtz		Grt Hbl Pl Ilm Qtz	
SV9	Cpx Hbl Pl Qtz	Cpx Hbl Pl Qtz		Bt
SK1	Grt Bt Qtz Pl Ilm	Grt Pl Qtz Kfs Ilm		Bt
SA10	Grt Hbl Bt Qtz Pl Cpx	Grt Hbl Bt Qtz Pl Cpx	Grt Hbl Bt Qtz Pl Cpx	Bt
SA13	Grt Hbl Bt Qtz Pl Ilm	Grt Hbl Bt Qtz Pl Ilm		Bt

Table 14.1. Table of mineralogy of the various samples analyzed by electron microprobe as well as the interpreted assemblages related to the various metamorphic episodes.

Samples S2 (from an A2 amphibolite) and SA13 (from a mafic boudin in the Sveabreen Formation) are characterised by hornblende, plagioclase, poikiloblastic garnet and accessory quartz and ilmenite. They both display a granoblastic texture. The development of biotite in sample SA13 is restricted to microfractures cross cutting earlier formed minerals.

Sample SA10 (from a porphyroclastic granite in the Sveabreen Formation) has a granoblastic texture and a strong planar fabric defined by quartz ribbons. Hornblende partially replaces clinopyroxene and is itself replaced by biotite. Garnet is poikiloblastic and contains inclusions of quartz. Plagioclase is antiperthitic with K-feldspar exsolution lamellae forming up to ~30vol%.

These lamellae form a trellised exsolution pattern.

Thermometry

Introduction

Most thermometers are based on the diffusion and exchange of Fe^{2+} and Mg between coexisting ferromagnesian silicates. A problem of thermometers is that diffusion of ions does not cease after maximum temperatures have been reached and thus the temperatures recorded commonly reflect the conditions at which diffusion ceased. These conditions will vary for different minerals and also for different rates of cooling. The foregoing discussion indicated that the rocks of the Sverdrupfjella remained under amphibolite grade conditions for relatively long periods. Thus it may be expected that temperatures suggested for M_1 may be similar to those for M_3 and reflect the blocking temperatures at the end of M_3. Because volume changes during ionic exchange are negligible, most thermometers are largely unaffected by changes in pressure. Therefore, the geothermometry methods will be applied first. The temperatures thus calculated will then be used in the various barometers.

Garnet-biotite thermometer

The garnet-biotite thermometer is based on the exchange of Fe and Mg between garnet and biotite. Numerous calibrations of this thermometer have been attempted (Perchuk and Lavrent'eva, 1983; Ferry and Spear, 1978; Indares and Martignole, 1985; Ganguly and Saxena, 1984; Goldman and Albee, 1977; Thompson, 1976).

A survey of these various calibrations by Chipera and Perkins (1988) suggested that the most reliable were those relying solely on a partitioning of Fe and Mg between garnet and biotite ($K = (X_{Mg}/X_{Fe})_{Grt}/(X_{Mg}/X_{Fe})_{Bt}$) namely the calibrations of Ferry and Spear (1978) and Perchuk and Lavrent'eva (1983). Chipera and Perkins (1988) concluded that the Ferry and Spear (1978) calibration resulted in temperature overestimates whereas the Perchuk and Lavrent'eva (1983) calibration yielded temperatures which were (a) comparable with other thermometers utilising different minerals and (b) consistent with field relationships.

Four samples containing garnet and biotite were selected for microprobe analysis (table 14.2). The temperatures calculated show values for biotite inclusions in garnet and biotite located at the margins of garnet grains. For samples JE39, SK1 and SA10, the rim temperatures are higher than the core or inclusion temperatures whereas for sample SLK1 the rim temperature derived is slightly lower than the core values. Generally the core and rim temperatures do not differ from each other by more than 10%. Most of the values calculated are $<600°C$. These values are at variance with the development of pre-F_1 anatectic veins and syn-F_2 pegmatitic

lenses. It is perhaps significant that of the values >600°C, most are from sample SA10, collected from the eastern part of the study area.

ASSUMED PRESSURE	JE39 INCLUSION	JE39 RIM	SK1 INCLUSION	SK1 RIM
2kb	600(548)	617(577)	541(452)	588(528)
3kb	594(552)	610(581)	535(456)	582(531)
4kb	588(556)	604(585)	529(459)	576(535)
5kb	582(560)	598(589)	523(462)	570(539)
6kb	576(564)	591(592)	518(462)	564(542)
7kb	569(567)	585(596)	512(469)	557(546)
8kb	563(571)	579(600)	506(472)	551(550)

ASSUMED PRESSURE	SLK1 INCLUSION	SLK1 RIM	SA10 INCLUSION	SA10 RIM
2kb	556(477)	549(464)	601(549)	634(604)
3kb	551(480)	543(468)	594(553)	626(608)
4kb	545(484)	537(471)	588(557)	619(612)
5kb	539(487)	531(475)	582(561)	613(616)
6kb	533(490)	525(478)	576(564)	606(620)
7kb	527(494)	520(481)	570(568)	600(624)
8kb	521(497)	514(485)	564(574)	594(628)
9kb	515(501)	508(488)	557(577)	587(632)
10kb	510(504)	502(491)	551(579)	581(636)

Table 14.2. Table showing temperatures calculated from biotite-garnet pairs. The values in parentheses are the result of the Ferry and Spear (1978) calibration whereas the values outside parentheses are calculated using the Perchuk and Lavrent'eva (1983) calibration. The samples in the top table are from the western part of the study area (shallower depths) whereas the values in the lower part are from the east and therefore possibly deeper areas.

Garnet-clinopyroxene thermometer.

Sample SLK50, collected from Salknappen from the eastern part of the study area, is the only one containing garnet + clinopyroxene. Application of garnet-clinopyroxene thermometers to an assemblage in which garnet and clinopyroxene are not in contact but are separated by symplectitic rims, assumes that the compositions of the garnet and clinopyroxene have remained unaltered during the change in P-T conditions resulting in the reactions producing the symplectitic rims. For this assumption, the compositions of the cores and rims of the garnet and clinopyroxene grains were used to calculate separate temperatures. The core compositions of garnet + clinopyroxene are interpreted as an M_1 assemblage whereas calculations utilising the grain rim compositions are interpreted as later re- equilibration values.

Numerous calibrations based on the assemblage garnet + clinopyroxene have been proposed (Raheim and Green, 1974a; Ellis and Green, 1979; Krogh, 1988; Pattison and Newton, 1989; Sengupta *et al.* 1989). The thermometer is based on the exchange of Fe and Mg between garnet and clinopyroxene. Ellis and Green (1979) recognised that the Fe-Mg exchange is also

influenced by the Ca content of garnet which may reach significant proportions.

SLK50 Grt-Cpx CORE-CORE COMPOSITIONS

ASSUMED P	KROGH	ELLIS & GREEN	PATTISON & NEWTON	SENGUPTA
6kb	712-718	746-753	600-659	586-589
7kb	714-721	748-755	606-665	589-592
8kb	717-724	750-758	611-670	592-595
9kb	720-727	753-761	616-767	595-598
10kb	723-730	756-763	622-681	598-601
11kb	726-732	758-766	627-687	601-604
12kb	728-735	761-769	633-692	604-607
13kb	732-738	764-772	639-698	607-610
14kb	734-741	767-774	644-704	610-613
15kb	737-744	769-777	650-709	613-616
16kb	740-747	772-780	655-715	616-619

SLK50 Grt-Cpx RIM-RIM COMPOSITIONS

ASSUMED P	KROGH	ELLIS & GREEN	PATTISON & NEWTON	SENGUPTA
6kb	682	718	554-607	624
7kb	684	720	559-612	627
8kb	687	722	564-618	630
9kb	690	725	570-623	633
10kb	693	728	575-629	636
11kb	695	730	581-634	640
12kb	698	733	586-640	644
13kb	701	736	592-646	646
14kb	704	739	598-651	649
15kb	707	741	603-657	652
16kb	709	744	609-662	655

Table 14.3. Table showing temperatures calculated using the various thermometers calibrated for garnet-clinopyroxene assemblages at pressures varying from 6 to 16kb. The table above represents core-core compositions whereas the table below represents rim-rim compositions.

Krogh (1988) combined and reinterpreted the experimental data of Ellis and Green (1979), Raheim and Green (1974a, 1974b), and Mori and Green (1978) to formulate his calibration. Krogh (1988) concluded that the Mg number of the garnet and Na^{cpx}_{M2} content have minor influences on the K_d which conflicts with the calibration of Pattison and Newton (1989).

The temperatures calculated from the garnet and clinopyroxene analyses using the calibrations of Ellis and Green (1979), Krogh (1988), Pattison and Newton (1989) and Sengupta *et al.* (1989) are presented in table 14.3. The temperature estimates lie between approximately 550-780°C with the Ellis and Green (1979) calibration yielding the highest temperatures whereas the Sengupta *et al.* (1989) calibration yields the lowest (Table 14.3). Pattison and Newton (1989) state that the calibration of Ellis and Green (1979) over-estimates temperatures by 100-150°C at 8kb, with the margin of error decreasing to 0 at 30kb. From table 14.3 it can be seen that the difference between these two calibrations is approximately 100°C.

The values calculated for the core compositions indicate temperatures approximately 30°C

higher than those of the rim, suggesting that either a degree of re-equilibration has occurred or that the garnets grew in a cooling environment.

Garnet-hornblende geothermometer

This thermometer is based on the exchange of Fe and Mg between garnet and hornblende. Graham and Powell (1984) developed an empirical geothermometer in which calibration was made against the garnet- clinopyroxene geothermometer of Ellis and Green (1979). Therefore, the accuracy of this thermometer should be viewed in the light of comments regarding the accuracy of Ellis and Green's estimates for garnet- clinopyroxene assemblages (see above). Ghent and Stout (1986) state that application of the garnet-hornblende geothermometer of Graham and Powell (1984) to their samples yielded higher temperatures than both the garnet-clinopyroxene calibration of Ellis and Green (1979) and, for rocks from the sillimanite zone, the garnet-biotite thermometer calibration of Ferry and Spear (1978). Ghent and Stout (1986) state that at lower grades (garnet zone), agreement between garnet-hornblende and garnet-biotite thermometers (calibration of Ferry and Spear, 1978) is much better. This statement must also be viewed in the light of the survey of Chipera and Perkins (1988) who concluded that the biotite-garnet thermometer of Ferry and Spear (1978) also tended to overestimate temperatures.

Graham and Powell (1984) assumed that all the Fe in hornblende was in the Fe^{2+} state. This assumption may be valid since Hsu (1968) has shown that the stability of almandine garnet is restricted to conditions below the QFM buffer. Thus hornblende in equilibrium with garnet is likely to contain negligible Fe^{3+}. To consider the possible influence of Fe^{3+}, temperatures were calculated using all the possible Fe^{3+} estimates provided by the calculation scheme RECAMP of Spear and Kimball (1984).

Graham and Powell (1984) provide compositional constraints on the amphiboles considered for their calibration and state that the Na content should not be <0.09, a condition met by the samples from the Sverdrupfjella. Graham and Powell (1984) ascribe relatively high Na contents to high pressures (10-30Kb).

Samples SA13, SLK50, S2 and JE39 contain both garnet and hornblende in contact with one another. The former two samples are from the eastern portion of the study area whereas the latter two samples are from the west. The temperatures calculated from this thermometer using analyses from four samples are shown in table 15.4.

Samples SA13 and SLK50 are from the eastern part of the study area and suggest that temperatures of at least $\sim 650°C$ prevailed during the M_2 metamorphism. In the western areas, samples JE39 and S2 provide estimates which range from 580-680°C.

	SA13	SLK50	S2	JE39
ALL $FE2^+$	655	627	682	583
SUM FM=13	617	578	630	488
SUM CA=15	650		679	

Table 14.4. Temperatures calculated from garnet-hornblende assemblages from samples SA13, SLK50, S2 and JE39. ALL FE2+ assumes that all Fe is Fe^{2+}. SUM FM = 13 recalculates Fe contents stoichiometrically assuming Si + Al + Ti + Fe^{3+} + Mg + Fe^{2+} + Mn = 13 and that Ca and Na are permitted in the M_4 site only and Na and K are in the A site. SUM CA = 15 assumes Si + Al + Ti + Fe^{3+} + Mg + Fe^{2+} + Mn + Ca = 15 with all Ca assigned to the M_4 site and all Na to the A site.

Conclusions

The temperatures suggested by garnet-biotite thermometry are at variance with the field relationships and therefore these values are considered to represent the temperatures at which Fe-Mg exchange ceased. In both the eastern and western areas, development of anatectic veins prior to F_1 and syn-F_2 and emplacement of the water-saturated Dalmatian Granite during D_3 suggest that temperatures exceeded 650°C. Consequently the higher temperatures given by the garnet-hornblende thermometer may be realistic estimates, but are probably best viewed as the temperatures at which the Fe and Mg diffusion ceased in these mineral pairs.

The temperatures suggested by garnet-clinopyroxene thermometry vary between 550-780°C. The lower values are inconsistent with evidence of anatexis. In the eastern part of the study area the temperatures during M_1/F_1, $M_2/F_2(D_2)$ and $M_3/F_3(D_3)$ were probably >650°C and in the west temperatures were probably ~650°C.

Barometers

Clinopyroxene-plagioclase-quartz barometers

These barometers are based on the increasing solution of the jadeite ($NaAlSiO_6$) and Ca-Tshermaks molecules ($CaAl_2SiO_6$, CATS) in clinopyroxene with increasing pressure. The CATS and jadeite contents of the clinopyroxenes in this study are low and may approximate ideal mixtures. Possible sources of error with these barometers are that superior quality analyses are required particularly with regard to clinopyroxene because the CATS and jadeite molecules are calculated on a charge balance basis and thus minor errors in the analysis of the major elements contained in clinopyroxene can result in significant variations in calculated pressures.

Four samples containing clinopyroxene + plagioclase + quartz from throughout the study area were analyzed namely SLK50, BK8, SV9 and SA10. Samples SLK50 and SA10 were collected from Salknappen in the east whereas samples BK8 and SV9 are from Brekkerista and Straumsvola in the west respectively. The computer program THERMO by Powell and Holland

(1988) was used to calculate the physical conditions of reaction for the following reactions (see Fig. 14.3 and 14.4):-

anorthite -> Ca-Tschermaks + quartz	I
albite + quartz -> jadeite	II
anorthite + jadeite -> Ca-Tschermacks + albite	III

The pyroxene end members were calculated after Cawthorn and Collerson (1974) and Fe^{3+} contents in the pyroxenes (see appendix 2) were calculated after Droop (1987). The activity (a) model for albite used is that of Newton (1986) whereas ideal mixing is assumed for the jadeite activity, particularly in view of the very low jadeite molecule contents in samples SLK50, BK8, SV9 and SA10 (see appendix 2). The activities for anorthite were calculated from Newton and Perkins (1982) and the mole fractions for CATS (see appendix 2) were used. Wood (1976) has shown that the solution of the Ca-Tshermaks component in clinopyroxene is essentially ideal such that the mole fraction $X_{CATS} = a_{CATS}$.

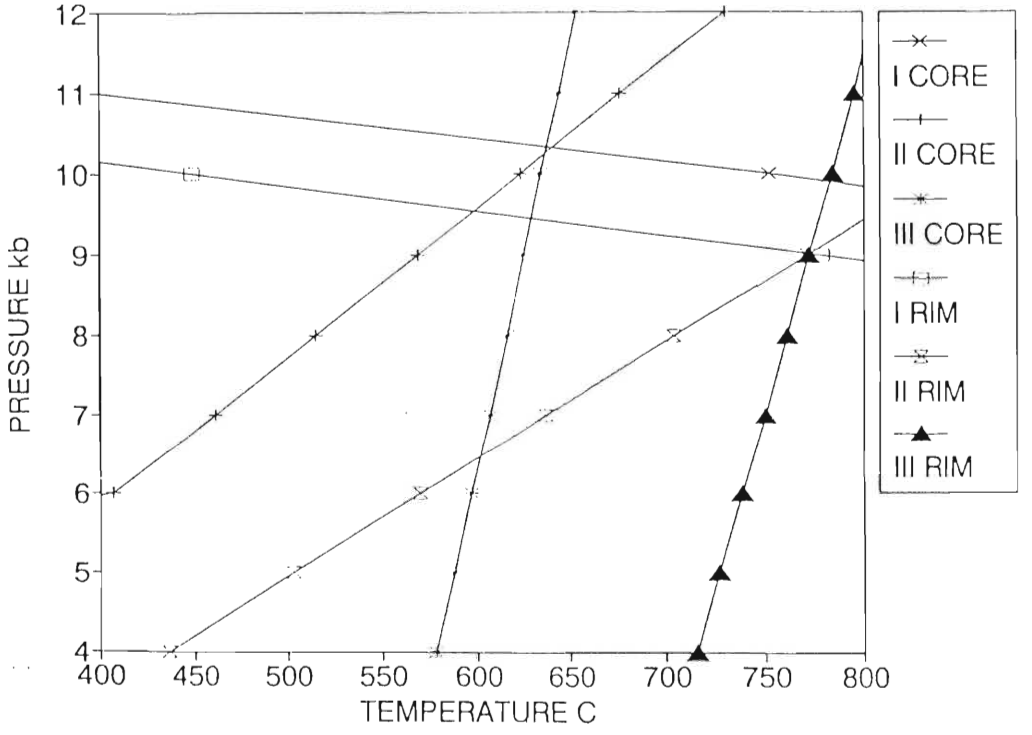

Figure 14.3 Reactions for sample SLK50 using average values for the core and rim compositions.

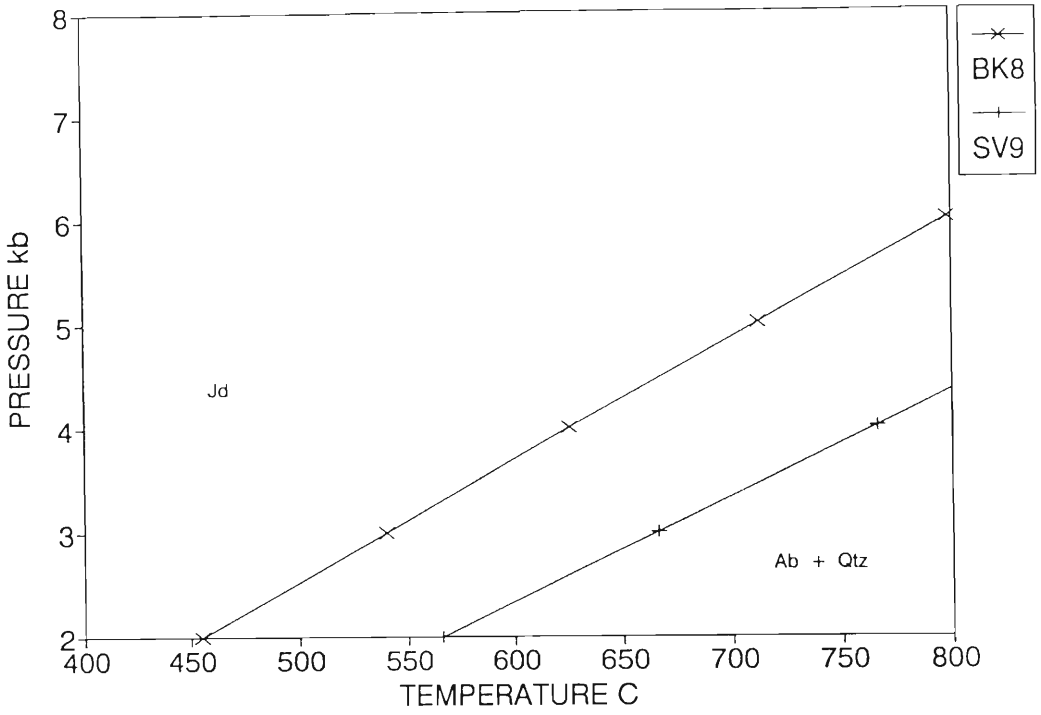

Figure 14.4. Calculated equilibria for the reaction albite + quartz -> jadeite for samples BK8 and SV9.

Figure 14.3 shows the reactions for sample SLK50 (from the east) using average values for the core and rim compositions. The reactions for the core compositions intersect at approximately 10.5kb and 640°C whereas those for the rim compositions intersect at approximately 9kb and 750°C.

Curves for reaction II were calculated for samples BK8 and SV9 (Fig. 14.4). These reactions suggest pressures of approximately 3-4.5kbs for the eastern part of the study area at temperatures of 650-700°C.

Discussion

Using the compositions of plagioclase and clinopyroxene from sample SA10 (from the east) did not yield realistic values for the reactions I,II or III which are at variance with sample SLK50 (also from the east). The discrepancy between samples SLK50 and SA10 may arise from the possibility that the porphyroclastic granitoid was emplaced subsequent to the higher pressure assemblages preserved in SLK50. The values suggested by the barometry on sample SLK50 are significantly lower than those indicated by the garnet-hornblende-plagioclase-quartz and garnet-clinopyroxene- plagioclase-quartz barometry (see below). Possible reasons for this are that either the barometer may have "closed" after the others or that the analyses of

clinopyroxene are not sufficiently accurate. The clinopyroxenes in SLK50 have fine exsolution lamellae which may contain exsolved Al_2O_3- rich phases.

The values calculated for sample BK8 nd SA10 are lower than those from other barometers applied (see GRIPS values for JE39 and S2). These low values could result from poor analyses of clinopyroxene. The low levels of CATS in these samples may similarly be related to the relatively sodic plagioclase in these rocks (see analyses in appendix 2.).

Garnet + Hornblende + Plagioclase + Quartz

Kohn and Spear (1989) have calibrated an empirical barometer utilising tshermakitic exchange in the assemblage garnet + hornblende + plagioclase + quartz. Four different models are presented by these authors and they recommend that an average of the four values from the different models be reported as well as the spread of the calculated pressures with the addition $\pm$0.5Kb as the precision. The results of the application of this barometer are shown in table 14.6. Also shown in table 14.6 are values derived for different values for the Fe^{3+} contents of the amphibole (estimated using RECAMP, Spear and Kimball, 1984). Kohn and Spear (1989) state that, in their calibration, Fe was calculated to a minimum value of Fe^{3+} consistent with amphibole stoichiometry (typically all Fe as Fe^{2+}).

The various models provided by the Kohn and Spear (1989) calibration show widely varying estimates for the different samples eg JE39 from the west shows pressures of 1.03 to 5.09kb with a mean of 3.15 kb at 700°C (all Fe as Fe2+, the recommended option)(table 14.6). Sample S2 from the west shows pressure estimates of 0.96 to 4.52kb with a mean of ~2.4kb at 700°C (all Fe as Fe^{2+}) (Table 14.6). Using the core compositions of minerals from sample SLK50 (from the east), pressures of between 5.46 and 11.9kb with a mean of ~9kb at 700°C are estimated (table 14.6). Using the rim compositions of minerals, pressures of 5.36 and 12.01kb with a mean of ~9kb at 700°C are estimated (Table 14.6). For sample SA13 from the east, pressures of 0.0 to 4.76 kb with a mean of 2.7kb at 700°C are estimated (Table 14.6).

Garnet + Rutile + Ilmenite + Plagioclase + Silica

Bohlen and Liotta (1986) have calibrated a barometer on the assemblage garnet + rutile + ilmenite + plagioclase + silica (GRIPS) resulting from the reaction:-

3plagioclase + 3quartz + 6ilmenite => grossular + 2almandine + 6rutile.

These authors state that this reaction has a relatively flat slope in P-T space and is therefore accurate with little temperature influence. The barometer is also largely governed by the

plagioclase and garnet compositions. The thermometer does require the recognition of rutile inclusions in the garnet.

SAMPLE NO.	TEMP °C	Mg MDL 1	Fe MDL 1	Mg MDL 2	Fe MDL 2	AVERAGE
JE39 (ALL FE2+)						
	400	5.89	3.51	4.07	0.31	3.90
	500	5.62	2.69	4.07	0.67	3.65
	600	5.36	1.86	4.07	1.04	3.4
	700	5.09	1.03	4.07	1.40	3.15
JE39 (FM=13)						
	400	7.37	5.46	5.30	0.65	5.21
	500	7.33	4.92	5.49	1.06	5.16
	600	7.28	4.38	5.68	1.47	5.1
	700	7.24	3.84	5.86	1.88	5.05
S2 (ALL FE2+)						
	400	5.68	2.34	4.41	-0.18	3.38
	500	5.29	1.41	4.32	0.19	3.05
	600	4.91	0.48	4.23	0.58	2.72
	700	4.52	0.44	4.14	0.96	2.39
S2 FM=13						
	400	6.41	3.29	5.54	0.50	4.15
	500	6.13	2.51	5.62	0.98	3.94
	600	5.85	1.72	5.69	1.46	3.72
	700	5.58	0.94	5.77	1.94	3.51
S2 CA=15						
	400	5.72	2.40	4.49	0.13	3.43
	500	5.35	1.48	4.41	0.26	3.11
	600	4.97	0.56	4.33	0.64	2.79
	700	4.59	-0.35	4.25	1.03	2.47
SLK50 CORE COMPOSITIONS ALL FE2+						
	500	10.75	8.81	10.94	4.28	8.65
	600	10.90	8.58	11.44	4.87	8.81
	700	11.06	8.34	11.93	5.46	8.98
	800	11.21	8.10	12.43	6.05	9.14
SLK50 RIM COMPOSITIONS ALL FE2+						
	500	10.81	8.71	11.04	4.16	8.62
	600	10.88	8.60	11.28	4.46	8.71
	700	11.11	8.25	12.01	5.36	8.96
	800	11.26	8.02	12.51	5.96	9.12
SA13 (ALL FE2+)						
	500	5.47	1.35	4.21	0.62	3.23
	600	5.11	0.48	4.11	1.13	2.96
	700	4.76	-0.39	4.01	1.64	2.69
SA13 FM=13						
	500	6.26	2.39	5.41	1.44	4.09
	600	6.00	1.65	5.46	2.05	3.93
	700	5.75	0.91	5.52	2.67	3.77
SA13 (CA=15)						
	500	5.35	1.45	4.34	0.72	3.3
	600	5.20	0.59	4.25	1.24	3.06
	700	4.85	-0.27	4.17	1.76	2.79

Table 14.6. Table showing the pressures calculated from the Kohn and Spear (1989) barometer for the different samples and stoichiometric calculations of Fe in hornblende after Spear and Kimball (1984).

If rutile is absent, the assumption that the activity of rutile = 1 provides a maximum possible pressure. Application of this barometer to garnet-amphibolites may also be bedeviled by the absence of quartz which renders the assumption of $a_{SiO2} = 1$ invalid. Analyzed samples which contain the necessary assemblages are JE39, S2 and SA13. The activity models used for garnet and plagioclase (temperature of 600°C assumed for calculation of activity) are those of Ganguly and Saxena (1984) and Newton and Perkins (1982) respectively. The ilmenite compositions were assumed to approach stoichiometry and therefore ideal-mixing is assumed for the ilmenite. Using the activities calculated, the reaction curves for samples S2, SA13 and JE29 are shown in figure 14.5.

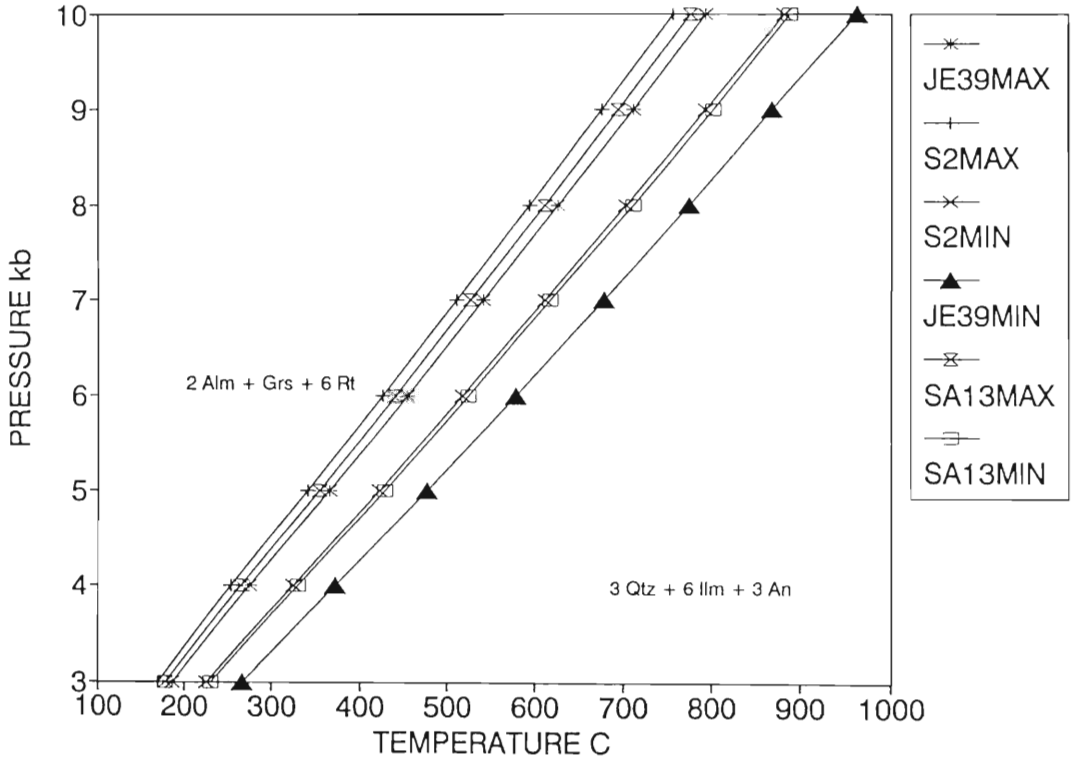

Figure 14.5. Maximum and minimum curves for the GRIPS assemblages for samples S2, JE39 and SA13.

The curves were calculated using the program of Powell and Holland (1988). For sample SA13 at temperatures of ~650°C (suggested by garnet-hornblende thermometry above) pressures of ~7.5-8.5kb are indicated (Fig. 14.5). For sample JE39, at temperatures of 550-600°C (suggested by garnet-biotite and garnet-hornblende thermometry) pressures of 5.8 to 7.2kb are indicated (Fig. 14.5). For sample S2 at temperatures of 600-700°C (suggested by garnet-hornblende thermometry) pressures of 6.8-9.0kb are indicated (Fig. 14.5). This value is

higher than the GRIPS value from sample JE39 (taken ~10km away at Jutulrora), the jadeite content values from samples BK8 (taken ~5km away) and SV9 (taken ~1km away) and the garnet- hornblende-plagioclase-quartz estimate from the same sample. A possible reason for difference from the GRIPS value for JE39, is that higher temperatures were applied derived from those calculated for S2 using the garnet-hornblende thermometer (Graham and Powell, 1984). If similar temperatures are assumed for JE39 then the pressures for JE39 are ~6-9kb and are therefore similar to S2.

Garnet + clinopyroxene + plagioclase + quartz

Only sample SLK50 has the necessary minerals for the application of this barometer. The barometer is based on the reaction:

clinopyroxene + plagioclase => garnet (grossular + almandine + pyrope) + quartz

Various authors have provided calibrations for this barometer (Moecher *et al.*, 1988; Newton and Perkins; 1982) dependant on activity models for clinopyroxene, plagioclase and garnet.

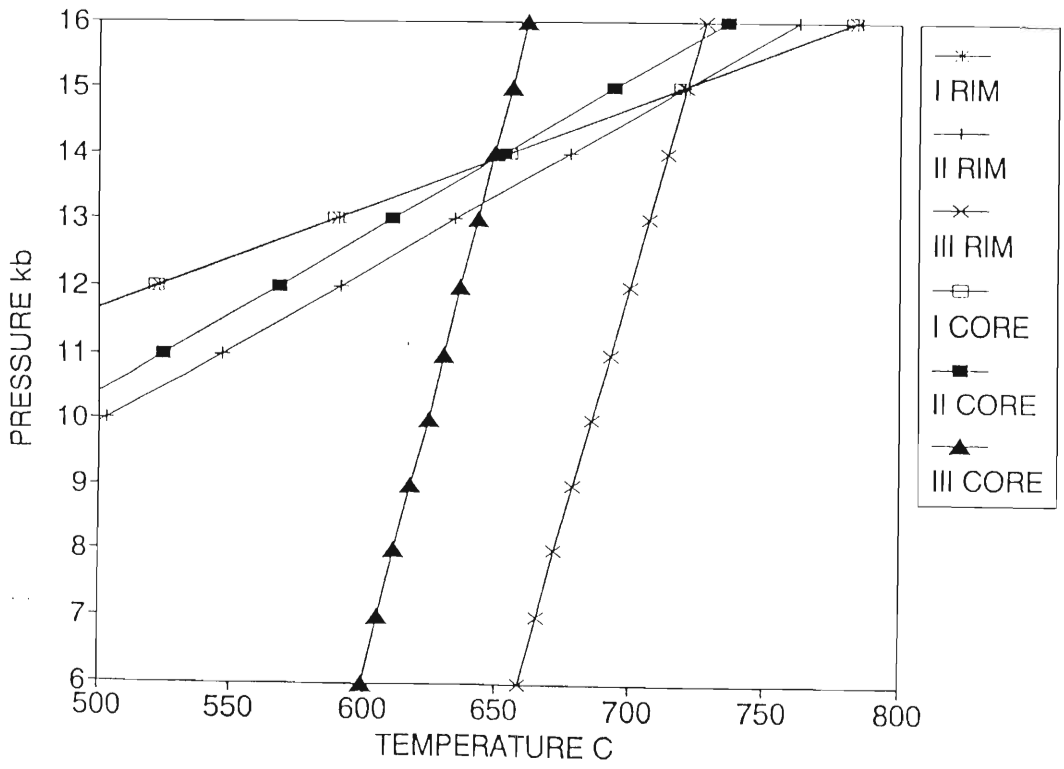

Figure 14.6. Maximum and minimum curves for the core and rim compositions for the garnet + clinopyroxene + quartz + plagioclase in sample SLK50.

The activity models used for these minerals are from Newton and Perkins (1982), Newton (1983) and Ganguly and Saxena (1984) respectively. These data were calculated and modelled using the computer program THERMO by Powell and Holland (1988). The reaction curves shown in figure 14.6 involve the following equilibria:-

$3Qtz + Alm + 2\,Grs = 3An + 3Hed$ I

$3Qtz + Py + 2Grs = 3An + 3Di$ II

$Alm + 3Di = Py + 3Hed$ III

The reaction curves I-III were calculated for the core and rim compositions of the garnet and clinopyroxene. At the temperatures indicated by the garnet-clinopyroxene and garnet-hornblende thermometers above and corroborated by the equilibria III above (core 600-750°C, rim 550-750°C) pressures of approximately 12 - 15kb are suggested (Fig. 14.6).

Conclusions

From the above estimates, pressures in the eastern part of the study area, deduced from anhydrous assemblages were high (10-16kb) (sample SLK50). Estimates of pressures of the order of 9kb are indicated by the garnet + hornblende + plagioclase + quartz equilibria (sample SLK50), the CATS and jadeite equilibria (sample SLK50), and the GRIPS equilibria (sample SLK13). Slightly lower values in the west are suggested (6-9kb) concomitant with lower temperatures.

Integration and discussion of the thermobarometry

The distribution of the samples lend themselves to division of the study area into two domains.

Thermobarometric data calculated above are plotted in figure 14.7 (eastern domain) and figure 14.8 (western domain). The data for the eastern part of the study area show that the rocks were characterised by an early M_1 anhydrous high pressure (10-16kb) assemblage of Grt + Cpx + Pl + Qtz which probably developed at temperatures between ~675-750°C (fig 14.7). These physical conditions encompass the intersections of curves 8, 11, 14, 15 and 16 (Table 14.7) and are based on the core compositions of minerals from sample SLK50.

The later (M_2)rim compositions of minerals and partially hydrated assemblages containing Cpx + Hbl + Grt + Pl + Qtz appear to indicate temperatures of ~600°C to 775°C and pressures of between 7 to 9.5kb (fig 14.7). These values are defined by the intersections of curves 5, 6, 7, 9, 10, 12 and 13 (Table 14.7). The temperatures for garnet-biotite pairs (curves 1,2,3,4, Fig.14.7) are lower than other calibrations and are considered to be the temperatures at which Fe-Mg diffusion ceased. Alternatively, they may reflect retrogressive biotite formation during M_3.

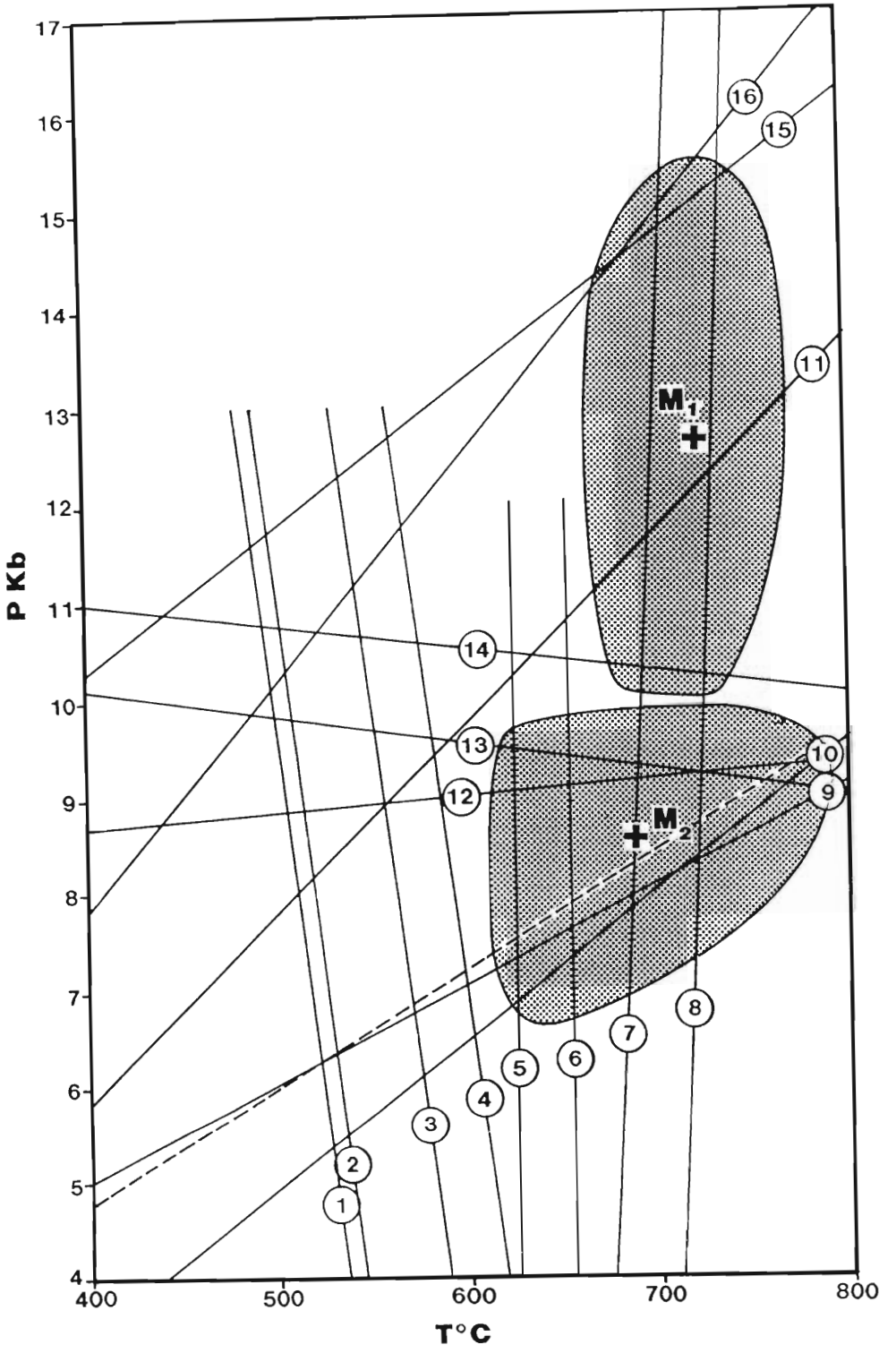

Figure 14.7. Summary of P-T values from the eastern area suggested by the different calculations discussed above. The dashed line represents a geothermal gradient of 25°C/km. The + signs represent the approximate mean values defined for the M_1 and M_2 physical conditions.

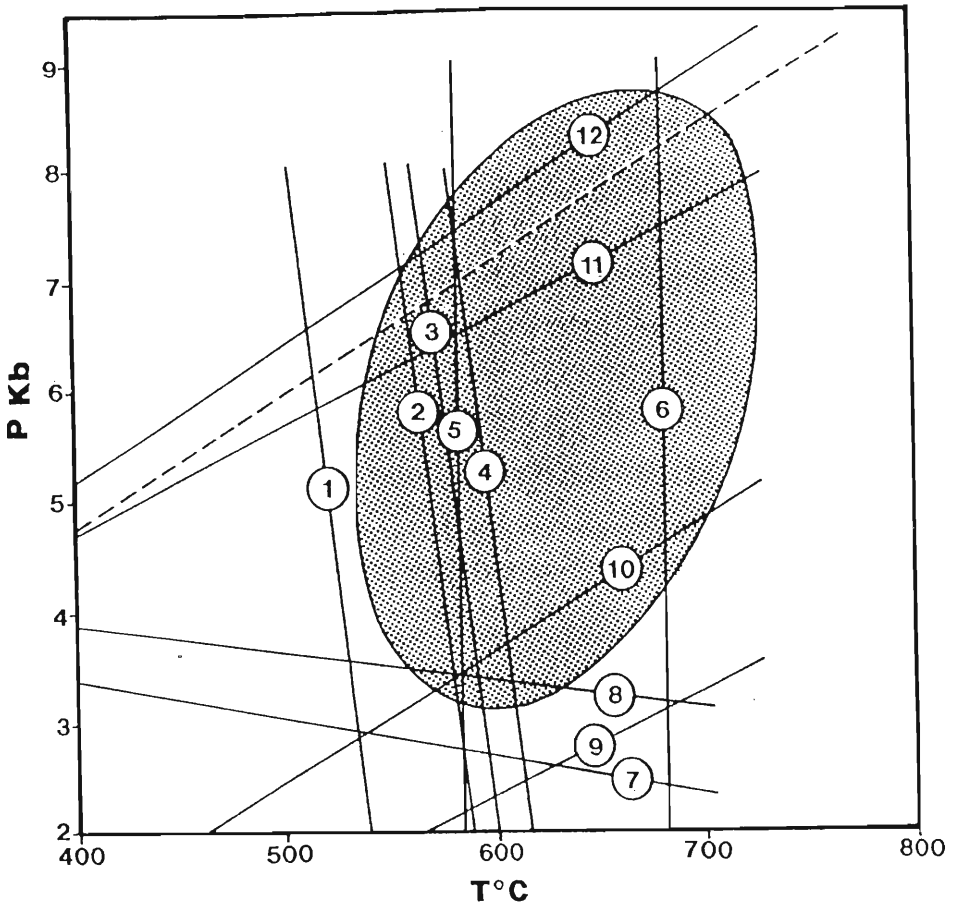

Figure 14.8. Summary of the P-T values from the western part of the study area suggested by calculated equilibria. The dashed line represents a geothermal gradient of 25°C/km.

The intersections of curves 2, 3, 4, 5, 6, 8, 10 and 11 (Fig. 14.8) define physical conditions in the western part of the study area of 550°C to 700°C and 3 to 8 kb. No clear definition between M_1 and M_2 is possible but the P-T conditions for sample S_2 from an amphibolite formed after M_1 suggest that P and T may have been higher during M_2 than M_1. Similarly, the garnet-biotite rim values are generally higher than the core values possibly supporting higher temperatures during M_2 or M_3. The data for the western part of the study area show that no such high pressure assemblages are preserved and no evidence has been recorded to suggest that such conditions were reached at any time. Curves 7 and 9 have been ignored because the physical conditions represented by their mutual intersections and intersections with curve 8 represent a geothermal gradient of >60°C/km. Geothermal gradients are generally in the range 15-30°C/km with extreme values from 5-60°C/km being recognised (Yardley, 1989;pp. 14-15).

THERMOBAROMETRY BASED ON MINERAL ASSEMBLAGES

In this section the metamorphic assemblages and reactions described from the Grey Gneisses (Chpt.3), the Banded Gneisses (Chpt4), the Fuglefjellet Formation (Chpt. 5) and the Sveabreen Formation (Chpt 6) and the Metamorphosed Intrusions (Chpt. 9) will be compared and discussed

further. The conditions of the reaction, 13An + 2Ab + 8Ed + H_2O = 19Qtz + 3 Grs + 10Prg described in the A3 amphibolite in chapter 9, are shown in figure 14.9.

CURVE NO.	CALIBRATION	COMMENT
1	Grt-Bt SLK1(rim)	
2	" SLK1(core)	
3	" SA10(core)	
4	" SA10(rim)	
5	Grt-Hbl SLK50	All Fe as Fe^{2+}
6	" SA13	"
7	Grt-Cpx SLK50 (rim)	Krogh (1989)calibration used as
8	" SLK50 (core)	approximation of mean.
9	Grt-Ru-Ilm-Pl-Qtz SA13	
10	Jd-Ab-Qtz SLK50 (rim)	
11	" SLK50 (core)	
12	Grt-Hbl-Pl-Qtz SLK50	All Fe as Fe^{2+}, mean value used
13	Cats-An-Qtz SLK50(rim)	
14	" SLK50(core)	
15	Gt-Pl-Cpx-Qtz (Fe) SLK50	
16	Gt-Pl-Cpx-Qtz (Mg) SLK50	

Table 14.7. Origin of curves 1-15 on Fig. 14.7

CURVE NO.	CALIBRATION	COMMENT
1	Grt-Bt SK1 (core)	
2	" SK1 (rim)	
3	" JE39 (core)	
4	" JE39 (rim)	
5	Grt-Hbl JE39	All Fe as Fe^{2+}
6	" S2	"
7	Grt-Hbl-Pl-Qtz S2	" , mean value used
8	" JE39	" , "
9	Jd-Ab-Qtz SV9	
10	" BK8	
11	Grt-Ru-Ilm-Pl-Qtz JE39	Mean value of core and rim used
12	" S2	"

Table 14.8. Origin of curves 1-11 on Fig. 14.8.

This reaction has been modelled using the program THERMO by Powell and Holland (1988). Assuming activities of 0.7 for the ferromagnesian phases (pargasite and edenite) and activities of 0.5 for the plagioclase end members, this reaction would occur at the physical conditions shown in figure 14.9.

Reactions 1-10 are shown in figure 14.10 and are presented in Table 14.9. The reactions are interpreted as being retrogressive and all require the introduction of H_2O during cooling. Consequently, before considering the conditions of reaction further, it is necessary to briefly consider the information regarding fluid compositions gleaned in previous chapters. Rock types

which commonly show mineralogical variations controlled by the composition of the fluid phase include magnesian and calcareous varieties.

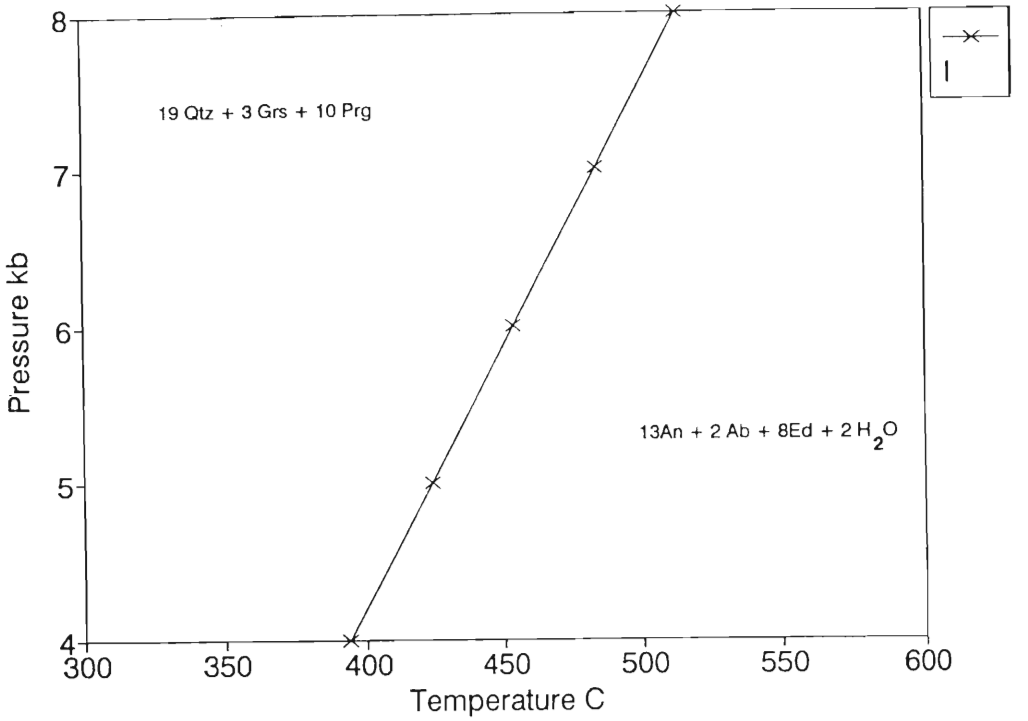

Figure 14.9 Metamorphic conditions applicable to the mineral assemblage in sample BK14. The mineral assemblage to the left of the diagram represents the product of the reaction whereas that on the right the reactants.

Magnesian assemblages in the Banded Gneisses of the Jutulrora Formation are consistent with a mixed (H_2O + CO_2) but H_2O-rich fluid. Grossular-bearing calc-silicate assemblages in the Banded Gneisses indicate that the fluid phase during metamorphism was H_2O-rich (page 60).

The mineral assemblages which define the higher grades of metamorphism in the magnesian rocks of the Fuglefjellet Formation do not constrain the fluid composition, however the formation of serpentine as a late retrogressive product serves to indicate that the fluid composition at that time was almost pure H_2O ($X_{H2O} > \sim 0.95$).

The mineral assemblages which define the higher grades of metamorphism in the carbonate rocks of the Fuglefjellet Formation do not constrain the fluid composition but it is reasonable to assume that the fluids were CO_2- rich. The retrogressive formation of brucite, serpentine and talc from tremolite, monticellite and, possibly, olivine (see pages 73-75) suggest that the fluid composition during the retrogressive stages was almost pure H_2O. Scapolite-bearing calc-silicate assemblages in the Fuglefjellet Formation suggest that the fluid composition in these rocks

contained significant CO_2 (possibly x_{CO2} >0.55). The partial replacement of the scapolite by zoisite/epidote suggests that during retrogression the fluid phase became increasingly enriched in H_2O.

1a. 4Phl + 6Zo + 15Qtz -> 6An + 3Hbl + 4Kfs + 4 H_2O
1b. 4Ann + 6Zo + 15Qtz -> 6An + 3 Fe-Hbl + 4Kfs + 4 H_2O
2. Ms + Ann + 3 Qtz -> Alm + 2Kfs + 2H_2O
3. Qtz + Ms -> Sil + Kfs + H_2O
4. Bt + Qtz -> Fs + Kfs + H_2O
5. 2Hbl -> 2An + 2Hd + 3Kfs + H_2O
6. 19 Qtz + 3Grs + 10Prg -> 13An + 2Ab + 8Ed + 2 H_2O
7. 4Zo + Qtz -> 5An + Gr + 2H_2O
8. 3Qtz + Hbl + 6Zo -> 10An + 4Hd + 4H_2O
9. Hbl + 4Spn + 26Zo -> 4Ilm + 9Grt + 31An + 14H_2O
10 2Hbl + 3Spn -> 3Ilm + 5Hd + 2An + 3Qtz + 2H_2O

Table 14.9. Reactions recognised in the Jutulrora, Fuglefjellet and Sveabreen Formations and the A3 amphibolites.

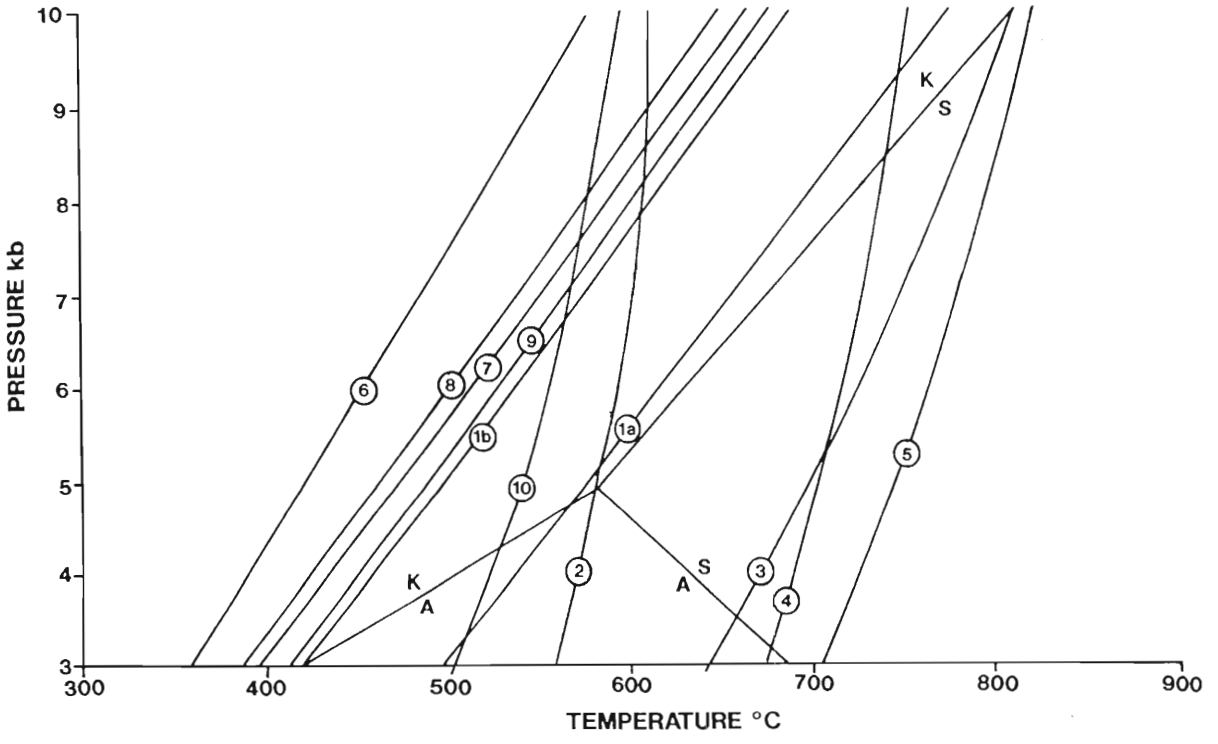

Figure 14.10. Summary of various reactions described in Chapters 3,4,5,6 and 9.

Besides these estimates of fluid-composition, there is little indication as to whether $p_{fluid} = P_{load}$ in the study area. Mineral assemblages in the Dalmatian Granite suggest that $p_{fluid} = P_{load}$ at least during D_3 (F_3) but no other indications of p_{fluid} have been recognised.

In conclusion, the above discussion suggests that during the retrogressive stages of metamorphism in the study area the fluid phase was dominantly H_2O-rich and probably $p_{fluid} = P_{load}$.

Significantly, the reaction curves (Fig. 14.10) are relatively steep indicating that they are dominantly thermally driven with pressure being subordinate. The reaction products are all located on the low temperature side of the curves requiring the introduction of H_2O.

Summary of thermobarometry

The thermobarometry suggests that rocks in the east at Salknappen were subjected to relatively high pressures (~12kb) and temperatures of the order 715°C during M_1 in the east and relatively low pressures in the west (Jutulrora) of approximately ~6 kb and temperatures of ~ 650°C. During D_2, the rocks in the east were elevated to shallower depths with pressures of approximately 8.5kb and temperatures of approximately 680°C being indicated. In the west, marginally higher temperatures (680°C) and pressures ~7kb are suggested by the post D_1/M_1 amphibolite although these differences are probably within or approaching analytical and calibration errors and therefore emphasis on the differences should be minimised. During D_3/M_3 temperatures and pressures in the east and west appear to have been similar and approximately 650°C and 6.5kb respectively. During and after D_3 many of the reactions recognised reflect hydration by a fluid phase dominated by H_2O during cooling.

P-T-t LOOP AND EVOLUTION OF THE STUDY AREA.

P-T-t loop

The P-T information from the thermobarometry and metamorphic history and the relevant information derived from the various intrusions (the Dalmatian Granite and the Kirwanveggan Dolerites) can be used to construct a provisional P-T time loop. This data is summarised in figure 14.11 on which various stages of evolution are identified. Construction of a complete loop is not feasible because of the lack of data from the prograde portion of the path. Spear *et al.* (1984) show that during the evolution of an orogenic belt, approximately one third of the time is spent at temperatures within ~50-100°C of the maximum temperatures. Therefore metamorphic assemblages produced in the earlier stages of the orogenic cycle, at lower temperatures, are unlikely to survive.

Stage 1 encompasses the metamorphic M_1 and structural evolution D_1 of the eastern and western domains. The timing of this event is constrained by the ages of the gneisses of the Jutulrora Formation and appears to have occurred at approximately 1000 to 900 Ma (Moyes

and Barton, 1990). At this time the rocks in the east were at greater depths.

Stage 2 was related to folding and thrust faulting associated with D_2 and is estimated to have occurred at approximately 800Ma $\pm$100. This event resulted in the tectonic stacking of the eastern domain over the west. Associated with this stage in the east is isothermal decompression indicated by the progression from the M_1 to M_2 conditions in figure 14.7. The timing of this stage is constrained by the age of the A2 amphibolites emplaced post-D_1 but pre-D_2. In the west, epidote-bearing pegmatitic lenses were formed axial planar to F_2 folds. The presence of epidote may be significant because experimental studies (Johannes, 1985) have shown that in partial melts, the assemblage anorthite + orthoclase + H_2O is replaced at higher pressures by zoisite + muscovite + quartz. This suggests that the western domain was depressed to greater depths (possibly from 6 to ~7) whereas the eastern domain was elevated to shallower levels (possibly ~12kb to ~6-7kb).

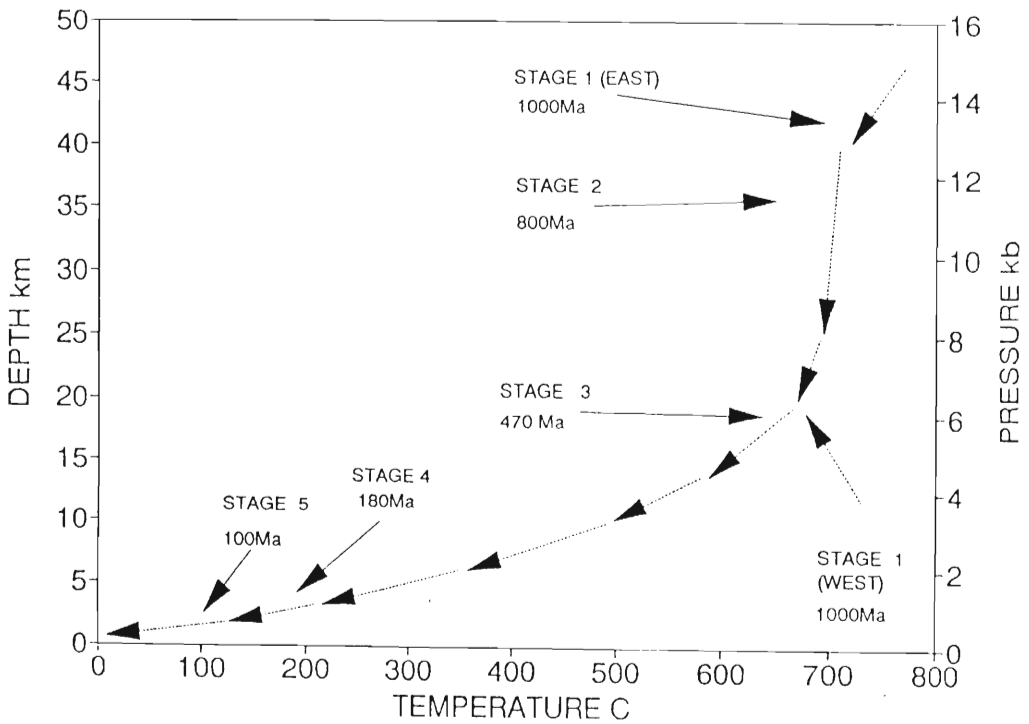

Figure 14.11. Diagram of the various stages of evolution recognised in the study area.

It is significant that the temperature in the west was not sufficiently elevated to cause large scale anatexis. This is similar to the scenario described by Spear *et al.* (1984) in which a relatively cold rock slab (eastern domain?) is thrust over a relatively warm rock slab (western domain) with the result that the P-T-t path in the hanging wall shows decreasing pressure and marginally increased temperature whereas the footwall shows increasing pressure and

marginally decreased temperature. In the western Sverdrupfjella temperatures recorded between the eastern and western domain do not vary greatly suggesting that the footwall and hanging wall were at similar temperatures.

Stage 3 involves the deformation during D_3 and thermal event (M_3)? associated with the intrusion of Dalmatian Granite during the Ross\Pan African orogeny (469$\pm$5Ma, Grantham *et al.*, 1991).

The period between Stage 3 and Stage 4 involves cooling and pressure reduction from M_3 conditions at ~470Ma to conditions at 180Ma associated with the igneous activity represented by the dolerite dykes and alkaline intrusions. Significantly, the reaction curves (Fig. 14.10) are relatively steep indicating that they are dominantly thermally driven with subordinate influence of pressure. The reaction products are all located on the low temperature side of the curves. The trajectory of variation in P-T space required to generate these reaction products requires that temperature varied significantly whereas pressure variations with time were minimal so that P-T evolution defines shallow trajectories crossing the steep reaction curves to give an isobaric cooling path (IBC), post M_3/D_3 (Harley, 1989).

Stage 4 involves processes related to the break up of Gondwanaland at ~170-180Ma (Cox, 1992). The presence of amygdales in dykes of the ~180Ma old (Harris *et al.*, 1991) Kirwanveggan Dolerite Suite provide evidence that at the time of emplacement, the cover was probably of the order of $\leq$0.5kb.

Evidence from the Kirwannveggan (200km to SW of the study area, Fig. 1.1) that lends support to assumptions of shallow depths includes the Kirwanveggan basalts and underlying sediments demonstrating that at ~180Ma ago the rocks of the Sverdrupfjella Group were exposed at surface. The presence of older unmetamorphosed sediments, the Urfell Group (Wolmarans and Kent, 1982) in the Kirwanveggan also provides evidence that the present levels of exposure of the Sverdrupfjella Group were already reached at approximately ~300Ma ago.

Stage 5 can be inferred from relationships in the Heimefrontfjella (~200km to the SW of the Kirwanveggan, Fig. 1.1) where fission-track dating on apatite (effective closure temperature ~100°C) shows two groups of ages (Jacobs, 1991). One group has ages around 100Ma and the other ages from 130-200Ma (Jacobs, 1991). Jacobs (1991) interprets the younger ages to represent rapid uplift and associated cooling during the Upper Cretaceous. The older ages are interpreted as mixed ages where temperatures were insufficient to anneal (reset) the apatite grains.

Discussion

Harley (1989) has reviewed the origin of granulites and related tectonothermal settings. He suggests that isothermal decompression (ITD) paths, typical of Stage 2, may be ascribed to either the later stages of thermal evolution of overthickened crust resulting from collision or

extensional settings within the footwall of a low-angle extensional detachment zone. In the latter case, the ITD path is formed at relatively shallow levels (5-2kb, Harley, 1989). In the Sverdrupfjella, thrust faulting associated with D_2 and the relatively higher pressures recorded by thermobarometry suggest the former environment is more likely.

Harley (1989) suggests that isobaric cooling paths (IBC) paths, similar to that defined by the period between stage 3 and stage 4, may arise in the following settings:-

(1.) Magmatic accretion into, and under, previously existing crust.

(2.) Extension of normal thickness crust with concomitant magmatic underplating.

(3.) Extension of normal thickness crust without additional magmatic accretion.

(4.) Tectonic thickening of extended crust back to normal thickness.

(5.) Extension of crust previously over-thickened in a collisional setting.

(6.) Thermal relaxation, through erosion, of lower-plate or lowermost continental material in a crustal section doubled in thickness by collision.

In the Sverdrupfjella, alternatives 1 and 2 are considered unlikely. The Dalmatian Granite was emplaced at approximately this time however the scale of magmatism is small. The tectonic activity associated with the emplacement of the Dalmatian Granite is compressional and consequently alternatives 2, 3 and 5 are similarly excluded. Alternative 4 does not match the tectonic evolution recognised in this study. An alternative which appears feasible is that described in 6 namely thermal relaxation through erosion.

CHAPTER 15
DISCUSSION OF TECTONIC SETTING AND CONCLUSIONS

TECTONIC SETTING

The thermobarometry and P-T-time loop formulated in chapter 14 suggest that the rocks of the western Sverdrupfjella were deformed and metamorphosed in a collisional tectonic setting. If one considers the distribution and types of lithologies in the study area, the following arrangement is apparent. Metapelitic to semi-metapelitic rocks, considered to have originally been shales and greywackes (Sveabreen Formation), and containing high grade metamorphosed mafic bodies of uncertain origin (intrusive or extrusive), were thrust over, at least in part, rocks of dominantly calcareous and quartzofeldspathic composition (the Fuglefjellet Formation), considered to be largely sedimentary in origin. West of the exposures of the Fuglefjellet Formation, the rocks of the Jutulrora Formation consist dominantly of quartzofeldspathic and mafic gneisses, regarded as a metamorphosed volcano-sedimentary sequence. It is important to note that those metamorphic rocks of sedimentary origin, likely to have been deposited in quieter and possibly deepwater environments (eugeosynclinal?), are farthest removed from the Ahlmannryggen terrane to the west. Located closer to the Ahlmannryggen terrane are the rocks of the Fuglefjellet Formation with their high component of metamorphosed carbonates, interpreted to represent a shallow water environment, possibly miogeosynclinal in nature. The dominantly volcanic Jutulrora Formation is located adjacent to the Ahlmannryggen terrane and possibly represents a volcanic chain similar to the Andes or a island-arc type of environment. Into these deformed volcano-sedimentary sequences a variety of granitic rocks were intruded at various times. The earliest intrusions namely the Jutulrora, Roerkulten and Brekkerista granites were emplaced possibly syn-D_1/M_1. The youngest granitic intrusions represented by the Dalmatian Granite and associated veins and pegmatites appear to have been emplaced during D_3/M_3.

Recent studies have attempted to relate the chemistry of granites (sensu lato) to the tectonic environments in which the granitic magmas were generated (Pearce *et al.*, 1984). The classification of Pearce *et al.* (1984) employs trace element signatures to determine the possible tectonic settings of magma generation. Such models have been based on the study of undeformed and unmetamorphosed Phanerozoic granites which are exposed in areas where there is little doubt regarding their tectonic settings or the nature of the probable source of their magmas. The extension of such models to granites which are older than the Phanerozoic and to those that have been metamorphosed and deformed is based on the assumption that plate tectonic processes have operated through time prior to the Phanerozoic and that metamorphism and deformation have not materially altered the trace element distributions on which the models are based.

Pearce *et al.* (1984) have utilised ORG normalised patterns of granites from various tectonic environments and have developed discriminant diagrams based on the Rb,Nb and Y contents of granitoids. Applying the discrimination diagrams of Pearce *et al.* (1984), the Nb vs Y contents of the Grey Gneisses are comparable with those of volcanic arc granitoids whereas the Rb vs Nb + Y distributions are comparable with volcanic arc and syn- collision granitoids (Fig. 3.11). Although it was concluded in chapter 8 that the Jutulrora, Roerkulten and Brekkerista granites were similar and therefore possibly derived from the same source, subtle differences are apparent. Based on the ORG-normalised "spidergrams" (Pearce *et al.*, 1984) the profile for the Roerkulten Granite (Fig. 8.3, p. 122) corresponds to a volcanic arc granite, being characterised by high K, Rb, Ba and Th concentrations as well as high Ce and Sm contents relative to Nb, Zr, Y and Yb (Fig. 8.3). The high Ce and Sm contents are interpreted to indicate a significant crustal component in the source regions of the granitic magmas (Pearce *et al.* 1984).

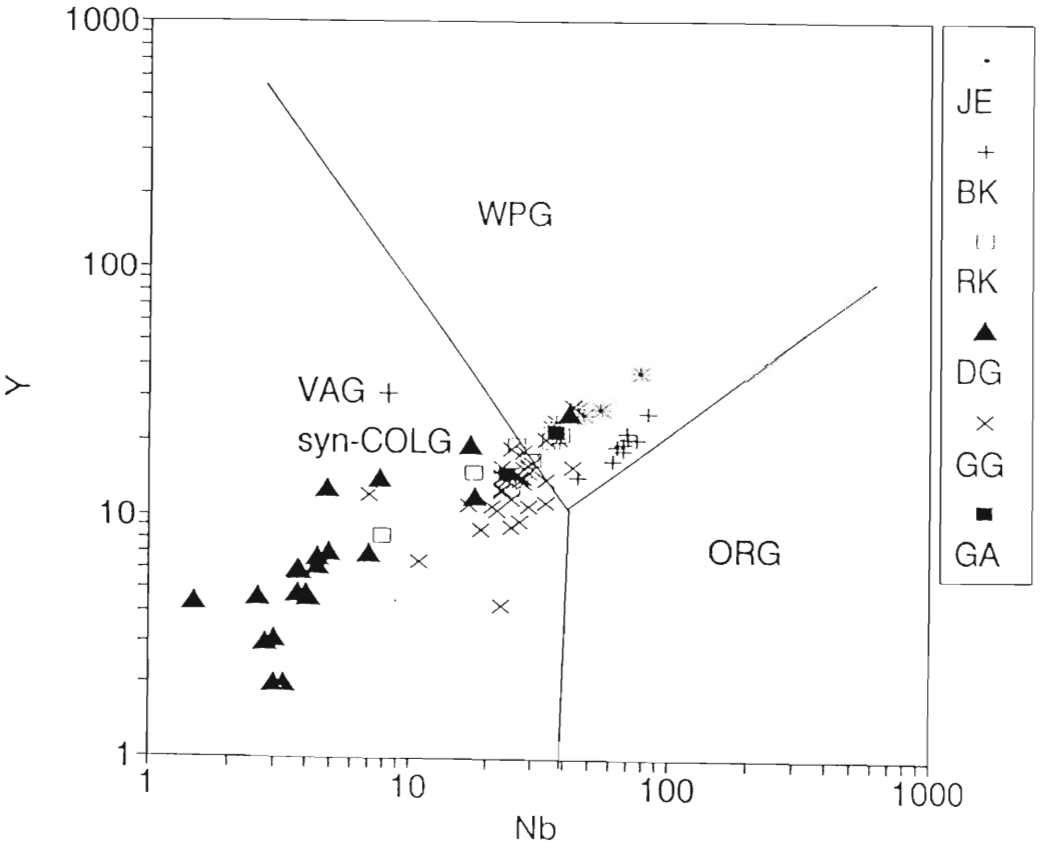

Figure 15.1. Nb vs Y for the Grey Gneiss Complex (GG), the Roerkulten (RK), Jutulrora (JE), Brekkerista (BK), Grey aplites (GA) and Dalmatian Granites (DG)(the latter including the late granitic veins). The different fields are from Pearce *et al.* (1984). VAG = volcanic arc granites, ORG = ocean ridge granites, WPG = within plate granites and syn-COLG = syn collision granites.

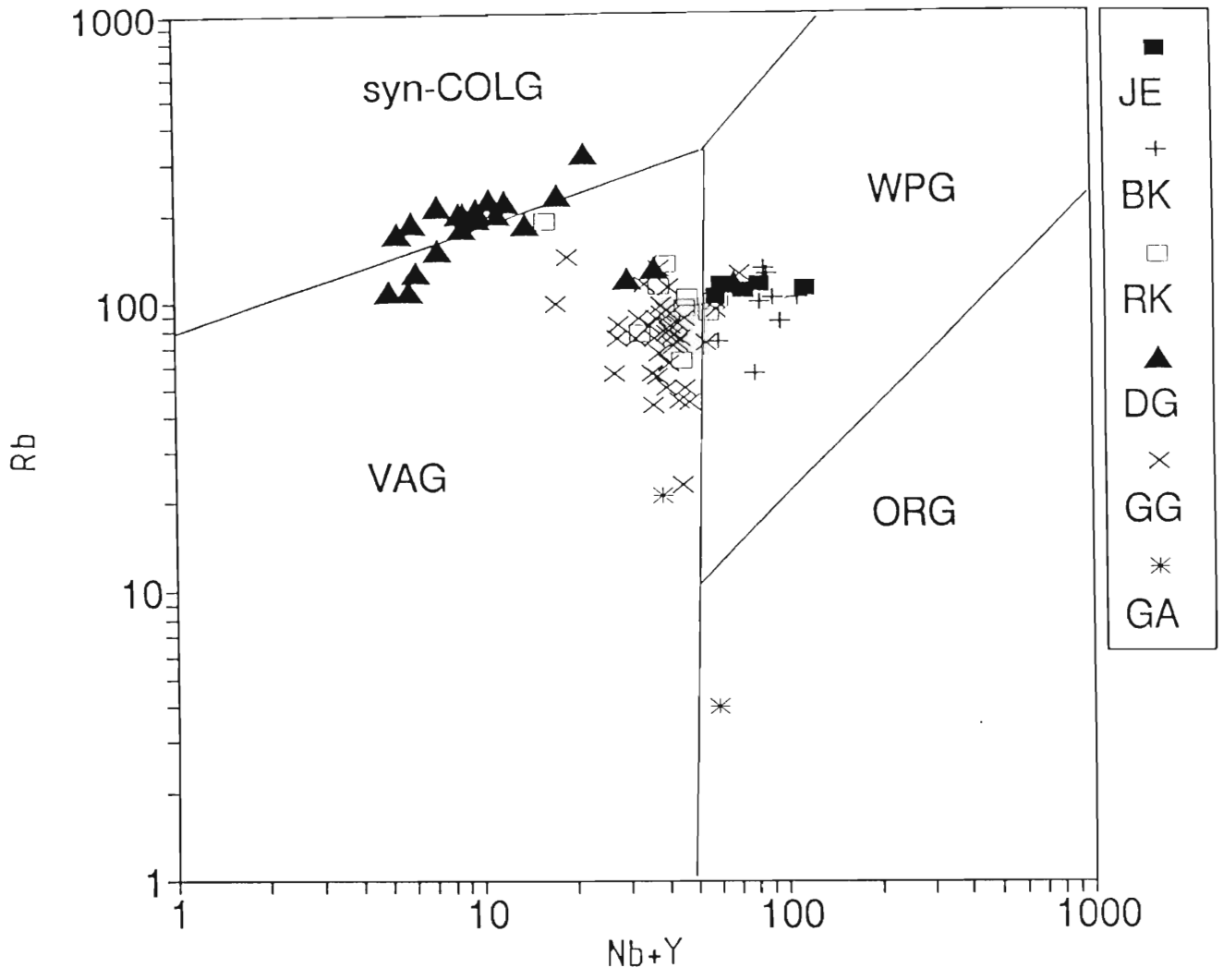

Figure 15.2. Rb vs Nb + Y for the Grey Gneiss Complex (GG), the Roerkulten (RK), Jutulrora (JE), Brekkerista (BK), Grey aplites (GA) and Dalmatian Granites (DG)(the latter including the late granitic veins). The different fields are from Pearce *et al.* (1984). VAG = volcanic arc granites, ORG = ocean ridge granites, WPG = within plate granites and syn-COLG = syn collision granites. (the latter including the late granitic veins). The different fields are from Pearce *et al.* (1984).

The ORG normalised profile (Fig. 8.3, page 122) for the Jutulrora Granite is difficult to distinguish from either within plate granites or volcanic arc granites. The Jutulrora Granite is characterised by low Yb values which, according to Pearce *et al.* (1984), are more characteristic of volcanic arc granites than within plate granites.

The Brekkerista Granite, with normalised Rb/Th ratios approximating unity and with high Rb/Nb and Th/Nb ratios (Fig. 8.3, p. 122) would appear to be characteristic of within-plate granites (Pearce *et al.*, 1984). However a low Yb content in the Brekkerista Granite relative to ORG is consistant with a volcanic-arc environment (Pearce *et al.*, 1984).

Classification of the Roerkulten, Jutulrora and, possibly, Brekkerista Granites as volcanic-arc granites appears to be consistent with the broadly calc-alkaline nature of the Grey Gneiss and Banded Gneiss Complexes of the Jutulrora Formation. Modelling discussed previously has shown that the presence of small proportions of various accessory minerals in the restite can cause significantly modifications that could result in erroneous tectonic classification.

Based on the discriminant diagrams of Pearce *et al.* (1984) the Roerkulten Granite samples plot mostly as volcanic-arc granites (figs. 15.1 and 15.2) whereas the Jutulrora Granite has trace element characteristics which, according Pearce *et al.* (1984), characterise within-plate granites. The Rb, Nb and Y contents of the Brekkerista Granite are consistent with within- plate granites (Figs. 15.1 and 15.2).

It is uncertain to what extent these discrimination diagrams may be applied. It may be significant that the Jutulrora and Brekkerista granites reflect compositions that lie along the within-plate and volcanic arc border. This may reflect an older crustal source at depth. The Roerkulten Granite on the other hand appears to have purely volcanic arc characteristics as do the Grey Gneisses of the Jutulrora Formation.

The grey aplites, which intrude the Brekkerista Granite, have relatively low Rb concentrations which, combined with their Nb + Y contents, suggest that they are either volcanic arc granitoids or oceanridge granitoids (only two samples) (Fig. 15.2). The latter possibility is discounted there are no other factors which support it. The Nb and Y contents are typical of within-plate granites (one sample) or volcanic-arc granites or syn-collision granites (one sample)(Fig. 15.1)

The profile of trace element variations for the Dalmatian Granite, characterised by low Ce, Zr and Sm contents relative to ORG (Fig. 10.6, p. 166) is suggestive of syn-collision granites (Pearce *et al.*, 1984). The Nb vs Y variation of the Dalmatian Granite would suggest that the Dalmatian Granite has characteristics of volcanic arc or syn-collision granites (Fig. 15.1). In terms of the Rb versus Nb + Y diagram the Dalmatian Granite has characteristics of syn-collision granites (Fig. 15.2), an interpretation which appears to be consistent with field relationships (chapter 10).

The next major crustal evolution episode to affect the area was the breakup of Gondwana at ~180Ma. Most reconstructions of Gondwana place western Dronning Maud Land adjacent to southeastern Africa (e.g. Martin and Hartnady, 1986). Recent comparisons of the geological evolution of southeastern Africa and western Dronning Maud Land (Grantham *et al.*, 1988; Grantham and Hunter, 1991; Groenewald *et al.*, 1991; Harris *et al.*, 1991) show that these two areas share many similarities. These authors suggest that the metamorphic terrane which underlies the Sverdrupfjella, Kirwanveggan and Heimefrontfjella mountains in Antarctica represent a continuation of the Mozambique Belt to the north and provides a link with the Natal-Namaqua belt to the south and east. This belt can be traced farther to the east and north, within a Gondwana framework, extending through Sri Lanka and East Antarctica. The extent of

this belt can be compared to the Grenvillian in the northern hemisphere which extends from the Urals in Russia in the east to southern California in the west (Bridgewater and Windley, 1973). Both belts are broadly of similar age and are characterised by the presence of intrusive charnockitic rocks. The breakup of Gondwana during the Jurassic appears to have followed this belt for much of its extent.

CONCLUSIONS

(1) The oldest rocks of the western sector of the H.U. Sverdrupfjella, the Jutulrora Formation, consist of tonalitic orthogneisses, interlayers of banded mafic to felsic ortho- and paragneisses. The Jutulrora Formation is interpreted to comprise calc-alkaline volcanic rocks interlayered with clastic sediments, originally constituting a volcanic arc sequence.

(2) The Jutulrora Formation is probably structurally overlain by the largely paragneissic, carbonate- dominated Fuglefjellet Formation. The Fuglefjellet Formation is considered to represent a miogeosynclinal shelf facies.

(3) The Fuglefjellet Formation is itself probably structurally overlain by the dominantly paragneissic Sveabreen Formation which consists of pelitic to quartzofeldspathic gneisses. This formation is considered to represent a eugeosynclinal facies.

(4) Three tabular granitic bodies, the Roerkulten, Jutulrora and Brekkerista Granites intruded the volcano-sedimentary rocks of the Jutulrora Formation. The trace and rare earth element chemistry of these granites suggest that allanite and sphene have played significant roles during their crystallization.

(5) Various phases of mafic intrusions, recognised as discordant amphibolites, are present as well as a phase of dioritic veining.

(6) Thin (up to 10m thick) sheet-like bodies of Dalmatian Granite were emplaced syntectonically with the Pan-African (or Ross) orogenic event (D_3) at ~470Ma. The magma from which this granite crystallized was generated by partial melting of crustal rocks at depths of approximately 6kb.

(7) Intrusions of Jurassic age include the alkaline complexes at Straumsvola and Tvora and numerous dolerite dykes; some of which clearly postdate the alkali intrusions. Amygdales in the dolerite dykes reflect crystallisation at shallow crustal depth.

(8) Five episodes of deformation are recognised. The first two deformation episodes resulted in folds (F_1 and F_2) which are co-planar and coaxial resulting in type 3 interference structures. Low angle thrust faulting was associated with D_2, the best example of which is recognised at Fuglefjellet. The vergence of folds and associated lineations suggest tectonic transport from the east toward the west during D_1 and D_2.

D_3 is characterized by folds and reverse faults. The fault planes and axial planes of the folds verge toward the east and south-east suggesting transport from the west and north-west. D_4

was a period of open folding which is difficult to quantify. Open dome and basin type folds are correlated with D_4.

D_5 is represented by normal faults and joints, developed largely in the rocks adjacent, and parallel, to the Jutulstraumen Glacier in the west. These joints affect the Tvora and Straumsvola Complexes and thus are post-Jurassic.

(9) Three major phases of metamorphic recrystallization and growth are recognised. These phases can be related to the deformational episodes. The dominant metamorphic assemblages define S_1 and S_2 planar fabrics and are interpreted to represent M_1 and M_2 metamorphic conditions. These assemblages are characteristic of upper amphibolite facies metamorphic conditions. Discordant mafic intrusions represented by amphibolites provide evidence of long periods during which the rocks were exposed to these metamorphic conditions. M_3 is dominated by the development of cross-cutting biotite which is commonly oriented axial planar to D_3 folds. In rocks from the eastern portion of the study area, thermobarometry suggests an isothermal decompression path from M_1 to M_2 to M_3 whereas in the west conditions during these phases of metamorphism appear to have remained broadly similar, possibly with marginally higher temperatures and pressures during M_2/D_2. After D_3/M3, an isobaric cooling path commensurate with erosion-induced cooling and pressure reduction is suggested.

(10) Comparison of the geology of the study area with that of southern Mozambique reveals many common facets. These similarities support reconstructions based on ocean floor magnetic anomalies which juxtapose Dronning Maud Land and southern Africa prior to the break up of Gondwana.

REFERENCES

Arth, J.G. (1976) Behaviour of trace elements during magmatic processes - a summary of theoretical models and their applications. U.S. Geol. Soc. Jnl. Res., 4, 41-47.

Asmerom, Y., Ikramuddin, M. and Kinart, K. (1988) Washington: implication for genesis of two-mica Cordilleran granites. Geology, 16, 431-435.

Barbey, P. and Cuney, M. (1982) K, Rb, Sr, Ba, U and Th geochemistry of Lapland Granulites (Fennoscandia) LILE fractionation controlling factors. Contrib. Mineral. Petrol., 81, 304-316.

Barker, F. (1961) Phase relations in cordierite-garnet-bearing Kinsman quartz monzonite and enclosing schist, New Hampshire. Amer. Mineral., 46, 1166-1176.

Benard, F., Moutou P. and Pichavant, M. (1984) Phase relations of tourmaline leucogranites and the significance of tourmaline in silicic magmas. Jnl. Geology., 93, 271-291.

Binns, R.A. (1969) Ferromagnesian minerals in high grade metamorphic rocks. Geol. Soc. Austr. Spec. paper, 2, 323-332.

Bohlen, S.R. and Liotta, J.J. (1986) A barometer for garnet amphibolites and garnet granulites. Jnl. Petrol. , 27,(5), 1025-1034.

Bridgewater, D. and Windley, B.F. (1973) Anorthosite, post orogenic granites, acid volcanic rocks and crustal development in the north Atlantic shield during the mid-Proterozoic. Spec. Publ. Geol. Soc. S. Afr., 3, 307-316.

Brown, G.C. (1982) Calc-alkaline intrusive rocks: their diversity, evolution, and relation to volcanic arcs. In Andesites, R.S. Thorpe (ed).,pp. 437-461, John Wiley & Sons.

Brown, T.H., Berman, R.G., and Perkins, E.H. (1988) GeO-Calc: software package for calculation and display of pressure-temperature- composition phase diagrams using an IBM or compatible personal computer. Computers and Geosciences, 14, 279-289.

Burnham, C.W., Holloway, J.R. and Davis, N.F. (1969) Thermodynamic properties of water to 1000°C and 10000 bars. Geol. Soc. Am. Spec. Pap., 132.

Carmichael, I.S.E., Turner, F.J., Verhoogen, J. (1974) Igneous Petrology. McGraw-Hill Book Co., New York. 739pp.

Cawthorn, R.G. and Collerson, K.D. (1974) The recalculation of pyroxene end-member parameters and the estimation of ferrous and ferric iron content from electron microprobe analysis. Amer. Mineral., 59, 1203- 1208.

Chappel, B.W. and White, A.J.R. (1974) Two contrasting granite types. Pacific Geol., 8, 173-174.

Chappel, B.W., White, A.J.R. and Wyborn, D. (1987) The importance of residual source material (restite) in granite petrogenesis. Jnl. Petrol., 28, 1111-1138.

Chayes, F. (1964) Variance-covariance relations in Harker diagrams of volcanic rock suites. Jnl. Petrol., 5, 219-237.

Chipera, S.J. and Perkins, D. (1988) Evaluation of biotite-garnet geothermometers : application to the English River subprovince Ontario. Contrib. Mineral. Petrol., 98, 40-48.

Chorlton, L.B. and Martin, R.F. (1978) The effect of boron on the granite solidus. Canadian Mineralogist, 16, 239-244.

Clarke, D.B. (1992) Granitoid rocks. Chapman and Hall, London. 283pp.

Cox, K.G. (1992,in press) Karoo igneous activity, and the early stages of the break-up of Gondwanaland. in Magmatism and the causes of continental Breakup. Storey, B.C., Alabaster, A. and Pankhurst, R.J. (eds). Geol. Soc. Lond. Spec. Publ.

Cox, K.G., Bell, J.D. and Pankhurst, R.J. (1979) The Interpretation of Igneous Rocks. George Allen and Unwin. London. 450pp.

Cox, K.G., Macdonald, R. and Hornung, G. (1967) Geochemical and petrogenetic provinces in the Karroo Basalts of southern Africa. Amer. Mineral., 52, 1451-1474.

Creaser, R.A., Price, R.C. and Wormald, R.J. (1991) A-type granites revisited: Assessment of a residual-source model. Geology, 19, 163-166.

Cullers, R.L. and Graf, J.L. (1984) Rare earth elements in igneous rocks of the continental crust: intermediate and silicic rocks - ore petrogenesis. pp. 275-316 In Rare Earth Element Geochemistry. Henderson P. (ed). Elsevier, Amsterdam. 510pp.

Daly, J.S., Cliff, R.A., and Yardley, B.W.D. (eds) (1989) Evolution of Metamorphic Belts. Geol. Soc. spec. publ. 43., Blackwell Sci. Publ., Oxford. 566 pp.

Davidson, L. and Park, R.G. (1978) Late Nagssugtoquidian stress orientation derived from deformed granodiorite dykes north of Holstein-borg, West Greenland. Quart. J. Geol. Soc. Lond., 135, 282-289.

Deer, W.A., Howie, R.A. and Zussman, J. (1966) An Introduction to Rock Forming Minerals. Longman, London. 528pp.

Deer, W.A., Howie, R.A. and Zussman, J. (1992) An Introduction to the Rock Forming Minerals 2nd Ed. Longman Scientific & Technical., Harlow. 696pp.

Drake, M.J. (1976) The oxidation state of europium as an indicator of oxygen fugacity. Geochim. Cosmochim. Acta., 39, 55-64.

Drake, M.J. and Weill, D.F. (1975) Partition of Sr, Ba, Ca, Y, Eu^{2+} and Eu^{3+} and other REE between plagioclase and magmatic liquid: an experimental study. Geochim. Cosmochim. Acta., 39, 689-712.

Droop, G.T.R. (1987) A general equation for estimating Fe^{3+} concentrations in ferromagnesian silicates and oxides from microprobe analyses using stoichiometric criteria. Min. Mag., 51, 431-436.

Eglington, B.M., Harmer, R.E. and Kerr, A. (1986) Petrographic, Rb-Sr isotope and geochemical characteristics of intrusive granitoids from the Port Edward - Port shepstone area, Natal. Trans. Geol. Soc. S. Afr., 89, 199-213 .

Eliston, J.N. (1984) Orbicules: an indication of the crystalisation of hydrosilicates. I. Earth Sci. Rev., 20, 265-344.

Ellison, A.J.G. and Hess, P.C. (1986) Solution behaviour of +4 cations in high silica melts : petrologic and geochemical implications. Contrib. Mineral. Petrol., 94, 343-351.

Ellis, D.J. and Green, D.H. (1979) An experimental study of the effects of Ca upon garnet clinopyroxene Fe-Mg exchange equilibria. Contrib. Mineral. Petrol., 71, 13-22.

Ewart, A. (1982) The mineralogy and petrology of Tertiary-Recent orogenic volcanic rocks: with special reference to the andesitic-basaltic compositional range. In Andesites. Thorpe, R.S. (ed).pp. 25-95, John Wiley and Sons.

Ferreira, E.P. (1986) 'n Sedimentologies - stratigrafiese ondersoek van die sedimentere gesteentes in die Ahlmannryggen, Antarktika (in Afrikaans) . MSc Thesis. University of Stellenbosch, South Africa, 176pp.

Ferry, J.M. and Spear, F.S. (1978) Experimental calibration of the partitioning of Fe and Mg between biotite and garnet. Contrib. Mineral. Petrol., 66, 113-117.

Fourcade, S. and Allegre, C.J. (1981) Trace element behaviour in granite genesis: a case study- the calc-alkaline association from the Querigut complex (Pyrenees, France). Contrib. Mineral. Petrol., 76, 177-195.

Fyfe, W.S. (1970) Some thoughts on granite magmas. In Mechanism of Igneous Intrusions. Newall G. and Rast. N. (eds). pp.201-216.

Ganguly, J. and Saxena, S.K. (1984) Mixing properties of aluminosilicate garnets: constraints from natural and experimental data, and applications to geothermo-barometry. Amer. Mineral., 69, 88-97.

Gavshon, R.D.J. and Erasmus, J.M. (1975) Precambrian metamorphic rocks of the Neumayerskarvet area, Kirwanveggan, western Dronning Maud Land. S. Afr. Jnl. Ant. Res., 5, 2-9.

Ghent, E.D. and Stout, M.Z. (1986) Garnet - hornblende thermometry, $CaMgSi_2O_6$ activity and the minimum pressure limits of metamorphism for garnet amphibolites. Jnl. Geology. , 94, 736-743.

Gill, J.B. (1981) Orogenic Andesites and Plate Tectonics . Springer- Verlag, Amsterdam, 390pp.

Goldman, D.S. and Albee, A.L. (1977) Correlation of Mg/Fe partitioning between garnet and biotite with O^{18}/O^{16} partitioning between quartz and magnetite. Am. Jnl. Sci. , 277, 750-767.

Graham, C.M. and Powell, R. (1984) A garnet-hornblende geothermometer: calibration testing and application to the Pelona Schist, southern California. Jnl. Metamorph. geol. , 2, 13-32.

Grantham, G.H. (1984) The tectonic, metamorphic and intrusive history of the Natal Mobile Belt between Glenmore and Port Edward, Natal. Unpubl. MSc. Univ. Natal (Pietermaritzburg). 243pp.

Grantham, G.H. and Hunter, D.R. (1991) The timing and nature of faulting and jointing adjacent to the Pencksokket, western Dronning Maud Land, Antarctica. pp. 47-51 in Geological Evolution of Antarctica. Thomson, M.R.A., Crame, J.A. and Thomson, J.W. (eds). Cambridge University Press, Cambridge.

Grantham, G.H., Groenewald, P.B. and Hunter, D.R. (1988) Geology of the northern H.U. Sverdrupfjella, western Dronning Maud Land and implications for Gondwana reconstructions. S. Afr. Jnl. Ant. Res. , 18, 2-10,

Grantham, G.H., Moyes, A.B. and Hunter, D.R. (1991) The age, petrogenesis and emplacement of the Dalmatian Granite, H.U. Sverdrupfjella, Dronning Maud Land, Antarctica. Antarct. Sci. , 3, 197-204.

Green, D.H. and Ringwood, A.E. (1967) An experimental investigation of the gabbro to eclogite transformation and its petrological implications. Geochim. Cosmochim. Acta. , 31, 767-833.

Green, T.H. and Pearson, N.J. (1986) REE partitioning between sphene and coexisting silicate liquid at high pressure and temperature. Chemical Geology , 55, 105-119.

Groenewald, P.B. and Hunter, D.R. (1991) Granulites of northern H.U. Sverdrupfjella, western Dronning Maud Land: metamorphic history from garnet-pyroxene assemblages, coronas and hydration reactions. pp. 61- 67 in Geological Evolution of Antarctica . Thomson, M.R.A., Crame, J.A. and Thomson, J.W. (eds). Int. symp. on Ant. Earth Sc., Cambridge.

Groenewald, P.B, Grantham, G.H. and Watkeys, M.K. (1991) Geological evidence for a Proterozoic to Mesozoic link between southeastern Africa and Dronning Maud Land, Antarctica. Jnl. Geol. Soc. Lond., 148, 1115-1123.

Gromet, L.P. and Silver, L.T. (1983) Rare-earth element distributions among minerals in a granodiorite and their petrogenetic implications. Geochim. Cosmochim. Acta, 47, 925-939.

Hamilton, D.L. and MacKenzie, W.S. (1965) Phase-equilibrium studies in the system $NaAlSiO_4$ (nepheline) - $KAlSiO_4$ (kalsilite) - SiO_2-H_2O. Min. Mag., 34, pp. 214-231.

Harley, S.L. (1989) The origins of granulites: a metamorphic perspective. Geol. Mag., 126, 215-247.

Harrison, T.M. and Watson, E.B. (1984) The behaviour of apatite during crustal anatexis: Equilibrium and kinetic considerations. Geochim. Cosmochim. Acta, 48, 1467-1477

Harrison, T.M. and Watson, E.B. (1986) Does anatexis deplete the lower crust in heat producing elements ?: implications from experimental studies. EOS, 16, 386.

Harris, C. and Rickard, R.S. (1987) Rare-earth-rich eudialite and dalyite from a peralkaline granite dyke at Straumsvola, Dronning Maud Land, Antarctica. Canadian Mineralogist, 25, 755-762.

Harris, C., Watters, B.R. and Groenewald, P.B. (1991) Geochemistry of the Mesozoic regional basic dykes of western Dronning Maud Land, Antarctica. Contrib. Mineral. Petrol., 107, 100-111.

Haskin, L.A. (1984) Petrogenetic modelling - use of rare earth elements. pp. 115-152 In Rare Earth Element Geochemistry. Henderson P. (ed). Elsevier, Amsterdam. 510pp.

Heard, R.G. (1976) An investigation of the metamorphic rocks of a portion of the Kirwanveggan, western Dronning Maud Land, Antarctica. Unpubl. rept. Geol. Surv. Pretoria.

Heier, K.S. and Thoresen, K. (1971) Geochemistry of high grade metamorphic rocks, Lofoten - Vesteralen, north Norway. Geochim. Cosmochim. Acta., 35, 89-99.

Henderson, P. (1982) Inorganic Geochemistry. Pergamon Press, Oxford. 353pp.

Henderson, P. (1984) General geochemical properties and abundances of the rare earth elements. pp. 1-32 In Rare Earth Element Geochemistry. Henderson P. (ed). Elsevier, Amsterdam. 510pp.

Henderson, P. (ed) (1984) Rare Earth Element Geochemistry. Elsevier. Amsterdam. 510pp.

Henry, D.J. and Guidotti, C.V. (1985) Tourmaline as a petrogenetic indicator mineral: an example from the staurolite grade metapelites of N.W. Maine. Amer. Mineral., 70, 1-15.

Hildreth, W. (1981) Gradients in silicic magma chambers: implications for lithospheric magmatism. Jnl. Geophys. Res., 86, 10153-10192.

Hjelle, A. (1972) Some observations on the geology of H.U. Sverdrupfjella, Dronning Maud Land. Norsk Polarinstitutt Arbok, 1972, 7-22.

Hsu, L.C. (1968) Selected phase equilibria in the system Al-Mn-Fe-Si-O-H. a model for garnet equilibria. Jnl. Petrol., 9, 40-83.

Indares, A. and Martignole, J. (1985) Biotite-garnet thermometry in the granulite facies: the influnece of Ti and Al in biotite. Amer. Mineral., 70, 272-278.

Irvine, T.N. (1982) Terminology for Layered Intrusions. Jnl. Petrol., 23, 127-162.

Irvine, T.N. and Barager, W.R.A. (1971) A guide to the chemical classification of the common volcanic rocks. Can. J. Earth Sci., 8, 523-548.

Jackson, M.P.A. (1976) High grade metamorphism and migmatization of the Namaqua Metamorphic Complex around Aus in the southern Namib desert, South west Africa. Precambrian Research Unit. Univ. Cape Town, Bull. 18, 299pp.

Jacobs, J. (1991) Structural evolution and cooling history of the Heimefrontfjella Mountains, western Dronning Maud Land, Antarctica. Berich. Polarforschung, 97, pp. 141.

Johannes, W. (1985) The significance of experimetal studies for the formation of migmatites. pp. 36-85 In Migmatites. Asworth J.R. (ed)., Blackie & Son Ltd. Glasgow. 302pp.

Kilpatrick, J.A. and Ellis, D.J. (1991) The Ardery Charnockite intrusions, Windmill Islands, Antarctica, representative of the widespread and unusual melting events producing charnockitic magmas in the Proterozoic of Gondwana. Gondwana Symp. Abs., Hobart, Tasmania, 48.

Kohn, M.J. and Spear, F.S. (1989) Empirical calibration of geobarometers for the assemblage garnet + hornblende + plagioclase + quartz. Amer. Mineral., 74, 77-84.

Kretz, R. (1983) Symbols for rock-forming minerals. Amer. Mineral., 68, 277-279.

Krogh, E.J. (1988) The garnet-clinopyroxene Fe-Mg geothermometer - a reinterpretation of existing experimental data. Contrib. Mineral. Petrol., 99, 44-48.

Le Maitre, R.W. (1976) Some problems of the projection of chemical data into mineralogical classifications. Contrib. Mineral. Petrol., 56, 181-189.

Loiselle, M.C. and Wones, D.R. (1979) Characteristics and origin of anorogenic granites. Geol. Soc. Am. Abstr. with programs, 11, 468.

London, D., Hervig, R.L. and Morgan, G.B. (1988) Melt-vapor solubilities and elemental partitioning in peraluminous granite-pegmatite systems : experimental results with Macusani glass at 200 MPa. Contrib. Mineral. Petrol. , 99, 360-373.

Luth, W.C. (1969) The systems $NaAlSi_3O_8$ and $KAlSi_3O_8$ - SiO_2 to 20 Kb and the relationship between H_2O content, pH_2O and P_{total} in granitic magmas. Am. Jnl. Sci., 267, 325-341.

Martin, A.K. and Hartnady, C.J.H. (1986) Plate tectonic development of the southwestern Indian Ocean : a revised reconstruction of East Antarctica and Africa. Jnl. Geophys. Res., 91 (B5) 86, 4767-4787.

McCarthy, T.S. and Hasty, R.A. (1976) Trace element distribution patterns and their relationship to the crystallisation of granitic melts. Geochim. Cosmochim. Acta, 40, 1351-1358.

McKenzie, D. (1985) The extraction of magma from the crust and mantle. Earth Planet. Sci. Lett., 74, 81-91.

Meineke, G.P. (1976) A structural investigation of the metamorphic rocks in a portion of the Kirwanveggan, western Dronning Maud Land, Antarctica. Unpubl. report geol. Surv., Pretoria.

Mendonidis, P. and Grantham, G.H. (1989) The distribution, petrology and geochemistry of the MunsterSuite, south coast, Natal. S. Afr. Jnl. Geol., 92, 377-388.

Miller, C.F and Mittlefehldt, D.W. (1982) Depletion of light rare-earth elements in felsic magmas. Geology, 10, 129-133.

Moecher, D.P., Essene, E.J. and Anovitz, L.M. (1988) Calculation and application of clinopyroxene-garnet-plagioclase-quartz barometers. Contrib. Mineral. Petrol., 100, 92-106.

Moller, P. and Muecke, G.K. (1984) Significance of europium anomalies in silicate melts and crystal-melt equilibria : a re-evaluation. Contrib. Mineral. Petrol., 87, 242-250.

Mori, T. and Green, D.H. (1978) Laboratory duplication of phase equilibria observed in natural lherzolites. J. Geology, 86, 87-97

Moore, J.G. (1965) Petrology of deep-sea basalt near Hawaii. Am. Jnl. Sci., 263, 40-52.

Moyes, A.B. and Barton, J.M. (1990) A review of isotopic data from western Dronning Maud Land, Antarctica. Zbl. Geo. Palaont. Teil I, 19-31.

Naney, M.T. (1983) Phase equilibria of rock-forming ferromagnesian silicates in granitic systems. Am. Jnl. Sci., 283, 993-1033.

Nash, W.P. and Crecraft, H.R. (1985) Partition coefficients for trace elements in silicic magmas. Geochim. Cosmochim. Acta, 49, 2309-2322.

Naslund, H.R. (1983) The effect of oxygen fugacity on liquid immiscibility in iron-bearing silicate systems. Am. Jnl. Sci., 283, 1034-1059.

Newton, R.C. (1983) Geobarometry of high-grade metamorphic rocks. Am. Jnl. Sci., 283, 1-28.

Newton, R.C. (1986) Metamorphic temperatures and pressures of group B and C eclogites. Geol. Soc. Am. Mem., 164, 17-30.

Newton, R.C. and Perkins, D. (1982) Thermodynamic calibration of geobarometers based on the assemblages garnet-plagioclase- orthopyroxene (cpx) - quartz. Amer. Mineral., 67, 203-222.

Norrish, K. and Hutton, J.T. (1969) An accurate X-ray spectrographic method for the analysis of a wide range of geological samples. Geochim. Cosmochim. Acta, 33, 43-453.

Pattison, D.R.M. and Newton, R.C. (1989) Reversed experimental calibration of the garnet-clinopyroxene Fe-Mg exchange thermometer. Contrib. Mineral. Petrol., 101-87-103.

Peacock, M.A. (1931) Classification of igneous rock series. Jnl. Geology., 39, 54-67.

Pearce, J.A., Harris, N.B.W. and Tindle, A.G. (1984) Trace element discrimination diagrams for the tectonic interpretation of granitic rocks. Jnl. Petrol., 25, 956-983.

Perchuk, L.L. and Lavrent'eva, I.V. (1983) Experimental investigation of exchange equilibria in the system cordierite-garnet-biotite. In: Saxena, S.K. (ed) Kinetics and Equilibrium in Mineral Reactions. Advances in Physical Geochemistry, 3, pp. 199-239, Springer-Verlag, New York.

Philpotts, J.A. (1970) Redox estimation from a calculation of Eu^{2+} and Eu^{3+} concentrations in natural phases. Earth Planet. Sci. Lett., 9, 257- 268.

Pichavant, M. (1981) An experimental study of the effect of boron on a water saturated haplogranite at 1kb vapour pressure. Contrib. Mineral. Petrol., 76, 430-439.

Pitcher, W.S. (1982) Granite type and tectonic environment. pp. 19-39 in Mountain Building Processes. ed Hsu, K.J. Academic Press. London.

Povondra, P. and Novak, M. (1986) Tourmalines in metamorphosed carbonate rocks from western Moravia, Czechoslovakia. Neues Jahrbuch fur Mineralogie Monatshefte, 6, 273-282.

Powell, R. (1978) Equilibrium Thermodynamics in Petrology. An Introduction. Harper & Row, London. 284pp.

Powell, R. and Holland, T.J.B. (1988) An internally consistent dataset with uncertainties and correlations : 3. Applications to geobarometry, worked examples and a computer program. Jnl. Metamorphic Petrol., 6, 173-204.

Pride, C. and Muecke, G.K. (1980) Rare earth element geochemistry of the Scourian complex N.W. Scotland - evidence for the granite-granulite link. Contrib. Mineral. Petrol., 73, 403-412.

Raheim, A. and Green, D.H. (1974a) Experimental determination of the temperature and pressure dependence of the Fe-Mg partition coefficient for coexisting garnet and clinopyroxene. Contrib. Mineral. Petrol., 48, 179-203.

Raheim, A. and Green, D.H. (1974b) Experimental petrology of lunar highland basalt composition and applications to models for the lunar interior. Jnl. Geology., 82, 607-622.

Ramsay, J.G. (1967) Folding and Fracturing of Rocks. McGraw-Hill Book Co., New York, 568pp.

Rapp, R.P. and Watson, E.B. (1986) Monazite solubility and dissolution kinetics: implications for the thorium and light rare earth chemistry of felsic magmas. Contrib. Mineral. Petrol.,94, 306-316.

Rapp, R.P., Ryerson, F.J. and Miller, C.F. (1986) Monazite and allanite in the crust: implications to the distribution of the LREEs, Y, U and Th. EOS, 67, 16, 386.

Ravich, M.G. and Solo'vev, D.S. (1966) Geology and Petrology of the Mountains of Central Queen Maud Land (East Antarctica). Trans. of Sci. Res. Inst. of Arct. Geol., Minist. of Geol. of U.S.S.R., vol. 141. 348pp. Trans. from Russian Israel Prog. for Sci. Trans. Jerus. 1969

Reinhardt, E.W. (1968) Phase relations in cordierite-bearing gneisses from Gananoque area, Ontario. Can. Jnl. Earth Sci., 5, 455-482.

Roots, E.F. (1953) Preliminary note on the geology of western Dronning Maud Land. Norsk geologisk Tidsskrift, 32, 17-33.

Roots, E.F. (1969) Geology of western Queen Maud Land. Plate VI, folio 12 - Geology. Antarctic map folio series. American Geophysical Union.

Sawkwa, W.N. and Chappel, B.W. (1988) Fractionation of uranium, thorium and rare earth elements in a vertically zoned granodiorite and implications for heat production distributions in the Sierra Nevada Batholith, California, U.S.A. Geochim. Cosmochim. Acta, 52, 1131-1143.

Schairer, J.F. (1950) The alkali-feldspar join in the system $NaAlSiO_4$- $KAlSiO_4$-SiO_2. Jnl. Geology., 58, 512-517.

Schoch, A.E. (1975) The Darling Granite batholith. Ann. Univ. Stell. Ser. A1 (geol), 1-104.

Schoch, A.E., Leygonie, F.E. and Burger, A.J. (1975) U-Pb ages for Cape Granites from the Saldanha Batholith: a prelimnary report. Trans. Geol. Soc. S. Afr., 78, 97-100.

Sengupta, P., Dasgupta, S., Bhattacharya, P.K. and Hariya, Y. (1989) Mixing behaviour in quaternary garnet solid solution and an extended Ellis and Green garnet-clinopyroxene geothermometer. Contrib. Mineral. Petrol., 103, 223-227.

Spear, F.S. and Kimball, K.L. (1984) Recamp. A FORTRAN IV program for estimating Fe^{3+} contents in amphibole. Computers and Geosciences., 10, 317-325.

Spear, F.S., Selverstone, J., Hickmott, D., Crowley, P. and Hodges, K.V. (1984) P-T paths from garnet zoning : a new technique for deciphering tectonic processes in crystalline terranes. Geology, 12, 87-90.

Stump, E., Smit, J.H. and Self, S. (1986) Timing of events during the late Proterozoic Orogeny, Antarctica: Geological evidence from the La Gorce Mountains. Geol. Soc. Amer. Bull., 97, 953-965.

Sun, S.-S. (1980) Lead isotopic study of young volcanic rocks from mid- ocean ridges, ocean islands and island arcs. Phil. Trans. R. Soc. Lond., A297, 409-45.

Sweeney, R.J. and Watkeys, M.K. (1990) A possible link between Mesozoic lithospheric architecture and Gondwana flood basalts. Jnl. Afr. Earth Sci., 10, 707-716.

Thomas, R.J. (1988) The petrology of the Oribi Gorge Suite: Kibaran granitoids from southern Natal. S. Afr. Jnl. Geol., 275-291.

Thompson, A.B. (1976) Mineral reactions in pelitic rocks; II Calculation of some P-T-X (Fe-Mg) phase relations. Am. Jnl. Sci., 276, 425-454.

Thompson, J.B. (1957) The graphical analysis of mineral assemblages in pelitic schists. Amer. Mineral., 42, 842-849.

Thornton, C.P. and Tuttle, O.F. (1960) Chemistry of igneous rocks. I. Differentiation index. Am. Jnl. Sci., 258., 664-684.

Tindle, A.G. and Pearce, J.A. (1981) Petrogenetic modelling of in situ fractional crystallisation in the zoned Loch Doon Pluton, Scotland. Contrib. Mineral. Petrol., 78, 196-207.

Tuttle, O.F. and Bowen, N.L. (1958) The origin of granite in the light of experimental studies in the system $NaAlSi_3O_8$-$KAlSi_3O_8$-SiO_2-H_2O. Geol. Soc. Am. Mem., 74.

Van Autenboer, T. (1972) Recent geological investigations in the Sor- Rondane Mountains, Belgicafjella, Dronning Maud Land. pp. 563-572 in Antarctic Geology and Geophysics. R.J. Adie (ed), Universiteits Forlaget, Oslo. 876pp.

Van den Kerkhof, A.M. (1988) The system CO2-CH4-N2 in fluid inclusions: theoretical modelling and geochemical applications. PhD thesis. Amsterdam (Free University). 206pp.

Van der Plas and Tobi, A.C. (1965) A graph for judging the reliability of point counting results. Am. J. Sci., 263, 87-90.

Wakita, H., Rey, P. and Schmitt, R.A. (1971) Abundances of 14 REE and 12 other trace elements in Apollo 12 samples: five igneous and one breccia rocks and four soils. Proc. 2nd Lunar Sci. Conf. p1319-1329.

Wallace, R.C. (1980) Metamorphic and associated rocks of the Kirwanveggen, Antarctica. Unpubl. rept. geol. surv., Pretoria.

Wall, V.J., Clemens, J.D. and Clarke, D.B. (1987) Models for granitoid evolution and source composition. Jnl. Geology., 95, 731-750.

Watson, E.B. (1978) Two liquid partition coefficients : experimental data and geochemical implications. Contrib. Mineral. Petrol., 56, 119-134.

Watson, E.B. (1979a) Apatite saturation in basic to intermediate magmas. Geophys. Res. Lett., 6, 937-940.

Watson, E.B. (1979b) Zircon saturation in felsic liquids: Experimental results and applications to trace element chemistry. Contrib. Mineral. Petrol., 70, 407-419.

Watson, E.B. and Capobianco, C.J. (1981) Phosphorous and the rare earth elements in felsic magmas: an assessment of the role of apatite. Geochim. Cosmochim. Acta, 45, 2349-2358.

Watson, E.B. and Harrison, T.M. (1983) Zircon saturation revisited: temperature and composition effects in a variety of crustal magma types. Earth Planet. Sci. Lett., 64, 295-304.

Weill, D.F. and Drake, M.J. (1973) Europium anomaly in plagioclase felspar experimental results and semi-quantitative model. Science, 180, 1059- 1060.

White, A.J.R. (1979) Sources of granite magmas. Geol. Soc. Am. Abs. with progr., 539.

Wickham, S.M. (1987) The segregation and emplacement of granite magmas. Jnl. Geol. Soc. Lond., 144, 281-297.

Winkler, H.G.F. (1976) Petrogenesis of Metamorphic Rocks (4th ed.). Springer Verlag. Heidelberg. 334pp.

Wolmarans, L.G. and Kent, L.E. (1982) Geological investigations in western Dronning Maud Land, Antarctica - a synthesis. S. Afr. Jnl. of Ant. Res., 93pp.

Wood, B.J. (1976) Mixing properties of tschermakitic clinopyroxenes. Amer. Mineral., 61, 599-602.

Wyllie, P.J., Huang, W., Stern, C.R. and Maaloe, S. (1976) Granitic magmas : possible and impossible sources, water contents and crystallization sequences. Can. Jnl. Earth Sci., 13, 1007-1019.

Yardley, B.W.D. (1989) An Introduction to Metamorphic Petrology. Longman Scientific and Technical, New York. 248pp.

APPENDIX 1

SAMPLING AND WHOLE ROCK ANALYTICAL DATA

The grain sizes of the various rock types were taken into consideration while sampling, recognising the transport logistical difficulties for large samples in Antarctica. Fresh samples free of surface weathering were collected. In the case of medium- to coarse-grained rocks samples of approximately 3 to 4kgs were collected whereas for fine-grained samples (eg dolerite dykes) samples of approximately 1 kg were collected. Sample site localities for the large nunataks (Jutulrora, Straumsvola, Brekkerista, Roerkulten, Joungane, Storjeon and Fuglefjellet) on the particular maps.

All samples were scrubbed with a nylon brush under running water, placed in an ultrasonic cleaner for 30 seconds and rinsed in distilled water thereafter. The samples were then dried in an oven at 120°C. After drying the samples were crushed to less than 1cm mesh size in a carbon steel jaw crusher. The crushed material was then "cone and quartered" until approximately 100g remained. The 100g samples were then milled to fine powder in a tungsten carbide swing mill. The swing mill was thoroughly cleaned with acetone between samples. Powdered samples were stored in sealed polyvinyl bottles.

X-Ray Flourescence Spectrometry

All the major and minor elements were analysed using the lithium tetraborate fusion method of Norish and Hutton (1969) whereas the trace elements were measured on pressed powder pellets.

Preparation of Norrish fusion discs

Approximately 0.5g of sample was weighed into silica crucibles which had been cleaned in a dilute solution of HCl and dried in a furnace. The sample was then placed in the furnace at 1000°C for 4hrs and then allowed to cool in a dessicator. The flux used for the fusion disc was preheated in Pt crucibles at 1000°C. Approximately 0.4g of the ashed sample were added to the spectroflux in a ratio of as close to 0.4g:2.2g of flux. The Pt crucibles were then placed in the furnace at 1000°C until the sample + flux had fused. The mixture was then allowed to anneal for three hours on a hot asbestos plate and then allowed to cool gradually.

Preparation of pressed powder pellets

Approximately 10g of sample were moistened and mixed with 1ml Mowiol solution in an agate mortar and pestle. The mixture was then compressed under 10tons in a piston cylinder for

a few seconds. The discs were then allowed to harden in an oven at 120°C for a few hours.

X-ray Flouresceence Spectrometry

All the chemical analyses of major, minor and trace elements (including La but excluding the remaining REE) on the rock samples were done on a Philips PW1404 X-ray flourescence spectrometer in the Department of Geology at the University of Natal. Calibration was controlled with a variety of international as well as in house rock and synthetic standards (see Table A1).

Prof. A.H. Wilson was responsible for the compilation of computer programmes used in the reduction of raw count data from the XRF. The following table, Table A1, shows the various instrumental settings used as well as the lower limits of detection.

Elt	Tube	Analyt. crystal	Collim.	Counter	Peak 2θ	Count time (s)	BG 2θ	Count time (s)	Std	LLD	Analyt. accuracy	Blank
SiO_2	Cr	Pet	Coarse	Flow	109.165	60	106.000	30	SiO_2 NIMD	100% 37.02%	0.004%	0.2%
Al_2O_3	Cr	"	"	"	145.040	60	139.160	30	NIML	13.9%	0.005%	0.5% SiO_2
Fe_2O_3	Au	LiF200	Fine	"	57.525	40	Blanks used		NIML	10.28%	0.001%	0.5% SiO_2 60%CaO40%SiO_2
MnO	Au	LiF200	"	"	62.990	40	"		NIML	0.78%	0.001%	0.5% SiO_2 60%CaO40%SiO_2
MgO	Cr	PX-1	Coarse	"	23.300	60	25.300	30	W-1	6.55%	0.011%	0.3% SiO_2
CaO	Cr	Pet	Fine	"	45.240	40	Blanks used		NIML	3.32%		SiO_2 40%$Fe_2O_3$60%SiO_2
K_2O	Cr	Pet	"	"	50.720	40	"		W-1	0.65%	0.003%	0.2% SiO_2 60%CaO40%SiO_2
TiO_2	Cr	Pet	"	"	36.720	40	"		W-1	1.05%	0.004%	0.2% SiO_2 60%CaO40%SiO_2
P_2O_5	Cr	Ge	Coarse	"	141.040	60	138.000 143.000	30 30	BR	1.1%	0.001%	0.2% SiO_2
Na_2O	Cr	PX-1	Fine	"	28.170	60	30.000	30	BR	3.1%	0.018%	2% SiO_2
Sc	Cr	LiF200	"	"	97.730	60	95.850 98.555	30 30	BCR	33ppm	0.3ppm	10% SiO_2 & $CaCO_3$
Ba	Cr	LiF220	"	"	115.275	60	114.500 116.500	30 30	W-1	160ppm	1ppm	±20% SiO_2 & MgO
Zn	Au	LiF200	"	"	41.795	60	39.65 46.70	30 30	NIMP	100ppm	0.3ppm	±10% SiO_2 & $CaCO_3$
Cu	Au	LiF200	"	"	45.040	60	39.65 46.70	30 30	W-1	110ppm	0.2ppm	±10% SiO_2 &$CaCO_3$
Ni	Au	LiF200	"	"	48.690	60	46.70 50.00	30 30	BR	260ppm	0.1ppm	±10% "
Cr	Au	LiF200	"	"	69.375	60	68.10 70.80	30 30	DB1	400ppm	0.6ppm	±10% SiO_2
V	Au	LiF220	"	"	123.220	60	117.10 123.80	30 30	W-1	260ppm	0.5ppm	±10% SiO_2
La	Au	LiF220	"	"	138.920	60	132.60 141.80	30 30	BR	80ppm	1.5ppm	±15% SiO_2
Zr	Rh	LiF220	"	Scint	32.045	60	29.30 34.89	30 30	AGV	230ppm	0.3ppm	±3% SiO_2
Sr	Rh	LiF220	"	"	35.830	60	34.89 36.90	30 30	W-1	190ppm	0.2ppm	±3% SiO_2
Nb	Rh	LiF220	"	"	30.420	60	29.45 34.80	30 30	GSP	23ppm	0.1ppm	±3% SiO_2
Y	Rh	LiF220	"	"	33.855	60	29.45 34.80	30 30	NIMG	45ppm	0.3ppm	±3% SiO_2
Rb	Rh	LiF220	"	"	37.960	60	34.80 41.10	30 30	NMIG	320ppm	0.4ppm	±2% SiO_2
Th	Rh	LiF220	"	"	39.250	100	36.90 41.10	30 30	GSP	105ppm	0.1ppm	±3% SiO_2

Table A1. Table showing the operating conditions for XRF analyses. All analyses were done at 50kV and 50mA. All samples were analysed using the Kα analytical lines except Ba which was analysed using the Lα analytical line.

APPENDIX 2
MICROPROBE ANALYSES AND PETROGRAPHIC DESCRIPTIONS

INTRODUCTION

Appendix 2 contains the petrographic descritions of those samples which were used for electron microprobe analyses and also contains the electron microprobe analyses with their calculated ionic formulas. The amphibole formulas were calculated using the program RECAMP by Spear and Kimball (1984). The Fe^{2+}/Fe^{3+} distrubutions for the pyroxenes were calculated after Droop (1987) and the pyroxene end members after Cawthorn and Collerson (1974). The list of abbreviations of mineral species at the back of this appendix is taken from Daly et al (1989) after Kretz (1983).

PETROGRAPHIC DESCRIPTIONS

Sample S2 - A2 AMPHIBOLITE

The rock is medium-grained (2mm grain size) and shows an equigranular granoblastic texture. Light to dark green pleochroic hornblende (58%) and untwinned plagioclase (25%) comprise the dominant minerals with minor garnet (10%), quartz (5%) and opaque minerals (2%). Garnet is poikiloblastic with inclusions of quartz, plagioclase and opaque minerals with accessory proportions of a red-brown mineral considered to be rutile. Locally garnet and hornblende are separated by a thin rind of plagioclase whereas generally hornblende and garnet are in contact. Plagioclase is locally partially saussuritized whereas garnet is locally chloritized.

Sample SA10 - Granitoid interlayered in the Sveabreen Formation

The rock is fine to medium grained (0.5mm) and displays a granoblastic texture. A strong planar fabric is defined by ribbons of recrystallised quartz, biotite and hornblende. The mineralogy includes quartz (10%), K- feldspar (25%), antipertite (25%), biotite (13%), hornblende (13%), garnet (8%) and clinopyroxene (3%). Clinopyroxene is partially replaced by light to dark green pleochroic hornblende. The antipertite is characterised by trellised exsolution lamellae of K-feldspar in plagioclase. These lamellae form up to 30% by volume.

Samples SLK1 and SK1 - Garnet-bearing Banded Gneiss

These rocks are (from Banded Gneisses of the Jutulrora Formation) characterised by porphyroblastic garnet which contains inclusions of quartz, feldspar and biotite. The garnet displays a pre-tectonic texture with the planar fabric being distorted about the garnets. The inclusions are randomly distributed in the garnet and do not show any preferred orientation or distribution. The quartz, feldspar, hornblende and biotite define a planar fabric.

Sample SA13 - Garnet bearing amphibolite in Sveabreen Formation

SA13 (from a mafic boudin in the Sveabreen Formation) is characterised by light to olive green pleochroic hornblende (50%), normally zoned plagioclase (35%), poikiloblastic garnet (5%) and accessory quartz (3%), biotite (3%), sphene (2%) and ilmenite (2%). The rock shows a granoblastic texture. Biotite is restricted to cracks. Locally hornblende and quartz are symplectitically intergrown. Garnet is poikiloblastic and contains inclusions of quartz and ilmenite. The ilmenite not included in garnet commonly forms vermicular intergrowths with hornblende.

Sample BK8 and SV9 - Banded Gneiss

Samples BK8 and SV9 (from Banded Gneisses of the Jutulrora Formation) are similar. Both samples are medium-grained, equigranular and show a weak planar fabric defined by plagioclase, clinopyroxene, hornblende and quartz. The grain boundaries are typically granoblastic. Hornblende partially replaces clinopyroxene and is itself locally partially replaced by biotite.

Sample JE39 - Garnet-bearing semipelite from Banded Gneiss

Sample JE39 (from Banded Gneisses of the Jutulrora Formation) is characterised by porphyroblastic garnets which contains inclusions of quartz, feldspar, biotite, rutile and hornblende. The garnet displays a pre-tectonic texture with the planar fabric being distorted about the garnets. The inclusions are randomly distributed in the garnet and do not show any preferred orientation or distribution. The quartz, feldspar, hornblende and biotite define a planar fabric. Biotite locally partially replaces hornblende and is developed marginal to garnet.

Sample SLK50 - Mafic boudin in Sveabreen Formation at Salknappen

Sample SLK50 (from a mafic boudin in the Sveabreen Formation) contains garnet (15%) + plagioclase (30%) + clinopyroxene (20%) + hornblende (30%) + quartz (5%) . The garnet and clinopyroxene are never in contact, being separated by symplectitic intergrowths of plagioclase + amphibole. Clinopyroxene, plagioclase, quartz and hornblende show a granoblastic texture. Clinopyroxene is commonly partially altered to hornblende. Hornblende/garnet grain boundaries appear to be stable forming granoblastic textures. The formation of hornblende + plagioclase + quartz symplectites between garnet and clinopyroxene is clearly a later reaction.

SAMPLE JE39

AMPHIBOLE 1		ALL Fe^{2+}	SUM FM=13	AV Fe^{3+}
SiO_2	42.72	6.310	6.203	6.256
Al_2O_3	15.56	2.709	2.664	2.686
Fe_2O_3	0.00	0.000	0.778	0.392
FeO	16.78	2.073	1.260	1.663
MnO	0.21	0.026	0.026	0.026
MgO	9.12	2.008	1.974	1.990
CaO	10.77	1.705	1.676	1.690
Na_2O	1.60	0.458	0.450	0.454
K_2O	0.50	0.094	0.093	0.093
TiO_2	0.88	0.098	0.096	0.097
Cr_2O_3	0.19	0.022	0.022	0.022
TOTAL	98.33			
	SUMFM	13.224	13.000	13.111
	$Fe^{2+}/Fe^{2+}+Mg$	0.508	0.390	0.455
	$Fe^{3+}/Fe^{3+}+Fe^{2+}$	0.000	0.382	0.191
	Aliv	1.690	1.797	1.744
	Alvi	1.019	0.867	0.942
	NAM4	0.072	0.324	0.199
	NA-A	0.386	0.126	0.255
	SUMA	0.481	0.219	0.349

SAMPLE JE39

AMPHIBOLE 2		ALL Fe^{2+}	SUM FM=13	AV Fe^{3+}
SiO_2	43.04	6.391	6.288	6.339
Al_2O_3	15.17	2.656	2.613	2.634
Fe_2O_3	0.00	0.000	0.743	0.375
FeO	16.99	2.110	1.333	1.718
MnO	0.13	0.016	0.016	0.016
MgO	8.97	1.985	1.953	1.969
CaO	10.97	1.745	1.717	1.731
Na_2O	1.54	0.443	0.436	0.440
K_2O	0.29	0.055	0.054	0.054
TiO_2	0.50	0.056	0.055	0.055
Cr_2O_3	0.10	0.012	0.012	0.012
TOTAL	97.70			
	SUMFM	13.213	13.000	13.106
	$Fe^{2+}/Fe^{2+}+Mg$	0.515	0.406	0.466
	$Fe^{3+}/Fe^{3+}+Fe^{2+}$	0.000	0.358	0.179
	Aliv	1.609	1.712	1.661
	Alvi	1.046	0.900	0.973
	NAM4	0.041	0.283	0.163
	NA-A	0.402	0.153	0.277
	SUMA	0.457	0.207	0.331

SAMPLE JE39

AMPHIBOLE 3		ALL Fe^{2+}	SUM FM=13	AV Fe^{3+}
SiO_2	44.09	6.441	6.330	6.385
Al_2O_3	14.98	2.580	2.535	2.558
Fe_2O_3	0.00	0.000	0.792	0.400
FeO	14.23	1.739	0.916	1.324
MgO	11.05	2.406	2.364	2.385
CaO	11.05	1.730	1.700	1.715
Na_2O	1.56	0.442	0.434	0.438
K_2O	0.30	0.056	0.055	0.055
TiO_2	0.57	0.063	0.062	0.062
TOTAL	97.83			
	SUMFM	13.228	13.000	13.113
	$Fe^{2+}/Fe^{2+}+Mg$	0.420	0.279	0.357
	$Fe^{3+}/Fe^{3+}+Fe^{2+}$	0.000	0.464	0.232
	Aliv	1.559	1.670	1.615
	Alvi	1.021	0.866	0.943
	NAM4	0.042	0.300	0.172
	NA-A	0.399	0.134	0.266
	SUMA	0.455	0.189	0.321

SAMPLE JE39

PLAGIOCLASE

ELT	WT%	IONPROP	AT PROP	CAT PRO
SiO_2	62.030	1.032	2.065	2.721
Al_2O_3	25.370	0.249	0.747	1.312
FeO	0.130	0.002	0.002	0.005
MgO	0.020	0.000	0.000	0.001
CaO	6.350	0.113	0.113	0.298
Na_2O	6.700	0.108	0.108	0.570
K_2O	0.050	0.001	0.001	0.003
TOTAL	100.650	1.505	3.035	4.910

XAn= 0.343 XAb= 0.654 XOr= 0.003

SAMPLE JE39

PLAGIOCLASE

ELT	WT%	IONPROP	AT PROP	CAT PRO
SiO_2	60.740	1.011	2.022	2.715
Al_2O_3	24.600	0.241	0.724	1.296
FeO	0.100	0.001	0.001	0.004
MgO	0.010	0.000	0.000	0.001
CaO	6.000	0.107	0.107	0.287
Na_2O	7.670	0.124	0.124	0.665
K_2O	0.060	0.001	0.001	0.003
TOTAL	99.180	1.485	2.979	4.971

XAn= 0.301 XAb= 0.696 XOr= 0.004

SAMPLE JE39
PLAGIOCLASE

ELT	WT%	IONPROP	AT PROP	CAT PRO
SiO_2	61.720	1.027	2.054	2.684
Al_2O_3	26.590	0.261	0.783	1.363
FeO	0.300	0.004	0.004	0.011
CaO	7.120	0.127	0.127	0.332
Na_2O	5.800	0.094	0.094	0.489
K_2O	0.020	0.000	0.000	0.001
TOTAL	101.550	1.513	3.062	4.880

XAn= 0.404 XAb= 0.595 XOr= 0.001

SAMPLE JE39
PLAGIOCLASE

ELT	WT%	IONPROP	AT PROP	CAT PRO
SiO_2	60.640	1.009	2.018	2.694
Al_2O_3	25.540	0.251	0.752	1.338
FeO	0.100	0.001	0.001	0.004
CaO	6.360	0.113	0.113	0.303
Na_2O	6.970	0.112	0.112	0.600
K_2O	0.004	0.000	0.000	0.000
TOTAL	99.614	1.487	2.997	4.938

XAn= 0.335 XAb= 0.665 XOr= 0.000

SAMPLE JE39
PLAGIOCLASE

ELT	WT%	IONPROP	AT PROP	CAT PRO
SiO_2	60.790	1.012	2.023	2.673
Al_2O_3	25.750	0.253	0.758	1.335
FeO	0.200	0.003	0.003	0.007
CaO	6.810	0.121	0.121	0.321
Na_2O	6.980	0.113	0.113	0.595
K_2O	0.910	0.010	0.010	0.051
TOTAL	101.440	1.511	3.028	4.983

XAn= 0.332 XAb= 0.615 XOr= 0.053

SAMPLE JE39
PLAGIOCLASE

ELT	WT%	IONPROP	AT PROP	CAT PRO
SiO_2	61.520	1.024	2.048	2.724
Al_2O_3	24.750	0.243	0.728	1.292
FeO	0.120	0.002	0.002	0.004
MgO	0.010	0.000	0.000	0.001
CaO	6.310	0.113	0.113	0.299
Na_2O	7.200	0.116	0.116	0.618
K_2O	0.030	0.000	0.000	0.002
TOTAL	99.940	1.498	3.007	4.940

XAn= 0.326 XAb= 0.672 XOr= 0.002

AMPLE JE39
IOTITE INCLUSION

LT	WT%	IONPROP	AT PROP	CAT PRO
iO_2	36.090	0.601	1.201	5.910
l_2O_3	18.340	0.180	0.540	3.541
eO	17.700	0.246	0.246	2.424
gO	13.360	0.331	0.331	3.260
a_2O	0.250	0.004	0.004	0.079
$_2O$	7.030	0.075	0.075	1.469
iO_2	1.670	0.021	0.042	0.206
OTAL	94.440	1.458	2.439	16.889

Ann= 0.426 XPhl= 0.574

AMPLE JE39
IOTITE INCLUSION

LT	WT%	IONPROP	AT PROP	CAT PRO
iO_2	35.540	0.591	1.183	5.858
l_2O_3	18.450	0.181	0.543	3.586
eO	17.280	0.241	0.241	2.382
gO	13.650	0.339	0.339	3.353
a_2O	0.300	0.005	0.005	0.096
$_2O$	7.010	0.074	0.074	1.474
iO_2	1.550	0.019	0.039	0.192
OTAL	93.780	1.450	2.423	16.942

Ann= 0.415 XPhl= 0.585

AMPLE JE39
IOTITE RIM GRAIN

LT	WT%	IONPROP	AT PROP	CAT PRO
iO_2	38.020	0.633	1.265	6.089
l_2O_3	17.260	0.169	0.508	3.259
eO	17.720	0.247	0.247	2.374
gO	12.590	0.312	0.312	3.005
a_2O	0.320	0.005	0.005	0.099
$_2O$	8.570	0.091	0.091	1.751
iO_2	2.540	0.032	0.064	0.306
r_2O_3	0.130	0.001	0.002	0.011
OTAL	97.150	1.490	2.494	16.895

Ann= 0.441 XPhl= 0.559

AMPLE JE39
ARNET

LT	WT%	WT% REC	IONPROP	AT PROP	CAT PRO
iO_2	37.530	37.530	0.625	1.249	2.986
l_2O_3	21.760	21.760	0.213	0.640	2.041
eO	30.370	30.370	0.423	0.423	2.021
nO	1.610	1.610	0.023	0.023	0.109
gO	3.820	3.820	0.095	0.095	0.453
aO	4.450	4.450	0.079	0.079	0.379
r_2O_3	0.080	0.080	0.001	0.001	0.003
OTAL	99.620	99.620	1.458	2.510	7.992

Alm= 0.682 XSp= 0.037 XPy= 0.153 XGrs= 0.128

SAMPLE JE39
GARNET

ELT	WT%	WT% REC	IONPROP	AT PROP	CAT PRO
SiO_2	37.350	37.350	0.622	1.243	2.976
Al_2O_3	21.750	21.750	0.213	0.640	2.043
FeO	29.330	29.330	0.408	0.408	1.954
MnO	1.310	1.310	0.018	0.018	0.088
MgO	4.480	4.480	0.111	0.111	0.532
CaO	4.730	4.730	0.084	0.084	0.404
Cr_2O_3	0.080	0.080	0.001	0.001	0.003
TOTAL	99.030	99.030	1.458	2.506	8.001

XAlm= 0.656 XSp= 0.030 XPy= 0.179 XGrs= 0.136

SAMPLE SLK50
PLAGIOCLASE

ELT	WT%	IONPROP	AT PROP	CAT PRO
SiO_2	48.600	0.809	1.618	2.220
Al_2O_3	33.180	0.325	0.976	1.787
CaO	15.690	0.280	0.280	0.768
Na_2O	2.450	0.040	0.040	0.217
K_2O	0.070	0.001	0.001	0.004
TOTAL	99.990	1.454	2.914	4.997

XAn= 0.776 XAb= 0.219 XOr= 0.004

SAMPLE SLK50
GARNET CORE

ELT	WT%	WT% REC	IONPROP	AT PROP	CAT PRO
SiO_2	38.650	38.650	0.643	1.286	2.969
Al_2O_3	22.540	22.540	0.221	0.663	2.041
FeO	18.800	18.800	0.262	0.262	1.208
MnO	0.440	0.440	0.006	0.006	0.029
MgO	6.190	6.190	0.154	0.154	0.709
CaO	12.810	12.810	0.228	0.228	1.054
TOTAL	99.430	99.430	1.514	2.600	8.010

XAlm= 0.403 XSp= 0.010 XPy= 0.236 XGrs= 0.352

SAMPLE SLK50
GARNET CORE

ELT	WT%	WT% REC	IONPROP	AT PROP	CAT PRO
SiO_2	38.860	38.860	0.647	1.293	2.962
Al_2O_3	22.780	22.780	0.223	0.670	2.047
FeO	19.280	19.280	0.268	0.268	1.229
MnO	0.490	0.490	0.007	0.007	0.032
MgO	6.220	6.220	0.154	0.154	0.707
CaO	12.720	12.720	0.227	0.227	1.039
TOTAL	100.350	100.350	1.526	2.620	8.015

XAlm= 0.409 XSp= 0.011 XPy= 0.235 XGrs= 0.346

SAMPLE SLK50
GARNET CORE

ELT	WT%	WT% REC	IONPROP	AT PROP	CAT PRO
SiO_2	38.400	38.400	0.639	1.278	2.945
Al_2O_3	22.510	22.510	0.221	0.662	2.036
FeO	18.890	18.890	0.263	0.263	1.212
MnO	0.480	0.480	0.007	0.007	0.031
MgO	6.150	6.150	0.153	0.153	0.703
CaO	13.280	13.280	0.237	0.237	1.091
TiO_2	0.160	0.160	0.002	0.004	0.009
TOTAL	99.870	99.870	1.521	2.604	8.028

XAlm= 0.399 XSp= 0.010 XPy= 0.231 XGrs= 0.359

SAMPLE SLK50
GARNET CORE

ELT	WT%	WT% REC	IONPROP	AT PROP	CAT PRO
SiO_2	38.810	38.810	0.646	1.292	2.964
Al_2O_3	22.730	22.730	0.223	0.669	2.047
FeO	18.630	18.630	0.259	0.259	1.190
MnO	0.450	0.450	0.006	0.006	0.029
MgO	6.090	6.090	0.151	0.151	0.693
CaO	13.150	13.150	0.234	0.234	1.076
TiO_2	0.110	0.110	0.001	0.003	0.006
TOTAL	99.970	99.970	1.521	2.615	8.006

XAlm= 0.398 XSp= 0.010 XPy= 0.232 XGrs= 0.360

SAMPLE SLK50
GARNET CORE

ELT	WT%	WT% REC	IONPROP	AT PROP	CAT PRO
SiO_2	39.020	39.020	0.649	1.299	2.969
Al_2O_3	22.750	22.750	0.223	0.670	2.041
FeO	18.940	18.940	0.264	0.264	1.205
MnO	0.450	0.450	0.006	0.006	0.029
MgO	6.230	6.230	0.155	0.155	0.706
CaO	12.800	12.800	0.228	0.228	1.044
TiO_2	0.150	0.150	0.002	0.004	0.009
TOTAL	100.340	100.340	1.527	2.625	8.002

XAlm= 0.404 XSp= 0.010 XPy= 0.237 XGrs= 0.350

SAMPLE SLK50
GARNET CORE

ELT	WT%	WT% REC	IONPROP	AT PROP	CAT PRO
SiO_2	38.910	38.910	0.648	1.295	2.967
Al_2O_3	22.800	22.800	0.224	0.671	2.050
FeO	18.640	18.640	0.259	0.259	1.189
MnO	0.460	0.460	0.006	0.006	0.030
MgO	6.230	6.230	0.155	0.155	0.708
CaO	13.040	13.040	0.233	0.233	1.065
TOTAL	100.080	100.080	1.524	2.619	8.008

XAlm= 0.397 XSp= 0.010 XPy= 0.237 XGrs= 0.356

SAMPLE SLK50
CLINOPYROXENE CORE

ELT	WT%	WT% REC	IONPROP	AT PROP	CAT PRO
SiO_2	51.130	51.130	0.851	1.702	1.874
Al_2O_3	6.490	6.490	0.064	0.191	0.281
FeO	4.860	4.860	0.068	0.068	0.149
MgO	13.200	13.200	0.327	0.327	0.721
CaO	23.370	23.370	0.417	0.417	0.918
Na_2O	0.640	0.640	0.010	0.010	0.045
TiO_2	0.350	0.350	0.004	0.009	0.010
TOTAL	100.040	100.040	1.741	2.724	3.998

EN	FS	WO	AC	JA	CATI	CAFE	CATS
0.393	0.081	0.437	0.000	0.025	0.005	0.000	0.059

SAMPLE SLK50
CLINOPYROXENE CORE

ELT	WT%	WT% REC	IONPROP	AT PROP	CAT PRO
SiO_2	50.810	50.810	0.846	1.691	1.878
Al_2O_3	6.360	6.360	0.062	0.187	0.277
FeO	4.720	4.720	0.066	0.066	0.146
MgO	12.970	12.970	0.322	0.322	0.714
CaO	23.400	23.400	0.417	0.417	0.927
Na_2O	0.610	0.610	0.010	0.010	0.044
TiO_2	0.340	0.340	0.004	0.009	0.009
TOTAL	99.210	99.210	1.727	2.701	0.000

EN	FS	WO	AC	JA	CATI	CAFE	CATS
0.390	0.080	0.442	0.000	0.024	0.005	0.000	0.059

SAMPLE SLK50
CLINOPYROXENE CORE

ELT	WT%	WT% REC	IONPROP	AT PROP	CAT PRO
SiO_2	52.180	52.180	0.868	1.737	1.902
Al_2O_3	5.360	5.360	0.053	0.158	0.230
FeO	4.630	4.630	0.064	0.064	0.141
MgO	13.630	13.630	0.338	0.338	0.741
CaO	23.910	23.910	0.426	0.426	0.934
Na_2O	0.370	0.370	0.006	0.006	0.026
TiO_2	0.380	0.380	0.005	0.010	0.010
TOTAL	100.460	100.460	1.761	2.739	0.000

EN	FS	WO	AC	JA	CATI	CAFE	CATS
0.402	0.077	0.452	0.000	0.014	0.006	0.000	0.050

SAMPLE SLK50
CLINOPYROXENE RIM

ELT	WT%	WT% REC	IONPROP	AT PROP	CAT PRO
SiO_2	50.540	50.540	0.841	1.682	1.884
Al_2O_3	5.330	5.330	0.052	0.157	0.234
FeO	7.070	7.070	0.098	0.098	0.220
MgO	12.990	12.990	0.322	0.322	0.722
CaO	22.730	22.730	0.405	0.405	0.908
Na_2O	0.320	0.320	0.005	0.005	0.023
TiO_2	0.350	0.350	0.004	0.009	0.010
TOTAL	99.330	99.330	1.729	2.679	4.001

EN	FS	WO	AC	JA	CATI	CAFE	CATS
0.385	0.118	0.428	0.000	0.012	0.005	0.000	0.051

SAMPLE SLK50
CLINOPYROXENE RIM

ELT	WT%	WT% REC	IONPROP	AT PROP	CAT PRO
SiO_2	51.440	51.440	0.856	1.712	1.924
Al_2O_3	3.410	3.410	0.033	0.100	0.150
FeO	7.810	7.810	0.109	0.109	0.244
MnO	0.110	0.110	0.002	0.002	0.003
MgO	13.890	13.890	0.344	0.344	0.774
CaO	21.890	21.890	0.390	0.390	0.877
Na_2O	0.310	0.310	0.005	0.005	0.022
TiO_2	0.260	0.260	0.003	0.007	0.007
TOTAL	99.120	99.120	1.743	2.669	4.004

EN	FS	WO	AC	JA	CATI	CAFE	CATS
0.404	0.127	0.424	0.000	0.012	0.004	0.000	0.030

SAMPLE SLK50
CLINOPYROXENE RIM

ELT	WT%	WT% REC	IONPROP	AT PROP	CAT PRO
SiO_2	50.280	50.280	0.837	1.673	1.886
Al_2O_3	5.210	5.210	0.051	0.153	0.230
FeO	7.610	7.610	0.106	0.106	0.239
MnO	0.110	0.110	0.002	0.002	0.003
MgO	13.190	13.190	0.327	0.327	0.738
CaO	21.560	21.560	0.384	0.384	0.867
Na_2O	0.400	0.400	0.006	0.006	0.029
K_2O	0.050	0.050	0.001	0.001	0.002
TiO_2	0.340	0.340	0.004	0.009	0.010
TOTAL	98.750	98.750	1.718	2.661	4.005

EN	FS	WO	AC	JA	CATI	CAFE	CATS
0.393	0.127	0.409	0.000	0.017	0.005	0.000	0.048

SAMPLE SLK50
CLINOPYROXENE RIM

ELT	WT%	WT% REC	IONPROP	AT PROP	CAT PRO
SiO_2	50.970	50.970	0.848	1.696	1.879
Al_2O_3	5.800	5.800	0.057	0.171	0.252
FeO	6.220	6.220	0.087	0.087	0.192
MgO	13.040	13.040	0.323	0.323	0.717
CaO	23.380	23.380	0.417	0.417	0.924
Na_2O	0.380	0.380	0.006	0.006	0.027
TiO_2	0.320	0.320	0.004	0.008	0.009
TOTAL	100.110	100.110	1.742	2.708	3.999

EN	FS	WO	AC	JA	CATI	CAFE	CATS
0.385	0.103	0.436	0.000	0.015	0.005	0.000	0.056

SAMPLE SLK50
GARNET RIM

ELT	WT%	WT% REC	IONPROP	AT PROP	CAT PRO
SiO_2	38.060	38.060	0.633	1.267	2.971
Al_2O_3	22.290	22.290	0.219	0.656	2.051
FeO	21.490	21.490	0.299	0.299	1.403
MnO	0.590	0.590	0.008	0.008	0.039
MgO	4.510	4.510	0.112	0.112	0.525
CaO	12.140	12.140	0.216	0.216	1.015
TOTAL	99.080	99.080	1.488	2.558	8.004

XAlm= 0.470 XSp= 0.013 XPy= 0.176 XGrs= 0.341

SAMPLE SLK50
GARNET RIM

ELT	WT%	WT% REC	IONPROP	AT PROP	CAT PRO
SiO_2	38.170	38.170	0.635	1.270	2.969
Al_2O_3	22.350	22.350	0.219	0.658	2.050
FeO	21.110	21.110	0.294	0.294	1.373
MnO	0.750	0.750	0.011	0.011	0.049
MgO	4.550	4.550	0.113	0.113	0.528
CaO	12.430	12.430	0.222	0.222	1.036
TOTAL	99.360	99.360	1.493	2.567	8.006

XAlm= 0.460 XSp= 0.017 XPy= 0.177 XGrs= 0.347

SAMPLE SLK50
HORNBLENDE RIM

		LOWER BOUND= ALL Fe^{2+}	UPPER BOUND= SUM Na=15	
		ALL Fe^{2+}	SUM Na=15	AV Fe^{3+}
SiO_2	51.52	SiO_2	7.367	7.299	7.333
Al_2O_3	5.90	Al_2O_3	0.995	0.985	0.990
Fe_2O_3	0.00	Fe_2O_3	0.000	0.419	0.211
FeO	9.80	FeO	1.172	0.742	0.956
MnO	0.12	MnO	0.015	0.014	0.014
MgO	16.79	MgO	3.578	3.545	3.561
CaO	11.79	CaO	1.806	1.790	1.798
Na_2O	0.60	Na_2O	0.166	0.165	0.166
K_2O	0.25	K_2O	0.046	0.045	0.045
TiO_2	0.37	TiO_2	0.040	0.039	0.040
Cr_2O_3	0.11	Cr_2O_3	0.012	0.012	0.012
TOTAL	97.25	SUMFM	13.165	13.045	13.105
		$Fe^{2+}/Fe^{2+}+Mg$	0.247	0.173	0.212
		$Fe^{3+}/Fe^{3+}+Fe^{2+}$	0.000	0.361	0.181
		Aliv	0.633	0.701	0.667
		Alvi	0.361	0.285	0.323
		NAM4	0.028	0.165	0.097
		NA-A	0.138	-0.000	0.069
		SUMA	0.184	0.045	0.114

SAMPLE SLK50
HORNBLENDE RIM

		LOWER BOUND= ALL Fe^{2+}	UPPER BOUND= SUM FM=13	
		ALL Fe^{2+}	SUM FM=13	AV Fe^{3+}
SiO_2	50.44	SiO_2	7.247	7.173	7.209
Al_2O_3	6.88	Al_2O_3	1.165	1.153	1.159
Fe_2O_3	0.00	Fe_2O_3	0.000	0.470	0.236
FeO	10.85	FeO	1.304	0.820	1.061
MgO	15.74	MgO	3.370	3.336	3.353
CaO	11.98	CaO	1.844	1.825	1.835
Na_2O	0.65	Na_2O	0.181	0.179	0.180
K_2O	0.30	K_2O	0.055	0.054	0.055
TiO_2	0.45	TiO_2	0.049	0.048	0.048
Cr_2O_3	0.15	Cr_2O_3	0.017	0.017	0.017
TOTAL	97.44	SUMFM	13.134	13.000	13.067
		$Fe^{2+}/Fe^{2+}+Mg$	0.279	0.197	0.240
		$Fe^{3+}/Fe^{3+}+Fe^{2+}$	0.000	0.365	0.182
		Aliv	0.753	0.827	0.791
		Alvi	0.412	0.326	0.369
		NAM4	0.021	0.175	0.098
		NA-A	0.160	0.005	0.082
		SUMA	0.215	0.059	0.136

SAMPLE SLK50
HORNBLENDE RIM

		LOWER BOUND= ALL Fe^{2+}	UPPER BOUND= SUM FM=13	
		ALL Fe^{2+}	SUM FM=13	AV Fe^{3+}
SiO_2	48.86	SiO_2 7.087	7.054	7.071
Al_2O_3	8.63	Al_2O_3 1.476	1.469	1.472
Fe_2O_3	0.00	Fe_2O_3 0.000	0.214	0.107
FeO	10.91	FeO 1.324	1.103	1.213
MgO	14.30	MgO 3.091	3.077	3.084
CaO	11.99	CaO 1.864	1.855	1.859
Na_2O	0.87	Na_2O 0.245	0.244	0.244
K_2O	0.49	K_2O 0.091	0.090	0.090
TiO_2	0.76	TiO_2 0.083	0.083	0.083
TOTAL	96.81	SUMFM 13.061	13.000	13.030
		$Fe^{2+}/Fe^{2+}+Mg$ 0.300	0.264	0.282
		$Fe^{3+}/Fe^{3+}+Fe^{2+}$ 0.000	0.162	0.081
		Aliv 0.913	0.946	0.929
		Alvi 0.563	0.523	0.543
		NAM4 0.076	0.145	0.111
		NA-A 0.169	0.098	0.134
		SUMA 0.260	0.189	0.224

SAMPLE SLK50
HORNBLENDE RIM

		LOWER BOUND= ALL Fe^{2+}	UPPER BOUND= SUM FM=13	
		ALL Fe^{2+}	SUM FM=13	AV Fe^{3+}
SiO_2	50.44	SiO_2 7.247	7.173	7.209
Al_2O_3	6.88	Al_2O_3 1.165	1.153	1.159
Fe_2O_3	0.00	Fe_2O_3 0.000	0.470	0.236
FeO	10.85	FeO 1.304	0.820	1.061
MgO	15.74	MgO 3.370	3.336	3.353
CaO	11.98	CaO 1.844	1.825	1.835
Na_2O	0.65	Na_2O 0.181	0.179	0.180
K_2O	0.30	K_2O 0.055	0.054	0.055
TiO_2	0.45	TiO_2 0.049	0.048	0.048
Cr_2O_3	0.15	Cr_2O_3 0.017	0.017	0.017
TOTAL	97.44	SUMFM 13.134	13.000	13.067
		$Fe^{2+}/Fe^{2+}+Mg$ 0.279	0.197	0.240
		$Fe^{3+}/Fe^{3+}+Fe^{2+}$ 0.000	0.365	0.182
		Aliv 0.753	0.827	0.791
		Alvi 0.412	0.326	0.369
		NAM4 0.021	0.175	0.098
		NA-A 0.160	0.005	0.082
		SUMA 0.215	0.059	0.136

SAMPLE SLK50

HORNBLENDE RIM

		LOWER BOUND= ALL Fe^{2+}		UPPER BOUND= SUM FM=13
			ALL Fe^{2+}	SUM FM=13	AV Fe^{3+}
SiO_2	48.86	SiO_2	7.087	7.054	7.071
Al_2O_3	8.63	Al_2O_3	1.476	1.469	1.472
Fe_2O_3	0.00	Fe_2O_3	0.000	0.214	0.107
FeO	10.91	FeO	1.324	1.103	1.213
MgO	14.30	MgO	3.091	3.077	3.084
CaO	11.99	CaO	1.864	1.855	1.859
Na_2O	0.87	Na_2O	0.245	0.244	0.244
K_2O	0.49	K_2O	0.091	0.090	0.090
TiO_2	0.76	TiO_2	0.083	0.083	0.083
TOTAL	96.81	SUMFM	13.061	13.000	13.030
		$Fe^{2+}/Fe^{2+}+Mg$	0.300	0.264	0.282
		$Fe^{3+}/Fe^{3+}+Fe^{2+}$	0.000	0.162	0.081
		Aliv	0.913	0.946	0.929
		Alvi	0.563	0.523	0.543
		NAM4	0.076	0.145	0.111
		NA-A	0.169	0.098	0.134
		SUMA	0.260	0.189	0.224

SAMPLE S2

GARNET

ELT	WT%	WT% REC	IONPROP	AT PROP	CAT PRO
SiO_2	37.990	37.990	0.632	1.264	3.021
Al_2O_3	21.030	21.030	0.206	0.619	1.972
FeO	25.690	25.690	0.358	0.358	1.709
MnO	1.320	1.320	0.019	0.019	0.089
MgO	2.980	2.980	0.074	0.074	0.353
CaO	9.810	9.810	0.175	0.175	0.836
TiO_2	0.110	0.110	0.001	0.003	0.007
TOTAL	98.930	98.930	1.465	2.511	7.986

XAlm= 0.572 XSp= 0.030 XPy= 0.118 XGrs= 0.280

SAMPLE S2

GARNET

ELT	WT%	WT% REC	IONPROP	AT PROP	CAT PRO
SiO_2	38.090	38.090	0.634	1.268	3.008
Al_2O_3	21.540	21.540	0.211	0.634	2.006
FeO	25.250	25.250	0.351	0.351	1.668
MnO	1.360	1.360	0.019	0.019	0.091
MgO	3.050	3.050	0.076	0.076	0.359
CaO	9.920	9.920	0.177	0.177	0.839
TiO_2	0.150	0.150	0.002	0.004	0.009
TOTAL	99.360	99.360	1.470	2.529	7.980

XAlm= 0.564 XSp= 0.031 XPy= 0.121 XGrs= 0.284

SAMPLE S2
GARNET

ELT	WT%	WT% REC	IONPROP	AT PROP	CAT PRO
SiO_2	38.400	38.400	0.639	1.278	3.004
Al_2O_3	21.700	21.700	0.213	0.639	2.001
FeO	25.110	25.110	0.349	0.349	1.643
MnO	0.530	0.530	0.007	0.007	0.035
MgO	2.550	2.550	0.063	0.063	0.297
CaO	11.940	11.940	0.213	0.213	1.001
Na_2O	0.070	0.070	0.001	0.001	0.011
TiO_2	0.090	0.090	0.001	0.002	0.005
TOTAL	100.390	100.390	1.487	2.553	7.996

XAlm= 0.552 XSp= 0.012 XPy= 0.100 XGrs= 0.336

SAMPLE S2
GARNET

ELT	WT%	WT% REC	IONPROP	AT PROP	CAT PRO
SiO_2	38.010	38.010	0.633	1.265	2.989
Al_2O_3	21.700	21.700	0.213	0.639	2.012
FeO	25.090	25.090	0.349	0.349	1.650
MnO	0.550	0.550	0.008	0.008	0.037
MgO	2.550	2.550	0.063	0.063	0.299
CaO	11.990	11.990	0.214	0.214	1.010
Na_2O	0.120	0.120	0.002	0.002	0.018
TOTAL	100.010	100.010	1.481	2.540	8.015

XAlm= 0.551 XSp= 0.012 XPy= 0.100 XGrs= 0.337

SAMPLE S2
PLAGIOCLASE

ELT	WT%	IONPROP	AT PROP	CAT PRO
SiO_2	60.290	1.003	2.007	2.645
Al_2O_3	26.560	0.261	0.782	1.374
FeO	0.290	0.004	0.004	0.011
MgO	0.013	0.000	0.000	0.001
CaO	7.940	0.142	0.142	0.373
Na_2O	6.220	0.100	0.100	0.529
K_2O	0.040	0.000	0.000	0.002
TOTAL	101.353	1.511	3.035	4.934

XAn= 0.413 XAb= 0.585 XOr= 0.002

SAMPLE S2
PLAGIOCLASE

ELT	WT%	IONPROP	AT PROP	CAT PRO
SiO_2	59.560	0.991	1.982	2.636
Al_2O_3	26.390	0.259	0.777	1.377
FeO	0.300	0.004	0.004	0.011
MgO	0.007	0.000	0.000	0.000
CaO	7.950	0.142	0.142	0.377
Na_2O	6.360	0.103	0.103	0.546
K_2O	0.050	0.001	0.001	0.003
TOTAL	100.617	1.499	3.008	4.950

XAn= 0.407 XAb= 0.590 XOr= 0.003

SAMPLE S2
PLAGIOCLASE

ELT	WT%	IONPROP	AT PROP	CAT PRO
SiO_2	57.910	0.964	1.927	2.576
Al_2O_3	27.430	0.269	0.807	1.439
FeO	0.330	0.005	0.005	0.012
MgO	0.010	0.000	0.000	0.001
CaO	8.960	0.160	0.160	0.427
Na_2O	5.750	0.093	0.093	0.496
K_2O	0.045	0.000	0.000	0.003
TOTAL	100.435	1.491	2.993	4.954

XAn= 0.461 XAb= 0.536 XOr= 0.003

SAMPLE S2
PLAGIOCLASE

ELT	WT%	IONPROP	AT PROP	CAT PRO
SiO_2	57.990	0.965	1.930	2.591
Al_2O_3	26.940	0.264	0.793	1.419
FeO	0.330	0.005	0.005	0.012
MgO	0.020	0.000	0.000	0.001
CaO	8.480	0.151	0.151	0.406
Na_2O	6.190	0.100	0.100	0.536
K_2O	0.050	0.001	0.001	0.003
TOTAL	100.000	1.486	2.980	4.969

XAn= 0.430 XAb= 0.567 XOr= 0.003

SAMPLE S2
HORNBLENDE

			LOWER BOUND= ALL Fe^{2+}	SUM Ca=15 SUM FM=13	UPPER BOUND= SUM FM=13 SUM Ca=15	SUM FM=13 AV Fe^{3+}
SiO_2	42.92	SiO_2	6.370	6.304	6.365	6.334
Al_2O_3	13.54	Al_2O_3	2.369	2.345	2.367	2.356
Fe_2O_3	0.00	Fe_2O_3	0.000	0.475	0.032	0.254
FeO	18.64	FeO	2.314	1.815	2.280	2.047
MgO	8.84	MgO	1.955	1.935	1.954	1.944
CaO	11.79	CaO	1.875	1.855	1.874	1.864
Na_2O	1.57	Na_2O	0.452	0.447	0.451	0.449
K_2O	0.86	K_2O	0.163	0.161	0.163	0.162
TiO_2	1.15	TiO_2	0.128	0.127	0.128	0.128
TOTAL	99.31	SUMFM	13.136	13.000	13.126	13.063
		$Fe^{2+}/Fe^{2+}+Mg$	0.542	0.484	0.539	0.513
		$Fe^{3+}/Fe^{3+}+Fe^{2+}$	0.000	0.207	0.014	0.110
		Aliv	1.630	1.696	1.635	1.666
		Alvi	0.738	0.648	0.732	0.690
		NAM4	-0.010	0.145	-0.000	0.073
		NA-A	0.462	0.303	0.451	0.377
		SUMA	0.625	0.464	0.614	0.539

SAMPLE S2
HORNBLENDE

			LOWER BOUND= ALL Fe^{2+}	SUM Ca=15 SUM FM=13	UPPER BOUND= SUM Ca=15	SUM FM=13 AV Fe^{3+}
SiO_2	43.04	SiO_2	6.376	6.309	6.372	6.340
Al_2O_3	13.50	Al_2O_3	2.358	2.333	2.356	2.345
Fe_2O_3	0.00	Fe_2O_3	0.000	0.479	0.030	0.256
FeO	18.75	FeO	2.323	1.820	2.292	2.055
MnO	0.12	MnO	0.015	0.015	0.015	0.015
MgO	8.75	MgO	1.932	1.912	1.930	1.921
CaO	11.80	CaO	1.873	1.853	1.872	1.863
Na_2O	1.57	Na_2O	0.451	0.446	0.451	0.448
K_2O	0.81	K_2O	0.153	0.151	0.153	0.152
TiO_2	1.20	TiO_2	0.134	0.132	0.134	0.133
TOTAL	99.54	SUMFM	13.137	13.000	13.128	13.064
		$Fe^{2+}/Fe^{2+}+Mg$	0.546	0.488	0.543	0.517
		$Fe^{3+}/Fe^{3+}+Fe^{2+}$	0.000	0.208	0.013	0.111
		Aliv	1.624	1.691	1.628	1.660
		Alvi	0.733	0.642	0.728	0.685
		NAM4	-0.010	0.147	0.000	0.074
		NA-A	0.461	0.300	0.451	0.375
		SUMA	0.614	0.451	0.604	0.527

SAMPLE S2
HORNBLENDE

			LOWER BOUND= ALL Fe^{2+}	SUM Ca=15 SUM FM=13	UPPER BOUND= SUM Ca=15	SUM FM=13 AV Fe^{3+}
SiO_2	42.55	SiO_2	6.380	6.321	6.370	6.345
Al_2O_3	13.22	Al_2O_3	2.337	2.315	2.333	2.324
Fe_2O_3	0.00	Fe_2O_3	0.000	0.425	0.072	0.249
FeO	18.63	FeO	2.336	1.889	2.261	2.074
MnO	0.10	MnO	0.013	0.013	0.013	0.013
MgO	8.63	MgO	1.928	1.911	1.925	1.918
CaO	11.84	CaO	1.902	1.885	1.899	1.892
Na_2O	1.55	Na_2O	0.451	0.446	0.450	0.448
K_2O	0.79	K_2O	0.151	0.150	0.151	0.150
TiO_2	1.13	TiO_2	0.127	0.126	0.127	0.127
TOTAL	98.44	SUMFM	13.121	13.000	13.101	13.050
		$Fe^{2+}/Fe^{2+}+Mg$	0.548	0.497	0.540	0.520
		$Fe^{3+}/Fe^{3+}+Fe^{2+}$	0.000	0.184	0.031	0.107
		Aliv	1.620	1.679	1.630	1.655
		Alvi	0.717	0.636	0.703	0.669
		NAM4	-0.023	0.115	-0.000	0.058
		NA-A	0.474	0.331	0.450	0.390
		SUMA	0.625	0.481	0.601	0.541

SAMPLE S2

HORNBLENDE

			LOWER BOUND= ALL Fe^{2+}	SUM Ca=15 SUM FM=13	UPPER BOUND= SUM FM=13 SUM Ca=15	AV Fe^{3+}
SiO_2	42.11	SiO_2	6.326	6.275	6.322	6.298
Al_2O_3	13.32	Al_2O_3	2.359	2.340	2.357	2.349
Fe_2O_3	0.00	Fe_2O_3	0.000	0.374	0.033	0.204
FeO	18.38	FeO	2.309	1.917	2.275	2.095
MnO	0.14	MnO	0.018	0.018	0.018	0.018
MgO	8.57	MgO	1.919	1.903	1.917	1.910
CaO	11.83	CaO	1.904	1.889	1.903	1.896
Na_2O	1.59	Na_2O	0.463	0.459	0.463	0.461
K_2O	0.80	K_2O	0.153	0.152	0.153	0.153
TiO_2	1.55	TiO_2	0.175	0.174	0.175	0.174
TOTAL	98.29	SUMFM	13.106	13.000	13.097	13.048
		$Fe^{2+}/Fe^{2+}+Mg$	0.546	0.502	0.543	0.523
		$Fe^{3+}/Fe^{3+}+Fe^{2+}$	0.000	0.163	0.014	0.089
		Aliv	1.674	1.725	1.678	1.702
		Alvi	0.685	0.615	0.679	0.647
		NAM4	-0.011	0.111	-0.000	0.056
		NA-A	0.474	0.348	0.463	0.405
		SUMA	0.627	0.500	0.616	0.558

SAMPLE BK8

CLINOPYROXENE CORE

ELT	WT%	WT% REC	IONPROP	AT PROP	CAT PRO
SiO_2	51.870	51.870	0.863	1.726	1.948
Al_2O_3	1.930	1.930	0.019	0.057	0.085
FeO	8.320	8.320	0.116	0.116	0.261
MnO	0.320	0.320	0.005	0.005	0.010
MgO	12.950	12.950	0.321	0.321	0.725
CaO	23.380	23.380	0.417	0.417	0.941
Na_2O	0.863	0.863	0.014	0.014	0.063
TiO_2	0.075	0.075	0.001	0.002	0.002
Cr_2O_3	0.087	0.087	0.001	0.001	0.002
TOTAL	99.795	99.795	1.756	2.659	4.038

EN	FS	WO	AC	JA	CATI	CAFE	CATS
0.364	0.131	0.467	0.000	0.032	0.001	0.001	0.005

SAMPLE BK8

CLINOPYROXENE CORE

ELT	WT%	WT% REC	IONPROP	AT PROP	CAT PRO
SiO_2	51.450	51.450	0.856	1.712	1.941
Al_2O_3	1.833	1.833	0.018	0.054	0.082
FeO	8.620	8.620	0.120	0.120	0.272
MnO	0.340	0.340	0.005	0.005	0.011
MgO	12.930	12.930	0.321	0.321	0.727
CaO	23.320	23.320	0.416	0.416	0.943
Na_2O	0.860	0.860	0.014	0.014	0.063
TiO_2	0.130	0.130	0.002	0.003	0.004
Cr_2O_3	0.110	0.110	0.001	0.001	0.002
TOTAL	99.593	99.593	1.752	2.646	4.045

EN	FS	WO	AC	JA	CATI	CAFE	CATS
0.362	0.136	0.465	0.000	0.031	0.002	0.001	0.003

SAMPLE BK8
PLAGIOCLASE

ELT	WT%	IONPROP	AT PROP	CAT PRO
SiO_2	62.440	1.039	2.078	2.796
Al_2O_3	22.690	0.223	0.668	1.198
CaO	4.780	0.085	0.085	0.229
Na_2O	8.650	0.140	0.140	0.751
K_2O	0.190	0.002	0.002	0.011
TOTAL	98.750	1.489	2.973	4.986

XAn= 0.231 XAb= 0.758 XOr= 0.011

SAMPLE BK8
PLAGIOCLASE

ELT	WT%	IONPROP	AT PROP	CAT PRO
SiO_2	62.540	1.041	2.082	2.784
Al_2O_3	22.920	0.225	0.675	1.203
CaO	5.010	0.089	0.089	0.239
Na_2O	8.910	0.144	0.144	0.769
K_2O	0.170	0.002	0.002	0.010
TOTAL	99.550	1.501	2.991	5.004

XAn= 0.235 XAb= 0.756 XOr= 0.009

SAMPLE BK8
PLAGIOCLASE

ELT	WT%	IONPROP	AT PROP	CAT PRO
SiO_2	62.300	1.037	2.074	2.802
Al_2O_3	22.360	0.219	0.658	1.186
CaO	4.820	0.086	0.086	0.232
Na_2O	8.740	0.141	0.141	0.762
K_2O	0.160	0.002	0.002	0.009
TOTAL	98.380	1.485	2.960	4.991

XAn= 0.231 XAb= 0.759 XOr= 0.009

SAMPLE BK8
CLINOPYROXENE RIM

ELT	WT%	WT% REC	IONPROP	AT PROP	CAT PRO
SiO_2	52.350	52.350	0.871	1.742	1.967
Al_2O_3	0.912	0.912	0.009	0.027	0.040
FeO	7.870	7.870	0.110	0.110	0.247
MnO	0.320	0.320	0.005	0.005	0.010
MgO	13.580	13.580	0.337	0.337	0.761
CaO	23.970	23.970	0.427	0.427	0.965
Na_2O	0.590	0.590	0.010	0.010	0.043
TOTAL	99.592	99.592	1.768	2.657	4.034

EN	FS	WO	AC	JA	CATI	CAFE	CATS
0.378	0.122	0.479	0.001	0.020	0.000	0.000	0.000

SAMPLE BK8
CLINOPYROXENE RIM

ELT	WT%	WT% REC	IONPROP	AT PROP	CAT PRO
SiO_2	52.090	52.090	0.867	1.734	1.969
Al_2O_3	0.943	0.943	0.009	0.028	0.042
FeO	7.896	7.896	0.110	0.110	0.250
MnO	0.275	0.275	0.004	0.004	0.009
MgO	13.540	13.540	0.336	0.336	0.763
CaO	23.590	23.590	0.421	0.421	0.956
Na_2O	0.591	0.591	0.010	0.010	0.043
TOTAL	98.925	98.925	1.756	2.641	4.031

EN	FS	WO	AC	JA	CATI	CAFE	CATS
0.380	0.124	0.475	0.001	0.021	0.000	0.000	0.000

SAMPLE SV9
PLAGIOCLASE

ELT	WT%	IONPROP	AT PROP	CAT PRO
SiO_2	60.790	1.012	2.023	2.651
Al_2O_3	26.140	0.256	0.769	1.344
FeO	0.190	0.003	0.003	0.007
CaO	7.930	0.141	0.141	0.371
Na_2O	7.060	0.114	0.114	0.597
K_2O	0.220	0.002	0.002	0.012
TOTAL	102.330	1.528	3.053	4.982

XAn= 0.378 XAb= 0.609 XOr= 0.012

SAMPLE SV9
PLAGIOCLASE

ELT	WT%	IONPROP	AT PROP	CAT PRO
SiO_2	59.050	0.983	1.965	2.655
Al_2O_3	25.190	0.247	0.741	1.335
CaO	7.830	0.140	0.140	0.377
Na_2O	6.300	0.102	0.102	0.549
K_2O	1.210	0.013	0.013	0.069
TOTAL	99.580	1.484	2.961	4.987

XAn= 0.379 XAb= 0.552 XOr= 0.070

SAMPLE SV9
PLAGIOCLASE

ELT	WT%	IONPROP	AT PROP	CAT PRO
SiO_2	59.640	0.993	1.985	2.651
Al_2O_3	25.630	0.251	0.754	1.343
CaO	7.910	0.141	0.141	0.377
Na_2O	6.940	0.112	0.112	0.598
K_2O	0.260	0.003	0.003	0.015
TOTAL	100.380	1.500	2.995	4.984

XAn= 0.381 XAb= 0.604 XOr= 0.015

SAMPLE SV9
PLAGIOCLASE

ELT	WT%	IONPROP	AT PROP	CAT PRO
SiO_2	60.240	1.002	2.005	2.671
Al_2O_3	25.270	0.248	0.744	1.321
CaO	7.430	0.132	0.132	0.353
Na_2O	7.350	0.119	0.119	0.632
K_2O	0.250	0.003	0.003	0.014
TOTAL	100.540	1.504	3.002	4.991

XAn= 0.353 XAb= 0.633 XOr= 0.014

SAMPLE SV9
CLINOPYROXENE

ELT	WT%	WT% REC	IONPROP	AT PROP	CAT PRO
SiO_2	52.800	52.800	0.879	1.757	1.957
Al_2O_3	1.400	1.400	0.014	0.041	0.061
Fe_2O_3	1.815	1.815	0.011	0.034	0.051
FeO	5.407	5.407	0.075	0.075	0.168
MnO	0.240	0.240	0.003	0.003	0.008
MgO	13.760	13.760	0.341	0.341	0.760
CaO	24.300	24.300	0.433	0.433	0.965
Na_2O	0.410	0.410	0.007	0.007	0.029
TiO_2	0.080	0.080	0.001	0.002	0.002
TOTAL	100.212	100.212	1.765	2.694	4.000

EN	FS	WO	AC	JA	CATI	CAFE	CATS
0.385	0.085	0.481	0.000	0.015	0.001	0.026	0.007

SAMPLE SV9
CLINOPYROXENE

ELT	WT%	WT% REC	IONPROP	AT PROP	CAT PRO
SiO_2	52.640	52.640	0.876	1.752	1.963
Al_2O_3	1.480	1.480	0.015	0.044	0.065
Fe_2O_3	1.201	1.201	0.008	0.023	0.034
FeO	5.749	5.749	0.080	0.080	0.179
MnO	0.270	0.270	0.004	0.004	0.009
MgO	13.550	13.550	0.336	0.336	0.753
CaO	24.130	24.130	0.430	0.430	0.964
Na_2O	0.420	0.420	0.007	0.007	0.030
TiO_2	0.100	0.100	0.001	0.003	0.003
TOTAL	99.540	99.540	1.756	2.678	4.000

EN	FS	WO	AC	JA	CATI	CAFE	CATS
0.384	0.091	0.483	0.000	0.015	0.001	0.017	0.007

SAMPLE SV9
CLINOPYROXENE

ELT	WT%	WT% REC	IONPROP	AT PROP	CAT PRO
SiO_2	52.520	52.520	0.874	1.748	1.959
Al_2O_3	1.420	1.420	0.014	0.042	0.062
Fe_2O_3	1.528	1.528	0.010	0.029	0.043
FeO	5.645	5.645	0.079	0.079	0.176
MnO	0.300	0.300	0.004	0.004	0.009
MgO	13.480	13.480	0.334	0.334	0.749
CaO	24.230	24.230	0.432	0.432	0.968
Na_2O	0.410	0.410	0.007	0.007	0.030
TiO_2	0.130	0.130	0.002	0.003	0.004
TOTAL	99.663	99.663	1.755	2.678	4.000

EN	FS	WO	AC	JA	CATI	CAFE	CATS
0.381	0.090	0.484	0.000	0.015	0.002	0.022	0.006

SAMPLE SV9
CLINOPYROXENE

ELT	WT%	WT% REC	IONPROP	AT PROP	CAT PRO
SiO_2	52.670	52.670	0.877	1.753	1.961
Al_2O_3	1.590	1.590	0.016	0.047	0.070
Fe_2O_3	1.065	1.065	0.007	0.020	0.030
FeO	6.111	6.111	0.085	0.085	0.190
MnO	0.250	0.250	0.004	0.004	0.008
MgO	13.520	13.520	0.335	0.335	0.750
CaO	23.990	23.990	0.428	0.428	0.957
Na_2O	0.410	0.410	0.007	0.007	0.030
TiO_2	0.130	0.130	0.002	0.003	0.004
TOTAL	99.737	99.737	1.759	2.681	4.000

EN	FS	WO	AC	JA	CATI	CAFE	CATS
0.383	0.097	0.479	0.000	0.015	0.002	0.015	0.008

SAMPLE SA10
CLINOPYROXENE

ELT	WT%	WT% REC	IONPROP	AT PROP	CAT PRO
SiO_2	50.040	50.040	0.833	1.666	1.958
Al_2O_3	0.732	0.732	0.007	0.022	0.034
Fe_2O_3	2.282	2.282	0.014	0.043	0.067
FeO	16.827	16.827	0.234	0.234	0.551
MnO	0.490	0.490	0.007	0.007	0.016
MgO	7.310	7.310	0.181	0.181	0.426
CaO	22.180	22.180	0.396	0.396	0.930
Na_2O	0.230	0.230	0.004	0.004	0.017
TOTAL	100.091	100.091	1.676	2.552	4.000

EN	FS	WO	AC	JA	CATI	CAFE	CATS
0.214	0.276	0.463	0.000	0.009	0.000	0.034	0.004

SAMPLE SA10
CLINOPYROXENE

ELT	WT%	WT% REC	IONPROP	AT PROP	CAT PRO
SiO_2	49.910	49.910	0.831	1.661	1.955
Al_2O_3	0.930	0.930	0.009	0.027	0.043
Fe_2O_3	2.159	2.159	0.014	0.041	0.064
FeO	16.657	16.657	0.232	0.232	0.546
MnO	0.480	0.480	0.007	0.007	0.016
MgO	7.270	7.270	0.180	0.180	0.424
CaO	22.020	22.020	0.393	0.393	0.924
Na_2O	0.320	0.320	0.005	0.005	0.024
TiO_2	0.130	0.130	0.002	0.003	0.004
TOTAL	99.876	99.876	1.672	2.549	4.000

EN	FS	WO	AC	JA	CATI	CAFE	CATS
0.214	0.275	0.462	0.000	0.012	0.002	0.032	0.003

SAMPLE SA10
GARNET CORE

ELT	WT%	WT% REC	IONPROP	AT PROP	CAT PRO
SiO_2	36.760	36.760	0.612	1.223	2.956
Al_2O_3	21.100	21.100	0.207	0.621	2.000
FeO	28.290	28.290	0.394	0.394	1.902
MnO	2.680	2.680	0.038	0.038	0.183
MgO	1.060	1.060	0.026	0.026	0.127
CaO	10.170	10.170	0.181	0.181	0.876
TOTAL	100.060	100.060	1.458	2.484	8.044

XAlm= 0.616 XSp= 0.059 XPy= 0.041 XGrs= 0.284

SAMPLE SA10
GARNET

ELT	WT%	WT% REC	IONPROP	AT PROP	CAT PRO
SiO_2	37.090	37.090	0.617	1.234	2.973
Al_2O_3	21.090	21.090	0.207	0.621	1.993
FeO	28.300	28.300	0.394	0.394	1.897
MnO	2.610	2.610	0.037	0.037	0.177
MgO	1.080	1.080	0.027	0.027	0.129
CaO	10.040	10.040	0.179	0.179	0.862
TOTAL	100.210	100.210	1.461	2.492	8.031

XAlm= 0.619 XSp= 0.058 XPy= 0.042 XGrs= 0.281

SAMPLE SA10
BIOTITE INCLUSION

ELT	WT%	IONPROP	AT PROP	CAT PRO
SiO_2	35.340	0.588	1.176	5.945
Al_2O_3	15.350	0.151	0.452	3.044
FeO	28.540	0.397	0.397	4.015
MnO	0.200	0.003	0.003	0.028
MgO	6.300	0.156	0.156	1.579
K_2O	9.110	0.097	0.097	1.955
TiO_2	3.730	0.047	0.093	0.472
TOTAL	98.570	1.438	2.374	17.039

XAnn= 0.718 XPhl= 0.282

SAMPLE SA10
BIOTITE INCLUSION

ELT	WT%	IONPROP	AT PROP	CAT PRO
SiO_2	35.020	0.583	1.166	5.923
Al_2O_3	15.490	0.152	0.456	3.089
FeO	28.060	0.391	0.391	3.969
MgO	6.320	0.157	0.157	1.593
K_2O	9.020	0.096	0.096	1.946
TiO_2	3.870	0.048	0.097	0.492
TOTAL	97.780	1.426	2.361	17.013

XAnn= 0.714 XPhl= 0.286

SAMPLE SA10
GARNET RIM

ELT	WT%	WT% REC	IONPROP	AT PROP	CAT PRO
SiO_2	36.840	36.840	0.613	1.226	2.951
Al_2O_3	21.260	21.260	0.209	0.626	2.007
FeO	28.330	28.330	0.394	0.394	1.898
MnO	3.090	3.090	0.044	0.044	0.210
MgO	1.070	1.070	0.027	0.027	0.128
CaO	9.940	9.940	0.177	0.177	0.853
TOTAL	100.530	100.530	1.463	2.493	8.046

XAlm= 0.615 XSp= 0.068 XPy= 0.041 XGrs= 0.276

SAMPLE SA10
GARNET RIM

ELT	WT%	WT% REC	IONPROP	AT PROP	CAT PRO
SiO_2	36.700	36.700	0.611	1.222	2.959
Al_2O_3	21.110	21.110	0.207	0.621	2.007
FeO	28.010	28.010	0.390	0.390	1.889
MnO	2.910	2.910	0.041	0.041	0.199
MgO	1.050	1.050	0.026	0.026	0.126
CaO	9.920	9.920	0.177	0.177	0.857
TOTAL	99.700	99.700	1.452	2.477	8.037

XAlm= 0.615 XSp= 0.065 XPy= 0.041 XGrs= 0.279

SAMPLE SA10
BIOTITE RIM

ELT	WT%	IONPROP	AT PROP	CAT PRO
SiO_2	35.160	0.585	1.170	5.909
Al_2O_3	14.800	0.145	0.436	2.932
FeO	29.140	0.406	0.406	4.096
MgO	5.600	0.139	0.139	1.403
K_2O	9.230	0.098	0.098	1.979
TiO_2	5.130	0.064	0.128	0.648
TOTAL	99.060	1.437	2.377	16.966

XAnn= 0.745 XPhl= 0.255

SAMPLE SA10
BIOTITE RIM

ELT	WT%	IONPROP	AT PROP	CAT PRO
SiO_2	34.830	0.580	1.159	5.917
Al_2O_3	14.690	0.144	0.432	2.942
FeO	28.810	0.401	0.401	4.093
MnO	0.140	0.002	0.002	0.020
MgO	5.470	0.136	0.136	1.385
Na_2O	0.090	0.001	0.001	0.030
K_2O	8.960	0.095	0.095	1.942
TiO_2	4.960	0.062	0.124	0.634
TOTAL	97.950	1.421	2.351	16.964

XAnn= 0.747 XPhl= 0.253

SAMPLE SA10
BIOTITE RIM

ELT	WT%	IONPROP	AT PROP	CAT PRO
SiO_2	34.650	0.577	1.153	5.896
Al_2O_3	14.460	0.142	0.426	2.901
FeO	29.340	0.408	0.408	4.176
MnO	0.150	0.002	0.002	0.022
MgO	5.630	0.140	0.140	1.428
K_2O	8.900	0.094	0.094	1.932
TiO_2	4.940	0.062	0.124	0.632
TOTAL	98.070	1.425	2.347	16.987

XAnn= 0.745 XPhl= 0.255

SAMPLE SA10
PLAGIOCLASE

ELT	WT%	IONPROP	AT PROP	CAT PRO
SiO_2	61.650	1.026	2.052	2.731
Al_2O_3	24.320	0.239	0.716	1.270
CaO	6.020	0.107	0.107	0.286
Na_2O	8.030	0.130	0.130	0.690
K_2O	0.120	0.001	0.001	0.007
TOTAL	100.140	1.503	3.006	4.983

XAn= 0.291 XAb= 0.702 XOr= 0.007

SAMPLE SA10
PLAGIOCLASE

ELT	WT%	IONPROP	AT PROP	CAT PRO
SiO_2	62.100	1.033	2.067	2.739
Al_2O_3	24.320	0.239	0.716	1.265
CaO	5.910	0.105	0.105	0.279
Na_2O	7.980	0.129	0.129	0.683
K_2O	0.130	0.001	0.001	0.007
TOTAL	100.440	1.508	3.018	4.973

XAn= 0.288 XAb= 0.704 XOr= 0.008

SAMPLE SA10
PLAGIOCLASE

ELT	WT%	IONPROP	AT PROP	CAT PRO
SiO_2	61.840	1.029	2.058	2.752
Al_2O_3	23.760	0.233	0.699	1.247
CaO	5.670	0.101	0.101	0.270
Na_2O	8.110	0.131	0.131	0.700
K_2O	0.190	0.002	0.002	0.011
TOTAL	99.570	1.496	2.991	4.980

XAn= 0.276 XAb= 0.713 XOr= 0.011

SAMPLE SA10
GARNET CORE

ELT	WT%	IONPROP	AT PROP	CAT PRO
SiO_2	37.050	0.617	1.233	2.966
Al_2O_3	21.490	0.211	0.632	2.028
FeO	33.510	0.466	0.466	2.243
MnO	2.220	0.031	0.031	0.151
MgO	2.700	0.067	0.067	0.322
CaO	3.630	0.065	0.065	0.311
TOTAL	100.600	1.457	2.495	8.021

XAlm= 0.741 XSp= 0.050 XPy= 0.106 XGrs= 0.103

SAMPLE SA10
GARNET CORE

ELT	WT%	IONPROP	AT PROP	CAT PRO
SiO_2	37.120	0.618	1.235	2.963
Al_2O_3	21.590	0.212	0.635	2.032
FeO	33.460	0.466	0.466	2.234
MnO	2.320	0.033	0.033	0.157
MgO	2.680	0.066	0.066	0.319
CaO	3.710	0.066	0.066	0.317
TOTAL	100.880	1.461	2.502	8.021

XAlm= 0.738 XSp= 0.052 XPy= 0.105 XGrs= 0.105

SAMPLE SA10
BIOTITE INCLUSION

ELT	WT%	IONPROP	AT PROP	CAT PRO
SiO_2	36.590	0.609	1.218	5.990
Al_2O_3	17.590	0.173	0.518	3.395
FeO	21.340	0.297	0.297	2.922
MgO	10.920	0.271	0.271	2.664
Na_2O	0.160	0.003	0.003	0.051
K_2O	8.600	0.091	0.091	1.796
TiO_2	1.700	0.021	0.043	0.209
TOTAL	96.900	1.464	2.440	17.027

XAnn= 0.523 XPhl= 0.477

SAMPLE SA10
BIOTITE INCLUSION

ELT	WT%	IONPROP	AT PROP	CAT PRO
SiO_2	35.700	0.594	1.188	5.889
Al_2O_3	17.740	0.174	0.522	3.450
FeO	21.660	0.301	0.301	2.988
MgO	11.040	0.274	0.274	2.714
Na_2O	0.190	0.003	0.003	0.061
K_2O	8.230	0.087	0.087	1.732
TiO_2	1.810	0.023	0.045	0.225
TOTAL	96.370	1.456	2.421	17.058

XAnn= 0.524 XPhl= 0.476

SAMPLE SA10
GARNET RIM

ELT	WT%	WT% REC	IONPROP	AT PROP	CAT PRO
SiO_2	37.070	37.070	0.617	1.234	2.982
Al_2O_3	21.130	21.130	0.207	0.622	2.004
FeO	33.440	33.440	0.465	0.465	2.250
MnO	2.620	2.620	0.037	0.037	0.179
MgO	2.230	2.230	0.055	0.055	0.267
CaO	3.870	3.870	0.069	0.069	0.334
TOTAL	100.360	100.360	1.451	2.482	8.016

XAlm= 0.743 XSp= 0.059 XPy= 0.088 XGrs= 0.110

SAMPLE SA10
GARNET RIM

ELT	WT%	WT% REC	IONPROP	AT PROP	CAT PRO
SiO_2	37.040	37.040	0.616	1.233	2.982
Al_2O_3	21.100	21.100	0.207	0.621	2.003
FeO	33.490	33.490	0.466	0.466	2.255
MnO	2.530	2.530	0.036	0.036	0.173
MgO	2.140	2.140	0.053	0.053	0.257
CaO	4.030	4.030	0.072	0.072	0.348
TOTAL	100.330	100.330	1.450	2.480	8.017

XAlm= 0.744 XSp= 0.057 XPy= 0.085 XGrs= 0.115

SAMPLE SA10
BIOTITE RIM

ELT	WT%	IONPROP	AT PROP	CAT PRO
SiO_2	36.640	0.610	1.220	5.993
Al_2O_3	17.800	0.175	0.524	3.433
FeO	20.510	0.285	0.285	2.806
MgO	10.860	0.269	0.269	2.647
Na_2O	0.270	0.004	0.004	0.086
K_2O	8.890	0.094	0.094	1.855
TiO_2	1.790	0.022	0.045	0.220
TOTAL	96.760	1.460	2.442	17.041

XAnn= 0.515 XPhl= 0.485

SAMPLE SA10
BIOTITE RIM

ELT	WT%	IONPROP	AT PROP	CAT PRO
SiO_2	36.980	0.615	1.231	5.983
Al_2O_3	17.980	0.176	0.529	3.430
FeO	20.770	0.289	0.289	2.810
MgO	11.130	0.276	0.276	2.684
Na_2O	0.190	0.003	0.003	0.060
K_2O	9.010	0.096	0.096	1.860
TiO_2	1.790	0.022	0.045	0.218
TOTAL	97.850	1.478	2.469	17.044

XAnn= 0.512 XPhl= 0.488

SAMPLE SLK1
GARNET CORE

ELT	WT%	WT% REC	IONPROP	AT PROP	CAT PRO
SiO_2	36.930	36.930	0.615	1.229	2.956
Al_2O_3	21.410	21.410	0.210	0.630	2.020
FeO	33.760	33.760	0.470	0.470	2.260
MnO	1.580	1.580	0.022	0.022	0.107
MgO	3.020	3.020	0.075	0.075	0.360
CaO	3.860	3.860	0.069	0.069	0.331
TOTAL	100.560	100.560	1.460	2.495	8.034

XAlm= 0.739 XSp= 0.035 XPy= 0.118 XGrs= 0.108

SAMPLE SLK1
GARNET CORE

ELT	WT%	WT% REC	IONPROP	AT PROP	CAT PRO
SiO_2	37.360	37.360	0.622	1.243	2.985
Al_2O_3	21.420	21.420	0.210	0.630	2.018
FeO	33.130	33.130	0.461	0.461	2.214
MnO	1.580	1.580	0.022	0.022	0.107
MgO	3.170	3.170	0.079	0.079	0.377
CaO	3.580	3.580	0.064	0.064	0.306
TOTAL	100.240	100.240	1.458	2.500	8.007

XAlm= 0.737 XSp= 0.036 XPy= 0.126 XGrs= 0.102

SAMPLE SLK1
BIOTITE INCLUSION

ELT	WT%	IONPROP	AT PROP	CAT PRO
SiO_2	36.690	0.611	1.221	5.972
Al_2O_3	18.290	0.179	0.538	3.510
FeO	18.090	0.252	0.252	2.463
MgO	12.410	0.308	0.308	3.010
CaO	0.150	0.003	0.003	0.026
Na_2O	0.320	0.005	0.005	0.101
K_2O	8.000	0.085	0.085	1.661
TiO_2	1.680	0.021	0.042	0.206
TOTAL	95.630	1.463	2.454	16.949

XAnn= 0.450 XPhl= 0.550

SAMPLE SLK1
BIOTITE INCLUSION

ELT	WT%	IONPROP	AT PROP	CAT PRO
SiO_2	36.130	0.601	1.203	5.975
Al_2O_3	17.960	0.176	0.529	3.502
FeO	18.220	0.254	0.254	2.520
MgO	12.140	0.301	0.301	2.992
CaO	0.330	0.006	0.006	0.058
Na_2O	0.410	0.007	0.007	0.131
K_2O	7.350	0.078	0.078	1.551
TiO_2	1.550	0.019	0.039	0.193
TOTAL	94.090	1.442	2.415	16.923

XAnn= 0.457 XPhl= 0.543

SAMPLE SLK1
GARNET RIM

ELT	WT%	WT% REC	IONPROP	AT PROP	CAT PRO
SiO_2	36.640	36.640	0.610	1.220	2.975
Al_2O_3	21.060	21.060	0.207	0.620	2.016
FeO	32.690	32.690	0.455	0.455	2.220
MnO	2.650	2.650	0.037	0.037	0.182
MgO	2.220	2.220	0.055	0.055	0.269
CaO	4.080	4.080	0.073	0.073	0.355
TOTAL	99.340	99.340	1.436	2.459	8.017

XAlm= 0.734 XSp= 0.060 XPy= 0.089 XGrs= 0.117

SAMPLE SLK1
GARNET RIM

ELT	WT%	WT% REC	IONPROP	AT PROP	CAT PRO
SiO_2	36.800	36.800	0.612	1.225	2.969
Al_2O_3	21.290	21.290	0.209	0.627	2.025
FeO	32.980	32.980	0.459	0.459	2.225
MnO	2.670	2.670	0.038	0.038	0.182
MgO	2.230	2.230	0.055	0.055	0.268
CaO	4.050	4.050	0.072	0.072	0.350
TOTAL	100.020	100.020	1.445	2.476	8.019

XAlm= 0.735 XSp= 0.060 XPy= 0.089 XGrs= 0.116

SAMPLE SLK1
BIOTITE RIM

ELT	WT%	IONPROP	AT PROP	CAT PRO
SiO_2	35.880	0.597	1.194	5.950
Al_2O_3	17.550	0.172	0.516	3.431
FeO	20.610	0.287	0.287	2.859
MgO	11.050	0.274	0.274	2.731
CaO	0.160	0.003	0.003	0.028
Na_2O	0.330	0.005	0.005	0.106
K_2O	8.120	0.086	0.086	1.718
TiO_2	1.630	0.020	0.041	0.203
Cr_2O_3	0.120	0.001	0.002	0.010
TOTAL	95.450	1.446	2.408	17.038

XAnn= 0.511 XPhl= 0.489

SAMPLE SLK1
BIOTITE RIM

ELT	WT%	IONPROP	AT PROP	CAT PRO
SiO_2	36.880	0.614	1.227	5.955
Al_2O_3	18.140	0.178	0.534	3.453
FeO	21.010	0.292	0.292	2.837
MgO	11.280	0.280	0.280	2.714
CaO	0.220	0.004	0.004	0.038
Na_2O	0.210	0.003	0.003	0.066
K_2O	8.230	0.087	0.087	1.695
TiO_2	1.730	0.022	0.043	0.210
Cr_2O_3	0.160	0.001	0.002	0.014
TOTAL	97.860	1.481	2.474	16.982

XAnn= 0.511 XPhl= 0.489

SAMPLE SA13
GARNET

ELT	WT%	WT% REC	IONPROP	AT PROP	CAT PRO
SiO_2	37.540	37.540	0.625	1.249	2.980
Al_2O_3	21.280	21.280	0.209	0.626	1.991
FeO	27.590	27.590	0.384	0.384	1.831
MnO	3.120	3.120	0.044	0.044	0.210
MgO	1.690	1.690	0.042	0.042	0.200
CaO	9.560	9.560	0.170	0.170	0.813
TOTAL	100.780	100.780	1.474	2.516	8.025

XAlm= 0.600 XSp= 0.069 XPy= 0.065 XGrs= 0.266

SAMPLE SA13
GARNET

ELT	WT%	WT% REC	IONPROP	AT PROP	CAT PRO
SiO_2	37.270	37.270	0.620	1.240	2.981
Al_2O_3	21.140	21.140	0.207	0.622	1.994
FeO	27.280	27.280	0.380	0.380	1.825
MnO	2.710	2.710	0.038	0.038	0.184
MgO	1.840	1.840	0.046	0.046	0.219
CaO	9.550	9.550	0.170	0.170	0.819
TOTAL	99.790	99.790	1.461	2.496	8.022

XAlm= 0.599 XSp= 0.060 XPy= 0.072 XGrs= 0.269

SAMPLE SA13

HORNBLENDE			LOWER BOUND= ALL Fe^{2+}	SUM Ca=15 SUM FM=13	UPPER BOUND= SUM FM=13 SUM Ca=15	AV Fe^{3+}
SiO_2	41.40	SiO_2	6.308	6.251	6.302	6.277
Al_2O_3	13.59	Al_2O_3	2.441	2.419	2.439	2.429
Fe_2O_3	0.00	Fe_2O_3	0.000	0.416	0.044	0.231
FeO	21.14	FeO	2.694	2.253	2.648	2.450
MnO	0.27	MnO	0.035	0.035	0.035	0.035
MgO	6.50	MgO	1.476	1.463	1.475	1.469
CaO	11.61	CaO	1.896	1.878	1.894	1.886
Na_2O	1.31	Na_2O	0.387	0.384	0.387	0.385
K_2O	1.02	K_2O	0.198	0.196	0.198	0.197
TiO_2	1.43	TiO_2	0.164	0.162	0.164	0.163
TOTAL	98.27	SUMFM	13.119	13.000	13.106	13.053
		$Fe^{2+}/Fe^{2+}+Mg$	0.646	0.606	0.642	0.625
		$Fe^{3+}/Fe^{3+}+Fe^{2+}$	0.000	0.156	0.016	0.086
		Aliv	1.692	1.749	1.698	1.723
		Alvi	0.750	0.671	0.741	0.706
		NAM4	-0.014	0.122	-0.000	0.061
		NA-A	0.401	0.262	0.387	0.324
		SUMA	0.600	0.459	0.585	0.521

SAMPLE SA13

HORNBLENDE			LOWER BOUND= ALL Fe^{2+}	SUM Ca=15 SUM FM=13	UPPER BOUND= SUM FM=13 SUM Ca=15	AV Fe^{3+}
SiO_2	41.08	SiO_2	6.259	6.188	6.240	6.214
Al_2O_3	13.48	Al_2O_3	2.421	2.394	2.414	2.404
Fe_2O_3	0.00	Fe_2O_3	0.000	0.520	0.140	0.331
FeO	21.62	FeO	2.755	2.203	2.606	2.404
MnO	0.27	MnO	0.035	0.034	0.035	0.035
MgO	6.63	MgO	1.505	1.488	1.501	1.495
CaO	11.62	CaO	1.897	1.876	1.891	1.883
Na_2O	1.43	Na_2O	0.422	0.418	0.421	0.419
K_2O	1.03	K_2O	0.200	0.198	0.200	0.199
TiO_2	1.51	TiO_2	0.173	0.171	0.173	0.172
P2O5	0.00	P2O5	0.000	0.000	0.000	0.000
Cr_2O_3	0.00	Cr_2O_3	0.000	0.000	0.000	0.000
NiO	0.00	NiO	0.000	0.000	0.000	0.000
TOTAL	98.67	SUMFM	13.149	13.000	13.109	13.054
		$Fe^{2+}/Fe^{2+}+Mg$	0.647	0.597	0.635	0.617
		$Fe^{3+}/Fe^{3+}+Fe^{2+}$	0.000	0.191	0.051	0.121
		Aliv	1.741	1.812	1.760	1.786
		Alvi	0.680	0.582	0.654	0.618
		NAM4	-0.046	0.124	0.000	0.062
		NA-A	0.468	0.293	0.421	0.357
		SUMA	0.669	0.491	0.621	0.556

SAMPLE SA13
PLAGIOCLASE

ELT	WT%	IONPROP	AT PROP	CAT PRO
SiO_2	57.620	0.959	1.918	2.615
Al_2O_3	25.610	0.251	0.754	1.370
CaO	8.530	0.152	0.152	0.415
Na_2O	6.760	0.109	0.109	0.595
K_2O	0.070	0.001	0.001	0.004
TOTAL	98.590	1.472	2.933	4.999

XAn= 0.409 XAb= 0.587 XOr= 0.004

SAMPLE SA13
PLAGIOCLASE

ELT	WT%	IONPROP	AT PROP	CAT PRO	
SiO_2	57.680	0.960	1.920	2.612	
Al_2O_3	25.700	0.252	0.756	1.372	
FeO	0.200	0.003	0.003	0.008	
CaO	8.500	0.152	0.152	0.412	
Na_2O	6.720	0.108	0.108	0.590	
K_2O	0.090	0.001	0.001	0.005	
TOTAL	98.890	98.890	1.476	2.940	5.000

XAn= 0.409 XAb= 0.586 XOr= 0.005

SAMPLE SA13
PLAGIOCLASE

ELT	WT%	IONPROP	AT PROP	CAT PRO
SiO_2	57.080	0.950	1.900	2.590
Al_2O_3	25.980	0.255	0.765	1.390
FeO	0.330	0.005	0.005	0.013
CaO	9.050	0.161	0.161	0.440
Na_2O	6.370	0.103	0.103	0.560
K_2O	0.070	0.001	0.001	0.004
TOTAL	98.880	1.474	2.934	4.997

XAn= 0.438 XAb= 0.558 XOr= 0.004

SAMPLE SA13
PLAGIOCLASE

ELT	WT%	IONPROP	AT PROP	CAT PRO
SiO_2	59.100	0.984	1.967	2.671
Al_2O_3	24.640	0.242	0.725	1.313
CaO	7.540	0.134	0.134	0.365
Na_2O	7.280	0.117	0.117	0.638
K_2O	0.170	0.002	0.002	0.010
TOTAL	98.730	1.479	2.946	4.997

XAn= 0.360 XAb= 0.630 XOr= 0.010

SAMPLE SA13
PLAGIOCLASE

ELT	WT%	IONPROP	AT PROP	CAT PRO
SiO_2	59.160	0.985	1.969	2.669
Al_2O_3	24.840	0.244	0.731	1.321
CaO	7.410	0.132	0.132	0.358
Na_2O	7.290	0.118	0.118	0.638
K_2O	0.130	0.001	0.001	0.007
TOTAL	98.830	1.479	2.951	4.993

XAn= 0.357 XAb= 0.636 XOr= 0.007

SAMPLE SA13
HORNBLENDE

LOWER BOUND= SUM Ca=15 UPPER BOUND= SUM FM=13

			ALL Fe^{2+}	SUM FM=13	SUM Ca=15	AV Fe^{3+}
SiO_2	41.41	SiO_2	6.386	6.332	6.383	6.357
Al_2O_3	12.58	Al_2O_3	2.287	2.268	2.286	2.277
Fe_2O_3	0.00	Fe_2O_3	0.000	0.386	0.021	0.204
FeO	20.97	FeO	2.704	2.295	2.682	2.488
MnO	0.23	MnO	0.030	0.030	0.030	0.030
MgO	6.75	MgO	1.551	1.538	1.551	1.544
CaO	11.48	CaO	1.897	1.881	1.896	1.888
Na_2O	1.45	Na_2O	0.434	0.430	0.433	0.432
K_2O	0.97	K_2O	0.191	0.189	0.191	0.190
TiO_2	1.31	TiO_2	0.152	0.151	0.152	0.151
TOTAL	97.15	SUMFM	13.110	13.000	13.104	13.052
		$Fe^{2+}/Fe^{2+}+Mg$	0.635	0.599	0.634	0.617
		$Fe^{3+}/Fe^{3+}+Fe^{2+}$	0.000	0.144	0.008	0.076
		Aliv	1.614	1.668	1.617	1.643
		Alvi	0.672	0.600	0.669	0.634
		NAM4	-0.007	0.119	0.000	0.060
		NA-A	0.440	0.311	0.433	0.372
		SUMA	0.631	0.500	0.624	0.562

SAMPLE SA13
HORNBLENDE

LOWER BOUND= SUM Ca=15 UPPER BOUND= SUM FM= 13

			ALL Fe^{2+}	SUM FM=13	SUM Ca=15	AV Fe^{3+}
SiO_2	42.11	SiO_2	6.395	6.329	6.390	6.359
Al_2O_3	12.77	Al_2O_3	2.286	2.263	2.284	2.273
Fe_2O_3	0.00	Fe_2O_3	0.000	0.475	0.036	0.257
FeO	21.47	FeO	2.727	2.223	2.689	2.455
MnO	0.22	MnO	0.028	0.028	0.028	0.028
MgO	6.84	MgO	1.548	1.532	1.547	1.539
CaO	11.53	CaO	1.876	1.857	1.875	1.866
Na_2O	1.41	Na_2O	0.415	0.411	0.415	0.413
K_2O	0.94	K_2O	0.182	0.180	0.182	0.181
TiO_2	1.33	TiO_2	0.152	0.150	0.152	0.151
TOTAL	98.62	SUMFM	13.136	13.000	13.125	13.062
		$Fe^{2+}/Fe^{2+}+Mg$	0.638	0.592	0.635	0.615
		$Fe^{3+}/Fe^{3+}+Fe^{2+}$	0.000	0.176	0.013	0.095
		Aliv	1.605	1.671	1.610	1.641
		Alvi	0.681	0.591	0.674	0.632
		NAM4	-0.012	0.143	0.000	0.072
		NA-A	0.427	0.268	0.415	0.341
		SUMA	0.609	0.448	0.597	0.522

MINERAL ABBREVIATONS

Acm	acmite	Dg	diginite	Mgs	magnesite
Act	actinolite	Di	diopside	Mrb	magnesioriebeckite
Agt	aegerine-augite	Dol	dolomite	Mag	magnetite
Ak	åkermanite	Drv	dravite	Mrg	margarite
Ab	albite	Eck	eckermannite	Mel	melilite
Aln	allanite	Ed	edenite	Mc	microcline
Alm	almandine	Elb	elbaite	Mo	molybdenite
Anl	analcite	En	enstatite	Mnz	monazite
Ant	anatase	Ep	epidote	Mtc	monticellite
And	andalusite	Fst	fassite	Mnt	montmorillonite
Adr	andradite	Fa	fayalite	Mul	mullite
Anh	anhydrite	Fac	ferroactinolite	Ms	muscovite
Ank	ankerite	Fed	ferroedenite	Ntr	natrolite
Ann	annite	Fs	ferrosilite	Ne	nepheline
An	anorthite	Fts	ferrotschermakite	Nrb	norbergite
Atg	antigorite	Fl	fluorite	Nsn	nosean
Ath	athophyllite	Fo	forsterite	Ol	olivine
Ap	apatite	Gn	galena	Omp	omphacite
Apo	apophyllite	Grt	garnet	Oam	orthoamphibole
Arg	aragonite	Ged	gedrite	Or	orthoclase
Arf	arfvedsonite	Gh	gehleite	Opx	orthopyroxene
Apy	arsenopyrite	Gbs	gibbsite	Pg	paragonite
Aug	augite	Glt	glauconite	Prg	pargasite
Ax	axinite	Gln	glaucophane	Pct	pectolite
Brt	barite	Gt	goethite	Pn	pentlandite
Brl	beryl	Gr	graphite	Per	periclase
Bt	biotite	Grs	grossularite	Prv	perovskite
Bhm	boehmite	Gru	grunerite	Phl	phlogopite
Bn	bornite	Gp	gypsum	Pgt	pigeonite
Brk	brookite	Hl	halite	Pl	plagioclase
Brc	brucite	Hs	hastingsite	Prh	prehnite
Bst	bustamte	Hyn	haüyne	Pen	protoenstatite
Cam	Ca clinoamphibole	Hd	hedenbergite	Pmp	pumpellyite
Cpx	Ca clinopyroxene	Hem	haematite	Py	pyrite
Cal	calcite	Hc	hercynite	Prp	pyrope
Ccn	cancrinite	Hul	heulandite	Prl	pyrophyllite
Crn	carnegieite	Hbl	hornblende	Po	pyrrhotite
Cst	cassiterite	Hu	humite	Qtz	quartz
Cls	celestite	Ill	illite	Rbk	riebekite
Cbz	chabazite	Ilm	ilmenite	Rds	rhodochrosite
Cc	chalcocite	Jd	jadeite	Rdn	rhodonite
Ccp	chalcopyrie	Jh	johannsenite	Rt	rutile
Chl	chlorite	Krs	kaersutite	Sa	sanidine
Cld	chloritoid	Kls	kalsilite	Spr	sapphirine
Chn	chondrodite	Kln	kaolinite	Scp	scapolite
Chr	chromite	Ktp	kataphorite	Srl	schorl
Ccl	chrysocolla	Kfs	K-feldspar	Srp	serpentine
Ctl	chrysotile	Krn	kornerupine	Sd	siderite
Cen	clinoenstatite	Ky	kyanite	Sil	sillimanite
Cfs	clinoferrosilite	Lmt	laumontite	Sdl	sodalite

Chu	clinohunite	Lws	lawsonite	Sps	spessartine
Czo	clinozoisite	Lpd	lepidolite	Sp	sphalerite
Crd	cordierite	Lct	leucite	Spn	sphene
Crn	corundum	Lm	limonite	Spl	spinel
Cv	covellite	Lz	lizardite	Spd	spodumene
Crs	cristobalite	Lo	loellingite	St	staurolite
Cum	cummingtonite	Mgh	maghemite	Stb	stilbite
Dsp	diaspore	Mkt	magnesiokatophorite	Stp	stilpnomelane
Str	strontianite	Tlc	talc	Tmp	thompsonite
Ttn	titanite	Tro	troilite	Wth	witherite
Toz	topaz	Ts	tschermakite	Wo	wollastonite
Tur	tourmaline	Usp	ulvöspinel	Wus	wustite
Tr	tremolite	Vrm	vermiculite	Zrn	zircon
Trd	tridymite	Ves	vesuvianite	Zo	zoisite

APPENDIX 3

PARTITION COEFFICIENTS

INTRODUCTION

This appendix presents a compilation of partition coefficients collected during the course of this study. The numbers in parentheses refer to the source (numbered in the reference list which follows the tables) of the particular coefficient. The letter in parentheses after the element in column 1 provides an indication of the rock type from which the coefficient was calculated eg (A) = acid and (B) = basic.

	Pl	Amph	Kks	Bt	Opx
La(B)	.14(2)	~.27(2)	.2-.01(10)	.2-17(10)	
La(B)		.17-.44(2)			
La(A)	~.32(2)	.85(2)	.404(13)	.32(2)	~.65(2)
La(A)	.24-.49(2)		.07-.1(11)		.5-.9(2)
La				.32(3)	
Ce(B)	~.14(2)	~.34(2)			~.02(2)
Ce(B)	.06-.3(2)	.09-.54(2)	.391(13)		.003-.04(2)
Ce(A)	~.24(2)	~1.2(2)	.04(2)	.04,.38(2)	~.46(2)
Ce(A)	.11-.4(2)	.43-1.8(2)			.08-1.03(2)
Ce	.1(4)		.02-.06(11)	.03(4)	.03(4)
Nd(B)	~.08(2)	.19(2)			.05(9)
Nd(B)	.02-.2(2)				.03,.06(2)
Nd(A)	~.19(2)	~3.2(9)	.03(2)	.04(2)	~.62(2)
Nd(A)	.06-29(2)	1-4.3(2)	.03-.04(11)		.11-1.2(2)
Sm(B)	.07(4)		.02(3)	.03(4)	.01(4)
Sm(B)	~.08	~.91(2)	.359(13)		~.05(2)
Sm(B)	.02-.2(2)	.34-1.46(2)			.01-.1(2)
Sm(A)	.13(9)	5.4(9)	.02(9)	.06-.39(9)	.7(9)
Eu(B)	~.32(2)	1.01(2)			.05(9)
Eu(B)	.06-.73(2)	.36-1.49(2)	2.1(13)		.02,.08(2)
Eu(A)	~2(2)	~3.6(9)	1.13(9)	.15,.33(2)	~.5(2)
Eu(A)	.82-4.2(2)	1.2-5.9(2)	3.3-6.5(11)		.11-1(2)
Eu	.3(4)			.03(4)	.013(4)
Eu+	.06(4)			.03(4)	.013(4)
Gd(B)	~.1(2)	1.1(2)			
Gd(B)	.03-.21(2)	.51-1.7(2)			
Gd(A)	~.16(2)		.07(12)	.08,.44(2)	~1.1(2)
Gd(A)	.11-.24(2)	1-10(12)			.17-2.2(2)
Dy(B)	~.09(2)	.64(2)			.12,.29(2)
Dy(B)	.01-.2(2)				
Dy(A)	~.13(2)	~9(2)	.04-.09(11)	.1(2)	~.7(2)
Dy(A)	.04-.45(2)	2.3-14(2)	.006(2)		.26-1.3(2)
Er(B)	~.08(2)	.48(2)			.16,.46(2)
Er(B)	.02-.24(2)				
Er(A)	~.05(2)	~8(2)	.006(2)	.16(2)	~.61(2)
Er(A)	.03-.08(2)	2.4(11)			.43-.73(2)
Yb(B)	.07(9)	.97(9)	.143(13)		.34(9)
Yb(A)	.08(9)	6.2(9)	.012(9)	.18,.67(2)	1(9)
Yb	.06(4)		.03-.04(11)	.04(4)	
Lu(B)	.08(9)	.89(9)	.126(13)		.11(9)

	Cpx	Gt	Ol	Phl	Qtz
La(B)	.08(2)	.03,.08(2)			
La(A)	~.6(2)	~.39(2)	.01-20(1)		.012-.018(11)
La(A)	.5-.8(2)	.28-.54(2)			.003(13)
Ce(B)	~.34(2)	.05(2)	.0009(2)	.03(2)	
Ce(B)	.17-.65(2)				
Ce(A)	~.9(2)	~.62(2)			.006-.018(11)
Ce(A)	.6-1.2(2)	.35-.93(2)	.01(16)		.003(13)
Ce	.1(4)		.001(4)		
Nd(B)	.6(2)		.007,.01(2)	.03(9)	
Nd(B)	.32-1.3(2)				
Nd(A)	~2.1(2)	~.63(9)			.009-.024(11)
Nd(A)	1.4-2.9(2)	.53-.73(2)			
Sm(B)	.26(4)		.002(4)	.03(9)	
Sm(B)	~.9	~.6(2)	~.009(2)		.004(13)
Sm(B)	.43-1.8(2)	.07-1.25(2)	.003-.015(2)		
Sm(A)	2.7(9)	2.2(9)			.008-.017(11)
Eu(B)	~.9(2)	~.9(2)	.008(9)	.03(9)	
Eu(B)	.48-2(2)	.07-1.25(2)	.006,.010(10)		
Eu(A)	~1.9(9)	.7(9)			.03-.08(11)
Eu(A)	1.6-2.3(2)	.17-1.37(2)			.013(13)
Eu			.002(4)		
Eu+	.3(4)		.002(4)		
Gd(B)	.82,.88(2)		.012(2)		
Gd(B)		2.1,5.2(2)			
Gd(A)	~3.1(2)	~7.7(2)			
Gd(A)	2-4.8(2)	5.3-13.6(2)			
Dy(B)	~1.1(2)		.009,.014(2)	.03(2)	
Dy(B)	.56-1.46(2)				
Dy(A)	~3.3(2)	29(2)			
Dy(A)	2.2-4(2)				.01-.017(11)
Er(B)	~1(2)		.009,.017(2)		
Er(B)	.53-1.3(2)				
Er(A)		43(2)			
Yb(B)	1.0(9)	30(9)	.002(4)		
Yb(A)	2.1(2)	43(9)			.024(13)
Yb	.28(4)		.002(4)		
Ho(B)		19(9)			
Ho(A)		28(9)			
Lu(B)	.8(9)	35(9)			.028(13)

	Spn	Ilm	Mag	Ap	Zr	Aln
La(B)	6(11)	.02-8(10)			26.6(14)	820(2)
La(B)	13-25(8)		.9(11)		3.3(14)	
La(A)	45(8)2-9(14)	7.1(11)	~.53(2)	+46.1,(14)		1331(14)
La(A)	60+(14)		.24-.88(2)	21.7(14)		2362(14)
Ce(B)	80(7)		~.61(2)	18-56(14)	2.5(4)	635(2)
Ce(B)	30-50(8)			~31(2)	~4.2(2)	2063(14)
Ce(A)	87(14)	7.8(11)	~.61(2)	17-53(2)	2.3-7.4(2)	
Ce(A)	90+(14)		.28-1.15(2)	+41.6,25.8(14)	2.4,23.5(14)	1279(14)
Nd(B)	88.3(9)			~50(2)	~3.6(2)	460(9)
Nd(B)	60-80(8)			21-81(2)	2-7.6(2,11)	874(14)
Nd(A)	103(14)		~.88(2)	+55.8,29(14)	22,2.2(14)	463(14)
Nd(A)	152(14)		.35-1.8(2)	27-81(14)		1400(14)
Sm(B)	20(8)			63(4)	3(4)	205(2)
Sm(B)	102(9)	6.5(11)		29-89(14)	3.7,17.7(14)	438(14)
Sm(B)	80-150(8)			+65,31.4(14)	3.14(14)	756(14)
Sm(A)	~200(8)		.9(9)	54(2)		
Sm(A)	340,204(14)		.07-1.4(16)			
Sm(A)	9-60(14)					
Eu(B)	70-150(8)		.58(2)	30(4)	3(4)	80(2)
Eu(B)				15-21(2)	1.1-5.2(2)	81(14)
Eu(A)	180(8)		~.58(2)	27(9)	3.4(9)	107(14)
Eu(A)	157,181(14)		.28-.96(2)	20-50(14)	12,3.14(14)	122(14)
Eu(A)				27.3,25.2(14)		
Eu+				60(4)	8(4)	
Gd(B)	100(8)		1.9(12)	22(2)		130(2)
Gd(A)	200(8)				13.9,12(14)	214(14)
Gd(A)	383(14)		.11-1(16)	79(14)		
Dy(B)		4.9(11)		~42(2)	~48(2)	
Dy(B)	50-70(8)		~1.7(11)	17-69(2)	38-54(2)	
Dy(A)	100-200(8)					
Er(B)	40-50(8)			~31(2)	~140(2)	
Er(B)			1.2(12)	14-51(2)	120-150(2)	
Er(A)	100-150(8)					
Yb(B)	60(7)	4.1(11)	.4(2)	24(4)	300(4)	8.9(2)
Yb(B)	20-40(8)				270(14)	22(14)
Yb(A)	80-100(8)			21(2)	280(9)	24.5(14)
Yb(A)	231,104(14)				225,490(14)	
Tb(A)	326,248(14)			60,34(14)	26.3,37(14)	204,71(14)
Tb(A)						235(14)
Ho(A)	360(14)			71(14)	84.6(14)	64(14)
Lu(A)	176,92(14)			60,12(14)	300,635(14)	22(14)
Lu(a)	7-11(14)			11-30(14)	323(14)	7.7(14)

	Cpx	Grt	Ol	Phl	Qtz
Ta(A)	~.06(15)		.02(15)		
Nb	.1(1)	.01(1)	.01(1)	1(1)	
Nb(A)	.01-.03(3)				
Y	.2(1)	2(1)	.01(1)	.03(1)	
Y(A)	4(1)	35(1)		2(1)	
Rb(B)	~.04(2)		~.006(2)	3.1(2)	
Rb(B)	.001-.28(2)		.0002-.011(2)		
Rb(A)	.09(2)	.009(2)	.01-.1(10)		.01(13)
Rb(A)					.012-.016(11)
Rb	.001(4)				
Ba(B)	~.07(2)	.02(16)	~.006(2)	1.1(2)	
Ba(B)	.002-.39(2)		.0001-.011(2)		
Ba(A)	.02,.06(2)	.017(2)	.01-.07(10)		.004-.015(11)
Ba(A)					.013(13)
Ba	.01-1(10)		.001(4)		
Sr(B)	~.14(2)		.01(2)	3.1(2)	
Sr(B)	.07-.43(2)		.0001-.02(2)		
Sr(A)			.01-.07(10)		
Sr	.1-1(10)		.001(4)		
Sc(B)	~2.7(2)	~4(2)	~.17(2)		
Sc(B)	1.7-3.2(2)	2.6-5.4(2)	.14-22(2)		
Sc(A)	~22(2)	~16(2)	7-10(10)		.01-.015(11)
Sc(A)	18-28(2)	10.2-20.2(2)			.009(13)
Th(B)		.01-3(10)			
Th(B)			.01-3(10)		.006-.01(11)
Th(A)	~.13(2)				
Th(A)	.01-.25(2)				.004(13)
Zr	.05-.22(3)	.3(1)	.01(1)	.6(1)	
Zr(A)	.6(1)	1.2(1)	.01-.1(10	2(1)	.38(13)
Hf	~.35(15)		.02(15)		.018-.057(11)
Ni(B)	~2.6(2)		~14(2)		
Ni(B)			8-19(2)		
Ni(A)		.6(16)	8-20(10)		
Ni	2(4)				
Cr(B)	~8.4(2)	.06,.29(2)		11(2)	
Cr(B)	4.7-20(2)		2.1,1.1(15)		
Cr(A)	90(2)				
Cr(A)					.1(13)
Cr	10(4)				
K(B)	~.03(2)		~.007(2)	2.7(2)	
K(B)	.002-.27(2)		.0002-.008(2)		
K(A)	.01-.06(16)	.02(2)	.01(16)		
K(A)					.011-.014(11)
K	.002(4)				
V(B)	~1.3(2)		.03(2)		
V(B)	.8-1.9(2)				
V(A)	.9-18(16)	8(16)	.08(16)		
V(A)	~1.1(16)				
Zn(B)	.41(2)		.7(2)		
Zn(A)		~2.6(2)			
Zn(A)		1.7-3.6(2)			
Co	1-20(10)	2(16)	3-20(10)		.019(13)
Co	~3(16)				
Ti	.3(1)	.3(1)	.02(1)	.9(1)	
Ti(A)			.04(1)		.015-.04(11)

	Pl	Amph	Kfs	Bt	Opx
Ta(A)	.004,.55(15)	1.3(16)	.01-.1(15)		.35(16)
Nb	.01(1)	.8(1)		1.8(1)	.15(1)
Nb(A)				4-9.5(11)	
Y	.03(1)	1(1)		.03(1)	.5(1)
Y(A)	.1(1)	6(1)		1-1.4(11)	.9(2)
Rb(B)	~.1(2)	~.25(2)		3.1(4)	.02,.03(2)
Rb(B)	.03-.5(2)	.04-.4(2)	.21(13)		
Rb(A)	~.09(2)		~.38(2)	3.3,3.5(2)	~.09(2)
Rb(A)	.02-.46(2)		.11-.8(2)		.0005-.29(2)
Rb	.07(4)	.011(5)	1.2-2.4(11)		.001(4)
Ba(B)	~.23(2)	~.31(2)			.012,.014(2)
Ba(B)	.05-.59(2)	.1-.44(2)			
Ba(A)	~.5(2)	.35(2)	~6.6(2)	6.4,8.7(2)	~.02(2)
Ba(A)	.3-.92(2)		2.7-12.9(2)	7-30(10)	.003-.03(2)
Ba	.2(4)	.05(5)		1.1(4)	.001(4)
Sr(B)	~1.8(2)	~.57(2)			.01,.02(2)
Sr(B)	1.3-2.9(2)	.19-1.02(2)	2(13)		
Sr(A)	~6(2)	3-10(10)	~9.4(2)	.12,.36(2)	
Sr(A)	1.5-8.8(2)		3.6-26(2)		.009,.05(2)
Sr	2.2(4)	.58(5)	4.5-7.3(11)	.08(4)	.01(4)
Sc(B)		2.2,4.2(2)			1.2(2)
Sc(B)		2-5(10)		3-20(10)	18(11)
Sc(A)	~.07(2)	11-100(10)	.01-.7(10)	11.3(2)	~6.9(2)
Sc(A)	.01-.2(2)	20(2)	.124(13)	5-20(11)	6-7.7(2)
Th(B)		.02-.15(10)			~.02(2)
Th(B)			.055(13)	.2-2(10)	.003-.05(2)
Th(A)	~.04(2)	.22(2)	.02-.03(11)	.31(2)	.11-.15(11)
Th(A)	.01-.09(2)	.3-2(10)	.01-.1(10)		
Zr	<.01(3)	.5(1)	.1-.3(10)	.8-2(11)	.03(1)
Zr(A)	.1(1)	4(1)	.01-.06(11)	.2-2(10)	.2(1)
Hf	~.09(15)				
Ni(B)			.32(13)	.79-1.8(11)	5(2)
Ni(B)	.01-.7(10)	.6-2(10)			1.4-4.4(2)
Ni(A)				.2-2(10)	
Ni	.01(4)		.2-1(10)	3.5(4)	4(4)
Cr(B)	.01-.8(10)	.1,1.6(2)			10(2)
Cr(B)		.05-10(10)	.02-.08(10)		
Cr(A)	~.2(2)	23-90(16)	.02-.08(10)	5-50(10)	~1.6(2)
Cr(A)	.03-.7(2)	~30(16)	.32(13)	19(2)	.6-3(2)
Cr	.01(4)			7(4)	2(4)
K(B)	~.17(2)	~.6(2)		2.7(4)	.01,.02(2)
K(B)	.02-.36(2)	.33-.86(2)			
K(A)	~.19(2)	.33(16)	~1.4(2)	2.5,5.6(2)	.01-.02(16)
K(A)	.08-.33(2)		.64-2.2(2)		.0006,.002
K	.2(4)			2.7(4)	.001(4)
V(B)					.6(2)
V(B)					
V(A)	.01(16)	6-45(16)			~6(2)
V(A)		~32(16)			4.4-10(2)
Zn(B)		.42,.69(2)			
Zn(A)	~.38(2)			20(2)	~.9(2)
Zn(A)	.26-.6(2)	7(2)	.19(13)		.8-1(2)
Co	.001-.1(10)	1-50(10)	.02-.8(10)	8-100(10)	3-15(16)
Co		~13(16)			~6(16)
Ti	.04(1)	1.5(1)			.1(1)
Ti(A)	.05(1)	7(1)			

	Spn	Ilm	Mag	Ru	Ap	Zr	Aln
Nb(B)		2.3(6)	.4(6)	16(1)			
Nb(A)	7.6(6)	4.6(6)	2.5(1)	26.5(6)	.01(1)		
Nb	5.3(10)	.8(3)	.7(6)	16(3)			
Y(B)			.2(1)		20(1)		
Y(A)			2(1)10		40(1)	60(1)	
Rb		.03-.8(10)	.039(15)				
Ba(A)			~.07(2)				
Ba(A)	2.4,<.6(14)	.03-1(10)	05-.08(2)		<.3(14)		
Sr(B)		.03-1(1)	.15(15)				
Sr(A)					3.6(14)		
Sc(B)			1-20(10)				0.46+(14)
Sc(A)	8,10(14)	11(10)	15(6)		0.4(14)		
Sc(A)			3.3-4.5(2)		.45(14)		
Sc			1-3(16)				
Th(B)			.03-2(10)				225(14)
Th(A)	17.1(14)	7.5(11)	~.11(2)				168(14)
Th(A)	16.5+(14)		.04-.2(2)				420(14)
Zr(B)		.28(1)	.45(15)		.1(1)		
V			24-63(16)				
V			~30(16)				
Zr(A)	8.6(14)	.28(3)	.1(1)		7.4(14)	280(2)	
Hf(A)	9.4(14)		.31(15)				2(14)
Hf(A)	10.1(14)						9.8(14)
Ni(A)		1.5-50(10)	93(15)				
Cr(B)		3(10)	14(15)			.2(4)	
Cr(A)			~11(2)				
Cr(A)			5-20(2)				
Cr		3(11)	164(11)				
Zn(A)			~28				
Zn(A)		125(11)	19-35(2)				
Co		2-40(10)	14(15)				
Ti(B)		50(1)	7.5(1)				
Ti(A)			12.5(1)		.1(1)		
Ta(A)	236(14)		.68(15)				3.2(14)
Ta(A)	142(14)						1.9(14)
U(A)	9.9(14)						<6.7(14)
U(A)	20.8(14)						14(14)

REFERENCES

1. Pearce J.A. and Norry M.J. (1979) Petrogenetic implications of Ti, Zr, Y, and Nb variations in volcanic rocks. Contrib. Mineral. Petrol., 69, 33-47.

2. Henderson, P. (1982) Inorganic Geochemistry. Pergamon Press, Oxford, England. 353pp.

3. McCallum I.S. and Charette M.P. (1978) Zr and Nb partition coefficients: implications for the genesis of mare basalts, KREEP and sea floor basalts. Geochim. Cosmochim. Acta, 42, 859-869.

4. Cox, K.G., Bell, J.D. and Pankhurst, R.J. (1979). The Interpretation of Igneous Rocks. George Allen and Unwin. London. 450pp.

5. McCarthy T.S. and Hasty R.A.(1978) Trace element distribution patterns and their relationship to the crystallisation of granitic melts. Geochim. Cosmochim. Acta, 40, 1351-1358.

6. Green T.H. and Pearson N.J. (1987) An experimental study of Nb and Ta partitioning between Ti-rich minerals and silicate liquids at high pressure and temperature. Geochim. Cosmochim. Acta, 51, 55-62.

7. Tindle, A.G. and Pearce, J.A. (1981) Petrogenetic modelling of in situ fractional crystallisation in the zoned Loch Doon pluton, Scotland. Contrib. Mineral. Petrol., 78, 196-207.

8. Green T.H and Pearson N.J. (1986) Rare earth element partitioning between sphene and coexisting silicate liquid at high pressure and temperature. Chem. Geol., 55, 105-109.

9. Henderson P.(ed)(1984) Rare Earth Element Geochemistry. Elsevier, Amsterdam. 510pp.

10. Lemarchand, F., Villemant, B. and Calas, G. (1987) Trace element distribution coefficients in alkaline series. Geochim. Cosmochim. Acta, 51, 1071-1081.

11. Nash, W.P. and Crecraft, H.R. (1985) Partition coefficients for trace elements in silicic magmas. Geochim. Cosmochim. Acta, 49, 2309-2322.

12. Cameron, K.L. and Cameron M. (1986) Whole-rock/groundmass differentiation trendsof rare earth elements in high silica rhyolites. Geochim. Cosmochin. Acta, 50, 759-769.

13. Zolensky M.E., Sylvester P.J. and James B.P. (1988) Origin and significance of blue colouration in quartz from Llano rhyolite (llanite), north central Llano County, Texas. Amer. Mineral., 73, 313-323.

14. Sawka W.S. (1988) REE and trace element variations in accessory minerals and hornblende from the strongly zoned McMurry Meadows Pluton, California. Trans. Roy. Soc. Edinburgh: Earth Sciences, 79, 157-168.

15. Francalanci L. (1989) Trace element partition coefficients for minerals in shoshonitic and calc-alkaline rocks from Stromboli Island. Neues. Jahrbuch. Miner. Abh., 160, 229-247.

16. Gill J. (1981) Orogenic Andesites and Plate Tectonics.(p200-201). Springer-Verlag. Berlin. 390pp.